Real-time Bioaerosol Analysis in the Healthcare Environment

A thesis submitted to
THE NATIONAL UNIVERSITY OF IRELAND, CORK

ucc
Coláiste na hOllscoile Corcaigh, Éire
University College Cork, Ireland

for the degree of
DOCTOR OF PHILOSOPHY
By

Mehael Fennelly

Based on Research carried out at

School of Chemistry, Department of Pathology
&
Environmental Research Institute

Supervisors
Professor Michael Prentice
and *Professor John Sodeau*

Head of School
Dr Humphrey Moynihan

University College Cork
January 2020

Table of Contents

Declaration

This is to certify that the work I am submitting is my own and has not been submitted for another degree, either at University College Cork or elsewhere. All external references and sources are clearly acknowledged and identified within the contents. I have read and understood the regulations of University College Cork concerning plagiarism.

_____

Mehael Fennelly

Dedication

In loving memory of my Dad

Quotation

“A man who dares to waste one hour of time has not discovered the value of life”

— Charles Darwin

Acknowledgements

Being a blow in from Kildare my journey to UCC first started with Eilish O'Donoghue, it was during my final year project that she instilled a belief in me that I had the ability to pursue a PhD and I am forever grateful for that. She then introduced me to Dave O'Connor who directed me down south to UCC. A big thanks has to go to Dave as throughout my PhD he has always been on hand to help with all WIBS related information and of course how to deal with the big man John Sodeau. From the first time I met John I knew we'd get along brilliantly, and for my time in UCC we did. From leaving notes of inspiration on my desk to helping me get in contact with various connections regarding the instrument, John has been a great supervisor and a great friend. This brings me along nicely to the second half of my two supervisors Mike Prentice. I can't begin to thank Mike enough for all he has done for me the past three years, from correcting some of the rubbish I wrote to driving this project on, without him this thesis would certainly not be finished nor near finished. I am eternally grateful for all his help throughout my PhD. It has been an absolute pleasure to have worked with two wonderful supervisors.

My three years down here have been spent in the CRAC lab, which has seen many people come and go. When I first moved down Paddy was my first point of contact about the WIBS and hitting the town, I am thankful for him sharing his expertise in both with me. Paul and Niall who have had to listen to me rant and rave every morning about everything from football to snooker, these three years wouldn't have been the same without ye. Of course, a massive thanks must go to Stig Hellebust, who's knowledge of stats and coding is never ending, and I am lucky to have had you in the group to juggle ideas with. Consequently, it was your MatLab program and code that spurred me on to write my own for R-studio. And to the rest of the CRAC members Emer, Hayley, Julien, Elena and past CRAC guys Dave H, Ian and Trev who have all also helped me, thank you. Katherine in micro who helped me with cultures and Paddy who kindly allowed me to use his MAS-100 and Aoife in Pathology for sorting out all the registrations and shipping's, this was all greatly appreciated.

Two people have had to put up with my moods and strops more than most have been my mother Hannah and girlfriend Laura. Ye have both been by my side and have reassured me a million times that everything would be fine and always tried to make

me smile whenever I was down and if it were not for the support from both of ye this would have been a real struggle.
Without the funding from the Healthcare Infection Society this project would not have been possible so a big thank you must go to them, and of course their generosity with conference and travel grants was always appreciated.
It is impossible to thank everyone who helped me along the way as there is quite a few but I would like all them to know that every bit of help whether it was small or big, was always appreciated.

Abstract

Airborne infection has been difficult to study in hospitals. Conventional sampling methods for airborne organisms are limited in sample time intervals (minutes to hours) and conventional culture requirements, restricting organism detection and only allowing retrospective analysis (days). This limits their usefulness in analysing air quality and risks of airborne transmission of infection. They provide limited data for standard setting and assessing the effect of interventions designed to increase air quality and decrease airborne infection risks. Direct continuous bioaerosol sampling is an established technology used to characterise ambient external air. Portable instruments such as the Wideband Integrated Bioaerosol Sensor (WIBS) combine laser particle size and shape detection with signals of particle viability (fluorescence from amino acids and NAD(P)H) characteristic of bioaerosols. This aim of this thesis was to investigate the utility of continuous monitoring approaches including WIBS and other instruments to characterise indoor air bioaerosols in hospital environments and evaluate the results of interventions designed to increase air quality.

The WIBS-4A was used to characterise airborne biological particles in a 4-bedded hospital respiratory ward bay over a 4-week period before and during a plasma air treatment intervention designed to increase air quality. Twice-daily conventional impaction and settle plates and surface swabs were carried out in parallel with continuous WIBS bioaerosol monitoring. No statistical difference between conventional culture counts was detected during the plasma air treatment period compared with the control. Cumulative continuous monitoring plotted diurnally revealed raw numbers of airborne fluorescent particles were lowest at night, with four striking recurrent fluorescent particle peaks during the daytime when the number of particles increased by over 200-fold compared to the nocturnal minimum. These peaks corresponded to observed nebuliser use on the ward. WIBS analysis of the two nebulised therapy drugs used on the ward defined a characteristic fluorescence signature for nebuliser aerosols. This allowed design of a threshold filter to remove interferent nebulised drugs from fluorescent particle counts which did not eliminate bacteria when applied to experimentally aerosolised bacteria.

Both raw and filtered WIBS data (excluding nebulised drug particles) showed a statistically significant ~28% reduction in fluorescent particles, ($P<0.05$), during the operation of the plasma disinfection unit. The clinical significance of this requires further study. The effect of footfall counts on bioaerosol concentrations was also monitored by deploying an infra-red footfall counter in tandem with the WIBS instrument. Both devices were successful in identifying that the highest footfall count coincided with the highest bioaerosol concentrations observed on the ward, which also coincided with the main morning staff shift change and handover. The cumulative filtered count data was used to devise a statistical threshold which could be the basis of a standard for the environment tested.

The WIBS-4A was used in conjunction with the nebulised drug signatures to show that a portable extractor tent (Demistifier 2000, Peace Medical) was 100% efficacious in preventing spread of nebulised bronchodilator drug aerosols. This confirmed that use of Extractor tents prevents spread of drug particles from nebulised therapy.

Air DNA samples were taken on six separate days over three months on the respiratory ward, and a preliminary analysis suggested that in most cases the largest single group at Phylum level were Firmicutes (*Clostridiaceae*/*Clostridiales* Families). Because these bacteria are potentially of gastrointestinal origin, it was hypothesized the source could be a communal lavatory that was present within the ward bay. A week-long WIBS campaign was therefore undertaken in a communal office toilet to investigate aerosol production from different toilet activities. Increased fluorescent particles were found in lavatory air on flushing after defaecation compared to other activities. Previous studies reporting the effect of toilet lids have found that they prevent the spread of visible droplets on flushing, however the effect on smaller particles was less clear cut. This study found that placing the lid down before flushing the toilet reduced the number of airborne fluorescent particles produced by flushing following defaecation, however it significantly increased particle size, shape, particle fluorescent intensity and residency time of defaecation-related particles in the air. A hypothesis is presented to account for this, involving acoustic reverberation magnification of flush-related turbulence by the lid, and implications of this for toilet design are discussed

This thesis highlights the ability of continuous bioaerosol detection by instruments such as WIBS to provide biologically meaningful characterisation of the healthcare environment. This characterisation facilitates airborne particle source attribution, allows provisional standard setting, and provides a powerful mode of assessment of the results of interventions designed to increase air quality.

List of abbreviations and acronyms

ACH	Air Changes per Hour
AF	Asymmetry Factor
AGI-30	All Glass Impinger 30
AP	Alkaline Phosphate
APS	Aerodynamic Particle Sizer
ASHRAE	American Society of Heating and Refrigerating and Air-Conditioning Engineers
BAC	Benzalkonium Chloride
BAM	Beta Attenuation Monitor
BC	Bacterial Counts
BA	*Bacillus atrophaeus*
BSE	Biological Sampling Efficiencies
CDC	Centres for Disease Control
CDI	*C. difficile* infections
CF	Cystic Fibrosis
CFOPD	Cystic Fibrosis Outpatients Department
CFU	Colony Forming Units
COPD	Chronic Obstructive Pulmonary Disease
CPC	Condensation Particle Counter
CPE	Carbapenemase Producing Enterobacterales
CRAB	*Carbapenem-resistant Acinetobacter baumannii*
CRE	*Carbapenem-resistant Enterobacteriaceae*
CRE	*Carbapenem-resistant Enterobacteriaceae*
CRTsA	*Carbapenem-resistant Pseudomonas aeruginosa*
CVE	Cardiovascular Event
Da	Particle Aerodynamic Size
DAPI	4.76-diamino-2-phenylindole
DMT	Droplet Measurement Technologies
DNA	Deoxyribonucleic Acid
ECU	Electronics Control Unit

EIA	Enzyme Immunoassay
ELISA	Enzyme-Linked Immunosorbent Assay
EOD	Equivalent Optical Diameter
EPA	Environmental Protection Agency
ES	Electrostatic
FAP	Fluorescent Aerosol Particles
FBAP	Fluorescent Biological Aerosol Particles
FEV	Forced Expiratory Volume
FIA	Fluorescent Immunoassay
FL	Fungal Load
FLIM	Fluorescent Lifetime Imaging
FM	Fluorescent Mean Intensity
FPF	Fluorescent Particle Fraction
FS	Fluorescent Polystyrene Latex Spheres
FT	Forced Trigger
HAI	Healthcare Associated Infections
HD	Hand Dryer
HEPA	High Efficiency Particle Air / Arrestance
HG	High Gain
HIV	Human Immunodeficiency Virus
HPA	Health Protection Agency
HPLC-UV	Ultraviolet High-Performance Liquid Chromatography
HRP	Horseradish Peroxide
HSE	Health Service Executive
HULIS	Humic-like Substances
HVAC	Heating, ventilation and air conditioning
IAQ	Indoor Air Quality
ICP-MS	Inductively Coupled Plasma Mass Spectrometry
ICU	Intensive Care Units
IHSAB	Irish Health Services Accreditation Board
IMA	Index of Microbial Air Contamination
INAB	Irish National Accreditation Board
INAES	Irish National Adverse Events Study
ISO	International Organization for Standardization

JAD	Jet Air Dryer
KR	*Kocuria rhizophila*
LEV	Local Exhaust Ventilation
LG	Low Gain
LIF	Light Induced Fluorescence
LOQ	Limit of Quantification
MAS-100	Microbial Air Monitoring system-100
MBS	Multi-parameter Bioaerosol Sensor
MDR	Multi-Drug Resistant
MDRO	Multi-Drug-Resistant Organisms
MDR-TB	Multi-Drug Resistant Tuberculosis
MERS	Middle East Respiratory Syndrome
MMD	Mass Median Diameter
MRSA	Methicillin-Resistant Staphylococcus Aureus
MS2	Bacteriophage MS2
MSLI	Multistage all Glass Liquid Impinger
NAD(P)H	Nicotinamide Adenine Dinucleotide Phosphate
NADH	Nicotinamide Adenine Dinucleotide
Nd:YAG	Neodymium:Yttrium Aluminium Garnet
NOAA	National Oceanic and Atmospheric Sciences Administration
PA-300	Particle Analyser – 300
PAH	Polycyclic Aromatic Hydrocarbons
PBAP	Primary Biological Aerosol Particles
PFU	Plaque Forming Units
PM	Particulate Matter
PMT	Photomultiplier Tube
PPS	Point Prevalence Surveys
PSL	Polystyrene Latex
PSE	Physical Sampling Efficiencies
qPCR	Quantitative Polymerase Chain Reaction
SARS	Severe Acute Respiratory Syndrome
SAS	Surface Air System
SDA	Sabourands Dextrose Agar
SIBS	Spectral Intensity Bioaerosol Sensor

SLIT	Sustained release Lipid Inhalation Targeting
SM	*Serratia marcescens*
SOA	Secondary Organic Aerosols
SPL	Sound Pressure Level
SSI	Surgical Site Infection
TB	Tuberculosis
TSA	Trypticase Soy Agar
TVC`	Total Viable Counts
UV-APS	Ultraviolet Aerodynamic Particle Sizer
VOC	Volatile Organic Compounds
VRE	*Vancomycin-resistant Enterococcus*
WC	Water Closet
WHO	World Health Organisation
WIBS	Wideband Integrated Bioaerosol Sensor

Chapter 1

Introduction to Bioaerosols and Bioaerosol Sampling Techniques

Table of Contents

1.1 Introduction

Aerosols constitute a significant portion of the Earth's atmosphere. This ubiquity within the atmosphere results in substantial ecological, health, and climatic effects to the planet. Aerosols are defined as suspensions of liquid or solid particles in a gas that possess a broad range of physical diameters, which span from the ultrafine (i.e., <100 nm) to the super coarse >10 μm (Seinfeld and Pandis, 2016, Zhu et al., 2002, Després et al., 2012). Primary Biological Aerosol Particles (PBAP) make up a substantial fraction of the total aerosol, and encompass particle types such as pollen, fungal spores, and bacterial cells/agglomerates amongst many others and we encounter many of these in the indoor environment. In fact bioaerosols are estimated to make up 5-35% of indoor particulate matter (Mandal and Brandl, 2011). These bioaerosols may originate from outdoor sources by passing through windows and doors (Nazaroff, 2004), or derive from human activity (Hospodsky et al., 2012).

High concentrations of both fungal and bacterial spores have been implicated in numerous diseases and health problems for humans and domestic animals. For example, respiratory problems, such as chronic obstructive pulmonary disease (COPD) and hypersensitivity pneumonitis have been conclusively linked to aeroallergen interactions within both humans and animals (Seguin et al., 2010, Sforza and Marinou, 2017). Several spore forming fungal species, including *Aspergillus fumigatus*, *Aspergillus flavus*, *Aspergillus parasiticus*, and *Alternaria alternata* are also known to produce mycotoxins (Sorenson, 1999, Weinhold, 2007). This fact is important because the inhalation of mycotoxins has been linked with diseases such as cancer, as well as renal failure (Peraica et al., 1999, Straus, 2009). Likewise, the long-term exposure to fine particulate matter (<2.5 μm) by inhalation and deposition in the respiratory tract, has been determined to be deleterious to public health and leads to increased risk of morbidity and mortality of sensitive groups (Pope III et al., 2002, Künzli et al., 2000, Fenger, 1999).

Some human diseases encountered in the healthcare setting can be spread by bioaerosols containing infectious microorganisms including severe acute respiratory syndrome (SARS) (Roy and Milton, 2004), H1N1 influenza (Lau et al., 2009), and the Middle East respiratory syndrome (MERS) (Kutter et al., 2018). Monitoring for

bioaerosols in the healthcare environment is one of the many tools that can be used to access the indoor air quality and the risk of infectious disease outbreaks (Lindsley et al., 2017). Bioaerosol monitoring may be appropriate during workplace health and exposure assessments, epidemiological investigations, research studies, or in situations deemed appropriate by the healthcare authorities. Sampling can also be used to evaluate healthcare environments before and after validation of microbial contamination (Lindsley et al., 2017).

1.2 Indoor Bioaerosols

Bioaerosols are established as agents of transmission of several infectious diseases, and their components are linked with the development and exacerbation of chronic respiratory illness (Hardin et al., 2003, Husman, 1996, Létourneau et al., 2010, Sax et al., 2015, Douwes et al., 2003, Flannigan et al., 2016, Morawska et al., 2013). The majority of people's existence is lived indoors, ~87% of life is spent indoors (Brasche and Bischof, 2005, Odeh and Hussein, 2016, Klepeis et al., 2001, Jenkins et al., 1992). This leads to extended exposure to indoor bioaerosols. Although outdoor particles have a high contribution to indoor bioaerosols (Chen and Zhao, 2011, Adams et al., 2013), bioaerosols emitted from indoor sources also contribute significantly to indoor bioaerosols (You et al., 2013, Morawska et al., 2008, Hospodsky et al., 2012). The known existence of harmful and potentially pathogenic indoor bioaerosols requires a streamlined classification and quantification of indoor bioaerosols to evaluate their effects, as well as identifying their sources. Potential sources aerosols indoors have been illustrated (Figure 1.1) by Marsh et al. (Marsh, 2016)

Figure 1.1 Sources of indoor bioaerosols in the indoor environment. Green dots represent beneficial microorganisms, red dots represent those harmful to health (Marsh, 2016)

Quantitative indoor and outdoor air monitoring has been used to relate human occupancy to indoor air bioaerosol concentrations (Hospodsky et al., 2012), with human occupancy a dominant factor in the levels of airborne bacteria detected by genomic analysis. Observations during occupancy revealed that direct human shedding along with particle resuspension from carpeted floors resulting from human activity significantly contributed to the elevated respirable particulate matter and bacterial concentrations, above background concentrations. Similarity between the bacteria associated with the human skin microbiome and those detected in indoor air highlight the importance of the human microbiota contribution to indoor air quality (Hospodsky et al., 2012).

Respiratory symptoms and lung function damage are the most extensively studied and undoubtedly among the most critical bioaerosol-associated health effects. Airborne bacteria and fungi cause or exacerbate respiratory diseases such as rhinitis, asthma, and pneumonia, which can even lead to death especially for those who are physiologically sensitive to them (Hardin et al., 2003, Husman, 1996, Shinn et al., 2003).

1.3 Human Bioaerosol Vectors

Studies using indoor/outdoor mass balance and receptor-based source apportionment models have shown that, supplementary to particles suspended in outdoor air, material resuspension from surfaces resultant from human activities is an important source of indoor bioaerosols (Ferro et al., 2004, Qian et al., 2014). Another significant source of bacteria is human oral and respiratory fluid emission from expiratory activities (Morawska et al., 2009, Chao et al., 2009) or the direct shedding of skin-associated microbiota (Weschler, 2016, Huttunen, 2018). The human epidermis can carry as many as 10^{12} microorganisms and the alimentary tract as many as 10^{14} microorganisms, each centimetre of our skin houses approximately 10^{6} bacteria (Luckey, 1972, Blaser et al., 2013, Grice et al., 2008). This potentially makes humans one of the greatest sources of bioaerosols in an enclosed environment. Respiration and shedding of millions of skin cells daily contribute greatly to the indoor environment thus making human occupancy and activity important factors in total concentration and community structure of indoor bioaerosols (Bhangar et al., 2015, Weschler, 2016, Huttunen, 2018). A pyrosequencing-based approach has even been used to quantitatively compare bacterial communities on objects and skin, to match the object associated with the individual with a high degree of certainty thus potentially providing forensic-style human DNA analysis (Fierer et al., 2010).

1.3.1 Occupancy

Although baseline quantitative information on bioaerosol emissions resulting from human occupancy is limited, several studies suggest that occupancy results in increased bioaerosol concentrations (Bhangar et al., 2014, Adam et al., 2015, Qian et al., 2014, Hospodsky et al., 2012). Previous studies on human bioaerosol emissions can be classified into 2 groups: controlled laboratory tests and observational assessments. Observational studies cannot differentiate between emissions from shedding (skin, hair, clothing etc.) and resuspension (from floor and contact surfaces). This is the probable explanation for the wide variation in bioaerosol emission concentrations produced per person in published literature. Controlled environment studies are designed to simulate certain environments and are usually conducted in a chamber fitted with a heating, ventilation and air conditioning (HVAC) system. This type of study can important information on emissions from specific sources, it can

differentiate between sources for example concentration of particles resuspended by walking and sitting can be calculated (Bhangar et al., 2015). Mean emissions of 14×10^6 cells h^{-1} $person^{-1}$ for bacteria were found in school classrooms (Hospodsky et al., 2015), compared with mean fluorescent particles concentration source strength of 2×10^6 particles h^{-1} $person^{-1}$ in university classrooms (Bhangar et al., 2014), and mean fluorescent particles concentration source strength of 0.9×10^6 particles h^{-1} $person^{-1}$ in simulated office conditions (Bhangar et al., 2015). An average emission rate of about 8.4×10^5 fluorescent particles h^{-1} $person^{-1}$ was found in a controlled environment (Xu et al., 2017). Lower emission concentrations are typically observed during controlled (Bhangar et al., 2015, Xu et al., 2017) compared with uncontrolled (Hospodsky et al., 2015, Bhangar et al., 2014) studies due to uncontrolled studies not differentiating between contributing processes. Literature suggests a breakdown of bioaerosol emissions to be approximately attributed to ~17% from breathing (Xu et al., 2017), ~18% from skin and clothing shedding (Qian et al., 2012) and ~65% from floor resuspension (Bhangar et al., 2015). Human emission rates may increase 5 to 6 fold by walking, as compared to sitting in a controlled setting (Bhangar et al., 2015).

Occupancy plays a role within the healthcare setting where associations have been made between surgical site infections (SSI) and the number of staffs in operating theatres. Simulation studies have shown that by increasing the number of people within a clean area close to an operating table that bacteria-carrying airborne particle concentrations would increase, especially for particles (5-10 μm) (Sadrizadeh et al., 2014). Using RNG k-ε turbulence modelling and Lagrangian air flow simulation they observed that under a constant air change rate that bacteria carrying particle deposition increases on increasing the number of people in critical areas. Consequently they recommended that only 5 – 6 staff should be present during infection prone surgery (Sadrizadeh et al., 2014). Similarly the number of staff influenced airborne bacterial counts collected within an operating theatre, with each additional staff present increasing bacterial counts by an average of 4.93 CFU/m^3 (Shaw et al., 2018). Positive correlations between SSI risk and personnel turnover has been observed during neurosurgical procedures (Wathen et al., 2016), with several other studies identifying increasing numbers of people in the operating room leading to increased SSI risk (Birgand et al., 2015). Actions from staff within operating theatres can also increase airborne particles. Unfolding surgical gowns, donning/doffing gloves and gowning

generate large number of airborne particles. ~20069 particles in the 0.3-5.0μm size range on average are generated (Noguchi et al., 2017).

In closed chamber experiments, a series of measurements were conducted to examine the short-term emission rates of particles in the "personal cloud" i.e. the totality of particles emitted from a clothed human being, in a sealed chamber. A positive correlation with physical activity on the emission rates of particles >1 μm was seen, but not for particles in the diameter range of 0.3-0.5 μm (You et al., 2013). Humans can be distinguished by their airborne bacterial emissions, as well as their contribution to settled particles within a 1.5 to 4-hour time frame. This has given substance to the idea that individual humans have their own personalised microbial cloud (Meadow et al., 2015). Similarly, an individual's "signature microbes" has been found to follow them from house to house. After an individual's relocation, the microbial community in the new house showed distinct similarities to the microbial community of the occupant's former house, suggesting rapid colonization by the family's microbiota. Direct contact with an indoor surface leaves a rapidly generated microbial signature characteristic of the occupants (Lax et al., 2014).

The survival of bacteria deposited on a surface depends on several factors including the precise geography of the surface, its moisture content, and the type of bioaerosol in terms of landscape acceptance e.g. tolerance to dry conditions. For example, most human pathogens are mesophiles which grow optimally at 35-37 °C, however they often adapt to survive in environments of human comfort i.e. 25 °C (Kowalski, 2016). As humans harbour distinguishably different microbial assemblages on various parts of their bodies (Costello et al., 2009, Findley et al., 2013), it can be assumed that different indoor surfaces could harbour different microbial communities depending on both specific body part in contact and the frequency of that contact. Such transmissions are possible even when contact is indirect, for example within a single classroom bacterial assemblages from four surface types, were suggestive of different source pools associated with the type of human contact each surface regularly encountered (Meadow et al., 2014).

These settled particles may become aerosolised from human activities such as walking or even sitting. Resuspension refers to previously deposited particles detaching from

surfaces and re-enter the air. This disturbance can often lead to an upsurge in inhalable particles within the indoor environment, with movements such as walking (Qian et al., 2008, Ferro et al., 2004, Tian et al., 2014) and vacuum cleaning (Veillette et al., 2013) emitting up to 10^7-10^8 particles minute^{-1}. To combat this, hospitals have made efforts to reduce the disturbance/generation of deposited/settled particles during cleaning. Design criteria for hospitals include specification of readily cleanable floor and wall surfaces, for example wall finishes must be washable and incorporate low volatile compound finishes to reduce moisture entrapment (Bartley et al., 2010). Surfaces are routinely cleaned, or cleaned and disinfected, according to predetermined cleaning protocols (hourly, daily, weekly, etc.) or when surfaces appear dirty, instances of spillages, and always post patient discharge (May and Pitt, 2012, Siani and Maillard, 2015). Cleaning is a key control factor for outbreaks of norovirus, *Vancomycin-resistant Enterococcus* (VRE), *C. difficile*, Methicillin-resistant *Staphylococcus aureus* (MRSA), etc (Dancer, 2009, Dancer, 2011, Davies, 2010). MRSA is known to resist desiccation and can survive in hospital dust for up to a year (Wagenvoort et al., 2000), thus it is imperative that cleaning efficiently removes these particles and not contribute to their dispersal. A cleaning manual by the Health Service Executive (HSE) supports the application of the Irish Health Services Accreditation Board (IHSAB) Hygiene Services Standards by providing guidance in the area of environmental cleanliness (National Hospitals, 2005). It recommends scrubbing machine tanks are emptied and decontaminated daily, vacuum cleaners are fitted with filters to not increase bacterial air contamination, and the use of damp dusting and wet cleaning to result in reduced bacterial air dispersal (National Hospitals, 2005).

1.3.2 Expiration

Breathing, coughing, sneezing and other human expiratory activities result in aerosol generation by wind shear force, plume from sneezing captured in Figure 1.2. Respiratory tract droplet atomisation arises from the passage of an air-stream at a sufficiently high speed over the surface of a liquid; aliquots of liquid are pulled from the surface, drawn thin and fragmented into columns of droplets (Hickey, 1996, Morawska, 2006). Each of these processes produces droplets of varying sizes originating from diverse areas of the upper respiratory tract (Loudon and Roberts, 1967, Chao et al., 2009, Yang et al., 2007, Stahlhofen et al., 1980, Milton et al., 2013),

and several studies have shown that these expelled aerosol particles may contain potentially infectious microorganisms (Morawska et al., 2009, Lindsley et al., 2012a, Fennelly et al., 2012).

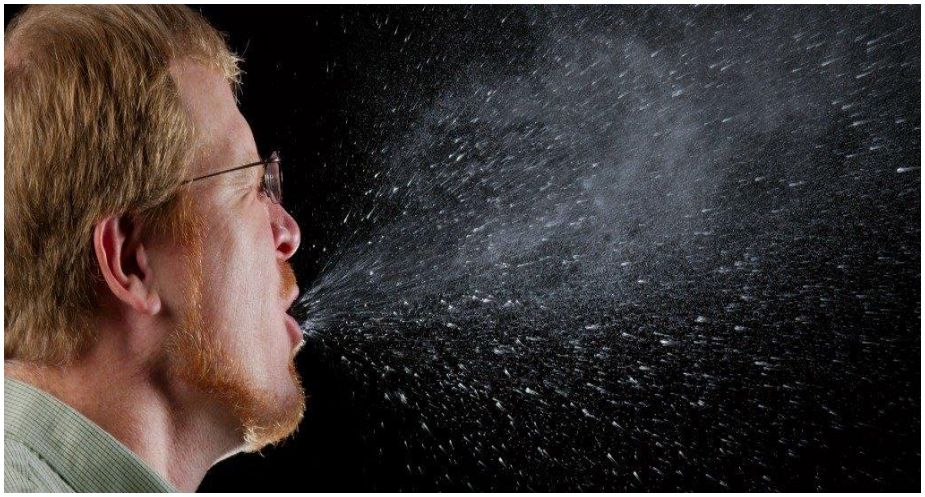

Figure 1.2 Plume of salivary droplets captured from man sneezing (Prevention, 2009)

Emphasis has been placed on human aerosol transmission in at least two airborne epidemics and one airborne pandemic in the last 20 years, the SARS pandemic in 2003 (Roy and Milton, 2004), the 2009 H1N1 influenza pandemic (Lau et al., 2009), and the 2014 MERS epidemic (Kutter et al., 2018). In addition, airborne outbreaks of other viruses (Kutter et al., 2018) and bacterial infections such as tuberculosis (Beggs et al., 2003) are well recognised. The World Health Organisation (WHO) and the US Centres for Disease Control (CDC) suggest only three infections as being transmitted through airborne routes tuberculosis (TB), chicken pox and measles (Siegel, 2007, Organization, 2014). In the cases of SARS and influenza, they are not generally considered airborne by WHO or CDC. These are considered to be opportunistic airborne infections, meaning they are typically spread through other routes i.e. droplet or contact, but under preferential conditions, aerosol-generating procedures, transmission can occur (Siegel, 2007, Organization, 2014, Seto, 2015). MRSA and its ability to be spread by aerial route has split opinions regarding its control. Ireland does not consider the airborne route as paramount and generally does not require negative pressure rooms for the care of patients colonised or infected with MRSA (Committee, 2013). Conversely the Netherlands require isolation rooms to have an antechamber and be negatively pressured (Van Rijen and Kluytmans, 2009). This differences in

approach highlights the disparity in opinions among clinicians on the significance of the airborne route for the spread of infection.

Exhaled breath is an important contributor to bioaerosol emissions, where exhaled particles can remain airborne and disperse (Milton et al., 2013, Gralton et al., 2011). Breathing can lead to an increase in bioaerosol emission of up to 17% (Xu et al., 2017) and exhaled breath may contain ~7000 CFU m^{-3} culturable bacteria (Xu et al., 2012). During tidal breathing, infectious aerosols can be generated by the release of small, pathogen-containing droplets, these rapidly evaporate into residual particles, which may be inhaled and deposited in the respiratory tract of others (Morawska, 2006, Atkinson and Wein, 2008, Gralton et al., 2011).

Cough-generated aerosols are of particular concern in disease transmission, coughing is a common symptom of respiratory infection, and the violent nature of expulsion during a cough generates aerosol particles that can travel up to 2 m or more away from an infected person (Zhu et al., 2006, Tang and Wan, 2013). This is of particular interest for the healthcare environment where a high percentage of the population may be immunocompromised and therefore susceptible to getting infected by infectious aerosols, but also capable of spreading infectious aerosols. A study of the size and quantity of aerosols produced by nine patients during coughing while they had Influenza and after they recovered showed that while infected with Influenza virus, they produced a significantly greater volume of aerosol particles (average 75400 particles $cough^{-1}$) compared to when they had recovered (average 52200 particles $cough^{-1}$). And although not significantly higher, their cough aerosol volume and number of particles produced per cough was higher than after they had recovered (Lindsley et al., 2012b). *Mycobacterium tuberculosis*, a major cause of morbidity and mortality worldwide, exacerbated by human immunodeficiency virus (HIV), is transmitted by fine aerosols. As part of a study of nosocomial TB transmission, culturable *M. tuberculosis* particles were collected, quantified and sized. It was discovered that a minority of patients with TB produced culturable cough aerosols and that there was a positive correlation between culturable cough aerosols and the strength of the cough (Fennelly et al., 2012).

Respiratory protective equipment is traditionally recommended for healthcare worker protection when in contact with open tuberculosis because of the aerosol risk. A minimum filtration efficiency of 95% (N95) is required. In contrast, for influenza, large droplet particles are believed to be the main infection risk and the CDC recommends that persons with influenza wear surgical masks protecting the mouth and nose from droplets when in contact with susceptible individuals (Control and Prevention, 2009). Conversely, medical attendants should also wear surgical masks when caring for patients with influenza. For the H1N1 pandemic in 2009, CDC recommended the used of N95 respirators by staff caring for patients. Recommendations for seasonal influenza only include performing aerosol provoking procedures as indications for N95 masks. Filter materials from N95, Surgical mask and "Doctor mask" had more than 95% filtration efficiency for 1.5 µm size particles, and close to 100% for 3 µm sized particles (Zou and Yao, 2015). But the efficiency of these respirators in shielding against bioaerosols depends on the fit (Xu et al., 2017).

1.4 Traditional Sampling Techniques

The objective of active bioaerosol sampling is to efficiently remove and collect a sample of representative biological particles from the air in a method that does not disturb the ability to detect the organisms (e.g. no modification of culturability or biological integrity) (Atlas and Bartha, 1981, Cox and Wathes, 1995, Haig et al., 2016).

The principle collection methods used can be broadly separated into four main categories: impactors, impingers, cyclones and filters (Grinshpun et al., 2016, Haig et al., 2016). Impactors collect airborne particles on to solid/semi-solid medium, and filters trap bioaerosol material on fine fibres or porous membrane surfaces, whereas impingers and cyclones collect airborne particles in a liquid medium (Grinshpun et al., 2016, Haig et al., 2016, Cox and Wathes, 1995). Passive or active sampling may be used, discussed further below (Haig et al., 2016, Breeding, 2003).

1.4.1 Passive Sampling

Passive sampling remains the most readily available, cheap and unobtrusive method of bioaerosol sampling and depends on the gravitational settling of airborne particles

onto substrate retained in a settle plate. Passive sampling does not disturb the surrounding air as it lacks any mechanical, moving part such as a pump (Hinds, 2012). Collected particles are normally enumerated in terms of the number of colony-forming units (CFU) within the area of the settle plates for the specified time-interval for example in units of CFU/m^2/hr (Haig et al., 2016, McCartney et al., 1997, Napoli et al., 2012). Although gravitational sampling has been explored and employed in bioaerosol sampling (Mainelis et al., 2002, Burge and Solomon, 1987), a combination of non-controllable factors, including particle settling, mean it is regarded as both quantitatively and qualitatively inaccurate and non-representative, and as a supplementary collection method to active sampling (Haig et al., 2016, Grinshpun et al., 2016). Larger, denser particles will spend less time airborne than smaller, lighter particles, and if the particle air speed surpasses the settling velocity the particle will continue to be suspended indefinitely and not sampled (Hinds, 2012). Furthermore, the source volume of air for the passively collected samples will be unknown as airflow, even within a built environment, will be affected by particle size and shape along with subtle changes in temperature (Haig et al., 2016, Hinds, 2012, Dietrich, 1982, Reponen et al., 2011). However, if the area of interest is the dust contamination of surfaces where the evaluation of the microbial fallout holds significance over particles suspended in air gravitational settling is useful (Haig et al., 2016). In an effort to standardise the use of settle plates a 1/1/1 approach was devised with consideration towards plate size, position and length of exposure (Pasquarella et al., 2000). The 1/1/1 scheme refers to the placing of 90 mm diameter Petri dishes at a height of 1 m above floor level, 1 m away from a wall, and an exposure time of 1 hr. The standardised method allows for a description of the surrounding atmosphere using an index of microbial air contamination (IMA). But studies within an operational ward using the method have found it to underestimate the actual contamination risk (Scaltriti et al., 2007, Napoli et al., 2012).

Several studies undertaken in hospital settings have shown that settle plates do not give an accurate reflection of what is present in the air when compared with active samplers and are comparatively insensitive to the collection of fungal spores (Sautour et al., 2007, Pasquarella et al., 2000, Pasquarella et al., 2012). Studies carried out in intensive care units at Aes Chemunex, Bruz, France presented variations in total viable microbial counts between surface and air sampling methods, suggesting that sources

of contamination may be different. Human activities significantly influenced the surface-settled organisms (Gaudart et al., 2013).

1.4.2 Active Sampling

To fully understand active sampling particle mass and inertia must first be discussed. Particle mass refers to its volume multiplied by its density, thus allowing two particles to have the same mass yet different volumes and densities (Hinds, 2012, Cox and Wathes, 1995). Considering instances where particles have the same density but differing volumes, the smaller particle will have a lower mass than the larger particle. Inertial mass of the particle is a measure of its resistance to acceleration (Force = Mass × Acceleration). If we consider two particles being carried by an airflow within a pipe, upon reaching a bend in the pipe where the airflow is redirected, the particle with the lesser mass will continue to travel along with the airflow streamline whereas the particle of mass above a certain threshold is more resistant to acceleration in the new direction and will impact onto the bend wall of the pipe, or a collection device located there. A particle impact where its mass doesn't allow it to follow the airflow is known as inertial impact (Hinds, 2012). This plays an important role within active samplers, where particles having the same density, but differing size will see larger particles yield more readily to inertial impaction than the smaller particles (Hinds, 2012). Smaller particles are collected more readily in the outflow from these sampling devices.

Impactors, Impingers and Cyclones are the main active samplers which will be discussed in detail later. Accurate samples require the active sampler to control five central elements.

1. Inlet to sampling device
2. Transport of air sample through device
3. Particle size selection
4. Collection medium
5. Pump and calibrated flow monitor.

The correct reflection of concentration and size distribution of airborne particles depends on the design of the inlet and air flow rate (Hinds, 1999, Hinds, 2012). In ventilation systems and other moving air streams this is achieved by isokinetic sampling, delivering a representative sample by considering the ratio of duct and

sampling probe diameters, air flows, and inlet orientation to the air stream to ensure successful capture of particles irrespective of size or inertia (Sippola and Nazaroff, 2004). Still air sampling is also affected by particle inertia where larger particles may evade the sampling probe, distorting the concentration in the sample collected. Larger particles may elude the sampling probe by the particle velocity increasing as it gets closer to the probe, proportionately increasing the particles stopping distance, allowing the particle to evade the probe (Hinds, 2012, Haig et al., 2016). Although sampling in still air is relatively more straightforward the probe inlet must be positioned horizontally to prevent any over or underestimation sampling bias (Grinshpun et al., 2016). To reduce the loss of air sample in conductive tubing the sample path must be as straight and direct as possible once the air sample is within the device (Haig et al., 2016). But for cases where this is not possible like cascade impactors, particle loss will occur through inertial impaction on the bends between the collection stages (Misra et al., 2002). If a device uses a sampling probe, particles loss may occur in the probe head or flexible connective tubing, as particles will be lodged on to the side wall and will not reach the sampling medium. For example, liquid-based bioaerosol samplers, where collection losses are experienced through evaporation of the collecting liquid and adhesion of the particles to the device walls. Once this occurs, the particles do not enter the collection liquid and the sampling process may therefore produce lower or false-negative results (Haig et al., 2016).

1.4.3 Impactors

Impaction is among the most commonly used of bioaerosol collection methods due to the combination of low cost and ease of handling and the ability to directly collect microorganisms directly onto growth agar without the need for post-sample processing (Li and Lin, 1999, Li, 1999, Nesa et al., 2001). Impactors employ a relatively simple collection technique. Generally, the impaction sampler separates particles from a sample stream by accelerating a sample stream and forcing a sudden change in sample aerosol direction, this centrifugal force causes particle/air separation based on particle inertia. Particles with high inertia get impacted onto the collecting substrate. Generally, impactors are particle aerodynamic diameter specific and employ a designed diameter cut-off point which is set to collect particles of a desired size. Particles larger than specification will get impacted onto the collection surface while

particles which do not meet the aerodynamic size criteria will advance through the sampler (Hinds, 1999). The greatest influences adversely affecting impactor performance are high background velocity, inlet loss and particle re-entrainment (Marple and Willeke, 1976, Willeke and Baron). This method is highly dependent on the microorganisms being collected to be viable and capable of growth on the specific nutrient media.

There are many varieties of commercially available impactors which differ by a few key characteristics; inlet size and shape, quantity of collection chambers and sample impaction surface (solid, semi-solid, filter or gelatine)(Kim et al., 2009). Variations in each of these characteristics will influence the sample collection and recovery efficiencies. Impactors can be operated either as individual single stage devices or as cascade samplers (Macher, 1989, Lawless, 2000, Andersen, 1958).

Impaction samplers can be subdivided into various categories including slit samplers, sieve and stacked sieve samplers and cascade impactors. Slit samplers generally use a single rectangular nozzle to suck in air. In this type of sampler drawn air is accelerated through its narrow slit and directed onto the surface of a rotating petri dish normally containing an agar media e.g. Burkard Spore Sampler. These were one of the first samplers used for airborne microorganism collection (Bourdillon et al., 1941) and have been successful in the collection of bioaerosols from both indoor (Bholah and Subratty, 2002) and outdoor (Hameed et al., 2009) environments. Sieve samplers are similar in that they accelerate drawn in air onto a culture media, however typically they have a circular shape with numerous inlet orifices in a perforated plate. Stacked sieve samplers are more commonly used. This type of sampler is one of the most widely operated air samplers i.e. the six-stage Andersen viable fractionating sampler (Andersen, 1958, Andersen, 1966, Xu and Yao, 2013, Grinshpun et al., 2016). This is also a cascade sampler, a size discriminating sampler which draws air through a series of slits that sequentially decrease in size in turn increasing air velocity from one stage to the next, causing larger particles to be deposited on the upper stage, while smaller particles that are capable of remaining in the airstream at a lower velocity will depart the airstream at higher velocities to be impacted onto the collection media further down (Cox and Wathes, 1995). For example, in the six-stage Andersen cascade sampler, particulates impact onto the agar medium of six Petri dishes, each below one

of a series of six stacked sieve plates (Knöppel and Wolkoff, 2013). The diameter of the 400 sieve plate perforations decreases progressively from 1.18 mm in the top plate to 0.25 mm in the bottom plate. As the air passes through continuously smaller holes the speed increases more than 20-fold between the initial and final stage. Subsequently, particles are organised by aerodynamic size (Knöppel and Wolkoff, 2013). Another widely used cascade sampler is the handheld, single stage, Microbial Air Monitoring system-100 (MAS-100), which consists of a single perforated plate with 400 holes each with a diameter of 0.7 mm through which air is drawn at a rate of 10.8 ms^{-1} and forced onto a solid culture plate. After passing through the airflow meter the sampling volume is then adjusted to 100 L/m^3. The MAS-100 is has been broadly used within a hospital setting, for example the MAS-100 was one of four impactors, along with a BioImpactor, Samplair and Omega, used to assess fungal spore collection efficiency in a hospital (Nesa et al., 2001). There was not a significant difference in the fungal spores observed between the four samplers, the MAS-100 as with the other samplers observed mainly moulds and sporadic *Aspergillus* (Nesa et al., 2001).

Similarly a comparative bacterial and fungal count study with a MAS-100 using malt extract agar collected the fungal genera *Cladosporium*, *Penicillium*, *Alternaria* and sparsely *Aspergillus* within a hospital environment (Gangneux et al., 2006).

While aerosolised bacterial and fungal spores can be collected separately over semi-solid (agar plates) and solid (glass slides) surfaces respectively (Hinds, 2012), generally culture based impactors are used to collect them together on agar plates (Li and Lin, 1999, Nesa et al., 2001, Yao and Mainelis, 2007a, Trunov et al., 2001). Apart from incubation at the required temperature, there is no post-collection processing required to tally microorganism counts, they are cultured and counted directly on the plate (Nesa et al., 2001, Yao and Mainelis, 2007a). The main weakness of using agar plates as a collection medium is in highly contaminated sample sites the culture plates become overloaded making enumeration extremely difficult, consequently requiring the use of the statistical "positive hole correction" in assessing highly loaded plates (Macher, 1989). Another theoretical drawback with using agar is particle bounce-off where aggregated particles, aerosolised spores agglomerating into chains and compacts, may deagglomerate at impaction and bounce off after impaction. Modified single stage impactors operating at a higher nozzle velocity have more efficient retention of particles of complex morphology. These convert a large portion of particle kinetic energy into vibrational excitation and heat, making bounce-off highly unlikely.

Alternatively, increased velocity may lead to significant bounce-off of bioaerosol particles on non-adhesive surfaces (Wittmaack et al., 2005).

Table 1.1 Approximate effective collection efficiency of 7 bioaerosol samplers (Yao and Mainelis, 2007b)

Sampler	Approximate Effective Collection Efficiency Percentages					
	Bacteria			Fungi		
	P. fluorescens	*E. coli*	*B. subtilis*	*C. cladosporium*	*A. versicolor*	*P. melinii*
MAS-100	<10	22	22	60	60	60
Microflow	<10	<10	<10	10	10	10
Bioculture	<10	<10	<10	10	10	10
SMA	<10	<10	<10	10	10	10
Millipore Air Tester	<10	<10	<10	60	60	60
RCS High Flow	30	30	30	80	80	80
SAS Super 180	20-30	20-30	20-30	90	90	90

The collection efficiency of seven different portable microbial samplers was tested with 3 bacterial (*Pseudomonas fluorescens*, *Escherichia coli* and *Bacillus Subtilis*) and 3 fungal species (*Cladosporium cladosporiodes*, *Aspergillus versicolor* ad *Penicillium melinii*). Table 1.1 shows the approximate effective collection efficiencies, this is the portion of aerosolised microorganisms collected onto agar media, all samplers shown Figure 1.3. Sampler collection efficiency was subsequently compared to the inhalation convention curves of the same microorganisms, reflecting the total deposition of particles in the respiratory system found by the American Conference of Governmental Industrial Hygienists (ACGIH) (ACGIH, 1999). The MAS-100 and SAS Super 180 matched the total deposition curves quite well for collecting bacteria and fungi. For example, total lung deposition fraction of *E. coli* was ~35% compared to 22% effective collection efficiency of MAS-100 sampler (Yao and Mainelis, 2007b).

Figure 1.3 (Left to Right) RCS High Flow, MicroFlow, BioCulture, Milipore, SAS Super 180, SMA MicroPortable and the MAS-100. Samplers examined by Yao and Mainelis et al. (Yao and Mainelis, 2007b).

1.4.4 Impingement

The first liquid impingers were developed as dust aerosol samplers and described by Greenberg and Smith in the early 1920's but were later adapted for the collection of airborne bacteria (Cown et al., 1957). Operating on a similar principle to the previously discussed impaction-based approach, impingement-based methods collect bioaerosols by channelling airflow through a nozzle and directing it into reservoir-filled liquid medium (Willeke et al., 1998, Kim et al., 2018). In its simplest form, the single stage "Greenberg-Smith impinger", the liquid impinger uses a vacuum pump to pull air through a narrow glass inlet tube onto the collecting medium, a glass platform submerged in liquid medium (Ghosh et al., 2015). As soon as the air impacts the liquid the air jet turbulence washes the particles from the platform and suspends them in the liquid medium (Driver et al., 2012). Upon sample completion, aliquots are cultured on growth media to count viable microorganisms (Henningson and Ahlberg, 1994, Kim et al., 2018). In terms of bioaerosol sampling, liquid impingers are generally used when enumerating specific microbial species and can also be used for non-culture DNA analysis (Nikaeen et al., 2018, Montagna et al., 2017b).

Impinger collection and recovery efficiencies vary depending on the sampler's inlet characteristics. The distance between the impinging jet and the base of the sampler directly affects the collection efficiency, originally the jet was 4 mm from the base, resulting in the jet disturbing the particles impinged in liquid media and causing them

to hit the sampler base, affecting the viability of the collected microorganisms (May and Harper, 1957). This led to the development of impingers which reduced particle impingement velocity in order to lessen the damage to cells caused by contact with the base of the sampler (May and Harper, 1957). In these samplers the air jet was introduced into the chamber at an angle, as in the Shipe sampler (Shipe et al., 1959), or introduced at a distance of 30 mm above the base, as in the All Glass Impinger 30 (AGI-30) (Kethley, 1958). The AGI-30 has also developed a curved inlet tube to replicate particle collection in the nasal passage (Davies, 1987). Airborne bacterial emissions from hospital incinerators in Illinois have been monitored using two aluminium inlet-fitted Shipe samplers (0.1 M phosphate buffer solution), resulting in concentration ranges from non-detectable to 1157 colonies/m^3 of air (Allen et al., 1989). Typically, impingers are operated with water or a sterilised buffered aqueous solution of similar viscosity and surface tension to water e.g. phosphate buffer. The type of liquid media may vary but normally they all have one common element i.e. liquids should be isotonic or buffered solution, protecting microorganisms form osmotic shock (Trouwborst et al., 1972, Walters et al., 1994). Glycerol, distilled water and mineral oil have proven efficient collection media for *Chlamydophila psittaci*, other bacterial and fungal spores (Van Droogenbroeck et al., 2009, Willeke et al., 1998, Näsman et al., 1999) and peptone in dissolved water has been used for *Escherichia coli* (Dungan and Leytem, 2016). However, water and similar liquids evaporate readily during sampling meaning sampling efficiency will vary with time. For example, the liquid in a AGI-30 evaporates in ~ 90 minutes when operated as recommended with flow rate of 1.25×10^4 cm^3 min^{-1} and filled with 20 ml of water (Lin et al., 1997).

Currently a wide variety of impingers are commercially available, ranging from the previously mentioned AGI-30, SKC Biosampler, multistage all glass liquid impinger (MSLI), and the Midget impinger with Personal Air Sampler. Since its implementation as a viable bioaerosol reference sampler, the AGI-30 has been the most widely used (Brachman et al., 1964). It is a single stage impinger consisting of a vacuumed cylindrical reservoir which contains 20 ml of a suitable collection liquid for concentrating bioaerosol from the air through the, earlier mentioned, centrally raised air jet (30 mm from the base). It is capable of a sampling rate of 12.5 $Lmin^{-1}$ via an electrically powered vacuum pump. The AGI-30 has been used extensively in the

enumeration and evaluation of bioaerosols in a hospital environment. Combining the AGI-30 impinger, collection medium of 20% broth, penicillin 300 units/ml and streptomycin 300 μg/ml, and petri dishes below the impinger orifice in the numeration and recovery of smallpox virus from patients and their environment was carried out at the infectious disease hospital in Madras (Downie et al., 1965). *Legionella pneumophila* was also isolated from 43 sites in two hospitals (40% of sites sampled). using an AGI liquid impinger containing 0.25% aqueous yeast extract (Barbaree et al., 1987). Recently the AGI impinger determined the prevalence of vancomycin and gentamicin resistant bacteria in the wards of four different education hospitals in Isfahan, Iran, recording average levels of bacteria ranging from 99 to 1079 CFU per m^3 (Mirhoseini et al., 2016). A major drawback with using the sampler is foaming induced with several collection media (protein or carbohydrate containing) (Dillon et al., 2005, Hermann et al., 2006).

Recently the all-glass, swirling aerosol impinger "Biosampler", has become the most popular liquid impinger. Biosampler operational design combines both centrifugation and impaction to trap bioaerosols into a swirling liquid. Typically it consists of an air inlet, three triangulated tangentially arranged nozzles and a collection vessel (Ghosh et al., 2015). The Biosampler draws in a sample through the nozzle, which is directed at a specific angle towards the inner surface of the cylindrical vessel wall. Together the inner surface of the curved vessel wall and swirling flow of previously ejected air deflect the sample flow laterally. Amalgamation of centrifugal forces and impaction push particles towards the curved inner surface. Diffusional motion may also throw submicron-sized particulates across the final short distance (Willeke et al., 1998). Biosampler had a better collection efficiency for particles ranging from 0.3-2.0 μm compared to the AGI-30. Other advantages of the Biosampler over the AGI-30 are its ability to use a non-evaporating, more viscous liquid extending the possible sampling time (0.5-4 hrs) (Dillon et al., 2005). The Biosampler has for example been used for bioaerosol analysis of indoor warm-water therapy pools. Pool air typically contained ~ 10^6 microbes per m^3 including *Mycobacterium avium* strains and a high portion of *Mycobacterium* spp overall (>30% of the microbes from the pool water) (Angenent et al., 2005).

1.4.5 Cyclone

Cyclone samplers use a nozzle to draw in an aerosol stream, aspirated air is then forced into a whirling motion. Particles within this airflow experience a centrifugal force proportional to their diameter, density and speed. The airflow forces particles of sufficient inertia towards the cyclone wall where they collide with the wall, separating from airflow and accumulate into the suspension liquid (Peng et al., 2005, Haig et al., 2016). Cyclones are less prone to particle bounce than impactors and can collect larger quantities of material (Lindsley et al., 2017).

One popular cyclone sampler is the Coriolis® µ (Bertin Technologies, Montigny le Bretonneux, France). This wet walled cyclonic sampler rapidly collects and concentrates biological particles into liquid at a high air flow rate (300 L/min). The sample liquid output is compatible with several rapid microbiological methods like PCR, immunoanalysis and flow cyclometry, with reliable results obtained within a few hours. The Coriolis® µ has successfully helped quantify and specify *Legionella* species in air. *L. pneumophila* was directly quantified, 4×10^3 cells/m^3, in a laboratory setting using a combination of the Coriolis® µ and micro-assay (Langer et al., 2012). Within 11 Italian healthcare facilities the Coriolis® µ quantified *Legionella* in bioaerosols by molecular investigation. Although Coriolis® culture methods alone did not show any air contamination when positive results were obtained by another culture-based method using Surface Air System (SAS) sampling (36.4% air contamination), the Coriolis® did show higher sensitivity for *Legionella* using a molecular method (72.7% air contamination) (Montagna et al., 2017b, Montagna et al., 2017a). Recently measurements of microbial contaminants within two French hospitals were made using the Coriolis® µ and the samples analysed by Quantitative Polymerase Chain Reaction (qPCR). It identified that the predominant bacterial flora at Rennes hospital was made up of *Micrococcus sp.*, *Bacillus sp.,* and *Burkholderia sp.*, and at the Nancy hospital, of *Staphylococcus sp.* , *Micrococcus sp.*, *Pseudomonas sp.*, and *Corynebacterium sp*. Regarding fungal flora, *Penicillium sp.*, *Aspergillus sp.*, *Cladosporium sp.*, and *Alternaria sp.* predominated at the Rennes hospital and *Basidiomycetes*, *Cryptococcus sp.*, *Cladosporium sp.*, *Penicillium sp.*, and *Aspergillus sp.* at the Nancy hospital (Baurès et al., 2018).

Figure 1.4 (Left to Right) OMNI-3000, SASS 2300, Coriolis®, BioSampler, BioCapture 650, SASS 3100, XMX-CV and ESP (Prototype), Gelatin filter not shown. The 9 bioaerosol samplers compared by Dybwab et al (Dybwad et al., 2014).

Table 1.2 Approximate Relative biological sampling efficiency of 9 bioaerosol samplers (Dybwad et al., 2014).

Relative Sampling efficiencies vs BioSampler													
Median Mass Aerosol Diameter (MMAD) µm		1			4								
Sampler	Test Agent	FS	BA		FS	BA		SM		KR		(MS2)	
	Analysis	FM*	C**	qPCR	FM	C	qPCR	C	qPCR	C	qPCR	C	qPCR
Coriolis		0.47	0.49	0.53	0.88	0.69	0.67	0.72	0.53	0.88	0.62	0.7	0.49
SASS 2300		0.05	0.1	0.08	0.13	0.43	0.39	1.6	0.57	0.85	0.39	0.63	0.57
SASS 3100		0.7	0.73	0.83	0.63	0.83	0.77	0.01	0.52	0.78	0.57	0.02	0.62
Gelatin filters		1.27	1.28	1.18	1.25	1.17	1.03	0.03	1.07	1.18	0.92	1.06	0.22
OMNI-3000		0.05	0.16	0.2	0.08	0.16	0.21						
BioCapture 650		0.24	0.22	0.22	0.74	0.78	0.6	0.18	0.46	0.9	0.57	0.72	0.68
ESP prototype		0.24	0.35	0.36	0.47	0.55	0.52	0.13	0.39	0.48	0.62	0.03	0.3
XMX-CV		0.05	0.22	0.19	1.07	1.26	1.11	2.63	0.98	1.45	1	0.21	0.16

* Fluorescent Microscopy (FM)

** Cultivation (C)

FS - fluorescent polystyrene latex spheres

BA - Bacillus atrophaeus

SM - Serratia marcescens

KR - Kocuria rhizophila

MS2 - Bacteriophage MS2

Biological sampling efficiencies (BSE) and Physical sampling efficiencies (PSE) of 9 bioaerosol samplers relative to a BioSampler reference sampler were determined for gram-negative and gram-positive vegetative bacteria, bacterial spores and viruses, see Table 1.2. The biological test agents included Gram-negative *Serratia marcescens* (SM) and gram positive, vegetative *Kocuria rhizophila* (KR) cells, *Bacillus atrophaeus* (BA) bacterial spores and Bacteriophage MS2 (MS2) viruses. Non-biological, fluorescent polystyrene latex spheres (FS) of two sizes, 1 µm and 4 µm, were analysed also. Apart from the gelatin filter the samplers all showed lower sampling efficiency for the FS compared to the reference sampler. Sampling efficiency differences between the samplers depended on particle size and stress-sensitivity. Wet collection methods had higher BSE than dry methods for stress-sensitive bioaerosols i.e. BG and KR were more resistant to stress than SM and MS2. Lower sampling efficiencies were the main reason for underestimation by other samplers compared to the Biosampler, however they could all collect more concentrated samples compared to the reference sampler.

1.4.6 Enzyme Immunosorbent Assays

Immunoassay is an analytical technique used to measure a target antigen i.e. the analyte. A key element of the immunoassay is the antibody or ligand, which binds a specific antigen or binding site. This binding of the antibody or antigen forms the foundation for immunoassay, where various systems have been developed to allow visual or instrumental analysis of this reaction.

Enzyme Immunoassay (EIA) are composed of different systems which can be used to quantify bioaerosols in air or dust samples. The basis of EIA is the binding of antibody or antigen to an enzyme, commonly horseradish peroxide (HRP) or alkaline phosphate (AP). The resultant enzyme activity, in the presence of a chromogenic substrate, gives a coloured end-product which can be used to quantitate the amount of antigen-antibody binding (Kontermann and Dübel, 2010). The most commercially available EIA is Enzyme-Linked Immunosorbent Assay (ELISA), and typically sandwich ELISA. Sandwich ELISA is used for the detection of airborne viruses and aeroallergens (Dillon et al., 2005, Leaderer et al., 2002). Here a capture antibody is bound to a solid surface, bioaerosol extract is added to the capture antibody and

incubated for a specified length of time, washed with phosphate buffer and probed with an enzyme labelled antibody allowing detection and quantification, through colorimetric change or fluorescence emission (Lindsley et al., 2017). Colour intensity is proportional to the quantity of antigen or analyte present in the sample. ELISA is highly specific and can be used on complex samples but does not distinguish between viable and non-viable aerosols.

1.4.7 Fluorescent Immunoassay

Fluorescent immunoassay (FIA) was first introduced by Coons *et al.* and exploits fluorescent-labelled antibodies to distinguish bacterial antigens (Coons et al., 1951). Since then several FIA techniques have evolved; (1) direct FIA detection of cell-bound antigens with fluorescent-labelled antibodies; (2) indirect FIA detection of cell-bound antigens using specific unlabelled antibodies and fluorescent anti-gamma globulin antibody; and (3) indirect FIA detection of serum antibody using antigen and fluorescent antibody (Jensen and Schafer, 1998, Meurant, 2012). A selection of fluorescent dyes may be employed, for example fluorescein, fluorescein isothiocyanate and rhodamine isothiocyanate (Symons, 1989). Samples are assessed and the number of fluorescent molecules are calculated under a fluorescent microscope (Jensen and Schafer, 1998). Bioaerosols including bacteria (Rule et al., 2007), fungi (Rydjord et al., 2007) and pollen (Rittenour et al., 2012) have been evaluated using a flow-cytometry-based approach with fluorescent-labelled antibodies. Although FIA is a trusted method of viral detection and quantification, it is limited by excessive cost and the necessity of a skilled technician in reading immunofluorescence (Lindsley et al., 2017).

1.4.8 Fluorescence Microscopy

Microscopic examination, identification and enumeration of airborne microbiological particles is performed by air samples being drawn on to glass slides or filters fitted on to samplers. For most microorganism's identification is not possible without processing the sample with a method designed to classify taxa or species. Fluorescent microscopy utilises ultraviolet or near-ultraviolet source of light to cause fluorescent compounds in a sample to emit light. The two common methods in determining the total count of environmental organisms are by exploiting the autofluorescence of

biological compounds relying on the naturally fluorescent components of a sample (Primary) (Pöhlker et al., 2012b) or by introducing fluorescent dyes to a sample thus not depending on any natural fluorescence (secondary) (Karlsson and Malmberg, 1989, Cox and Wathes, 1995). For example direct-count methods used to tally environmental organisms commonly apply acridine orange (Palmgren, 1991, Ramsay, 1978, Scholefield et al., 1985) or 4.76-diamino-2-phenylindole (DAPI) fluorescent dyes (Morikawa and Yanagida, 1981, Otto, 1990).

1.4.9 Fluorescent Lifetime Imaging

Fluorescent Lifetime Imaging (FLIM) is a technique that maps out the spatial distribution of the fluorescent lifetimes within microscopic images of fixed as well as living cells. The first FLIM instrument was defined as early as 1959 (Venetta, 1959) and created on a frequency-domain microscope arrangement, only permitting single point measurements. Lakowicz *et al.* and Gabella *et al.* were among the first groups to perform time resolved fluorescence imaging in single cells (Lakowicz et al., 1992, Gadella et al., 1993). Fluorochromes are not just characterised by their excitation and emission spectra, but also by their unique lifetime. Fluorescent lifetime is the average time the fluorophore remains in the excited state before descending to the ground state, a basic physical parameter that is independent of fluorescence excitation and unlike fluorescence intensity, is not subject to artefacts due to fluorophore concentrations, but can be affected by protein binding of the fluorophore. Fluorescent lifetime is not only dependant on the molecules chemical structure but highly sensitivity to its environment (pH, polarity, refractive index of medium, temperature) for example NADH has a lifetime of ~0.4 nanosecond in water but can be ~20 times longer when bound to dehydrogenase (Piersma et al., 1998) and similarly Tryptophan lifetime varies in different tryptophan-containing proteins (Beechem and Brand, 1985). This provides a foundation for mapping spatial variations of the lifetime in response to variations in the environment, providing information on the biomolecule's action or state *in vivo*. Thus, fluorescence lifetime is a reliable direct quantitative measure of fluorophore concentration and state which when applied to key fluorescent metabolic intermediate molecules such as NADH can be used to characterise individual bacteria.

1.5 Hospital Microbial Standards

Several studies have shown that the hospital environment is regularly contaminated with potential pathogens that pose a risk of cross-transmission to patients (Schwegman, 2009, Eames et al., 2009). Air sampling studies have even shown that MRSA can be detected in areas with no known MRSA-positive patients, showing how easily areas can be contaminated by pathogens from patients that do not presently reside there (Creamer et al., 2014). Microbial air monitoring has even been used to assess novel air disinfection units in reducing total viable counts (TVC) (O'Brien et al., 2012). However, a significant problem encountered in assessing hospital air quality is the lack of specification and uniformity in existing standards. No standardised air sampling protocols for hospitals are currently available other than for operating rooms, and comparisons between studies are difficult because of varying methodologies used to assess microbial air quality, with variability among air sampling devices documented (Cooper et al., Ghosh et al., 2015, Lindsley et al., 2017, Haig et al., 2016, Mbareche et al., 2018).

Different operating rooms standards are available, Table 1.3. Ireland follows the Health Technical Memorandum (HTM) 03-01 for its operating theatre standards (Centre, 2008). In the UK, the Health Technical Memorandum 03-01 sets standards for both conventional and ultra-clean operating theatres. These specify an empty operating theatre should not have CFU greater than 35 CFU/m^3, an active operating theatre should not exceed 180 CFU/ m^3 for an average 5-minute period. Ultra-clean theatre air is defined as that containing no more than 10 CFU/m^3 (Health/Estates and Division, 2007). For German operating room standards, sampling while operations are not performed, it is expected class 1a rooms should contain < 1 CFU/50cm/hr, and class 1b <5 CFU/50cm/hr, with acceptable levels of dust contamination, particles > 0.5 µm, to be 4000 particles/m^3 (DIN, 2008). France classifies rooms as M1 < 1 CFU/m^3, M10 < 10 CFU/m^3 and M100 < 100 CFU/m^3. M1 refers to risk class 4, M10 to class 3 and M100 as class 2 (Norme, 2003). Risk class 4 microorganisms are those that cause serious diseases in humans and constitute a danger to those directly exposed to them and pose a high risk of spread. Class 3 organisms can cause serious illness in humans and constitute a danger for people directly exposed to them and pose risk of spread. Class 2 cause illness in humans and constitute a danger for people directly

exposed to them, spread in community is unlikely (Norme, 2003). Finland bases their levels on studies (Intag, 1975) by the American Society of Heating and Refrigerating and Air-Conditioning Engineers (ASHRAE) where 100 CFU/m^3 is the recommended maximum level for general surgery, and during high risk operations lower levels of 10 CFU/m^3 are recommended (Kalliokoski, 2003). The Legislation in Poland uses an information source from a Ministry of Health and Social Welfare publication from 1984 (Kruczkowski et al., 1984). In this hospital guideline rooms fall into 3 groups, depending on acceptable levels of bacteria in the air:

(I) the strictest level with acceptable bacteria concentrations of up to 70 CFU/m^3, rooms include highly aseptic operating theatres, sterile boxes, infusion liquids labs and special burn wards

(II) acceptable bacteria concentrations of up to 300 CFU/m^3 rooms include aseptic theatres, septic operating theatres, intensive care unit (ICU) and wards, premature infant wards, postoperative rooms, patient and surgeon prep rooms and sterilisation rooms.

(III) allowing bacteria concentrations of up to 700 CFU/m^3. Rooms include among others delivery rooms, endoscopy rooms, X-ray rooms, blood drawing rooms, diagnostic labs and apparatus rooms.

Table 1.3 Microbial cleanliness guidelines for selected Hospital Rooms.

Switzerland (Krankenhausinstitut, 1987)		Germany (DIN, 2008)		Finland (Kalliokoski, 2003)		France (Norme, 2003)		UK (Health/Estates and Division, 2007)	
Class	CFU/ m^3	Class	CFU/ 50cm/hr	Risk level	CFU/m^3	Class	CFU/m^3	Class	CFU/m^3/5min
I	≤ 10	Ia	≤ 1	High	≤ 10	M1	≤ 1	Conventional (Empty)	≤ 35
II	50	Ib	≤ 5	Normal	100	M10	≤ 10	Conventional (Active)	≤ 180
IIb	200					M100	≤ 100	Ultra-Clean	≤ 10
III	500								

Portuguese legislation on indoor air quality outlines that indoor bacteria concentration should be lower than outdoor concentration, plus 350 CFU/m^3 (Government, 2013). Other guidelines on airborne bacteria relate to medical devices. Good Manufacturing Practices Guideline (EudraLex) established air cleanliness requirements for medical device manufacturing, Table 1.4 and Table 1.5. That document recommends a total aerobic count limit of <1 CFU/m3 in class A rooms (similar to International Organization for Standardization (ISO) 6), 10 CFU/m^3 in class B rooms (similar to ISO 7) and <100 CFU/m^3 in class C rooms (similar to ISO8) (EudraLex).

Table 1.4 Volume 4 EU Guidelines to Good Manufacturing Practice Medicinal Products for Human and Veterinary Use (EudraLex).

Grade	Max concentration limits (particles/m^3 of air) per particle size greater than or equal to the dimensions considered below			
	At Rest		In Operation	
	0.5 µm	5 µm	0.5 µm	5 µm
A	3520	20	3520	20
B	3520	29	352000	2900
C	352000	2900	3520000	29000
D	3520000	29000	-	-

Grade	Recommended Limits for Microbial Containment [a]			
	Air Sample CFU/m^3	Settle Plates (diam. 90 mm) CFU/4hours [b]	Contact Plates (diam. 55 mm) CFU/plate	Glove Print 5 fingers CFU/gloves
A	<1	<1	<1	<1
B	10	5	5	5
C	100	50	25	-
D	200	100	50	-

(a) Average values

(b) Individual settle plates may be exposed for less than 4 hours

Table 1.5 Classification and maximum concentration limits (air particles / m^3) of clean rooms and zones as indicated by the UNI Standard EN ISO 14644-1 (ISO, 2015)

Number (N) of ISO classification	Max concentration limits (particles/m^3 of air) per particle size greater than or equal to the dimensions considered below					
	0.1µm	0.2 µm	0.3 µm	0.5 µm	1 µm	5 µm
ISO class 1	10	2				
ISO class 2	100	24	10	4		
ISO class 3	1000	237	102	35	8	
ISO class 4	10000	2370	1020	352	83	
ISO class 5	100000	23700	10200	3520	832	29
ISO class 6	1000000	237000	102000	35200	8320	293
ISO class 7				352000	83200	2930
ISO class 8				3520000	832000	29300
ISO class 9				35200000	8320000	293000

As mentioned previously, very limited standards for airborne microorganisms exist for hospital areas outside of operating theatres, but monitoring has been reported in hospital rooms (Ortiz et al., 2009), hospital clean rooms (Li and Hou, 2003), a pneumological ward (Augustowska and Dutkiewicz, 2006), an emergency service (Verde et al., 2015), a surgical ward (Verde et al., 2015, Asif et al., 2018), in ICU (Dougall et al., 2019) and maternity wards (Ortiz et al., 2009). As can be seen from Table 1.6, variability in both bacterial concentrations and instrumentation can be seen.

Table 1.6 Summary of bacterial concentrations at various hospital sites

Location	Site	Bacterial Concentration (CFU/m^3)		Instrument	Culture Media	Reference
		Average	Range			
Murcia, Spain	Operating Theatre	25.6	1.67-157	MAS-100	Plate Count Agar	(Ortiz et al., 2009)
	Hospital Rooms*	124.4	4.12-1293			
	Maternity Ward*	67	14.33-224			
Islamabad, Pakistan	Operation theatre Emergency	221	60-466.7	Gillian 5000	Trypticase soy agar (TSA)	(Asif et al., 2018)
	Operation theatre General	236.2	60-460			
	Surgical Ward	369.9	20-1038.5			
	General Medicine Ward	383.9	100-840			
	Emergency Service	1028.9	280-2280			
	Out-patient department	1649.7	380-3577			
Korea	Lobby A	870	380-1800	Anderson Single Stage	TSA	(Park et al., 2013)
	Lobby B	6620	50-2300			
	Lobby C	760	280-1800			
	Lobby D	680	330-1800			
	Lobby E	540	270-1700			
	Lobby F	200	80-450			
Sebutal, Portugal	Operating Theatre		12-170	MAS-100	TSA	(Verde et al., 2015)
	Emergency Service		240-736			
	Surgical Ward		99-495			
Lublin, Poland	Pneumological Ward		257.1-436.3	Own device	Blood Agar	(Augustowska and Dutkiewicz, 2006)
Modena, Italy	Operating Theatre	25.8**	13-82**	Single Stage Slit Impactor	TSA	(Scaltriti et al., 2007)
	Instrument Area	7.9	0-25	Gravitational settling		
	Surgeon Area	5.2	0-25			
	Anaesthesia Equipment Area	6.2	0-18			
Taiwan	Clean Room Class 100		0-32	Anderson 1-STG	TSA	(Li and Hou, 2003)
	Clean Room Class 100000		1-423			
	Operating Theatre 10000	88	13-336			
Scotland	Intensive Care Unit	104.4	12-510	SAS Super-180	TSA	(Dougall et al., 2019)

This variability in observation and lack of objective standards makes it very difficult to determine the effect of airborne microbiological contamination in the general healthcare environment.

New EU/WHO hospital air contamination limits based on patient risk using a 3-class system is being developed. This will set allowable number of bacterial CFU within different healthcare environments. However it must be noted that these guidelines are based on previously operationally developed standards, Table 1.7, for microbial cleanliness in Switzerland from 1987 (Krankenhausinstitut, 1987).

Table 1.7 Room classifications as per Swiss microbial cleanliness guidelines.

Class I Rooms	Class II Rooms	Class III Rooms
Operating theatres (transplantology)	Operating theatre (lower requirements)	ICU (coronary disease)
Orthopaedics	Emergency wards	X-ray rooms
Cardiosurgery	Preoperative rooms	Central sterilization rooms
Patient rooms (extensive burns)	Corridors in operating suites	Surgeries and wards
Specialist laboratories	Premature infant wards and delivery rooms	Changing rooms
ICU (immunosuppressive therapy after bone marrow transplantation)	ICU (surgery and internal departments)	Delivery rooms and children wards
	Patients with less severe burns	Control rooms
		Gym halls
		Central bed stations
		Sterile storerooms
		Laboratories
		Corridoes
		Kitchens
		Laundry rooms

1.6 Modern Real-Time Air Sampling Techniques

More recently, the use of fluorescence detection in the real-time monitoring of ambient particles has grown in popularity, and has been utilized in several widely differing environments (Gabey et al., 2011, O'Connor et al., 2015a, Huffman et al., 2010). The popularity of these instruments have surged for several reasons, including: (i) superior time resolution (millisecond) and continuous real-time readouts in comparison to most traditional techniques which sample over a fixed interval and require processing over days or weeks to yield data ; (ii) the techniques are non-destructive; and, (iii) the processing requires few consumables for operation, and generally does not require an extensively trained operator to extract the data when compared to some of the more subjective conventional methods. It should be noted that while these instruments were designed for the detection of PBAP, the presence of interfering non-biological fluorescent particles may contribute to the total fluorescent count. The concentration values are therefore generally reported as fluorescent aerosol particles (FAP) to reflect the contribution of this unknown component.

1.6.1 Fluorescence

Intrinsic fluorescence (also known as autofluorescence) of PBAP is caused by the presence of naturally occurring fluorescent molecular components (bio-fluorophores) within the sampled particle.

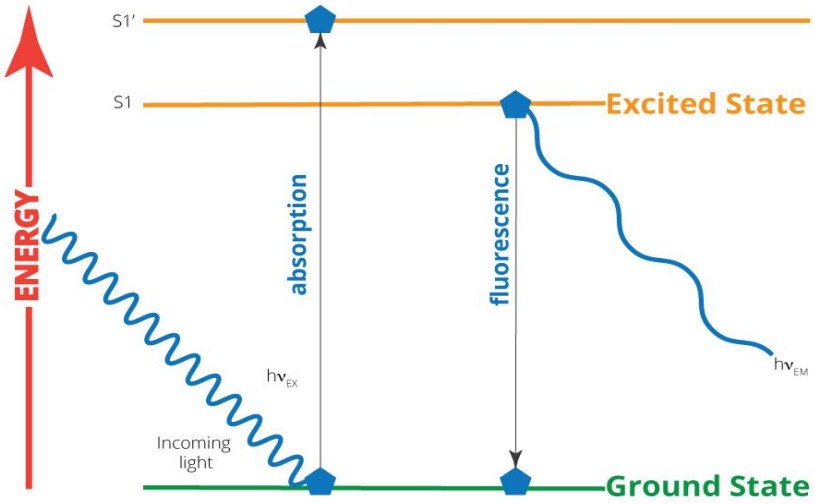

Figure 1.5 Jablonski diagram illustrating the processes of fluorescence by absorption of higher photon energy by a fluorophore and subsequent emission of lower photon energy, resulting in fluorescence during the fluorescence-lifetime (Instruments, 2019).

Extensive reviews on the subject are available (Pöhlker et al., 2012a, Pöhlker et al., 2013, Roshchina, 2008), and only a brief overview of them will be given here. A summary of the characteristic spectra of different compounds is presented in Table 1.8.

The predominant fluorescent molecules found in PBAP are amino acids**,** which are the fundamental building blocks of peptides and proteins, and are common to all life (Weber and Teale, 1957). Of the 20 candidate amino acids, only tyrosine, phenylalanine, and tryptophan are fluorescent (due to their aromatic components) and have absorption/excitation maxima between 260–280 nm. Of the three, tryptophan is known to be the predominant fluorescent species, with as much as 90% of protein fluorescence being attributable to its presence. This enhanced contribution is due to its higher quantum yield when compared to the other amino acids (Pöhlker et al., 2012a). A plethora of other structural chemicals common to many microorganisms or other airborne particles of biological origin**,** including cellulose, chitin, lignin, and

sporopollenin, absorb and re-emit light (Kunit and Puxbaum, 1996, Roshchina, 2008, Pöhlker et al., 2012a, Winiwarter et al., 2009). Sporopollenin, for instance, is a complex biopolymer consisting of carotenoids and phenylalanine which serves as the outermost shell of atmospheric particles, such as pollen (Mel'nikova et al., 1997). Several studies have used the fluorescence signature of sporopollenin and other pollen grain components to distinguish them from other particles in laboratory and outdoor settings (O'Connor et al., 2011, O'Connor et al., 2014). The exact composition of the observed fluorescence in pollen is likely due to a host of bio-fluorophores, such as phenols (emission between 440–480 nm), carotenoids (emission between 500–560 nm), azulene (emission between 440–460 nm), and anthocyanin (emission between 450–470 and 600–640 nm). While sporopollenin as a structural component exclusively relates to pollen, several other fluorescing structural materials are found in other PBAP species. One such component is cellulose, which is an abundant organic molecule that is found in the cell walls of plants, plant debris, fungi, algae, and even bacteria. It is excited over a broad spectrum (250–350 nm) but exhibits rather weak fluorescence in its pure form. Its fluorescence can however be enhanced by the presence of proximal phenolic compounds, with the resultant maxima being observed between 440–460 nm (Pöhlker et al., 2012a). Chitin is another structural component that is present in all fungi. It exhibits maximum fluorescent emission at ~410 nm and its excitation maximum is observed at ~335 nm (Jabaji-Hare et al., 1984, Pöhlker et al., 2012a). Other structural chemicals, such as lignin, one of the most plentiful polymers that is found in the natural world, has also been noted as a fluorescent component observed in certain PBAP, particularly in the cell walls of plants and algae (Pöhlker et al., 2012a). Lignin exhibits fluorescence emission maxima at ~360 nm upon excitation at wavelengths ranging from 240 to 320 nm (Albinsson et al., 1999).

Coenzymes are further category of fluorescent PBAP components that contribute to atmospherically relevant bioaerosol fluorescence. Coenzymes, such as Nicotinamide Adenine Dinucleotide (NADH) and Nicotinamide Adenine Dinucleotide Phosphate (NAD(P)H), are typically present in many PBAP. These coenzymes can be utilized as markers for living cells due to their rapid depletion within several hours of cell death. These coenzymes are directly excited at 340 nm, but can also be excited at 295 nm when energy transfer from nearby photo-excited species occurs (Pöhlker et al., 2012a). Vitamins and flavins are also capable of contributing to observed fluorescent signals from PBAP. Flavins act as metabolic redox carriers and are omnipresent in

microorganisms. Riboflavin (vitamin B_2) in particular is an important contributor to PBAP fluorescence. Its absorption maximum in solution is at 266.5 nm, with a further broader, lower energy peak being observed at ~450 nm. Its fluorescence maximum is observed at ~525 nm with quantum yields of 0.36 in acetone and 0.37 in dioxane (Kozioł and Knobloch, 1965, Pöhlker et al., 2012a). Other vitamins, such as vitamin A, C, D, K, and the other B vitamins are also potential fluorescent contributors, and have been previously discussed in detail (Pöhlker et al., 2012a).

Given the wide variety of colours exhibited by PBAP, it should come as little surprise that PBAP can contain many differing pigments. Many of these pigments are fluorescent, and, therefore, likely contribute to overall PBAP fluorescence emission. Pigments, such as chlorophyll-a, chlorophyll–b, and melanin, are ubiquitous in nature and are present in various environmentally significant aerobiological organisms. Both fungal spores and bacteria have been found to have high melanin content. The presence of chlorophyll-a has been suggested as a potentially useful individual marker for the discrimination of grass pollen and other atmospherically relevant PBAP (O'Connor et al., 2014). The Chlorophylls are generally excited between 390–470 nm, yielding a distinctive emission between 630–730 nm. Melanin, in contrast, has absorption maxima between 469–471 nm, with a prominent emission band between 543–548 nm.

Nucleic acids (DNA) are another biofluorophore with the potential to add to observed PBAP fluorescence signals. Solution-phase DNA fluoresces between ~280–370 nm upon excitation at 270 nm, with the emission maxima shifting to between 350–470 nm when the excitation source is changed to 320 nm (Pisarevskii et al., 1966). Those ranges are the same as those that are expected for pollen and fungal spore fluorescence (O'Connor et al., 2011, O'Connor et al., 2014), however it should be noted that the fluorescence intensity of DNA is rather weak due to its low quantum yields of 10^{-4} to 10^{-5}, and, as such, is not a significant contributor to overall FAP signal intensity (Morgan and Daniels, 1980, Lakowicz et al., 2001).

Secondary metabolites**,** such as alkaloids, terpenes, and phenols represent other classes of fluorescent molecules present in a variety of PBAP. The terpenoid's fluorescence wavelengths range between 420 and 480 nm (Roshchina, 2008). This spectral range

originates from changes in the extent of conjugation that is found in the larger terpenes, with shifts to longer wavelengths associated with increasing conjugation. It has also been reported that several monoterpenes exhibit emission between ~405–430 nm when excited between 310 and 380 nm (Pöhlker et al., 2012a). Of the terpenoids, azulenes have been extensively studied, as they are known constituents of pollen grains. Azulenes, when linked with cellulose, exhibit fluorescence with two emission peaks apparent, the first between 440–460 nm and the second between 620 and 650 nm. Phenols are another secondary metabolite that can be observed on the surface of biofluorophores such as sporopollenin or imbedded in the surface of cell walls. Many phenolics are well known fluorophores in their own regard with emission observed between 400–500 nm when excited in the UV range (Roshchina et al., 1997). Finally, one of the most varied of the secondary metabolites are the alkaloids, which occur in microorganisms such as fungi and bacteria, amongst others. Alkaloids are a diverse group of natural plant compounds, which contain at least one nitrogen in a heterocyclic ring (Saxena, 2007, Roshchina, 2008). Given the wide variety of alkaloids that are found in nature, it is not surprising that this class of compound exhibits wide variations in the observed excitation and emission spectral ranges. Earlier studies have noted excitation ranges between 360–380 nm, leading to fluorescence in the visible spectrum between 410–600 nm (Saxena, 2007, Roshchina, 2008, Pöhlker et al., 2012a).

Table 1.8 Table of fluorophore excitation and emission wavelengths.

Fluorophore	Excitation Wavelengths (nm)	Emission Wavelengths (nm)
Amino acids	260–295	280–360
NADH and NADPH	290–295, 340–366	440–470
Flavins	450–488	520–560
Cellulose	250–350	350–500
Chitin	335	413
Lignin	240–320	360
Melanin	469–471	543–548
Sporopollenin	300–550	400–650
Chlorophyll	390–470	630–730
Flavonoids	365	440–610
Carotenoids	400–500	520–560
Alkaloids	360–380	410–600
Nucleic acids (DNA)	270, 320	280–370 and 350–470
Terpenoids	250–395	400–725
Phenolic compounds	300–380	400–500

Fluorescent compounds are ubiquitous in both biological and non-biological airborne particulate matter. This presents significant challenges when measuring fluorescence on atmospheric samples due to the contribution of non-biological derived fluorescence to the overall fluorescence intensity, which can lead to a potential overestimation of FBAP concentrations (Pöhlker et al., 2012a).

1.6.2 Ultraviolet Aerodynamic Particle Sizer (UV-APS)

The Ultraviolet Aerodynamic Particle Sizer (UV-APS) was the first commercially available single particle fluorescence-based, real-time biological aerosol sensors. The commercial models are based on a prototype instrument that has been detailed previously (Hairston et al., 1997). To determine the fluorescence/sizing signals pertaining to a wide variety of different PBAP species, the UV-APS has been a central feature of extensive indoor and outdoor field campaigns, as well as laboratory-based experiments (Huffman et al., 2010, Huffman et al., 2012, Morawska et al., 2008). The instrument evaluates the aerodynamic size and total fluorescence intensity of individual particles, in addition to their concentrations. A laser is used to determine the particle size, as well as to induce PBAP fluorescence.

The UV-APS determines the sizes of particles in a different manner to the other devices discussed below. The UV-APS determines the particle aerodynamic size (D_a), as opposed to optical instruments that estimate optical size based on optical scatter (Mie theory). The D_a is determined by measuring particle velocity relative to air velocity within an accelerating airflow. The time of flight of each particle is measured as the particles in the flow pass through two sequentially positioned laser beams (680 nm). The particle size is then obtained by collecting the scattered 680 nm light, using a suitable detector, followed by comparison to a calibrated library of size values (Brosseau et al., 2000, Kulkarni et al., 2011).

The instrument samples ambient air with an overall flow rate of 5 L min^{-1}. This flow then bifurcates, and 1 L min^{-1} of the flow is used as the sample flow. The remaining air is channeled in a laminar sheath that directs and focuses the particle stream to the center flow. Preceding the size parameter measurement, the particle fluorescent counts and intensities are measured using a 355 nm diode-pumped, frequency-tripled

Neodymium:Yttrium Aluminium Garnet (Nd:YAG) laser. An ellipsoidal mirror is then used to capture any fluorescent emission from excited particles, with both long pass (410 nm) and short pass filters (630 nm) being used to differentiate between emission and scattered light. The sensitivity of photomultipler tubes (PMT) decreases dramatically above 600 nm, meaning that only fluorescence signals between 410 and 600 nm are actually measured. The number of particles, as well as their aerodynamic size and fluorescence intensities, are then recorded. The UV-APS has seen significantly used in a wide variety of locations and environments, the majority of which are described below, Table 1.9.

Table 1.9 Published studies of ambient Fluorescent Biological Aerosol Particles (FBAP) detected by UV-APS.

Location	Site	Length	Particle Type Analyzed	Concentration Values (Mean or Peak)	Reference
Mainz, Germany	Semi-urban	4 months	FAPs (1–20 μm)	30 L^{-1} (mean)	(Huffman et al., 2010)
Central Amazonia, Brazil	Rainforest	~1 month	FAPs (>1 μm)	73 L^{-1} (mean)	(Huffman et al., 2012, Pöschl et al., 2010)
Colorado, USA	High altitude	~2 months	FAPs (>0.54 μm)	30 ± 10 L^{-1} (mean)	(Hallar et al., 2011)
Colorado, U.S.A	Semi-arid forest	10 months	FBAPs	15 ± 24 L^{-1} (spring) (mean); 30 ± 30 L^{-1} (summer) (mean); 17 ± 31 L^{-1} (fall) (mean); 5.3 ± 6.3 L^{-1} (winter) (mean)	(Schumacher et al., 2013)
Colorado, U.S.A	Semi-arid, forest	35 days	FAPs (0.3–20 μm)	30 L^{-1} (dry periods) (mean)	(Huffman et al., 2013)
Colorado, U.S.A	Forest	~1 month	FAPs (0.5–20 μm)	~400 L^{-1} (peak)	(Gosselin et al., 2016)
Beijing, China	Wastewater plant	NA	FAPs	>2 μm 6.533 L^{-1} (peak); <2 μm 3.867 L^{-1} (peak)	(Li et al., 2016)
Beijing, China	Urban	2 weeks	FAPs	500 L^{-1} (peak)	(Wei et al., 2016)
Beijing, China	Subway	~1 month	FAPs	2.5×10^3 L^{-1}	(Fan et al., 2016)
Multiple sites, China	Urban	March–April	FAPs (0.5–20 μm)	N/A	(Li et al., 2013)
Multiple sites,China	Urban	12 days	FAPs	5 to 470 L^{-1} (range), 79 L^{-1} (mean)	(Wei et al., 2015)
Helsinki, Finland	Urban	23 days (winter); ~60 days (summer)	FAPs (0.5–15 μm)	10–28 L^{-1} (range), 15 L^{-1} (mean)	(Saari et al., 2015b)
Hyytiälä, Finland	Boreal forest	18 months	FAPs	15 ± 24 L^{-1} (spring) (mean); 46 ± 48 L^{-1} (summer) (mean); 27 ± 32 L^{-1} (fall) (mean); 4 ± 46 L^{-1} (winter) (mean)	(Schumacher et al., 2013)
Hyytiälä, Finland	Boreal forest	2 years	FAPs (1–20 μm)	500 L^{-1} (peak)	(Manninen et al., 2014)
Killarney, Ireland	Rural	~1 month	FAPs (0.5–20 μm)	~55 L^{-1} (peak)	(Healy et al., 2014)
India	High-altitude site	11 weeks	FAPs (>1 μm)	20 ± 20 L^{-1} (mean); ~520 L^{-1} (peak)	(Valsan et al., 2016)

1.6.3 Wideband Integrated Bioaerosol Detector (WIBS)

The Wideband Integrated Bioaerosol Sensor (WIBS) is a single aerosol particle fluorescence monitor that uses light-induced fluorescence (LIF) to detect fluorescent aerosol particles (FAP) in real-time. The original instrument was invented by Professor Paul Kaye and co-workers at the University of Hertfordshire. It is now commercially available from Droplet Measurement Technologies (DMT) and is one of the most widely-used instruments for monitoring PBAP in real-time. The WIBS was originally developed for defence applications to enable the detection of airborne particles (Kaye et al., 2014). It offers the ability to characterize the size and asymmetry (shape) of individual fluorescent and non-fluorescent particles by assessing the forward and sideways optical scatter, along with the spectrally unresolved fluorescent intensity of each particle at a millisecond time resolution. There have been several versions of the WIBS available, from Models 3 and 4 prototypes, to the commercial version 4A. Observations have been made in many different external environments and a few indoor environments, Table 1.10.

Table 1.10 Comparison between results of studies utilizing various models of the WIBS instrument. Equivalent Optical Diameter (EOD) is recorded in the μm size range. Number-concentrations of FAP is reported in L^{-1}. (Numbers in parentheses are the fraction of fluorescent particles from the total particles collected as a %).

Site Location	WIBS Model	Site Category	Season	EOD Range	N_{FL1}	N_{FL2}	N_{FL3}	N_{FAP}	References
Manchester, England	3	Urban	Winter	0.8–20	29 (3%)	52 (6%)	110 (11%)	-	(Gabey et al., 2011)
Borneo, Malaysia	3	Rainforest	Summer	0.8–20	-	-	-	150	(Gabey et al., 2011)
Puy de Dôme mountain, France	3	High-altitude	Summer	0.8–20	12 (4.4%)	-	95 (35.2%)	-	(Gabey et al., 2013)
Cork, Ireland	4	Coastal	Summer	3.0–31	~25	~11	~2	(~15%)	(O'Connor et al., 2015a)
Killarney, Ireland	4	Rural	Summer	0.5–13	-	-	-	-	(Healy et al., 2014)
Karlsruhe, Germany	4	Semi-rural	1-Year	0.8–16	-	-	-	31 (7.3%)	(Toprak and Schnaiter, 2013)
Southern U.S.A	4	High-altitude	Autumn	1.0–10	-	-	-	(24%)	(Perring et al., 2015)
Jungfrau, Switzerland	4	High-altitude	Winter	>0.8	-	-	-	6.3 ± 5.7	(Crawford et al., 2016)
Nanjing, China	4a	Suburban	Autumn	1.0–15	570 (4.6%)	3350 (25.3%)	2090 (15.6%)	-	(Yu et al., 2016)
Vancouver, Canada	4a	Coastal	Autumn	0.5–10	-	-	-	(7.8%)	(Mason et al., 2015)
Colorado, U.S.A	3/4	Rural Forest	1-Year	0.8–20	-	-	-	(7.12 %)/(4.02%)	(Crawford et al., 2014)
North Carolina, U.S.A	4a	Urban	Autumn	0.5–15	-	-	-	(41.63%)	(Wright et al., 2014)
Denver, U.S.A	4a	High-altitude	Autumn	0.8–12	-	-	-	69 (11%)	(Twohy et al., 2016)
Nanyang, Singapore	4a	Indoor	-	1.0–10	-	-	-	(~50%)	(Zhou et al., 2017)
Beijing, China	4a	Indoor	Spring	0.5–10	-	-	-	(4.37%)	(Xie et al., 2017)
Beijing, China	4a	Urban	Winter	>0.8	155 (3.3%)	551 (11.4%)	79.4 (1.5%)	642 (13.3%)	(Yue et al., 2017)

1.6.4 BioScout

BioScout is an optical LIF real-time bioaerosol system developed at TUT (Tampere University of Technology), before being commercialized by Environics Ltd (Saari et al., 2013). The BioScout unit utilises a 405 nm continuous wave laser diode operating at 200 mW optical power, to induce autofluorescence from individual bio-particles. The autofluorescence and the scattered light are collected via an elliptical mirror, before being separated using a beam-splitter and focused onto two PMTs. The scattered light is then used to examine the optical particle size, whilst the autofluorescence is isolated from the scattered light using a 442 nm long-pass filter prior to detection at the PMT. The fluorescence intensity is then organised into sixteen intensity channels. The BioScout manufacturers specify a working particle size analysis range from 0.5–10 μm and a time resolution of 1 s. Newer models of the BioScout also include an additional functionality, enabling secondary air sampling of bio-aerosols using filter substrates, which can then be used for subsequent biological analysis.

The BioScout has been comparatively tested against the well-studied UV-APS, under both laboratory conditions and in field campaigns. The laboratory results of an initial study indicated that the BioScout had a higher fluorescent particle detection efficiency for aerosolized fungal spores (*Aspergillus versicolor*, *Penicillium brevicompactum*, and *Penicillium expansum*), aerosolized bacterial spores (*Bacillus atrophaeus* and *Bacillus thuringiensis*), and the common biochemicals (ovalbumin, tryptophan, and riboflavin) when compared to the UV-APS system (Saari et al., 2013). The authors speculate that the higher fluorescent particle fraction (FPF) values observed with the BioScout are due to its more powerful laser, when compared to the UV-APS system. They also note the possibility that the variation of detectors and emission bands that are utilised within each system, might also contribute to the observed difference in fluorescence sensitivity (405 nm excitation for the BioScout and 355 nm excitation for the UV-APS). The UV-APS did however fare better with biochemical particle analysis of NADH, with substantially higher FPF values being observed when compared to the BioScout. The higher FPF values observed for NADH when monitoring using the UV-APS, were attributed to the near coincidence of the excitation peak of NADH with that of the UV-APS 355 nm laser line (Agranovski et al., 2004). When examining the particle size responses of each instrument, the study noted that the UV-APS appeared

to possess better size resolution, whereas the BioScout appeared to demonstrate more efficient particle counting with smaller particle sizes. Discretion is required when making such comparisons since the two instruments use differing measurement modalities. The UV-APS measures the aerodynamic diameter of particles, whilst the BioScout measures optical diameter, which is dependent on the optical properties of the particles.

A second laboratory study also compared the UV-APS and BioScout systems when examining the fluorescent properties of aerosolized fungal spores. Comparisons between instruments were made as a function of the fungal species under examination (*Aspergillus versicolor*, *Cladosporium cladosporioides* and *Penicillium brevicompactum*), their cultivation time, growth substrate and the air exposure velocity (Saari et al., 2015a). The study concluded that all of these factors had an impact on the detection efficiency of fungal spores when utilising fluorescence-based systems. When the two systems were compared, the difference in the observed FPF values were less striking than the previous study and were found to be broadly comparable for both instruments. However, in two cases, the age of two spore varieties led to statistically significant differences in the compared FPF values. The FPF values that were observed with the BioScout were higher (in the case of four-month-old *A. versicolor*) and lower (in the case of four-month-old *P. brevicompactum*) when compared to the UV-APS. The authors attributed these FPF variations between the two systems to the differing fluorescent compounds produced within late stage *Aspergillus versicolor* and *Penicillium brevicompactum* spores, coupled with the dissimilar excitation wavelengths used within each system.

The BioScout and a UV-APS system were also compared in a study involving a summer and winter measurement campaign examining FAP and size distributions in suburban and urbans sites in the Helsinki metropolitan area, Finland (Saari et al., 2015b). Two FAP modes were detected during the summer period at 0.5–1.5 µm (fine) and 1.5–5 µm (coarse). The results showed a high correlation between the instruments for the total particle count for both modes, in spite of the different modalities utilised for their measurement (*vide supra*). Comparison of the UV-APS and BioScout FAP detection efficiencies also suggested that the BioScout demonstrated 2.6× and 9.7× higher detection efficiencies for the coarse and fine modes, respectively. Again, the

authors attributed the observed efficiencies to the higher laser intensity of the BioScout and the good signal to noise ratio of the fluorescence signal that is associated with the system.

Overall, given the observed FAP detection efficiencies that are associated with the use of the 405 nm excitation line within the BioScout system, and notwithstanding the line's relative insensitivity to NADH, it appears that this excitation wavelength may prove interesting in the continued development of instrumentation for the real-time detection of airborne microorganisms (Saari et al., 2013).

1.6.5 Intercomparisons of the Real-Time Fluorescence Devices

It is of interest to comparatively examine the available real-time fluorescence bioaerosol instruments by summarizing intercomparison campaigns that have been undertaken in field and laboratory settings.

Table 1.11 outlines the operational parameters of each of the instruments. The most readily apparent observation is the variety of excitation sources that are used by the instruments with both the UV-APS and BioScout favouring lasers, while the WIBS utilizes multiple flash lamps. The devices all use an excitation wavelength between 370–405 nm (to coincide with NAD(P)H and flavin light absorption maxima amongst others), the WIBS also exploits a shorter wavelength excitation source to discriminate between particles. The 280 nm wavelength flash lamp was included as it provides the required wavelength to excite amino acids, which are constituents of all the biological particles. This additional wavelength facility is absent in the other instruments, which may reduce their ability to detect certain fluorescing particle types. Several laboratory experiments using the WIBS and bacteria have highlighted the importance of the 280 nm wavelength (Channel A or FL1) for bacterial detection. In these studies, aerosolized bacterial samples were observed to fluoresce almost exclusively in channel A (with little if any fluorescence noted in the other detection channels) (Hernandez et al., 2016).

Table 1.11 Specifications of the online real-time devices.

Device	WIBS-4/4A	UV-APS	Bio-Scout
Excitation (nm) and/or scatter source	280/370 nm (two Xe flashlamps)	355-nm UV laser (30 mJ)	405 nm laser diode
Fluorescence detection range	310–400 nm and 420–650 nm	430–580 nm	>442 nm
Size detection range (µm)	0.5–12 HG; 3–30 LG (WIBS-4) or 0.5–20 µm (WIBS-4A)	0.5–20 µm	0.5–10 µm
Time resolution	Millisecond	1 s–18 h (5 min generally)	1 s
Sample flow	0.24 L/min (WIBS-4); 0.3 L/min (WIBS-4A)	1 L/min	2 L/min
Total flow	2.4 L/min (WIBS-4); 2.5/0.3 L/min (WIBS-4A)	5 L/min	2 L/min

Both the UV-APS and the BioScout have also been used to detect bacteria in a laboratory setting. In one study, both instruments were subjected in parallel to a variety of test aerosols in order to ascertain their fluorescent particle fraction (FPF). The aerosols used varied from bacteria to a number of dispersed bio-chemicals. In the majority of cases, the BioScout described a greater fraction of the aerosols as fluorescent. Overall, the BioScout FPF values varied between 0.34–0.77 for single bacterial spores, while the UV-APS FPF values for the bacterial spores were significantly lower (between 0.13–0.17). Interestingly, smaller particles of the same particle type comprised lower fluorescent fractions of the total. These results suggest that these particles did not produce sufficient fluorescence emission to enable their detection by the instruments, and were thus below the instrument detection limit, rather than being non-fluorescent in nature. However, the UV-APS did return far higher fluorescent fractions for the bio-chemical NAD(P)H. This finding was not surprising given the 355 nm laser used by the UV-APS excites in the excitation range (340–366 nm) of NAD(P)H, whereas the BioScout laser does not (405 nm). Thus, this study suggests that the BioScout is potentially more sensitive than the UV-APS for the detection of bacterial cells, but the ability of the UV-APS to induce NAD(P)H fluorescence may prove to be of greater interest in the detection of viable or metabolically active biological particles (Saari et al., 2013).

Other laboratory studies have shown that the UV-APS can detect fluorescence from individual bacterial cells (*B. subtilis*), however, very little fluorescence from bacterial endospores was noted (Agranovski et al., 2003). To explain their results, the authors suggested that bacterial endospores are dormant (i.e., lack metabolic activity), and

therefore do not contain sufficient concentrations of NAD(P)H to elicit a response above the instrumental sensitivity threshold.

The second excitation channel incorporated into the WIBS may also allow for the enhanced detection of fungal spores in comparison to the other instruments. As was observed for bacteria samples, several laboratory studies have also shown that fluorescence channel A is the most likely to characterize fungal spores (Hernandez et al., 2016, O'Connor et al., 2013). One study showed that for a particular fungal spore species tested ~80% of the fungal spore numbers could be characterized as "A-type" particles (Hernandez et al., 2016). This specific information cannot be obtained using the UV-APS or the BioScout due to their inability to excite particles at 280 nm. However, laboratory studies have shown that while the UV-APS and the BioScout can detect fungal spores (Kanaani et al., 2007, Kanaani et al., 2008, Saari et al., 2015a) (implying other excitation wavelengths and detection bands are still useful), the question as to what fraction of the total fungal spore concentration they sample in comparison to the WIBS has not been answered.

Parallel sampling of the aforementioned instruments during field studies has also allowed for the direct comparison of their capabilities. For instance, the BioScout and the UV-APS have been the subject of a comparative study in an urban environment (Saari et al., 2013). Both of the instruments correlated well for fluorescent particles >1.5 µm (R = 0.83) and <1.5 µm (R = 0.92). One significant difference noted was the concentration of fluorescent particles that were sampled with the BioScout, which showed 2.6× and 9.7× values for the coarse and fine FAP, respectively (Saari et al., 2015b). Similarly, the WIBS and the UV-APS have been stationed together during a field campaign in Killarney Ireland. Importantly, both returned virtually identical total particle concentrations, implying that total particle counts obtained for both instruments may considered as equivalent. Furthermore, the FL3 channel intensities obtained with the WIBS correlated well with the UV-APS fluorescent counts. In contrast, the WIBS FL3 counts were measured to be far higher than those provided by the UV-APS (by a factor of ~2). In this study, the WIBS instrumental data led to a bi-modal distribution of particle sizes at ~3–4 and ~1–2 µm. This distribution was not observed using the UV-APS, with only the larger mode being registered. This sizing result possibly indicates that the WIBS approach is more suited for the detection

bacteria when compared to the UV-APS. Collections from both of the instruments were positively correlated with those that were obtained using traditional impaction/optical microscopy methodologies. This important feature has been subsequently confirmed for WIBS and traditional measurements at a number of locations (O'Connor et al., 2014). Real-time instrumentation tends to return larger concentration values than those that are obtained using a traditional sampler (O'Connor et al., 2015b, O'Connor et al., 2014). This finding is most likely due to the poor collection efficiencies of the traditional samplers, coupled with operator error when counting large concentrations by eye. WIBS results also correlate well with those obtained from fungal spore tracer methods (Gosselin et al., 2016). For example, it has been found that WIBS results were within ~13% of the spore count estimated by a tracer method. The UV-APS approach has also been contrasted with off-line sampling methods (e.g., AGI-30 impingers) and the studies have shown good agreement (Kanaani et al., 2008).

The capability of each instrument to evaluate particulate size ranges also varies. The WIBS and the UV-APS can effectively sample larger biological particles (>20 µm depending on the version and instrument), whereas the BioScout size range cut-off size is 10 µm, and therefore precludes it from the detection of larger fungal spores and pollen. The WIBS instrument is the only reviewed instrument that has been successfully used to detect pollen in both laboratory and outdoor environments. In addition, the instrument has been shown to respond to a host of different fungal spores and pollen grains in terms of fluorescence signals, sizing, and asymmetry factors, but PBAP identification at the species level still remains elusive.

Finally, the flow rates of the three instruments differ significantly (Table 1.11). The UV-APS with its 5 L/min flow rate is the largest of the three, which provides advantages to ambient outdoor sampling as vertical sampling lines are generally used. This feature allows for more effective sampling of fast-moving particles during windy periods.

1.7 Future Instrumental Development

Newer instrumental techniques based on the premise of single particle fluorescence continue to be developed. These instruments offer greater sensitivity and even the prospect of spectrally resolved fluorescence spectra. Among the most promising instruments are the Particle Analyser - 300 (PA-300), the Spectral Intensity Bioaerosol Sensor (SIBS), and the Multi-parameter Bioaerosol Sensor (MBS), manufactured by Plair SA, Droplet Measurement Technologies, and the University of Hertfordshire/DSTL, respectively. In principle, these instruments function similarly to those discussed above. However, such devices are designed to give additional information over the full fluorescence emission wavelength ranges to aid with actual identification of the FAP/PBAP by essentially determining the individual spectroscopic "fingerprints" for specific biological species. An overview of each instrument is given below. Although they are all commercially available, there are to date little or no peer reviewed publications to confirm their capabilities.

1.7.1 PA-300

This instrument is based on the work of Kiselev et al. (Kiselev et al., 2011, Kiselev et al., 2013) and uses both optical scatter and spectrally resolved fluorescence for the identification of biological particles by providing a near complete spectrum for each particle. The instrument has an air-flow rate of 2 L min^{-1}, and initially passes particles through a red laser beam (658 nm) to yield time-resolved scattering data. The signals are recorded by two photo-detectors that also characterize the optical shape, size, and surface properties. The manufacturers claim that the instrument can measure particles in the size range of 1–100 μm, which represents a far larger span than any of the instrumentation described above. Subsequent to the initial laser excitation, a second laser beam (377 nm) excites the particles and the resultant fluorescence signals are recorded using a diffraction grating and an array of 32 photo-detectors (32 equal bins with overall range 390–600 nm). Again, the span is far greater than the instruments mentioned hitherto. Additionally, and unique to the PA-300, the phosphorescence of individual particles can also be recorded. This will allow for the further investigation of the intrinsic photophysical properties of biological particles, and possibly aid in the discrimination between biological species.

Only one peer-reviewed publication is currently available on the use of the PA-300 (Crouzy et al., 2016), which sought to analyze the performance of the PA-300 with regard to pollen identification and airborne particle concentrations. The spectral measurements were made in parallel to a manual reference measurement instrument (Hirst-type volumetric sampler/optical microscopy) during a Swiss pollen season (14th February–31st August 2016). The studies were made at the MeteoSwiss site in Payerne, Switzerland. The PA-300 that was used on this campaign was modified to provide an inlet system, which increased the factory standard sampling levels. A concentrator provided by Plair SA and based on the virtual impactor principle, was also used in conjunction with a second pump (flow rate 30 L min^{-1}). A good correlation between the expected and measured values (r = 0.88) was calculated when comparing 16 different pollen types. To simplify the pollen counting process, only particles fluorescing between 390 nm and 600 nm and with sizes <9 μm were analyzed. The PA-300 measurements recorded ~25 times more events than the manual sampling approach. There was a high correlation between the two methodologies (r = 0.95) for total pollen counts. This trend was also noted for individual species, such as grass pollen (r = 0.83), amongst others. These observations are of great interest given that grass pollen is generally considered to be the greatest contributor to hay fever (Crouzy et al., 2016). Recently, an extended version of the PA-300 has been developed, the PA-1000. It has enhanced capabilities for the detection of aerosols down to 0.5 μm. The PA-1000 can also provide time-resolved excited state lifetimes of individual particles. This has the potential to provide an additional intrinsic physical property with which to discriminate between particles possessing similar physical and spectral characteristics. Previous work has demonstrated that individual particles can be discriminated on the basis of their excited state lifetimes, albeit in an off-line capacity. A study by O'Connor et al. (2014) (O'Connor et al., 2014) showed that different species of pollen returned different lifetime values based on their photophysical properties (O'Connor et al., 2014).However, there are currently no peer reviewed reports that are available documenting its use.

1.7.2 WIBS-4+ and WIBS-Neo

During a laboratory study that measured the fluorescence spectra and the lifetimes of individual pollen grains, the biomolecule chlorophyll-a was shown to be a possible biomarker for grass pollen due to its unique fluorescence peak at 670 nm (O'Connor et al., 2014). It is suggested that this biomarker could be used to specifically characterize grass pollen, as opposed to tree pollen, which does not give rise to the same signal (O'Connor et al., 2014). Therefore, to specifically detect chlorophyll-a fluorescence, an upgrade of the WIBS-4 was developed and termed the WIBS-4+. This instrument provides two additional fluorescence data channels, FL4 and FL5. The FL4 signals derive from the excitation of particles at 280 nm, while FL5 signals come from the excitation of particles at 370 nm. Potential emission from chlorophyll-a is recorded by a photomultiplier in the 600–750 nm range. The WIBS-Neo is conceptually the same as the WIBS-4A but incorporates a working particle size range of 0.5–50 µm, has improved sensitivity and the capability of measuring fluorescence lifetimes. However, no peer-reviewed papers are available on either the WIBS-4+ or the WIBS-Neo as of this time.

1.7.3 Multiparameter Bioaerosol Spectrometer (MBS)

Although being the first of the next generation of real-time techniques for airborne PBAP/FAP analysis to be developed, there is only one peer-reviewed publication that reports the use of an MBS (Ruske et al., 2017). The MBS is an evolution of the WIBS technology and provides data relating to the size (1–20 microns), shape, and autofluorescence of individual airborne particles. However, where the WIBS-3 and WIBS-4(A) only record particle fluorescence over two ranges, 310–400 nm and 420–650 nm, the MBS provides spectral distribution histograms over eight wavelength bands: 300–335 nm, 340–385 nm, 390–435 nm, 440–485 nm, 490–535 nm, 540–575 nm, 580–615 nm, and 620–655 nm. The end-result is comparable to a traditional spectrum because individual fluorescing particles give rise to specific spectral distributions. When combined with the ability to determine FAP size and shape using an arrangement of two 512-pixel CMOS detector arrays to record high-resolution data, improved discrimination between biological and non-biological particles would appear to be possible with this instrument arrangement (Ruske et al., 2017).

The MBS operates by drawing ambient aerosol at a rate of ~1.5 L min^{-1} through an inlet tube before being split. Parts of this flow are then used as both a "bleed flow" (to maintain inner optical chamber cleanliness) and as a "sheath flow" to surround and direct the remaining 300 mL min^{-1} sample flow. Particles that are confined in this sample flow are forced through the so-called "sensing volume", which is the juncture between the particle detection laser beam and the sample airflow column. Here, individual particles are first irradiated by a low-power laser beam (12 mW at 635 nm) and the subsequent light scatter from the laser pulse is collected by a lens assembly, while a small proportion of this light is directed by a pellicle beam splitter to a photodiode trigger detector. The voltage output pulse of this detector is proportional to the light intensity and is used to determine particle size. The trigger detector signal also induces the firing of a second, high-power pulsed laser (250 mW at 635 nm) to irradiate the particle with sufficient intensity to allow two CMOS linear detector arrays to then capture the morphology and orientation elements associated with spatial light scattering pattern of the particle. About 10 μs after particle detection, an intense UV pulse (at 280 nm) illuminates the particle for ~1 μs, resulting in fluorescence of the analyte particles. The fluorescence is then focused onto the spectrometer optics. The eight channel PMT records a fluorescence spectrum between 310–650 nm after which the electronics control unit (ECU) digitizes and documents the information. The particle then exits the chamber and the process is repeated for further particles. The total time taken to measure one particle is 30 μs, meaning that the system has the potential to count particles at a rate greater than 1000 particles per second. However, the xenon lamp has a recharge time of ~5 ms, which then becomes a limiting factor, and reduces the data collection rate to ~100 particles s^{-1} equivalent to 2×10^4 particles L^{-1} (Ruske et al., 2017).

1.7.4 SIBS

SIBS is also based on the WIBS instrument design and uses several identical components. However, like the MBS, it provides additional spectral information by recording 32 combined channels of fluorescence intensity per particle. It also has the ability to determine fluorescence lifetimes of particles. The SIBS measures particles with sizes in the lower sub-micron range (≥ 0.1 μm). No peer-reviewed publications are yet available regarding the use and efficacy of this technique in either field or

laboratory settings. Comparison between the parameters for the previously discussed future instrumentation compiled in Table 1.12.

Table 1.12 Comparison between reported instrumental parameters of future instrumentation.

Parameter	PA-300	PA-1000	MBS	WIBS-4+	WIBS-Neo	SIBS
Excitation source	337 nm UV-laser beam	263 nm UV-laser beam	280 nm Xenon flashtubes	280 and 370 nm Xenon flashtubes	280 and 370 nm Xenon flashtubes	280 and 370 nm Xenon flashtubes
Aerosol sampling flow rate	2.0 L min^{-1}	2.8 L min^{-1}	0.30 L min^{-1}	0.30 L min^{-1}	0.30 L min^{-1}	0.30 L min^{-1}
Sizing method	Optical Diameter (D_o) by Mie theory	Optical Diameter (D_o) by Mie theory	Optical Diameter (D_o) by Mie theory	Optical Diameter (D_o) by Mie theory	Optical Diameter (D_o) by Mie theory	Optical Diameter (D_o) by Mie theory
Particle size range	1–100 µm	0.5–100 µm	1–20 µm	High-Gain = 0.5–12 µm Low-Gain = 3–31 µm	0.5–50 µm	N/A
Fluorescence	32 equal bins between 390–600 nm	32 equal bins between range 290–660 nm	300–335 nm, 340–385 nm, 390–435 nm, 440–485 nm, 490-535 nm, 540–575 nm, 580–615 nm, 620–655 nm	FL1 λ_{ex} = 280 nm, λ_{em} = 310–400 nm FL2 λ_{ex} = 280 nm λ_{em} = 420–650 nm FL3 λ_{ex} = 370 nm λ_{em} = 420–650 nm FL4 λ_{ex} = 280 nm λ_{em} = 600–750 nm FL5 λ_{ex} = 370 nm λ_{em} = 600–750 nm	FL1 λ_{ex} = 280 nm, λ_{em} = 310–400 nm FL2 λ_{ex} = 280 nm λ_{em} = 420–650 nm FL3 λ_{ex} = 370 nm λ_{em} = 420–650 nm	16 channels between 300–720 nm

1.7.5 Real-time Fluorescent Monitoring in Hospitals

Limited real-time fluorescence monitoring of hospital bioaerosols has been reported, Table 1.13, a study of a respiratory ward at St James's University Hospital in Leeds, United Kingdom, at several settings between two hospitals in Brisbane, Australia and an operating theatre in Hefei, China (Roberts et al., 2006, Pereira et al., 2017, Dai et al., 2015).

The previous real-time studies of fluorescent particle bioaerosol detection in hospital wards using different instruments showed average fluorescent particle concentrations ranging from 0 – 0.09 $\times 10^6$ part./m^3 (mean 0.03×10^5) in a children's hospital and higher values 0.05– 0.48 $\times 10$ part./m^3 (mean 0.06×10^6) in an adult hospital (Pereira et al., 2017). Total particle concentrations in the children's hospital ranged from 0.19–0.51 $\times 10^6$ part./m^3 (mean 0.06×10^6 part./m^3) , at the adults hospital total particle concentrations ranged from 0.67– 1.67 $\times 10^6$ part./m^3 (mean 1.20×10^6 part./m^3), Table 1.13.

Table 1.13 Summary of previous Particle concentrations at various hospital sites

Location	Area	Particle Counts ($\times 10^6$ part/m^3)				Instrument	Ref
		Fluorescent mean.	Fluorescent Range	Total mean.	Total Range		
Australia, Brisbane	Adult Pulmonary Ward	0.05	0.02 - 0.1	1.28	0.84 - 1.83	UV-APS	(Pereira et al., 2017)
	Adult Spirometry Lab	0.07	0.11 - 0.24	1.46	0.57 - 1.84		
	Adult Outpatients Waiting	0.04	0.01 - 1.11	0.91	0.61 - 1.35		
	Adult Overall	0.06	0.05 - 0.48	1.2	0.67 - 1.67		
	Children Pulmonary Ward	0.03	0.0 - 0.06	0.4	0.26 - 0.58		
	Children Spirometry Lab	0.04	0.0 - 0.14	0.65	0.27 - 0.76		
	Children Outpatients Waiting	0.02	0.0 - 0.07	0.15	0.06 - 0.21		
	Children Overall	0.03	0.0 - 0.09	0.33	0.19 - 0.51		
China, Hefei	Operating Theatre (During Operation)	0.08				BAC-6825	(Dai et al., 2015)
	Operating Theatre (Preparation phase)	0.12					
	Operating Theatre (Static Condition)	0.02					

1.8 Research Aims and Objectives

The aim of this thesis is to determine if methods and technology previously applied to aerobiology of the external environment can characterise the healthcare environment.

Objectives

1. To determine if continuous monitoring technology including spectrometry utilising light-induced-fluorescence (LIF) can successfully monitor aerosols of biological origin in the healthcare environment in real-time (Chapter 3).
2. To determine the likely sources of aerosols of biological origin revealed by LIF spectroscopy in different healthcare environments (Chapter 3,4,6).
3. To assess the effects of different interventions on biological aerosols in the healthcare environment using continuous monitoring technology (Chapters 3,4,5,6).

Chapter 3 details how real-time monitoring using LIF can reveal bioaerosol generating procedures, identify viable aerosols by fluorescent signatures, determine the effectiveness of air treatment devices and efficiency of aerosol dispersal interventions. Specifically, Chapter 3 will discuss the use of the WIBS instrument in monitoring bioaerosols on a respiratory ward at CUH. The effectiveness of a plasma disinfection unit on air particle concentrations will be analysed using both real-time monitoring (WIBS and AirNode) and conventional sampling (MAS-100, settle plates, swab analysis and Coriolis μ). Movement activity was also monitored using a footfall counter with correlations assessed between footfall counts, particle concentrations and bacterial loads. Preliminary analysis on the respiratory ward noted diurnally plotted fluorescent particle counts resolved into four distinct peaks, corresponding to times of nebuliser therapy.

In Chapter 4 analysis of in vitro WIBS-4A observations of in vitro nebulised bacteria previously gathered by Dr Stig Hellebust and Dr David O'Connor is used to provide a fingerprint of airborne bacteria which allows establishment in Chapter 5 of a bioinformatic method of filtering out specific fluorescent interferants (nebulised drugs detected in Chapter 3) from WIBS-4A and WIBS-4+ observations. Subsequently in Chapter 5 an extractor tent used to reduce the known risk of TB transmission during sputum induction is conclusively shown to limit the dispersal of nebulised drugs. The effectiveness of the extractor tent (Demistifier 2000, Peace Medical) was verified by

continuous monitoring of particle dispersal from a nebuliser, within the tent, using a real-time bioaerosol detector.

Chapter 6 investigates the bioaerosol generation associated with different toilet activities and interventions from a shared office lavatory. All toilet activities were logged allowing for comparisons and associations to be generated between the activities and particle data. The intervention analysed was the toilet lid, with data collected with and without toilet lid usage compared. To further control variables related to the flush process, experiments with artificial stool were performed in the same toilet. Paradoxically, enhanced persistence of airborne flush-associated particles was noted with the lid-down position.

Finally, Chapter 7 includes a summary of the work and outlines future work in the area.

1.9 References

ACGIH 1999. Particle size-selective sampling for particulate air contaminants.

ADAM, R. I., BHANGAR, S., PASUT, W., ARENS, E. A., TAYLOR, J. W., LINDOW, S. E., NAZAROFF, W. W. & BRUNS, T. D. 2015. Correction: Chamber Bioaerosol Study: Outdoor Air and Human Occupants as Sources of Indoor Airborne Microbes. *PloS one,* 10**,** e0133221.

ADAMS, R. I., MILETTO, M., TAYLOR, J. W. & BRUNS, T. D. 2013. Dispersal in microbes: fungi in indoor air are dominated by outdoor air and show dispersal limitation at short distances. *The ISME journal,* 7**,** 1262.

AGRANOVSKI, V., RISTOVSKI, Z., HARGREAVES, M., BLACKALL, P. J. & MORAWSKA, L. 2003. Real-time measurement of bacterial aerosols with the UVAPS: performance evaluation. *Journal of Aerosol Science,* 34**,** 301-317.

AGRANOVSKI, V., RISTOVSKI, Z. D., AYOKO, G. A. & MORAWSKA, L. 2004. Performance evaluation of the UVAPS in measuring biological aerosols: fluorescence spectra from NAD (P) H coenzymes and riboflavin. *Aerosol Science and Technology,* 38**,** 354-364.

ALBINSSON, B., LI, S., LUNDQUIST, K. & STOMBERG, R. 1999. The origin of lignin fluorescence. *Journal of Molecular Structure,* 508**,** 19-27.

ALLEN, R. J., BRENNIMAN, G. R., LOGUE, R. R. & STRAND, V. A. 1989. Emission of airborne bacteria from a hospital incinerator. *JAPCA,* 39**,** 164-168.

ANDERSEN, A. 1966. A sampler for respiratory health hazard assessment. *American Industrial Hygiene Association Journal,* 27**,** 160-165.

ANDERSEN, A. A. 1958. New sampler for the collection, sizing, and enumeration of viable airborne particles. *Journal of Bacteriology,* 76**,** 471.

ANGENENT, L. T., KELLEY, S. T., AMAND, A. S., PACE, N. R. & HERNANDEZ, M. T. 2005. Molecular identification of potential pathogens in water and air of a hospital therapy pool. *Proceedings of the National Academy of Sciences of the United States of America,* 102**,** 4860-4865.

ASIF, A., ZEESHAN, M., HASHMI, I., ZAHID, U. & BHATTI, M. F. 2018. Microbial quality assessment of indoor air in a large hospital building during winter and spring seasons. *Building and Environment,* 135**,** 68-73.

ATKINSON, M. P. & WEIN, L. M. 2008. Quantifying the routes of transmission for pandemic influenza. *Bulletin of mathematical biology,* 70**,** 820-867.

ATLAS, R. M. & BARTHA, R. 1981. *Microbial ecology: fundamentals and applications,* Addison-Wesley Publishing Company.

AUGUSTOWSKA, M. & DUTKIEWICZ, J. 2006. Variability of airborne microflora in a hospital ward within a period of one year. *Annals of Agricultural and Environmental Medicine,* 13**,** 99-106.

BARBAREE, J., GORMAN, G., MARTIN, W., FIELDS, B. & MORRILL, W. 1987. Protocol for sampling environmental sites for legionellae. *Applied and Environmental Microbiology,* 53**,** 1454-1458.

BARTLEY, J. M., OLMSTED, R. N. & HAAS, J. 2010. Current views of health care design and construction: practical implications for safer, cleaner environments. *American Journal of Infection Control,* 38**,** S1-S12.

BAURÈS, E., BLANCHARD, O., MERCIER, F., SURGET, E., LE CANN, P., RIVIER, A., GANGNEUX, J.-P. & FLORENTIN, A. 2018. Indoor air quality in two French hospitals: measurement of chemical and microbiological contaminants. *Science of the total environment,* 642**,** 168-179.

BEECHEM, J. M. & BRAND, L. 1985. Time-resolved fluorescence of proteins. *Annual review of biochemistry,* 54**,** 43-71.

BEGGS, C., NOAKES, C., SLEIGH, P., FLETCHER, L. & SIDDIQI, K. 2003. The transmission of tuberculosis in confined spaces: an analytical review of alternative epidemiological models. *The international journal of tuberculosis and lung disease,* 7**,** 1015-1026.

BHANGAR, S., ADAMS, R. I., PASUT, W., HUFFMAN, J., ARENS, E. A., TAYLOR, J. W., BRUNS, T. D. & NAZAROFF, W. W. 2015. Chamber bioaerosol study: human emissions of size-resolved fluorescent biological aerosol particles. *Indoor Air*.

BHANGAR, S., HUFFMAN, J. & NAZAROFF, W. 2014. Size-resolved fluorescent biological aerosol particle concentrations and occupant emissions in a university classroom. *Indoor air,* 24**,** 604-617.

BHOLAH, R. & SUBRATTY, A. 2002. Indoor biological contaminants and symptoms of sick building syndrome in office buildings in Mauritius. *International journal of environmental health research,* 12**,** 93-98.

BIRGAND, G., SALIOU, P. & LUCET, J.-C. 2015. Influence of staff behavior on infectious risk in operating rooms: what is the evidence? *infection control & hospital epidemiology,* 36**,** 93-106.

BLASER, M., BORK, P., FRASER, C., KNIGHT, R. & WANG, J. 2013. The microbiome explored: recent insights and future challenges. *Nature Reviews Microbiology,* 11**,** 213.

BOURDILLON, R., LIDWELL, O. & THOMAS, J. C. 1941. A slit sampler for collecting and counting air-borne bacteria. *Epidemiology & Infection,* 41**,** 197-224.

BRACHMAN, P. S., EHRLICH, R., EICHENWALD, H. F., GABELLI, V. J., KETHLEY, T., MADIN, S. H., MALTMAN, J. R., MIDDLEBROOK, G., MORTON, J. D. & SILVER, I. H. 1964. Standard sampler for assay of airborne microorganisms. *Science,* 144**,** 1295.

BRASCHE, S. & BISCHOF, W. 2005. Daily time spent indoors in German homes–baseline data for the assessment of indoor exposure of German occupants. *International journal of hygiene and environmental health,* 208**,** 247-253.

BREEDING, D. C. 2003. Bioaerosol evaluation in indoor environments. *Occupational health & safety (Waco, Tex.),* 72**,** 58.

BROSSEAU, L. M., VESLEY, D., RICE, N., GOODELL, K., NELLIS, M. & HAIRSTON, P. 2000. Differences in detected fluorescence among several bacterial species measured with a direct-reading particle sizer and fluorescence detector. *Aerosol Science & Technology,* 32**,** 545-558.

BURGE, H. A. & SOLOMON, W. R. 1987. Sampling and analysis of biological aerosols. *Atmospheric Environment (1967),* 21**,** 451-456.

CENTRE, H. P. S. 2008. Infection Prevention and Control Building Guidelines for Acute Hospitals in Ireland. *Strategy for the control of Antimicrobial Resistance in Ireland (SARI)*.

CHAO, C. Y. H., WAN, M. P., MORAWSKA, L., JOHNSON, G. R., RISTOVSKI, Z., HARGREAVES, M., MENGERSEN, K., CORBETT, S., LI, Y. & XIE, X. 2009. Characterization of expiration air jets and droplet size distributions immediately at the mouth opening. *Journal of Aerosol Science,* 40**,** 122-133.

CHEN, C. & ZHAO, B. 2011. Review of relationship between indoor and outdoor particles: I/O ratio, infiltration factor and penetration factor. *Atmospheric Environment,* 45**,** 275-288.

COMMITTEE, N. C. E. 2013. Prevention and control methicillin-resistant staphylococcus aureus (MRSA) national clinical guideline No. 2.
CONTROL, C. F. D. & PREVENTION 2009. Interim guidance for novel H1N1 flu (swine flu): taking care of a sick person in your home. *Accessed May,* 6.
COONS, A. H., LEDUC, E. H. & KAPLAN, M. H. 1951. Localization of antigen in tissue cells: VI. The fate of injected foreign proteins in the mouse. *Journal of Experimental Medicine,* 93**,** 173-188.
COOPER, C. W., AITHINNE, K. A., FLOYD, E. L., STEVENSON, B. S. & JOHNSON, D. L. A comparison of air sampling methods for Clostridium difficile endospore aerosol. *Aerobiologia***,** 1-10.
COSTELLO, E. K., LAUBER, C. L., HAMADY, M., FIERER, N., GORDON, J. I. & KNIGHT, R. 2009. Bacterial community variation in human body habitats across space and time. *Science,* 326**,** 1694-1697.
COWN, W., KETHLEY, T. & FINCHER, E. 1957. The critical-orifice liquid impinger as a sampler for bacterial aerosols. *Applied Microbiology,* 5**,** 119.
COX, C. S. & WATHES, C. M. 1995. *Bioaerosols handbook*, crc press.
CRAWFORD, I., LLOYD, G., HERRMANN, E., HOYLE, C., BOWER, K., CONNOLLY, P., FLYNN, M., KAYE, P., CHOULARTON, T. & GALLAGHER, M. 2016. Observations of fluorescent aerosol–cloud interactions in the free troposphere at the High-Altitude Research Station Jungfraujoch. *Atmospheric Chemistry and Physics,* 16**,** 2273-2284.
CRAWFORD, I., ROBINSON, N., FLYNN, M., FOOT, V., GALLAGHER, M., HUFFMAN, J., STANLEY, W. & KAYE, P. H. 2014. Characterisation of bioaerosol emissions from a Colorado pine forest: results from the BEACHON-RoMBAS experiment. *Atmospheric Chemistry and Physics,* 14**,** 8559-8578.
CREAMER, E., SHORE, A. C., DEASY, E. C., GALVIN, S., DOLAN, A., WALLEY, N., MCHUGH, S., FITZGERALD-HUGHES, D., SULLIVAN, D. J. & CUNNEY, R. 2014. Air and surface contamination patterns of meticillin-resistant Staphylococcus aureus on eight acute hospital wards. *Journal of Hospital Infection,* 86**,** 201-208.
CROUZY, B., STELLA, M., KONZELMANN, T., CALPINI, B. & CLOT, B. 2016. All-optical automatic pollen identification: Towards an operational system. *Atmospheric Environment,* 140**,** 202-212.
DAI, C., ZHANG, Y., MA, X., YIN, M., ZHENG, H., GU, X., XIE, S., JIA, H., ZHANG, L. & ZHANG, W. 2015. Real-time measurements of airborne biologic particles using fluorescent particle counter to evaluate microbial contamination: results of a comparative study in an operating theater. *American Journal of Infection Control*, 43**,** 78-81.
DANCER, S. J. 2009. The role of environmental cleaning in the control of hospital-acquired infection. *Journal of Hospital Infection,* 73**,** 378-385.
DANCER, S. J. 2011. Hospital cleaning in the 21st century. *European journal of clinical microbiology & infectious diseases,* 30**,** 1473-1481.
DAVIES, C. N. 1987. The aerobiological pathway of microorganisms. By C. S. Cox. John Wiley & Sons. 1987. Pp. 293. £32.00. *Quarterly Journal of the Royal Meteorological Society,* 113**,** 1403-1404.
DAVIES, S. 2010. Fragmented management, hospital contract cleaning and infection control. *Policy & Politics,* 38**,** 445-463.
DESPRÉS, V. R., HUFFMAN, J. A., BURROWS, S. M., HOOSE, C., SAFATOV, A. S., BURYAK, G., FRÖHLICH-NOWOISKY, J., ELBERT, W.,

ANDREAE, M. O. & PÖSCHL, U. 2012. Primary biological aerosol particles in the atmosphere: a review. *Tellus B,* 64.
DIETRICH, W. E. 1982. Settling velocity of natural particles. *Water resources research,* 18**,** 1615-1626.
DILLON, H. K., HEINSOHN, P. A., MILLER, J. D. & COMMITTEE, A. I. H. A. B. 2005. *Field Guide for the Determination of Biological Contaminants in Environmental Samples*, American Industrial Hygiene Association.
DIN, D. 2008. Raumlufttechnik e Teil 4: Raumlufttechnische Anlagen in Gebäuden und Räumen des Gesundheitswesens. *Berlin, Germany: Deutsches Institut für Normung eV*.
DOUGALL, L. R., BOOTH, M., KHOO, E., HOOD, H., MACGREGOR, S., ANDERSON, J., TIMOSHKIN, I. & MACLEAN, M. 2019. Continuous Monitoring of Aerial Bioburden within Intensive Care Isolation Rooms and Identification of 'High Risk'Activities. *Journal of Hospital Infection*.
DOUWES, J., THORNE, P., PEARCE, N. & HEEDERIK, D. 2003. Bioaerosol health effects and exposure assessment: progress and prospects. *Annals of Occupational Hygiene,* 47**,** 187-200.
DOWNIE, A., MEIKLEJOHN, M., VINCENT, L. S., RAO, A., BABU, B. S. & KEMPE, C. 1965. The recovery of smallpox virus from patients and their environment in a smallpox hospital. *Bulletin of the World Health Organization,* 33**,** 615.
DRIVER, J., BAKER, S. R. & MCCALLUM, D. 2012. *Residential Exposure Assessment: A Sourcebook*, Springer US.
DUNGAN, R. S. & LEYTEM, A. B. 2016. Recovery of culturable Escherichia coli O157: H7 during operation of a liquid-based bioaerosol sampler. *Aerosol Science and Technology,* 50**,** 71-75.
DYBWAD, M., SKOGAN, G. & BLATNY, J. M. 2014. Comparative testing and evaluation of nine different air samplers: end-to-end sampling efficiencies as specific performance measurements for bioaerosol applications. *Aerosol Science and Technology,* 48**,** 282-295.
EAMES, I., TANG, J., LI, Y. & WILSON, P. 2009. Airborne transmission of disease in hospitals. The Royal Society.
EUDRALEX Good Manufacturing Practice, Medicinal Products for Human and Veterinary Use.
FAN, H., LI, X., DENG, J., DA, G., GEHIN, E. & YAO, M. 2016. Time-dependent size-resolved bacterial and fungal aerosols in Beijing subway. *Aerosol and Air Quality Research,* 10**,** 1-11.
FENGER, J. 1999. Urban air quality. *Atmospheric environment,* 33**,** 4877-4900.
FENNELLY, K. P., JONES-LÓPEZ, E. C., AYAKAKA, I., KIM, S., MENYHA, H., KIRENGA, B., MUCHWA, C., JOLOBA, M., DRYDEN-PETERSON, S. & REILLY, N. 2012. Variability of infectious aerosols produced during coughing by patients with pulmonary tuberculosis. *American journal of respiratory and critical care medicine,* 186**,** 450-457.
FERRO, A. R., KOPPERUD, R. J. & HILDEMANN, L. M. 2004. Source strengths for indoor human activities that resuspend particulate matter. *Environmental science & technology,* 38**,** 1759-1764.
FIERER, N., LAUBER, C. L., ZHOU, N., MCDONALD, D., COSTELLO, E. K. & KNIGHT, R. 2010. Forensic identification using skin bacterial communities. *Proceedings of the National Academy of Sciences,* 107**,** 6477-6481.

FINDLEY, K., OH, J., YANG, J., CONLAN, S., DEMING, C., MEYER, J. A., SCHOENFELD, D., NOMICOS, E., PARK, M. & KONG, H. H. 2013. Topographic diversity of fungal and bacterial communities in human skin. *Nature,* 498**,** 367-370.

FLANNIGAN, B., SAMSON, R. A. & MILLER, J. D. 2016. *Microorganisms in Home and Indoor Work Environments: Diversity, Health Impacts, Investigation and Control, Second Edition,* CRC Press.

GABEY, A., STANLEY, W., GALLAGHER, M. & KAYE, P. H. 2011. The fluorescence properties of aerosol larger than 0.8 μm in urban and tropical rainforest locations. *Atmospheric Chemistry and Physics,* 11**,** 5491-5504.

GABEY, A., VAITILINGOM, M., FRENEY, E., BOULON, J., SELLEGRI, K., GALLAGHER, M., CRAWFORD, I., ROBINSON, N., STANLEY, W. & KAYE, P. H. 2013. Observations of fluorescent and biological aerosol at a high-altitude site in central France. *Atmospheric Chemistry and Physics,* 13**,** 7415-7428.

GADELLA, T. W., JOVIN, T. M. & CLEGG, R. M. 1993. Fluorescence lifetime imaging microscopy (FLIM): spatial resolution of microstructures on the nanosecond time scale. *Biophysical chemistry,* 48**,** 221-239.

GANGNEUX, J.-P., ROBERT-GANGNEUX, F., GICQUEL, G., TANQUEREL, J.-J., CHEVRIER, S., POISSON, M., AUPÉE, M. & GUIGUEN, C. 2006. Bacterial and fungal counts in hospital air: comparative yields for 4 sieve impactor air samplers with 2 culture media. *Infection control & hospital epidemiology,* 27**,** 1405-1408.

GAUDART, J., CLOUTMAN-GREEN, E., GUILLAS, S., D'ARCY, N., HARTLEY, J. C., GANT, V. & KLEIN, N. 2013. Healthcare environments and spatial variability of healthcare associated infection risk: cross-sectional surveys. *PLoS One,* 8**,** e76249.

GHOSH, B., LAL, H. & SRIVASTAVA, A. 2015. Review of bioaerosols in indoor environment with special reference to sampling, analysis and control mechanisms. *Environment international,* 85**,** 254-272.

GOSSELIN, M. I., RATHNAYAKE, C. M., CRAWFORD, I., PÖHLKER, C., FRÖHLICH-NOWOISKY, J., SCHMER, B., DESPRÉS, V. R., ENGLING, G., GALLAGHER, M. & STONE, E. 2016. Fluorescent bioaerosol particle, molecular tracer, and fungal spore concentrations during dry and rainy periods in a semi-arid forest. *Atmospheric Chemistry and Physics,* 16**,** 15165-15184.

GOVERNMENT, P. 2013. Ordinance n.o. 353-A/2013. Diario da Republica.

GRALTON, J., TOVEY, E., MCLAWS, M.-L. & RAWLINSON, W. D. 2011. The role of particle size in aerosolised pathogen transmission: a review. *Journal of Infection,* 62**,** 1-13.

GRICE, E. A., KONG, H. H., RENAUD, G., YOUNG, A. C., BOUFFARD, G. G., BLAKESLEY, R. W., WOLFSBERG, T. G., TURNER, M. L. & SEGRE, J. A. 2008. A diversity profile of the human skin microbiota. *Genome research,* 18**,** 1043-1050.

GRINSHPUN, S. A., BUTTNER, M. P., MAINELIS, G. & WILLEKE, K. 2016. Sampling for airborne microorganisms. *Manual of Environmental Microbiology, Fourth Edition.* American Society of Microbiology.

HAIG, C., MACKAY, W., WALKER, J. & WILLIAMS, C. 2016. Bioaerosol sampling: sampling mechanisms, bioefficiency and field studies. *Journal of Hospital Infection,* 93**,** 242-255.

HAIRSTON, P. P., HO, J. & QUANT, F. R. 1997. Design of an instrument for real-time detection of bioaerosols using simultaneous measurement of particle aerodynamic size and intrinsic fluorescence. *Journal of Aerosol Science,* 28**,** 471-482.

HALLAR, A., CHIROKOVA, G., MCCUBBIN, I., PAINTER, T. H., WIEDINMYER, C. & DODSON, C. 2011. Atmospheric bioaerosols transported via dust storms in the western United States. *Geophysical Research Letters,* 38.

HAMEED, A. A., KHODER, M., YUOSRA, S., OSMAN, A. & GHANEM, S. 2009. Diurnal distribution of airborne bacteria and fungi in the atmosphere of Helwan area, Egypt. *Science of the Total Environment,* 407**,** 6217-6222.

HARDIN, B. D., KELMAN, B. J. & SAXON, A. 2003. Adverse human health effects associated with molds in the indoor environment. *Journal of occupational and environmental medicine/American College of Occupational and Environmental Medicine,* 45**,** 470-478.

HEALTH/ESTATES, D. O. & DIVISION, F. 2007. Health Technical Memorandum 03-01: Specialised Ventilation for Healthcare Premises. Part A-Design and Installation. The Stationery Office Norwich, UK.

HEALY, D., HUFFMAN, J., O'CONNOR, D., PÖHLKER, C., PÖSCHL, U. & SODEAU, J. 2014. Ambient measurements of biological aerosol particles near Killarney, Ireland: a comparison between real-time fluorescence and microscopy techniques. *Atmospheric Chemistry and Physics,* 14**,** 8055-8069.

HENNINGSON, E. W. & AHLBERG, M. S. 1994. Evaluation of microbiological aerosol samplers: a review. *Journal of Aerosol Science,* 25**,** 1459-1492.

HERMANN, J. R., HOFF, S. J., YOON, K.-J., BURKHARDT, A. C., EVANS, R. B. & ZIMMERMAN, J. J. 2006. Optimization of a sampling system for recovery and detection of airborne porcine reproductive and respiratory syndrome virus and swine influenza virus. *Applied and environmental microbiology,* 72**,** 4811-4818.

HERNANDEZ, M., PERRING, A. E., MCCABE, K., KOK, G., GRANGER, G. & BAUMGARDNER, D. 2016. Chamber catalogues of optical and fluorescent signatures distinguish bioaerosol classes. *Atmospheric Measurement Techniques,* 9**,** 3283-3292.

HICKEY, A. J. 1996. *Inhalation aerosols: physical and biological basis for therapy*, CRC Press.

HINDS, W. C. 1999. Aerosol Technology: Properties. *Behavior, and Measurement of airborne Particles (2nd.*

HINDS, W. C. 2012. *Aerosol Technology: Properties, Behavior, and Measurement of Airborne Particles*, Wiley.

HOSPODSKY, D., QIAN, J., NAZAROFF, W. W., YAMAMOTO, N., BIBBY, K., RISMANI-YAZDI, H. & PECCIA, J. 2012. Human occupancy as a source of indoor airborne bacteria. *PloS one,* 7**,** e34867.

HOSPODSKY, D., YAMAMOTO, N., NAZAROFF, W., MILLER, D., GORTHALA, S. & PECCIA, J. 2015. Characterizing airborne fungal and bacterial concentrations and emission rates in six occupied children's classrooms. *Indoor air,* 25**,** 641-652.

HUFFMAN, J., SINHA, B., GARLAND, R., SNEE-POLLMANN, A., GUNTHE, S., ARTAXO, P., MARTIN, S., ANDREAE, M. & PÖSCHL, U. 2012. Size distributions and temporal variations of biological aerosol particles in the Amazon rainforest characterized by microscopy and real-time UV-APS

fluorescence techniques during AMAZE-08. *Atmospheric Chemistry and Physics,* 12**,** 11997-12019.
HUFFMAN, J., TREUTLEIN, B. & PÖSCHL, U. 2010. Fluorescent biological aerosol particle concentrations and size distributions measured with an Ultraviolet Aerodynamic Particle Sizer (UV-APS) in Central Europe. *Atmospheric Chemistry and Physics,* 10**,** 3215-3233.
HUFFMAN, J. A., PRENNI, A., DEMOTT, P., PÖHLKER, C., MASON, R., ROBINSON, N., FRÖHLICH-NOWOISKY, J., TOBO, Y., DESPRÉS, V. & GARCIA, E. 2013. High concentrations of biological aerosol particles and ice nuclei during and after rain. *Atmospheric Chemistry and Physics,* 13**,** 6151.
HUSMAN, T. 1996. Health effects of indoor-air microorganisms. *Scandinavian journal of work, environment & health***,** 5-13.
HUTTUNEN, K. 2018. Indoor Air Pollution. *Clinical Handbook of Air Pollution-Related Diseases.* Springer.
INSTRUMENTS, W. P. 2019. *Ca2+ Detection in Muscle Tissue using Fluorescence Spectroscopy* [Online]. Available: https://www.wpiinc.com/blog/post/ca-sup-2-sup-detection-in-muscle-tissue-using-fluorescence-spectroscopy [Accessed July 3 2019].
INTAG, C. 1975. An investigation of the importance of air flow in control of post-operative infections. *ASHRAE J.*
ISO, I. 2015. 14644-1: 2015, Cleanrooms and associated controlled environments–Part 1: Classification of air cleanliness by particle concentration. *Polish Standardization Committee*.
JABAJI-HARE, S., PERUMALLA, C. & KENDRICK, W. 1984. Autofluorescence of vesicles, arbuscules, and intercellular hyphae of a vesicular–arbuscular fungus in leek (Allium porrum) roots. *Canadian journal of botany,* 62**,** 2665-2669.
JENKINS, P. L., PHILLIPS, T. J., MULBERG, E. J. & HUI, S. P. 1992. Activity patterns of Californians: use of and proximity to indoor pollutant sources. *Atmospheric Environment. Part A. General Topics,* 26**,** 2141-2148.
JENSEN, P. A. & SCHAFER, M. P. 1998. Sampling and characterization of bioaerosols. *NIOSH manual of analytical methods,* 1**,** 82-112.
KALLIOKOSKI, P. 2003. Risks caused by airborne microbes in hospitals-source control is important. *Indoor and Built Environment,* 12**,** 41-46.
KANAANI, H., HARGREAVES, M., RISTOVSKI, Z. & MORAWSKA, L. 2007. Performance assessment of UVAPS: Influence of fungal spore age and air exposure. *Journal of Aerosol Science,* 38**,** 83-96.
KANAANI, H., HARGREAVES, M., SMITH, J., RISTOVSKI, Z., AGRANOVSKI, V. & MORAWSKA, L. 2008. Performance of UVAPS with respect to detection of airborne fungi. *Journal of Aerosol Science,* 39**,** 175-189.
KARLSSON, K. & MALMBERG, P. 1989. Characterization of exposure to molds and actinomycetes in agricultural dusts by scanning electron microscopy, fluorescence microscopy and the culture method. *Scandinavian journal of work, environment & health***,** 353-359.
KAYE, P. H., STANLEY, W. R. & FOOT, E. V. J. 2014. *Fluid-Borne Particle Detector*. US 13/957,655.
KETHLEY, T. W. 1958. The effect of relative humidity and temperature on the effectiveness of samplers used in aerobiological studies. Georgia Institute of Technology.

KIM, K.-H., KABIR, E. & JAHAN, S. A. 2018. Airborne bioaerosols and their impact on human health. *Journal of Environmental Sciences,* 67**,** 23-35.

KIM, Y., PLATT, U., GU, M. B. & IWAHASHI, H. 2009. *Atmospheric and Biological Environmental Monitoring,* Springer Netherlands.

KISELEV, D., BONACINA, L. & WOLF, J.-P. 2011. Individual bioaerosol particle discrimination by multi-photon excited fluorescence. *Optics express,* 19**,** 24516-24521.

KISELEV, D., BONACINA, L. & WOLF, J.-P. 2013. A flash-lamp based device for fluorescence detection and identification of individual pollen grains. *Review of Scientific Instruments,* 84**,** 033302.

KLEPEIS, N. E., NELSON, W. C., OTT, W. R., ROBINSON, J. P., TSANG, A. M., SWITZER, P., BEHAR, J. V., HERN, S. C. & ENGELMANN, W. H. 2001. The National Human Activity Pattern Survey (NHAPS): a resource for assessing exposure to environmental pollutants. *Journal of Exposure Science and Environmental Epidemiology,* 11**,** 231.

KNÖPPEL, H. & WOLKOFF, P. 2013. *Chemical, Microbiological, Health and Comfort Aspects of Indoor Air Quality - State of the Art in SBS,* Springer Netherlands.

KONTERMANN, R. E. & DÜBEL, S. 2010. *Antibody Engineering,* Springer Berlin Heidelberg.

KOWALSKI, W. 2016. *Hospital Airborne Infection Control,* CRC Press.

KOZIOŁ, J. & KNOBLOCH, E. 1965. The solvent effect on the fluorescence and light absorption of riboflavin and lumiflavin. *Biochimica et Biophysica Acta (BBA)-Biophysics including Photosynthesis,* 102**,** 289-300.

KRANKENHAUSINSTITUT, S. 1987. Richtlinie für den Bau, Betrieb und die Überwachung von lüftungstechnischen Anlagen in Spitälern. Aarau: Krankenhausinstitut (in German).

KRUCZKOWSKI, P., KOLENDARSKI, W. & SIKORSKI, J. 1984. Wytyczne projektowania szpitali ogólnych. *Instalacje sanitarne. Zeszyt,* 5.

KULKARNI, P., BARON, P. A. & WILLEKE, K. 2011. *Aerosol Measurement: Principles, Techniques, and Applications,* Wiley.

KUNIT, M. & PUXBAUM, H. 1996. Enzymatic determination of the cellulose content of atmospheric aerosols. *Atmospheric Environment,* 30**,** 1233-1236.

KÜNZLI, N., KAISER, R., MEDINA, S., STUDNICKA, M., CHANEL, O., FILLIGER, P., HERRY, M., HORAK, F., PUYBONNIEUX-TEXIER, V. & QUÉNEL, P. 2000. Public-health impact of outdoor and traffic-related air pollution: a European assessment. *The Lancet,* 356**,** 795-801.

KUTTER, J. S., SPRONKEN, M. I., FRAAIJ, P. L., FOUCHIER, R. A. & HERFST, S. 2018. Transmission routes of respiratory viruses among humans. *Current opinion in virology,* 28**,** 142-151.

LAKOWICZ, J. R., SHEN, B., GRYCZYNSKI, Z., D'AURIA, S. & GRYCZYNSKI, I. 2001. Intrinsic fluorescence from DNA can be enhanced by metallic particles. *Biochemical and Biophysical Research Communications,* 286**,** 875-879.

LAKOWICZ, J. R., SZMACINSKI, H., NOWACZYK, K. & JOHNSON, M. L. 1992. Fluorescence lifetime imaging of free and protein-bound NADH. *Proceedings of the National Academy of Sciences,* 89**,** 1271-1275.

LANGER, V., HARTMANN, G., NIESSNER, R. & SEIDEL, M. 2012. Rapid quantification of bioaerosols containing L. pneumophila by Coriolis® μ air

sampler and chemiluminescence antibody microarrays. *Journal of Aerosol Science,* 48**,** 46-55.
LAU, J. T., GRIFFITHS, S., CHOI, K. C. & TSUI, H. Y. 2009. Widespread public misconception in the early phase of the H1N1 influenza epidemic. *Journal of infection,* 59**,** 122-127.
LAWLESS, P. 2000. Improvements in the positive-hole correction for multijet aerosol impactors collecting viable microorganisms. *Journal of Aerosol Science,* 31**,** 743-744.
LAX, S., SMITH, D. P., HAMPTON-MARCELL, J., OWENS, S. M., HANDLEY, K. M., SCOTT, N. M., GIBBONS, S. M., LARSEN, P., SHOGAN, B. D. & WEISS, S. 2014. Longitudinal analysis of microbial interaction between humans and the indoor environment. *Science,* 345**,** 1048-1052.
LEADERER, B. P., BELANGER, K., TRICHE, E., HOLFORD, T., GOLD, D. R., KIM, Y., JANKUN, T., REN, P., MCSHARRY JE, J.-E. & PLATTS-MILLS, T. A. 2002. Dust mite, cockroach, cat, and dog allergen concentrations in homes of asthmatic children in the northeastern United States: impact of socioeconomic factors and population density. *Environmental health perspectives,* 110**,** 419-425.
LÉTOURNEAU, V., NEHMÉ, B., MÉRIAUX, A., MASSÉ, D., CORMIER, Y. & DUCHAINE, C. 2010. Human pathogens and tetracycline-resistant bacteria in bioaerosols of swine confinement buildings and in nasal flora of hog producers. *International journal of hygiene and environmental health,* 213**,** 444-449.
LI, C.-S. 1999. Sampling performance of impactors for bacterial bioaerosols. *Aerosol Science & Technology,* 30**,** 280-287.
LI, C.-S. & HOU, P.-A. 2003. Bioaerosol characteristics in hospital clean rooms. *Science of the Total Environment,* 305**,** 169-176.
LI, C.-S. & LIN, Y.-C. 1999. Sampling performance of impactors for fungal spores and yeast cells. *Aerosol Science & Technology,* 31**,** 226-230.
LI, J., LI, M., SHEN, F., ZOU, Z., YAO, M. & WU, C.-Y. 2013. Characterization of biological aerosol exposure risks from automobile air conditioning system. *Environmental science & technology,* 47**,** 10660-10666.
LI, J., ZHOU, L., ZHANG, X., XU, C., DONG, L. & YAO, M. 2016. Bioaerosol emissions and detection of airborne antibiotic resistance genes from a wastewater treatment plant. *Atmospheric Environment,* 124**,** 404-412.
LIN, X., WILLEKE, K., ULEVICIUS, V. & GRINSHPUN, S. A. 1997. Effect of sampling time on the collection efficiency of all-glass impingers. *American Industrial Hygiene Association Journal,* 58**,** 480-488.
LINDSLEY, W. G., GREEN, B. J., BLACHERE, F. M., MARTIN, S. B., LAW, B., JENSEN, P. & SCHAFER, M. 2017. Sampling and characterization of bioaerosols. *NIOSH manual of analytical methods. 5th ed. Cincinnati (OH): National Institute for Occupational Safety and Health*.
LINDSLEY, W. G., KING, W. P., THEWLIS, R. E., REYNOLDS, J. S., PANDAY, K., CAO, G. & SZALAJDA, J. V. 2012a. Dispersion and exposure to a cough-generated aerosol in a simulated medical examination room. *Journal of Occupational and Environmental Hygiene,* 9**,** 681-690.
LINDSLEY, W. G., PEARCE, T. A., HUDNALL, J. B., DAVIS, K. A., DAVIS, S. M., FISHER, M. A., KHAKOO, R., PALMER, J. E., CLARK, K. E. & CELIK, I. 2012b. Quantity and size distribution of cough-generated aerosol particles

produced by influenza patients during and after illness. *Journal of occupational and environmental hygiene,* 9**,** 443-449.
LOUDON, R. G. & ROBERTS, R. M. 1967. Droplet Expulsion from the Respiratory TRACT 1, 2. *American Review of Respiratory Disease,* 95**,** 435-442.
LUCKEY, T. 1972. Introduction to intestinal microecology. *The American journal of clinical nutrition,* 25**,** 1292-1294.
MACHER, J. M. 1989. Positive-hole correction of multiple-jet impactors for collecting viable microorganisms. *The American Industrial Hygiene Association Journal,* 50**,** 561-568.
MAINELIS, G., ADHIKARI, A., WILLEKE, K., LEE, S.-A., REPONEN, T. & GRINSHPUN, S. A. 2002. Collection of airborne microorganisms by a new electrostatic precipitator. *Journal of Aerosol Science,* 33**,** 1417-1432.
MANDAL, J. & BRANDL, H. 2011. Bioaerosols in indoor environment-a review with special reference to residential and occupational locations. *The Open Environmental & Biological Monitoring Journal,* 4.
MANNINEN, H. E., BÄCK, J., SIHTO-NISSILÄ, S.-L., HUFFMAN, J. A., PESSI, A.-M., HILTUNEN, V., AALTO, P. P., HIDALGO FERNÁNDEZ, P. J., HARI, P. & SAARTO, A. 2014. Patterns in airborne pollen and other primary biological aerosol particles (PBAP), and their contribution to aerosol mass and number in a boreal forest.
MARPLE, V. A. & WILLEKE, K. 1976. Impactor design. *Atmospheric Environment (1967),* 10**,** 891-896.
MARSH, A. S. 2016. FAQ: Microbiology of Built Environments: Report on an American Academy of Microbiology Colloquium held in Washington, DC, in September 2015.
MASON, R., SI, M., LI, J., CHOU, C., DICKIE, R., TOOM-SAUNTRY, D., PÖHLKER, C., YAKOBI-HANCOCK, J., LADINO, L. & JONES, K. 2015. Ice nucleating particles at a coastal marine boundary layer site: correlations with aerosol type and meteorological conditions. *Atmospheric Chemistry and Physics,* 15**,** 12547-12566.
MAY, D. & PITT, M. 2012. Environmental cleaning in UK healthcare since the NHS Plan: a policy and evidence based context. *Facilities,* 30**,** 6-22.
MAY, K. & HARPER, G. 1957. The efficiency of various liquid impinger samplers in bacterial aerosols. *British Journal of Industrial Medicine,* 14**,** 287.
MBARECHE, H., VEILLETTE, M., BILODEAU, G. J. & DUCHAINE, C. 2018. Bioaerosol sampler choice should consider efficiency and ability of samplers to cover microbial diversity. *Appl. Environ. Microbiol.,* 84**,** e01589-18.
MCCARTNEY, H., FITT, B. D. & SCHMECHEL, D. 1997. Sampling bioaerosols in plant pathology. *Journal of Aerosol Science,* 28**,** 349-364.
MEADOW, J. F., ALTRICHTER, A. E., BATEMAN, A. C., STENSON, J., BROWN, G., GREEN, J. L. & BOHANNAN, B. J. 2015. Humans differ in their personal microbial cloud. *PeerJ,* 3**,** e1258.
MEADOW, J. F., ALTRICHTER, A. E., KEMBEL, S. W., MORIYAMA, M., O'CONNOR, T. K., WOMACK, A. M., BROWN, G., GREEN, J. L. & BOHANNAN, B. J. 2014. Bacterial communities on classroom surfaces vary with human contact. *Microbiome,* 2**,** 7.
MEL'NIKOVA, Y. V., ROSHCHINA, V. & KARNAUKHOV, V. 1997. Microspectrofluorimetry of intact plant pollen. *Biophysics,* 1**,** 243-251.
MEURANT, G. 2012. *Immunoassay: A Practical Guide,* Elsevier Science.

MILTON, D. K., FABIAN, M. P., COWLING, B. J., GRANTHAM, M. L. & MCDEVITT, J. J. 2013. Influenza virus aerosols in human exhaled breath: particle size, culturability, and effect of surgical masks. *PLoS pathogens,* 9**,** e1003205.

MIRHOSEINI, S. H., NIKAEEN, M., KHANAHMAD, H. & HASSANZADEH, A. 2016. Occurrence of airborne vancomycin-and gentamicin-resistant bacteria in various hospital wards in Isfahan, Iran. *Advanced biomedical research,* 5.

MISRA, C., SINGH, M., SHEN, S., SIOUTAS, C. & HALL, P. M. 2002. Development and evaluation of a personal cascade impactor sampler (PCIS). *Journal of Aerosol Science,* 33**,** 1027-1047.

MONTAGNA, M., DE GIGLIO, O., CRISTINA, M., NAPOLI, C., PACIFICO, C., AGODI, A., BALDOVIN, T., CASINI, B., CONIGLIO, M. & D'ERRICO, M. 2017a. Evaluation of Legionella air contamination in healthcare facilities by different sampling methods: An Italian multicenter study. *International journal of environmental research and public health,* 14**,** 670.

MONTAGNA, M. T., DE GIGLIO, O., CRISTINA, M. L., ALBERTINI, R., PASQUARELLA, C., GROUP, G.-S. W., GROUP, A. W. & GROUP, S. W. 2017b. Legionella indoor air contamination in healthcare environments. *Indoor Air Quality in Healthcare Facilities.* Springer.

MORAWSKA, L. 2006. Droplet fate in indoor environments, or can we prevent the spread of infection? *Indoor air,* 16**,** 335-347.

MORAWSKA, L., AFSHARI, A., BAE, G., BUONANNO, G., CHAO, C. Y. H., HÄNNINEN, O., HOFMANN, W., ISAXON, C., JAYARATNE, E. R. & PASANEN, P. 2013. Indoor aerosols: from personal exposure to risk assessment. *Indoor Air,* 23**,** 462-487.

MORAWSKA, L., JOHNSON, G., RISTOVSKI, Z., HARGREAVES, M., MENGERSEN, K., CHAO, C., WAN, M. P., LI, Y., XIE, X. & KATOSHEVSKI, D. Droplets expelled during human expiratory activities and their origin. International Conference on Indoor Air Quality and Climate, 2008.

MORAWSKA, L., JOHNSON, G., RISTOVSKI, Z., HARGREAVES, M., MENGERSEN, K., CORBETT, S., CHAO, C. Y. H., LI, Y. & KATOSHEVSKI, D. 2009. Size distribution and sites of origin of droplets expelled from the human respiratory tract during expiratory activities. *Journal of Aerosol Science,* 40**,** 256-269.

MORGAN, J. P. & DANIELS, M. 1980. Excited states of DNA and its components at room temperature—III. Spectra, polarisation and quantum yields of emissions from ApA and poly rA. *Photochemistry and Photobiology,* 31**,** 101-113.

MORIKAWA, K. & YANAGIDA, M. 1981. Visualization of individual DNA molecules in solution by light microscopy: DAPI staining method. *Journal of biochemistry,* 89**,** 693-696.

NAPOLI, C., MARCOTRIGIANO, V. & MONTAGNA, M. T. 2012. Air sampling procedures to evaluate microbial contamination: a comparison between active and passive methods in operating theatres. *BMC Public Health,* 12**,** 594.

NÄSMAN, Å., BLOMQUIST, G. & LEVIN, J.-O. 1999. Air sampling of fungal spores on filters. An investigation on passive sampling and viability. *Journal of Environmental Monitoring,* 1**,** 361-365.

NATIONAL HOSPITALS, O. 2005. HSE National Cleaning Standards Manual.

NAZAROFF, W. W. 2004. Indoor particle dynamics. *Indoor air,* 14**,** 175-183.

NESA, D., LORTHOLARY, J., BOUAKLINE, A., BORDES, M., CHANDENIER, J., DEROUIN, F. & GANGNEUX, J.-P. 2001. Comparative performance of impactor air samplers for quantification of fungal contamination. *Journal of Hospital Infection,* 47**,** 149-155.

NIKAEEN, M., SHAMSIZADEH, Z. & MIRHOSEINI, S. H. 2018. Direct Monitoring of Gram-negative Agents of Nosocomial Infections in Hospital Air by a PCR-based Approach. *Aerosol and Air Quality Research,* 18**,** 2612-2617.

NOGUCHI, C., KOSEKI, H., HORIUCHI, H., YONEKURA, A., TOMITA, M., HIGUCHI, T., SUNAGAWA, S. & OSAKI, M. 2017. Factors contributing to airborne particle dispersal in the operating room. *BMC surgery,* 17**,** 78.

NORME, N. 2003. S 90351. *Établissements de santé. Salles propres et environnements maîtrisés apparentés. Exigences relatives pour la maîtrise de la contamination aéroportée*.

O'CONNOR, D. J., HEALY, D. A. & SODEAU, J. R. 2013. The on-line detection of biological particle emissions from selected agricultural materials using the WIBS-4 (Waveband Integrated Bioaerosol Sensor) technique. *Atmospheric environment,* 80**,** 415-425.

O'CONNOR, D. J., LOVERA, P., IACOPINO, D., O'RIORDAN, A., HEALY, D. A. & SODEAU, J. R. 2014. Using spectral analysis and fluorescence lifetimes to discriminate between grass and tree pollen for aerobiological applications. *Analytical Methods,* 6**,** 1633-1639.

O'BRIEN, D., STEVENS, N., FITZGERALD-HUGHES, D. & HUMPHREYS, H. 2012. Effect of a novel air disinfection system on airborne micro-organisms in a hospital outpatient clinic. *Journal of Hospital Infection,* 80**,** 98-99.

O'CONNOR, D., HEALY, D. & SODEAU, J. 2015a. A 1-month online monitoring campaign of ambient fungal spore concentrations in the harbour region of Cork, Ireland. *Aerobiologia***,** 1-20.

O'CONNOR, D. J., HEALY, D. A., HELLEBUST, S., BUTERS, J. T. & SODEAU, J. R. 2014. Using the WIBS-4 (Waveband Integrated Bioaerosol Sensor) technique for the on-line detection of pollen grains. *Aerosol Science and Technology,* 48**,** 341-349.

O'CONNOR, D. J., HEALY, D. A. & SODEAU, J. R. 2015b. A 1-month online monitoring campaign of ambient fungal spore concentrations in the harbour region of Cork, Ireland. *Aerobiologia,* 31**,** 295-314.

O'CONNOR, D. J., IACOPINO, D., HEALY, D. A., O'SULLIVAN, D. & SODEAU, J. R. 2011. The intrinsic fluorescence spectra of selected pollen and fungal spores. *Atmospheric Environment,* 45**,** 6451-6458.

ODEH, I. & HUSSEIN, T. 2016. Activity Pattern of Urban Adult Students in an Eastern Mediterranean Society. *International journal of environmental research and public health,* 13**,** 960.

ORGANIZATION, W. H. 2014. *Infection prevention and control of epidemic-and pandemic-prone acute respiratory infections in health care*, World Health Organization.

ORTIZ, G., YAGÜE, G., SEGOVIA, M. & CATALÁN, V. 2009. A study of air microbe levels in different areas of a hospital. *Current microbiology,* 59**,** 53.

OTTO, F. 1990. DAPI staining of fixed cells for high-resolution flow cytometry of nuclear DNA. *Methods in cell biology,* 33**,** 105-110.

PALMGREN, M. G. 1991. Acridine orange as a probe for measuring pH gradients across membranes: mechanism and limitations. *Analytical biochemistry,* 192**,** 316-321.

PASQUARELLA, C., PITZURRA, O. & SAVINO, A. 2000. The index of microbial air contamination. *Journal of hospital infection,* 46**,** 241-256.

PASQUARELLA, C., VITALI, P., SACCANI, E., MANOTTI, P., BOCCUNI, C., UGOLOTTI, M., SIGNORELLI, C., MARIOTTI, F., SANSEBASTIANO, G. & ALBERTINI, R. 2012. Microbial air monitoring in operating theatres: experience at the University Hospital of Parma. *Journal of Hospital Infection,* 81**,** 50-57.

PENG, W., HOFFMANN, A., DRIES, H., REGELINK, M. & STEIN, L. 2005. Experimental study of the vortex end in centrifugal separators: the nature of the vortex end. *Chemical Engineering Science,* 60**,** 6919-6928.

PERAICA, M., RADIC, B., LUCIC, A. & PAVLOVIC, M. 1999. Toxic effects of mycotoxins in humans. *Bulletin of the World Health Organization,* 77**,** 754-766.

PEREIRA, M. L., KNIBBS, L. D., HE, C., GRZYBOWSKI, P., JOHNSON, G. R., HUFFMAN, J. A., BELL, S. C., WAINWRIGHT, C. E., MATTE, D. L. & DOMINSKI, F. H. 2017. Sources and dynamics of fluorescent particles in hospitals. *Indoor Air*.

PERRING, A., SCHWARZ, J., BAUMGARDNER, D., HERNANDEZ, M., SPRACKLEN, D., HEALD, C., GAO, R., KOK, G., MCMEEKING, G. & MCQUAID, J. 2015. Airborne observations of regional variation in fluorescent aerosol across the United States. *Journal of Geophysical Research: Atmospheres,* 120**,** 1153-1170.

PIERSMA, S. R., VISSER, A. J., DE VRIES, S. & DUINE, J. A. 1998. Optical spectroscopy of nicotinoprotein alcohol dehydrogenase from Amycolatopsis methanolica: a comparison with horse liver alcohol dehydrogenase and UDP-galactose epimerase. *Biochemistry,* 37**,** 3068-3077.

PISAREVSKII, A., CHERENKEVICH, S. & ANDRIANOV, V. 1966. Fluorescence spectrum and quantum yield of DNA in solution. *Journal of Applied Spectroscopy,* 5**,** 452-454.

PÖHLKER, C., HUFFMAN, J. & POSCHL, U. 2012a. Autofluorescence of atmospheric bioaerosols-fluorescent biomolecules and potential interferences. *Atmos. Meas. Tech,* 5**,** 37-71.

PÖHLKER, C., HUFFMAN, J. & PÖSCHL, U. 2012b. Autofluorescence of atmospheric bioaerosols–fluorescent biomolecules and potential interferences. *Atmospheric Measurement Techniques,* 5**,** 37-71.

PÖHLKER, C., HUFFMAN, J. A., FÖRSTER, J.-D. & PÖSCHL, U. 2013. Autofluorescence of atmospheric bioaerosols: spectral fingerprints and taxonomic trends of pollen. *Atmospheric Measurement Techniques,* 6**,** 3369-3392.

POPE III, C. A., BURNETT, R. T., THUN, M. J., CALLE, E. E., KREWSKI, D., ITO, K. & THURSTON, G. D. 2002. Lung cancer, cardiopulmonary mortality, and long-term exposure to fine particulate air pollution. *Jama,* 287**,** 1132-1141.

PÖSCHL, U., MARTIN, S., SINHA, B., CHEN, Q., GUNTHE, S., HUFFMAN, J., BORRMANN, S., FARMER, D., GARLAND, R. & HELAS, G. 2010. Rainforest aerosols as biogenic nuclei of clouds and precipitation in the Amazon. *science,* 329**,** 1513-1516.

PREVENTION, C. F. D. C. A. 2009. *Public Health Image Library* [Online]. Centers for Disease Control and Prevention. Available: https://phil.cdc.gov/details.aspx?pid=11162 [Accessed July 3 2019].

QIAN, J., FERRO, A. R. & FOWLER, K. R. 2008. Estimating the resuspension rate and residence time of indoor particles. *Journal of the Air & Waste Management Association,* 58**,** 502-516.

QIAN, J., HOSPODSKY, D., YAMAMOTO, N., NAZAROFF, W. W. & PECCIA, J. 2012. Size-resolved emission rates of airborne bacteria and fungi in an occupied classroom. *Indoor air,* 22**,** 339-351.

QIAN, J., PECCIA, J. & FERRO, A. R. 2014. Walking-induced particle resuspension in indoor environments. *Atmospheric Environment,* 89**,** 464-481.

RAMSAY, A. J. 1978. Direct counts of bacteria by a modified acridine orange method in relation to their heterotrophic activity. *New Zealand Journal of Marine and Freshwater Research,* 12**,** 265-269.

REPONEN, T., WILLEKE, K., GRINSHPUN, S. & NEVALAINEN, A. 2011. Biological particle sampling. *Aerosol Measurement: Principles, Techniques, and Applications, Third Edition***,** 549-570.

RITTENOUR, W. R., HAMILTON, R. G., BEEZHOLD, D. H. & GREEN, B. J. 2012. Immunologic, spectrophotometric and nucleic acid based methods for the detection and quantification of airborne pollen. *Journal of immunological methods,* 383**,** 47-53.

ROBERTS, K., HATHWAY, A., FLETCHER, L., BEGGS, C., ELLIOTT, M. & SLEIGH, P. 2006. Bioaerosol production on a respiratory ward. *Indoor and Built Environment,* 15**,** 35-40.

ROSHCHINA, V., MEL'NIKOVA, E. & KOVALEVA, L. 1997. Changes in fluorescence during development of the male gametophyte. *Russian Journal of Plant Physiology,* 44**,** 36-44.

ROSHCHINA, V. A. V. 2008. *Fluorescing world of plant secreting cells,* Science Publishers.

ROY, C. J. & MILTON, D. K. 2004. Airborne transmission of communicable infection-the elusive pathway. ARMY MEDICAL RESEARCH INST OF INFECTIOUS DISEASES FORT DETRICK MD ….

RULE, A. M., KESAVAN, J., SCHWAB, K. J. & BUCKLEY, T. J. 2007. Application of flow cytometry for the assessment of preservation and recovery efficiency of bioaerosol samplers spiked with Pantoea agglomerans. *Environmental science & technology,* 41**,** 2467-2472.

RUSKE, S., TOPPING, D. O., FOOT, V. E., KAYE, P. H., STANLEY, W. R., CRAWFORD, I., MORSE, A. P. & GALLAGHER, M. W. 2017. Evaluation of machine learning algorithms for classification of primary biological aerosol using a new UV-LIF spectrometer. *Atmospheric Measurement Techniques,* 10**,** 695.

RYDJORD, B., NAMORK, E., NYGAARD, U. C., WIKER, H. G. & HETLAND, G. 2007. Quantification and characterisation of IgG binding to mould spores by flow cytometry and scanning electron microscopy. *Journal of immunological methods,* 323**,** 123-131.

SAARI, S., MENSAH-ATTIPOE, J., REPONEN, T., VEIJALAINEN, A., SALMELA, A., PASANEN, P. & KESKINEN, J. 2015a. Effects of fungal species, cultivation time, growth substrate, and air exposure velocity on the fluorescence properties of airborne fungal spores. *Indoor air,* 25**,** 653-661.

SAARI, S., NIEMI, J., RÖNKKÖ, T., KUULUVAINEN, H., JÄRVINEN, A., PIRJOLA, L., AURELA, M., HILLAMO, R. & KESKINEN, J. 2015b. Seasonal and diurnal variations of fluorescent bioaerosol concentration and

size distribution in the urban environment. *Aerosol and Air Quality Research,* 15**,** 572-581.

SAARI, S., REPONEN, T. & KESKINEN, J. 2013. Performance of Two Fluorescence-Based Real-Time Bioaerosol Detectors: BioScout vs. UVAPS. *Aerosol Science and Technology,* 48**,** 371-378.

SADRIZADEH, S., TAMMELIN, A., EKOLIND, P. & HOLMBERG, S. 2014. Influence of staff number and internal constellation on surgical site infection in an operating room. *Particuology,* 13**,** 42-51.

SAUTOUR, M., SIXT, N., DALLE, F., L'OLLIVIER, C., CALINON, C., FOURQUENET, V., THIBAUT, C., JURY, H., LAFON, I. & AHO, S. 2007. Prospective survey of indoor fungal contamination in hospital during a period of building construction. *Journal of Hospital infection,* 67**,** 367-373.

SAX, H., BLOEMBERG, G., HASSE, B., SOMMERSTEIN, R., KOHLER, P., ACHERMANN, Y., RÖSSLE, M., FALK, V., KUSTER, S. P. & BÖTTGER, E. C. 2015. Prolonged outbreak of Mycobacterium chimaera infection after open-chest heart surgery. *Clinical Infectious Diseases,* 61**,** 67-75.

SAXENA, P. B. 2007. *Chemistry of Alkaloids*, 4383/4 - A, Ansari Road, Darya Ganj, New Delhi - 110002, India, Discovery Publishing House Pvt. Limited, 4383/4 - A, Ansari Road, Darya Ganj, New Delhi - 110002, India.

SCALTRITI, S., CENCETTI, S., ROVESTI, S., MARCHESI, I., BARGELLINI, A. & BORELLA, P. 2007. Risk factors for particulate and microbial contamination of air in operating theatres. *Journal of Hospital Infection,* 66**,** 320-326.

SCHOLEFIELD, J., MANSON, R., JOHNSTON, R. & SCOTT, R. 1985. The use of acridine orange staining and image analysis to detect bacteriuria. *Urological research,* 13**,** 141-142.

SCHUMACHER, C., PÖHLKER, C., AALTO, P., HILTUNEN, V., PETÄJÄ, T., KULMALA, M., PÖSCHL, U. & HUFFMAN, J. 2013. Seasonal cycles of fluorescent biological aerosol particles in boreal and semi-arid forests of Finland and Colorado. *Atmospheric chemistry and physics,* 13**,** 11987-12001.

SCHWEGMAN, D. 2009. Prevention of Cross Transmission of Microorganisms is Essential to Preventing Outbreaks of Hospital Acquired Infections. *Emory University*.

SEGUIN, V., LEMAUVIEL-LAVENANT, S., GARON, D., BOUCHART, V., GALLARD, Y., BLANCHET, B., DIQUELOU, S., PERSONENI, E., GAUDUCHON, P. & OURRY, A. 2010. Effect of agricultural and environmental factors on the hay characteristics involved in equine respiratory disease. *Agriculture, ecosystems & environment,* 135**,** 206-215.

SEINFELD, J. H. & PANDIS, S. N. 2016. *Atmospheric Chemistry and Physics: From Air Pollution to Climate Change*, Wiley.

SETO, W. 2015. Airborne transmission and precautions: facts and myths. *Journal of Hospital Infection,* 89**,** 225-228.

SFORZA, G. G. R. & MARINOU, A. 2017. Hypersensitivity pneumonitis: a complex lung disease. *Clinical and Molecular Allergy,* 15**,** 6.

SHAW, L. F., CHEN, I. H., CHEN, C. S., WU, H. H., LAI, L. S., CHEN, Y. Y. & DER WANG, F. 2018. Factors influencing microbial colonies in the air of operating rooms. *BMC infectious diseases,* 18**,** 4.

SHINN, E. A., GRIFFIN, D. W. & SEBA, D. B. 2003. Atmospheric transport of mold spores in clouds of desert dust. *Archives of Environmental & Occupational Health,* 58**,** 498.

SHIPE, E., TYLER, M. & CHAPMAN, D. 1959. Bacterial Aerosol Samplers: II. Development and Evaluation of the Shipe Sampler. *Applied microbiology,* 7**,** 349.

SIANI, H. & MAILLARD, J.-Y. 2015. Best practice in healthcare environment decontamination. *European Journal of Clinical Microbiology & Infectious Diseases,* 34**,** 1-11.

SIEGEL, J. D. 2007. Healthcare Infection Control Practices Advisory Committee 2007 Guideline for isolation precautions: preventing transmission of infectious agents in healthcare settings. *http://www. cdc. gov/ncidod/dhqp/gl_isolation. html*.

SIPPOLA, M. R. & NAZAROFF, W. W. 2004. Experiments measuring particle deposition from fully developed turbulent flow in ventilation ducts. *Aerosol Science and technology,* 38**,** 914-925.

SORENSON, W. 1999. Fungal spores: hazardous to health? *Environmental Health Perspectives,* 107**,** 469-472.

STAHLHOFEN, W., GEBHART, J. & HEYDER, J. 1980. Experimental determination of the regional deposition of aerosol particles in the human respiratory tract. *The American Industrial Hygiene Association Journal,* 41**,** 385-398a.

STRAUS, D. C. 2009. Molds, mycotoxins, and sick building syndrome. *Toxicology and industrial health,* 25**,** 617-635.

SYMONS, R. H. 1989. *Nucleic Acid Probes,* Taylor & Francis.

TANG, C.-S. & WAN, G.-H. 2013. Air quality monitoring of the post-operative recovery room and locations surrounding operating theaters in a medical center in Taiwan. *PloS one,* 8**,** e61093.

TIAN, Y., SUL, K., QIAN, J., MONDAL, S. & FERRO, A. R. 2014. A comparative study of walking-induced dust resuspension using a consistent test mechanism. *Indoor Air,* 24**,** 592-603.

TOPRAK, E. & SCHNAITER, M. 2013. Fluorescent biological aerosol particles measured with the Waveband Integrated Bioaerosol Sensor WIBS-4: laboratory tests combined with a one year field study. *Atmospheric Chemistry and Physics,* 13**,** 225.

TROUWBORST, T., DE JONG, J. & WINKLER, K. 1972. Mechanism of inactivation in aerosols of bacteriophage T1. *Journal of General Virology,* 15**,** 235-242.

TRUNOV, M., TRAKUMAS, S., WILLEKE, K., GRINSHPUN, S. A. & REPONEN, T. 2001. Collection of bioaerosol particles by impaction: effect of fungal spore agglomeration and bounce. *Aerosol Science & Technology,* 35**,** 617-624.

TWOHY, C. H., MCMEEKING, G. R., DEMOTT, P. J., MCCLUSKEY, C. S., HILL, T. C., BURROWS, S. M., KULKARNI, G. R., TANARHTE, M., KAFLE, D. N. & TOOHEY, D. W. 2016. Abundance of fluorescent biological aerosol particles at temperatures conducive to the formation of mixed-phase and cirrus clouds. *Atmospheric Chemistry and Physics,* 16**,** 8205-8225.

VALSAN, A., RAVIKRISHNA, R., BIJU, C., PÖHLKER, C., DESPRÉS, V., HUFFMAN, J., PÖSCHL, U. & GUNTHE, S. 2016. Fluorescent biological aerosol particle measurements at a tropical high-altitude site in southern India during the southwest monsoon season. *Atmospheric Chemistry and Physics,* 16**,** 9805-9830.

VAN DROOGENBROECK, C., VAN RISSEGHEM, M., BRAECKMAN, L. & VANROMPAY, D. 2009. Evaluation of bioaerosol sampling techniques for

the detection of Chlamydophila psittaci in contaminated air. *Veterinary microbiology,* 135**,** 31-37.

VAN RIJEN, M. M. L. & KLUYTMANS, J. 2009. Costs and benefits of the MRSA Search and Destroy policy in a Dutch hospital. *European Journal of Clinical Microbiology & Infectious Diseases,* 28**,** 1245-1252.

VEILLETTE, M., KNIBBS, L. D., PELLETIER, A., CHARLEBOIS, R., LECOURS, P. B., HE, C., MORAWSKA, L. & DUCHAINE, C. 2013. Microbial contents of vacuum cleaner bag dust and emitted bioaerosols and their implications for human exposure indoors. *Appl. Environ. Microbiol.,* 79**,** 6331-6336.

VENETTA, B. D. 1959. Microscope phase fluorometer for determining the fluorescence lifetimes of fluorochromes. *Review of Scientific Instruments,* 30**,** 450-457.

VERDE, S. C., ALMEIDA, S. M., MATOS, J., GUERREIRO, D., MENESES, M., FARIA, T., BOTELHO, D., SANTOS, M. & VIEGAS, C. 2015. Microbiological assessment of indoor air quality at different hospital sites. *Research in microbiology,* 166**,** 557-563.

WAGENVOORT, J., SLUIJSMANS, W. & PENDERS, R. 2000. Better environmental survival of outbreak vs. sporadic MRSA isolates. *Journal of Hospital Infection,* 45**,** 231-234.

WALTERS, M., MILTON, D., LARSSON, L. & FORD, T. 1994. Airborne environmental endotoxin: a cross-validation of sampling and analysis techniques. *Applied and environmental microbiology,* 60**,** 996-1005.

WATHEN, C., KSHETTRY, V. R., KRISHNANEY, A., GORDON, S. M., FRASER, T., BENZEL, E. C., MODIC, M. T., BUTLER, S. & MACHADO, A. G. 2016. The association between operating room personnel and turnover with surgical site infection in more than 12 000 neurosurgical cases. *Neurosurgery,* 79**,** 889-894.

WEBER, G. & TEALE, F. 1957. Determination of the absolute quantum yield of fluorescent solutions. *Transactions of the Faraday Society,* 53**,** 646-655.

WEI, K., ZHENG, Y., LI, J., SHEN, F., ZOU, Z., FAN, H., LI, X., WU, C.-Y. & YAO, M. 2015. Microbial aerosol characteristics in highly polluted and near-pristine environments featuring different climatic conditions. *Science bulletin,* 60**,** 1439-1447.

WEI, K., ZOU, Z., ZHENG, Y., LI, J., SHEN, F., WU, C.-Y., WU, Y., HU, M. & YAO, M. 2016. Ambient bioaerosol particle dynamics observed during haze and sunny days in Beijing. *Science of the Total Environment,* 550**,** 751-759.

WEINHOLD, B. 2007. A spreading concern: inhalational health effects of mold. National Institute of Environmental Health Sciences.

WESCHLER, C. J. 2016. Roles of the human occupant in indoor chemistry. *Indoor air,* 26**,** 6-24.

WILLEKE, K. & BARON, P. A. Aerosol measurement.

WILLEKE, K., LIN, X. & GRINSHPUN, S. A. 1998. Improved aerosol collection by combined impaction and centrifugal motion. *Aerosol Science and Technology,* 28**,** 439-456.

WINIWARTER, W., BAUER, H., CASEIRO, A. & PUXBAUM, H. 2009. Quantifying emissions of primary biological aerosol particle mass in Europe. *Atmospheric Environment,* 43**,** 1403-1409.

WITTMAACK, K., WEHNES, H., HEINZMANN, U. & AGERER, R. 2005. An overview on bioaerosols viewed by scanning electron microscopy. *Science of the Total Environment,* 346**,** 244-255.

WRIGHT, T. P., HADER, J. D., MCMEEKING, G. R. & PETTERS, M. D. 2014. High relative humidity as a trigger for widespread release of ice nuclei. *Aerosol Science and Technology,* 48**,** i-v.

XIE, Y., FAJARDO, O. A., YAN, W., ZHAO, B. & JIANG, J. 2017. Six-day measurement of size-resolved indoor fluorescent bioaerosols of outdoor origin in an office. *Particuology,* 31**,** 161-169.

XU, C., WU, C.-Y. & YAO, M. 2017. Fluorescent Bioaerosol Particles Resulting from Human Occupancy with and without Respirators. *Aerosol and Air Quality Research,* 17**,** 198-208 (lxv.

XU, Z., SHEN, F., LI, X., WU, Y., CHEN, Q., JIE, X. & YAO, M. 2012. Molecular and microscopic analysis of bacteria and viruses in exhaled breath collected using a simple impaction and condensing method. *PLoS One,* 7**,** e41137.

XU, Z. & YAO, M. 2013. Monitoring of bioaerosol inhalation risks in different environments using a six-stage Andersen sampler and the PCR-DGGE method. *Environmental monitoring and assessment,* 185**,** 3993-4003.

YANG, S., LEE, G. W., CHEN, C.-M., WU, C.-C. & YU, K.-P. 2007. The size and concentration of droplets generated by coughing in human subjects. *Journal of Aerosol Medicine,* 20**,** 484-494.

YAO, M. & MAINELIS, G. 2007a. Analysis of portable impactor performance for enumeration of viable bioaerosols. *Journal of occupational and environmental hygiene,* 4**,** 514-524.

YAO, M. & MAINELIS, G. 2007b. Use of portable microbial samplers for estimating inhalation exposure to viable biological agents. *Journal of Exposure Science and Environmental Epidemiology,* 17**,** 31.

YOU, R., CUI, W., CHEN, C. & ZHAO, B. 2013. Measuring the short-term emission rates of particles in the "personal cloud" with different clothes and activity intensities in a sealed chamber. *Aerosol and Air Quality Research,* 13**,** 911-921.

YU, X., WANG, Z., ZHANG, M., KUHN, U., XIE, Z., CHENG, Y., PÖSCHL, U. & SU, H. 2016. Ambient measurement of fluorescent aerosol particles with a WIBS in the Yangtze River Delta of China: potential impacts of combustion-related aerosol particles. *Atmospheric Chemistry and Physics,* 16**,** 11337-11348.

YUE, S., REN, H., FAN, S., WEI, L., ZHAO, J., BAO, M., HOU, S., ZHAN, J., ZHAO, W. & REN, L. 2017. High Abundance of Fluorescent Biological Aerosol Particles in Winter Beijing, China. *ACS Earth and Space Chemistry*.

ZHOU, J., FANG, W., CAO, Q., YANG, L., CHANG, V. C. & NAZAROFF, W. W. 2017. Influence of moisturizer and relative humidity on human emissions of fluorescent biological aerosol particles. *Indoor Air,* 27**,** 587-598.

ZHU, S., KATO, S. & YANG, J.-H. 2006. Study on transport characteristics of saliva droplets produced by coughing in a calm indoor environment. *Building and Environment,* 41**,** 1691-1702.

ZHU, Y., HINDS, W. C., KIM, S., SHEN, S. & SIOUTAS, C. 2002. Study of ultrafine particles near a major highway with heavy-duty diesel traffic. *Atmospheric Environment,* 36**,** 4323-4335.

ZOU, Z. & YAO, M. 2015. Airflow resistance and bio-filtering performance of carbon nanotube filters and current facepiece respirators. *Journal of Aerosol Science,* 79**,** 61-71.

Chapter 2

Materials and Methods

Table of Contents

2.1 Wideband Integrated Bioaerosol Sensor

2.1.1 Development and Operation

The Wideband Integrated Bioaerosol Sensor (WIBS) is a single aerosol particle fluorescence monitor that uses light-induced fluorescence (LIF) to detect fluorescent aerosol particles (FAP) in real-time, Figure 2.1 and Table 2.1. The original instrument was invented by Professor Paul Kaye and co-workers at the University of Hertfordshire. It is now commercially available from Droplet Measurement Technologies (DMT) and is one of the most widely used instruments for monitoring PBAP in real-time. The WIBS was originally developed for defence applications to enable the detection of airborne particles (Kaye et al., 2014). It offers the ability to characterize the size and asymmetry (shape) of individual fluorescent and non-fluorescent particles by assessing the forward and sideways optical scatter, along with the spectrally unresolved fluorescent intensity of each particle at a millisecond time resolution. There have been several versions of the WIBS available, from Models 3 and 4 prototypes, to the commercial version 4A.

Figure 2.1 Outer Components WIBS-4+ (Black), WIBS-4A (Silver) (Top), Internal Components Wibs-4+ (middle) and WIBS-4A (Technologies, 2014a).

Table 2.1 Principal Components of the WIBS-4+ and 4A

	WIBS-4+	WIBS-4A
1	Aerosol Inlet	
2	USB and power connectors, air sample outflow, LED indicators	
3	Oversize particle trap	
4	Pump	
5	Main optical chamber	
6	Xenon sources	
7	Fluorescence detector channels	
8	Quadrant PMT, particle “shape” detector	
9	Power distribution board	
10	Analog acquisition and digitisation board	
11	Extra xenon source	

With regard to their operation, there are a number of differences between the prototype WIBS-4 and commercially available WIBS-4A. The prototype WIBS-4 draws in ambient air at a rate of 2.4 L min^{-1}. Approximately 2.2 L min^{-1} of the initial aerosol flow is filtered and reintroduced as a sheath flow to confine the remaining 0.2 L min^{-1} sample (Kaye et al., 2014). With the commercially available WIBS-4A instruments, the analyte particles are pumped into the main optical chamber at a rate of 2.5 L min^{-1}. Part of this flow, ~0.3 L min^{-1}, is then directed as sample flow. The remaining 2.2 L min^{-1} of the air flow is filtered before forming a sheath flow to constrain the sample flow as a vertical column, which sequentially aligns the incoming particles (Technologies, 2014b).

2.1.2 WIBS-4a

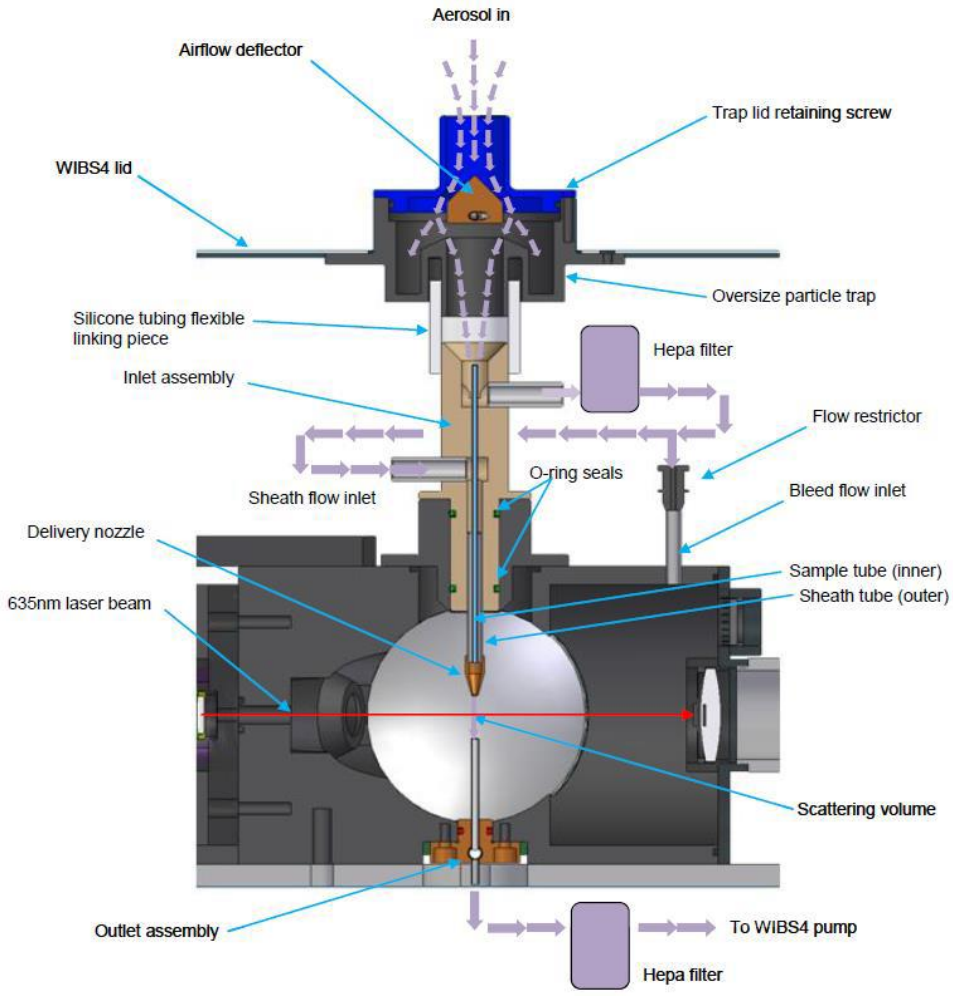

Figure 2.2 WIBS-4a Aerosol Flow (Technologies, 2014a)

Both WIBS models use a combination of the sheath flow and a small bleed flow to constantly purge the optical chamber of any extraneous particles. The initial detection of the particle uses a continuous-wave red diode laser at 635 nm that illuminates the particles flowing into the optical chamber. Scattering of the laser light is used for both the sizing of particles (based on Mie theory) and to determine a basic particle "shape" using a so-called asymmetry factor (AF). As with most optical particle counters, the WIBS-4 and WIBS-4A apply a particle size calibration that is based on a theoretical curve, which assumes that the particles are spherical and of a specified refractive index. Both prototype and commercial WIBS use a calibration curve that is calculated using standard monodispersed polystyrene latex (PSL) microsphere aerosols. These spheres have a quoted refractive index of 1.58 ± 0.2 (Technologies, 2014b). As the

calibration curve is based on PSL spheres, the size data that is produced should be treated as an estimate, especially when measuring spherical particles of disparate refractive index or non-spherical solid particles. The WIBS-4 prototype contains a size selection utility allowing for the user to select one size fraction of the ambient air sample to perform data analysis on. In practice, this is controlled via a sensitive dual gain function with two switchable settings: High Gain (HG) and Low Gain (LG). Smaller size particles that are in the range between 0.5 and 12 μm are monitored in HG, whereas larger sized (more highly fluorescent) particles in the range between 3 and 31 μm are detected in LG. The commercially available models (WIBS-4A) have a single gain setting, which evaluates particles between 0.5–20 μm. Use of the gain settings affect WIBS particle sizing range, however, it should be noted that this is an instrumental limit rather than a fundamental limit with regard to light scatter sizing. Particle shape is assessed through the azimuthal distribution of the forward scattered light. The forward scattered light falls on a quadrant photomultiplier tube (PMT) detector where the scattering pattern of the particle is sampled at four angular offsets.

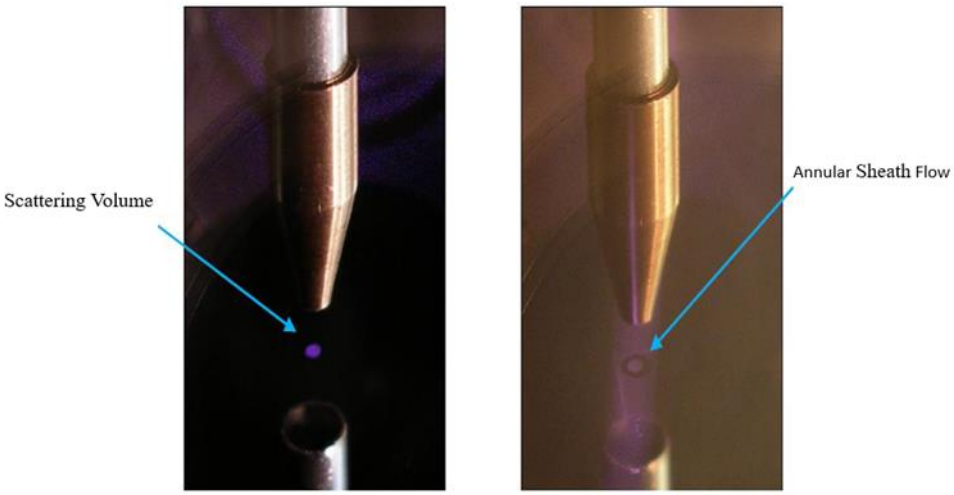

Figure 2.3 Smoke Visualisation of Scattering Volume and its Surrounding Clean Sheath Flow (Technologies, 2014a)

For each of the scatter intensities that are recorded by the quadrants, the root-mean-square variation around the mean value outputs produces a numerical value between 0–100 AF units, with 0 being a perfect sphere and 100 denoting long rod-like fibrous particles. The fluorescence characteristics of the individual particles are then interrogated using two xenon flash lamps (Xe_1, Xe_2). They are tuned to excite at the maxima absorption wavelengths of the biofluorophores tryptophan (280 nm) and

NAD(P)H (370 nm), by delivering two sequential ultraviolet pulses at 280 nm and 370 nm. Fluorescence emission following these excitation pulses is detected in two detector bands: 310–400 nm (Band I) and 420–650 nm (Band II). Thus, once a particle has been detected by the laser (after ~10 μs), the first xenon light source (280 nm) is triggered which induces fluorescence that is detected in two bands. Following this sequence, the second xenon flash lamp (370 nm) is triggered (after a further 10 μs) resulting in another excitation of the particle. Subsequent measurement in both the first and second detector bands follows, however the wavelength data from the first band (310–400nm) is discarded due to interference from the excitation pulse (370 nm) (Healy et al., 2012a). Hence, for individual particles, three fluorescence measurements are recorded: (a) Excitation at 280 nm, emission in Band I (termed FL1); (b) Excitation at 280 nm, emission in Band II (termed FL2); and, (c) Excitation at 370 nm, emission in Band II (termed FL3).

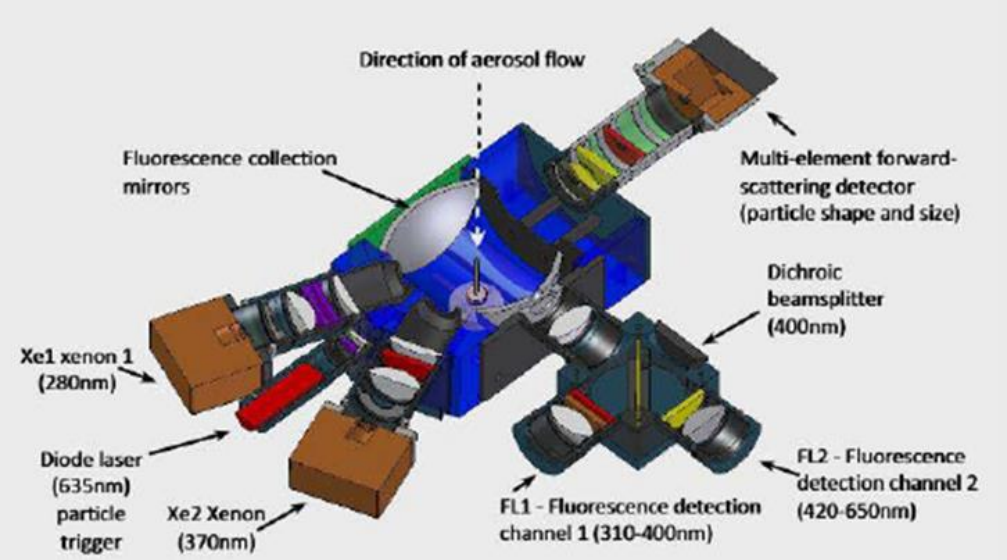

Figure 2.4 Schematic of the Optical Chamber of the WIBS-4a (Technologies, 2014a)

While the flash lamps are tuned to excite at the maxima of the biofluorophores tryptophan and NAD(P)H, it should be emphasized that a host of other PBAP fluorophores, such as cellulose and light harvesting pigments, like the chlorophylls, can also contribute to the luminescence signals (*vide supra*). Humic-like Substances (HULIS), Secondary Organic Aerosols (SOA), Polycyclic Aromatic Hydrocarbons (PAH), and other important atmospheric chemicals can also fluoresce in the spectral regions relevant to WIBS technology, but often with much smaller quantum yields than the biologicals. However, the possibility remains that they may still contribute to

the overall WIBS data-sets and related FAP numbers. Where results are suspected to have large quantities of these potentially interfering non-biological materials present, the data analyst must take extra attention when interpreting the WIBS measurements. There are also several differences in the instrumental configurations of the early prototype WIBS-3 and the WIBS-4. The WIBS-4 included several upgrades from the WIBS-3, such as improvements to its optical configuration, optical filters, UV delivery, and sample inlet system (Healy et al., 2012a, Stanley et al., 2011, Gabey et al., 2010). However, the most significant difference was made in the separation of two detection bands. The WIBS-3 has two detection bands that overlap (FL1 = 320–600 nm; FL2/FL3 = 410–600 nm), whereas, within the WIBS-4 and WIBS-4A, this overlap does not occur. This constrains the bands in which a particle fluoresces, allowing for the FL2 channel to more completely differentiate information from the FL1 channel. WIBS data-sets also contain particle numbers, size and "shape" parameters, along with the three individual fluorescence intensity characteristics. Perring et al. (Perring et al., 2015) conducted a dual campaign using a WIBS-4 in Florida and California and subsequently developed a new annotation system. They categorized particle fluorescence into one of seven types, depending on the three forms of fluorescence signals detected by the WIBS (Perring et al., 2015). These categories consider each channel individually (FL1, FL2, and FL3), but also includes all possible combinations, as shown in Table 1.13 Such cataloguing nomenclature allows for a greater degree of individual particle classification since the particle fluorescence intensities could previously only be placed into one or more of the FL channels, depending on their fluorescence. Thus, the designations used in Table 1.13 allow for a more detailed understanding of ambient particles fluorescent characteristics.

Table 2.2 Wideband Integrated Bioaerosol Sensor (WIBS) channel annotation matrix. Channels are matched with excitation wavelength and emission waveband.

Channel	Excitation (nm)	Emission (nm)
A	280	310–400
B	280	420–650
C	370	420–650
AB	280	310–400 420–650
AC	280	310–400
	370	420–650
BC	280 370	420–650
ABC	280	310–400 420–650
	370	420–650

This categorization system denotes particles that fluoresce above the threshold in only one channel as either types A, B, or C (depending on the excitation and emission wavelengths of the particle, as indicated in Table 2.2). Particles fluorescing in only two channels are classified as types AB, AC, and BC; while, particles that fluoresce in all of the channels are categorized as type ABC (Perring et al., 2015). Using this method of classification, it is hoped that more complex environments can be better characterized by reference to the many different types of FAP which are observed.

The processing of the collected data is arguably the most challenging step in distinguishing between PBAP and interfering non-biological fluorescent compounds. This is in part due to the rather large data sets (>10,000,000 particles with each of the five variables), which can be routinely collected during a campaign. In an effort to simplify the subsequent analyses, the WIBS data is reduced into discrete concentration time-series. In an effort to extract useful data from these large sets, Robinson et al., 2013 have used hierarchical agglomerative cluster analysis (Robinson et al., 2013). The technique was first applied to the measurement of various fluorescent and non-fluorescent PSL. Excellent separation was achieved, with the cluster analysis successfully classifying the majority of the particles correctly (Robinson et al., 2013). The methodology was then applied to two separate simultaneous ambient WIBS data sets that were recorded in a forest site in Colorado, USA (Robinson et al., 2013). The authors suggested the following criteria as essential for WIBS single-particle data analysis: (i) Simplification procedures should not include any assumptions about the types of particles present in the dataset, since this would prevent the identification of

PBAP, which have not been previously characterised using similar measurements; and, (ii) As several types of PBAP can be present in a wide range of concentrations, assumptions regarding relative group sizes should not be required. When the analysis method is applied and differences between the WIBS-3 and WIBS-4 are taken into consideration, the average measurement values of the clusters were qualitatively similar. Ambient cluster results were related to aerosol types by comparison of the cluster measurements averages and time-series to the available literature. By applying the cluster analysis to the collected ambient data sets, bacterial agglomerations, fungal smut spores, and other fungal spores were suggested as separate cluster identities. The approach was tested and verified on a controlled data set of PSL measurements, and were successfully applied to a subset of WIBS measurements, with the remaining measurements being accredited to the previously resolved clusters (Robinson et al., 2013).

2.1.3 Laboratory Studies

Many laboratory experiments have been performed to evaluate the counting efficiency of the WIBS. The particle counting efficiency of the WIBS-4 has been measured using PSL microspheres in size ranges between 0.3 and 30 μm (Healy et al., 2012b). The experiment compared the results of a WIBS-4 particle count to the results that were obtained using a commercially available reference instrument, the condensation particle counter (CPC, TSI, Model 3010, Minnesota, USA) (Healy et al., 2012b). A parameter termed D_{50} was used to define the diameter of particles with a number concentration ratio for WIBS-4/CPC experiments that is equal to 50% counting efficiency (i.e., WIBS counted 50% of that seen by the CPC). A D_{100} was likewise defined as 100% counting efficiency (i.e., both instruments counted equal amounts at a given size value) (Healy et al., 2012b). The lower-end counting efficiency curve was then defined in specific size regimes (D_{50} ~0.489 μm and D_{100} ~0.690 μm) (Healy et al., 2012b).

The WIBS-4 sensitivity that was surrounding the analysis and discrimination of biological and non-biological aerosols has also been the subject of many studies (*vide infra*). However, in an effort to distinguish between major classes of airborne microbes and pollen, numerous studies have sought to measure the optical fluorescence signals,

which would enable this distinction to be made. The sensitivity for PBAP discrimination using the WIBS-4 was investigated by Healy *et al.* (Healy et al., 2012a). Fifteen samples from two separate taxonomic kingdoms, *Plantae* (8) and *Fungi* (7), along with two non-fluorescing chemical solids (common salt and chalk), were systematically introduced into the WIBS-4, and more than 2000 individual-particle measurements were then recorded for each sample type (Healy et al., 2012a). The ability of the WIBS-4 to discriminate between chemical particles and the pollen and fungal spores was then explored through the classification of FAP signatures. Discrimination between the particles was made on the basis of five measurable characteristics (size, AF, FL1, FL2, and FL3) (Healy et al., 2012a). The use of these variables demonstrated that some spore and pollen sample signals could be separated from each other, according to the normalised fluorescence data that was obtained in the FL1/FL3 axis. Most interestingly, grass pollen was shown to be separable from other pollen (Healy et al., 2012a). Based on these results, it was suggested that using a combination of three-dimensional (3-D) plots of normalised fluorescence coupled with size measurements, may enable the instrument to be used as an early warning system for the presence of bio-aerosols (Healy et al., 2012a).

The sensitivity of a WIBS-4 for discriminating chemical and biological aerosols was evaluated using a series of environmental chamber experiments (Toprak and Schnaiter, 2013). The number-concentrations and size distribution of the aerosols in the chamber experiments were measured by an assortment of instruments, including the WIBS-4, an Aerodynamic Particle Sizer (APS), and a CPC. The laboratory tests supported and clarified the accuracy of the previously defined fluorescence thresholds of the WIBS. The results further demonstrated the ability of the WIBS to discriminate between biological and non-biological aerosols, with the study concluding that some non-biological particles (PAH, mineral dust, and ammonium sulfate) may cause interference for individual WIBS channel signals. However, it was found that using a combination of two fluorescent channels provided adequate discrimination between biological and non-biological aerosols (Toprak and Schnaiter, 2013). For example, the authors found that using a combination of FL1 and FL3 channels, an aerosolised ammonium sulfate-fungal spore mixture could be readily discriminated (Toprak and Schnaiter, 2013).

Hernadez *et al.* (Hernandez et al., 2016) has compiled an aerobiological reference catalogue of more than 50 pure cultures of common bioaerosols (bacteria, fungi, and pollen) using a WIBS-4A (Hernandez et al., 2016). The catalogue visualizes size, shape, and fluorescent channel emission intensities of the investigated samples, which allows for discrimination between the major classes of airborne microbes and pollen. The main discriminators used were: (i) The utilization of the ABC category nomenclature; (ii) The average fluorescence intensity within each of these categories; and, (iii) The average Equivalent Optical Diameter (EOD) (Hernandez et al., 2016). Based on the application of the discriminators, common fluorescence patterns for each of the bioaerosol classes were observed. For instance, most aerosolized bacterial cultures that accumulated with EOD < 1.5 μm displayed weak fluorescence intensities predominantly in the fluorescence type A category. However, a breakdown of this general trend was noted for *Bacillus subtilis*, which dominated in the AB category. Fungal spores were noted to exhibit a higher EOD range (2–9 μm), but encompassed several fluorescence types: A, AB, BC, and ABC, with most giving rise to type A and AB. Although pollen grain signals overlapped with those of several fungal spores with respect to EOD ranges, the former largely exhibited higher fluorescence intensities because they contain more biofluorophores (due to their larger size). Type C fluorescence was more dominant with fungal spores when compared to pollen grains, which displayed only as BC and ABC types (Hernandez et al., 2016). Under defined conditions (i.e., relative humidity, temperature and culture conditions), it was suggested that key components of airborne samples could be distinguished by measuring optical diameters and fluorescence intensity (Hernandez et al., 2016).

Using the same ABC categorization system as described above, a chamber-type experiment was performed, which used a WIBS-4A to evaluate the release of fluorescent particles that were associated with human shedding while walking (Zhou et al., 2017). The monitoring was carried out in a small office room (39.5 m^3), with the only air-exchange occurring through air filtration (Zhou et al., 2017). A mean emission rate of fluorescent particles in the range 1–10 μm was calculated to be 6.8–7.5 million particles/person/hour. This value is equivalent to ~0.3 mg/person/hour. Of the total fluorescent particles, 90% were associated with the categories ABC, AB, and A. Particles in the ABC channel were the highest contributors making up to 40% of the total number (particles >1 μm) and ~70% of mass emission rates of fluorescent

particles (Zhou et al., 2017). The fluorescent particles demonstrated a lognormal distribution, with a mean geometric diameter within the 2.5–4 μm range. The ABC category showed a higher lognormal size distribution with a value of 4 μm for the mean diameter. This value was 1.5 μm greater than that observed for the A and AB categories. The AF (shape) parameter of the fluorescent particles also increased with size (Zhou et al., 2017). Another component of this study sought to measure the influence of applied moisturiser (jojoba oil) on the frictional interactions between skin and clothing. The oil application resulted in a significant increase in emissions rates, with factors between 2–5× noted. However, the emissions that were related to the moisturiser were due to smaller particle sizes and the mass emissions rate was lower with moisturiser than without. Moisturiser use also increased the emissions of category A particles, which is a possible indication of abiotic interference that is associated with their use (Zhou et al., 2017).

The instrumental fluorescence detection limit is determined by measuring the fluorescence emission signal when no particles are present in the optical chamber. This is undertaken by putting the WIBS instrument into a setting known as "forced trigger" mode. This mode essentially causes the flash lamps within the WIBS to fire on empty space while the pump is off. Background fluorescent values from the forced trigger mode are then collected for each channel. In general, the average of these values plus 3× standard deviations of the mean fluorescence intensity in each channel (FL1, FL2, and FL3) are then used as the cut-off thresholds. In more recent times, alternate threshold strategies utilizing increased thresholds to aid in the detection, classification, and discrimination of ambient bio-particles from interfering particles have been suggested (Savage et al., 2017). Savage *et al.* (Savage et al., 2017) systematically evaluated fluorescence thresholds for the WIBS-4A using sixty-nine types of aerosol material, which included size-resolved biological particles (i.e., bacteria, fungal spores and pollen), and chemical interferents (i.e., soot, smoke and HULIS) (Savage et al., 2017). A broad separation between the two classification types was observed using size and shape parameters in conjunction with the Perring (2015) (Perring et al., 2015) particle classification system. Using these different classification systems, the role that particle size plays in controlling fluorescent properties was assessed. This was carried out with the inclusion of a new threshold calculation whereby the fluorescent threshold was raised from the usual forced trigger (FT) + 3σ to FT + 9σ. This results in weakly

fluorescing aerobiologically insignificant particles under the previous threshold being reassigned as non-fluorescent under the new FT + 9σ criteria. The authors concluded that while it does not reduce the fraction of aerosol considered biological, it does significantly reduce fluorescence interference to almost zero for most particle types (Savage et al., 2017).

Currently, no standard fluorescent calibration method exists for real-time, single-particle fluorescence instruments. However, Robinson *et al.* 2013 has proposed a method that uses size-selected particles containing a known mass of fluorophore to calibrate the fluorescence detection of a WIBS-4A (Robinson et al., 2017). This approach was attempted using mixed tryptophan-ammonium sulfate particles to calibrate one detector (FL1) and pure quinine particles to calibrate the other (FL2). Based on the resulting fluorescence and mass relationship data, the tryptophan-ammonium sulfate particles displayed a linear relationship. The pure quinine particles gave non-linear signals, suggesting that only a portion of the quinine mass contributes to the observed fluorescence (Robinson et al., 2017). Both of the materials produced a repeatable response between observed fluorescence and particle mass. This procedure should provide the data to: establish appropriate detector gains (absolute response); estimate limits of detection; improve the repeatability of instrument set-up; and, enable more meaningful instrument comparisons (Robinson et al., 2017).

2.1.4 Field Campaigns and the Indoor Environment

All versions of the WIBS instrument (3, 4 and 4A) have been used in field campaigns within vastly contrasting settings. All of the studies focussed on the detection and quantification of PBAP concentrations in relation to the total particle load. Many of the studies used standard reference and/or other additional UV-light induced fluorescence (UV-LIF) techniques to assess the capabilities of the WIBS approach (Gabey et al., 2011, Gabey et al., 2013, Crawford et al., 2014, Healy et al., 2014, Toprak and Schnaiter, 2013, Yu et al., 2016). Some examples of these studies are shown in Table 1.9. For example, the particle morphology and fluorescence signals (FL1, FL2, and FL3 channels) of aerosolized materials in the size ranges between 0.8–20 μm have been investigated in two dissimilar environments, an urban city center (Manchester, United Kingdom (UK), December 2009) and a remote, tropical forest

(Borneo, Malaysia, June/July 2008) (Gabey et al., 2011). The FL1, FL2, and FL3 channels represented 3%, 6%, and 11% of the total aerosol counts over the Manchester study, with two dominant size modes being recorded for the fluorescent material, one at 0.8–1.2 μm and a second at 2–4 μm (Gabey et al., 2011). A large variation in the fluorescence and total aerosol concentration was evident throughout the day, with non-fluorescent particles peaking between 05:00–10:00 and 17:00–19:00, and the fluorescent particles concentrations peaking strongly at 09:00–10:00. Due to the concentrations of non-fluorescent and fluorescent particles peaking at a similar morning period, it was suggested that the release of SOA particles from traffic activity may have impacted on these results. Given the particle size profile and the fact that SOA can absorb and fluoresce at the same excitation/emission wavelengths that are associated with biological particles, they likely represent possible interferents in this study.

In the Borneo study, a clear diurnal pattern was observed under the rainforest canopy, with FAP concentrations being recorded at a minimum of 50–100 L^{-1} in late morning. This period was followed by strong temporal fluctuations before reaching 4000 L^{-1} in mid-afternoon. Stable concentrations spanning 1000–2500 L^{-1} were measured between midnight and sunrise. Above the canopy, FAP ranged from 50–100 L^{-1} during the day to 200–400 L^{-1} at night. The transient fluctuations that were seen in the under-storey were not observed (Gabey et al., 2011). FAP accounted for 55% of the total aerosol that was monitored beneath the canopy and fell to 28% above it (for particles between 0.8–20 μm). Both sites exhibited a size mode at 2 μm < D_o < 4 μm, which consisted primarily of FAP. These accounted for 75% of the under-storey and 57% and above-canopy coarse particles ($D_o \geq 2.5$ μm) (Gabey et al., 2011). It was suggested that a potential link between FAP concentrations and relative humidity existed as the highest FAP concentrations were measured at RH ≥ 80%. This behavior appears to be consistent with fungal spore releases (Gabey et al., 2011).

A WIBS-3 instrument was also used in the determination of FAP in the 0.8–20 μm size range at Puy de Dôme, a high-altitude site in France during the summer of 2010. A mean total aerosol concentration of 270 L^{-1}, with a modal size of 2 μm, was observed (Gabey et al., 2013). The mean fluorescent particle concentration determined in the FL1 channel was 12 L^{-1}, whilst those that were associated with the FL3 channel

were found to be 95 L^{-1}. The FL1 channel concentrations did not vary much throughout the campaign, but the FL3 concentrations followed a strong diurnal cycle that peaked at night (Gabey et al., 2013, Gabey et al., 2011).

WIBS-3 and WIBS-4 instruments were also used to characterize bioaerosol emissions from a Colorado pine forest (Crawford et al., 2014). Both sets of WIBS data were analysed using the previously discussed cluster analysis (*vide supra*) (Crawford et al., 2014, Robinson et al., 2013). Based on the collected data, all of the fluorescent clusters showed diurnal fluctuations along the forest floor, with minimum concentrations observed at midday (50–100 L^{-1}) and maximum concentrations at night (200–300 L^{-1}) (Crawford et al., 2014). The cluster behaviours were then compared against those expected for bioaerosols. It was shown that one cluster exhibited the greatest enhancement and highest concentration during sustained wet periods. This behaviour is consistent with that previously reported for fungal spores (O'Connor et al., 2015). A separate cluster dominated the dry periods, which showed characteristics similar to that of bacterial spores (Crawford et al., 2014).

Other notable field measurements include a month-long study, (August–September 2011) performed at Killarney National Park, Ireland. This work compared the use of two real-time fluorescence instruments, the WIBS-4 and a UV-APS. The results were compared with those obtained from a single-stage particle Hirst-type impactor and standard optical microscopic analysis (Healy et al., 2014). Both of the approaches were used to enumerate, categorise, and compare the captured particles/bioaerosols by examining the FAP data in relation to the optical microscopy results. The WIBS and UV-APS showed qualitatively comparable results, with elevated fluorescent bio-particle concentrations at night being noted when maximum RH values and minimum temperatures were measured (Healy et al., 2014). Both real-time instruments sampled through the same inlet throughout the campaign, with the mean coarse particle number-concentrations (D_o > 1 μm) measured at 32800 L^{-1} and 32400 L^{-1} for WIBS-4 and UV-APS, respectively. This observation indicated that there was no significant sampling losses between the instruments (Healy et al., 2014). Quantitatively, the two instruments gave results that correlated well with R^2 = 0.90 for the mean total particle concentrations over the campaign (Healy et al., 2014). A correlation was clearly observed (integrated number concentrations) between the total biological fungal spore

concentrations from the impaction techniques and the WIBS and UV-APS. The fluorescence values of both the instruments showed periodic high and low concentration fluctuations, with concomitant peaks and troughs being measured using optical microscopy occurring at similar time periods as the WIBS-4 FL2 and FL3 channels. However, it should be noted that the FL1 channels bore little temporal similarity (Healy et al., 2014). The FL1 channel was dominated by particles with D_o < 2 μm and fluorescent particle concentrations ~ 10^2 L^{-1} (Healy et al., 2014). Such an observation is to be expected since optical microscopy counting is not accurate in this smaller size regime. When comparing the spore number concentrations with each WIBS channel showed R^2 values of 0.05, 0.29, and 0.38 for FL1, FL2, and FL3, respectively. Each of the comparisons suggests that the impaction/optical microscopy method undercounts the WIBS by factors of 3–14× (Healy et al., 2014). Finally, it was concluded that the results provided by the three WIBS fluorescence channels provide analytical advantages for bioaerosol classification when compared to the single channel detection approach offered by the UV-APS (Healy et al., 2014).

During another semi-rural field campaign located in Karlsruhe, Germany, the WIBS FAP concentration data were shown to exhibit seasonal and diurnal variations. Seasonal maximum mean FAP concentrations of 46 L^{-1} were measured in the summer, with a decline in mean FAP concentration of 19 L^{-1} towards winter. The mean FAP concentration over the year was 31 L^{-1} (Toprak and Schnaiter, 2013). The contribution of FAP to the total aerosol concentrations again varied throughout the year, being highest in summer (10.6%) and lowest in Winter (3.87%), with a yearly mean of 7.34% (for particles between 0.8–16 μm) (Toprak and Schnaiter, 2013). Diurnal FAP concentrations increased after sunset, reaching their highest concentrations during late nights and early mornings. In contrast, total aerosol concentrations were normally highest during the daytime with a decrease noted towards the evening, followed by a sharp decrease after sunset (Toprak and Schnaiter, 2013). No correlation was found between FAP concentrations and temperature, precipitation, wind direction, or wind speed. Nevertheless, clear correlations (R^2 = 0.924 and R^2 = 0.911 for spring and summer respectively) were observed between RH and FAP concentrations. The FAP concentrations increased significantly for RH conditions in the 75–95% RH range. However, lower values for the correlation coefficients were observed during both the autumn (R^2 = 0.541) and winter months (R^2 = 0.652) (Toprak and Schnaiter, 2013).

The varying concentrations of FAP, monitored as a function of altitude, have also been investigated. For example, sampling has been carried out near the surface and subsequently compared to measurements made at 1000 m above ground-level, for a wide range of longitudes across the U.S.A between Florida and California. In this study, a WIBS-4A was utilized to make measurements aboard the airship "Gondola" (Perring et al., 2015). FAP counting was recorded for the range between 1–10 μm, revealing particle concentrations, ranging from 2.1–8.7 × 10 particles L^{-1}. These Figures are representative of ~24% of the total particle number (Perring et al., 2015). Diverse size distributions and distinctive fluorescent characteristics were apparent for these regions. For instance, FAP between 1–4 μm in diameter were observed in the Eastern States which is consistent with the presence of mould spores, whilst larger particles between 3–10 μm diameter were sampled in the Western States, where FAP contributions to the total particle concentration were much more variable (Perring et al., 2015). This study showed that FAP can contribute significantly to the overall particulates in arid as well as humid environments, and that there are significant sources of bioaerosols in each area, but they may well be of differing types (Perring et al., 2015).

The fluorescence characteristics of aerosol particles in the polluted atmospheric area of Nanjing, Yangtze River Delta, China also been investigated (Yu et al., 2016). Day-to-day and diurnal variations of FAP were observed and the concentrations were found to be dominated by the FL2 channel, with a mean of 3400 particles L^{-1}, followed by FL3 (2100 L^{-1}) and FL1 (600 L^{-1}). These values are much larger than those found in Amazon (93 L^{-1}), Borneo (150 L^{-1}), and Hyytiälä (23 L^{-1}) (Gabey et al., 2011, Huffman et al., 2012, Toprak and Schnaiter, 2013), indicating that in the China study, the observed concentrations of FAP were ~1–2× greater. The work also suggests a size dependence for the fractions measured as well as a contribution by diverse FAP types. In the FL3 channel, the 1–2 μm range was reportedly dominated by combustion related particles, with the majority of FAP/biological particles apparent in the 2–5 μm range (Yu et al., 2016). A strong correlation (R^2 = 0.75) between FL1 and the $M_{BC}/PM_{0.8}$ (Mass concentration of black carbon/mass concentration of particles in the size range 0.006–0.8 μm) is suggestive of a large contribution from anthropogenic emissions (Yu et al., 2016). The high fluorescence values measured, when combined with the strong correlation between FL1 and $M_{BC}/PM_{0.8}$, suggest that directly using the three

fluorescent channels of the WIBS may not be appropriate for indexing PBAP in significantly polluted areas (Yu et al., 2016).

The WIBS-4A was further used in a study that investigated indoor (office) versus outdoor size-resolved concentrations of fluorescent aerosols. The measurements were undertaken over a period of six continuous days (144 h) in an office located in the campus of Tsinghua University, Beijing, China. The office was 5.1 × 2.7 m^2 in area, 2.8 m high and void of any outside influence i.e., the only indoor source of air was from a filtration system (Xie et al., 2017). The WIBS was fitted with an automated control box (KLD2OS 2-way motorised ball valve; Tianjin Kailida Control Technology Development Co., Tianjin, China, allowing for both indoor and outdoor sampling) and a timer device, which permitted the WIBS-4A to switch between indoor and outdoor measurements every 5 min. The results showed that measurements in the FL1 channel for both indoor and outdoor FAP fitted a bimodal lognormal distribution, with the first peak ranging from 1.35–1.5 μm and the second occurring within the range, 2.1 and 2.25 μm. The R^2 values between indoors and outdoors was 0.938 for the smaller size range and 0.935 for the larger range (Xie et al., 2017). A lognormal distribution was also shown to fit the AF dataset, with values for all outdoor and all indoor aerosols peaking at 11–11.5, and a correlation coefficient of R^2 = 0.992 being noted between the outdoor and indoor AF values (Xie et al., 2017). Linear regression of indoor versus outdoor fluorescent bioaerosol concentrations showed that all of the size ranges from 0.5 to 2.5 μm exhibited very similar profiles with concentrations of indoor and outdoor FAP increasing linearly with respect to each other. However, as particle size increased, the slopes become less steep, possibly reflecting a higher loss rate for larger fluorescent bioaerosols as they enter the building envelope (Xie et al., 2017). The time series of the size resolved indoor versus outdoor bioaerosols were also determined using a mass balance equation to model their relationship. Periodic fluctuations throughout all of the size ranges in outdoor non-fluorescent versus fluorescent bioaerosols were also reflected in the indoor concentrations, albeit with a considerable reduction in concentrations, and also with a time lag. Mean concentrations of fluorescent particles made up less than 10% of all the aerosols, leading to similar variations in the non-fluorescent and fluorescent number-concentrations (Xie et al., 2017).

2.2 AirNode Airvisual

AirVisual Airnode (IQAir China, Beijing, China) is a low-cost, portable, continuous light scattering laser air quality monitor that uses artificial intelligence in combination with a Particulate matter ($PM_{2.5}$) laser sensor to measure and predict air pollution. AirNode detects $PM_{2.5}$ along with CO_2, temperature and relative humidity levels in the environment. AirNode accuracy depends on auto-calibration which simultaneously considers a variation of factors including temperature, humidity and outlying data points.

Table 2.3 Air Quality Index (AQI) as defined by the EPA.

Air Quality (4-bands)	Index (1-10);	Ozone Running 8-hour mean (ug/m^3)	Nitrogen dioxide 1-hour mean (ug/m^3)	Sulphur dioxide 1-hour mean (ug/m^3)	$PM_{2.5}$ Running 24-hour mean (ug/m^3)	PM_{10} Running 24-hour mean (ug/m^3)
Good	1	0-33	0-67	0-29	0-11	0-16
	2	34-65	68-134	30-59	12-23	17-33
	3	67-100	135-200	60-89	24-35	34-50
Fair	4	101-120	201-267	90-119	36-41	51-58
	5	121-140	268-334	120-149	42-47	59-66
	6	141-160	335-400	150-179	48-53	67-75
Poor	7	161-187	401-467	180-236	54-58	76-83
	8	188-213	468-534	237-295	59-64	84-91
	9	214-204	535-600	296-354	65-70	92-100
Very Poor	10	≥241	≥601	≥355	≥71	≥101

The device uses an Air Quality Index (AQI) system for reporting the severity of air quality levels. The index ranges from 0-500, where higher index values indicate higher levels of air pollution, as defined by the Environmental Protection Agency (EPA) (Organization, 2010), see Table 2.3 The Airnode indicates each AQI level with an AQI icon, see Figure 2.5.

** Sensitive groups include people with respiratory or heart disease, children and the elderly

Figure 2.5 Airnode AQI icons.

CO_2 readings are indicated by a CO_2 gauge which indicates CO_2 levels in the room, the more the gauge fills the darker the colour will get indicating higher CO_2 ppm concentration, see CO_2 icon index Figure 2.6.

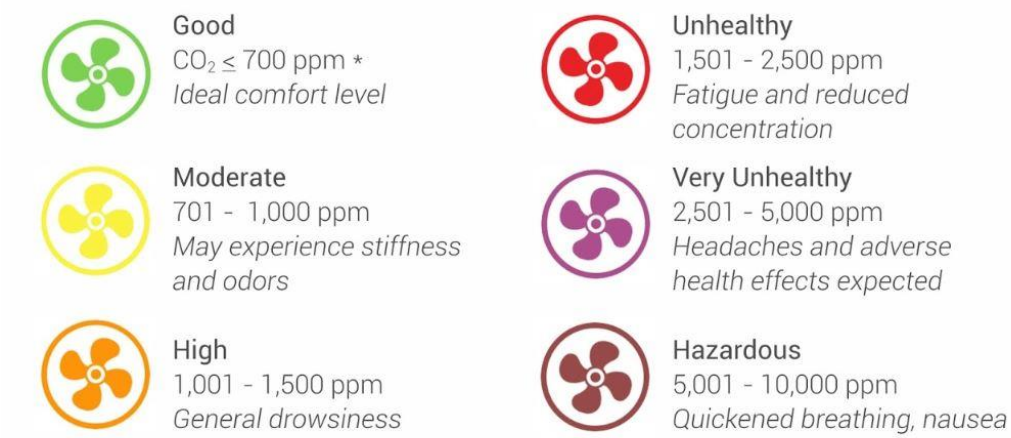

Figure 2.6 CO2 index, concentrations defined by colour.

To date there has been relatively few studies reporting the performances of the Airvisual Airnode (Feenstra et al., 2019, Li et al., Singer and Delp, 2018). The AirVisual had highly correlated and quantitative (within a factor of 2) results vs. the reference sampler (Grimm Mini Wide-Range Aerosol Spectrometer Model 1.371) for large cooking, combustion sources and dust suspension. However, it missed sources

with little mass exceeding 0.3µm particles (Singer and Delp, 2018). Hourly measurements of ambient $PM_{2.5}$ of the AirVisual was tested against a federally equivalent method (FEM), the Met One Attenuation Monitor (BAM), at an ambient air monitoring station in California, US. Triplicate analysis with the AirVisual showed relatively high linearity (r^2 = 0.69 - 0.7) and a low mean biased error (MBE) (0.2-3.4 µg/m^3) and mean absolute error (MAE) (4.4-5.3 µg/m^3) in comparison to the BAM. MBE provides a indicates the tendency of the AirVisual to over- or under-estimate the BAM $PM_{2.5}$ concentration. The MAE takes the absolute value of the hourly differences between the sensor and the BAM. The high correlation and low MBE/MAE indicate the AirVisual could accurately track ambient $PM_{2.5}$ concentration as well as the FEM BAM (Feenstra et al., 2019).

2.2.2 WIBS-4+

As described in introduction section 1.5.2 during a laboratory study that measured the fluorescence spectra and the lifetimes of individual pollen grains, the biomolecule chlorophyll-a was shown to be a possible biomarker for grass pollen due to its unique fluorescence peak at 670 nm (O'Connor et al., 2014). It is suggested that this biomarker could be used to specifically characterize grass pollen, as opposed to tree pollen, which does not give rise to the same signal (O'Connor et al., 2014). Therefore, to specifically detect chlorophyll-a fluorescence, an upgrade of the WIBS-4 was developed and termed the WIBS-4+. This instrument provides two additional fluorescence data channels, FL4 and FL5. The FL4 signals derive from the excitation of particles at 280 nm, while FL5 signals come from the excitation of particles at 370 nm. Potential emission from chlorophyll-a is recorded by a photomultiplier in the 600–750 nm range. Continuing the categorization system developed by Perring et al. the WIBS-4+ can additionally denote particles that fluoresce above the threshold in only one channel as either types D and E as well as A, B and C depending on the excitation and emission wavelengths of the particle, as indicated in Table 2.4 (Perring et al., 2015). This leads to an additional 21 categories, these consider each channel individually (FL1, FL2, FL3, FL4 and FL5), but also includes all possible combinations.

Table 2.4 Five basic fluorescent categorisations, when all possible combinations considered 28 categories exist.

Channel	Excitation (nm)	Emission (nm)
A	280	310–400
B	280	420–650
C	370	420–650
D	280	600-750
E	370	600-750

2.3 **MAS-100**

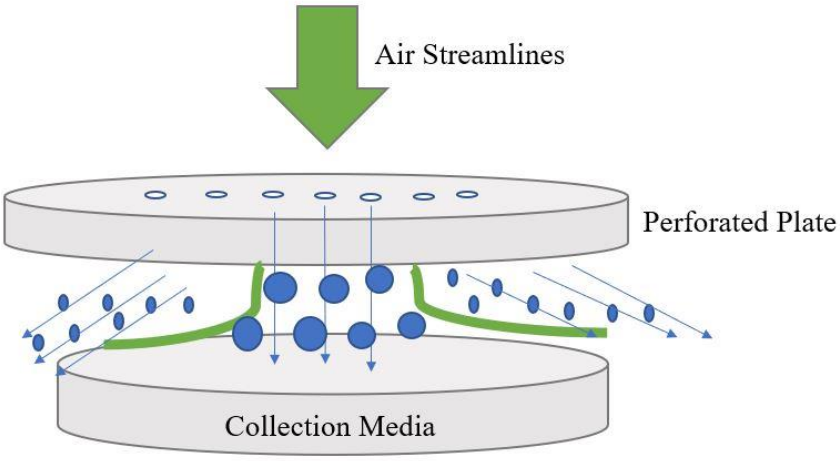

Figure 2.7 Particle airflow in the MAS-100 impactor.

A Microbial Air Monitoring system-100 (MAS-100) air sampler (MERCK, Darmstadt, Germany) was the impaction sampling apparatus used in the study. The MAS-100 is a sieve impaction sampler based on the Andersen impaction principles. Impactors use the inertia of the particle to assist collection. As air is passed through an array of nozzles to channel a jet of particle-laden air across a gap towards the collection media. Figure 2.7 the air flow (Green) of the jet will follow a set of streamlines through the sampler. As the collection media diverts the streamlines, with air flowing past the plate, particles with sufficiently low inertia will be carried by the streamlines, however particles with higher inertia will be collected.

Figure 2.8 MAS-100.

The MAS-100 consists of a single perforated plate with 400 holes, each with a diameter of 0.7 mm through which air is drawn at a rate of 10.8ms^{-1} and forced onto a solid culture plate. After passing through the airflow meter the sampling volume is then adjusted to 100 L/m^3. It has been broadly used within hospital settings, these have been described in Chapter 1, section 1.4.3.

For the ward study the MAS-100 was operated according to impaction principle, with an air intake of 100 L/min, with the impaction speed of 10.8 ms^{-1}, this velocity guarantees that all particles > 1 µm are collected (Meier and Zingre, 2000). The above mentioned characteristics allowed the sampler to collect microorganisms with diameter ≥1 µm, complying with ISO/CD 14698-1 "Cleanrooms and associated controlled environments – Biocontamination control" (STANDARD and ISO, 2003). The sampler head was thoroughly cleaned with 70% ethanol between samples. Since the low cut-off size of the sampler is ~1 µm, there is a likelihood that a sizable fraction of bacteria-containing particles <1 µm in diameter may be excluded from the sample. Thus, the impaction study results should be a lower limit of the bacterial numbers in air. Samples were collected ~1 m off the floor to simulate the breathing zone. Bacterial counts were assessed using tryptic soy agar (TSA) and fungal loads using Sabourauds Dextrose Agar (SDA) in 90 mm petri dishes and plates were incubated at 30 °C for 5 days. An independent, Irish National Accreditation Board (INAB) accredited

company, Curam Medical, provided the TSA and SDA for active air sampling and passive settle plate analysis. Collection, incubation and counting was performed by Curam Medical.

2.4 **Cyclonic Air Sampler**

Figure 2.9 Coriolis µ® main components.

The cyclone sampler Coriolis µ® (Bertin, Montigny le Bretonneux, France) was used as the impingement sampler. The Coriolis is based on a cyclone type operation, concentrating airborne biological particles, in the size range of 0.5 – 20 µm and concentrate them into a liquid sample. Air is first aspirated into the cone (pre-filled with collection fluid) in a whirling motion creating a vortex. Centrifugal force pulls the particles against the wall and separates them from air to be concentrated in the liquid, diagram of operating principle shown in Figure 2.9.

Figure 2.10 Operating principle of the Coriolis μ®.

Biological and physical efficiency of the Coriolis μ® are certified by an independent testing agency HPA (health Protection Agency, Porton Down, UK) corresponding to the standard requirements of ISO 14698-1 (Standard, 2003). According to the ISO 14698-1 standard this device has an impact speed high enough to allow capture of particle down to ~1 μm but low enough not to damage fragile viable particles. The optimal flow rate of the instrument is 300 L/min. So far, the Coriolis μ® has been mainly used in comparative studies, previously described in Chapter 1, section 1.4.5. Prior to sampling on the respiratory ward 10 ml of PBS with Triton X-100 0.005% was added to the sampling cone and screwed on to the sampler. The sampling time for all samples was 10 minutes with 300 L/min as the sampling volume flow rate. The samplers air flowing cane and air intake were thoroughly cleaned with 70% ethanol between samples. DNA was extracted using a Mobio Powersoil kit. V3/V4 region of 16S rRNA gene was amplified, Illumina Libraries prepared with Nextera ®XT DNA kit, sequenced by MiSeq (500 cycles) and metagenomic analysis by MG-RAST server.

2.5 **Footfall Counter**

Figure 2.11 IRC5716-NW Gazelle DualView IP Counter 60° Master Unit.

An IRC5716-NW Gazelle DualView IP Counter 60 ° Master Unit footfall counter (Axiomatic Technology, Nottingham, United Kingdom) was used to monitor activity i.e. footfall in and out of the respiratory ward and Cystic Fibrosis Outpatients Department (CFOPD) gym. The 19 x 11 cm unit contains imaging optics, sensors, signal processing and interfacing electronics. The sensor has a 60 ° opening angle allowing it to cover an area of 1.97 – 4.52 m^2 depending on mounting height.

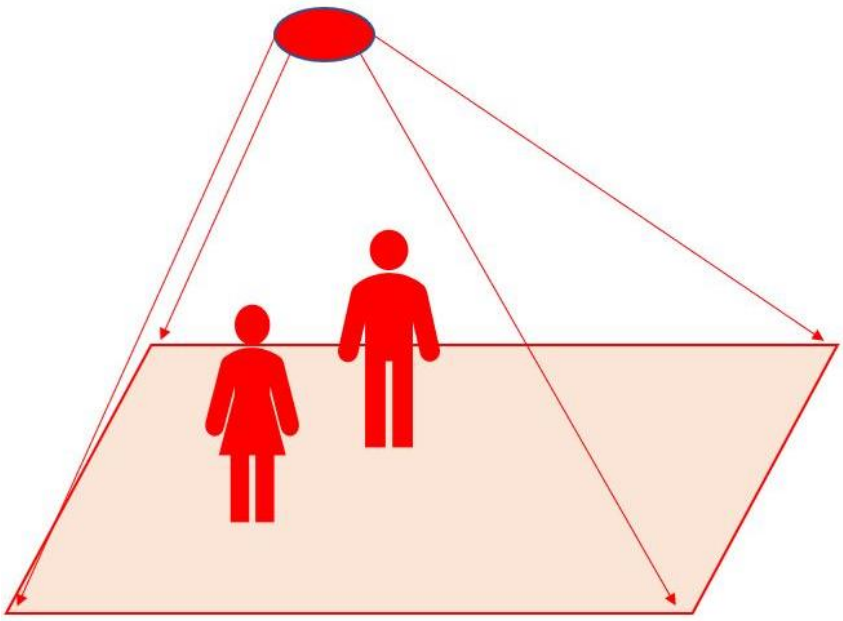

Figure 2.12 Sensor thermal image from footfall counter.

The sensors are designed to detect the heat emitted by people passing underneath it as infrared radiation, it uses this thermal image to differentiate between the floor and the

people passing under the counter Figure 2.12 The sensor measures people count based on this temperature difference. Brightness does not affect the people counter. It defines the entry and exit areas for people using two freely adjustable lines, making it possible to detect and count people going in and out. In the respiratory ward (Chapter 3) it was mounted at a height of 2.4m and 0.6m in from the door. Eight virtual counting lines were remotely defined by the Axiomatic operator using a portable PC setup tool, and people are counted as they pass each line, this is then summed for individual one-minute periods.

2.6 Statistical Analysis

All WIBS data was imported into MATLAB (Math Works Inc., USA) and processed further into appropriate files, subsets and matrices. They were then analysed with MATLAB and graphed using R Studio 1.1.383. Similarly, microbial data from the MAS-100 and settle plate testing were examined by Curam Medical and compiled into excel sheets which were then analysed and graphed by the author using R Studio 1.1.383.

2.7 References

CRAWFORD, I., ROBINSON, N., FLYNN, M., FOOT, V., GALLAGHER, M., HUFFMAN, J., STANLEY, W. & KAYE, P. H. 2014. Characterisation of bioaerosol emissions from a Colorado pine forest: results from the BEACHON-RoMBAS experiment. *Atmospheric Chemistry and Physics,* 14**,** 8559-8578.

FEENSTRA, B., PAPAPOSTOLOU, V., HASHEMINASSAB, S., ZHANG, H., DER BOGHOSSIAN, B., COCKER, D. & POLIDORI, A. 2019. Performance evaluation of twelve low-cost PM2. 5 sensors at an ambient air monitoring site. *Atmospheric Environment,* 216**,** 116946.

GABEY, A., GALLAGHER, M., WHITEHEAD, J., DORSEY, J., KAYE, P. H. & STANLEY, W. 2010. Measurements and comparison of primary biological aerosol above and below a tropical forest canopy using a dual channel fluorescence spectrometer. *Atmospheric Chemistry and Physics,* 10**,** 4453-4466.

GABEY, A., STANLEY, W., GALLAGHER, M. & KAYE, P. H. 2011. The fluorescence properties of aerosol larger than 0.8 μm in urban and tropical rainforest locations. *Atmospheric Chemistry and Physics,* 11**,** 5491-5504.

GABEY, A., VAITILINGOM, M., FRENEY, E., BOULON, J., SELLEGRI, K., GALLAGHER, M., CRAWFORD, I., ROBINSON, N., STANLEY, W. & KAYE, P. H. 2013. Observations of fluorescent and biological aerosol at a high-altitude site in central France. *Atmospheric Chemistry and Physics,* 13**,** 7415-7428.

HEALY, D., HUFFMAN, J., O'CONNOR, D., PÖHLKER, C., PÖSCHL, U. & SODEAU, J. 2014. Ambient measurements of biological aerosol particles near Killarney, Ireland: a comparison between real-time fluorescence and microscopy techniques. *Atmospheric Chemistry and Physics,* 14**,** 8055-8069.

HEALY, D. A., O'CONNOR, D. J., BURKE, A. M. & SODEAU, J. R. 2012a. A laboratory assessment of the Waveband Integrated Bioaerosol Sensor (WIBS-4) using individual samples of pollen and fungal spore material. *Atmospheric environment,* 60**,** 534-543.

HEALY, D. A., O'CONNOR, D. J. & SODEAU, J. R. 2012b. Measurement of the particle counting efficiency of the "Waveband Integrated Bioaerosol Sensor" model number 4 (WIBS-4). *Journal of Aerosol Science,* 47**,** 94-99.

HERNANDEZ, M., PERRING, A. E., MCCABE, K., KOK, G., GRANGER, G. & BAUMGARDNER, D. 2016. Chamber catalogues of optical and fluorescent signatures distinguish bioaerosol classes. *Atmospheric Measurement Techniques,* 9**,** 3283-3292.

HUFFMAN, J., SINHA, B., GARLAND, R., SNEE-POLLMANN, A., GUNTHE, S., ARTAXO, P., MARTIN, S., ANDREAE, M. & PÖSCHL, U. 2012. Size distributions and temporal variations of biological aerosol particles in the Amazon rainforest characterized by microscopy and real-time UV-APS fluorescence techniques during AMAZE-08. *Atmospheric Chemistry and Physics,* 12**,** 11997-12019.

KAYE, P. H., STANLEY, W. R. & FOOT, E. V. J. 2014. *Fluid-Borne Particle Detector*. US 13/957,655.

LI, J., MATTEWAL, S. K., PATEL, S. & BISWAS, P. Evaluation of Nine Low-cost-sensor-based Particulate Matter Monitors 29.

MEIER, R. & ZINGRE, H. 2000. Qualification of air sampler systems: the MAS-100. *Swiss Chem,* 7-15.

O'CONNOR, D. J., LOVERA, P., IACOPINO, D., O'RIORDAN, A., HEALY, D. A. & SODEAU, J. R. 2014. Using spectral analysis and fluorescence lifetimes to discriminate between grass and tree pollen for aerobiological applications. *Analytical Methods,* 6**,** 1633-1639.

O'CONNOR, D., HEALY, D. & SODEAU, J. 2015. A 1-month online monitoring campaign of ambient fungal spore concentrations in the harbour region of Cork, Ireland. *Aerobiologia***,** 1-20.

ORGANIZATION, W. H. 2010. WHO guidelines for indoor air quality: selected pollutants.

PERRING, A., SCHWARZ, J., BAUMGARDNER, D., HERNANDEZ, M., SPRACKLEN, D., HEALD, C., GAO, R., KOK, G., MCMEEKING, G. & MCQUAID, J. 2015. Airborne observations of regional variation in fluorescent aerosol across the United States. *Journal of Geophysical Research: Atmospheres,* 120**,** 1153-1170.

ROBINSON, E. S., GAO, R.-S., SCHWARZ, J. P., FAHEY, D. W. & PERRING, A. E. 2017. Fluorescence calibration method for single-particle aerosol fluorescence instruments. *Atmospheric Measurement Techniques,* 10**,** 1755.

ROBINSON, N. H., ALLAN, J., HUFFMAN, J., KAYE, P. H., FOOT, V. & GALLAGHER, M. 2013. Cluster analysis of WIBS single-particle bioaerosol data. *Atmospheric Measurement Techniques,* 6**,** 337.

SAVAGE, N., KRENTZ, C., KÖNEMANN, T., HAN, T. T., MAINELIS, G., PÖHLKER, C. & HUFFMAN, J. A. 2017. Systematic Characterization and Fluorescence Threshold Strategies for the Wideband Integrated Bioaerosol Sensor (WIBS) Using Size-Resolved Biological and Interfering Particles. *Atmos. Meas. Tech. Discuss.,* 2017**,** 1-41.

SINGER, B. & DELP, W. 2018. Response of consumer and research grade indoor air quality monitors to residential sources of fine particles. *Indoor air,* 28**,** 624-639.

STANDARD, B. & ISO, B. 2003. Cleanrooms and associated controlled environments—Biocontamination control—.

STANDARD, I. 2003. 14698-1 (2003), Cleanrooms and Associated Controlled Environments–Biocontamination Control Part 1: General Principals and Methods. *International Organization for Standardization, Geneva*.

STANLEY, W. R., KAYE, P. H., FOOT, V. E., BARRINGTON, S. J., GALLAGHER, M. & GABEY, A. 2011. Continuous bioaerosol monitoring in a tropical environment using a UV fluorescence particle spectrometer. *Atmospheric Science Letters,* 12**,** 195-199.

TECHNOLOGIES, D. M. 2014a. Wideband Integrated Bioaerosol Sensor (WIBS-4a) Operator Manual. USA: Droplet Measurement Technologies.

TECHNOLOGIES, D. M. 2014b. Wideband Integrated Bioaerosol Sensor (WIBS-4a) Operator Manual. USA: Droplet Measurement Technologies.

TOPRAK, E. & SCHNAITER, M. 2013. Fluorescent biological aerosol particles measured with the Waveband Integrated Bioaerosol Sensor WIBS-4: laboratory tests combined with a one year field study. *Atmospheric Chemistry and Physics,* 13**,** 225.

XIE, Y., FAJARDO, O. A., YAN, W., ZHAO, B. & JIANG, J. 2017. Six-day measurement of size-resolved indoor fluorescent bioaerosols of outdoor origin in an office. *Particuology,* 31**,** 161-169.

YU, X., WANG, Z., ZHANG, M., KUHN, U., XIE, Z., CHENG, Y., PÖSCHL, U. & SU, H. 2016. Ambient measurement of fluorescent aerosol particles with a WIBS in the Yangtze River Delta of China: potential impacts of combustion-related aerosol particles. *Atmospheric Chemistry and Physics,* 16**,** 11337-11348.

ZHOU, J., FANG, W., CAO, Q., YANG, L., CHANG, V. C. & NAZAROFF, W. W. 2017. Influence of moisturizer and relative humidity on human emissions of fluorescent biological aerosol particles. *Indoor Air,* 27**,** 587-598.

Chapter 3

The Effect of Plasma Treatment on Air Quality in a Hospital Ward Monitored by Conventional Culture and a Bioaerosol Detector

Table of Contents

3.1 Introduction

Unfortunately, nosocomial infections, or healthcare associated infections (HAI) are ubiquitous in public health. HAIs cause a persistent and significant threat to patients resulting in considerable morbidity and mortality to patients, while imposing a financial burden on healthcare trusts. The World Health Organisation (WHO) reports that HAI affect hundreds of millions of patients worldwide, and that 6-7 in every 100 patients will acquire at least one HAI (Allegranzi et al., 2017, Wałaszek et al., 2016). A retrospective review of the National Point Prevalence Surveys (PPS) carried out in 2012 using the Irish National Adverse Events Study (INAES) showed that HAI prevalence in Ireland was 6.1% , with an average of 10 additional bed days attributed to HAI adverse events, costing € 9400 per event, equating to an annual cost of € 121 million to the Irish healthcare system (Murchan et al., 2018). In England a £ 1 billion cost is attributed to HAI annually (Office, 2009, Health and Excellence, 2012). Data from the European Centre for Disease Prevention and Control (ECDC), show on any given day in Europe ~ 80,000 patients will develop at least one HAI, the most frequent of which is lower respiratory tract infection (23.4%) (Prevention et al., 2013). Resulting in 16,000,000 extra days of hospital stay while contributing directly to 37,000 and indirectly to 110,000 deaths annually, consequently costing the economy ~£ 7 billion (Prevention et al., 2013). HAIs have continued to be transmitted despite the implementation of infection control policies (Siegel, 2007, Assiri et al., 2013, Wilson et al., 2016).

Although there are many routes to infection spread, airborne transport is among the most significant from an infection control point of view. This has been emphasized by three airborne epidemics and an airborne pandemic in the last 20 years, the severe acute respiratory syndrome (SARS) pandemic in 2003 (Roy and Milton, 2004), the 2009 H1N1 influenza pandemic (Lau et al., 2009), and the 2014 Middle East respiratory syndrome (MERS) epidemic (Kutter et al., 2018).

Aerobiology plays a fundamental role in the transmission of infectious diseases thus poor indoor air quality (IAQ) can significantly contribute to the prevalence of HAI, with all respiratory pathogens having the potential to cause HAIs (Lim et al., 2010, Warfel et al., 2012, Azimi and Stephens, 2013, Kowalski, 2016, Ijaz et al., 2016,

Kowalski, 2007). Varying proportions of HAI have been ascribed to airborne transmission, some suggest it is responsible for 10-20% of endemic HAI (Brachman, 1971), 20-24% of post-operative wound infections (Kundsin, 1980) and a third of all HAIs (Kowalski, 2007). The role of aerosol or airborne transmission has been well documented with air sampling techniques. Both culture and molecular methods have been utilised for the detection of bacteria, in particular the sensitive and rapid detection of *M. tuberculosis* using filter/real-time quantitative polymerase chain reaction (qPCR) techniques (Mastorides et al., 1999, Chen and Li, 2005, Vadrot et al., 2004) and the detection of viable *M. tuberculosis* aerosols using Anderson cascade air samplers (Tobias et al., 2005, Fennelly et al., 2004).

Although hospitals are subject to similar infectious challenges common to all indoor environments like offices and commercial buildings, a distinguishing factor comes in the form of their high-density populations of potentially contagious and immunocompromised occupants (Fernstrom and Goldblatt, 2013). It is recognised that many nosocomial pathogens e.g. *methicillin-resistant Staphylococcus* (MRSA) (Layton et al., 1993, Bures et al., 2000, Sexton et al., 2006), c*arbapenem-resistant Enterobacteriaceae* (CRE) (Goodman et al., 2016, Kotsanas et al., 2013), *Aspergillus* (Anaissie et al., 2002, Haiduven, 2009, O'Gorman, 2011), *Legionella* (Muder et al., 1983, Streifel, 1996, Cassier et al., 2013) etc. have an environmental reservoir within the hospital setting. Although the mechanism of acquisition from the environment is not consistently clear, it is well documented that MRSA (Shiomori et al., 2002), *Legionella* (Cassier et al., 2013) and *Aspergillus* (O'Gorman, 2011) are disseminated via aerial routes in the clinical environment.

Numerous human activities have been linked with processes which instigate the production and introduction of droplets with potentially infectious contents into indoor air;

- Expiratory activities – breathing, speaking, coughing, sneezing etc (aerosol generation by wind shear force)
- Using water utilities – showering, tap water, toilets (potentially atomise infectious bioaerosols within water supply or in plumbing systems)
- Wet-cleaning of indoor surfaces

The above processes generate aerosols of distinctive characteristics regarding size and initial speed. These two characteristics are critically important for the fate of aerosolised particles in air, for example the distance an aerosol travels, change in size as a function of temperature and relative humidity along with survival and location deposition (Morawska et al., 2009, Morawska, 2006, Lindsley et al., 2012, Lindsley et al., 2015, Gerba et al., 1975, Xie et al., 2009, Stelzer-Braid et al., 2009, Barker and Jones, 2005, Tang et al., 2006).

Hospitals have made efforts to reduce the disturbance/generation of deposited/settled particles during cleaning. Surfaces are routinely cleaned, or cleaned and disinfected, according to predetermined cleaning protocols (hourly, daily, weekly, etc.) or when surfaces appear dirty, instances of spillages, and always post patient discharge (May and Pitt, 2012, Siani and Maillard, 2015). Cleaning is a key control factor for outbreaks of norovirus, Vancomycin-resistant enterococci (VRE), *C. difficile*, MRSA, etc (Dancer, 2009, Dancer, 2011, Davies, 2010). MRSA is known to resist desiccation and can survive in hospital dust for up to a year (Wagenvoort et al., 2000), thus it is imperative that cleaning efficiently removes these particles and does not contribute to their dispersal. A cleaning manual by the Health Service Executive (HSE) supports the application of the Irish Health Services Accreditation Board (IHSAB) Hygiene Services Standards by providing guidance in the area of environmental cleanliness (National Hospitals, 2005). It recommends that scrubbing machine tanks are emptied and decontaminated daily, vacuum cleaners should be fitted with filters to minimise bacterial air contamination, and damp dusting and wet cleaning should be used to reduce bacterial air dispersal (National Hospitals, 2005).

Historically, conventional airborne microorganism levels have been studied in parts of the hospital environment where patient contamination by organisms transmitted from others or the environment was recognised to be harmful, such as operating theatres (Verde et al., 2015, Ortiz et al., 2009, Scaltriti et al., 2007). Empirical airborne microorganism standards for operating theatres have been developed (Health/Estates and Division, 2007). Limited standards for airborne microorganisms exist for other hospital areas, but monitoring data has been reported from hospital rooms (Ortiz et al., 2009), hospital clean rooms (Li and Hou, 2003), a pneumological ward (Augustowska and Dutkiewicz, 2006), an emergency service (Verde et al., 2015), surgical wards

(Verde et al., 2015, Asif et al., 2018), intensive care units (ICU) (Dougall et al., 2019) and maternity wards (Ortiz et al., 2009) .Some real-time monitoring of hospital bioaerosols has been reported, including a study of a respiratory ward at St James's University Hospital in Leeds, United Kingdom and in several settings within two hospitals in Brisbane, Australia (Roberts et al., 2006, Pereira et al., 2017).

Filtration, the physical removal of particulates from air, is the foremost step in attaining acceptable indoor air quality. To improve air quality without renovating the existing heating, hospital ventilating, and air-conditioning (HVAC) system, the system may be augmented by a "portable air cleaner". The Centre for Disease Control and Prevention (CDC) recognises portable, industrial-grade, HEPA (High Efficiency Particle Air / Arrestance) filtration devices as a supplemental means of increasing the effective number of air changes per hour (ACH) in controlled environments (Chinn and Sehulster, 2003). Many air treatment devices have been developed to remove biological particles from hospital air in addition to HEPA filters (First, 1998, Qian et al., 2010), including nanofiber mats (Wang et al., 2013), UV irradiation (Lin and Li, 2002), cold plasma (Kapustina and Volodina, 2004) and electrostatic air filtering (ES) (Zhuang et al., 2000). However, objective evaluation of their efficacy has been difficult to determine (von Vogelsang et al., 2018, Balikhin et al., 2016, Obee et al., 2016, Fox, 1994).

The current study relates to a four-bedded bay in an adult respiratory ward at Cork University Hospital. The ward is ventilated by a heat recovery ventilation system with a HEPA filtered unit delivering 12 air changes per hour. Because of the nature of the ward, many patients receive nebulised drug therapy three or more times per day. Preliminary observations with a bioaerosol detector (Wideband Integrated Bioaerosol Sensor, described below) found great variability in biological particle numbers (defined as particles less than 10 microns in diameter fluorescing when excited at wavelengths typical of tryptophan or NADPH-associated fluorescence) from second to second during the day. Aggregate data summed over 15 minutes in observations taken over a week suggested an underlying diurnal pattern to particle counts.

Bioaerosol generation procedures relating to ward footfall and noted ward events were assessed using the WIBS, culture and footfall counter counts. Because the ward had

been refurbished with various antimicrobial devices, including plasma air treatment, which had not yet been activated it was decided to test the effect of activating the plasma air treatment. The effect on particle counts using the WIBS device and bacterial numbers cultured using conventional air and surface sampling would be assessed. A period of at least 14 days observations without plasma treatment was to be compared with a period of at least 14 days treatment with plasma treatment. Preliminary studies had revealed no significant day to day differences in WIBS counts

3.2 Methods

3.2.1 Instrumentation

Several instruments were utilised throughout this study, locations marked in Figure 3.1. Below is a brief description of each instrument.

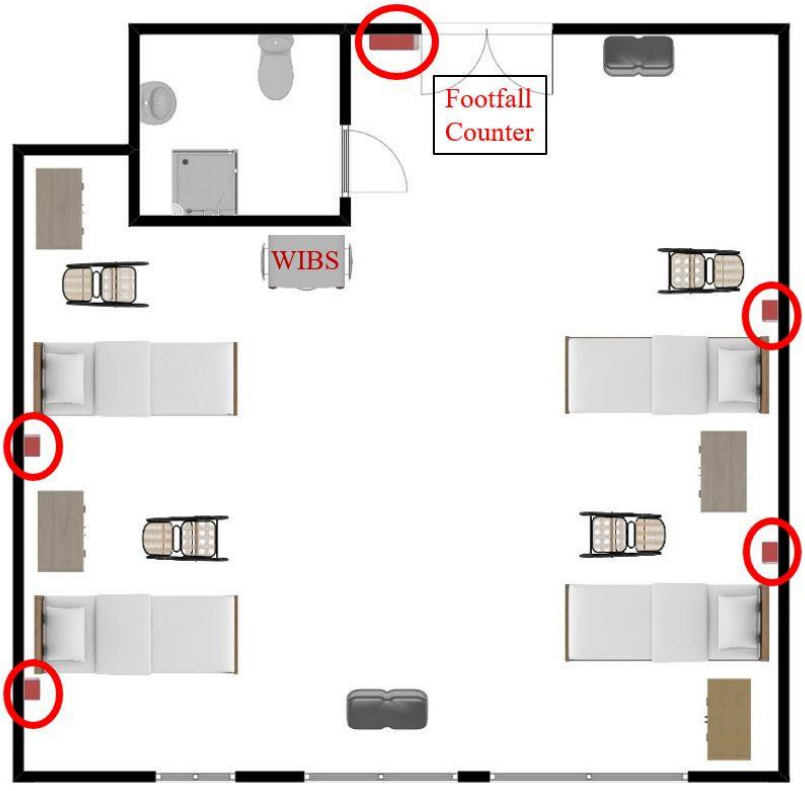

Figure 3.1 Schematic of respiratory ward. Plasma disinfection units circled in red. Footfall counter on ceiling in front of door

3.2.2 Wideband Integrated Bioaerosol Sensor

Real-time airborne particle data was recorded using a Wideband Integrated Bioaerosol Sensor-4a (Droplet Measurement Technologies, Boulder, Colorado, USA). The

Wideband Integrated Bioaerosol Sensor (WIBS) is a single aerosol particle fluorescence monitor that uses light-induced fluorescence (LIF) to detect fluorescent aerosol particles (FAP) in real-time. It provides particle size (0.5-12 µm), shape and fluorescent intensity in 3 channels. Initial detection of the particle is made using a continuous-wave red diode laser at 635 nm that illuminates the particles flowing into the optical chamber. Scattering of the laser light is used for both the sizing of particles (based on Mie theory) and to determine a basic particle "shape" using a so-called asymmetry factor (AF). The fluorescence characteristics of the individual particles are then interrogated using two xenon flash lamps (Xe_1, Xe_2). These are tuned to excite at the maxima absorption wavelengths of the biofluorophores tryptophan (280 nm) and NAD(P)H (370 nm). Fluorescence emission following these excitation pulses is detected in two detector bands: 310–400 nm (Band I) and 420–650 nm (Band II) (Healy et al., 2012). More details on the operation of the WIBS-4a are provided by Kaye et al. (Kaye et al., 2014), Fennelly et al. (Fennelly et al., 2017) and in section 2.1.1. The categorisation system of Perring *et al.* was used to categorise particles.

3.2.3 Airnode AirVisual

AirVisual Airnode (IQAir China, Beijing, China) is a low-cost, portable, continuous light scattering laser air quality monitor that uses artificial intelligence in combination with a particulate matter ($PM_{2.5}$) laser sensor to measure and predict air pollution. AirNode detects $PM_{2.5}$ along with CO_2, temperature and relative humidity levels in the environment. AirNode operation was described in section 2.2 The Airnode device was only available for the 2-weeks of the campaign where the plasma disinfection unit was on. Data was downloaded via local Wi-Fi network using devices SAMBA protocol.

3.2.4 Microbial plate samples

Impaction and settle plate samples were taken during twice daily visits to the ward over 4 weeks Monday – Friday. Samples were taken at 2 timepoints 11:30 and 13:00 (times which preliminary WIBS observation suggested provided different particle counts). A Microbial Air Monitoring system-100 (MAS-100) air sampler (MERCK, Darmstadt, Germany) with a sampling head of 400 holes × 0.7 mm was the impaction sampling apparatus used in the study. The MAS is a sieve impaction sampler based on

the Andersen impaction principles. The operation principles of the MAS-100 and plate collection procedure were previously discussed in section 2.3.

3.2.5 Impingement

The cyclone sampler Coriolis μ® (Bertin, Montigny le Bretonneux, France) was used as the impingement sampler. The Coriolis μ® operation and DNA extraction methods were earlier described in section 2.4.

3.2.6 Swab Samples

Figure 3.2 Swab Sampling sites. (A) Top of patient locker, (B) Top of patient electrical unit and (C) Top of Isolation room door.

Cotton swabs were used, and swabbing was carried out at sites indicated in Figure 3.2. The specific sites were chosen as they are not sites that were normally cleaned on a daily basis, hence surface counts would probably not be influences by regular

cleaning. The swab tip was wetted in sterile water and run over the entire 10 cm^2 swab site horizontally, vertically, and diagonally before streaked out onto TSA and SDA plates horizontally and vertically. Plates were then incubated at 30 °C for 5 days.

3.2.7 Footfall Counter

An Irisys Gazelle footfall counter (Axiomatic Technology, Nottingham, United Kingdom) was used to monitor ward activity i.e. footfall in and out of the ward. The sensors are described in detail in section 2.5

3.2.8 Plasma disinfection unit

The plasma disinfection unit used in this study was an air treatment device comprised of an electrostatic precipitator and a plasma generator. This unit captures airborne contaminants and generates a plasma discharge field to effectively sterilise air contaminants. Electrostatic precipitators have been used exclusively as highly efficient filtration devices in the removal of fine particles from a flowing gas using the force of an induced electrostatic charge, while minimally impeding the flow of gases through the unit (Deane et al., 2016). Other units have used plasma radicals for sterilisation of air filter mediums, where plasma discharge generates active radicals which flow upstream to a medium filter and inactivate any bacteria or viruses trapped by the filter. Essentially the electrostatic precipitator charges airborne particle within its proximity and immediately directs them to an inactivation zone created by the plasma generator. The airborne particles are directed between the electrostatic precipitator and the plasma activation zone by a voltage applied between them. Plasma generators are effective in inactivating airborne viruses (Nishikawa and Nojima, 2003, Wu et al., 2015) and bacteria (Lai et al., 2016). The plasma generator in this unit creates an inactivation zone where plasma is released and inactivates airborne pollutant material. The airborne material may be subdivided into 3 groups (i) airborne pathogens, (ii) airborne allergens and (iii) airborne volatile organic compounds (VOC). A detailed description of the unit and its operations are provided by Deane et al. (Deane et al., 2015, Deane et al., 2016).

3.3 Statistical Analysis

The WIBS-4A records raw data as CSV files on a directly connected laptop which was accessible remotely via a Wi-Fi connection. A single CSV file records a maximum of 30,000 particles or up to a maximum duration of 3 hrs. During the four-week measurement period (15th March 2018 – 26th April 2018) a total of 2502 raw Excel files were collected. 2-weeks of observations were collected when the air purifying device was turned off (15th March – 3rd April 18) and 2-weeks collected when the air purifier device was turned on (4th– 26th April 18). The data were imported into MATLAB (Math Works Inc., USA) and processed further into appropriate files, subsets and matrices. They were then analysed with MATLAB and graphed using R Studio 1.1.383.

3.3.1 Statistical Analysis

All p-values were calculated using appropriate statistical tests (t-test for parametric data and Mann-Whitney U for non-parametric), the significance of the p-values was found using the benjamini-hochberg method, this is a less stringent method than Bonferroni and is used to control the false discovery rate.

3.4 Results

3.4.1 Colony forming units (CFU) from air samples, swabs and fluorescent particle concentrations at two sampling time points during different plasma disinfection unit operations.

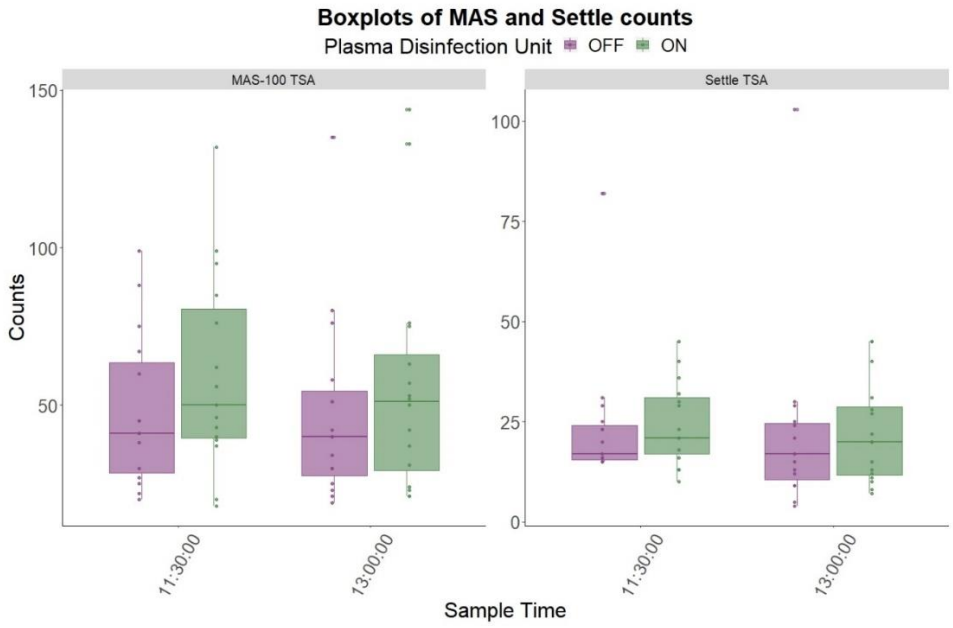

Figure 3.3 Boxplots of MAS-100 (left) and Settle Plate (right) samples taken at two Sampling Times. Each panel is split into the two-sample period 11:30 (left) and 13:00(right). Boxplots coloured by plasma disinfection unit operation on (green) and off (purple).

Results (Table 3.1) showed no significant difference in CFU/m^3 for the MAS-100 (P=0.34, P=0.45) or settle plate (P=0.43, P=0.53) samples for either the 11:30 or the 13:00 sampling intervals between the plasma treatment and control non-treatment period. Although an insignificant difference the CFU mean, Table 3.1, and median, boxplots Figure 3.3, increased during the plasma disinfection period for MAS-100 and settle plate samples.

Table 3.1 Summary statistics for MAS-100 and settle plate samples with p-values calculated between plasma disinfection period and control period.

Sample	Time	N	On		Off		P-value
			CFU				
			Mean ± sd	5th - 95th	Mean ± sd	5th - 95th	
MAS-100*	11:30:00	20	509 ± 368	189 - 927	507 ± 284	209 - 941	0.34
	13:00:00		629 ± 439	210 - 1391	526 ± 273	199 - 1103	0.45
Settle**	11:30:00	20	25 ± 10	12.1 - 42	24 ± 17	15 - 46	0.43
	13:00:00		23 ± 13	7.7 - 45	22 ± 24	4.7 - 52	0.53

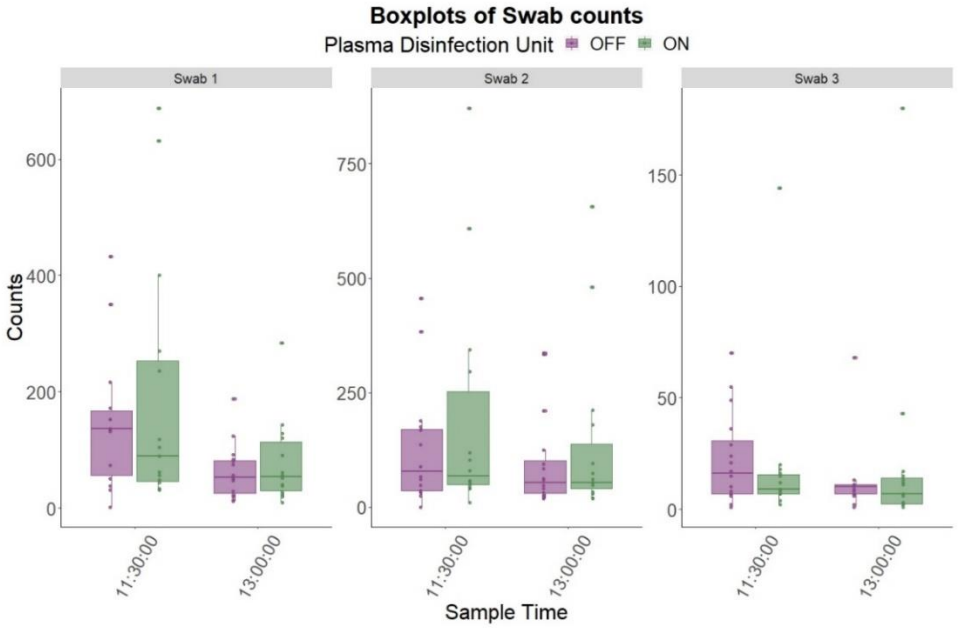

Figure 3.4 Boxplots of swab samples taken at 3 different areas at 2 sampling times swab 1 (left) swab 2 (middle) and swab 3 (right). Each panel is split into the two-sample period 11:30 (left) and 13:00(right). Boxplots coloured by plasma disinfection unit operation on (green) and off (purple).

Like the MAS-100 and settle plate samples, the swab samples taken at 3 different areas showed no significant difference for either sampling intervals between the plasma disinfection and control non-treatment period. The swabs taken within the ward (swab 1 and swab 2) resulted in higher CFU/m^3 than the swab 3 sample. This is due to the sample are for swab 3 being consistently cleaned, whereas swab site for swab 1 and swab 2 were not consistently cleaned. recorded means, Table 3.2, and medians, boxplots Figure 3.4, for swab 1 and swab 2 were higher at 11:30 than 13:00, suggesting

that the overnight accumulation was collected with the first 11:30 sample. However, this not observed for swab 3, again due to consistent cleaning by staff.

Table 3.2 Summary statistics for swab samples with p-values calculated between plasma disinfection period and control period.

Sample	Time	N	On		Off		p-value
			CFU/m^3				
			Mean ± sd	5th - 95th	Mean ± sd	5th - 95th	
Swab 1	11:30:00	20	190 ± 211	31 - 649	148 ± 116	21 - 379	0.81
	13:00:00		78 ± 70	17 192	63 ± 46	13 - 143	0.743
Swab 2	11:30:00		195 ± 247	29 - 700	124 ± 125	35 - 46	0.662
	13:00:00		138 ± 180	20 - 533	96 ± 102	20 - 335	0.621
Swab 3	11:30:00		19 ± 34	3 - 57	22 ± 20	2 - 59	0.302
	13:00:00		21 ± 44	2 - 84	13 ± 16	2 - 35	0.945

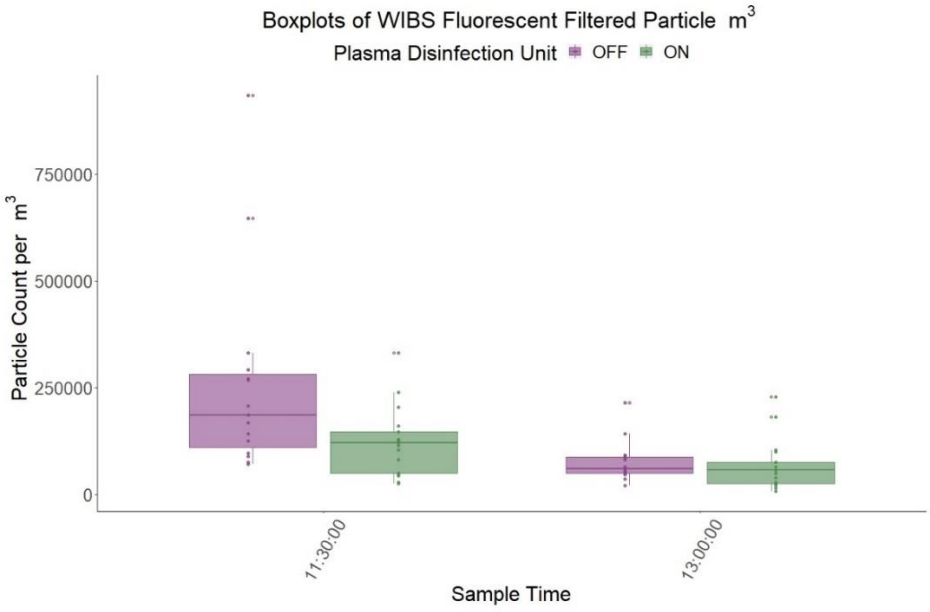

Figure 3.5 Boxplots of WIBS fluorescent filtered counts taken at 3 different areas at 2 sampling times. Panel is split into the two-sample period 11:30 (left) and 13:00 (right). Boxplots coloured by plasma disinfection unit operation on (green) and off (purple).

Analysing WIBS fluorescent filtered counts made at the two time points used for culture-based samples, 11:30 and 13:00, no significant difference was observed in fluorescent filtered particles counts for the two periods. From Figure 3.5 and Table 3.3 both periods displayed decreases in particle counts. When the plasma disinfection unit

system was on the time period of 11:30 demonstrated a significant decrease of 1.38×10^6 particles per m^3 between the plasma disinfection and control non-treatment period (P=0.02). A lower decrease was observed at the 13:00 interval with fluorescent filtered counts reducing by 9×10^4 particles per m^3.

Table 3.3 Summary statistics for swab samples with p-values calculated between plasma disinfection period and control period.

Sample	Time	N	On		Off		p-value
			Particles / m^3 ($\times10^6$)				
			Mean ± sd	5th - 95th	Mean ± sd	5th - 95th	
WIBS	11:30:00	20	1.22 ± 0.86	0.29 - 2.58	2.60 ± 2.37	0.74 - 7.33	0.02
	13:00:00		0.67 ± 0.59	0.13-1.91	0.76 ± 0.48	0.31 - 1.64	0.77

Using two sampling time intervals no sampling method observed a significant difference in either CFU nor particle counts between a 2-week control period and a 2-week period using air disinfection units. This indicates that the plasma disinfection units have no effect on biological particles during those sampling intervals.

3.5 Correlations between air samples, swabs and WIBS counts.

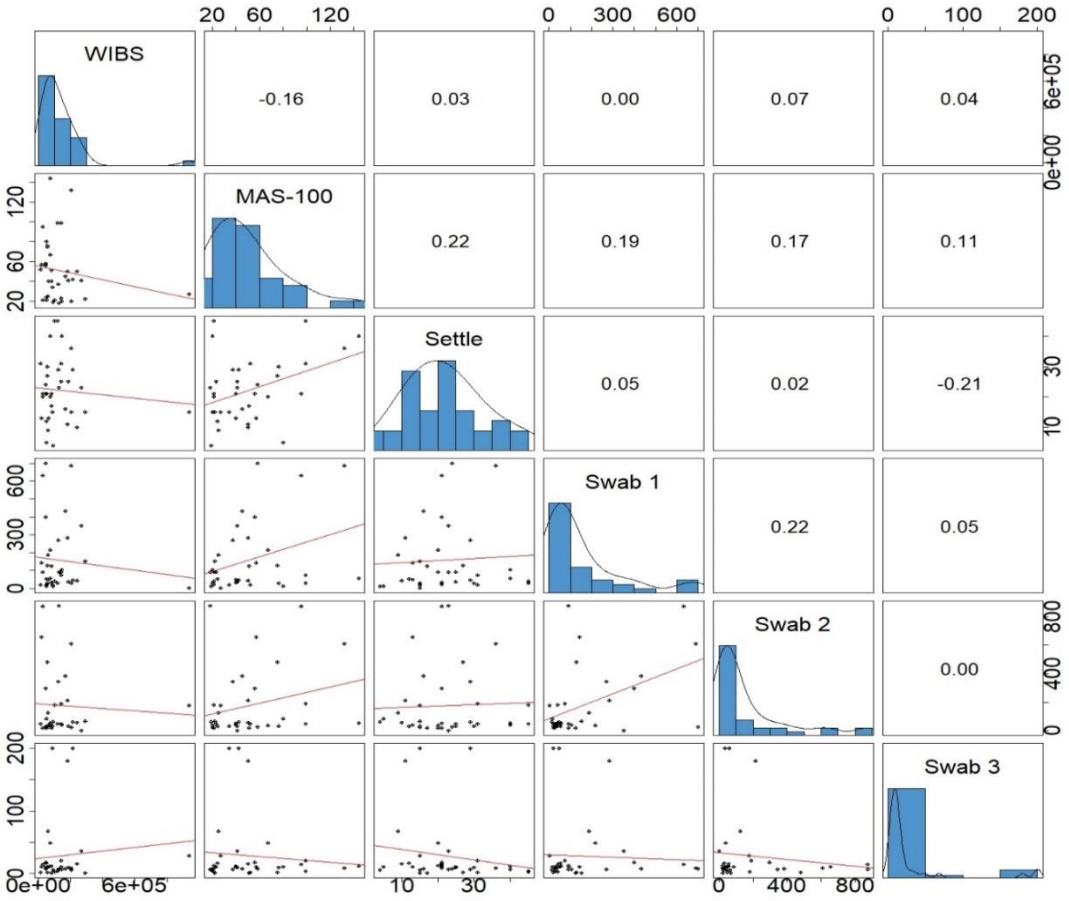

Figure 3.6 Spearman correlation matrix of conventional samples and fluorescent filtered WIBS counts.

A correlation matrix is a table showing correlation coefficients between variables. The above correlation matrix shows correlation coefficients between the WIBS fluorescent particle counts and the five conventional tests. The line of going from the top left to the bottom right is the main diagonal, which shows each variables histogram distribution. Each cell in the bottom half of the table shows the scatterplot between two variables and each cell in the top half represents the spearman correlation coefficient between two variables. This matrix is symmetrical, with the correlation shown above the main diagonal being a correlation of those scatterplots below the main diagonal. Stars over correlations would represent different statistical significance i.e. * $P < 0.05$, ** $P < 0.01$ and ***$P<0.001$.

Figure 3.6 shows the correlation matrix for the conventional counts and WIBS fluorescent filtered particle counts. No statistically significant correlation exists between any of the counts (no asterisks present over any correlation coefficient). However, some weak spearman rank correlations exist between the MAS-100 and Settle plate samples ($r(36) = +0.22$, $P > 0.05$), and between Swab 1 and Swab 2 ($r(36)= +0.22$, $P > 0.05$).

The lack of correlation between any sampling method would suggest that sampling at two time points is not enough in gathering information on specific environments. This may have an impact on analysing air treatment devices, whereby two sampling periods may not be enough to accurately determine a devices efficiency in improving air quality.

3.6 **Coriolis Sampling**

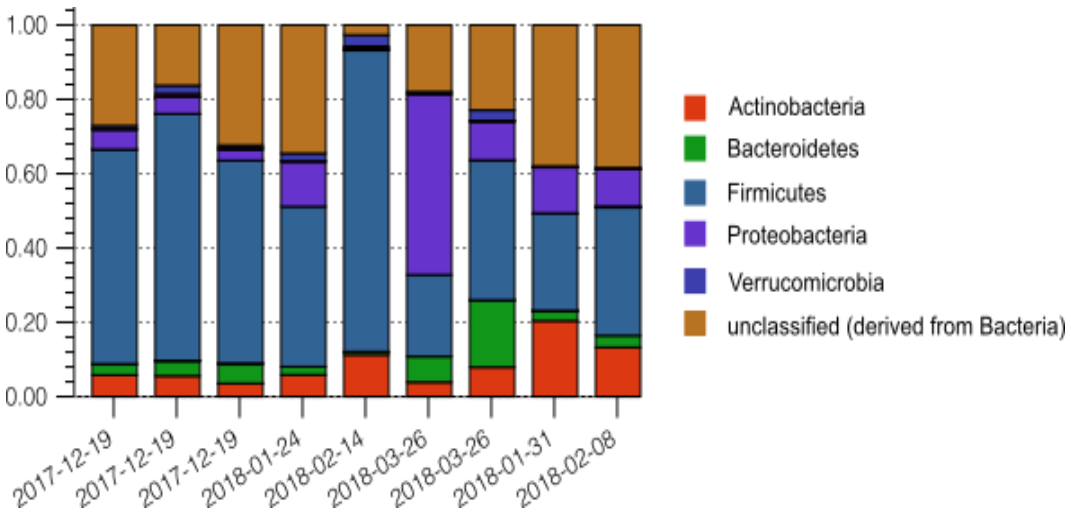

Figure 3.7 Phyla quantification from DNA sampling

For 8 out of 9 air DNA samples taken on six separate days over three months on the ward the largest single group at Phylum level were *Firmicutes*. Most belonged to *Clostridiaceae*/*Clostridiales* Families. *Actinobacteria* formed the next commonest phylum in 5/9 samples, comprising common gastrointestinal species and *Micrococcaceae*. *Proteobacteria* (72-99% *Gammaproteobacteria*) were the second commonest phylum in 4 samples with a low DNA content and the commonest attributable phylum in a sequenced negative control sample.

A large portion of the Coriolis air sample sequences belonged to the phyla *Firmicutes*, *Bacteroidetes*, *Actinobacteria* and *Bacteroidetes*. Both *Firmicutes* and *Bacteroidetes* are commonly associated with the human gut (Claesson et al., 2009, Ismail et al., 2011, Armougom et al., 2009). It has been suggested that indirect airborne faecal contamination may occur through toilet flushing (Best et al., 2012, Aithinne et al., 2019). Considering the ward has a communal toilet which facilitates the four patients it is possible that the aerosols generated within this toilet are escaping and rescinding in the ward air.

3.7 WIBS-4A particle concentrations observations

3.7.1 Overall fluorescent particle counts

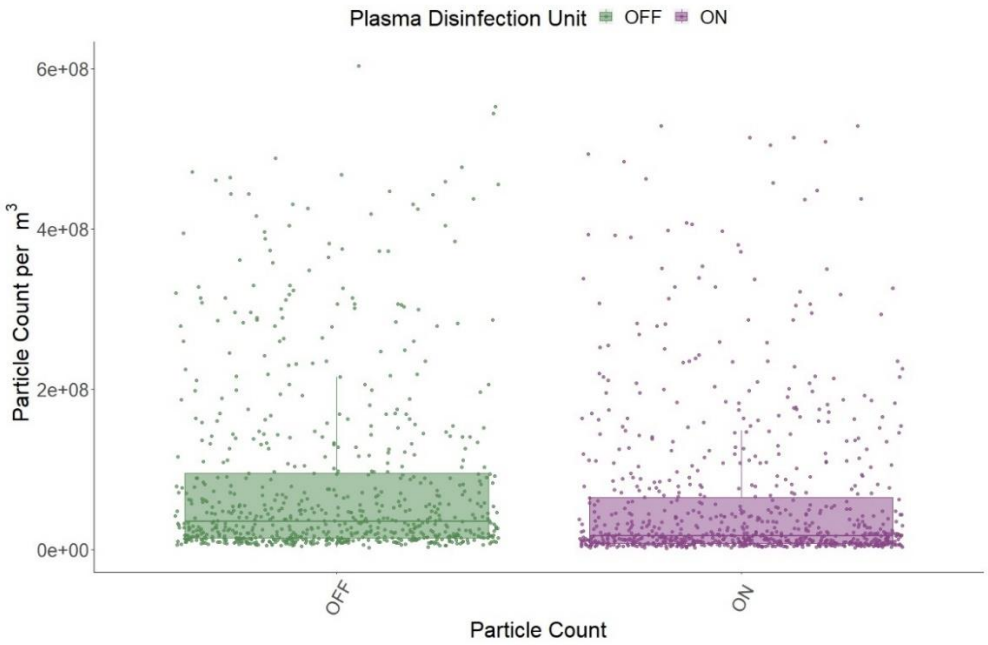

Figure 3.8 Boxplots of unfiltered fluorescent particle counts. Dots represent a single thirty-minute period (summed), all half hour periods over the campaign shown. Boxplots coloured by plasma disinfection unit operation on (green) and off (purple). A summed period refers to all time points within that period added together to get a concentration observed for the full period i.e. thirty-minute summed period refers to summing up of all thirty-minute interval concentrations for that period.

A significant difference ($P < 0.01$), (Table 3.4), was found between total fluorescent particle counts obtained when the plasma disinfection units activated, and the control

period, Figure 3.8. A significant decrease was observed for fluorescent particle counts over different time intervals, Table 3.4. Significant reduction of ~ 4.5×10^7 particles/m^3, 2.3×10^7 particles/m^3 and 0.8×10^6 particles/m^3 were observed with air disinfection unit in operation for hour, thirty-minute and minute intervals, respectively.

Table 3.4 Summary statistics for time-interval summed fluorescent counts with p-values calculated between air disinfection period and control period.

Time Interval	Particle type	On		Off		p-value
		$\times10^6$ particles / m^3				
		Mean ± sd	5th - 95th	Mean ± sd	5th - 95th	
Hour	Fluorescent	120.9 ± 2.0	9.0 - 473.5	166.3 ± 2.0	16.1 - 574.4	<0.01
Thirty-minute		60.5 ± 1.6	4.2 – 283.1	83.4 ± 1.5	7.6 - 349.3	<0.01
Minute		2.0 ± 3.7	0.1- 10.7	2.8 ± 4.1	0.2 - 12.7	<0.01

As explained in the materials and method chapter particle “shape” is determined using a so-called asymmetry factor (AF). Essentially it is determined from the azimuthal distribution of forward scattered light, the scattered light falls on a quadrant PMT detector where the scattering pattern of the particle is sampled at four angular offsets. For each of the scatter intensities that are recorded by the quadrants, the root-mean-square variation around the mean value outputs produces a numerical value between 0–100 AF units, with 0 being a perfect sphere and 100 denoting long rod-like fibrous particles.

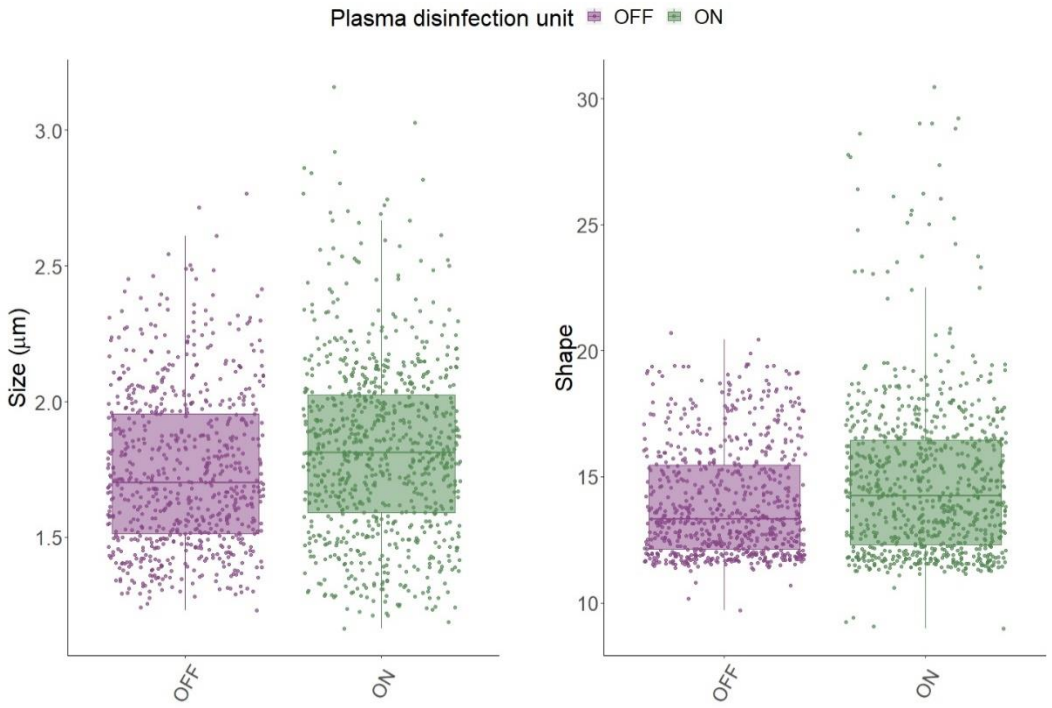

Figure 3.9 Boxplots of unfiltered fluorescent particle size (µm) (left) and shape (right). Dots represent a single thirty-minute period (mean), all half hour periods over the campaign shown. Boxplots coloured by plasma disinfection unit operation on (green) and off (purple).

Both the overall thirty-minute unfiltered fluorescent particle size (µm) and shape means were significantly increased during the plasma disinfection unit phase compared to the control phase (Figure 3.9). The operation of the plasma disinfection units was associated with an increase in particle size (µm) (1.74 ± 0.35 µm to 1.82 ± 0.44 µm, $P<0.01$), Table 3.5. Similarly, the overall hourly average fluorescent particle shape (sphericity) significantly increased (14.00 ± 2.41 to 14.80 ± 3.49, $P<0.01$) with the air disinfection units on (Table 3.5). Examining Figures 3.9, higher variation i.e. larger boxplot range, is noted during times of nebulisation therapy for both particle size (µm) and shape.

Table 3.5 Summary statistics for fluorescent particle size (µm) and shape with p-values calculated between air disinfection period and control period.

Particle Type	Characteristic	On		Off		p-value
		Mean ± sd	5^{th} - 95^{th}	Mean ± sd	5^{th} - 95^{th}	
Fluorescent	Size (µm)	1.82 ± 0.44	1.26 - 2.59	1.74 ± 0.35	1.32 - 2.40	<0.01
	Shape	14.80 ± 3.49	11.32 - 20.50	14.00 ± 2.41	11.51 - 18.8	<0.01

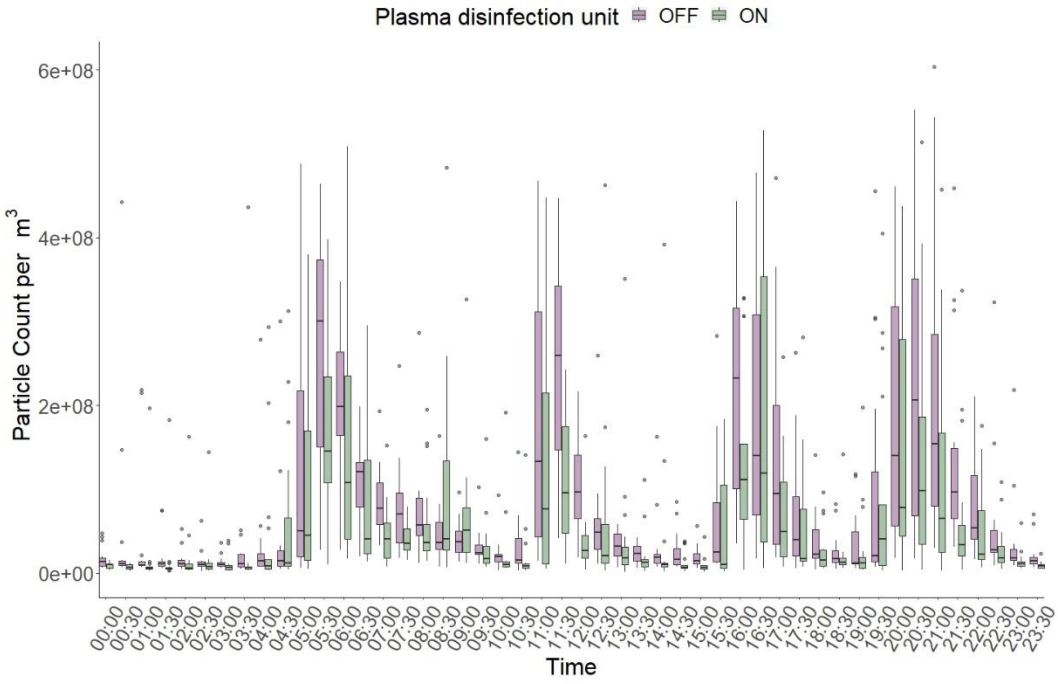

Figure 3.10 Boxplots of thirty-minute summed fluorescent particle counts. Boxplots coloured by plasma disinfection unit operation on (green) and off (purple).

Majority of half hourly diurnal counts presented lower mean fluorescent counts when plasma disinfection was in operation (Figure 3.10). Previously, section 3.4.1, considering all periods (minute, half hourly or hourly) a statistically significant ($P<0.01$) reduction is observed for particle counts with the plasma disinfection unit in operation. But only seven out of 48 individual half hour time period showed a statistically significant reduction in fluorescent filtered particles counts with plasma disinfection unit in operation compared to the control period. Of the seven, five were early morning / late night periods (00:00-01:30, 23:00-23:30) and two at mid-day (12:00 and 15:00)

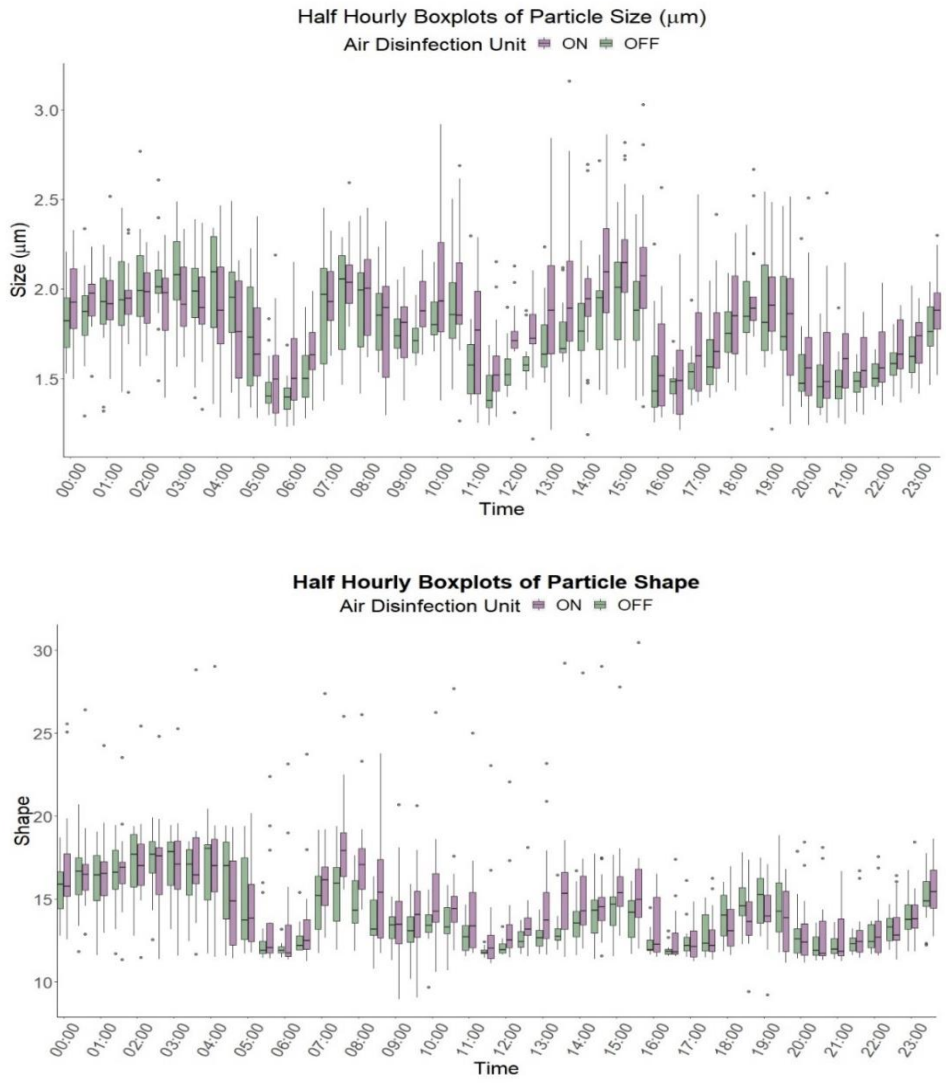

Figure 3.11 Thirty-minute mean boxplots of fluorescent particle size (µm) and shape. Boxplots coloured by plasma disinfection unit operation on (green) and off (purple).

From the half hourly mean timeseries boxplots (Figure 3.11) the approximate nebulisation times, ~05:00, 11:00, 16:00, and 20:00, the mass of nebulised aerosols released correspond to an immediate decrease in size (µm) and shape (dip going towards zero, increase in sphericity).

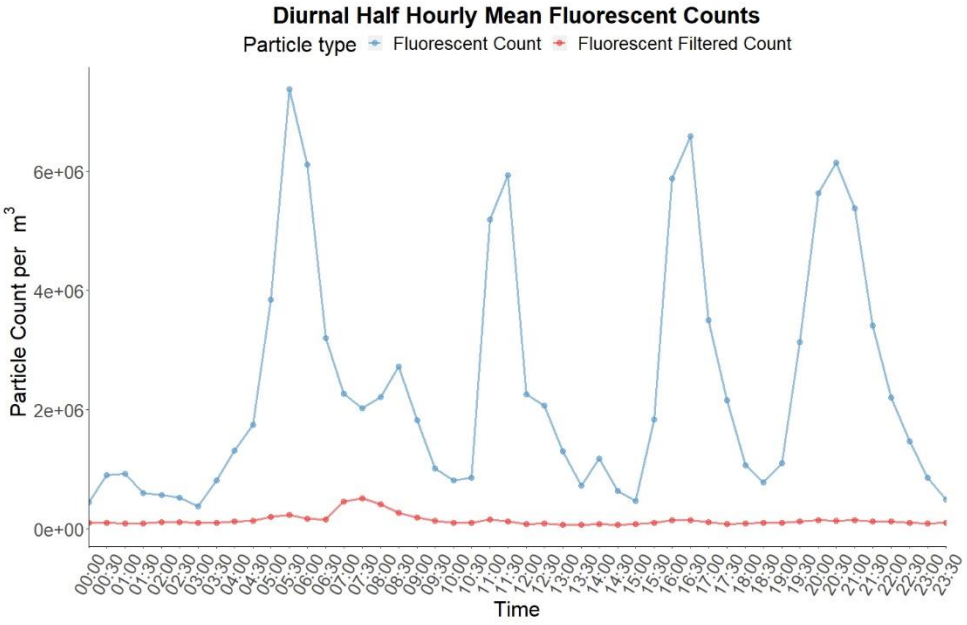

Figure 3.12 Diurnal line graph of thirty-minute mean fluorescent (blue) and fluorescent filtered (red) particle counts per m^3.

The raw fluorescent particle counts, Figure 3.12, from the WIBS device showed large intermittent particle showers. When these were analysed on a diurnal plot of 15-minute (or longer) rolling averages, they resolved into four daily particle peaks) with a trough from 00:00-04:00, (Figure 3.12). It was noted that these diurnal peaks, shown in Figure 3.12, coincided with known times of nebulised drug administration on the ward, which could give rise to fluorescent airborne particles. Compared to the nocturnal baseline (counts over the period of 00:00-04:00), peaks from nebulisation therapy leads to an average 29550% increase in fluorescent particle count, based on 30-minute summed intervals, when the plasma treatment device was on and a 21195% increase with the unit powered off.

Air chamber experiments (Chapter 4) were carried out with WIBS and the nebulised drugs used on the ward to obtain characteristic fluorescent drug particle fingerprints. This data was used in signal processing of the raw WIBS counts to remove particles with signals compatible with being nebulised drugs, counts processed in this way were designated as filtered counts. Figure 3.13 shows signal filtered particle counts (red) on the same scale as the fluorescent unfiltered (blue). When comparing fluorescent with

fluorescent filtered particle concentrations over the same time periods, nebuliser usage led to a 1564% (×~15.5) increase in hourly average particle concentration.

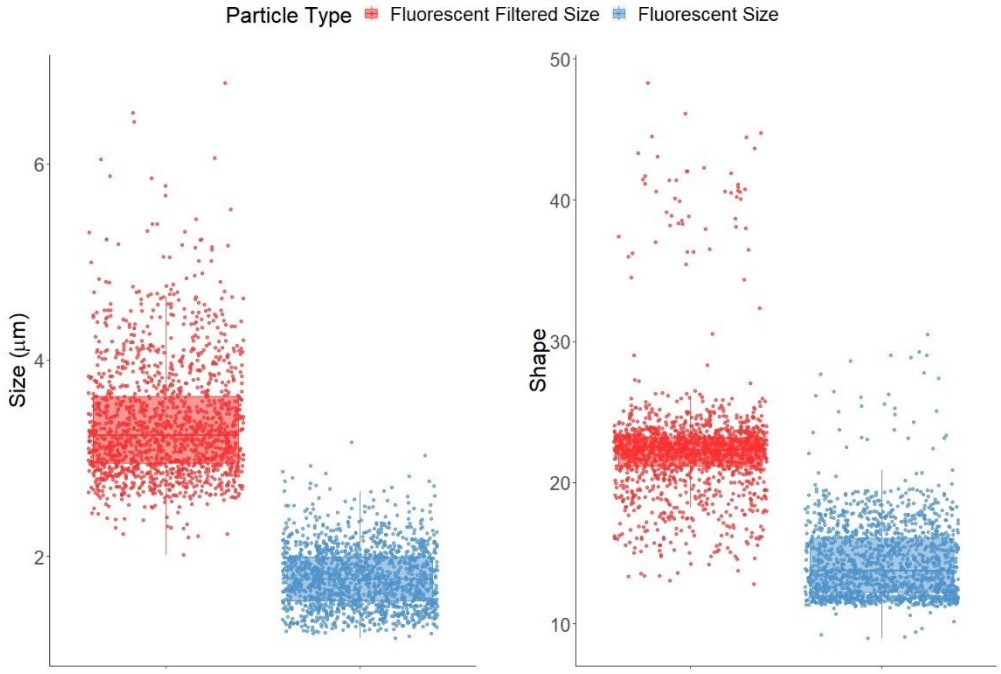

Figure 3.13 Jitter boxplots of half hour mean fluorescent filtered (Blue) and filtered (Red) particle size (µm) (left) and shape (right).

The raw fluorescent particles (blue) were significantly smaller than the filtered fluorescent particles (red) (1.78 ± 0.40 µm vs 3.36 ± 1.19 µm, $p < 0.01$) (Figure 3.13, Table 3.6). Similarly, as with size (µm), the fluorescent filtered particles shape displayed less sphericity than the fluorescent unfiltered particles which more spherical (14.42 ± 3. 06 vs 22.40 ± 5.44, $p< 0.01$) (Figure 3.13, Table 3.6)

Table 3.6 Summary statistics for fluorescent particle size (µm) and shape with p-values calculated between fluorescent and fluorescent filtered particles.

Characteristic	Type	Mean ± sd	5th - 95th	p-value
Size (µm)	Fluorescent	1.78 ± 0.40	1.29 - 2.5	<0.01
	Fluorescent Filtered	3.36 ± 1.19	2.12 - 5.5	
Shape	Fluorescent	14.42 ± 3.06	11.40 - 19.63	<0.01
	Fluorescent Filtered	22.40 ± 5.44	14.85 - 31.47	

3.7.2 Overall fluorescent filtered counts

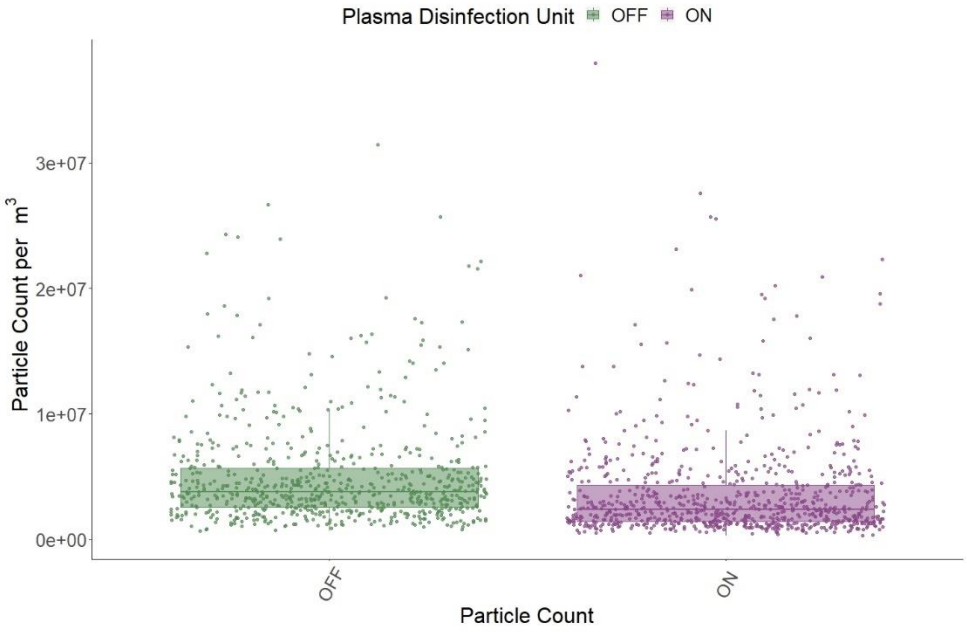

Figure 3.14 Boxplots of unfiltered fluorescent particle counts. Dots represent a single thirty-minute period (summed), all half hour periods over the campaign shown. Boxplots coloured by plasma disinfection unit operation on (green) and off (purple).

A significant difference ($P < 0.01$), (Table 3.7), was found between total fluorescent filtered particle counts obtained when the plasma disinfection units activated, and the control period. A significant decrease was observed for fluorescent filtered particle counts over different time intervals, Table 3.7. When compared to the control period the plasma disinfection period oversaw significant reduction of ~ 2.6×10^6 particles/m^3, 1.3×10^6 particles/m^3 and 5×10^4 particles/m^3 were observed with air disinfection unit in operation for hour, thirty-minute and minute intervals respectively.

Table 3.7 Summary statistics for time-interval summed fluorescent filtered counts with p-values calculated between air disinfection period and control period.

Time Interval	Particle type	On		Off		p-value
		$\times10^6$ particles / m^3				
		Mean ± sd	5th - 95th	Mean ± sd	5th - 95th	
Hour	Fluorescent Filtered	7.27 ± 0.06	1.88 - 19	9.86 ± 0.07	2.86 - 26.4	<0.01
Thirty-minute		3.63 ± 0.05	0.85 - 10.7	4.95 ± 0.06	1.35 - 13.4	<0.01
Minute		0.121 ± 0.15	0.02 - 0.39	0.17 ± 0.16	0.038 - 0.47	<0.01

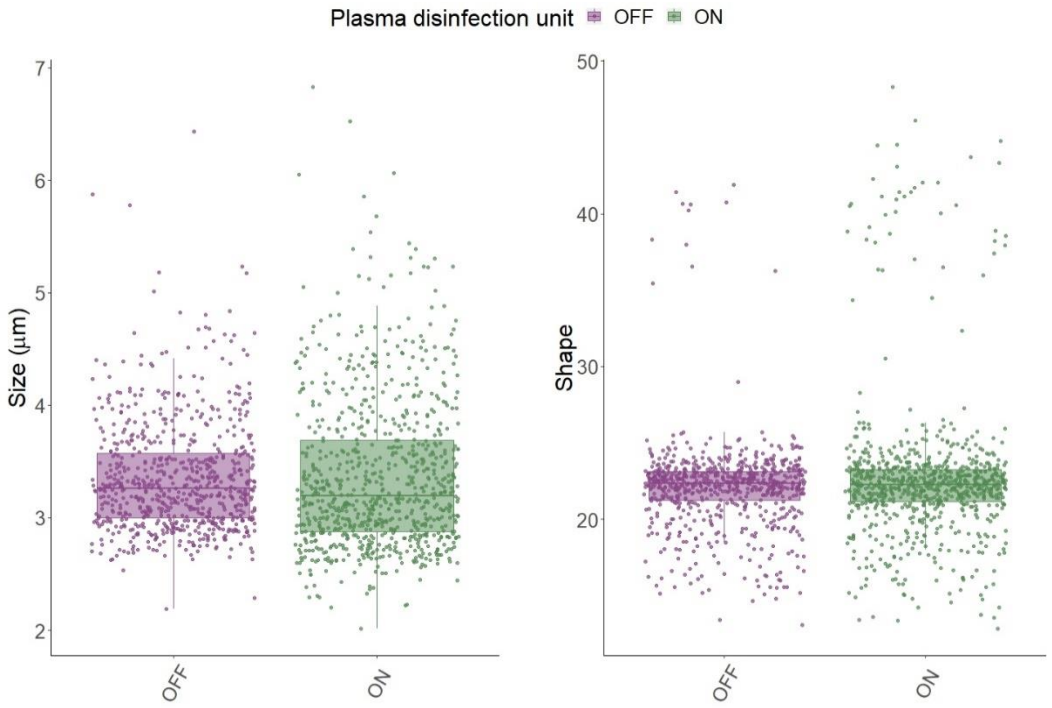

Figure 3.15 Boxplots of fluorescent filtered particle size (µm) (left) and shape (right). Dots represent a single thirty-minute period (mean), all half hour periods over the campaign shown. Boxplots coloured by plasma disinfection unit operation on (green) and off (purple).

During the operation of the plasma disinfection unit the overall hourly average fluorescent filtered particle size (µm) was not significantly different from the control period (3.36 ± 1.37 to 3.36 ± 0.96, P = 0.3), Figure 3.15. Similarly, the particle shape did not differ significantly during plasma operation (22.69 ± 6.29 to 22.08 ± 4.27, P=0.05) (Table 3.8).

Table 3.8 Summary statistics for thirty-minute mean fluorescent filtered particle size (µm) and shape with p-values calculated between air disinfection period and control period.

Particle Type	Characteristic	On		Off		p-value
		Mean ± sd	5^{th} - 95^{th}	Mean ± sd	5^{th} - 95^{th}	
Fluorescent Filtered	Size (µm)	3.36 ± 1.37	2.03 - 5.92	3.36 ± 0.96	2.28 - 5.1	0.3
	Shape	22.69 ± 6.29	14.36 - 35.17	22.08 ± 4.27	15.39 - 28.32	0.05

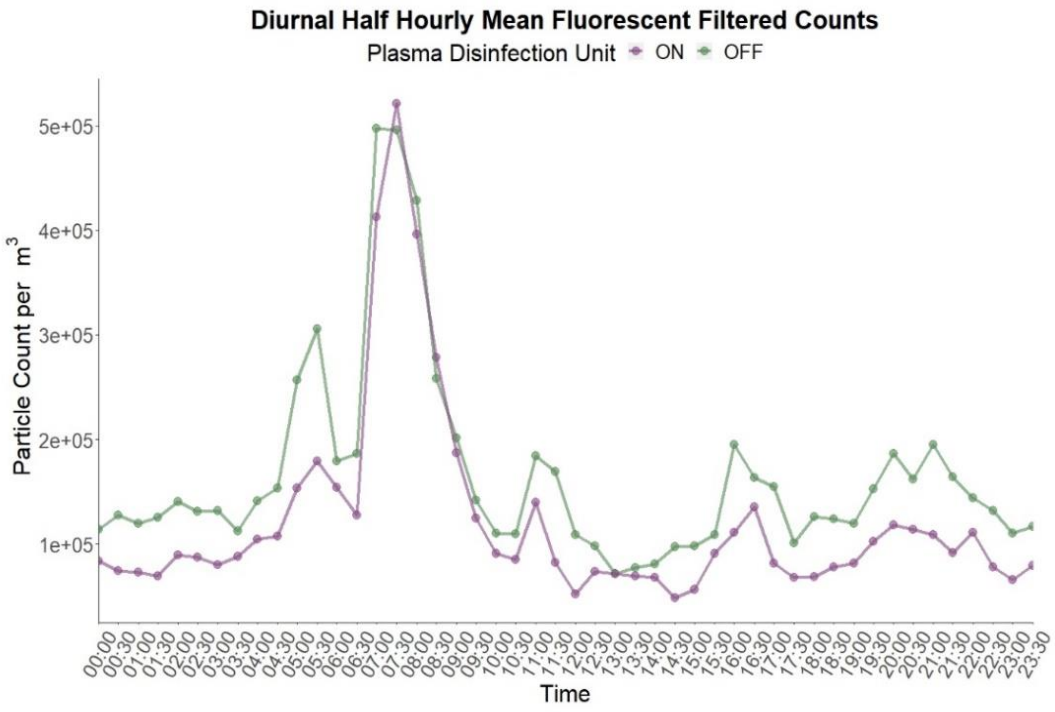

Figure 3.16 Diurnal line graph of thirty-minute mean fluorescent filtered particle counts per m^3. Line and points coloured by plasma disinfection unit operation on (green) and off (purple).

Diurnal plotting of filtered counts showed one major daily peak 07:00-08:30, (Figure 3.16), this period will be discussed further in section 3.5.3. Yet less prominent peaks at early morning (05:00), mid-morning (11:00) and afternoon (16:00) indicate that some nebuliser related particles remained, and that filtering did not eradicate all nebuliser particles from the fluorescent filtered data set.

The fluorescent (Table 3.4) and fluorescent filtered particles per m^3 (Table 3.7) observations showed significant ($P<0.01$) reduction in particles per m^3 with plasma disinfection unit in operation when compared to the control period. The data collected in both tables shows the large variation in particles per m^3 that can occur in minute periods, for example the 5^{th} to 95^{th} percentile range for fluorescent filtered counts per m^3 differed by 4.5×10^5. This would again indicate the inadequacy of the conventional sampling methods for measuring difference in air quality, where the WIBS can examine 100,000's of time points with relative ease conventional sampling cannot severely limiting its ability to accurately access air purification devices.

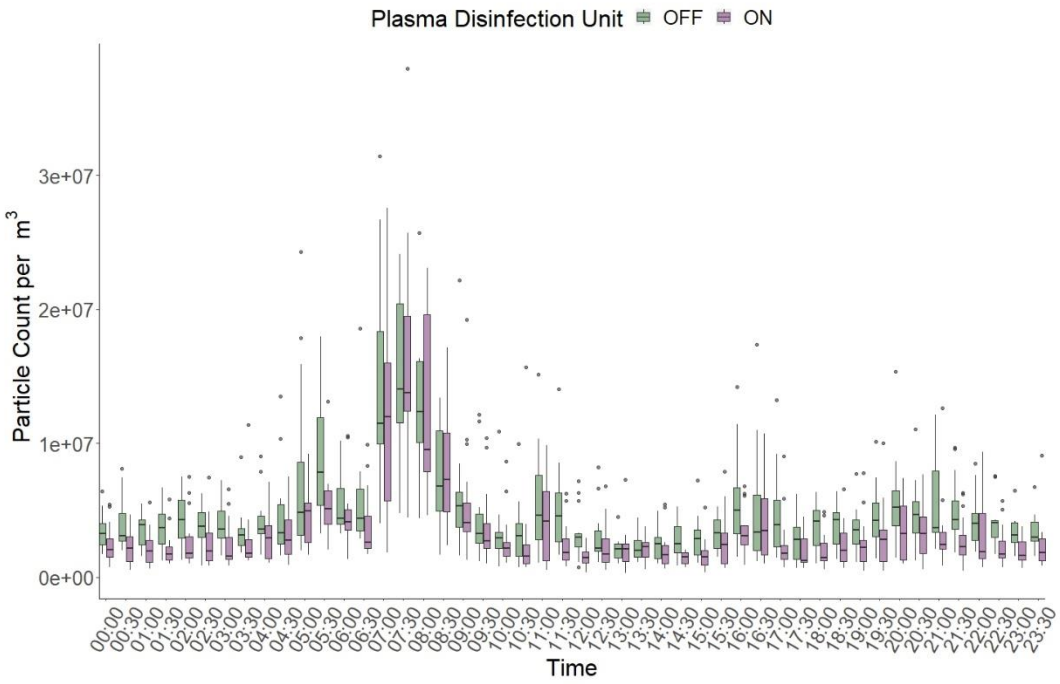

Figure 3.17 Boxplots of thirty-minute summed filtered fluorescent particle counts. Boxplots coloured by plasma disinfection unit operation on (green) and off (purple).

Nearly all half hourly diurnal counts showed lower mean filtered fluorescent counts when plasma disinfection was in operation (Figure 3.17). As stated previously, section 3.4.2, in all periods measured (minute, half hourly or hourly) a statistically significant ($P<0.01$) reduction in particle counts with the plasma disinfection unit in operation was noted. However, as with fluorescent particle counts (Figure 3.10), the underlying fluorescent filtered particle counts within these time periods are highly variable, subsequently looking at each half hour time periods individually (Figure 3.17) all but 2 half hourly diurnal counts, 07:00-07:30 and 08:30-09:00, presented lower mean filtered fluorescent counts when plasma disinfection was in operation. And interestingly no individual half hour time period showed a statistically significant reduction in fluorescent filtered particles counts with plasma disinfection unit in operation compared to the control period.

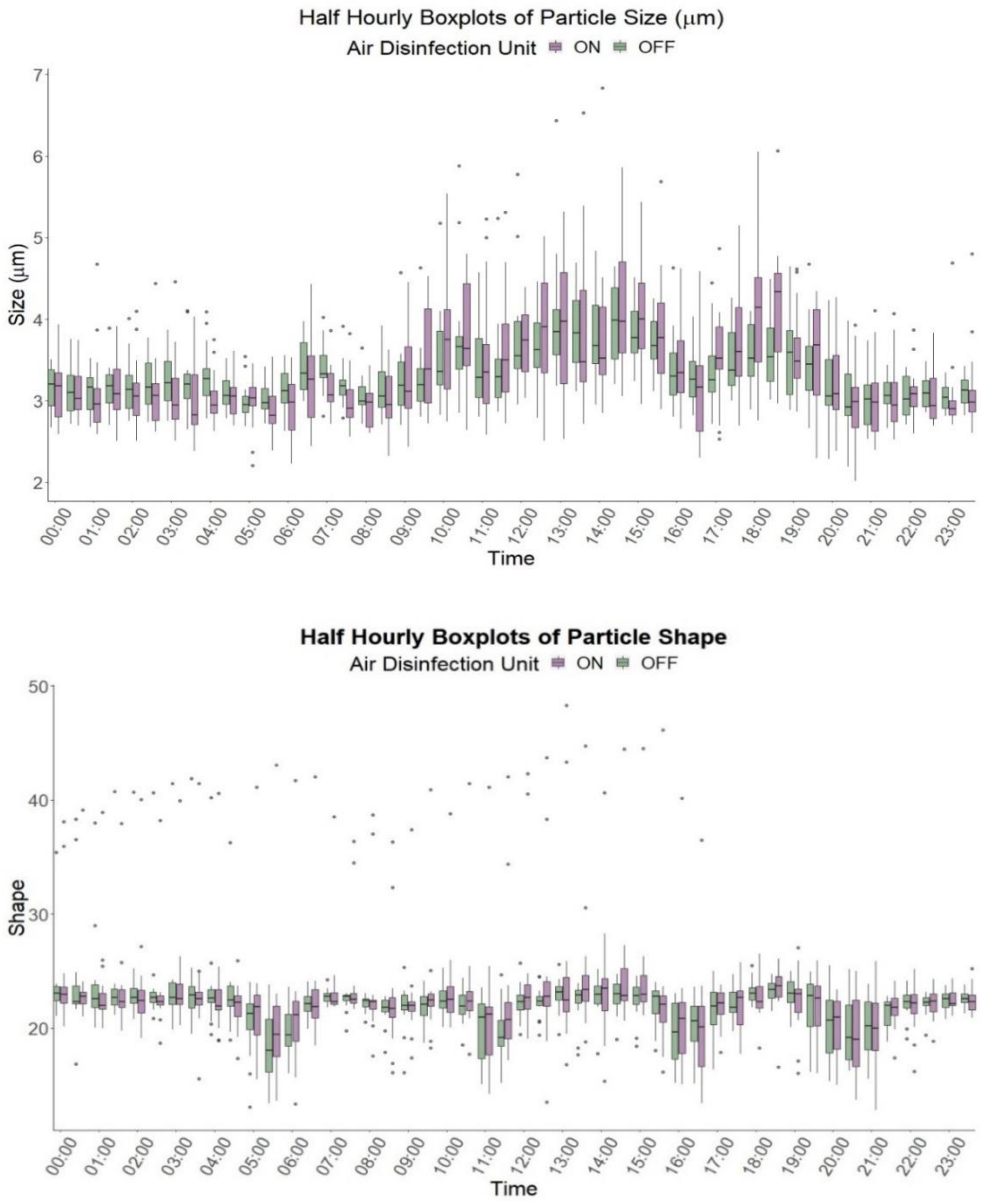

Figure 3.18 Thirty-minute mean boxplots of fluorescent filtered particle size (µm) (top) and shape (bottom). Boxplots coloured by plasma disinfection unit operation on (green) and off (purple).

From Figure 3.18, the size is lowest during the night-time period between 00:00-04:00, however from 09:00-20:00 the particle size (µm) increases, this suggests two things; the increase in footfall stimulates the resuspension of larger particles that may have settled on surfaces or larger particles are transported in by footfall and emitted from occupants. However, from both characteristics in Figure 3.18, there are troughs in size (µm) and shape during nebulisation therapy where nebuliser particles are still being considered fluorescent post-thresholding.

3.8 Effect of plasma disinfection unit on the percentage of Total particles showing a filtered fluorescent signal

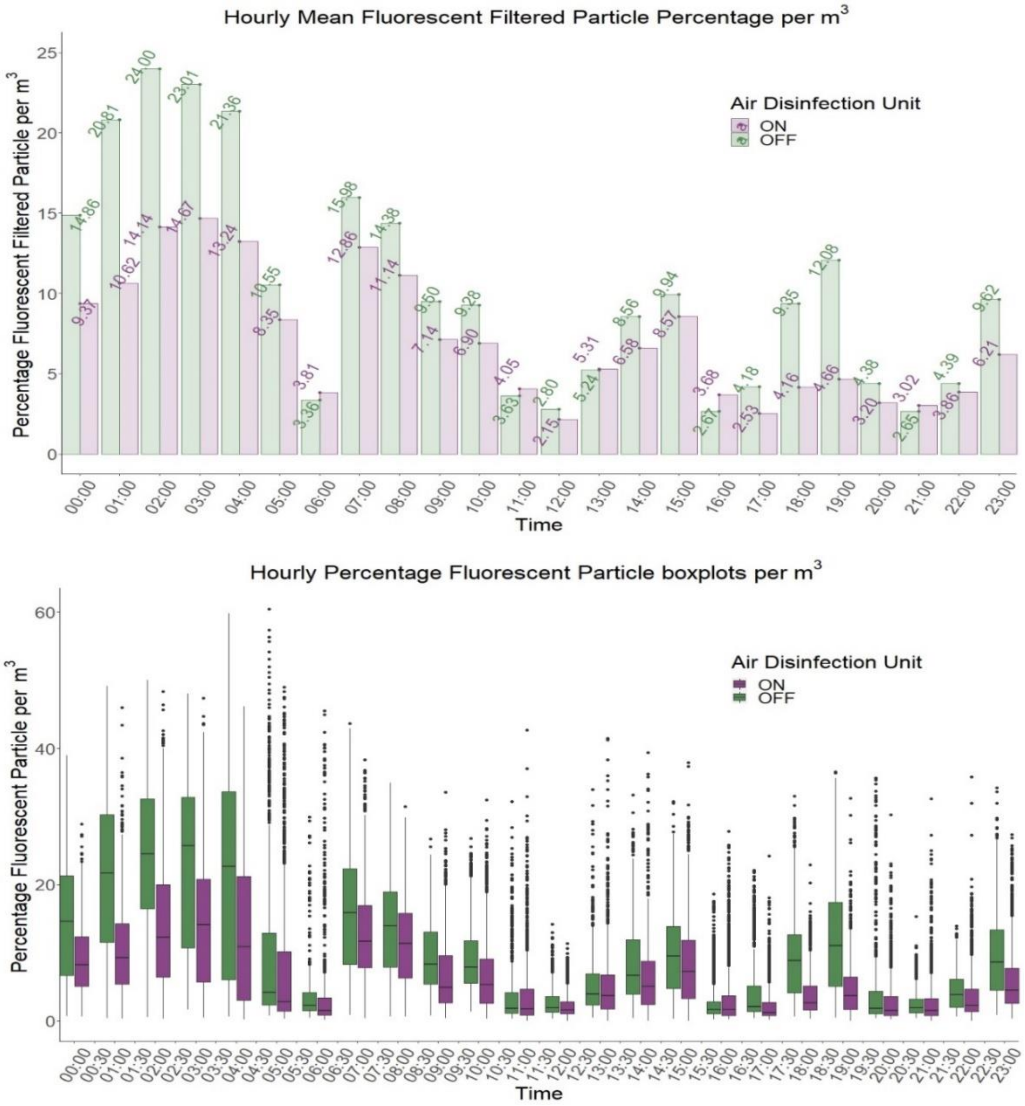

Figure 3.19 (Top) Hourly percentage filtered fluorescent particle bar graph with the plasma disinfection units ON and OFF. (Bottom) Hourly percentage filtered fluorescent particle boxplots with the plasma disinfection units ON and OFF.

The percentage of total particles showing a filtered fluorescent signal varies greatly throughout the day, Figure 3.19, highest observed in the early morning, 00:00 – 04:30, and lower during the day, 07:00-23:00. Operation of the plasma disinfection units was associated with a significant decrease in the percentage of aerosol particles showing a filtered fluorescent signal ($P < 0.01$) over all one, thirty- and sixty-minute intervals.

3.9 Effect of plasma disinfection unit on aerosol peaks

3.9.1 Unfiltered fluorescent peaks (Nebuliser related)

Nebulised drug particle signals were characterised via laboratory analysis of Ipramol and Ventolin nebulised aerosols, see Chapter 4. The decay of signals fitting these characteristics from their peak values (in particle counts measured over one minute) during the 4-week study was used to calculate a fluorescent nebulised particle reduction rate. Below we compare the reduction rates of the nebulised aerosol particles in respect of plasma disinfection unit activity.

Table 3.9 Summary statistics for nebuliser reduction rates with the plasma disinfection unit on and off.

Plasma disinfection unit	Nebuliser reduction rate (fluorescent particle/min)		P-value
	Mean ± sd	5^{th} – 95^{th}	
ON	2322 ± 962	1107 - 4290	<0.01
OFF	1753 ± 572	978 - 2889	

Operation of plasma disinfection units was associated with a significant decrease in fluorescent particles corresponding to nebulised aerosols ($P < 0.01$). The rate decreased from an average 1753 particles per minute to 2322 particles per minute (32%) when the plasma disinfection units were turned on. This corresponded to a reduction of 978-2889 particles per minute (5^{th} – 95^{th} percentiles), when the unit was off to 1107-4290 (5^{th} – 95^{th} percentiles) with the unit turned on, Table 3.9.

3.9.2 Fluorescent filtered peaks (outside of nebuliser times)

The production and decay of nebuliser-signal filtered counts from their peak values (in particle counts measured over one minute) during the 4-week campaign was used to calculate a filtered fluorescent particle production and reduction rates. Below we compare the reduction rates of the nebulised aerosol particles in respect of plasma disinfection unit activity (Table 3.10).

Table 3.10 Summary statistics for filtered fluorescent peak production rates with the plasma disinfection unit on and off.

Plasma disinfection unit	Nebuliser reduction rate (fluorescent particle/min)		P-value
	Mean ± sd	5^{th} – 95^{th}	
ON	14534.9 ± 13062	3101.7 - 42245.7	0.64
OFF	14949.8 ± 12133	4080.5 - 38070.2	

From Table 3.10 the rate of unfiltered fluorescent aerosol particles (at times unrelated to nebuliser-peaks) decreased from peak levels of 14950 to 14535 particles per minute with plasma disinfection, a ~3% decrease. This decrease was not significant (P=0.64).
Table 3.11 Summary statistics for filtered fluorescent peak reduction rates with the plasma disinfection unit on and off.

Plasma disinfection unit	Nebuliser reduction rate (fluorescent particle/min)		P-value
	Mean ± sd	5^{th} – 95^{th}	
ON	8301.54 ± 5438.5	2725.4 - 18565.2	<0.01
OFF	5674.4 ± 3043.9	2314.3 - 10340.9	

The rate of filtered fluorescent aerosol peaks (at times unrelated to nebuliser-peaks) significantly decreases from 8302 to 5675 (P<0.01) a ~32decrease with plasma disinfection units in comparison to when the units were off (Table 3.11).

3.10 **Fluorescent Signal Categorisation**

Applying the Perring *et al.* (Perring, 2016) categorisation system both total fluorescent particles and filtered fluorescent particles were largely recorded in the A category of the WIBS.

3.10.1 Fluorescent particle categorisation

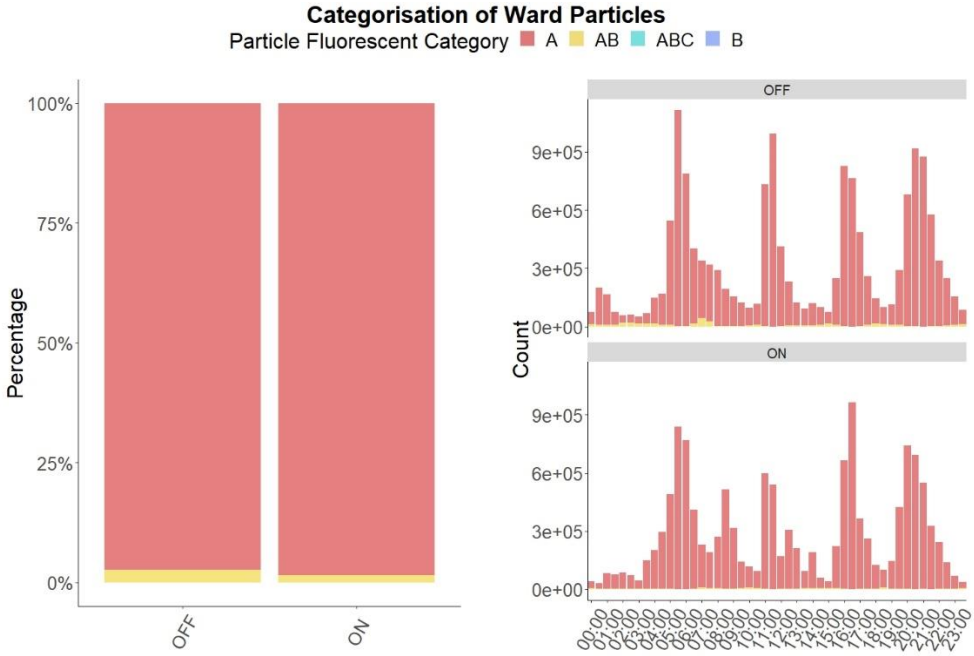

Figure 3.20 Fluorescence properties of fluorescent unfiltered aerosols on the ward. Stacked bar chart panel (Left) represents the % of fluorescent particles in each fluorescent type. Panel (Right) shows the overall half hourly particle count distribution in each type. Fluorescence type distribution is defined by excitation and emission from any of three possible channels alone (A, B or C) or in any combination.

The fluorescent aerosols produced from nebulising the drugs were dominated by a single fluorescence type (A), Figure 3.20. Although the nebulised drugs result in high numbers of AB type, and relatively low in the B and ABC channel, Table 3.12. Two of the four particle types showed significant difference with air disinfection unit operation. The mean number of fluorescent particles presenting in type A significantly ($P<0.001$) fell from 4281.36 to 4014.16 with air disinfection unit operation. Similarly, with the air disinfection unit operational the mean counts in the AB channel significantly decreased from 828.17 to 740.19 ($P<0.001$), no other category showed

significant difference in number of particles in fluorescent type between air disinfection unit operations.

Table 3.12 Fluorescent types and quantities observed for air plasma disinfection unit on and off.

Aid Disinfection Unit	Mean number in Fluorescent Type			
	A	B	AB	ABC
OFF	4281.36	69.10	828.17	31.00
ON	4014.16	63.34	740.19	14.69
P-value[A]	<0.001	0.360	<0.001	1

3.10.2 Fluorescent filtered particle categorisation

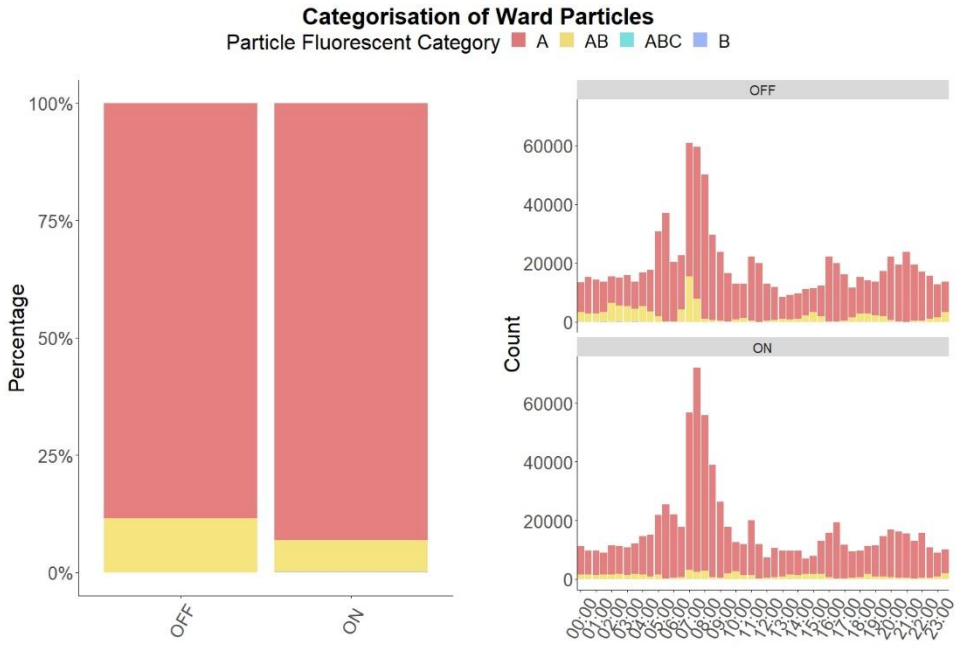

Figure 3.21 Fluorescence properties of fluorescent filtered aerosols on the ward. Stacked bar chart panel (Left) represents the % of fluorescent particles in each fluorescent type. Panel (Right) shows the overall half hourly particle count distribution in each type.

Figure 3.21 shows that the fluorescent filtered aerosols produced from nebulising the drugs were dominated by a single fluorescence type (A), although the fluorescent filtered particles did present in quite high in the AB type and relatively low in the B and ABC channel, Table 3.13.

Type AB was the only fluorescent type that showed a significant difference when the air disinfection unit was in operation. The mean number of fluorescent particles presenting as type AB significantly decreased from 516.7 to 417.37 with the air disinfection unit operation ($P<0.001$). No other category showed a significant difference in the number of particles in fluorescent type with air disinfection unit operations.

Table 3.13 Fluorescent types and quantities observed for air plasma disinfection unit on and off.

Aid Disinfection Unit	Mean number in Fluorescent Type			
	A	B	AB	ABC
OFF	2522.63	16.70	516.70	10.00
ON	2240.47	25.86	417.37	6.00
P-value	0.171	0.143	<0.001	0.5

3.11 **Footfall Counts**

3.11.1 Footfall count throughout the campaign

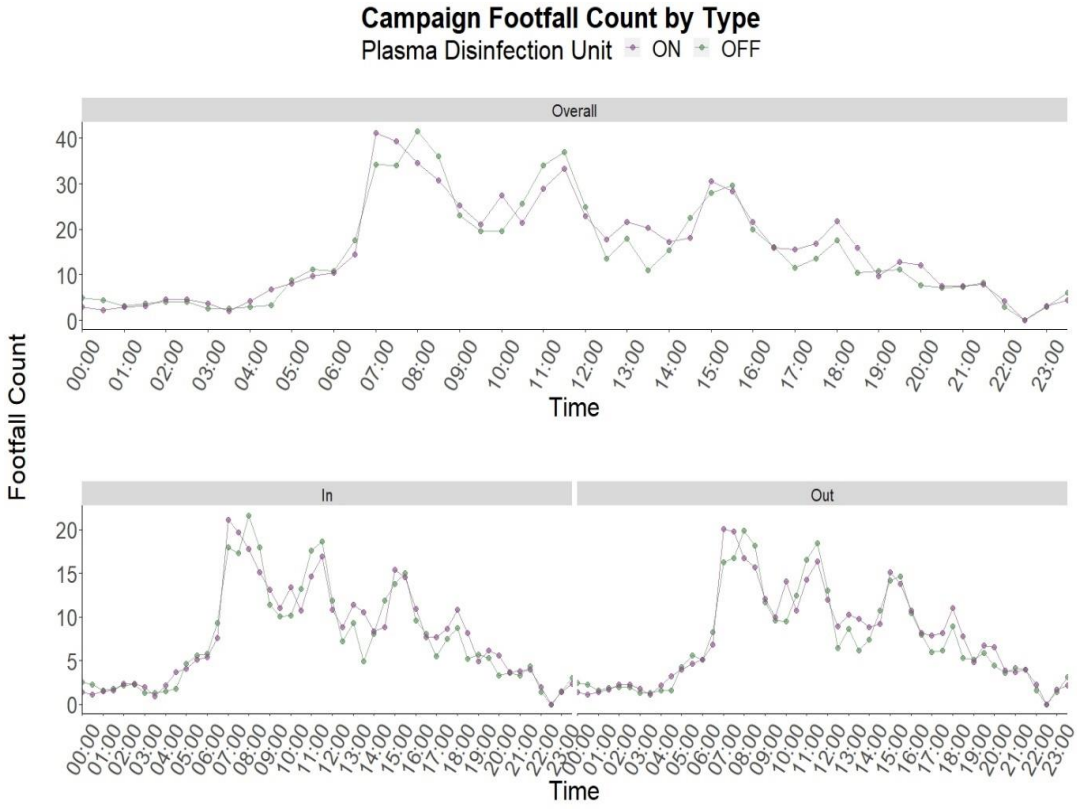

Figure 3.22 Mean footfall counts on the ward over the study. (Top) Overall footfall count (In and Out). Footfall into the ward and out of the ward.

In total, 5504 half hourly footfall counts were recorded during the study. The mean and summed half hourly footfall counts stayed consistent over the two observation periods when plotted diurnally (Figure 3.22), with no significant difference ($P<0.01$) calculated for footfall counts between plasma air disinfection and control periods, for any time-interval. Mean footfall counts were lowest overnight 00:00 – 04:30 and peaked in the mornings at 07:00 (41±10) with the plasma disinfection unit on and at 08:00 (42±15) with the units was off. This was followed by 2 further peaks at 11:30 (35±12) and 15:00 (29±12), with less significant peaks occur at 13:00 (20±12) and 18:00 (20±9).

3.11.2 Ward events fitting morning fluorescent filtered particle peak

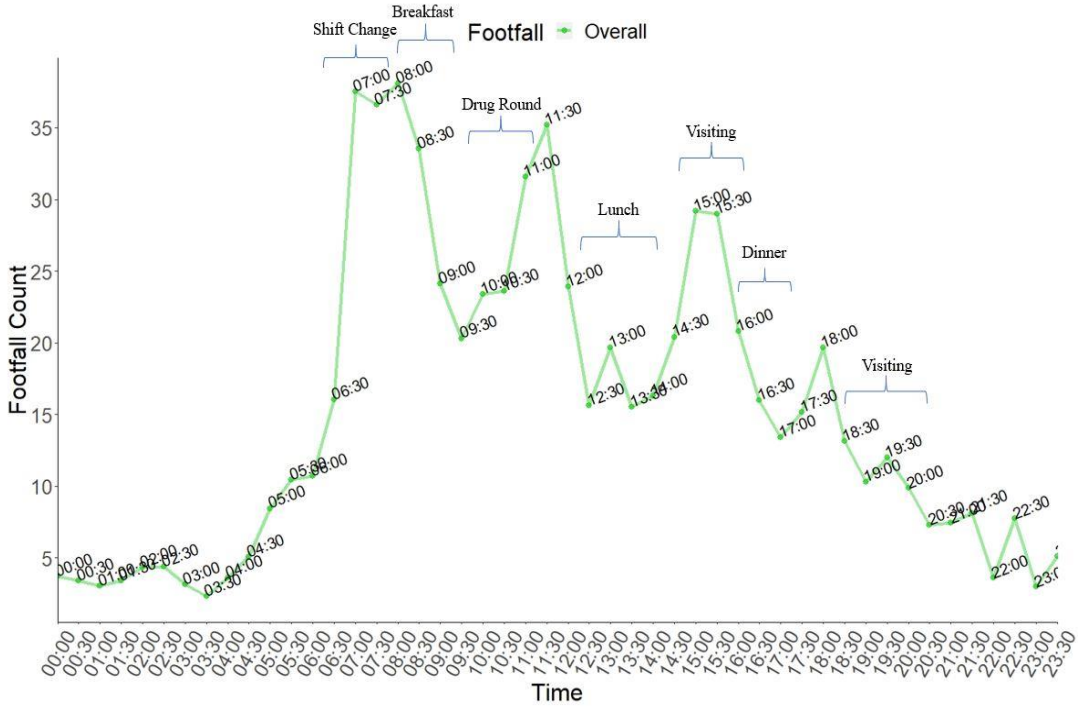

Figure 3.23 Overall footfall with approximate times of events fitted.

Footfall peaks, Figure 3.23, showed a consistent diurnal pattern which coincides with regular events on the ward occur at times of day with, nurses on the ward worked day and night shifts, day shift staff (6-9) arrived for handover at 07:45 and night shift staff (3) at 20:00. Meals were served to the patients beds at 08:00-08:30, 12:30-13:00 and 16:30-17:00 and drug rounds were made at 10:30, visiting time was –14:00-16:00 and 18:30-20:30. Beds were not made at a specific time but over the course of the morning 08:30-10:00, but if a patient was discharged the bed would be stripped and remade (Figure 3.23). On site observations suggested visiting times were not strictly enforced so visiting may come before or after official visiting hours.

Night shift to day shift nursing handover was the likeliest single daily event accounting for the morning fluorescent filtered particle peak. Nurses on the ward worked day and night shifts, where the day shift staff arrived for shift handover at 07:45 and night shift staff for a handover at 20:00. Six to nine staff would arrive for night to day handover, in comparison only three-night staff would arrive for the day to night handover. Shift handover involved a meeting directly outside of the respiratory ward bay being monitored with movement of chairs before and after the meeting. In addition, although

hospital policy is for nurses to change into uniform in a locker room away from the ward after travelling to work, during the period of the study it was noted that some staff were travelling in uniform and depositing outdoor coats in treatment room cupboards adjacent to the bay being studied.

3.11.3 Footfall count fitted with WIBS fluorescent filtered data

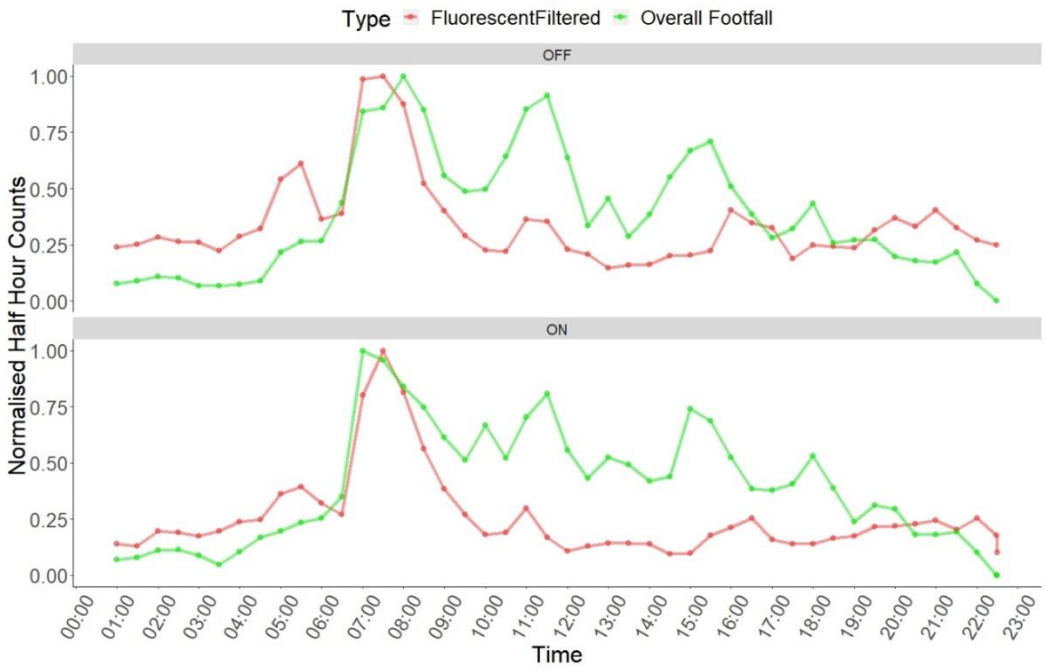

Figure 3.24 Normalised diurnal line graph with thirty-minute summed fluorescent filtered particle concentrations (red) and overall footfall (green). Panel split by plasma disinfection operation; on (top) and off (bottom).

The highest footfall interval of 07:00-08:30 (Figure 3.24), coincide with the highest fluorescent filtered particle concentrations. No statistically significant difference in fluorescent filtered particle concentrations with operation of the plasma disinfection unit was noted during this period ($P > 0.01$).

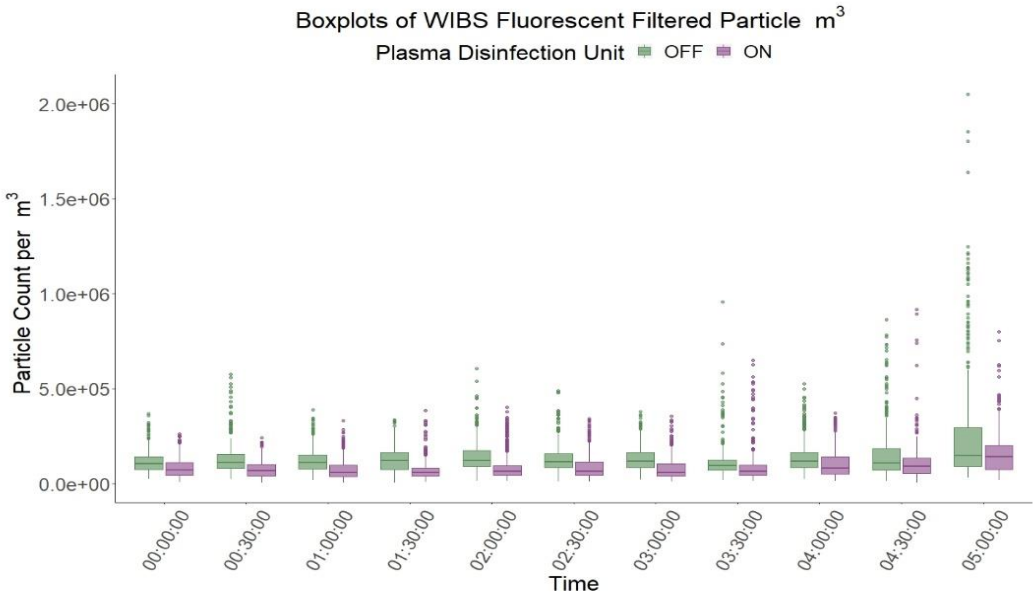

Figure 3.25 Boxplots of thirty-minute summed morning fluorescent filtered particle concentrations. Boxplots coloured by plasma disinfection unit operation on (purple) and off (green).

Figure 3.22 revealed that overall footfall was lowest during early morning from 00:00 – 04:30, ranging from 0 – 9.5 overall footfall counts per 30 min (25^{th} – 75^{th} percentile) (Table 3.14). This period of low footfall also coincides with the period of lowest particle counts. Boxplots of half-hourly mean counts overnight, (Figure 3.25) showed a decrease in fluorescent particle counts and distribution through all periods, however no individual period was significantly, ($P<0.05$) decreased with plasma disinfection in operation. But looking at the period as a whole (00:00 – 05:00) a significant decrease in fluorescent filtered particles was observed during plasma disinfection unit operation ($P<0.05$).

Table 3.14 Thirty-minute mean footfall and fluorescent particle counts per m^3

Time Interval	Plasma disinfection operation			
	On		Off	
	Footfall	Particle/m^3 ($\times 10^6$)	Footfall	Particle/m^3 ($\times 10^6$)
00:00:00	2.9	2.5	5	3.4
00:30:00	2.1	2.3	4.4	3.9
01:00:00	2.7	2.2	3.1	3.5
01:30:00	3	2.1	3.6	3.8
02:00:00	4.3	2.7	4.1	4.3
02:30:00	4.6	2.6	4.1	3.7
03:00:00	3.5	2.4	2.6	4.0
03:30:00	2	2.7	2.6	3.4
04:00:00	4	3.1	3	4.2
04:30:00	6.4	3.2	3.4	4.6
05:00:00	8.1	4.7	8.8	7.8

During the period of highest footfall two of the three time periods showed lower fluorescent filtered counts, but one period (07:00-07:30) demonstrate higher mean counts when plasma disinfection unit was powered on than during the control period (Table 3.15).

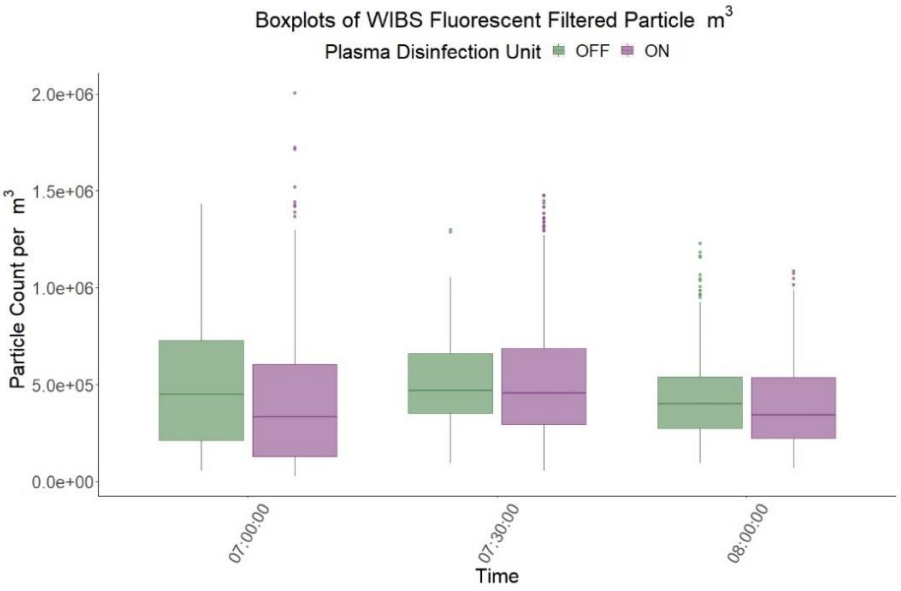

Figure 3.26 Boxplots of thirty-minute summed fluorescent filtered particle concentrations for the peak morning period. Boxplots coloured by plasma disinfection unit operation on (purple) and off (green).

Exploring each time period individually, Figure 3.26 and Table 3.15, the period of 06:30-07:00 revealed a mean fluorescent filtered particle concentration of $12.2\times10^6 \pm 7.07\times10^6$ particles/m^3 during plasma disinfection period increasing to $14.8\times10^6 \pm 7.98\times10^6$ particles/m^3, (P = 0.53), during the control period. Likewise, at 07:30-08:00 the mean fluorescent filtered particle concentrations increased form $12.1\times10^6 \pm 6.13\times10^6$ particles/m^3 with plasma disinfection unit on, to $13.0\times10^6 \pm 5.25\times10^6$ particles/m^3 with the units off, (P = 0.94).

However, an increase in fluorescent filtered particle was observed during the 07:00-07:30 period, with $15.6\times10^6 \pm 8.49\times10^6$ particles/m^3 with plasma disinfection units in operation from $14.9\times10^6 \pm 6.08\times10^6$ particles/m^3 during the control period, (P = 0.48).

Table 3.15 Summary statistics of the 07:00-08:00 period, mean footfall and fluorescent filtered counts.

Time Interval	Plasma disinfection operation			
	On		Off	
	Footfall	Particle/m^3 ($\times10^6$)	Footfall	Particle/m^3 ($\times10^6$)
07:00:00	40	12.2	34	14.8
07:30:00	39	15.6	34	14.9
08:00:00	35	12.1	42	13

3.11.4 Footfall correlations

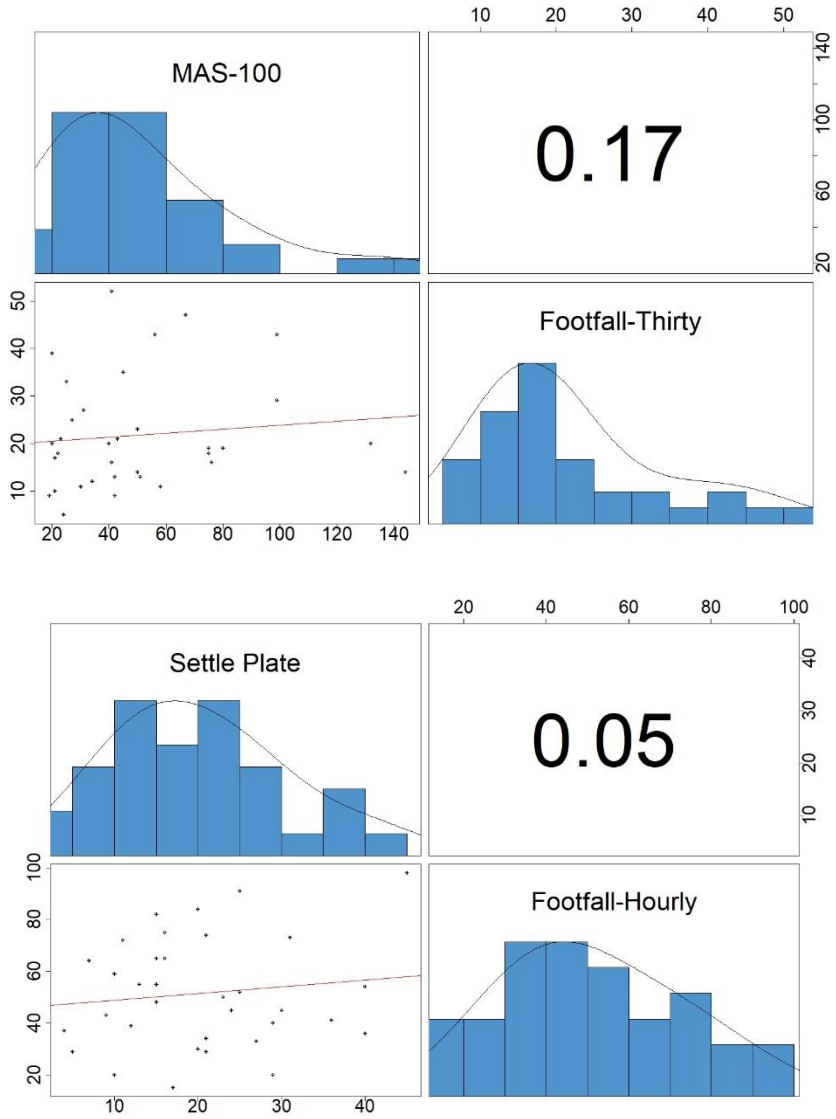

Figure 3.27 Spearman correlation matrix for MAS-100 air samples and thirty-minute footfall counts prior to sample period (top) and settle plate with corresponding hour footfall counts during sample period (bottom).

A spearman correlation matrix (Figure 3.27, top) was constructed using the MAS-100 air sample counts and prior footfall counts which had a low and insignificant correlation with the MAS-100 counts ($r(34) = +0.17$, $P > 0.05$). Equally the spearman correlation matrix constructed for settle plate counts and footfall during the sample period (Figure 3.27, bottom) found no correlation ($r(34) = +0.05$, $P > 0.05$).

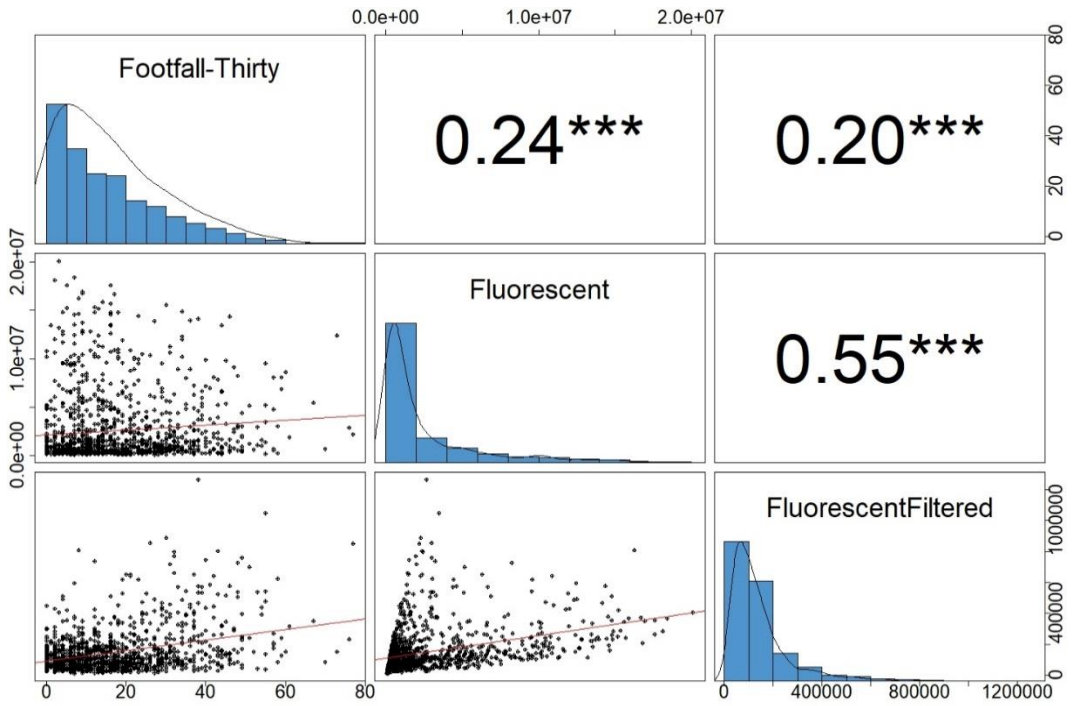

Figure 3.28 Spearman correlation matrix for thirty-minute footfall counts with corresponding fluorescent and fluorescent filtered particle counts per m^3.

The spearman correlation matrix (Figure 3.28) highlights the significant but weak correlations between footfall counts and WIBS particle observation. Overall footfall counts had low and insignificant correlation with the fluorescent particle counts ($r(1232) = +0.24$, $P > 0.001$). Similarly, overall footfall had a low, but significant correlation with fluorescent filtered counts ($r(1232) = +0.20$, $P > 0.001$). Although footfall had a higher spearman correlation coefficient with fluorescent particle counts compared to fluorescent filtered counts, both were low correlations. However, the spearman correlation matrix was constructed from corresponding footfall and WIBS over 1,232 timepoints.

From the diurnal line graph for footfall and fluorescent filtered particle counts (Figure 3.24) the highest concentration of particle counts coincided with the highest footfall period, 07:00-08:30, but the constructed correlation matrix (Figure 3.28) produced a significant, but low correlation coefficient. This would suggest that although footfall is a major contributor to early bioaerosol concentrations, it is not the only bioaerosol producing event in the ward.

3.12 **Ward Observations**

Continuous air monitoring within an intensive care isolation room reported increases of 122 CFU/m^3 associated with a patient being assisted out of bed (Dougall et al., 2019), indicating that even mundane tasks like getting out of bed may produce bioaerosols. Mean counts of airborne methicillin resistant-*Staphylococcus aureus* (MRSA) from infected patients have been reported as 4.7 CFU/m^3 during rest periods (before bed making), increasing to 116 CFU/m^3 during bed sheet changes. Levels were shown to remain elevated for at least 15 minutes after activities finished (Shiomori et al., 2002), again, suggesting that movements of patients lying in bed and rustling the bed covers can result in bioaerosol generation. During conventional sampling I noticed some ward events that could only be noted if present. Two bed making events that occurred and were noted during the campaign are shown below.

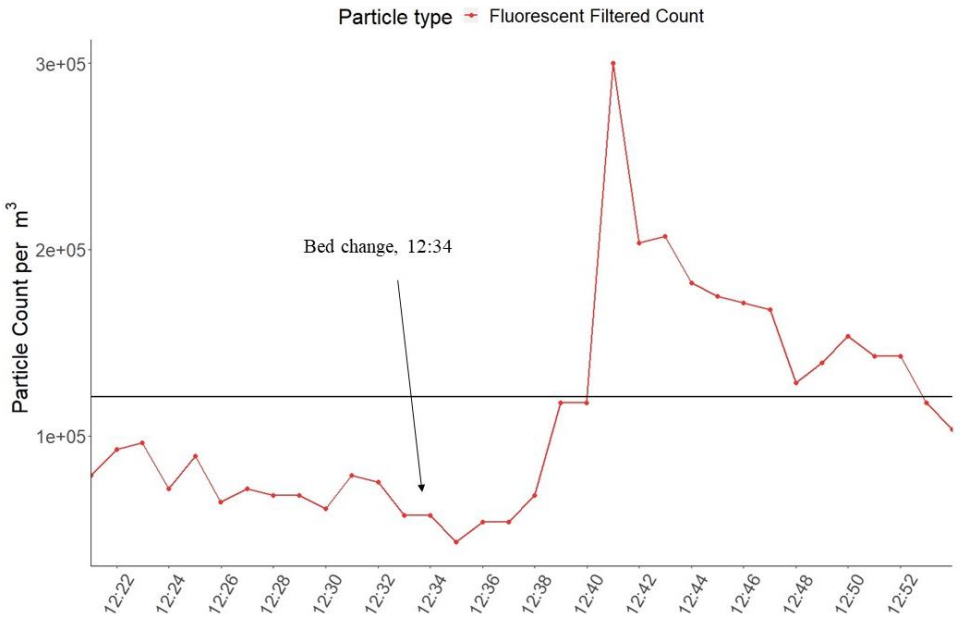

Figure 3.29 Fluorescent filtered particle concentrations during bed change on 22nd March 2018. The mean fluorescent filtered count denoted by the black line, the start of bed change is highlighted.

During the bed change pobserved on the 22nd March, Figure 3.29, the fluorescent filtered concentration reached a peak concentration of 2.99×10^5 counts per m^3 at 12:42 ~eight minutes after bed changing had started. This is ~5-fold increase from when the bed change commenced at 12:34 6.07×10^4 counts per m^3. Particle

concentration remained above the mean fluorescent filtered concentrations for ~ 12 minutes before falling below the mean concentration.

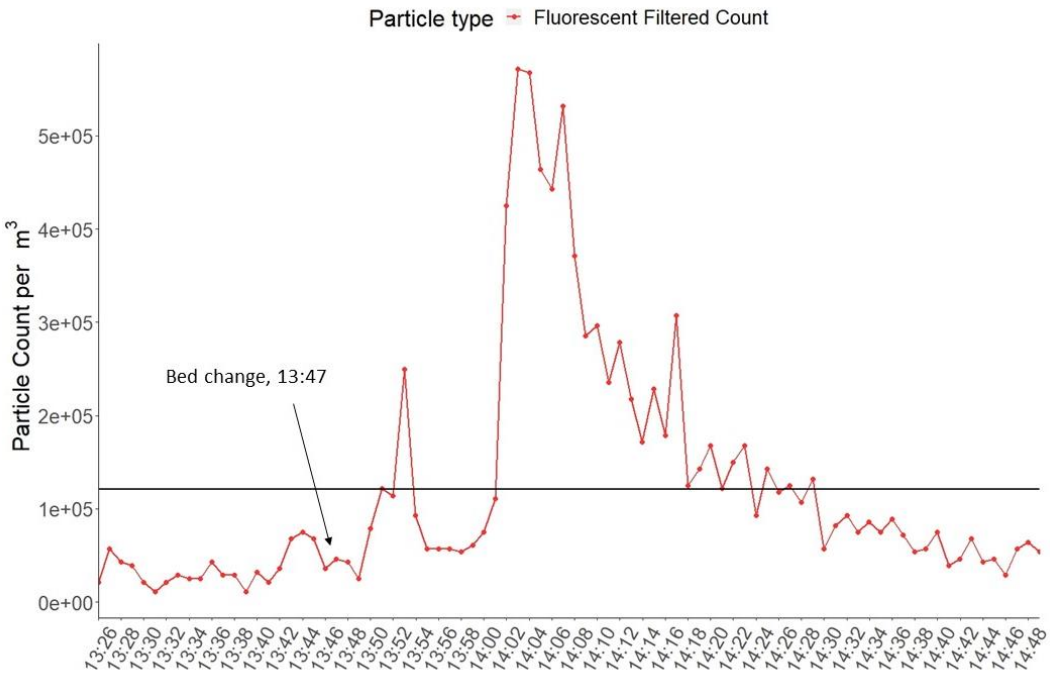

Figure 3.30 Fluorescent filtered particle concentrations during bed change on 18th April 2018. Mean fluorescent filtered count denoted by black line, start of bed change highlighted.

The bed change observed on the 18th April (Figure 3.30) exhibits two increases. Initially an increase in fluorescent filtered concentrations was observed at 13:52 reaching a maximum concentration of 2.5×10^5 counts per m^3, 6-fold higher than the initial bed change concentration (0.42×10^5 counts per m^3 at 13:47) and remained above the mean for ~ one minute. However, a second subsequently larger increase in particle concentrations started to occur at 13:58 and reached a peak concentration of 5.7×10^5 counts per m^3, ~2.2 fold larger than the first peak, at 13:03, and ~14 fold larger than the initial change concentration.

3.13 Airnode concentrations

3.13.1 Airnode $PM_{2.5}$ counts

Airnode data was collected during the two-weeks with the plasma disinfection unit active, but it was unavailable during the control period, therefore, no plasma disinfection unit comparison could be performed using the AirNode.

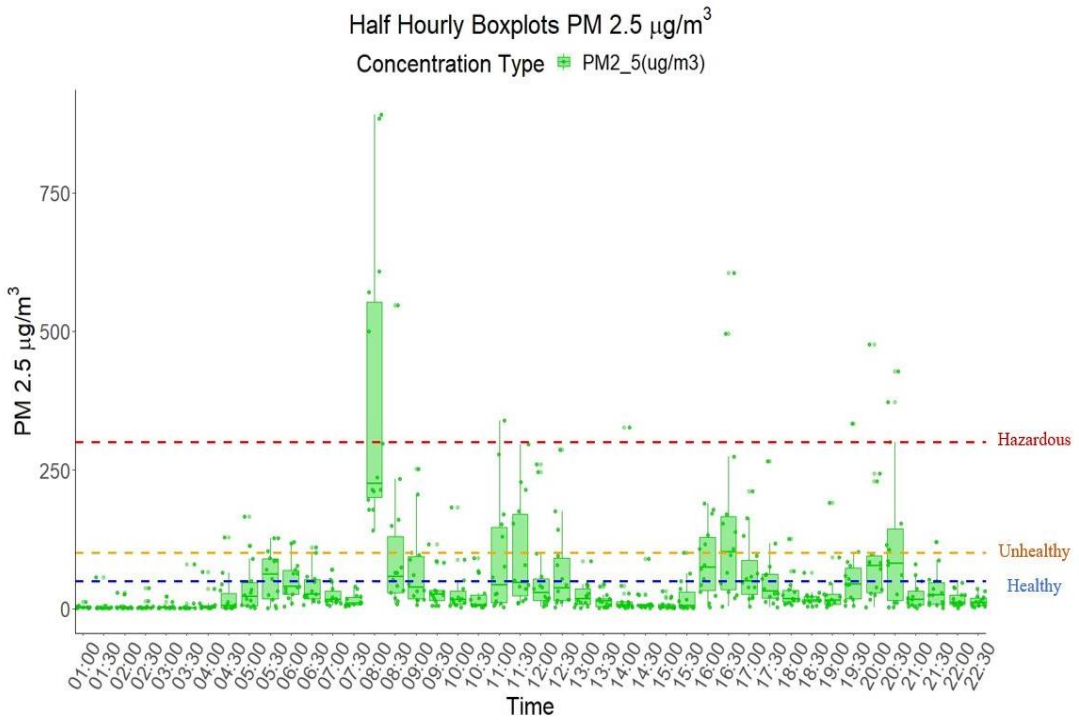

Figure 3.31 Boxplots of Airnode data with hazardous (red), unhealthy (orange) and healthy (blue) levels marked with coloured dotted lines. These marked levels are for illustration and based upon the EPA AQI limits.

The most prominent $PM_{2.5}$ concentration peak was clearly in the unhealthy / hazardous limit for $PM_{2.5}$ (Figure 3.31). This coincided with the most prominent peak detected for the fluorescent filtered (Figure 3.22). Other less prominent peaks were noted during times of nebuliser usage, like the fluorescent particle concentrations (Figure 3.10). However, the nebuliser aerosol concentrations reported by the AirNode were considerably less than those of the WIBS.

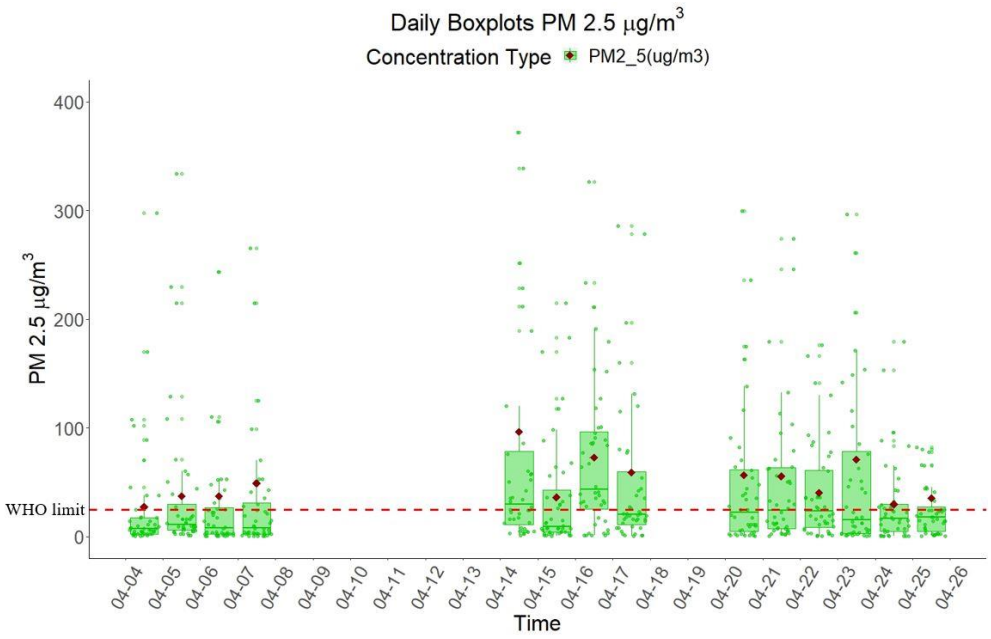

Figure 3.32 Daily Boxplots of AirNode $PM_{2.5}$ counts with mean highlighted. Red dot represents the mean calculated for that day and red line is $PM_{2.5}$ daily limit from WHO guidelines.

The mean daily $PM_{2.5}$ concentration was 50.2 ± 19.7 µg/m^3, and all 14 days monitored by the AirNode exceeded that WHO daily limit of 25 µg/m^3 (red line, Figure 3.32).

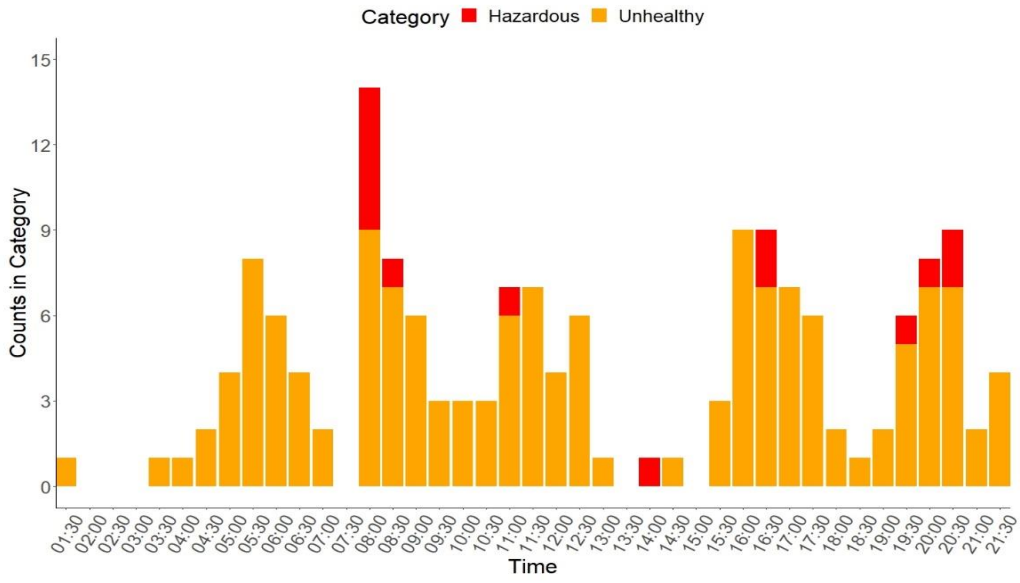

Figure 3.33 Count of hazardous (red) and unhealthy (orange) concentrations of $PM_{2.5}$ from the two-week period.

Of the 616 $PM_{2.5}$ measurements by the AirNode, 455 were classed as healthy, 147 as unhealthy and 14 as hazardous. Figure 3.33 illustrates the number of counts that were

classified as unhealthy and hazardous for $PM_{2.5}$ concentrations per thirty-minutes over the two-week period. The highest counts for both hazardous and unhealthy classified levels of $PM_{2.5}$ occurred during the 07:00-07:30 time period (Figure 3.33), the same period with the highest footfall and fluorescent filtered particle counts (Figure 3.24).

3.13.2 Airnode correlations

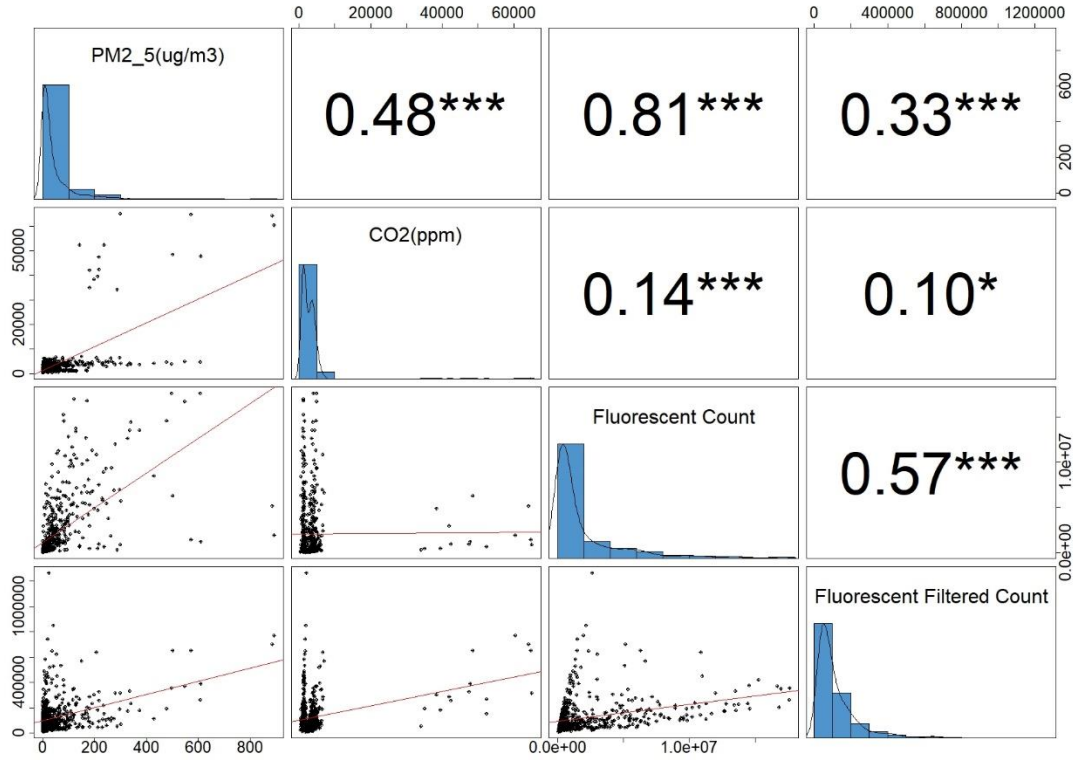

Figure 3.34 Spearman correlation matrix for $PM_{2.5}$, CO_2, fluorescent and fluorescent filtered particle counts.

$PM_{2.5}$ concentrations from the AirNode (Figure 3.34) showed a strong correlation with the unfiltered fluorescent particle counts from the WIBS-4a ($r(616) = +0.81$, $P<0.001$), demonstrating its ability to identify nebuliser-related particles. The $PM_{2.5}$ concentrations showed a lower correlation with filtered fluorescent particle counts from the WIBS-4a ($r(616) = +0.37$, $P<0.001$).

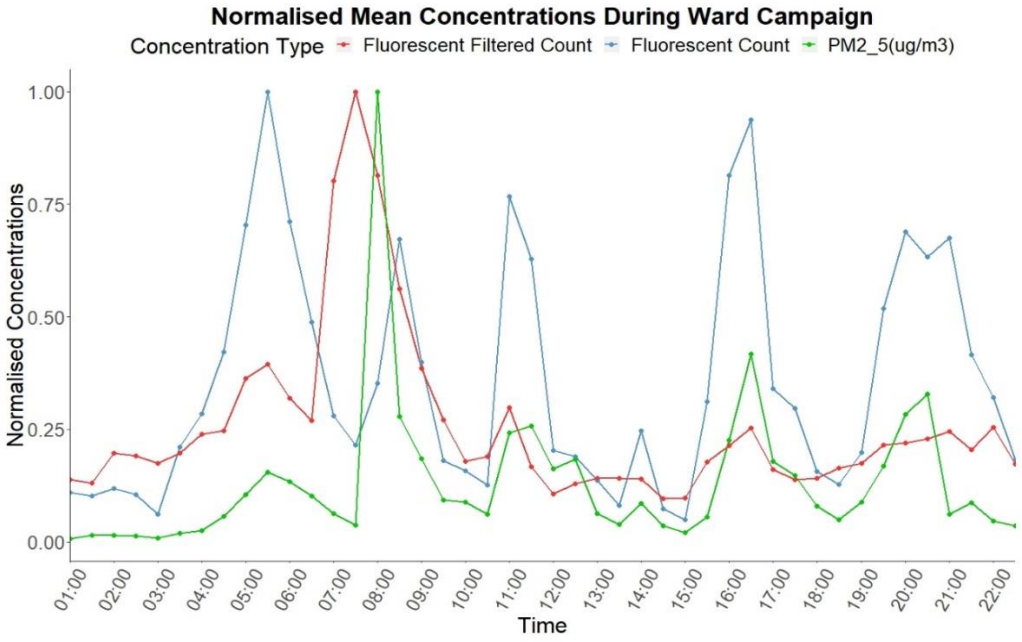

Figure 3.35 Half Hourly averaged fluorescent particle counts (blue) and filtered fluorescent particle counts (red) with the Airnode $PM_{2.5}$ (green).

Although $PM_{2.5}$ had a higher correlation with fluorescent counts than the filtered fluorescent counts (Figure 3.34), examining Figure 3.35 shows the most prominent peak of $PM_{2.5}$ (green), 07:00-07:30, emanates after the most prominent peak in filtered fluorescent counts (red) over the 06:30-07:00 period. This suggests that although the AirNode is registering the nebuliser aerosols, it is more sensitive to the actual bioaerosol particles.

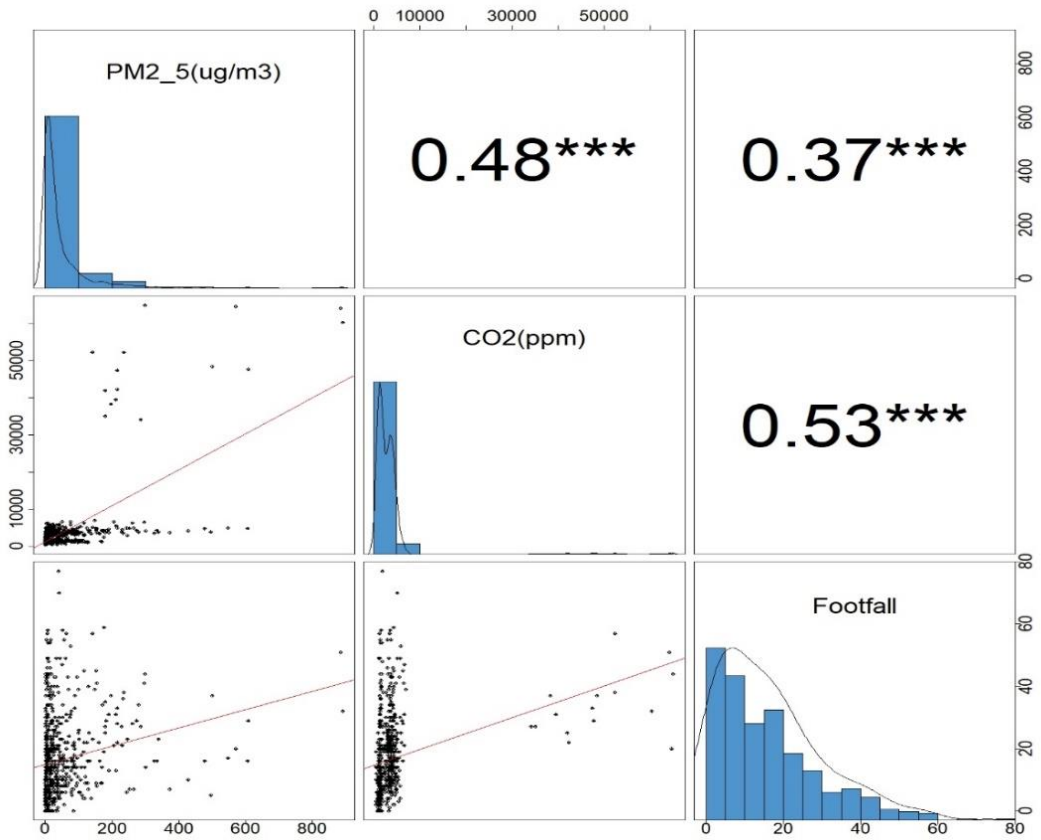

Figure 3.36 Spearman correlation matrix for $PM_{2.5}$, CO_2 and overall footfall counts.

Overall footfall counts had a medium and significant correlation with both AirNode measurements, $PM_{2.5}$ ($r(616) = +0.37$, $P<0.001$) and CO_2 concentrations ($r(616) = +0.53$, $P<0.001$), Figure 3.36. The $PM_{2.5}$ concentrations had a strong and significant correlations with CO_2 concentrations ($r(616) = +0.48$, $P<0.001$). Similar to peaking after the fluorescent filtered peak, the $PM_{2.5}$ peak also followed the period of highest footfall, 07:00 (41±10) (Figure 3.36).

3.14 **Nebuliser exposure rates**

Inhalation rates for individuals during various activity levels within a 24-hour simulated activity pattern were estimated as a function of VO_2, body weight, age and gender. The mean short-term inhalation rates, calculated for children and adults performing various activities, ranged from 3×10^{-3} - 5.8×10^{-2} m^3/min. The lowest was male child <1 year sleeping and the highest a male adult aged 51-61 of age during high-intensity activities (US Environmental Protection Agency, 2009). The daily mean ventilation rate during light activity for a male aged 41-51 years old was 1.4×10^{-2} and for female in same age range was 1.2×10^{-2}, giving a mean of 1.3×10^{-2} between males and females (US Environmental Protection Agency, 2009). The background ambient aerosols, as calculated by the average particles during the early morning period 00:00-04:00 ($8.24\times10^5 \pm 4.14\times10^5$, $6.26\times10^5 \pm 3.60\times10^5$ for Plasma unit off and on respectively), were subtracted from the nebuliser times in an effort to isolate nebuliser particles. Based on this and the average nebuliser particles produced during a half hour period, we calculated the percentage of exhaled drug that could be potentially be inhaled by a healthcare worker or bystander during patient nebuliser therapy, Table 3.16. Exhaled aerosols were estimated to be ~29% of nominal drug (0.725 mg) (McGrath et al., 2019) and the percentage of aerosol inhaled and immediately exhaled was ~ 13% (0.325 mg) (Clay and Clarke, 1987).

Table 3.16 Thirty-minute averaged aerosol exposure during nebuliser times.

Nebuliser Time	% of exhaled drug		% of inhaled and immediately exhaled drug		% Difference Plasma Unit
	Plasma Disinfection Unit				
	Off	On	Off	On	
05:00:00	3.60	2.89	8.04	6.45	24.551
05:30:00	4.90	3.78	10.92	8.42	29.624
11:00:00	4.54	3.78	10.13	8.44	20.064
11:30:00	4.17	2.33	9.31	5.21	78.824
16:00:00	5.90	4.46	13.17	9.96	32.199
16:30:00	4.59	5.46	10.24	12.19	-15.975
20:00:00	5.24	5.10	11.69	11.37	2.861
20:30:00	5.66	4.54	12.62	10.12	24.742

Values provided in table 3.16 are average values for nebuliser particle concentrations. We could not discriminate between which patients used the nebulisers and the distance

they were from the instrument. The highest exposure to the nebuliser aerosols was at 16:00:00 -17:00:00 where bystanders were estimated to be exposed to 4.46-5.90% (0.032 mg – 0.043 mg) of the exhaled nebuliser aerosols and 9.96-13.17% (0.0033 mg – 0.0042 mg) of inhaled and immediately exhaled aerosols per half hour.

3.15 **Conclusion**

This study characterised the indoor air of a four-bedded bay in a hospital respiratory ward using conventional plate count cultures of air and surface samples and real time continuous biological particle air sampling over a total of 20 days. Movement activity was likewise continuously monitored by an infra-red people counter at the entrance to the bay.

3.15.1 Ward Observations

The cumulative continuous monitoring observations revealed that counts were lowest at night, with four striking recurrent fluorescent particle peaks during the daytime when the number of particles increased by over 200-fold compared to the nocturnal minimum (00:00-04:30 hrs) (Figure 3.12). These peaks corresponded to observed nebuliser use on the ward. When the characteristic fluorescence signal of nebulised drug particles was determined and removed from the data to leave filtered fluorescent counts, one large daily peak between 07:00-08:30, 5-fold higher than the nocturnal minimum, remained (Figure 3.16). Higher rates of MRSA in air samples were recovered by Creamer *et al*. in the early morning between 07:30-09:00 compared with other times, with rates of MRSA declining throughout the day (Creamer et al., 2014). They suggested that patients may shed more skin scales during the night while sleeping however, they did mention that some ward activity may have taken place before 07:30 (Creamer et al., 2014). Similarly, the observed WIBS fluorescent filtered particle counts peaked at a similar time (Figure 3.16). The timing of this filtered fluorescent particle peak corresponded to the arrival of the nursing day shift and the main nursing handover meeting held in the adjacent corridor, and the maximum movement in and out of the bay as detected by infra-red footfall count (Figure 3.22). Footfall counts obtained from an infra-red people counter made simultaneously with airborne particle counts also gave four daily peaks when analysed on a cumulative diurnal scale. Footfall counts correlated slightly better with overall unfiltered fluorescent particle concentrations ($r = +0.24$, $P < 0.001$), than the overall filtered fluorescent counts including nebulised drug particles ($r = +0.20$, $P < 0.001$), Figure 3.28 This may be explained by footfall peaks coinciding with times to nebuliser usage. Strong and significant correlations exist between the $PM_{2.5}$ ($r = +0.37$, $P < 0.001$) and CO_2 ($r = +0.53$, $P < 0.001$) concentrations recorded by the AirNode and overall footfall

counts (Figure 3.36). These observations confirm the enhanced observational sensitivity arising from continuous particle monitoring compared to intermittent conventional cultures.

The association between filtered fluorescent particle counts, $PM_{2.5}$, footfall and occupant activities suggest that these particle counts represent bioaerosols. Occupant activities within an indoor environment are known to raise levels of inhalable bioaerosols, with walking as a significant contributor to bioaerosol concentrations through both loss of skin particles attached to clothing and the resuspension of particles disturbed from the floor (Gomes et al., 2007, Qian et al., 2014, Tian et al., 2014). Direct human shedding from skin, hair and nose along with resuspension contributes to the elevated respirable particulate matter and bacterial genome equivalents measured by quantitative PCR above background concentrations associated with human occupancy (Hospodsky et al., 2012). Occupancy of school classrooms has shown significant increases of airborne bacteria (81-fold), fungal spores (15-fold) and PM mass concentrations (9-fold), when compared to background vacant conditions (Hospodsky et al., 2015). A single published environmental monitoring study of air contamination levels in an ICU across a 24-hour time period showed significant variance across sampling periods, with peaks directly related to room activity, particularly with increased staff presence or use of large equipment (Dougall et al., 2019). Dougall *et al.* consistently linked numbers of staff in patients' rooms to levels of air contamination. When more than 2 staff were present in the room, a 154.7% increase in average airborne bacteria was observed, this widened to an average 197.1% when more than 3 staff were present (Dougall et al., 2019).

Bed sheet changes have previously been implicated in any increase in the aerial dispersal of bacteria. Significant increases of CFU/m^3 from 4.7 CFU/m^3 to 116 CFU/m^3 of MRSA were reported, with these levels remaining elevated for up to 15 minutes after initial change (Shiomori et al., 2002). Another study in a burns patient unit related bed changing with significantly high levels of airborne bacteria, up to 2614 CFU/m^3, lasting up to one hour after bed sheet change had occurred (Bache et al., 2015). Recently Dougall *et al.* observed an average increase of 145.3% in CFU of airborne bacteria with bed changes (Dougall et al., 2019). Figure 3.29 shows bioaerosol concentrations remain elevated above mean levels for ~12 minutes after the

initial bed change, similar to observations form Shiomori *et al.* (Shiomori et al., 2002), this was a ~400% increase in bioaerosol concentration from the initial bed change concentration, and ~150% above the fluorescent filtered mean concentration. Figure 3.30 exhibits two increases in fluorescent filtered particle concentrations after the initial bed change, the first being a ~6-fold (+525%) increase on the initial bed change concentration, however, the second larger peak observed 8 minutes after the first peak was ~14 fold (+1325%) larger than the initial bed change concentration. Both Figure 3.29 and 3.30 show larger increases in particle concentrations than the increases in CFU/m^3 observed in previous studies (Shiomori et al., 2002, Dougall et al., 2019). This could be due to a few reasons. The WIBS is not constricted by poor time resolution and can continuously sample for hours without missing any time point, whereas conventional sampling times are severely limited to instrument sampling intervals. Furthermore, conventional sampling is restricted by the organisms it can culture, whereas the WIBS samples all particles and then segregates them from dust etc., according to the fluorescent intensities observed from their biological components.

3.15.2 Plasma disinfection unit effect on air quality

We observed the effect of activating plasma disinfection units on air in the ward using conventional and real-time air sampling techniques over a control time period without plasma disinfection and a test period with plasma disinfection. The daily patterns of particle count and footfall were retained across both periods of observation (Figure 3.24).

Conventional testing of air samples by impact and settle plates found no significant difference in CFU counts between these periods at either of the two time points 11:30 and 13:00 ($P > 0.01$) (Table 3.1). Unlike the intensive care unit (ICU) study our study did not find any statistical difference linking CFU by conventional samples to different occupancy levels (Figure 3.27), the ITU study by Dougall *et al.* obtained 97 impaction samples, sampling every 15 minutes for 10 hours. This study only sampled air twice daily, at the same time points. Footfall data collected in section 3.11, revealed that within each half hour time period, there was little footfall variability, but there was variability between periods (Figure 3.22). Neither the MAS-100 ($r(34) = +0.07$, $P >$

0.01) nor settle plate counts ($r(34) = +0.20$, $P > 0.01$) showed correlation with footfall counts (Figure 3.27), this may be due to samples taken at limited time points. Interestingly, no significant difference was detected in WIBS-4A counts recorded over the same time period as air impact/settle plates were taken ($P > 0.01$), Table 3.3.

Continuous WIBS-4A observation revealed a significant decrease during plasma disinfection operation of both overall fluorescent and fluorescent filtered mean particle counts compared with the control period (Tables 3.4 and 3.7). Approximately 27% fewer unfiltered fluorescent particles (which in the daytime were largely nebulised drug particles) and ~28% fluorescent signal-filtered particles (processed to remove the effect of nebulised drug particles) were found when plasma disinfection was active. However, Figures 3.10 and Figures 3.16 show that underlying fluorescent and filtered fluorescent counts are highly variable within time periods. Only seven thirty-minute time periods of fluorescent counts experienced a significant reduction in particle counts, five of which occurred at periods of low footfall (Figure 3.10). The plasma disinfection unit is associated with a non-significant decrease in all periods of fluorescent filtered particles, apart from the time periods associated with highest footfall and highest particle concentration which witnessed a non-significant increase in particle concentrations (Figure 3.17).

Unfiltered fluorescent aerosol particles (largely nebuliser-related) increased from 1753 to 2322 particles per minute with plasma disinfection, a 33% increase, Table 3.9. No significant difference was observed in filtered fluorescent peaks ($P=0.64$), however, filtered fluorescent aerosol peaks, at times associated with nebuliser usage, significantly increased ($P<0.01$) by ~32% with plasma disinfection units on in comparison to when the plasma units were off (Table 3.10 & 3.11).

A study cataloguing the fluorescent signatures of aerosolised bioaerosols showed that bacteria fell into a common fluorescent pattern, <1.5 µm in size, and all but one bacterial aerosol was dominated by the single fluorescent type A (Perring, 2016). Cataloguing the fluorescent signatures of the fluorescent filtered particles on the ward found that the majority lay within the type A fluorescent signature, Figure 3.21, however in larger sizes than presented by Perring et al., The size range of particles were larger at 3-4 µm, Figure 3.15. This may be explained by sampling in ambient air

as opposed to a controlled laboratory experiment in ambient air. bacterial cells have a tendency to agglomerate (Wang et al., 2008, Lighthart, 1997) and are not often seen as singular particles, as was seen in the laboratory experiment (Perring, 2016). The air disinfection unit did not significantly affect the number of fluorescent type A particles, but it did significantly reduce the number of particles of type AB, Table 3.13. This suggests it may have a significantly greater effect in removing some bacteria (bioaerosols presenting as AB) but not others (bioaerosol exhibiting type A).

No significant difference was observed for total particle counts ($P>0.05$), but the fluorescent filtered particle counts fell ($P<0.01$). This would indicate that the air disinfection unit was eliminating the biological components in the particles, without destroying the particles (Table 3.4 and Table 3.7). The plasma disinfection units were associated with an overall reduction in fluorescent filtered particles, with a decrease (non-significant) recorded for the majority of time periods. However, at the time periods which displayed the highest fluorescent filtered particles concentration, the particles did not decrease, but in fact increased when compared to the control period. Fluorescent unfiltered particles concentrations significantly decreased at several thirty-minute intervals, suggesting the plasma may work more effectively on nebuliser related aerosols. There are several possible reasons why plasma might have a greater effect in reducing nebulised drug particles than airborne bacteria. Firstly, a plasma effect on nebulised liquid particles might include evaporation of smaller particles (increasing mean particle size - Figure 3.9) and could be more effective than the damaging of bacterial cells induced by plasma (Mai-Prochnow et al., 2014, Laroussi et al., 2003) in reducing the number of fluorescent particles. There could also be a source location effect, with the nebulised particles source being local within the bay and the bacterial and fungal particles representing events in the corridor and ward station during the shift handover between nurses. This has implications for unit placement with regards to particle reservoir location. Previous reports revealed the importance of portable air cleaner placement, where the positioning may result in a factor of 2.5 change in overall particle removal (Novoselac and Siegel, 2009). Another reason could be that the nebuliser solutions are made up in dilute hydrochloric acid (HCL), HCL is a polarised neutral electrophile, meaning it tends to gain electrons, possibly making it more favourable to gain an electron from the negative electrode and thus more attracted to the plasma field. Bacterial cell on the other hand are

negatively charged due to the presence of teichoic acid linked to either the peptidoglycan or underlying plasma membrane (Silhavy et al., 2010).

3.15.3 Nebuliser related aerosols

The potential secondary exposure to exhaled nebuliser-related aerosol emissions for bystanders during the average nebuliser treatment was examined in section 3.14, table 3.16. Although the background ambient aerosols, as calculated by the average particles during the early morning period were subtracted, it may not have explicitly removed all ambient aerosols. However, it was calculated that from 16:00-17:00 a bystander was exposed to 0.032 mg – 0.043 mg (of exhaled nebuliser aerosols) and 0.0033 mg – 0.0042 mg (of inhaled and immediately exhaled aerosols) per half hour. Nevertheless, there are several factors which may influence inhalation dose, age, weight, activity level etc (US Environmental Protection Agency, 2009), all of which will affect the quantity of aerosols inhaled. Room dimensions, air turbulence, ventilation and temperature may alter the distribution of the aerosols in the ward (Ciuzas et al., 2015, Kumar et al., 2016). Although the exposure may only be in low doses in short time periods, healthcare workers who may be working in the vicinity of several patients over days, weeks and years may be susceptible to chronic low dose occupational exposure (Goodson III et al., 2015). The implications and inhalation rates of this are further examined in chapter 5.

3.15.4 AirNode Air monitor

The emergence of "low-cost" and novel air quality sensors has caused a paradigm shift in air quality measurements from standardised government operated networks, using reference instruments, to mixed networks where emergent sensor/monitor technologies supplement reference-grade monitors as documented by the U.S. EPA (Snyder et al., 2013, Morawska et al., 2018). Similarly, in Europe Borrego *et al.* suggest the use of microsensors, if supported by the proper post processing and data modelling tools, have the ability to support and complement standard monitoring procedures (Borrego et al., 2016, Borrego et al., 2018).

In this study the AirVisual showed high and significant correlation with the unfiltered WIBS data (r=+0.81) and a relatively lower correlation with the filtered WIBS data (r

= +0.33), see Figure 3.34. However, the most prominent peak of $PM_{2.5}$ concentration at 07:00-07:30 lags ~ 30 minutes after the most prominent filtered WIBS peak at 06:30-07:00. Although the AirVisual sensor correlates highly with the unfiltered WIBS counts, the normalised ratio of the mean half hourly concentrations with the WIBS counts was quite low (Figure 3.35), suggesting the AirVisual device does not quantify the nebuliser aerosols to the same extent as the WIBS does. This may be down to the scattering ability of the two devices. The WIBS uses a sheath flow to constrain particles as a vertical column and allows the 635 nm laser to illuminate individual particles flowing into the optical chamber. The scattering of this light allows individual particles to be sized based on mie theory. Whereas within the AirVisual Node is a measuring chamber where a laser beam is shone onto particles, this light is irradiated in all directions from the particle scattering allowing its sensor to calculate the concentration of particles in the chamber. However, this does not identify individual particles, so in the case of nebulisation where large quantities of aerosols are produced the chamber may become flooded with particles, causing the laser scatter to hit masses of aerosol particles instead of individual particles. This results in a weaker signal, as it is measuring the scatter from a mass of aerosol instead of singular particles. Perhaps after a certain concentration enters the chamber, it saturates consequently reporting low concentrations.

Measurements by the AirNode device showed that all 14 days had an average above the 25 $\mu g/m^3$ limit (Figure 3.32). The World Health Organisation guidelines for air quality state that over a 24hr period the average 99^{th} percentile limit for $PM_{2.5}$ should not exceed 25 $\mu g/m^3$ with an annual mean of 10 $\mu g/m^3$ (Krzyzanowski and Cohen, 2008, Organization, 2010). European Union directive 2008/50/EC guidelines on ambient air quality, specify that an annual average $PM_{2.5}$ concentration should not exceed a higher, upper assessment limit of 20 $\mu g/m^3$ (UNION, 2008). WHO estimates that 92% of people are exposed to $PM_{2.5}$ concentrations exceeding the annual mean of 10 $\mu g/m^3$ (Organization, 2016). Portuguese hospital legislation has followed WHO guidelines and implemented the limit for $PM_{2.5}$, legislating that concentrations should not exceed 25 $\mu g/m^3$ in the hospital environment (Government, 2013).The International Agency for Research on Cancer (IARC) classified particulate matter (PM) as a Group 1 carcinogen in 2013 (Loomis et al., 2013). Fine particulate matter $PM_{2.5}$, particles with aerodynamic diameter less than 2.5 µm, have been linked to many

adverse health effects including respiratory illness (Xing et al., 2016), cardiovascular disease (Dabass et al., 2016, Turner et al., 2017), lung cancer (Vinikoor-Imler et al., 2011), reproductive issues (Wu et al., 2016), and premature death (Cohen et al., 2018). It is estimated that in 2015 ~4.2 million people died prematurely due to $PM_{2.5}$ exposure, putting $PM_{2.5}$ in the top five morality risk factors worldwide (Cohen et al., 2018).

3.15.5 Comparison of microbial cultures

As previously documented in chapter 1, section 1.5 no specific protocol or standard to be used in general ward air sampling is available, but the Health Technical Memorandum 03-01 sets standards for both conventional and ultra-clean operating theatres (Health/Estates and Division, 2007). However, new EU/WHO hospital air contamination limits based on patient risk using a 3-class system are being developed. That will set allowable numbers of bacterial CFU within selective healthcare environments. These guidelines are based on previously developed standards for microbial cleanliness in Switzerland from 1987 (Krankenhausinstitut, 1987).

The colony count of air collected during the study was on average 509 CFU/m^3 at 11:30, and 629 CFU/m^3 at 13:00. This would see the respiratory ward fall into the Class III room as per Swiss guidelines (Chapter 1, Table 1.3). Comparing the mean cultured bacterial counts to those from previous studies, compiled in Chapter 1, Table 1.16, the bacterial counts collected during this study were higher than operating theatre levels, but the boxplot shown in Figure 3.37. shows that bacterial counts from this study are not an outlier compared to all the other means.

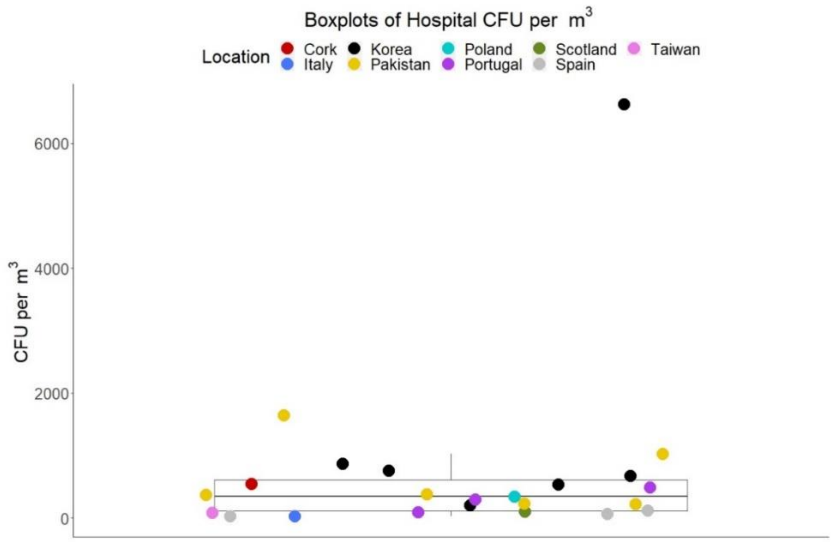

Figure 3.37 Boxplot of mean hospital CFU/m^3 from Table 1.16. The coloured dots represent the different locations, this study (Cork) is the red-coloured dot.

Table 3.17 Summary of previous bacterial concentrations at various hospital sites with the inclusion of this study.

Location	Site	Bacterial Concentration (CFU/m^3)		Instrument	Culture Media	Reference
		Average	Range			
Murcia, Spain	Operating Theatre	25.6	1.67-157	MAS-100	Plate Count Agar	(Ortiz et al., 2009)
	Hospital Rooms*	124.4	4.12-1293			
	Maternity Ward*	67	14.33-224			
Islamabad, Pakistan	Operation theatre Emergency	221	60-466.7	Gillian 5000	TSA	(Asif et al., 2018)
	Operation theatre General	236.2	60-460			
	Surgical Ward	369.9	20-1038.5			
	General Medicine Ward	383.9	100-840			
	Emergency Service	1028.9	280-2280			
	Out-patient department	1649.7	380-3577			
Korea	Lobby A	870	380-1800	Anderson Single Stage	TSA	(Park et al., 2013)
	Lobby B	6620	50-2300			
	Lobby C	760	280-1800			
	Lobby D	680	330-1800			
	Lobby E	540	270-1700			
	Lobby F	200	80-450			
Setubal, Portugal	Operating Theatre		12-170	MAS-100	TSA	(Verde et al., 2015)
	Emergency Service		240-736			
	Surgical Ward		99-495			
Lublin, Poland	Pneumological Ward		257.1-436.3	Own device	Blood Agar	(Augustowska and Dutkiewicz, 2006)
Modena, Italy	Operating Theatre	25.8**	13-82**	Single Stage Slit Impactor	TSA	(Scaltriti et al., 2007)
	Instrument Area	7.9	0-25	Gravitational settling		
	Surgeon Area	5.2	0-25			
	Anaesthesia Equipment Area	6.2	0-18			
Taiwan	Clean Room Class 100		0-32	Anderson 1-STG	TSA	(Li and Hou, 2003)
	Clean Room Class 100000		1-423			
	Operating Theatre 10000	88	13-336			
Scotland	Intensive Care Unit	104.4	12-510	Surface Air System (SAS) Super-180	TSA	(Dougall et al., 2019)
Cork, Ireland	Respiratory Ward	542.75	189-1391	MAS-100	TSA	
		23.5	10-52	Gravitational		

Table 3.18 Summary of previous Particle concentrations at various hospital sites.

Location	Area	Particle Counts ($\times 10^6$ part/m^3)				Instrument	Ref
		Fluorescent mean	Fluorescent Range	Total mean	Total Range		
Australia, Brisbane	Adult Pulmonary Ward	0.05	0.02 - 0.1	1.28	0.84 - 1.83	UV-APS	(Pereira et al., 2017)
	Adult Spirometry Lab	0.07	0.11 - 0.24	1.46	0.57 - 1.84		
	Adult Outpatients Waiting	0.04	0.01 - 1.11	0.91	0.61 - 1.35		
	Adult Overall	0.06	0.05 - 0.48	1.2	0.67 - 1.67		
	Children Pulmonary Ward	0.03	0.0 - 0.06	0.4	0.26 - 0.58		
	Children Spirometry Lab	0.04	0.0 - 0.14	0.65	0.27 - 0.76		
	Children Outpatients Waiting	0.02	0.0 - 0.07	0.15	0.06 - 0.21		
	Children Overall	0.03	0.0 - 0.09	0.33	0.19 - 0.51		
China, Hefie	Operating Theatre (During Operation)	0.08				BAC-6825	(Dai et al., 2015)
	Operating Theatre (Preparation phase)	0.12					
	Operating Theatre (Static Condition)	0.02					
Ireland, Cork	Respiratory Ward	0.121	0.032 - 0.30	4.29	0.45 - 13.3	WIBS-4A	

A previous real-time study of fluorescent particle bioaerosol detection in hospital wards using a different instrument showed average fluorescent particle concentrations ranging from 0 – 0.09 $\times 10^6$ part./m^3 (mean 0.03 $\times$ 10^5) in a children's hospital and higher values 0.05 – 0.48 $\times$10 part./m^3 (mean 0.06 $\times$ 10^6) in an adult hospital (Pereira et al., 2017), Table 3.18. In comparison, the ward in this study had a mean fluorescent filtered particle concentration of 0.121 $\times$ 10^6 particles/m^3, similar to that reported from the adult ward in Australia (Pereira et al., 2017). Total particle concentrations in the children's hospital ranged from 0.19 – 0.51 $\times 10^6$ particles/m^3 (mean 0.06 $\times$ 10^6 particles/m^3), and at the adult hospital total particle concentrations ranged from 0.67 – 1.67 $\times$ 10^6 particles/m^3 (mean 1.20 $\times$ 10^6 particles/m^3). A higher total particle concentration mean was detected during this study, 3.92 $\times 10^6$ particles/m^3, a 226.7% increase.

Similarities exists between the Pereira *et al.* study and ours, they found bioaerosol concentrations increased with nebulised drug therapy, and ward activity. Although Pereira *et al.* found increases in fluorescent particle concentrations from the average 0.03$\times 10^6$ to 0.08$\times 10^6$ particles/m^3 concentrations during a documented case of

nebulisation therapy, they were not to the extent of WIBS nebuliser concentrations. The WIBS and the UVAPS are not directly comparable because of the different frequencies involved, the WIBS excites particles at 270 nm and 380 nm, however, the UVAPS only excites particles at 380 nm, which in turn misses the main excitation wavelength for salbutamol, 278 nm (Bi et al., 2013, Srichana et al., 2003). Pereira *et al.* observed that night-time bioaerosol concentrations were 3.3 and 9.0 times lower at night than day for total and fluorescent particles, respectively. Smaller decreases were noted in our respiratory ward with the night-time 0.29 and 0.36 times lower than day for total and fluorescent filtered concentrations, respectively.

3.16 **Future work**

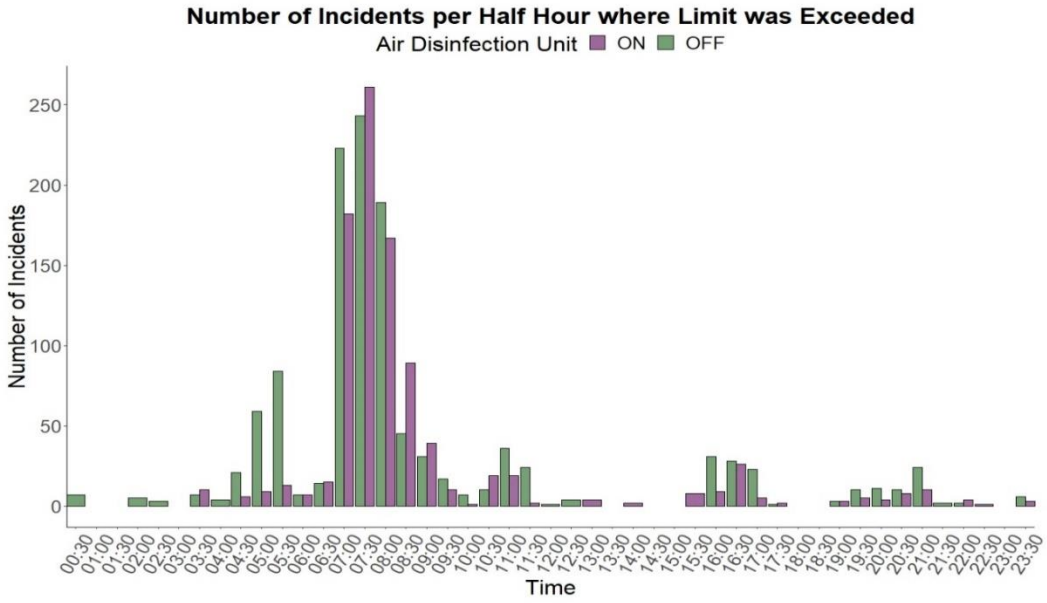

Figure 3.38 Number of incidents per half hour time interval over the full campaign.

The prospect of using real-time analysis as an early warning system with regards to bioaerosols produced is a possibility. With continuous WIBS-4A observation in future studies it would be relatively easy to propose and integrate an early warning system into the WIBS data collection. For example if one set a fluorescent filtered aerosol particle limit as the mean + three-times the standard deviation (mean + 3σ) (447000 part/m^3) for this study dataset, out of 46012-minute observations, the 3σ limit was exceeded 2135 times (943 with plasma disinfection unit on vs. 1199 with plasma disinfection unit off, P=0.655). Figure 3.38 shows that the half hour time periods from

07:00 – 08:00, coinciding with highest footfall, have the vast majority of incidents above 3σ.

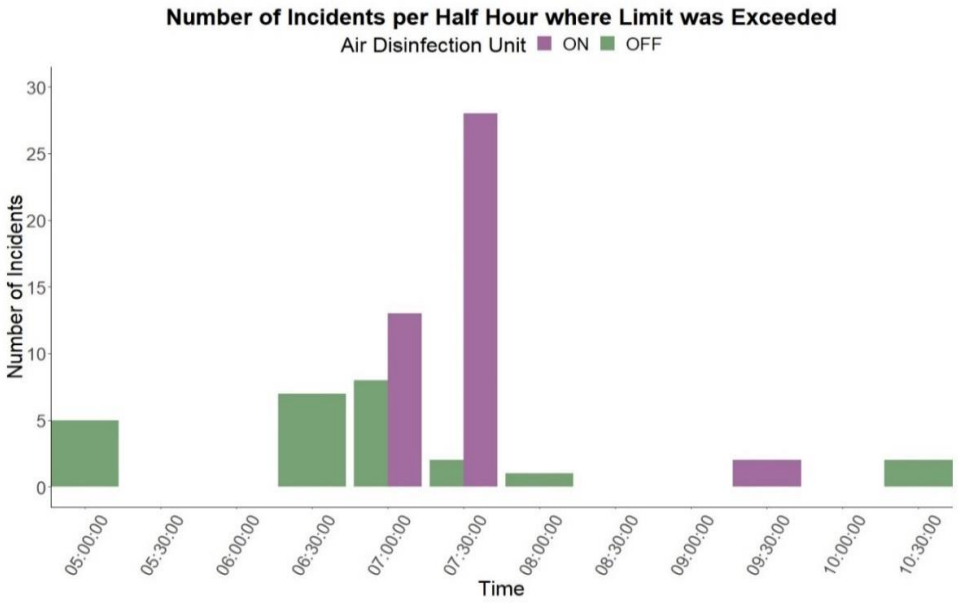

Figure 3.39 Number of incidents per half hour time interval over the full study (32 days)

If the threshold is increased to the mean + seven-times the standard deviation (mean + 7σ) (1215393 part/m^3), out of the 46012-minute observations, 68 minutes exceed the limit and all individual threshold breaches were in the morning 05:00-10:30 (Figure 3.39). This is the period when the cumulative diurnal fluorescent filtered particle counts and AirVisual $PM_{2.5}$ counts were highest (Figure 3.35). An insignificant increase in incidents breaking the threshold was observed with plasma (purple) compared to the control period (green) (43 with plasma disinfection unit on vs. 25 with plasma disinfection unit off, P=0.237).

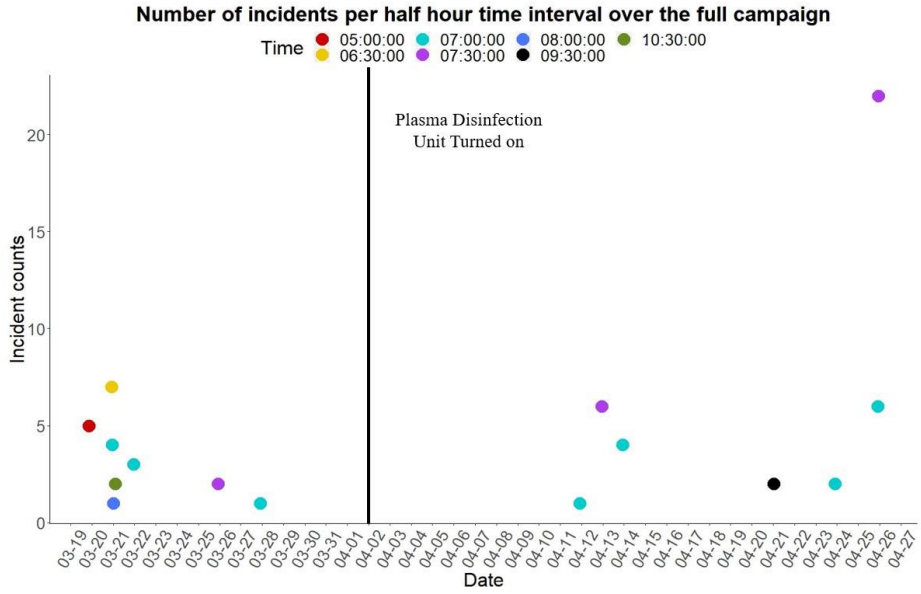

Figure 3.40 Incidents of 7σ excision per half hour time interval over the full study. Points coloured by time of threshold excision and y-axis is the count of excision per that half hour period.

Compressing this down into half hour period per day, see Figure 3.40, the limit was exceeded on 11 days, and multiple times some days. This illustrates that a background particle level could be defined by continuous observation in a locality with an early warning metric for limit breaches. It must be noted that on the 26th April, the limit was breached 28 times between 07:00-08:00, this is large outlier within the dataset.

3.17 **Conclusion**

The WIBS provides real-time biological air monitoring previously not possible by conventional sampling methods. One of the most impressive abilities of the instrument is its capability in identifying specific time periods which are bioaerosol generating, something which is impossible with conventional sampling methods. This can identify periods which may seem harmless but may generate significant amounts of bioaerosols. Here we identified staff changeover as being the most significant bioaerosol generating period. Significantly the WIBS can provide analysis of air disinfection systems, and every time period providing an overall evaluation of systems based on millions of time points, as opposed to 20-30 that are collected via conventional methods. This is noteworthy as the WIBS could help tune air disinfection systems to react to particle generating events as opposed to being constantly on, like

the early warning system, discussed section 4.6. Another important feature of the instrument is its remote, online monitoring. Where conventional sampling requires onsite presence, the WIBS can be left onsite with remote access via laptop and wi-fi dongle. This also allows the WIBS to synchronise its data up accurately with other instruments i.e. the footfall counter, where particle counts, and footfall data could be analysed side by side. The footfall counter allowed us to remotely accumulate footfall data over the 4-week study to accurately detail the movement in and out of the ward and to construct a consistent diurnal pattern allowing us to see high traffic times without being present on the ward. Being able to accurately correlate footfall counts with fluorescent particle counts revealed which activities were bioaerosol generating. In addition to quantifying bioaerosols the WIBS utilises its 3 fluorescent channels together and these channels have the potential to map certain areas with fluorescent signatures. In doing this, the WIBS can then monitor any changes that may occur, or the effect alterations have to an areas fluorescent signature i.e. what effect certain systems have to the microbial particle types generated in an area.

One potential weakness of the instrument is its sensitivity to fluorescent interferants, which in this case is illustrated by nebuliser therapy drugs flooding the instrument's fluorescence detectors. Incidentally this interferant instigated further research into the mass of aerosols produced by nebuliser therapy, the implications of which will be discussed further in Chapter 5. A practical problem with remote monitoring was experienced in a public environment like the hospital ward in that, despite enclosure in a box members of the public attempted to tamper with the instrument, and the instrument was unplugged several times on the ward by both staff and patients despite extensive coverage with warning notices. However, overall the WIBS successfully investigated the effectiveness of the novel intervention of plasma disinfection unit in removing bioaerosols from a hospital environment.

3.18 **References**

AITHINNE, K. A., COOPER, C. W., LYNCH, R. A. & JOHNSON, D. L. 2019. Toilet plume aerosol generation rate and environmental contamination following bowl water inoculation with Clostridium difficile spores. *American journal of infection control,* 47**,** 515-520.

ALLEGRANZI, B., NEJAD, S. B. & PITTET, D. 2017. The burden of healthcare-associated infection. *Hand hygiene: a handbook for medical professionals. 1st edition ed. hospital medicine: current concepts. Hoboken: Wiley***,** 1-7.

ANAISSIE, E. J., STRATTON, S. L., DIGNANI, M. C., SUMMERBELL, R. C., REX, J. H., MONSON, T. P., SPENCER, T., KASAI, M., FRANCESCONI, A. & WALSH, T. J. 2002. Pathogenic Aspergillus species recovered from a hospital water system: a 3-year prospective study. *Clinical Infectious Diseases,* 34**,** 780-789.

ARMOUGOM, F., HENRY, M., VIALETTES, B., RACCAH, D. & RAOULT, D. 2009. Monitoring bacterial community of human gut microbiota reveals an increase in Lactobacillus in obese patients and Methanogens in anorexic patients. *PloS one,* 4**,** e7125.

ASIF, A., ZEESHAN, M., HASHMI, I., ZAHID, U. & BHATTI, M. F. 2018. Microbial quality assessment of indoor air in a large hospital building during winter and spring seasons. *Building and Environment,* 135**,** 68-73.

ASSIRI, A., MCGEER, A., PERL, T. M., PRICE, C. S., AL RABEEAH, A. A., CUMMINGS, D. A., ALABDULLATIF, Z. N., ASSAD, M., ALMULHIM, A. & MAKHDOOM, H. 2013. Hospital outbreak of Middle East respiratory syndrome coronavirus. *New England Journal of Medicine,* 369**,** 407-416.

AUGUSTOWSKA, M. & DUTKIEWICZ, J. 2006. Variability of airborne microflora in a hospital ward within a period of one year. *Annals of Agricultural and Environmental Medicine,* 13**,** 99-106.

AZIMI, P. & STEPHENS, B. 2013. HVAC filtration for controlling infectious airborne disease transmission in indoor environments: Predicting risk reductions and operational costs. *Building and Environment,* 70**,** 150-160.

BACHE, S. E., MACLEAN, M., GETTINBY, G., ANDERSON, J. G., MACGREGOR, S. J. & TAGGART, I. 2015. Airborne bacterial dispersal during and after dressing and bed changes on burns patients. *Burns,* 41**,** 39-48.

BALIKHIN, I., BERESTENKO, V., DOMASHNEV, I., KABATCHKOV, E., KURKIN, E., TROITSKI, V. & NAKHAEV, V. 2016. Photocatalytic recyclers for purification and disinfection of indoor air in medical institutions. *Biomedical Engineering,* 49**,** 389-393.

BARKER, J. & JONES, M. 2005. The potential spread of infection caused by aerosol contamination of surfaces after flushing a domestic toilet. *Journal of applied microbiology,* 99**,** 339-347.

BEST, E., SANDOE, J. & WILCOX, M. 2012. Potential for aerosolization of Clostridium difficile after flushing toilets: the role of toilet lids in reducing environmental contamination risk. *Journal of Hospital Infection,* 80**,** 1-5.

BI, S., PANG, B., ZHAO, T., WANG, T., WANG, Y. & YAN, L. 2013. Binding characteristics of salbutamol with DNA by spectral methods. *Spectrochimica Acta Part A: Molecular and Biomolecular Spectroscopy,* 111**,** 182-187.

BORREGO, C., COSTA, A., GINJA, J., AMORIM, M., COUTINHO, M., KARATZAS, K., SIOUMIS, T., KATSIFARAKIS, N., KONSTANTINIDIS, K. & DE VITO, S. 2016. Assessment of air quality microsensors versus

reference methods: The EuNetAir joint exercise. *Atmospheric Environment,* 147**,** 246-263.

BORREGO, C., GINJA, J., COUTINHO, M., RIBEIRO, C., KARATZAS, K., SIOUMIS, T., KATSIFARAKIS, N., KONSTANTINIDIS, K., DE VITO, S. & ESPOSITO, E. 2018. Assessment of air quality microsensors versus reference methods: The EuNetAir Joint Exercise–Part II. *Atmospheric environment,* 193**,** 127-142.

BRACHMAN, P. Hospital-acquired infection—airborne or not? Proceedings of the International Conference on Hospital-Acquired Infections, 1971. American Hospital Association, 189-192.

BURES, S., FISHBAIN, J. T., UYEHARA, C. F., PARKER, J. M. & BERG, B. W. 2000. Computer keyboards and faucet handles as reservoirs of nosocomial pathogens in the intensive care unit. *American journal of infection control,* 28**,** 465-471.

CASSIER, P., LANDELLE, C., REYROLLE, M., NICOLLE, M., SLIMANI, S., ETIENNE, J., VANHEMS, P. & JARRAUD, S. 2013. Hospital washbasin water: risk of legionella-contaminated aerosol inhalation. *Journal of Hospital Infection,* 85**,** 308-311.

CHEN, P.-S. & LI, C.-S. 2005. Quantification of airborne Mycobacterium tuberculosis in health care setting using real-time qPCR coupled to an air-sampling filter method. *Aerosol Science and Technology,* 39**,** 371-376.

CHINN, R. Y. & SEHULSTER, L. 2003. Guidelines for environmental infection control in health-care facilities; recommendations of CDC and Healthcare Infection Control Practices Advisory Committee (HICPAC).

CIUZAS, D., PRASAUSKAS, T., KRUGLY, E., SIDARAVICIUTE, R., JURELIONIS, A., SEDUIKYTE, L., KAUNELIENE, V., WIERZBICKA, A. & MARTUZEVICIUS, D. 2015. Characterization of indoor aerosol temporal variations for the real-time management of indoor air quality. *Atmospheric environment,* 118**,** 107-117.

CLAESSON, M. J., O'SULLIVAN, O., WANG, Q., NIKKILÄ, J., MARCHESI, J. R., SMIDT, H., DE VOS, W. M., ROSS, R. P. & O'TOOLE, P. W. 2009. Comparative analysis of pyrosequencing and a phylogenetic microarray for exploring microbial community structures in the human distal intestine. *PloS one,* 4**,** e6669.

CLAY, M. M. & CLARKE, S. W. 1987. Wastage of drug from nebulisers: a review. *Journal of the Royal Society of Medicine,* 80**,** 38-39.

COHEN, A., BRAUER, M. & BURNETT, R. 2018. Estimates and 25-year trends of the global burden of disease attributable to ambient air pollution: an analysis of data from the Global Burden of Diseases Study 2015 (vol 389, pg 1907, 2017). *Lancet,* 391**,** 1576-1576.

CREAMER, E., SHORE, A. C., DEASY, E. C., GALVIN, S., DOLAN, A., WALLEY, N., MCHUGH, S., FITZGERALD-HUGHES, D., SULLIVAN, D. J. & CUNNEY, R. 2014. Air and surface contamination patterns of meticillin-resistant Staphylococcus aureus on eight acute hospital wards. *Journal of Hospital Infection,* 86**,** 201-208.

DABASS, A., TALBOTT, E. O., VENKAT, A., RAGER, J., MARSH, G. M., SHARMA, R. K. & HOLGUIN, F. 2016. Association of exposure to particulate matter (PM2. 5) air pollution and biomarkers of cardiovascular disease risk in adult NHANES participants (2001–2008). *International journal of hygiene and environmental health,* 219**,** 301-310.

DANCER, S. J. 2009. The role of environmental cleaning in the control of hospital-acquired infection. *Journal of Hospital Infection,* 73**,** 378-385.
DANCER, S. J. 2011. Hospital cleaning in the 21st century. *European journal of clinical microbiology & infectious diseases,* 30**,** 1473-1481.
DAVIES, S. 2010. Fragmented management, hospital contract cleaning and infection control. *Policy & Politics,* 38**,** 445-463.
DEANE, G., MAUGHAN, K. & SOBERON, F. 2015. Coil Assembly for Plasma Generation. Google Patents.
DEANE, G., MAUGHAN, K., SOBERON, F. & O'CONNOR, N. 2016. Air Treatment Device Having A Plasma Coil Electrostatic Precipitator Assembly. Google Patents.
DOUGALL, L. R., BOOTH, M., KHOO, E., HOOD, H., MACGREGOR, S., ANDERSON, J., TIMOSHKIN, I. & MACLEAN, M. 2019. Continuous Monitoring of Aerial Bioburden within Intensive Care Isolation Rooms and Identification of 'High Risk'Activities. *Journal of Hospital Infection*.
FENNELLY, K. P., MARTYNY, J. W., FULTON, K. E., ORME, I. M., CAVE, D. M. & HEIFETS, L. B. 2004. Cough-generated aerosols of Mycobacterium tuberculosis: a new method to study infectiousness. *American journal of respiratory and critical care medicine,* 169**,** 604-609.
FENNELLY, M. J., SEWELL, G., PRENTICE, M. B., O'CONNOR, D. J. & SODEAU, J. R. 2017. The Use of Real-Time Fluorescence Instrumentation to Monitor Ambient Primary Biological Aerosol Particles (PBAP). *Atmosphere,* 9**,** 1.
FERNSTROM, A. & GOLDBLATT, M. 2013. Aerobiology and its role in the transmission of infectious diseases. *Journal of pathogens,* 2013.
FIRST, M. W. 1998. Hepa Filters. *Journal of the American Biological Safety Association,* 3**,** 33-42.
FOX, R. W. 1994. Air cleaners: a review. *Journal of allergy and clinical immunology,* 94**,** 413-416.
GERBA, C. P., WALLIS, C. & MELNICK, J. L. 1975. Microbiological hazards of household toilets: droplet production and the fate of residual organisms. *Applied microbiology,* 30**,** 229-237.
GOMES, C., FREIHAUT, J. & BAHNFLETH, W. 2007. Resuspension of allergen-containing particles under mechanical and aerodynamic disturbances from human walking. *Atmospheric Environment,* 41**,** 5257-5270.
GOODMAN, K., SIMNER, P., TAMMA, P. & MILSTONE, A. 2016. Infection control implications of heterogeneous resistance mechanisms in carbapenem-resistant Enterobacteriaceae (CRE). *Expert review of anti-infective therapy,* 14**,** 95-108.
GOODSON III, W. H., LOWE, L., CARPENTER, D. O., GILBERTSON, M., MANAF ALI, A., LOPEZ DE CERAIN SALSAMENDI, A., LASFAR, A., CARNERO, A., AZQUETA, A. & AMEDEI, A. 2015. Assessing the carcinogenic potential of low-dose exposures to chemical mixtures in the environment: the challenge ahead. *Carcinogenesis,* 36**,** S254-S296.
GOVERNMENT, P. 2013. Ordinance n.o. 353-A/2013. Diario da Republica.
HAIDUVEN, D. 2009. Nosocomial aspergillosis and building construction. *Medical mycology,* 47**,** S210-S216.
HEALTH, N. I. F. & EXCELLENCE, C. 2012. Infection: prevention and control of healthcare-associated infections in primary and community care. *NICE Google Scholar*.

HEALTH/ESTATES, D. O. & DIVISION, F. 2007. Health Technical Memorandum 03-01: Specialised Ventilation for Healthcare Premises. Part A-Design and Installation. The Stationery Office Norwich, UK.

HEALY, D. A., O'CONNOR, D. J., BURKE, A. M. & SODEAU, J. R. 2012. A laboratory assessment of the Waveband Integrated Bioaerosol Sensor (WIBS-4) using individual samples of pollen and fungal spore material. *Atmospheric environment,* 60**,** 534-543.

HOSPODSKY, D., QIAN, J., NAZAROFF, W. W., YAMAMOTO, N., BIBBY, K., RISMANI-YAZDI, H. & PECCIA, J. 2012. Human occupancy as a source of indoor airborne bacteria. *PloS one,* 7**,** e34867.

HOSPODSKY, D., YAMAMOTO, N., NAZAROFF, W., MILLER, D., GORTHALA, S. & PECCIA, J. 2015. Characterizing airborne fungal and bacterial concentrations and emission rates in six occupied children's classrooms. *Indoor air,* 25**,** 641-652.

IJAZ, M. K., ZARGAR, B., WRIGHT, K. E., RUBINO, J. R. & SATTAR, S. A. 2016. Generic aspects of the airborne spread of human pathogens indoors and emerging air decontamination technologies. *American Journal of Infection Control,* 44**,** S109-S120.

ISMAIL, N. A., RAGAB, S. H., ELBAKY, A. A., SHOEIB, A. R., ALHOSARY, Y. & FEKRY, D. 2011. Frequency of Firmicutes and Bacteroidetes in gut microbiota in obese and normal weight Egyptian children and adults. *Archives of medical science: AMS,* 7**,** 501.

KAPUSTINA, E. & VOLODINA, E. 2004. Air decontamination and the fine filtration system" Potok 150MK". *Aviakosmicheskaia i ekologicheskaia meditsina= Aerospace and environmental medicine,* 38**,** 57-58.

KAYE, P. H., STANLEY, W. R. & FOOT, E. V. J. 2014. *Fluid-Borne Particle Detector*. US 13/957,655.

KOTSANAS, D., WIJESOORIYA, W., KORMAN, T. M., GILLESPIE, E. E., WRIGHT, L., SNOOK, K., WILLIAMS, N., BELL, J. M., LI, H. Y. & STUART, R. L. 2013. "Down the drain": carbapenem-resistant bacteria in intensive care unit patients and handwashing sinks. *Medical Journal of Australia,* 198**,** 267-269.

KOWALSKI, W. 2007. Hospital-Acquired Infections. *HPAC Engineering*.

KOWALSKI, W. 2016. *Hospital Airborne Infection Control*, CRC Press.

KRANKENHAUSINSTITUT, S. 1987. Richtlinie für den Bau, Betrieb und die Überwachung von lüftungstechnischen Anlagen in Spitälern. Aarau: Krankenhausinstitut (in German).

KRZYZANOWSKI, M. & COHEN, A. 2008. Update of WHO air quality guidelines. *Air Quality, Atmosphere & Health,* 1**,** 7-13.

KUMAR, P., SKOULOUDIS, A. N., BELL, M., VIANA, M., CAROTTA, M. C., BISKOS, G. & MORAWSKA, L. 2016. Real-time sensors for indoor air monitoring and challenges ahead in deploying them to urban buildings. *Science of the Total Environment,* 560**,** 150-159.

KUNDSIN, R. B. 1980. Documentation of airborne infection during surgery. *Annals of the New York Academy of Sciences,* 353**,** 255-261.

KUTTER, J. S., SPRONKEN, M. I., FRAAIJ, P. L., FOUCHIER, R. A. & HERFST, S. 2018. Transmission routes of respiratory viruses among humans. *Current opinion in virology,* 28**,** 142-151.

LAI, A., CHEUNG, A., WONG, M. & LI, W. 2016. Evaluation of cold plasma inactivation efficacy against different airborne bacteria in ventilation duct flow. *Building and Environment,* 98**,** 39-46.

LAROUSSI, M., MENDIS, D. & ROSENBERG, M. 2003. Plasma interaction with microbes. *New Journal of Physics,* 5**,** 41.

LAU, J. T., GRIFFITHS, S., CHOI, K. C. & TSUI, H. Y. 2009. Widespread public misconception in the early phase of the H1N1 influenza epidemic. *Journal of infection,* 59**,** 122-127.

LAYTON, M. C., PEREZ, M., HEALD, P. & PATTERSON, J. E. 1993. An outbreak of mupirocin-resistant Staphylococcus aureus on a dermatology ward associated with an environmental reservoir. *Infection Control & Hospital Epidemiology,* 14**,** 369-375.

LI, C.-S. & HOU, P.-A. 2003. Bioaerosol characteristics in hospital clean rooms. *Science of the Total Environment,* 305**,** 169-176.

LIGHTHART, B. 1997. The ecology of bacteria in the alfresco atmosphere. *FEMS Microbiology Ecology,* 23**,** 263-274.

LIM, T., CHO, J. & KIM, B. S. 2010. The predictions of infection risk of indoor airborne transmission of diseases in high-rise hospitals: Tracer gas simulation. *Energy and Buildings,* 42**,** 1172-1181.

LIN, C.-Y. & LI, C.-S. 2002. Control effectiveness of ultraviolet germicidal irradiation on bioaerosols. *Aerosol science and technology,* 36**,** 474-478.

LINDSLEY, W. G., NOTI, J. D., BLACHERE, F. M., THEWLIS, R. E., MARTIN, S. B., OTHUMPANGAT, S., NOORBAKHSH, B., GOLDSMITH, W. T., VISHNU, A. & PALMER, J. E. 2015. Viable influenza A virus in airborne particles from human coughs. *Journal of occupational and environmental hygiene,* 12**,** 107-113.

LINDSLEY, W. G., PEARCE, T. A., HUDNALL, J. B., DAVIS, K. A., DAVIS, S. M., FISHER, M. A., KHAKOO, R., PALMER, J. E., CLARK, K. E. & CELIK, I. 2012. Quantity and size distribution of cough-generated aerosol particles produced by influenza patients during and after illness. *Journal of occupational and environmental hygiene,* 9**,** 443-449.

LOOMIS, D., GROSSE, Y., LAUBY-SECRETAN, B., EL GHISSASSI, F., BOUVARD, V., BENBRAHIM-TALLAA, L., GUHA, N., BAAN, R., MATTOCK, H. & STRAIF, K. 2013. The carcinogenicity of outdoor air pollution. *The lancet oncology,* 14**,** 1262-1263.

MAI-PROCHNOW, A., MURPHY, A. B., MCLEAN, K. M., KONG, M. G. & OSTRIKOV, K. K. 2014. Atmospheric pressure plasmas: infection control and bacterial responses. *International journal of antimicrobial agents,* 43**,** 508-517.

MASTORIDES, S. M., OEHLER, R. L., GREENE, J. N., SINNOTT IV, J. T., KRANIK, M. & SANDIN, R. L. 1999. The detection of airborne Mycobacterium tuberculosis using micropore membrane air sampling and polymerase chain reaction. *Chest,* 115**,** 19-25.

MAY, D. & PITT, M. 2012. Environmental cleaning in UK healthcare since the NHS Plan: a policy and evidence based context. *Facilities,* 30**,** 6-22.

MCGRATH, J. A., O'SULLIVAN, A., BENNETT, G., O'TOOLE, C., JOYCE, M., BYRNE, M. A. & MACLOUGHLIN, R. 2019. Investigation of the quantity of exhaled aerosols released into the environment during nebulisation. *Pharmaceutics,* 11**,** 75.

MORAWSKA, L. 2006. Droplet fate in indoor environments, or can we prevent the spread of infection? *Indoor air,* 16**,** 335-347.

MORAWSKA, L., JOHNSON, G., RISTOVSKI, Z., HARGREAVES, M., MENGERSEN, K., CORBETT, S., CHAO, C. Y. H., LI, Y. & KATOSHEVSKI, D. 2009. Size distribution and sites of origin of droplets expelled from the human respiratory tract during expiratory activities. *Journal of Aerosol Science,* 40**,** 256-269.

MORAWSKA, L., THAI, P. K., LIU, X., ASUMADU-SAKYI, A., AYOKO, G., BARTONOVA, A., BEDINI, A., CHAI, F., CHRISTENSEN, B. & DUNBABIN, M. 2018. Applications of low-cost sensing technologies for air quality monitoring and exposure assessment: How far have they gone? *Environment international,* 116**,** 286-299.

MUDER, R. R., VICTOR, L. Y., MCCLURE, J. K., KROBOTH, F. J., KOMINOS, S. D. & LUMISH, R. M. 1983. Nosocomial Legionnaires' disease uncovered in a prospective pneumonia study: implications for underdiagnosis. *Jama,* 249**,** 3184-3188.

MURCHAN, S., MURPHY, H. & BURNS, K. 2018. Point Prevalence Survey of Hospital-Acquired Infections & Antimicrobial Use in European Acute Care Hospitals. NATIONAL REPORT: IRELAND.

NATIONAL HOSPITALS, O. 2005. HSE National Cleaning Standards Manual.

NISHIKAWA, K. & NOJIMA, H. 2003. Airborn virus inactivation technology using cluster ions generated by discharge plasma. *Sharp Tech J,* 86**,** 10-15.

NOVOSELAC, A. & SIEGEL, J. A. 2009. Impact of placement of portable air cleaning devices in multizone residential environments. *Building and Environment,* 44**,** 2348-2356.

O'GORMAN, C. M. 2011. Airborne Aspergillus fumigatus conidia: a risk factor for aspergillosis. *Fungal biology reviews,* 25**,** 151-157.

OBEE, T. N., HAY, S. O., BRANDES, S. D. & COLKET, M. B. 2016. Method and system for using an ozone generating device for air purification. Google Patents.

OFFICE, G. B. N. A. 2009. *Reducing healthcare associated infections in hospitals in England*, Stationery Office.

ORGANIZATION, W. H. 2010. WHO guidelines for indoor air quality: selected pollutants.

ORGANIZATION, W. H. 2016. Ambient air pollution: A global assessment of exposure and burden of disease.

ORTIZ, G., YAGÜE, G., SEGOVIA, M. & CATALÁN, V. 2009. A study of air microbe levels in different areas of a hospital. *Current microbiology,* 59**,** 53.

PEREIRA, M. L., KNIBBS, L. D., HE, C., GRZYBOWSKI, P., JOHNSON, G. R., HUFFMAN, J. A., BELL, S. C., WAINWRIGHT, C. E., MATTE, D. L. & DOMINSKI, F. H. 2017. Sources and dynamics of fluorescent particles in hospitals. *Indoor Air*.

PERRING, A. E. 2016. Chamber catalogues of optical and fluorescent signatures distinguish bioaerosol classes. *Atmospheric Measurement Techniques,* 9**,** 3283.

PREVENTION, E. C. F. D., CONTROL, SUETENS, C., HOPKINS, S., KOLMAN, J. & HÖGBERG, L. D. 2013. *Point Prevalence Survey of Healthcare-associated Infections and Antimicrobial Use in European Acute Care Hospitals: 2011-2012*, Publications Office of the European Union.

QIAN, H., LI, Y., SUN, H., NIELSEN, P. V., HUANG, X. & ZHENG, X. Particle removal efficiency of the portable HEPA air cleaner in a simulated hospital ward. Building Simulation, 2010. Springer, 215-224.

QIAN, J., PECCIA, J. & FERRO, A. R. 2014. Walking-induced particle resuspension in indoor environments. *Atmospheric Environment,* 89**,** 464-481.

ROBERTS, K., HATHWAY, A., FLETCHER, L., BEGGS, C., ELLIOTT, M. & SLEIGH, P. 2006. Bioaerosol production on a respiratory ward. *Indoor and Built Environment,* 15**,** 35-40.

ROY, C. J. & MILTON, D. K. 2004. Airborne transmission of communicable infection-the elusive pathway. ARMY MEDICAL RESEARCH INST OF INFECTIOUS DISEASES FORT DETRICK MD ….

SCALTRITI, S., CENCETTI, S., ROVESTI, S., MARCHESI, I., BARGELLINI, A. & BORELLA, P. 2007. Risk factors for particulate and microbial contamination of air in operating theatres. *Journal of Hospital Infection,* 66**,** 320-326.

SEXTON, T., CLARKE, P., O'NEILL, E., DILLANE, T. & HUMPHREYS, H. 2006. Environmental reservoirs of methicillin-resistant Staphylococcus aureus in isolation rooms: correlation with patient isolates and implications for hospital hygiene. *Journal of Hospital Infection,* 62**,** 187-194.

SHIOMORI, T., MIYAMOTO, H., MAKISHIMA, K., YOSHIDA, M., FUJIYOSHI, T., UDAKA, T., INABA, T. & HIRAKI, N. 2002. Evaluation of bedmaking-related airborne and surface methicillin-resistant Staphylococcus aureus contamination. *Journal of Hospital Infection,* 50**,** 30-35.

SIANI, H. & MAILLARD, J.-Y. 2015. Best practice in healthcare environment decontamination. *European Journal of Clinical Microbiology & Infectious Diseases,* 34**,** 1-11.

SIEGEL, J. D. 2007. Healthcare Infection Control Practices Advisory Committee 2007 Guideline for isolation precautions: preventing transmission of infectious agents in healthcare settings. *http://www. cdc. gov/ncidod/dhqp/gl_isolation. html*.

SILHAVY, T. J., KAHNE, D. & WALKER, S. 2010. The bacterial cell envelope. *Cold Spring Harbor perspectives in biology,* 2**,** a000414.

SNYDER, E. G., WATKINS, T. H., SOLOMON, P. A., THOMA, E. D., WILLIAMS, R. W., HAGLER, G. S., SHELOW, D., HINDIN, D. A., KILARU, V. J. & PREUSS, P. W. 2013. The changing paradigm of air pollution monitoring. ACS Publications.

SRICHANA, T., SUEDEE, R. & SRISUDJAI, P. 2003. Application of spectrofluorometry for evaluation of dry powder inhalers in vitro. *Die Pharmazie-An International Journal of Pharmaceutical Sciences,* 58**,** 125-129.

STELZER-BRAID, S., OLIVER, B. G., BLAZEY, A. J., ARGENT, E., NEWSOME, T. P., RAWLINSON, W. D. & TOVEY, E. R. 2009. Exhalation of respiratory viruses by breathing, coughing, and talking. *Journal of medical virology,* 81**,** 1674-1679.

STREIFEL, A. J. 1996. *Controlling aspergillosis and Legionella in hospitals*, Boca Raton: Lewis Publishers.

TANG, J., LI, Y., EAMES, I., CHAN, P. & RIDGWAY, G. 2006. Factors involved in the aerosol transmission of infection and control of ventilation in healthcare premises. *Journal of Hospital Infection,* 64**,** 100-114.

TIAN, Y., SUL, K., QIAN, J., MONDAL, S. & FERRO, A. R. 2014. A comparative study of walking-induced dust resuspension using a consistent test mechanism. *Indoor Air,* 24**,** 592-603.

TOBIAS, H. J., SCHAFER, M. P., PITESKY, M., FERGENSON, D. P., HORN, J., FRANK, M. & GARD, E. E. 2005. Bioaerosol mass spectrometry for rapid detection of individual airborne Mycobacterium tuberculosis H37Ra particles. *Appl. Environ. Microbiol.,* 71**,** 6086-6095.

TURNER, M. C., COHEN, A., BURNETT, R. T., JERRETT, M., DIVER, W. R., GAPSTUR, S. M., KREWSKI, D., SAMET, J. M. & POPE III, C. A. 2017. Interactions between cigarette smoking and ambient PM2. 5 for cardiovascular mortality. *Environmental research,* 154**,** 304-310.

UNION, P. 2008. Directive 2008/50/EC of the European Parliament and of the Council of 21 May 2008 on ambient air quality and cleaner air for Europe. *Official Journal of the European Union*.

US ENVIRONMENTAL PROTECTION AGENCY 2009. Metabolically Derived Human Ventilation Rates: A Revised Approach Based upon Oxygen Consumption Rates. USEPA Washington, DC.

VADROT, C., BEX, V., MOUILLESEAUX, A., SQUINAZI, F. & DARBORD, J.-C. 2004. Detection of Mycobacterium tuberculosis complex by PCR in hospital air samples. *Journal of Hospital Infection,* 58**,** 262-267.

VERDE, S. C., ALMEIDA, S. M., MATOS, J., GUERREIRO, D., MENESES, M., FARIA, T., BOTELHO, D., SANTOS, M. & VIEGAS, C. 2015. Microbiological assessment of indoor air quality at different hospital sites. *Research in microbiology,* 166**,** 557-563.

VINIKOOR-IMLER, L. C., DAVIS, J. A. & LUBEN, T. J. 2011. An ecologic analysis of county-level PM2. 5 concentrations and lung cancer incidence and mortality. *International journal of environmental research and public health,* 8**,** 1865-1871.

VON VOGELSANG, A.-C., FÖRANDER, P., ARVIDSSON, M. & LÖWENHIELM, P. 2018. Effect of mobile laminar airflow units on airborne bacterial contamination during neurosurgical procedures. *Journal of Hospital Infection,* 99**,** 271-278.

WAGENVOORT, J., SLUIJSMANS, W. & PENDERS, R. 2000. Better environmental survival of outbreak vs. sporadic MRSA isolates. *Journal of Hospital Infection,* 45**,** 231-234.

WAŁASZEK, M., KOSIARSKA, A., GNIADEK, A., KOŁPA, M., WOLAK, Z., DOBROŚ, W. & SIADEK, J. 2016. The risk factors for hospital-acquired pneumonia in the Intensive Care Unit. *Przegl Epidemiol,* 70**,** 15-20.

WANG, C.-C., FANG, G.-C. & LEE, L.-Y. 2008. The study of ambient air bioaerosols during summer daytime and nighttime periods in Taichung, Central Taiwan. *Environmental Forensics,* 9**,** 6-14.

WANG, N., RAZA, A., SI, Y., YU, J., SUN, G. & DING, B. 2013. Tortuously structured polyvinyl chloride/polyurethane fibrous membranes for high-efficiency fine particulate filtration. *Journal of colloid and interface science,* 398**,** 240-246.

WARFEL, J. M., BEREN, J. & MERKEL, T. J. 2012. Airborne transmission of Bordetella pertussis. *The Journal of infectious diseases,* 206**,** 902-906.

WILSON, A., LIVERMORE, D., OTTER, J., WARREN, R., JENKS, P., ENOCH, D., NEWSHOLME, W., OPPENHEIM, B., LEANORD, A. & MCNULTY, C. 2016. Prevention and control of multi-drug-resistant Gram-negative

bacteria: recommendations from a Joint Working Party. *Journal of Hospital Infection,* 92**,** S1-S44.

WU, J., LAURENT, O., LI, L., HU, J. & KLEEMAN, M. 2016. Adverse Reproductive Health Outcomes and Exposure to Gaseous and Particulate-Matter Air Pollution in Pregnant Women. *Research report (Health Effects Institute)***,** 1-58.

WU, Y., LIANG, Y., WEI, K., LI, W., YAO, M., ZHANG, J. & GRINSHPUN, S. A. 2015. MS2 virus inactivation by atmospheric-pressure cold plasma using different gas carriers and power levels. *Appl. Environ. Microbiol.,* 81**,** 996-1002.

XIE, X., LI, Y., SUN, H. & LIU, L. 2009. Exhaled droplets due to talking and coughing. *Journal of the Royal Society Interface***,** rsif20090388.

XING, Y.-F., XU, Y.-H., SHI, M.-H. & LIAN, Y.-X. 2016. The impact of PM2. 5 on the human respiratory system. *Journal of thoracic disease,* 8**,** E69.

ZHUANG, Y., KIM, Y. J., LEE, T. G. & BISWAS, P. 2000. Experimental and theoretical studies of ultra-fine particle behavior in electrostatic precipitators. *Journal of electrostatics,* 48**,** 245-260.

3.19 **Appendix**

3.19.1 All time interval counts for fluorescent and fluorescent filtered

Table 3.19 Summary statistics of mean half hourly fluorescent and fluorescent filtered particle counts with P-values and adjusted P-values.

Time	Mean Fluorescent Count $\times 10^6$ particles / m^3			P-value	Adjusted P-value	Mean Fluorescent Filtered Count $\times 10^5$ particles / m^3			P-value	Adjusted P-value
	Plasma Disinfection Unit		Difference			Plasma Disinfection Unit		Difference		
	OFF	ON		MWU[A]	H[B]	OFF	ON		MWU[A]	H[B]
00:00	0.61	0.30	0.31	0.01	0.45	1.14	0.84	0.30	0.037	0.941
00:30	1.65	0.24	1.41	0.00	0.04	1.28	0.75	0.53	0.006	0.21
01:00	1.29	0.59	0.70	0.00	0.02	1.20	0.73	0.47	0.003	0.131
01:30	0.65	0.55	0.10	0.00	0.02	1.25	0.69	0.56	0.005	0.174
02:00	0.52	0.61	-0.09	0.05	0.79	1.41	0.90	0.51	0.015	0.448
02:30	0.51	0.55	-0.04	0.23	0.79	1.31	0.88	0.43	0.054	0.941
03:00	0.43	0.33	0.10	0.01	0.37	1.32	0.81	0.51	0.004	0.144
03:30	0.56	1.04	-0.48	0.00	0.14	1.12	0.88	0.25	0.014	0.424
04:00	1.20	1.42	-0.22	0.13	0.79	1.41	1.05	0.36	0.153	0.941
04:30	1.38	2.08	-0.70	0.79	0.79	1.53	1.08	0.46	0.174	0.941
05:00	4.34	3.42	0.91	0.68	0.79	2.57	1.53	1.03	0.37	0.941
05:30	9.05	5.91	3.14	0.11	0.79	3.06	1.79	1.27	0.013	0.406
06:00	6.94	5.39	1.55	0.09	0.79	1.79	1.54	0.26	0.355	0.941
06:30	3.61	2.85	0.76	0.10	0.79	1.87	1.27	0.59	0.014	0.424
07:00	2.95	1.66	1.29	0.01	0.21	4.97	4.13	0.85	0.526	0.941
07:30	2.74	1.39	1.35	0.01	0.37	4.96	5.21	-0.26	0.941	0.941
08:00	2.49	1.97	0.52	0.15	0.79	4.29	3.96	0.33	0.478	0.941
08:30	1.73	3.60	-1.87	0.39	0.79	2.58	2.78	-0.20	0.865	0.941
09:00	1.36	2.24	-0.88	0.37	0.79	2.01	1.87	0.14	0.478	0.941
09:30	1.04	0.99	0.05	0.06	0.79	1.42	1.25	0.17	0.461	0.941
10:00	0.80	0.83	-0.03	0.01	0.21	1.10	0.91	0.20	0.131	0.941
10:30	1.08	0.66	0.41	0.01	0.21	1.10	0.85	0.24	0.069	0.941
11:00	6.28	4.23	2.05	0.11	0.79	1.84	1.39	0.45	0.411	0.941
11:30	8.48	3.74	4.73	0.00	0.12	1.69	0.83	0.87	0.004	0.16
12:00	3.46	1.20	2.26	0.00	0.04	1.09	0.52	0.57	0.001	0.046
12:30	1.95	2.17	-0.22	0.13	0.79	0.98	0.74	0.24	0.097	0.941
13:00	1.11	1.46	-0.36	0.11	0.79	0.72	0.72	0.00	0.71	0.941
13:30	0.79	0.67	0.11	0.02	0.64	0.77	0.70	0.08	0.791	0.941
14:00	1.02	1.33	-0.31	0.02	0.55	0.81	0.68	0.13	0.189	0.941
14:30	0.88	0.42	0.46	0.00	0.10	0.97	0.49	0.48	0.001	0.067
15:00	0.65	0.31	0.34	0.00	0.04	0.98	0.56	0.42	0.005	0.193
15:30	2.12	1.58	0.54	0.05	0.79	1.09	0.91	0.18	0.142	0.941
16:00	7.24	4.67	2.56	0.11	0.79	1.95	1.11	0.84	0.045	0.941
16:30	6.40	6.75	-0.35	0.79	0.79	1.63	1.36	0.28	0.734	0.941
17:00	4.61	2.52	2.09	0.15	0.79	1.55	0.81	0.74	0.006	0.21
17:30	2.50	1.85	0.65	0.19	0.79	1.01	0.68	0.33	0.097	0.941

18:00	1.29	0.88	0.41	0.13	0.79	1.26	0.68	0.58	0.003	0.131
18:30	0.86	0.71	0.15	0.23	0.79	1.24	0.78	0.45	0.013	0.406
19:00	1.16	1.04	0.13	0.37	0.79	1.20	0.81	0.39	0.023	0.633
19:30	3.32	2.97	0.34	0.50	0.79	1.53	1.02	0.51	0.022	0.614
20:00	6.09	5.24	0.85	0.53	0.79	1.86	1.19	0.68	0.069	0.941
20:30	7.67	4.80	2.87	0.11	0.79	1.62	1.14	0.48	0.069	0.941
21:00	7.11	3.86	3.26	0.04	0.79	1.95	1.09	0.86	0.005	0.174
21:30	4.70	2.27	2.42	0.00	0.11	1.64	0.92	0.73	0.003	0.131
22:00	2.76	1.71	1.05	0.02	0.59	1.44	1.11	0.34	0.069	0.941
22:30	2.02	0.98	1.04	0.02	0.68	1.32	0.78	0.54	0.002	0.106
23:00	1.28	0.49	0.79	0.00	0.06	1.10	0.66	0.44	0.002	0.102
23:30	0.70	0.31	0.39	0.00	0.02	1.17	0.79	0.37	0.003	0.132

[A] Mann Whitney U [H] Hochberg

3.20 **Nebuliser Peak Identification**

The nebuliser associated peaks were noisy, so in order to analyse these peaks, the data was smoothed to remove noise. Smoothing data is a forecasting method that averages values over multiple periods in order to reduce noise and uncover patterns in data. The simplest and most straightforward is the moving average. This method selects several nearby points and averages them to estimate a trend. When calculating a simple moving average, you use an odd number of points so that the calculation is symmetric. For example, to calculate a 5-point moving average, the formula is:

$$\hat{y}_t = \frac{y_{t-2} + y_{t-1} + y_t + y_{t+1} + y_{t+2}}{5}$$

where *t* is the time step that you are smoothing at and 5 is the number of points being used to calculate the average, often denoted ask. For the ward data we can see the data is quite noisy, so in order to determine the rates at which peaks are reduced before and after the plasma disinfection unit was turned on, i.e. nebuliser peaks or human traffic peaks this moving average is useful. As the number of points used for the average increases, the curve becomes smoother and smoother. Choosing a value for *k* is a balance between eliminating noise while still capturing the data's true structure. For our study data, the 12-minute moving average ($k = 12$) eliminated some noise without removing the data's true pattern.

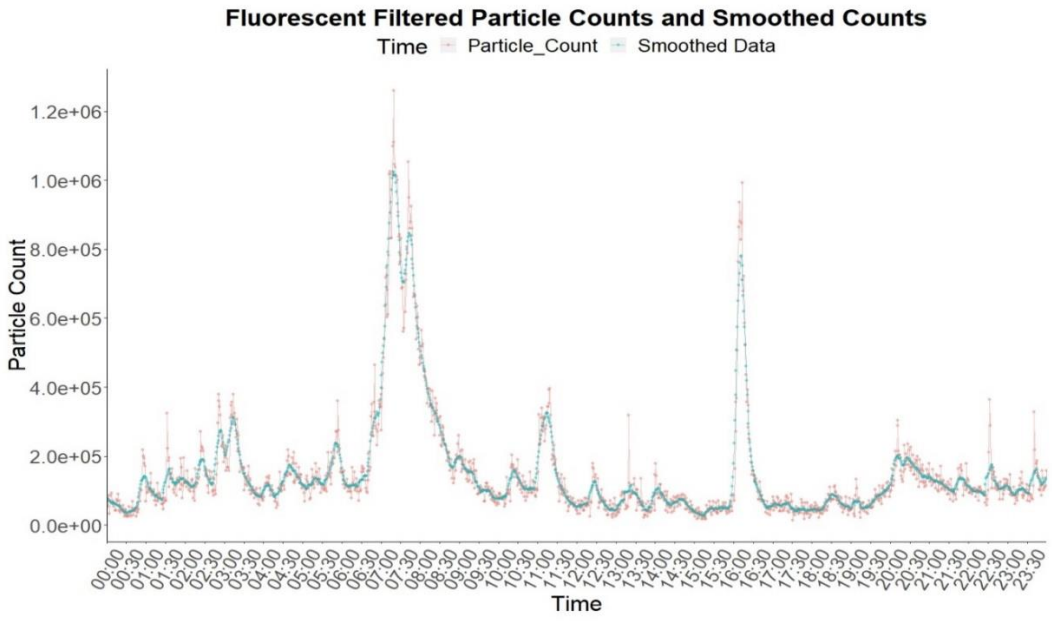

Figure 3.41 Single day isolated for data smoothing using moving average approach k = 12, smoothed data (blue) superimposed on the original particle counts (pink).

This allows peaks and valleys in dataset to be analysed without noise interference allowing accurate reduction rates to be calculated, see Figure 3.41.

Chapter 4

Laboratory Tests Of Nebulised Drugs and Nebulised Bacteria

Table of Contents

4.1 Introduction

The instrumental fluorescence detection limit of the WIBS is determined by measuring the fluorescence emission signal when no particles are present in the optical chamber (Fennelly et al., 2017). This is undertaken by putting the WIBS instrument into a setting known as “forced trigger” (FT) mode. This mode essentially causes the flash lamps within the WIBS to fire on empty space while the pump is off. Background fluorescent intensity values from the forced trigger mode are then collected for each channel over an undefined period of time, but usually 10 minutes. In general, the mean of these values in each channel (FL1, FL2, and FL3) plus 3× standard deviation (σ) has been used as the minimum cut-off threshold for particle fluorescence. In more recent times, alternate threshold strategies utilizing increased thresholds to aid in the detection, classification, and discrimination of ambient bio-particles from interfering particles have been suggested (Savage et al., 2017). Savage et al. (Savage et al., 2017) systematically evaluated fluorescence thresholds for the WIBS-4A using sixty-nine types of aerosol material, which included size-resolved biological particles (i.e., bacteria, fungal spores and pollen), and known chemical interferents (i.e., soot, smoke and atmospheric humic-like substances or HULIS) (Savage et al., 2017). A broad separation between the fluorescence signals of biological particles and chemical interferents was obtained using size and shape parameters in conjunction with the Perring (Perring et al., 2015) fluorescence channel particle classification system. Using these different classification systems, the role that particle size plays in controlling fluorescent properties was assessed. This led to a new threshold calculation whereby the fluorescent threshold was raised from the usual FT + 3σ to FT + 9σ. This results in weakly-fluorescing aerobiologically-insignificant particles under the previous threshold being reassigned as non-fluorescent under the new FT + 9σ criteria. The authors concluded that while it does not reduce the fraction of aerosol considered biological, it does significantly reduce fluorescence interference to almost zero for most particle types (Savage et al., 2017).

Perring *et al.* (Perring et al., 2015) conducted a dual campaign using an airborne WIBS-4 over Florida and California and subsequently developed a new particle classification system. They categorized particle fluorescence into one of seven types, depending on the different combinations of the three possible channels of fluorescence

signal above threshold detected by the WIBS (Perring et al., 2015). These categories consider each channel individually (FL1, FL2, and FL3), but also include all possible combinations, as shown in Table 4.1 Such cataloguing nomenclature allows for a greater degree of individual particle classification since the particle fluorescence intensities could previously only be placed into one or more of the FL channels, depending on their fluorescence. Thus, the designations used in Table 4.1 allow for a more detailed understanding of the fluorescent characteristics of ambient particles.

Table 4.1 Wideband Integrated Bioaerosol Sensor (WIBS-4A) channel annotation matrix. Channels are matched with excitation wavelength and emission waveband.

Channel	Excitation (nm)	Emission (nm)
A	280	310–400
B	280	420–650
C	370	420–650
AB	280	310–400 420–650
AC	280 370	310–400 420–650
BC	280 370	420–650
ABC	280	310–400 420–650
	370	420–650

This categorization system denotes particles that fluoresce above the threshold in only one channel as either types A, B, or C (depending on the excitation and emission wavelengths of the particle, as indicated in Table 4.1). Particles fluorescing in only two channels are classified as types AB, AC, and BC; while, particles that fluoresce in all of the channels are categorized as type ABC (Perring et al., 2015). As the WIBS determines characteristics of individual particles it is possible to detect more than one category of fluorescence signal from a single sample of known content e.g. spores of a single fungus.

Continuing the categorization system developed by Perring *et al.* the WIBS-4+ has two additional channels allowing particle designation as either types D and E as well as A, B and C (depending on the excitation and emission wavelengths of the particle, as indicated in Table 4.2 (Perring et al., 2015). This leads to an additional 21 categories, these consider each channel individually (FL1, FL2, FL3, FL4 and FL5), but also includes all possible combinations.

Table 4.2 Wideband Integrated Bioaerosol Sensor (WIBS-4+) channel annotation matrix. Channels are matched with excitation wavelength and emission waveband.

Channel	Excitation (nm)	Emission (nm)
A	280	310–400
B	280	420–650
C	370	420–650
D	280	600-750
E	370	600-750

I hypothesized that most of the fluorescence signature of an aqueous drug solution would come from the drug and that this would have a characteristic consistent signal different from a viable bacterium. Thus, gathering a fluorescent signature from the drug solutions would allow discrimination between nebulised drug and viable bacterium. Analysis and comparison of nebulised therapy drugs using the two versions of the WIBS instrument (4A and 4+) was carried out in order to define a characteristic fluorescence signature for nebuliser aerosols to develop a data filtering threshold for ward data. Using *in vitro* WIBS4A observations previously gathered by Dr Stig Hellebust and Dr David O'Connor, the author compared and categorised particle size and particle fluorescence in defined bacteria-containing liquid aerosols.

4.2 Method

4.2.1 Nebuliser Analysis

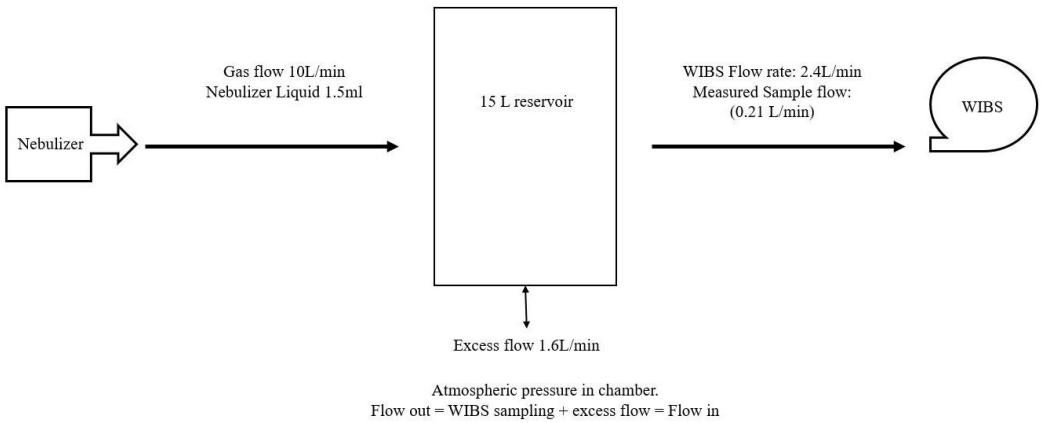

Figure 4.1 Schematic outlining the experimental procedure employed.

The experiment was carried out in a Class II biological safety cabinet. The nebulizer pump used was the PARI TurboBOY SX (PARI Medical Ltd, Surrey, UK), used in combination with the PARI LC SPRINT Nebuliser. This combination is designed to produce a total output rate of 600 mg/min with aerosol particles having a mass median diameter of 3.5 µm and mass percentage below 5 µm of 67%. The Respirable Drug Delivery Rate (RDDR), a measure of therapeutically useful quantity of medication that can be deposited in the lung in each unit of time, is designed to be ~100 – 140 µg/min.

The instrument used was the WIBS-4a, as previously described in the methods section. A 15 L reservoir chamber was the medium from which the nebuliser aerosols were sampled. The nebulizer air flow was ~10 L/min to replicate that used for nebulisers on the ward. However, continuous sampling at this flow rate into a closed volume was not possible due to the large numbers of aerosol particles produced, which caused the WIBS software to crash. Thus, the nebuliser pump was turned on for 3 seconds which produced a large quantity of aerosols which could be characterised.

4.2.2 Samples

These were Ventolin® Nebules® (GlaxoSmithKline Ltd, Dublin, Ireland), the active ingredient being each pack is 2.5 mg salbutamol (as sulphate) in 2.5 ml. Other ingredients are sodium chloride, water for injections and dilute hydrochloric acid.
Also, Ipramol® Steri-Neb® (IVAX Pharmaceuticals UK, Cheshire, UK), the active ingredients in each pack being 0.5 mg of ipratropium bromide (as the monohydrate) and 2.5 mg of salbutamol (as the sulphate) in 2.5 ml was the second. Other ingredients are sodium chloride, water for injections and dilute hydrochloric acid.

4.2.3 Bacterial nebulisation

Bacterial concentrations (1×10^2, 1×10^3, 1×10^5, and 1×10^6 CFU/ml) were dispersed in water and nebulised. The nebulisation flow rate remained constant throughout, *E. coli* K12: 4 L/min, *Bacillus atropheus*: 1.6 L/min.

4.2.4 Bacterial samples

E. coli K12 ATCC 15597 and *Bacillus atrophaeus* DSM 7264/ATCC 49337 were grown overnight in Luria broth at 37 ºC. Cultures were centrifuged and freeze-dried Known numbers of bacteria per microgram were resuspended in distilled water immediately before use.

4.3 Instruments

Two WIBS instruments were used for testing. The availability of the WIBS 4+ allowed a wider range of excitation and fluorescence to be assessed.

4.3.1 WIBS-4a

Real-time airborne particle data was recorded using a Wideband Integrated Bioaerosol Sensor-4a (Droplet Measurement Technologies, Boulder, Colorado, USA). The Wideband Integrated Bioaerosol Sensor (WIBS) is a single aerosol particle fluorescence monitor that uses light-induced fluorescence (LIF) to detect fluorescent aerosol particles (FAP) in real-time. It provides particle size (0.5-12 µm), shape and fluorescent intensity in 3 channels. Initial detection of the particle is made using a continuous-wave red diode laser at 635 nm that illuminates the particles flowing into the optical chamber. Scattering of the laser light is used for both the sizing of particles (based on Mie theory) and to determine a basic particle "shape" using a so-called asymmetry factor (AF). The fluorescence characteristics of the individual particles are then interrogated using two xenon flash lamps (Xe_1, Xe_2). These are tuned to excite at the maxima absorption wavelengths of the biofluorophores tryptophan (280 nm) and NAD(P)H (370 nm). Fluorescence emission following these excitation pulses is detected in two detector bands: 310–400 nm (Band I) and 420–650 nm (Band II) (Healy et al., 2012a). More details on the operation of the WIBS-4a are provided by Kaye et al. (Kaye et al., 2014), Fennelly et al. (Fennelly et al., 2017) and detailed in section 2.1.1.

4.3.2 WIBS-4+

The WIBS-4+ is a prototype instrument (University of Hertfordshire, Hertfordshire, UK), an upgrade of the WIBS-4 with additional fluorescence channels. As described in introduction section 1.5.2, during a laboratory study that measured the fluorescence spectra and the lifetimes of individual pollen grains, the biomolecule chlorophyll-a was shown to be a possible biomarker for grass pollen due to its unique fluorescence peak at 670 nm (O'Connor et al., 2014). Grass pollen, but not tree pollen, gives this signal (O'Connor et al., 2014). To specifically detect chlorophyll-a fluorescence, and therefore grass pollen the WIBS-4+ was developed. This instrument provides two additional fluorescence data channels, FL4 and FL5. The FL4 signals derive from the

excitation of particles at 280 nm, while FL5 signals come from the excitation of particles at 370 nm. Potential emission from chlorophyll-a is recorded by a photomultiplier in the 600–750 nm range.

4.4 Results

4.4.1 Analysis of nebulised distilled water

Nebulised drugs are made up using water for injection. Sterile water for injection, USP, is a sterile, nonpyrogenic, distilled water. below is the analysis of aerosolised, in-house distilled water.

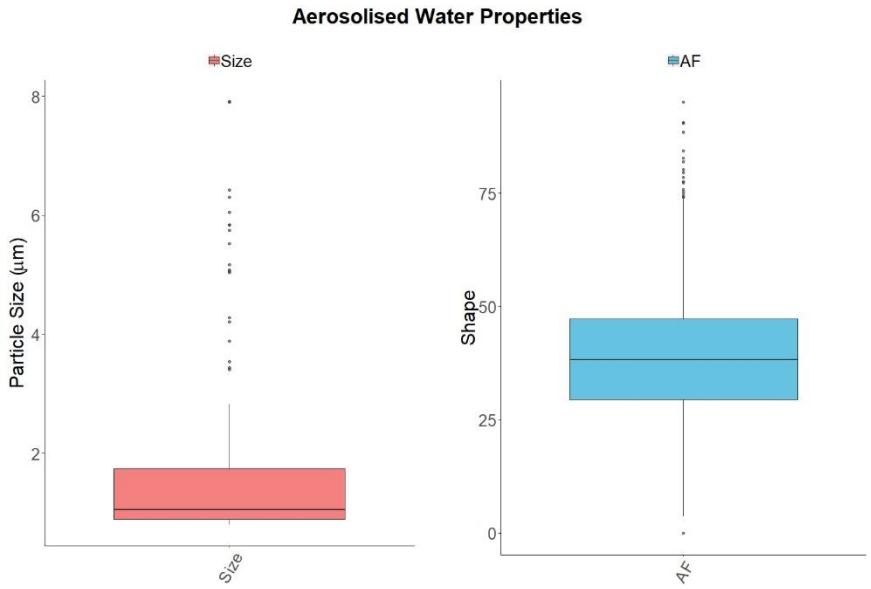

Figure 4.2 Boxplots of physical particle characteristics of detected aerosols generated by nebulizing distilled water Size (µm) (red, left panel) and Shape or asymmetry factor (AF) (blue, right panel)

Figure 4.2 shows water aerosol size (µm) and shape or asymmetry factor (AF). Aerosol size varies (1.87 µm ± 1.72 µm) over the full detection range. For each of the scatter intensities that are recorded by the quadrants, the root-mean-square variation around the mean value outputs produces a numerical value between 0–100 AF units, with 0 being a perfect sphere and 100 denoting long rod-like fibrous particles. The shape of the particles was towards the mid-range of AF, between spherical and rod shaped, (39.47±14.31), suggesting they may be distorted from spherical towards rod shaped during nebulisation, potentially caused by agglomeration where assemblages of particles may have formed.

Table 4.3 Statistical summary of the physical characteristics and fluorescent intensities of aerosols from nebulised distilled water

	Mean ± standard deviation				
	Physical characteristic		Fluorescent intensities		
Distilled Water	AF	Size (μm)	FL1	FL2	FL3
	39.47±14.31	1.87 ± 1.72	26.67±9	98.40±18.29	438.07±46.25

Figure 4.3 shows boxplots of the observed particle fluorescence signals from individual water aerosols. A statistical summary is shown for each channel and subsequent fluorescent thresholds, mean + 3σ and mean + 9σ, calculated using water aerosols as a background, Table 4.4.

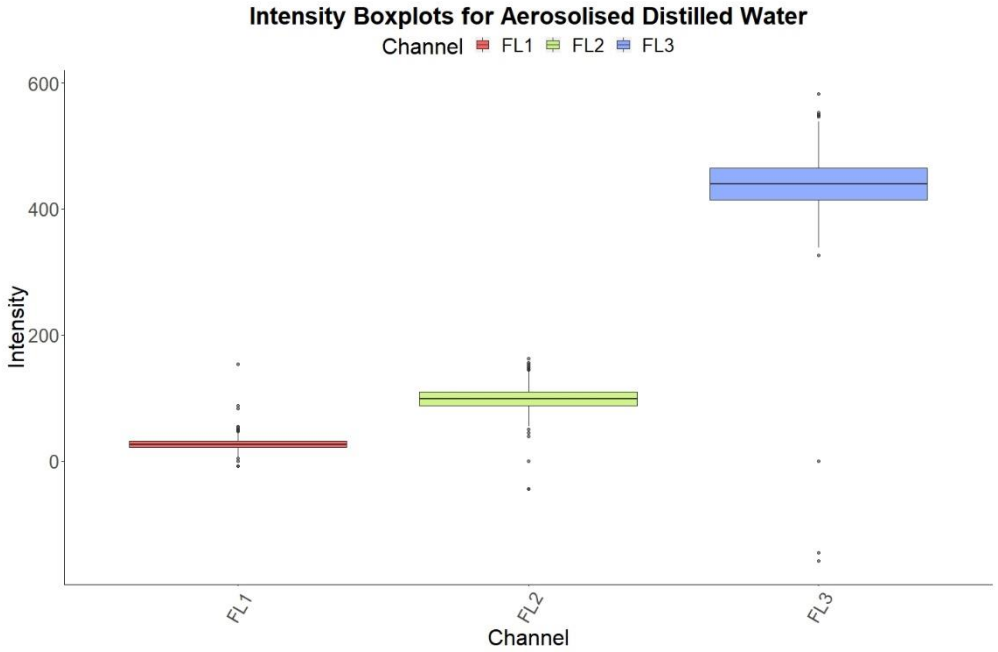

Figure 4.3 Boxplots of particle characteristics of detected aerosols generated by nebulizing distilled water Size (μm) (red, left panel) and Shape (blue, right panel)

Figure 4.3 and Table 4.4 confirm that distilled water exhibits high fluorescent intensity in the FL3 channel nearly 20-fold higher than the particle intensity in the FL1, and 5-fold higher than the FL2 channel. The distilled water here was distilled in house and may not be contaminant free, some of which may be fluorophores with excitation at 370 nm and emission in the 420-650 nm waveband.

Table 4.4 Mean and standard deviation (SD) of fluorescent intensities recorded in each channel with fluorescent thresholds using the standards Mean + 3σ and higher Mean + 9σ

	Channel	Mean ± sd	Mean + 3σ	Mean + 9σ
Water	FL1	26.67 ± 9.0	53.67	107.66
	FL2	98.40 ± 18.29	153.27	263.02
	FL3	438.07 ± 46.25	576.80	854.27

4.4.2 Nebuliser Analysis WIBS-4A

All 255,317 particles sampled by the WIBS instrument during the experiment were fluorescent. Triplicate samples were taken for both solutions. A total of 113,007 particles were collected for Ipramol® Steri-Neb® and 142,310 for Ventolin® Nebules®. It is quite unusual that all particles that were analysed by the WIBS were considered fluorescent. In ambient environments, it is usually between 10-15% fluorescence, see Table 1.10 in section 1.6.3.

Table 4.5 Summary of Nebulised drug physical characteristics observed by the WIBS-4A.

Drug	Characteristic	Percentiles					Statistics	
		5.00	25.00	50.00	75.00	95.00	Mean	SD
Ipramol	Size (µm)	0.58	0.98	1.25	1.54	1.96	1.27	0.43
	Shape (AF:0-100)	1	3	6	9	15	6.59	4.44
Ventolin	Size (µm)	0.60	1.00	1.31	1.60	2.06	1.32	0.46
	Shape (AF:0-100)	6	9	11	14	18	11.46	3.95

Both size (µm) and shape were statistically significantly different ($P<0.001$) between the two nebuliser solutions, although, the magnitude of these differences were small, Ventolin particles were on average slightly larger (~0.05 µm) and less spherical (Asymmetry Factor, AF +5) than Ipramol.

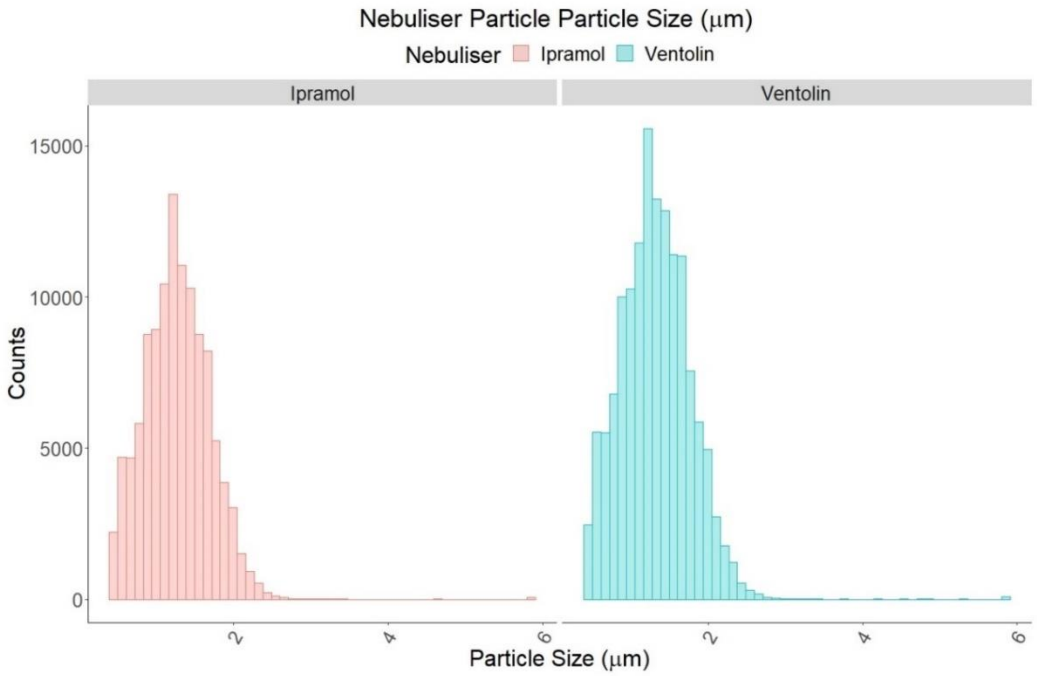

Figure 4.4 Histogram of aerosol size (μm) distribution of nebulised Ipramol and Ventolin recorded by the WIBS-4A

Both Ipramol and Ventolin form a slightly right skewed distribution. The main distribution peak is slightly off centre, with the size tailing off to the larger size range. The instrumental limit for detection could explain this. The WIBS-4A, when set to high-gain mode as described in the materials and methods section, will size aerosols in the 0.5-12 μm range. However, a lower limit of 0.70 μm was applied to this data set in correspondence to the lower-end counting efficiency for specific size regimes D_{50} ~0.489 μm (the diameter of particles at which WIBS counting efficiency is 50% of a reference method) and D_{100} ~0.690 μm (the diameter of particles at which WIBS counting efficiency is 100% of a reference method) reported by Healy *et al*. (Healy et al., 2012b). Setting the lower limit to examine aerosols > 0.70 μm may have caused the skewed distribution by not including aerosols < 0.70 μm.

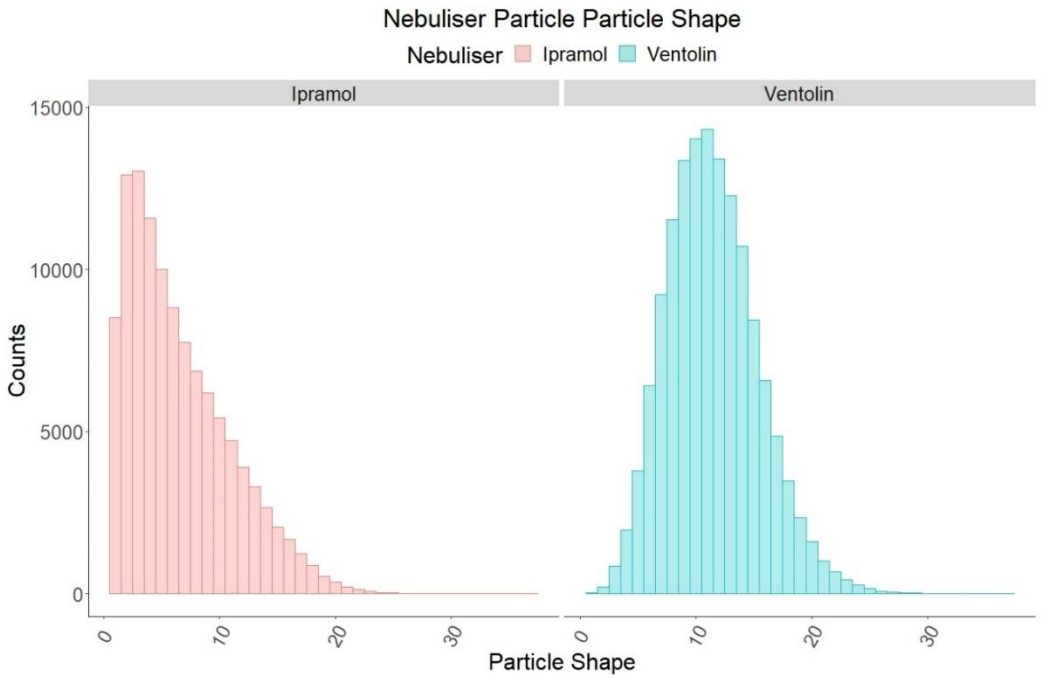

Figure 4.5 Histogram of Asymmetry Factor distribution of nebulised Ipramol and Ventolin recorded by the WIBS-4A

From Figure 4.5, Ipramol shows a highly right skewed shape distribution. The mean AF for Ipramol was 6.59, however from the histogram we can see a clear skew towards an AF of 0. Unlike Ipramol, Ventolin presents a normal distribution with even variation around the mean of 11.46.

4.4.3 Nebuliser Fluorescent Characteristics

Table 4.6 gives a summary of the fluorescence characteristics of nebulised drug particles as characterised by the WIBS. For both drugs, most fluorescence was observed in the FL1 channel (excitation at 280 nm, emission in Band I (310-400 nm)) where it was strongly fluorescent. These correspond to Type A particles (Figure 4.7). Excitation at 280 nm, emission in Band II (420–650 nm) (termed FL2) and excitation at 370 nm, emission in Band II (termed FL3) had lower fluorescent intensity.

Table 4.6 Summary statistics of the fluorescence characteristics of nebulised drug particles collected by the WIBS-4A

Drug	Fluorescent Channel	Percentiles					Statistics	
		5.00	25.00	50.00	75.00	95.00	Mean	SD
Ipramol	FL1	104	140	194	301	687	267.95	228.22
	FL2	11	15	18	21	34	20.64	21.99
	FL3	23	27	30	34	42	32.57	21.03
Ventolin	FL1	101	135	189	298	690	264.03	228.22
	FL2	11	15	18	22	48	23.45	25.98
	FL3	23	28	31	35	50	34.75	23.88

As can be seen from Table 4.6 and Figure 4.6, both nebulised drugs recorded highest mean fluorescent particle intensity in the FL1 channel (264.03 - 267.95). The largest variation in particle intensity was also observed in the FL1 channel, standard deviation ±228.22. Fluorescent intensity channel boxplots, Figure 4.6, show the FL1 channel is frequently saturated for both nebulised drugs (intensity >2047). Approximately, 10 and 9-fold lower fluorescent intensities were recorded for the FL2 and FL3 channels, while also featuring lower variation in intensities standard deviation ±21.03 - ±25.98.

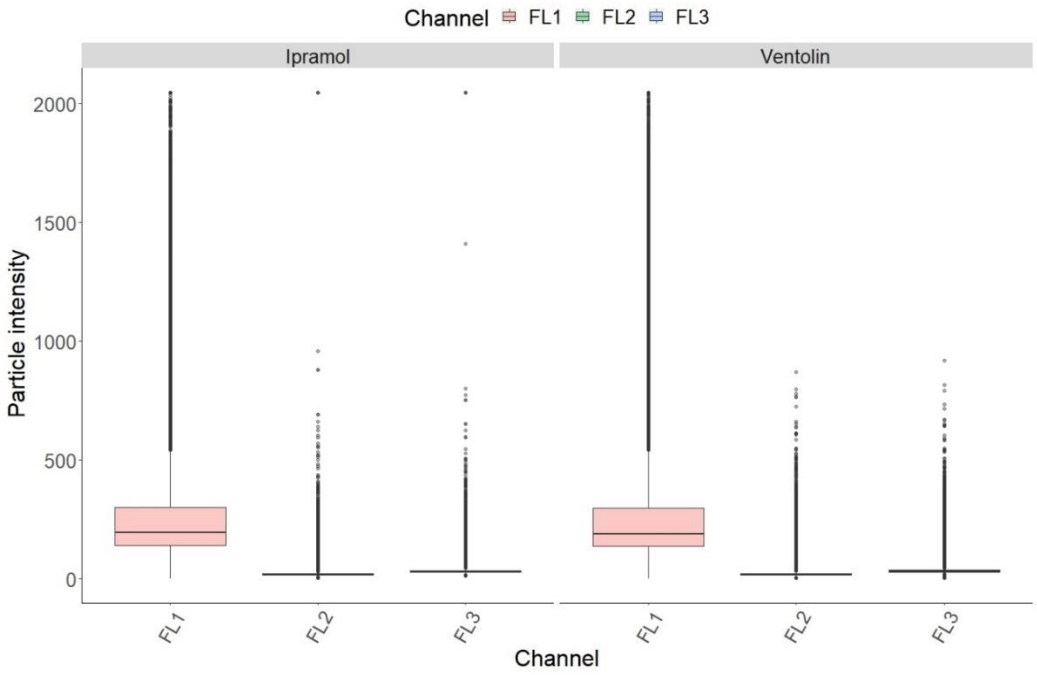

Figure 4.6 Boxplots of fluorescent signals recorded in each channel by nebulised drug.

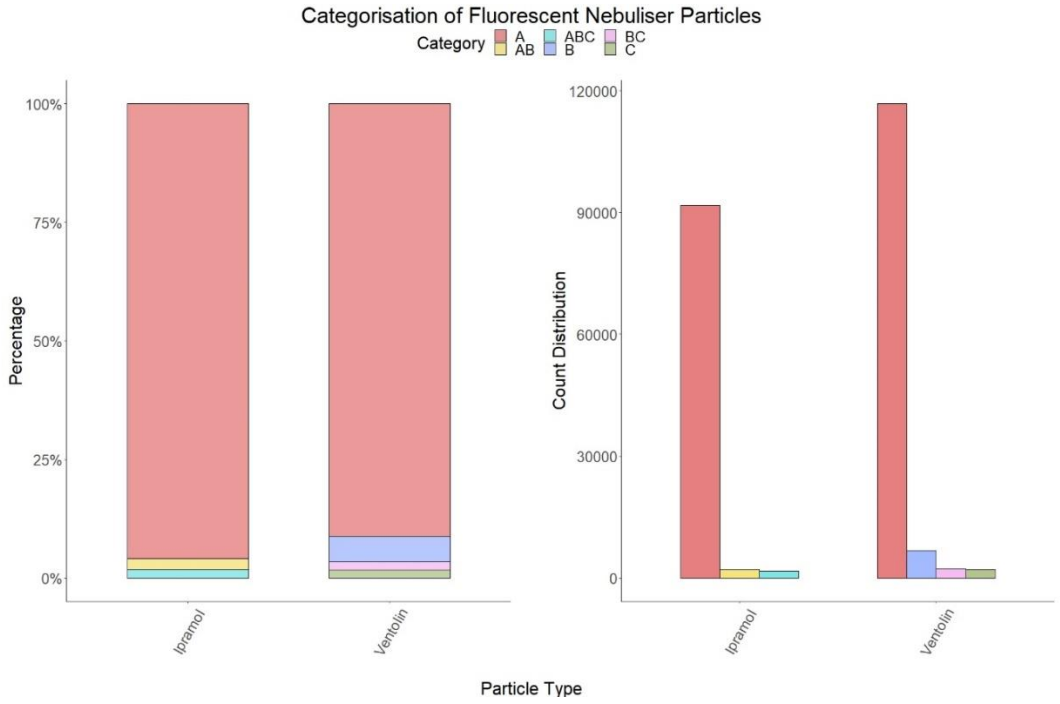

Figure 4.7 fluorescence properties of nebulised drug solutions. Stacked bar chart panel (Left) represents the % of fluorescent particles in each fluorescent type. Panel (Right) shows the overall particle count distribution in each type. Fluorescence type distribution is defined by excitation and emission from any of three possible channels alone (A, B or C) or in any combination.

Following the annotation introduced by Perring *et al.* particle fluorescence was categorized as one of seven types, which considers each of three fluorescence bandwidths individually, as well as in all possible combinations, Table 4.1, Figure 4.7.

Table 4.7 of fluorescent types and quantities observed for both nebulised drugs.

Drug	Number in Fluorescent Type					
	A	B	C	AB	BC	ABC
Ipramol	91764	NA	NA	2110	NA	1757
Ventolin	116808	6831	2110	NA	2286	NA

The fluorescent aerosols produced from nebulising the drugs were dominated by a single fluorescence type (A). Although the nebulised drugs presented in several other fluorescence types i.e. B, C, AB, BC and ABC, it was dominated by the A channel, Table 4.7

4.4.4 Nebuliser Analysis WIBS-4+

All 123,807 particles sampled by the WIBS instrument during the experiment were fluorescent. Triplicate samples were taken for both solutions. A total of 63,813 particles collected for Ipramol® Steri-Neb® and 59,994 for Ventolin® Nebules®.

Table 4.8 shows the physical characteristics of the nebulised drug collected by the WIBS instrument in the laboratory.

Table 4.8 Summary of nebulised drug physical characteristics observed by the WIBS-4+.

Drug	Characteristic	Percentiles					Statistics	
		5	25	50	75	95	Mean	SD
Ipramol	Size (µm)	0.59	0.75	1	1.34	1.85	1.09	0.41
	Shape	3.44	6.35	8.78	11.51	16.05	9.15	3.90
Ventolin	Size (µm)	0.59	0.75	0.97	1.34	1.84	1.08	0.40
	Shape	3.44	6.37	8.79	11.51	16.05	9.16	3.91

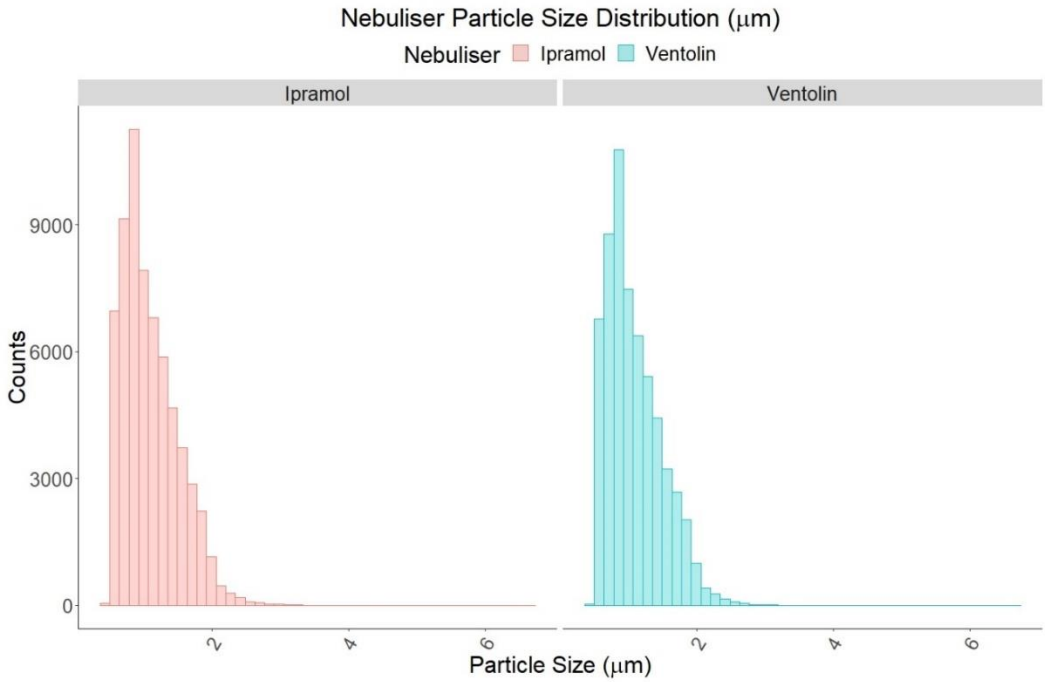

Figure 4.8 Histogram of aerosol size (µm) distribution of nebulised Ipramol and Ventolin recorded by the WIBS-4+.

Like the WIBS-4A histograms of size Ipramol and Ventolin in Figure 4.4, both nebulised drugs formed a slightly right skewed distribution, Figure 4.8. Again, the

main distribution peak was slightly off centre, with the size tailing off to the larger size range. The instrumental limit for detection for the WIBS-4+, has not been reported. However, it should be very close to that of the WIBS-4A considering the only difference should be the added fluorescent channels. In theory with the WIBS-4+ set to high-gain mode as described it, should size aerosols in the 0.5-12 µm range. Considering the lower limits of detections set for the WIBS-4a, a lower limit of 0.70 µm was also applied to this data set. Thus, setting this lower limit aerosols > 0.70 µm may have caused the skewed distribution by not including aerosols < 0.70 µm, explain the right skew.

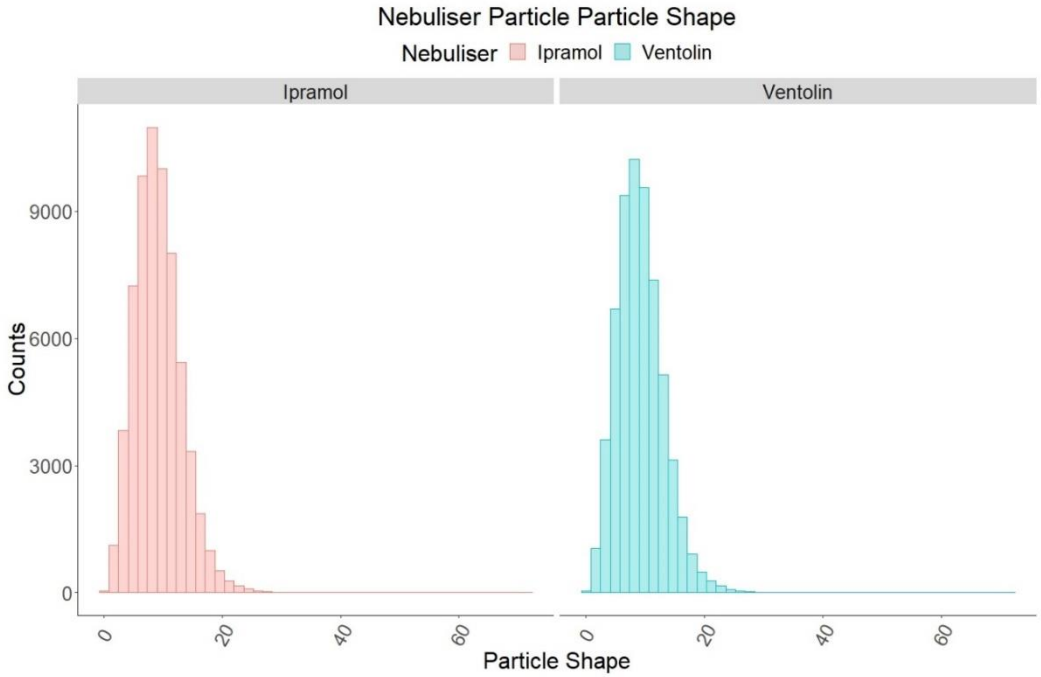

Figure 4.9 Histogram of aerosol shape distribution of nebulised Ipramol and Ventolin recorded by the WIBS-4+

Unlike the shape analysis for Ipramol using the WIBS-4a, Figure 4.5, no right skewed distribution was present in the WIBS-4+ analysis of Ipramol, Figure 4.9. It was instead presenting a normal distribution like the nebulised Ventolin, with even variation around the mean shape of 9.16.

4.4.5 Nebuliser Fluorescent Characteristics

Table 4.9 gives a summary of the fluorescence characteristics of nebulised drug particles as characterised by the WIBS-4+. The fluorescent intensity observed in the FL1 channel (excitation at 280 nm, emission in Band I (310-400 nm)), FL2 (excitation at 280 nm, emission in Band II (420–650 nm)) and FL3 (excitation at 370 nm, emission in Band II) had lower fluorescent intensity than the particles presented in the FL4 (excitation of particles at 280 nm, emission in Band III (600–750 nm)) and FL5 (excitation of particles at 370 nm, emission in Band III (600–750 nm))

Table 4.9 Summary statistics of the fluorescence characteristics of nebulised drug particles collected by the WIBS-4+

Drug	Fluorescent channel	Percentiles					Statistics
		5	25	50	75	95	Mean ± sd
Ipramol	FL1	79	94	107	125	205	119.61 ± 55.13
	FL2	116	134	150	172	241	160.67 ± 48.82
	FL3	150	169	187	216	313	204.44 ± 73.60
	FL4	219	237	266	480	1160	432.13 ± 346.74
	FL5	51	64	203	340	1097	295.83 ± 375.15
Ventolin	FL1	76	92	107	132	198	120.20 ± 50.98
	FL2	108	125	149	193	247	163.40 ± 52.69
	FL3	143	161	176	197	264	186.20 ± 48.97
	FL4	209	226	247	462	1071	406.33 ± 326.06
	FL5	46	58	204	325	1003	278.76 ± 352.64

From Table 4.9 and Figure 4.10, it can be seen that both nebulised drugs recorded the highest mean fluorescent particle intensity in the FL4 channel (406.33 – 432.16). The largest variation in particle intensity is observed in the FL5 channel, standard deviation ±352.64 - ±375.16. Figure 4.10 fluorescent intensity channel boxplots show that the FL4 and FL5 channel was frequently saturated for both nebulised drugs. Large variation for the remaining 3 channels, FL1 - FL3, were observed in the boxplots, Figure 4.10, although these channels do not saturate as frequently as the FL4 and FL5 and they do record particles of high intensity.

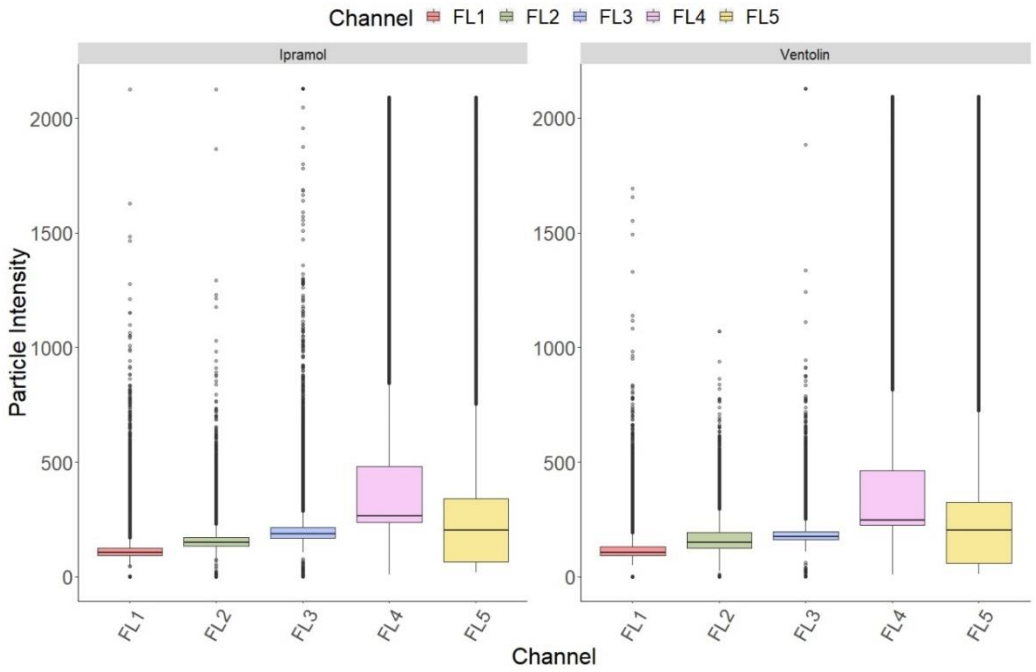

Figure 4.10 Boxplots of fluorescent signals recorded in each channel by WIBS 4+ for each nebulised drug. Boxplots coloured by channel, panel (left) Ipramol and (right) Ventolin.

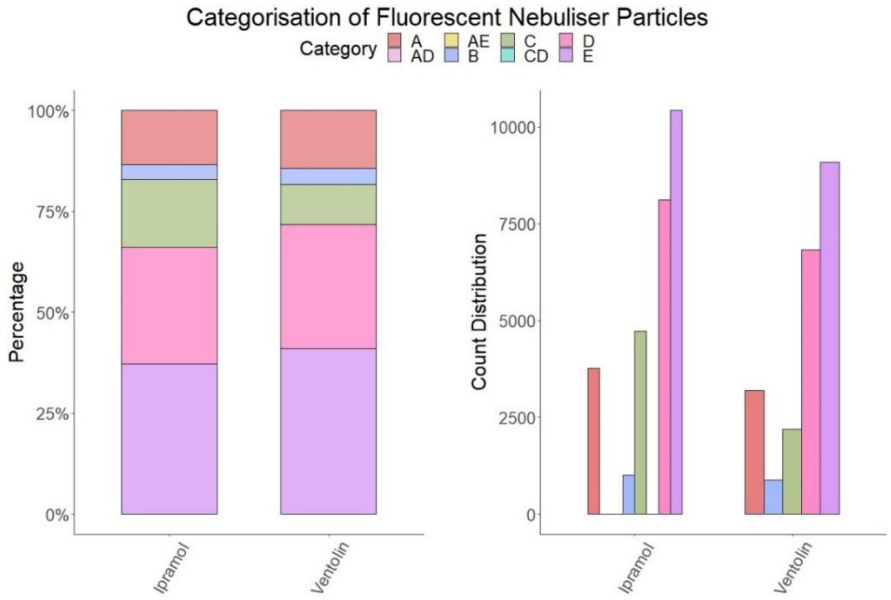

Figure 4.11 Fluorescence properties of nebulised drug solutions measured by WIBS 4+. Stacked bar chart panel (Left) represents the % of fluorescent particles in each fluorescent type. Panel (Right) shows the overall particle count distribution in each type. Fluorescence type distribution is defined by excitation and emission from any of five possible channels alone (A, B, C, D or E) or in any combination.

Expanding on the annotation introduced by Perring *et al.* for the WIBS-4A, which considers each of three fluorescence bandwidths individually, as well as in all possible combinations, particle fluorescence reported by the WIBS-4+ was categorized as one of 28 types. The fluorescent types recorded during drug nebulisation are tabulated in Table 4.10. The fluorescent aerosols produced from nebulising the drugs were dominated by a two-fluorescence type (D and E); together they contributed to ~70% of the fluorescent particle type, Figure 4.11. The remaining nebulised drugs present in three other fluorescence types i.e. A, B and C, Table 4.10, with Ipramol presenting three individual particles as fluorescent type AD and CD, while the three remaining particles for Ventolin presented are fluorescent type AE.

Table 4.10 of fluorescent types and quantities observed for both nebulised drugs.

Drug	Number in Category							
	A	AD	AE	B	C	CD	D	E
Ipramol	3771	2	NA	1000	4717	1	8123	10426
Ventolin	3194	NA	3	875	2186	NA	6819	9096

4.5 **Instrumental comparison**

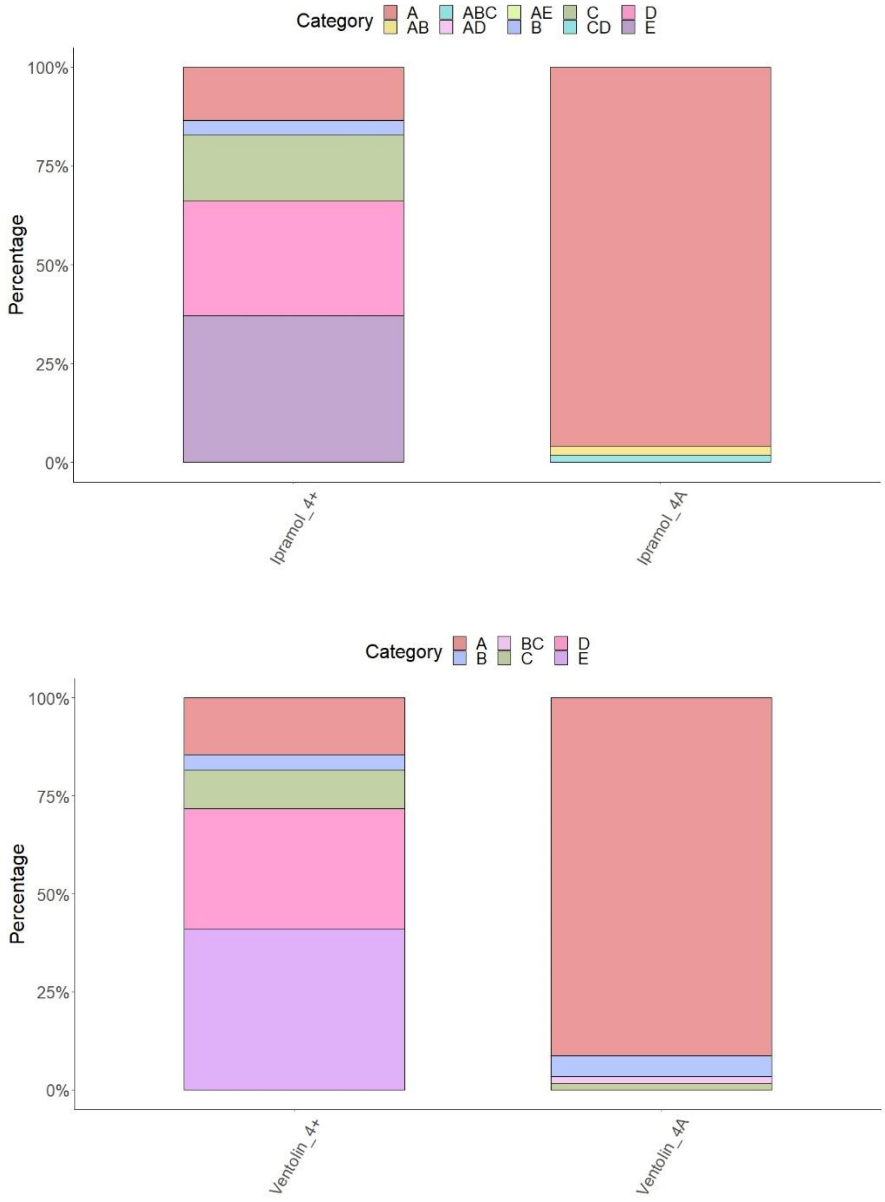

Figure 4.12 Comparison of fluorescence type distributions for two different WIBS instruments from the nebulised drugs used in this analysis. The top panel shows distributions for nebulised Ipramol for the WIBS-4+ (left) and DMT WIBS-A (right). The bottom panel shows the fluorescence type distributions from nebulised Ventolin for WIBS-4+ (left) and DMT WIBS-A (right).

A comparison of fluorescence type distributions for the two different WIBS instruments, is shown in Figure 4.12. The WIBS-4A, classifying a higher portion of nebuliser aerosols in the A channel, compared to the WIBS-4+ prototype. The WIBS-4+ classifies a large portion, ~70% of nebuliser aerosols into the D and E, these type classifications use the new photomultiplier detector.

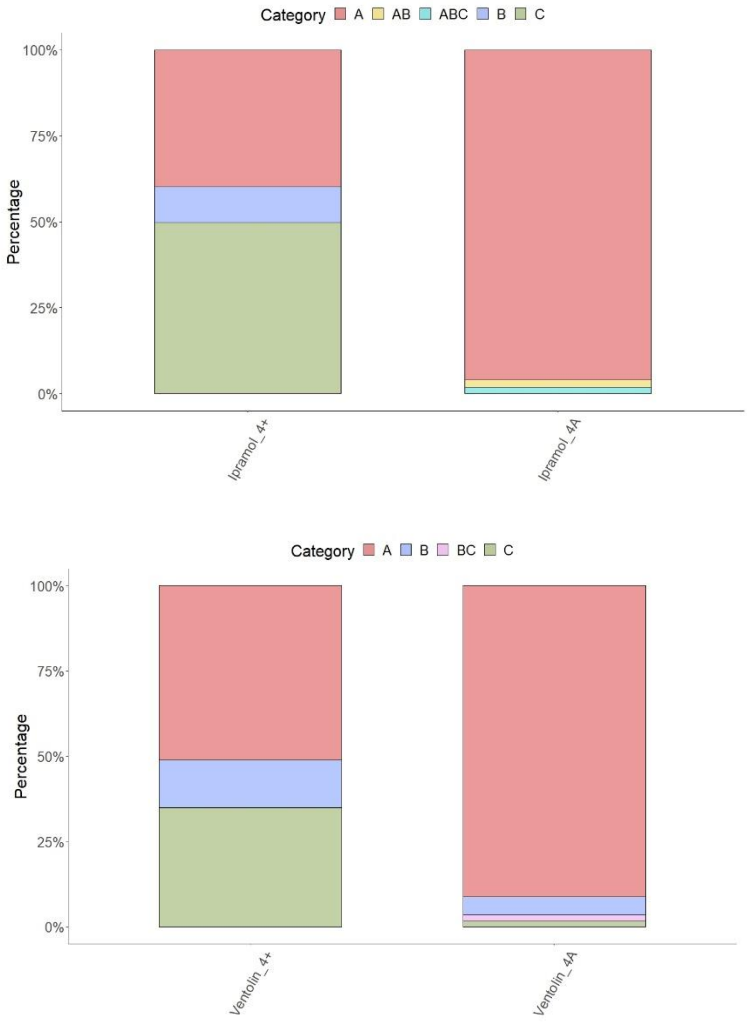

Figure 4.13 Comparison of fluorescence type distributions for two different WIBS instruments, using only common channels. from the nebulised drugs used in this analysis. The top panel shows distributions for nebulised Ipramol for the WIBS-4+ (left) and DMT WIBS-A (right). The bottom panel shows the fluorescence type distributions for nebulised Ventolin for WIBS-4+ (left) and DMT WIBS-A (right).

Comparison of fluorescence type distributions for two different WIBS instruments using only common fluorescent channels, i.e. the D and E type are excluded from the WIBS-4+ graphs, Figure 4.13. After removing the added channel classification from the WIBS-4+ data it classifies a smaller percentage (~40-50%) of the nebulised aerosols from both drugs into the A channel than the WIBS 4A, with the remaining ~50-60% split into the C channel (35-50%) and B channel (10-15%).

4.5.2 Nebuliser threshold

In order to create a filter to remove nebuliser data from data collected on wards where patients regularly use nebuliser therapy, it was decided to use a new threshold calculation whereby the fluorescent threshold was raised from the usual forced trigger values of FT + 3σ , FT + 7σ, or FT + 9σ based (Savage et al., 2017) to absolute fluorescent intensity mean (FM) + 3σ , FM + 7σ, FM + 9σ based on nebuliser signal values from the laboratory. Instead of instrumental background fluorescent values, this fluorescent threshold is based on non-biological fluorescent particle interference.

Table 4.11 Nebulised drug particles fluorescent intensity and physical characteristic laboratory statistics calculated forced triggers FM + 3σ, FM + 7σ and FM + 9σ based on nebuliser signals observed by the WIBS-4A.

Statistic	Ipramol					Ventolin				
	FL1	FL2	FL3	Size	Shape	FL1	FL2	FL3	Size	Shape
Mean	267.95	20.64	32.57	1.27	6.59	264.03	23.45	34.75	1.32	11.46
St. Dev	228.22	21.99	21.03	0.43	4.44	228.22	25.98	23.88	0.46	3.95
FM + 9σ	2321.93	218.55	221.84	5.14	46.55	2318.07	257.27	249.67	5.46	47.19
FM + 7σ	1865.51	174.54	179.77	4.29	37.67	1861.54	205.31	201.94	4.54	39.15
FM + 3σ	952.62	86.59	95.66	2.56	19.91	948.67	101.39	106.41	2.7	23.33

This would result in fluorescent nebuliser particles over the forced trigger threshold being reassigned as non-fluorescent if under FM + 3σ, FM + 7σ or FM + 9σ criteria. The FM + 9σ threshold completely filters out all particles that fluoresce in the FL1 channel by putting the threshold above the intensity maximum (FL1 intensity > 2047). The FM + 3σ threshold has little effect on the nebulised drug counts, so the FM + 7σ threshold was used (Figure 4.13). The mean FM + 7σ recorded for Ipramol and Ventolin was used (FL1 > 1863.53, FL2 > 189.93, and FL3 > 190.86) because both drugs were used on the ward on most days for which data was available.

Applying this threshold significantly reduces fluorescence interference from nebuliser particles, see Figure 4.14 and Table 4.12.

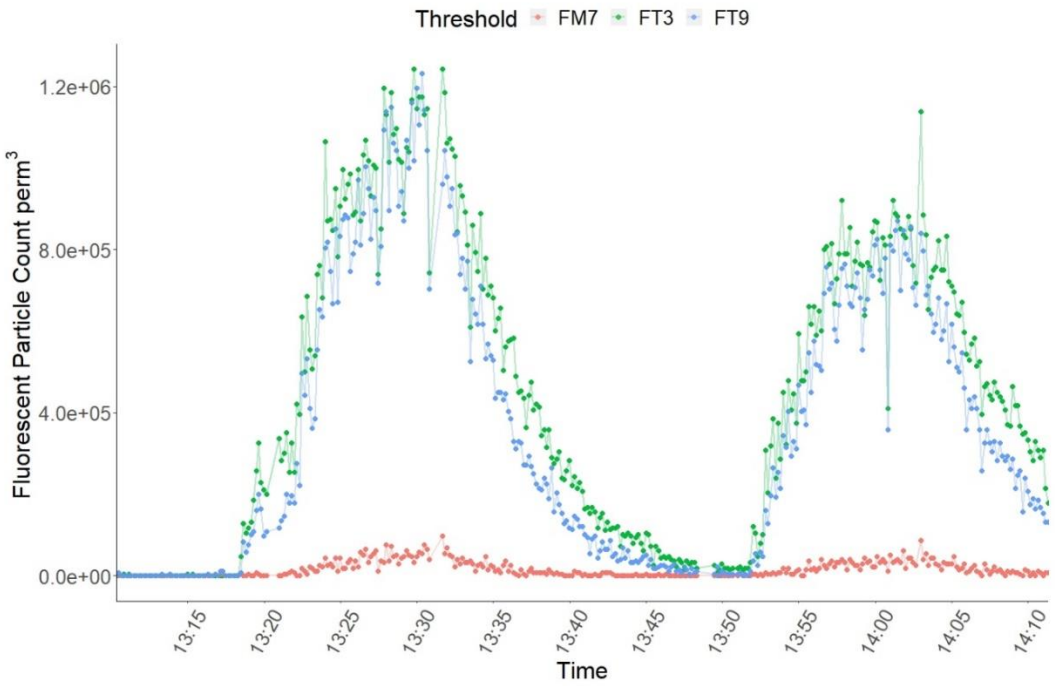

Figure 4.14 Fluorescent particle counts from nebuliser drugs during a controlled experiment coloured by different fluorescent intensity thresholds.

Table 4.12 Statistics of nebulised drug fluorescent particles counts under different thresholds. Instrument calculated thresholds using forced trigger (FT3, mean + 3σ) and (FT9, mean + 3σ) and lab calculated threshold (FM7, FM + 7σ).

Nebulised drug	Threshold	Fluorescent particle count		Fluorescent particle counts ($\times 10^4$ m^{-3})		% Decrease with lab threshold
		Mean ± SD	Max	Mean ± SD	Max	
Ventolin	FM7	5.66 ± 4.38	24	2.02 ± 1.56	8.57	
	FT3	161.95 ± 64.58	319	57.83 ± 23.06	113.91	96.51
	FT9	133.05 ± 65.93	244	47.51 ± 2.35	87.13	95.75
Ipramol	FM7	4.98±5.83	27	1.78 ± 2.08	9.64	
	FT3	144.16±108.32	348	51.48 ± 3.87	124.27	96.55
	FT9	117.93±105.01	345	42.11 ± 3.75	123.2	95.78
Background	FM7	0.13 ± 0.36	2	.046 ± .13	0.71	
	FT3	0.77 ± 1.01	5	2.60±3.61	1.79	83.12
	FT9	0.26 ± 0.55	3	0.091 ± 0.20	1.07	50

Nebulising drug aerosols into an outpatient's room resulted in a significant increase in fluorescent particle counts from 0.77-161.95, (~ 20932.5 %), on average compared to background fluorescence using the instrument calculated forced trigger (FT3), Table

4.13. Applying the lab calculated the threshold (FM7), the fluorescent particle counts increases on average from 0.13 - 5.66, (~4253.9 %), compared to background fluorescence, Table 4.12. A large increase in fluorescent particle counts was still observed with the higher forced trigger-based threshold (FT9) as proposed by Savage *et al*. Using the FT9 threshold resulted in an average 43380.8% fluorescent particle count increase during drug nebulisation, compared to background, and average increase in fluorescent particle counts compared to the FM7 threshold of ~2250.71%.

4.6 Bacterial nebulisation study with WIBS 4A

4.6.1 Analysis of nebulised liquid bacteria samples

In order to identify bacteria-associated particles, the higher fluorescent threshold, mean + 9σ was used as a cut off. This increased threshold is to aid the detection, classification, and discrimination of ambient bio-particles from interfering distilled water particles.

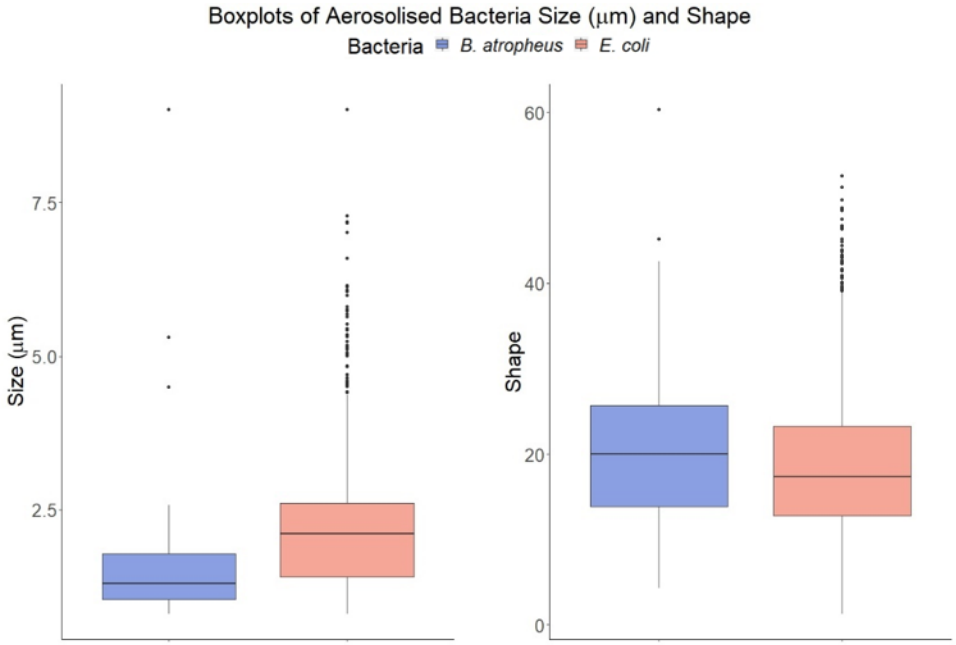

Figure 4.15 Boxplots of particle size (µm) (left panel) and asymmetry factor (AF) (right panel) of fluorescent particles from nebulized distilled water with *B. atropheus* (blue) and with dispersed *E.coli* bacteria (red).

Both the size (µm) and shape of the bacteria differed significantly, Figure 4.15 and Table 4.14. Although the observed size (µm) for *E. coli* (2.16 ± 0.97 µm) was significantly larger than nebulised *B. atropheus* (1.50 ± 0.48 µm), the *B. atropheus* particles were significantly larger in shape i.e. less spherical than those recorded for *E. coli*, Table 4.15.

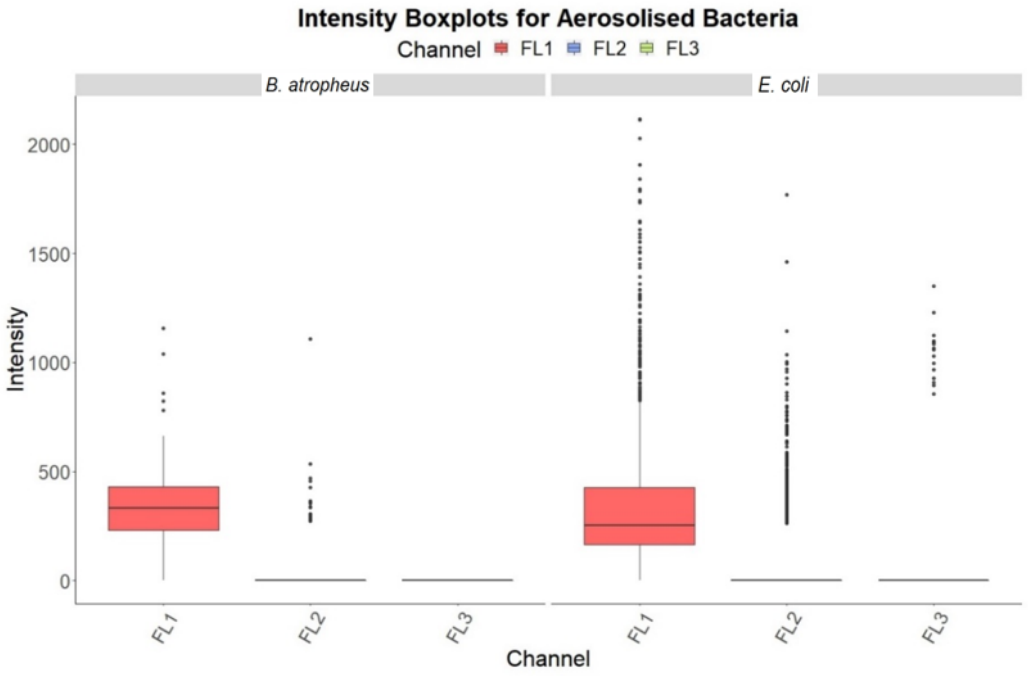

Figure 4.16 Boxplots of fluorescent particle intensities of detected aerosols generated by nebulizing distilled water with *B. atropheus* (left panel) and aerosols generated by nebulizing distilled water with dispersed *E. coli* bacteria (right panel).

Similar results were obtained with dispersions of *B. atropheus* in distilled water. The percentages of bacterial aerosols in the nebulized bacterial dispersion of Bacillus were 23-70 %, 10-30 % and 0-10 %, respectively, for channels FL1, FL2 and FL3, Table 4.14. The FL1 shows the highest fluorescent intensity out of all the channels (346.42±174.46 and 353.78±304.94), for *B. atropheus* and *E. coli* respectively.

Table 4.13 Statistical summary of the physical characteristics and fluorescent intensities of aerosols from nebulised B. atropheus and E. coli.

Mean ± standard deviation					
Bacteria	Physical characteristics		Fluorescent intensities		
	AF	Size (µm)	FL1	FL2	FL3
Bacillus	20.61 ± 8.95	1.50 ± 0.48	346.42 ± 174.46	50.25 ± 143.47	NA
E. coli	18.69 ± 8.34	2.16 ± 0.97	353.78 ± 304.94	84.44 ± 183.74	8.87 ± 96.62
P-value	<0.01	<0.01	0.49	<0.01	<0.01

Interestingly the shape of both fluorescent nebulised bacteria aerosols was more spherical than the water droplets, section 4.4.1.1. *E. coli* was significantly ~0.6 µm larger than *B. atropheus*, while also being slightly, but significantly more spherical, AF of ~2.0 less. Both bacterial aerosols presented highest fluorescent intensity in the FL1 channel followed by 3-fold decrease in intensities observed in FL2 and lowest intensities observed in the FL3 channel. The slightly variable flow rate may be one reason for shape being more spherical that the water droplets, the mean droplet diameter has been reported to decreases with the increase of the flow rate of aeration gas, this also may alter the shape (Ochowiak and Matuszak, 2017).

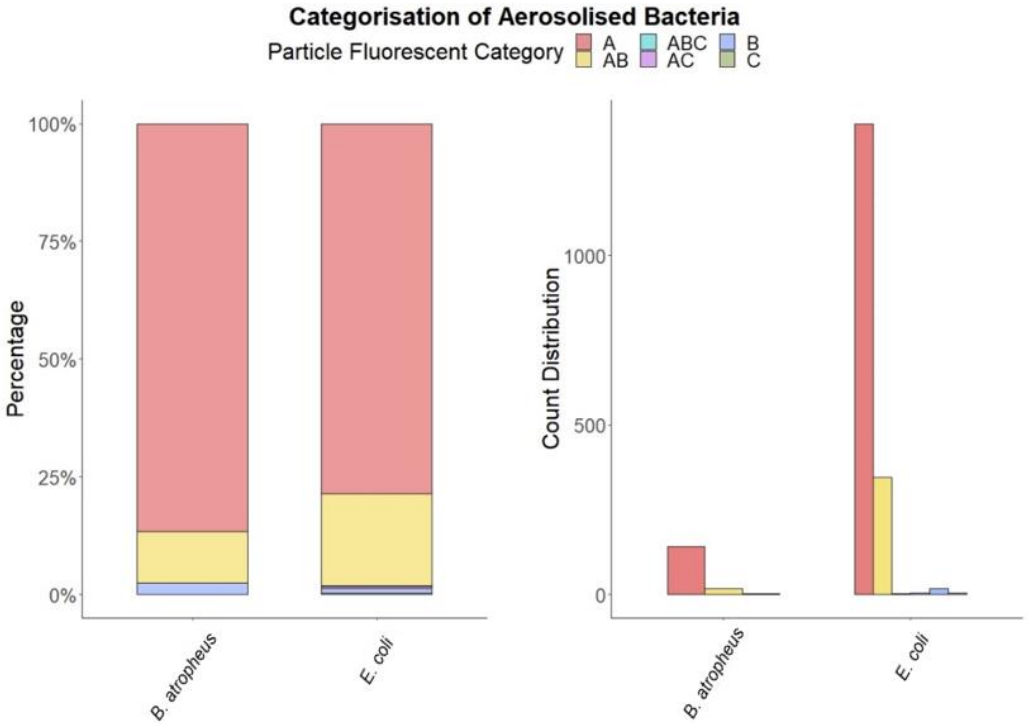

Figure 4.17 Fluorescent properties of nebulised bacteria samples. Stacked bar chart panel (Left) represents the % of fluorescent particles in each fluorescent type. Panel (Right) shows the overall particle count distribution in each type. Each bar chart is split showing detected aerosols from nebulized distilled water with *B. atropheus* (left) and the *E. coli* bacteria (right).

Table 4.14 of nebulised *B. atropheus* and *E. coli* aerosol categorisation, showing the number of particles that fall into each category.

Bacteria	Number in Fluorescent Type					
	A	AB	B	C	AC	ABC
E. Coli	1389	346	18	6	6	3
B. atropheus	143	18	4	NA	NA	NA

Both aerosolised bacterial samples share a common fluorescent signature, Figure 4.17. Both sets of aerosolised bacteria particles were dominated by the fluorescent type A, *E. coli* presented ~23% in the AB categorisation and remaining ~5% in the B, C, AC and ABC, while *B. atropheus* showed ~10% in the AB and the remining ~2% as fluorescent type B.

4.7 **Thresholds to nebulised bacteria**

Applying the nebuliser threshold, discussed in section 4.5.2, to the aerosolised bacteria dataset, results in a large increase in particles being classed as fluorescent, Table 4.15. This is mainly down to the specificity of the nebuliser threshold, which is designed to filter particles with a similar fluorescent signature to nebuliser aerosols, whereas the bacterial dataset has interference from the distilled water fluorescence, as discussed 4.4.1. The distilled water shows high fluorescent intensity in the FL3 channel (438.07 ± 46.25), whereas nebuliser aerosols do not exhibit such a high fluorescent intensity in the FL3 channel (32.57 ± 21.03). So, using the nebuliser threshold would not eliminate the distilled water interference. However, applying the nebuliser threshold to aerosolised bacteria data pre-filtered to eliminate distilled water interference, results in no significant difference in the number of particles classed as fluorescent. In fact, applying the nebuliser threshold to the pre-filtered data only changes the classification of 1 *E. coli* particle from fluorescent to non-fluorescent.

Table 4.15 Particle classification and count in each class under different threshold.

Bacteria	Particle Classification	Number of particles by threshold		
		FM7	DWT*	DWT+FM7**
B. atropheus	Fluorescent	10072	252	252
	Non	20	9840	9840
E. Coli	Fluorescent	21117	2386	2387
	Non	30	18761	18762

*Distilled water threshold

**Distilled water threshold and nebuliser threshold.

This shows the nebuliser threshold only targets nebuliser related aerosols and does not filter out airborne bacteria.

4.8 Comparison with fluorescent signatures collect in literature

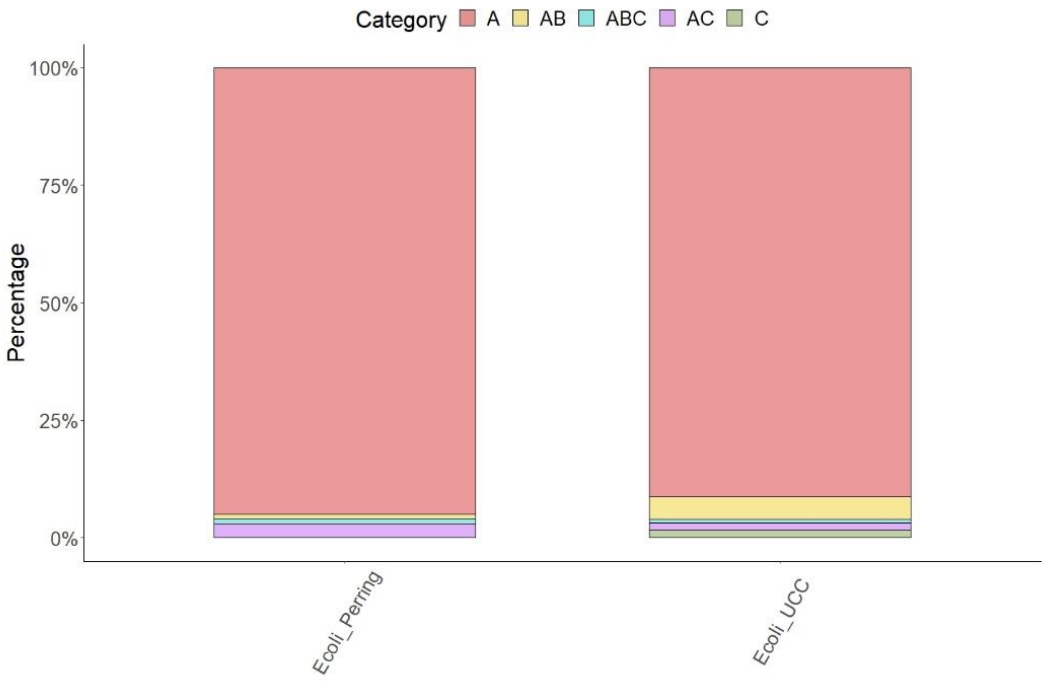

Figure 4.18 Fluorescent properties of aerosolised *E. coli* sample from Perring et al. (left) and nebulised *E. coli* in this study (right). Stacked bar chart panel represents the % of fluorescent particles in each fluorescent type.

The nebulised *E. coli* analysed in this study exhibits a similar fluorescent type to that of the aerosolised *E. coli* by Perring *et al.*, Figure 4.18. Both report a large portion of aerosols as type A, Table 4.16. The recorded size range of *E. coli* in both studies differs by ~1.2 µm, the size of fluorescent *E. coli* particles analysed here were 2.16 ± 0.97 µm, Figure 4.18, in comparison Perring *et al.* recorded a smaller average size of 0.9 ± 0.4 µm

Table 4.16 Nebulised *E. coli* aerosol categorisation from UCC WIBS and Perring et al. WIBS, table showing the number of particles that fall into each category at different concentrations.

Bacteria	Percentage of fluorescent particles in Fluorescent Type					
	A	AB	B	C	AC	ABC
*E.coli*_UCC	79	20	1	NA	NA	NA
*E.coli*_Perring	95	1	NA	NA	3	1

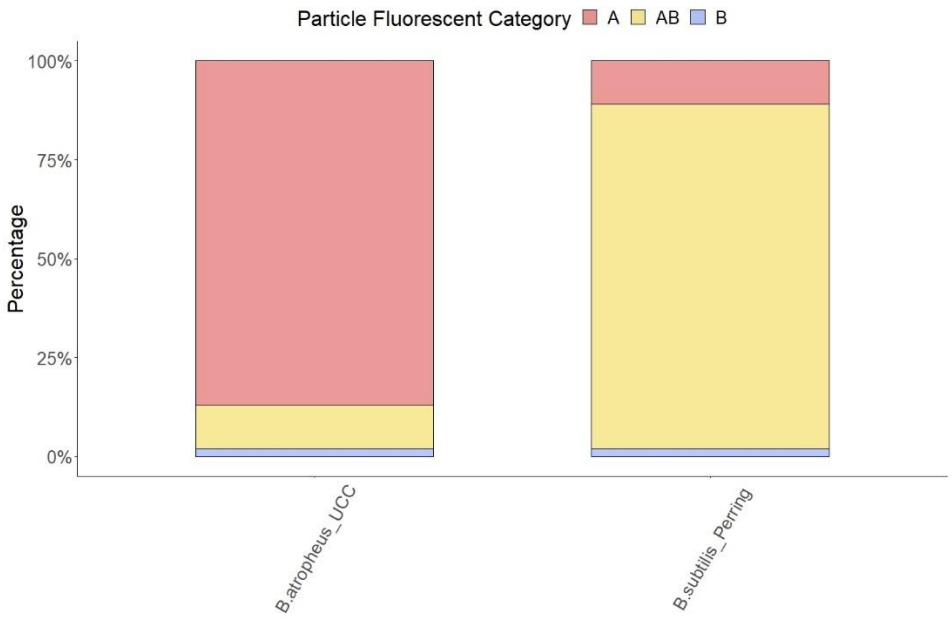

Figure 4.19 Fluorescent properties of aerosolised *B. subtilis* sample from Perring *et al.* (left) and nebulised *B. atropheus* in this study (right). The stacked bar chart panel represents the % of fluorescent particles in each fluorescent type.

The fluorescent signatures differ greatly, Figure 4.19, between *B. atropheus* examined with the UCC WIBS and the *B. subtilis* assessed by Perring *et al.* The *B. atropheus* nebulised mainly produced the fluorescent type A, contrastingly with the *B. subtilis* by Perring *et al.* which presented mainly as fluorescent type AB, Table 4.17.

Table 4.17 Nebulised *B. athropheus* aerosol categorisation using the UCC WIBS and *B. subtilis* nebulised by Perring et al., showing the number of particles that fall into each category at different concentrations.

Bacteria	Percentage of fluorescent particles in Fluorescent Type					
	A	AB	B	C	AC	ABC
*B.atropheus*_UCC	87	11	2	NA	NA	NA
*B.subtilis*_Perring	11	87	2	NA	NA	NA

4.9 Analysis of bacteria at different concentrations

4.9.1 *E. coli* at different known concentrations

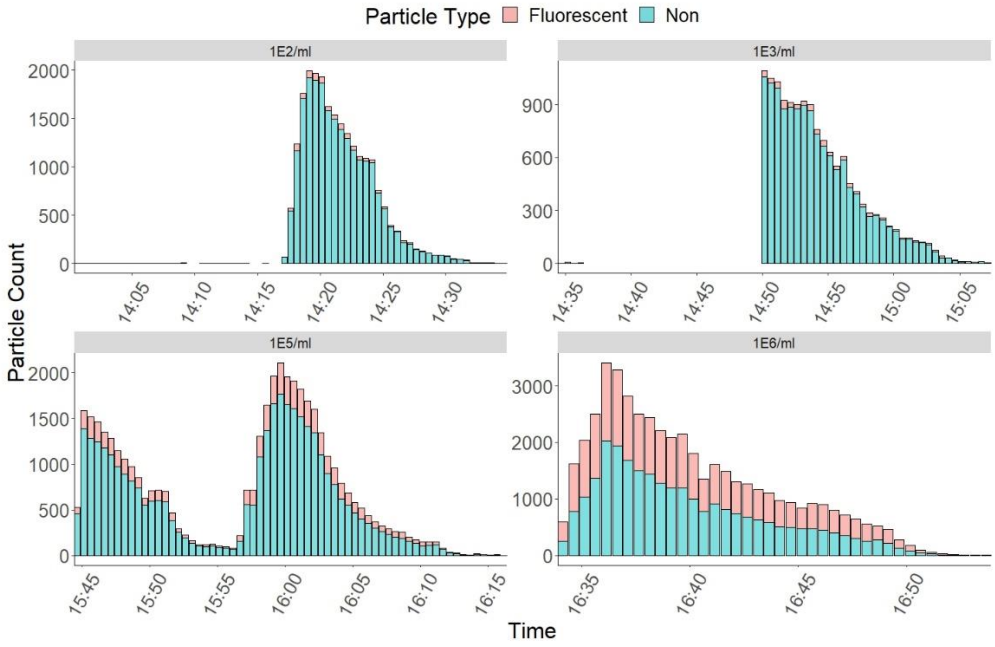

Figure 4.20 *E. coli* particle counts per 30 seconds coloured by fluorescent (red) and non-fluorescent (blue) at different bacterial concentrations per ml 1×10^2 (top left), 1×10^3 (top right), 1×10^5 (bottom left), and 1×10^6. (bottom right).

Figure 4.20 and Table 4.18 show that increasing the concentration of bacteria in the liquid suspension increases the number of fluorescent particles detected, while the number of non-fluorescent particles remains relatively stable (although a large variation was noted within samples, SD range 361.02 – 596.43 particle counts, Table 4.18) due to the flow being approximately constant. The mean ratio of fluorescent to non-fluorescent over the period of nebulisation increased with increased bacterial particle concentrations, Table 4.18. increasing the bacterial concentration nebulised from 1×10^2 /ml to 1×10^6 /ml results in the average ratio of fluorescent particles to non-fluorescent particles increasing from 0.06 to 0.82, Table 4.18.

Table 4.18 Statistical summary of the Fluorescent and non-fluorescent particle counts from nebulised *E. coli* at different concentrations.

Particle Type	Concentration			
	1×10^2 /ml	1×10^3 /ml	1×10^5 /ml	1×10^6 /ml
	Mean ± SD Particle Counts			
Fluorescent	23.08 ± 23.55	15.14 ± 12.5	115.52±97.54	535.25 ± 393.04
Non-fluorescent	369.00±596.43	352.69±361.02	558.08±531.95	656.4 ± 562.53
Ratio of Fluorescent: Non-Fluorescent	0.06	0.04	0.21	0.82

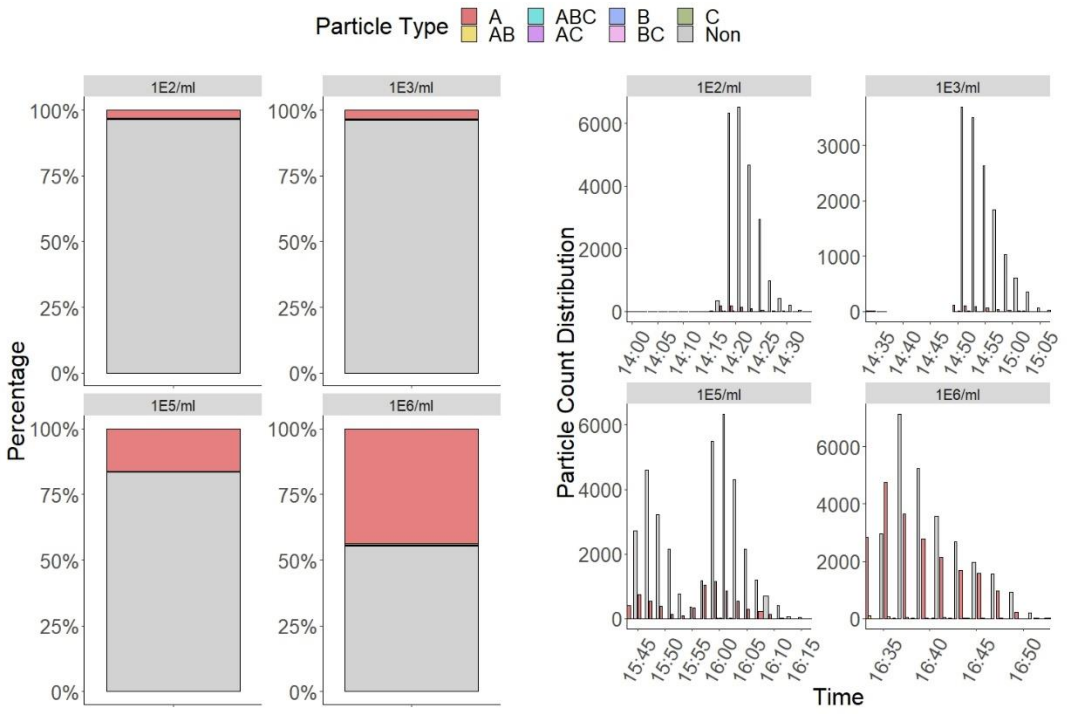

Figure 4.21 Fluorescent properties of all particles from nebulised *E. coli* samples. Stacked bar chart panel (Left) represents the % of fluorescent particles in each fluorescent type by bacterial concentrations. Panel (Right) shows the overall particle count distribution in each type.

In terms of fluorescent signature, increasing the bacterial concentration results in an increase in fluorescent particles categorised as the fluorescent type A, Figure 4.21 and Table 4.19. Increasing particle concentration increased the number of particles that were type A, but WIBS also increases in particle categorised as type AB. Increasing from 1×10^5 /ml to 1×10^6 /ml resulted in a tenfold increase of particles categorised as AB (3.08 ± 2.91 to 34.4 ± 27.48)

Table 4.19 Nebulised *E. coli* aerosol categorisation, showing the number of particles that fall into each category at different concentrations.

Concentration CFU/ml	Fluorescent Type						
	A	AB	ABC	AC	B	BC	Non
	Mean ± SD Particle Counts						
1×10^2	63.64 ± 76.37	8.75 ± 10.82	2.16 ± 1.17	NA	6.6 ± 5.78	1.5 ± 0.71	1250.5 ± 2251.78
1×10^3	57.25 ± 43.05	2.43 ± 1.39	3.4 ± 3.36	NA	3.56 ± 2.74	1.33 ± 0.58	1250.45 ± 1431.65
1×10^5	405.53± 362.13	3.08 ± 2.91	1.6 ± 1.34	NA	5.42 ± 5.47	1.29 ± 0.49	2101± 2031
1×10^6	2060.9 ± 1488.86	34.4 ± 27.48	1.29± 0.76	1.5± 0.71	13 ± 8.97	2.75 ± 2.06	2625.6± 2242.17

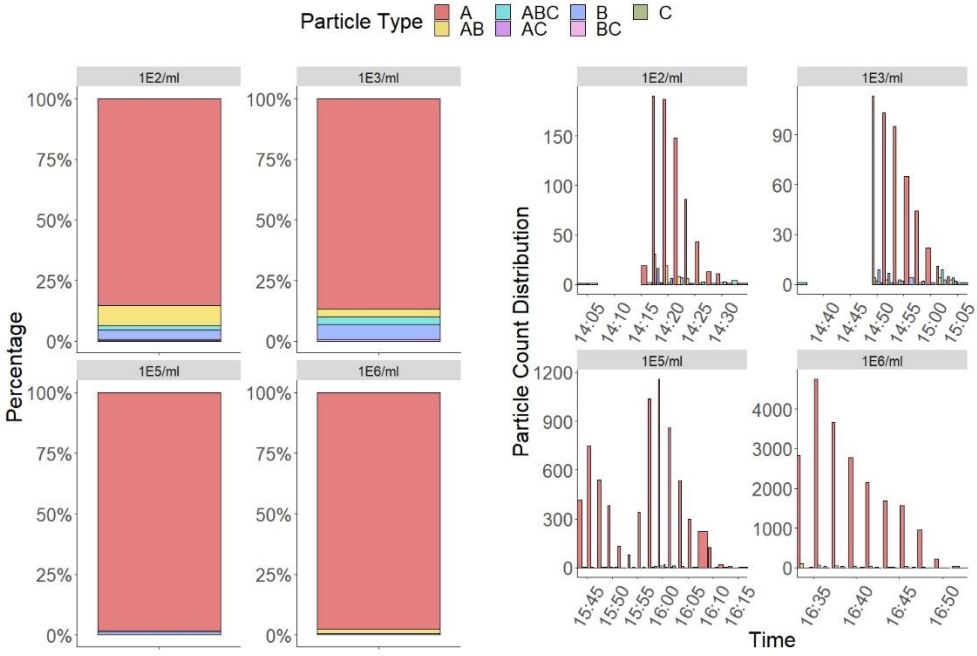

Figure 4.22 Fluorescent properties of fluorescent particles of nebulised *E. coli* samples. Stacked bar chart panel (Left) represents the % of fluorescent particles in each fluorescent type by bacterial concentrations, panel (right) shows the overall particle count distribution in each type.

Looking specifically at the fluorescent particles it can be seen from Figure 4.22 and Table 4.20, that the percentage of fluorescent *E. coli* particles categorised as type B, AB, AC, and ABC decreases while type A categorised particles increase as the concentrations increase. This could be down to larger percentage of water aerosolised in the lower concentration samples. Section 4.4.1, shows that water shows high

fluorescence in the FL2 and FL3 channel, therefore this could be water aerosols containing small quantities of bacteria. This would allow them to break the FL1 threshold and be classed as fluorescent but still fluoresce highly in the FL2 and FL3 channels.

Table 4.20 Nebulised *E. coli* aerosol categorisation, showing the number of particles that fall into each category at different concentrations

Concentration	Fluorescent Type					
	A	AB	ABC	AC	B	BC
	Percentage of Type					
1×10^2 /ml	76.99	10.59	2.62	2.62	7.99	1.81
1×103 /ml	84.23	3.57	5.00	5.00	5.23	1.96
1×10^5 /ml	97.27	0.74	0.38	0.38	1.30	0.31
1×10^6 /ml	97.50	1.63	0.06	0.06	0.61	0.13

4.9.2 *Bacillus atrophaeus* at unknown concentrations

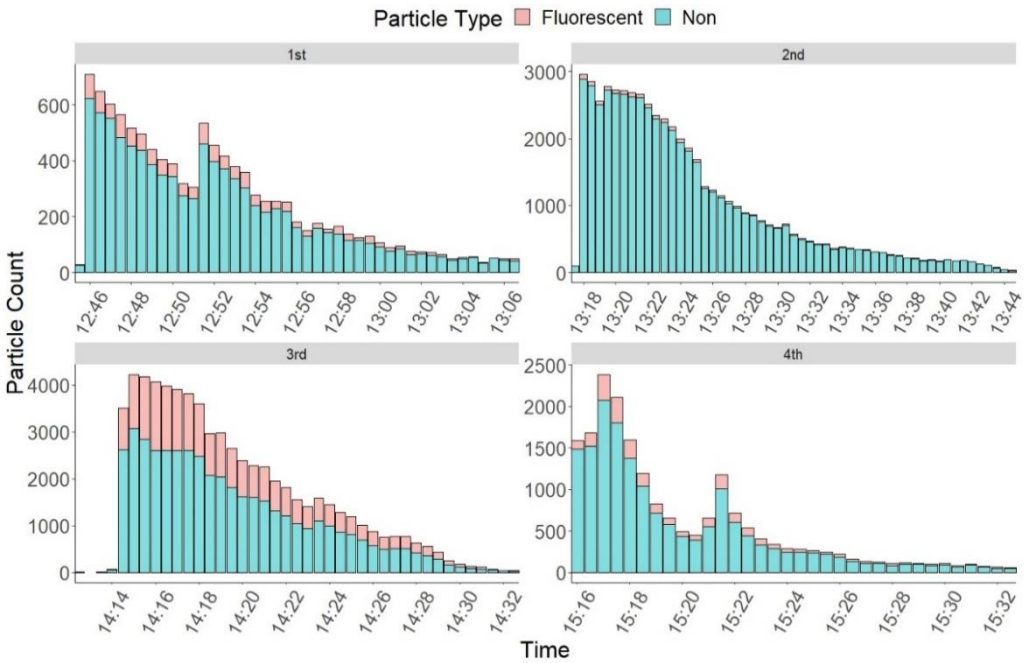

Figure 4.23 *B. athropheus* particle counts per 30 seconds coloured by fluorescent (red) and non-fluorescent (blue) at randomly injected bacterial concentrations. The different panels represent different bacterial concentrations.

Figure 4.23 and Table 4.21 show that nebulising random concentrations of bacteria in the liquid suspension results in different numbers of fluorescent particles detected, while the number of non-fluorescent particles remains relatively stable (although large variation was noted within samples, SD range 219.14 – 1121.67 particle counts, Table 4.21) due to flow being approximately constant. The mean ratio of fluorescent to non-fluorescent over the period of nebulisation changed with different bacterial particle concentrations, Table 4.21. The bacterial concentration nebulised ranged from 1×10^2 /ml to 1×10^6 /ml and the results show average ratio of fluorescent particles to non-fluorescent particles increasing ranging from 0.02 to 0.47, Table 4.21.

Table 4.21 Statistical summary of the Fluorescent and non-fluorescent particle counts from nebulised *E. coli* at different concentrations.

Particle Type	Concentration			
	Sample mean ± sd			
	1st	2nd	3rd	4th
Fluorescent	30.86 ± 24.44	23.75 ± 21.41	523.2 ± 450.87	75.44 ± 80.95
Non-fluorescent	219.14 ± 171.59	971.8 ± 949.029	1121.67 ± 981.12	496.21 ± 556.95
Ratio of Fluorescent: Non-Fluorescent	0.14	0.02	0.47	0.15

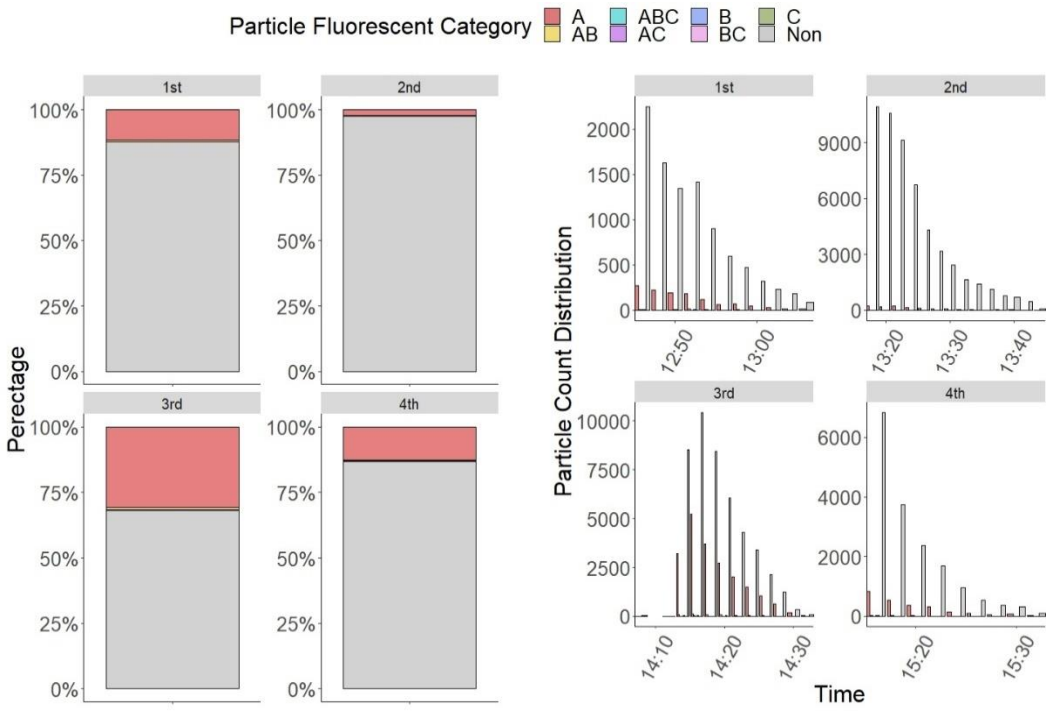

Figure 4.24 Fluorescent properties of all particles from nebulised *B. athropheus* samples. Stacked bar chart panel (Left) represents the % of fluorescent particles in each fluorescent type by bacterial concentrations. Panel (Right) shows the overall particle count distribution in each type.

In terms of fluorescent signature, the different bacterial concentration results in different fluorescent particles categorised as fluorescent type A, Figure 4.24 and Table 4.22. Sample 3 showed the highest particle concentration presenting as fluorescent type A, and also resulted in the highest number of particles presenting as the other fluorescent types B, C, AB, and ABC. Sample 3 showed a seven-fold increase compared to the next highest presenting type A channel (72.08 ± 77.75 to 482.09 ± 438.87), with sample 4.

Table 4.22 Nebulised *B. athropheus* aerosol categorisation, showing the number of particles that fall into each category at different concentrations.

Sample	Fluorescent Type							
	A	AB	ABC	AC	B	BC	C	Non
	Mean ± SD							
1st	28.81 ± 23.09	2.69 ± 1.66	1	NA	1.44 ± 0.88	1	NA	219.13 ± 171.58
2nd	23.17 ± 20.35	1.35 ± 0.49	1	NA	1.56 ± 0.96	1	NA	971.8 ± 949.03
3rd	482.09 ± 438.87	11.67 ± 9.42	2.2 ± 1.70	1.37 ± 0.74	4.25 ± 3.09	1.36 ± 0.50	3.33 ± 2.51	1068.76 ± 986.41
4th	72.08 ± 77.75	3 ± 2.40	1.16 ± 0.41	Na	2.18 ± 1.90	NA	1	496.20 ± 556.96

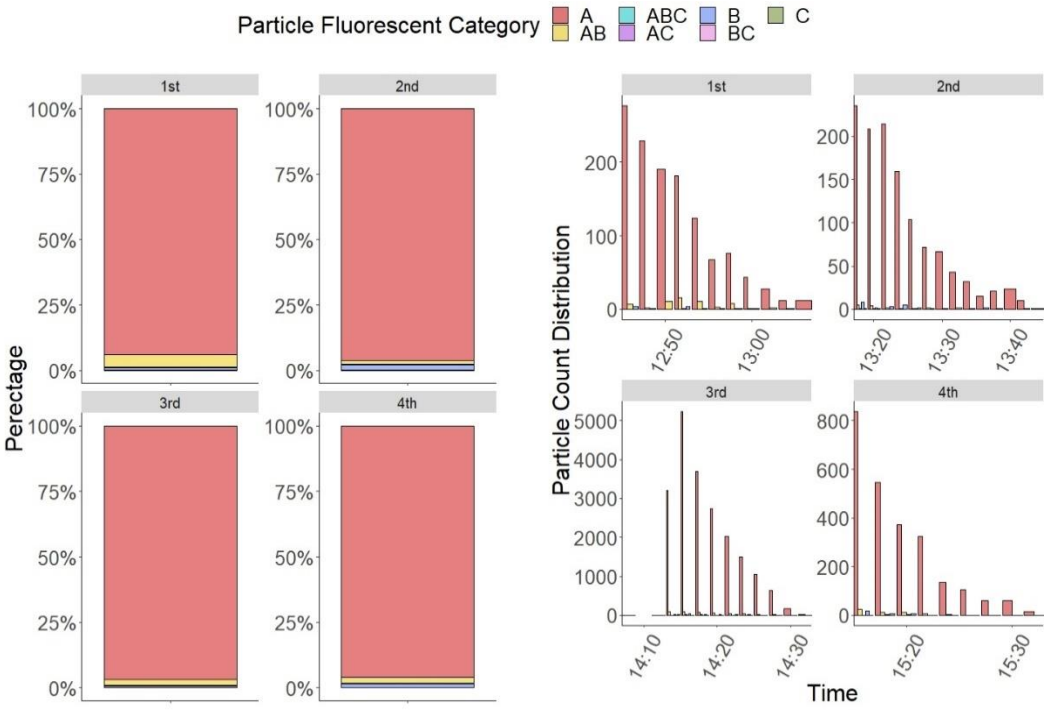

Figure 4.25 Fluorescent properties of fluorescent particles of nebulised *B. athropheus* samples. Stacked bar chart panel (Left) represents the % of fluorescent particles in each fluorescent type by bacterial concentrations, panel (right) shows the overall particle count distribution in each type.

Looking specifically at the fluorescent particles, Figure 4.25 and table 4.23 the percentage of fluorescent *B. athropheus* particles categorised as type B, AB, AC, and ABC varied through the concentrations. The 3rd and 4th samples had the highest percentage of particles presenting as type A, whereas the 1st and 2nd samples had higher

percentages in the other fluorescent types B, C, AC, BC, and ABC. This resembled the analysis of *E. coli*, section 4.9.1, where the percentage of type A *E. coli* particles increased while the percentage of particles in the remaining categories decreased as the concentration of bacteria in the solution increased.

Table 4.23 Nebulised *B. atrophaeus* aerosol categorisation, showing the number of particles that fall into each category at different concentrations

Sample	Fluorescent Type						
	A	AB	ABC	AC	B	BC	C
	Percentage of Type						
1st	75	7	3	0	4	3	9
2nd	80	5	3	0	5	3	3
3rd	96	2	0	0	1	0	0
4th	92	4	1	0	3	0	0

An analysis of the known concentrations of nebulised *E. coli,* section 4.9.1, showed that increasing the bacterial particle concentration nebulised, increased the number of fluorescent particles, the ratio of fluorescent to non-fluorescent particles and the percentage of particles presenting as type A fluorescent type. Although the *B. athropheus* solutions were nebulised at random times, we can from the analysis of *E. coli*, interpret which samples were which concentrations. Sample 3 resulted in the highest mean (523.2 ± 450.87), highest fluorescent to non-fluorescent particle ratio (0.47) and had the highest mean particles as type A (482.09 ± 438.87, 96%) suggesting it would be the highest concentration, 1×10^6 CFU/ml. Although the 1st and 4th sample resulted in similar fluorescent to non-fluorescent particle ratios, the 4th sample had higher mean fluorescent particles (75.44 ± 80.95) and resulted in the second highest concentration of particles presenting as type A (72.08 ± 77.75, 92%), suggesting it was the second highest concentration sample 1×10^5 CFU/ml. The 1st and 2nd sample had the lowest concentrations, they were quite close in mean fluorescent counts (1st = 30.86 ± 24.44, 2nd = 23.75 ± 21.41), although the 2nd sample had a lower ratio of fluorescent to non-fluorescent particles 0.02 compared to the 1st samples 0.14, and the second sample had much high numbers of non-fluorescent particles present compared to the 1st sample, due to having an approximate flow rate. Where they were distinguishable was with the 2nd sample having a higher percentage of fluorescent particle as type A (80%), and a lower percentage of particles with as the other fluorescent types (3-5%)

compared to the 1st samples type A (75%) and other fluorescent types (3-9%), sample 2 had 1×10^3 CFU/ml and sample 1 had 1×10^2 CFU/ml.

4.10 **Conclusion**

The WIBS instrument found aerosols produced from nebulisers were made up of polydisperse particles of varying size, as established in the literature (Mercer, 1973, Mercer, 2012). The particle size distribution of therapeutic aerosols was approximately a log normal distribution , as described (Hinds, 2012, O'Callaghan and Barry, 1997). It could be anticipated that both nebuliser solutions would exhibit high fluorescent intensity in the FL1 channel category A particles (280 nm excitation, 310–400 nm emission) due to the presence of salbutamol as an active ingredient in both drugs (2.5 mg / 2 ml in Ventolin and Ipramol). Salbutamol is known to absorb light at 278 nm and strongly emits fluorescence at 306 nm when excited at 278 nm. (Bi et al., 2013, Srichana et al., 2003) . These observers recorded spectra from 280 to 450 nm. Evaluations of dry salbutamol sulphate inhaler powders using a ultraviolet high performance liquid chromatography (HPLC-UV) found increasing the dosage solutions of salbutamol sulphate resulted in an increase in fluorescent intensity (Srichana et al., 2003). This was the case for the WIBS-4A, where a large portion of the nebuliser aerosols measured were classified as fluorescent type A. However, this differs using the prototype WIBS-4+, where ~70% of the nebuliser aerosols were classed as type D and E i.e. particles were excited at 280 and 370 nm, respectively, and emissions were recorded in the 600-750 nm waveband (Figure 4.11). However, Pandya et al., recording spectra 400-700 nm, reported excitation of salbutamol at 279.6 nm with a major emission peak at 609.8 nm, which would fall into the D and E categories which formed the largest two parts of the salbutamol signal in the WIBS-4+ (Pandya et al., 2010). The higher fluorescence intensity observed in the D and E categories of the WIBS4+ should also have been apparent in the B and C categories of the WIBS4A which also recorded at up to 650 nm (Table 4.1).

Sections 4.5.2 show the capabilities of the instrument to create and apply filters to remove specific fluorescent interferants. Using the lab developed threshold, a significant decrease in aerosolised nebuliser particles was observed, a ~95% decrease compared to the standard threshold used. Applying these thresholds to bacterial

aerosols showed no significant difference in the classification of bacterial aerosols as fluorescent. In fact, there was only 1 particle change classification from fluorescent to non-fluorescent when the nebuliser threshold was applied, section 4.7 and Table 4.15. This shows the threshold only filters out nebuliser related aerosols and does not unintentionally remove airborne bacteria from the datasets. This also shows that known fluorescent interferants within an indoor environment could possibly be filtered out, with reducing the number of bioaerosol particles in the dataset.

The current instrument manufacturer, Droplet Measurement Technologies (DMT), calibrates detector gains based on photomultiplier fluorescence detection from monodisperse tests using commercially available polystyrene latex (PSL) fluorescent microspheres. The intensity of PSL fluorescent ionospheres is known to vary between manufacturing batches and can degrade considerably over time, even with correct cold storage. Overall, this provides consistency across different instruments, but the lack of an absolute calibration means that there may be noticeable variability in fluorescence signal recovery of a bioaerosol between instruments. Differences have been reported between prototype WIBS from Cranfield University and production line WIBS from DMT. A laboratory comparison between a retail production line WIBS-4A from DMT and another prototype WIBS instrument owned by the Chemical Sciences Division of the National Oceanic and Atmospheric Sciences Administration (NOAA), Colorado, showed different spectral classification of a subset of aerosolised bioaerosols (Perring, 2016). They observed the NOAA WIBS was classifying a higher portion of bioaerosols in the B and C channel, which uses the same photomultiplier detector, than the commercial WIBS. The lab experiments presented here reported a similar difference between the production line WIBS and a WIBS prototype developed for UCC, where the commercially bought WIBS classified the majority of fluorescent nebulised drug particles as type A, whereas the UCC WIBS classified a higher portion of the nebulised drugs as type B and C, when comparing common channels only, Figure 4.13. The UCC developed WIBS has additional fluorescent channels where a large portion of the fluorescent nebulised drugs signature was recorded, but also saturated the channel by exhibiting high fluorescent intensity, Figure 4.11 Finding these differences in spectral classification confirms that different WIBS instrumentation, while in theory configured the same and challenged under the same conditions, can report somewhat different fluorescence distributions.

A study cataloguing the fluorescent signatures of aerosolised bioaerosols showed bacteria fell into a common fluorescent pattern, <1.5 µm in size and all but one bacterial aerosol was dominated by the single fluorescent type A (Perring, 2016). One of the bacterial samples aerosolised by Perring *et al.* was *E. coli* K-12, which is also aerosolised in this experiment. The nebulised *E. coli* analysed in this study exhibits a similar fluorescent type to that of the aerosolised *E. coli* by Perring *et al.*, Figure 4.18. However, the percentage of *E. coli* presenting as AB fluorescent type is higher with the UCC WIBS-4A, but as discussed earlier in the section this may be down to the calibration of the detector by the manufacturer. Also, the recorded size range of *E. coli* in both studies differed by ~1.2 µm, the size of fluorescent *E. coli* particles analysed here were 2.16 ± 0.97 µm, in comparison Perring *et al.* recorded a smaller average size of 0.9 ± 0.4 µm (Perring, 2016). In their experiment they nebulised through a humidifier which would have dried the particles before they entered the chamber, whereas a particle dryer was not used in our experiment, so the water droplets increased the *E. coli* particle size. For the published bacterial dataset from Perring *et al*. they presented one noticeable outlier, *Bacillus subtilis*, whose fluorescent signature displayed largely as AB fluorescent type. Although our experiment used a different species of *Bacillus*, *B. atropheus*, the fluorescent signatures differ greatly, see Figure 4.19. As *Bacillus* is a spore forming bacterial strain, the preparation of samples may affect whether they are composed of vegetative bacteria or mostly spores. This may affect the fluorescent signature, thus explaining the difference between the sample analysed here and the sample referenced by Perring *et al.*

Section 4.9.1 illustrated the fluorescent properties of *E. coli* at different bacterial concentrations. It found that by increasing the concentration of bacteria in the liquid suspension, the number of fluorescent particles detected increased, but the number of non-fluorescent particles remained relatively stable (within experimental variation) due to flow being approximately constant, Table 4.18. But also, the fluorescent signatures in certain channels increased, i.e. type A categorised fluorescent particles increased ~10% from 1×10^2 /ml to 1×10^6 /ml. Knowing that different concentrations helped identify randomly nebulised concentrations of *Bacillus*. This may also have implications when sampling in areas where bacterial concentrations could vary over time, meaning the identical bacterial species may give different fluorescent characteristics at different concentrations.

However, this lab study demonstrates the ability of the instrument to detect bacterial aerosols, at different concentrations, but also shows the advantage of having different channels, in which different types of biological aerosols exhibit different responses. This has increased importance in indoor facilities where different areas have different microbiological community structures. The WIBS has the potential to map certain areas with fluorescent signatures and has the ability to monitor any changes that may occur, or the effect alterations to areas have on its fluorescent signature.

4.11 **References**

BI, S., PANG, B., ZHAO, T., WANG, T., WANG, Y. & YAN, L. 2013. Binding characteristics of salbutamol with DNA by spectral methods. *Spectrochimica Acta Part A: Molecular and Biomolecular Spectroscopy,* 111**,** 182-187.

FENNELLY, M. J., SEWELL, G., PRENTICE, M. B., O'CONNOR, D. J. & SODEAU, J. R. 2017. The Use of Real-Time Fluorescence Instrumentation to Monitor Ambient Primary Biological Aerosol Particles (PBAP). *Atmosphere,* 9**,** 1.

HEALY, D. A., O'CONNOR, D. J., BURKE, A. M. & SODEAU, J. R. 2012a. A laboratory assessment of the Waveband Integrated Bioaerosol Sensor (WIBS-4) using individual samples of pollen and fungal spore material. *Atmospheric environment,* 60**,** 534-543.

HEALY, D. A., O'CONNOR, D. J. & SODEAU, J. R. 2012b. Measurement of the particle counting efficiency of the "Waveband Integrated Bioaerosol Sensor" model number 4 (WIBS-4). *Journal of Aerosol Science,* 47**,** 94-99.

HINDS, W. C. 2012. *Aerosol Technology: Properties, Behavior, and Measurement of Airborne Particles*, Wiley.

KAYE, P. H., STANLEY, W. R. & FOOT, E. V. J. 2014. *Fluid-Borne Particle Detector*. US 13/957,655.

MERCER, T. 2012. *Aerosol technology in hazard evaluation*, Elsevier.

MERCER, T. T. 1973. Production and characterization of aerosols. *Archives of internal medicine,* 131**,** 39-50.

O'CALLAGHAN, C. & BARRY, P. W. 1997. The science of nebulised drug delivery. *Thorax,* 52**,** S31.

O'CONNOR, D. J., LOVERA, P., IACOPINO, D., O'RIORDAN, A., HEALY, D. A. & SODEAU, J. R. 2014. Using spectral analysis and fluorescence lifetimes to discriminate between grass and tree pollen for aerobiological applications. *Analytical Methods,* 6**,** 1633-1639.

OCHOWIAK, M. & MATUSZAK, M. 2017. The effect of additional aeration of liquid on the atomization process for a pneumatic nebulizer. *European Journal of Pharmaceutical Sciences,* 97**,** 99-105.

PANDYA, H. N., BERAWALA, H. H., KHATRI, D. M. & MEHTA, P. J. 2010. Spectrofluorimetric estimation of salbutamol sulphate in different dosage forms by formation of inclusion complex with β-cyclodextrin. *Pharmaceutical methods,* 1**,** 49.

PERRING, A., SCHWARZ, J., BAUMGARDNER, D., HERNANDEZ, M., SPRACKLEN, D., HEALD, C., GAO, R., KOK, G., MCMEEKING, G. & MCQUAID, J. 2015. Airborne observations of regional variation in fluorescent aerosol across the United States. *Journal of Geophysical Research: Atmospheres,* 120**,** 1153-1170.

PERRING, A. E. 2016. Chamber catalogues of optical and fluorescent signatures distinguish bioaerosol classes. *Atmospheric Measurement Techniques,* 9**,** 3283.

SAVAGE, N., KRENTZ, C., KÖNEMANN, T., HAN, T. T., MAINELIS, G., PÖHLKER, C. & HUFFMAN, J. A. 2017. Systematic Characterization and Fluorescence Threshold Strategies for the Wideband Integrated Bioaerosol Sensor (WIBS) Using Size-Resolved Biological and Interfering Particles. *Atmos. Meas. Tech. Discuss.,* 2017**,** 1-41.

SRICHANA, T., SUEDEE, R. & SRISUDJAI, P. 2003. Application of spectrofluorometry for evaluation of dry powder inhalers in vitro. *Die Pharmazie-An International Journal of Pharmaceutical Sciences,* 58**,** 125-129.

Chapter 5

Prevention of Nebulised Drug Dispersal using an Extractor Tent

Table of Contents

5.1 Introduction

Infectious aerosols from coughing, sneezing and talking can transmit disease from person-to-person by deposition in the respiratory tract. While numerous particle sizes are generated by these activities, those <10 µm in diameter remain suspended in air for long periods of time increasing the risk of inhalation, and particles <5 µm are most likely to cause infection in the lower respiratory tract (Sirignano, 2010, Morawska et al., 2009, Stilianakis and Drossinos, 2010, Seto, 2015). The Severe Acute Respiratory Syndrome (SARS) pandemic of 2003, the emergence of Multi-Drug Resistant (MDR) *Mycobacterium tuberculosis*, and persistent threat of a new influenza pandemic have heightened interest in the aerosol transmission of disease. Evidence exists supporting the aerosol transmission of SARS (Yu et al., 2004, Li et al., 2005, Varia et al., 2003), and tuberculosis (TB) (Fennelly et al., 2004, Nardell, 2004, Control and Prevention, 2006, Fennelly et al., 2012).

Several medical procedures involving the respiratory tract, including intubation, non-invasive ventilation and nebuliser therapy, are known to be 'aerosol generating' (Davies et al., 2009, Organization, 2008). Aerosols from these procedures may be exhaled from patients and can be unintentionally inhaled by healthcare workers (HCW) and family members. The exhaled dose of aerosolised drug is the amount of drug that was exhaled by the breathing patient. Deliberate aerosolisation by a nebuliser is a common method of drug delivery to the respiratory tract. A nebuliser is a device that converts liquid into polydisperse aerosol droplets suitable for inhalation (O'Callaghan and Barry, 1997, Health and Excellence, 2010). In the commonest type, a conventional jet nebuliser, the liquid drug solution is broken up into polydisperse droplets by compressed air and the larger droplets are then removed by baffles, where they amalgamate and fall back into the reservoir to be recirculated (Clay and Clarke, 1987b). Most of the drug released from the nebuliser is in particles of 1-5 µm diameter. Studies with radiolabelled inhaled aerosolised drug particles show that that during inhalation only 44% of inhaled aerosols with mass median diameter of 10.3 µm reached the lungs, while 79% of aerosols with mass median diameter (MMD) of 1.8 µm are deposited in the lungs (Clay and Clarke, 1987a). In addition, two thirds of the prescribed dose is released from the nebuliser during expiration (unless specific triggering of nebulisation during inhalation is employed), passing into the surrounding

air, the combination of this with the particle size, leaving only ~10% of the nominal dose to reach the lungs (O'Callaghan and Barry, 1997, Clay and Clarke, 1987b, Kradjan and Lakshminarayan, 1985). *In vitro* studies examining the mechanical ventilation of a patient with and without expiratory filters reported that > 45% of the nominal dose could become 'second-hand medical aerosol' (Ari et al., 2016). More recently a study by McGrath *et al.* investigated the proportion of drug exhaled using collection filters on nebuliser exhalation ports. They attributed ~30% of the nominal dose being exhaled using a standard compressor-driven jet nebuliser.

Several studies have highlighted concerns regarding the adverse effects of secondary exposure to nebulised aerosols (inhalation by people other than the intended patient) mainly with respect to cytotoxic drugs like cisplatin (Wittgen et al., 2006, Wittgen et al., 2007), the neurotoxic antiprotozoal/antifungal drug pentamidine (O'Riordan and Smaldone, 1992) and the potentially teratogenic antiviral drug ribavirin (Krilov, 2002). Health services recognise this risk. For example, in the USA, the National Institute for Occupational Safety and Health, part of the Centres for Disease Control (NIOSH,CDC) provides guidelines for the administration of cytotoxic drugs by nebuliser, recommending they are administered to patients inside tents, in negative pressure rooms with all healthcare workers dressed in in full barrier protection (Wittgen et al., 2007, Connor et al., 2008, Gardenhire et al., 2017).

Another potential side effect of secondary drug exposure is allergy. Studies have found that likelihood of asthma increases twofold along with significant associations with bronchial hyperresponsiveness following entry into a health care profession when performing tasks that involve aerosolized medication administration (Delclos et al., 2007).

Finally, there is some evidence for a role of nebuliser use in infection transmission. The most extreme are studies using nebulisers to challenge animals with aerosolised pathogens, in order to study respiratory infection (Peterson et al., 2007, Agar et al., 2008). *Yersinia pestis* and *Bacillus anthracis*, both biological warfare agents which when inhaled are highly fatal, were successfully aerosolised using a three-jet Collison nebuliser and in both instances the aerosolised pathogens successfully infected the lungs of experimental animals (Peterson et al., 2007, Agar et al., 2008).

In clinical practice patients requiring nebuliser therapy are likely to have air flow obstruction due to asthma or chronic obstructive pulmonary disease (COPD) and are therefore more likely to be coughing and wheezing spontaneously, and it is plausible that the flow from the nebuliser could disseminate additional cough-associated droplets (Simonds et al., 2010). Exhaled particles from patients are likely to have a mass median aerodynamic diameter of <2 μm, and particles in this range have a tendency to remain suspended in air for extended periods in time (Nazaroff, 2004, Sirignano, 2010, Morawska et al., 2009). In cases where low concentration exposure to infectious agents is enough for transmission, then exhaled aerosols may pose serious risk (Gortazar et al., 2014). Studies by Simonds et al. did not detect any additional droplet-sized particles with nebuliser use (Simonds et al., 2010). However using droplets as a proxy for dissemination is a limitation, as dissemination risk can only be determined through air sampling for specific agents in the vicinity of individuals with influenza, SARS, TB or other airborne pathogens (O'neil et al., 2017).

There is conflicting evidence that nebulisers may have played a role in the transmission of SARS in two major hospital outbreaks. The hospital index patient in the Toronto outbreak received nebulised salbutamol treatment in the emergency department and transmitted SARS to two patients 1.5 m and 5 m away in the ED, respectively. However, all three patients were cared for by the same nurse (Varia et al., 2003). Nurses who administered nebuliser therapy to SARS patients in Toronto were not found to be significantly more at risk of infection in two retrospective cohort studies. (Loeb et al., 2004, Raboud et al., 2010). In the Hong Kong outbreak, bronchodilator nebuliser therapy of the index case was also believed to have contributed to the high attack rate among hospital staff and patients (Lee et al., 2003). However, a retrospective cohort study found efficient transmission had begun before nebuliser therapy was initiated, and being present on the ward during nebuliser therapy, did not increase the risk of infection (Wong et al., 2004). Small nebuliser-derived aerosols may of course remain suspended in the air beyond the period of nebuliser use, confounding this result. Multi-drug resistant tuberculosis (MDR-TB) infection has been linked with the usage of aerosolised pentamidine, whereby nebulised drug administration to outpatients with tuberculosis in clinic rooms with positive pressure relative to treatment and waiting areas was associated with a greater

risk of MDR-TB transmission to other patients attending an human immunodeficiency virus (HIV) clinic (Beck-Sagué et al., 1992).

Contamination of nebulisers with environmental fungi or bacteria is well recognised to carry a risk of respiratory infection in the patient using the nebuliser. Environmental bacteria or fungi have been readily isolated from the home and hospital environment of patients with cystic fibrosis (CF) (Pitchford et al., 1987, Hutchinson et al., 1996, Jakobsson et al., 1997, Vassal et al., 2000, Mastro et al., 1991), asthma and other chronic pulmonary diseases that require nebuliser use. Treatment guidelines for the management of CF (Mogayzel Jr et al., 2013, Heijerman et al., 2009), asthma (Bateman et al., 2008) and COPD (Vestbo et al., 2013) recommend inhaled therapy as a route to administer medication. Gram-negative bacilli, predominantly *Pseudomonas* sp. were isolated from 61% of patient nebuliser solutions and aerosols in a study from New Zealand (Jones et al., 1985). A similar study at the University of Southampton (UK) revealed that up to a third of nebulisers used in domiciliary practice were contaminated with inhalable concentrations of Gram positive cocci (Barnes et al., 1987). More recently, a study showed that 66.7% of home nebulisers used by asthmatic children were contaminated by staphylococci and *Pseudomonas* spp. (Cohen et al., 2006), and 65% of home nebulisers used by CF patients (Blau et al., 2007) were contaminated by *Pseudomonas* sp. The high prevalence of fungal colonisation and infection among CF patients led Peckham *et al.* to assess fungal contamination of nebuliser devices. The study tested 170 nebuliser devices from 149 subjects with 57.7% of subjects having positive fungal cultures from one of their devices *Candida guilliermodi* was the most frequently recovered yeast (Peckham et al., 2016). Forty-four nebuliser sets from elderly patients with COPD were tested, and 73% were contaminated with microorganisms at >100 CFU/plate. Potentially pathogenic bacteria were recovered from 13 of the 44 nebulisers with isolates of *Staphylococcus aureus*, *Pseudomonas aeruginosa*, multidrug-resistant *Serratia marcesans, Escherichia coli* and multidrug resistant *Klebsiella* spp, *Enterobacteriaceae* and the fungus, *Fusarium oxysporum* (Jarvis et al., 2014).

Thus far the only airway treatment delivery procedure for which there is clear evidence for aerosol production is endotracheal intubation (Bivas-Benita et al., 2005). Bronchoscopy and sputum induction have long been associated with nosocomial

transmission of TB (Larson et al., 2003, McWilliams et al., 2002). More recently bronchoscopy, and respiratory and airway suctioning resulted in above baseline (background) values for the detection of H1N1 in aerosols (Thompson et al., 2013). Little research has been undertaken looking at the mass of aerosols produced from nebulisers and the pathogen carrying potential of aerosols expelled. Simulation studies have modelled the dispersal of exhaled air and aerosolised droplets during nebuliser therapy (Hui et al., 2009). Using smoke particles as an indicator it was determined that for patients with normal lung function, particles were dispersed 0.45 m laterally. This distance increased with decreasing lung function, 0.54 m at mild lung injury and then >0.8 m with severe lung injury (Hui et al., 2009). Environmental exposure is also of interest where aerosolised antibacterial agents may deposit on surfaces, exposed to ambient bacteria in concentrations that may be well below the level to kill the bacteria. Low concentration exposure of antibiotics is associated with development of antibiotic resistant species (Eames et al., 2009, Tornimbene et al., 2018).

It is common practice to use nebulised sterile saline solution to induce sputum induction in patients without spontaneous sputum production (Weiszhar and Horvath, 2013). To reduce the known risk of TB transmission during sputum induction, engineering controls are commonly put in place to control airflow and remove infectious particles, similar to the regulated aerosolisation of cytotoxic drugs, previously mentioned. The two main types of engineering controls are local exhaust ventilation (LEV) devices and negative pressure isolation rooms. LEV devices are in principle the most efficient control method involving capturing infectious particles close to the point of generation, thus preventing the dispersion of particles to other areas. The preferred type of LEV is a complete enclosure (booth or tent) surrounding the patient with exhaust air passage via a high-efficiency particulate air (HEPA)-filter (Francis, 1999, Gore and Smith, 2011). Tents have flexible walls with rigid frames and require minor assembly and disassembly (Gore and Smith, 2011). Although LEV devices of this type are in widespread use, their efficacy at reducing dispersal or nebuliser aerosols has not been formally demonstrated. As discussed in Chapter 2, during the 4-week study, 4 consistent diurnal peaks were observed, coinciding with known times of nebulised drug administration on the ward. These peaks from nebulisation therapy lead to an average 29550% increase in fluorescent particle count compared to background levels. The efficacy of an extractor tent (Demistifier 2000,

Peace Medical) on reducing aerosol dispersal of nebulised bronchodilator drugs, as used on the ward during the 4-weeks study, was determined by continuous monitoring of particle dispersal from a nebuliser with a bioaerosol detector.

5.2 Methods

5.2.1 Laboratory Characterisation of Nebulised Drug Particles by WIBS

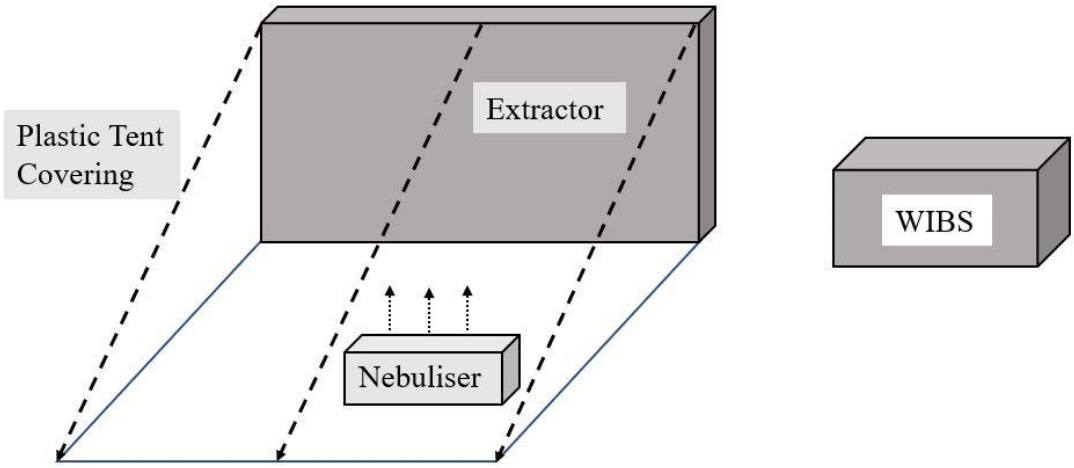

Figure 5.1 Schematic of experimental set up.

Figure 5.1 outlines the experimental procedure employed. The nebulizer pump used was the PARI TurboBOY SX (PARI Medical Ltd, Surrey, UK), and the nebuliser solutions were Ventolin® Nebules® (GlaxoSmithKline Ltd, Dublin, Ireland) and Ipramol® Steri-Neb® (IVAX Pharmaceuticals UK, Cheshire, UK). The instrument used was the WIBS-4a, as previously described in the methods section. The nebulizer air flow was ~10 L/min to replicate that used for nebulisers on the ward, Chapter 2. The experiment was conducted without a subject inhaling from the nebuliser.

5.2.2 Setting

The study was conducted in an unoccupied TB outpatients' room at St. James's Hospital, Dublin on 19th July 2019. The room did not have a heating, ventilation and air conditioning (HVAC) system. The LEV device used in the room was the Demistifier 2000, a tent-style mobile, HEPA-filtered isolation device (Demistifier, Peace Medical, Orange, New Jersey, USA) (Figure 5.2). The Demistifier 2000 has an extract fan expelling internal air via a filter pack containing two filters including a

HEPA fibre silicate filter that removes 99.99% of airborne particles 0.3 µm or more in diameter. The second filter is a carbon (charcoal) prefilter which captures large airborne particles. This prefilter incorporates the Aegis Antimicrobial System which is designed to prevent surface colony growth by chemically bonding to prefilter fibres and destroying all micro-organisms it contacts. The Aegis antimicrobial prefilter is treated with Aegis, an anti-microbial agent permanently bonded to the filter media. The Aegis is effective against Gram positive bacteria, Gram negative bacteria and moulds, mildew, fungi and yeasts. The Demistifier 2000 is designed to isolate a patient in a loose-skirted PVC enclosure reaching to the floor. As the fan operates, air is drawn upward from around the bottom of the skirt and flows through the HEPA filter system at a rate of 240-360 air changes per hour.

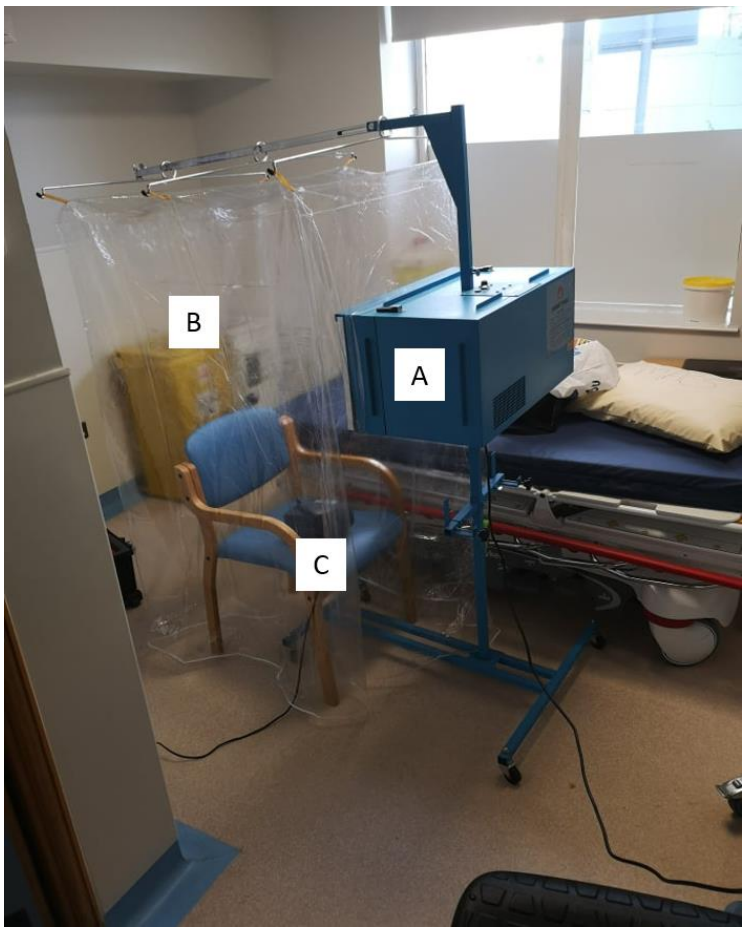

Figure 5.2 Demistifier 2000 set up in TB room, (A) filtration system containing the prefilter, HEPA filter and carbon filter, (B) plastic tent covering and (C) nebuliser pump.

5.2.3 Wideband Integrated Bioaerosol Sensor

Real-time airborne particle data was recorded using a Wideband Integrated Bioaerosol Sensor-4a (Droplet Measurement Technologies, Boulder, Colorado, USA). The Wideband Integrated Bioaerosol Sensor (WIBS) is a single aerosol particle fluorescence monitor that uses light-induced fluorescence (LIF) to detect fluorescent aerosol particles (FAP) in real-time. It provides particle size (0.5-12 µm), shape and fluorescent intensity in 3 channels. Initial detection of the particle is made using a continuous-wave red diode laser at 635 nm that illuminates the particles flowing into the optical chamber. Scattering of the laser light is used for both the sizing of particles (based on Mie theory) and to determine a basic particle "shape" using a so-called asymmetry factor (AF). The fluorescence characteristics of the individual particles are then interrogated using two xenon flash lamps (Xe_1, Xe_2). These are tuned to excite at the maxima absorption wavelengths of the biofluorophores tryptophan (280 nm) and NAD(P)H (370 nm). Fluorescence emission following these excitation pulses is detected in two detector bands: 310–400 nm (Band I) and 420–650 nm (Band II) (Healy et al., 2012). More details on the operation of the WIBS-4a are provided by Kaye et al. (Kaye et al., 2014), Fennelly et al. (Fennelly et al., 2017) and further details on instrument in section 2.1.1.

5.2.4 Samples

PARI TurboBOY SX (PARI Medical Ltd, Surrey, UK) was the compressor pump used in combination with the PARI LC SPRINT Nebuliser to nebulise the solutions. This is designed to produce a total output rate of 600 mg/min with aerosol particles having a mass median diameter of 3.5 µm and mass percentage below 5 µm of 67%. It delivers a high Respirable Drug Delivery Rate (RDDR), a measure of therapeutically useful quantity of medication that can be deposited in the lung in a given unit of time, in this case ~100 – 140 µg/min.

Ventolin® Nebules® (GlaxoSmithKline Ltd, Dublin, Ireland) were the active ingredient in each pack as 2.5 mg salbutamol (as sulphate). Other ingredients were sodium chloride, water for injections and dilute hydrochloric acid.

Ipramol® Steri-Neb® (IVAX Pharmaceuticals UK, Cheshire, UK), was the active ingredients in each pack as 0. 5 mg of ipratropium bromide (as the monohydrate) and 2.5 mg of salbutamol (as the sulfate). Other ingredients were sodium chloride, water for injections and dilute hydrochloric acid.

5.2.5 Statistical Analysis

The WIBS-4A records raw data as CSV files on a directly connected laptop. A single CSV file records a maximum of 30,000 particles or up to a maximum duration of 3 hrs. During the 3hour measurement period (19th July 2019) a total of 22 raw Excel files were collected. The data were imported into MATLAB (Math Works Inc., USA) and processed further into appropriate files, subsets and matrices. They were then summed into 10 second intervals and analysed and graphed using R Studio 1.1.383.

5.3 Results

5.3.1 Controlled TB Ward nebuliser experiments

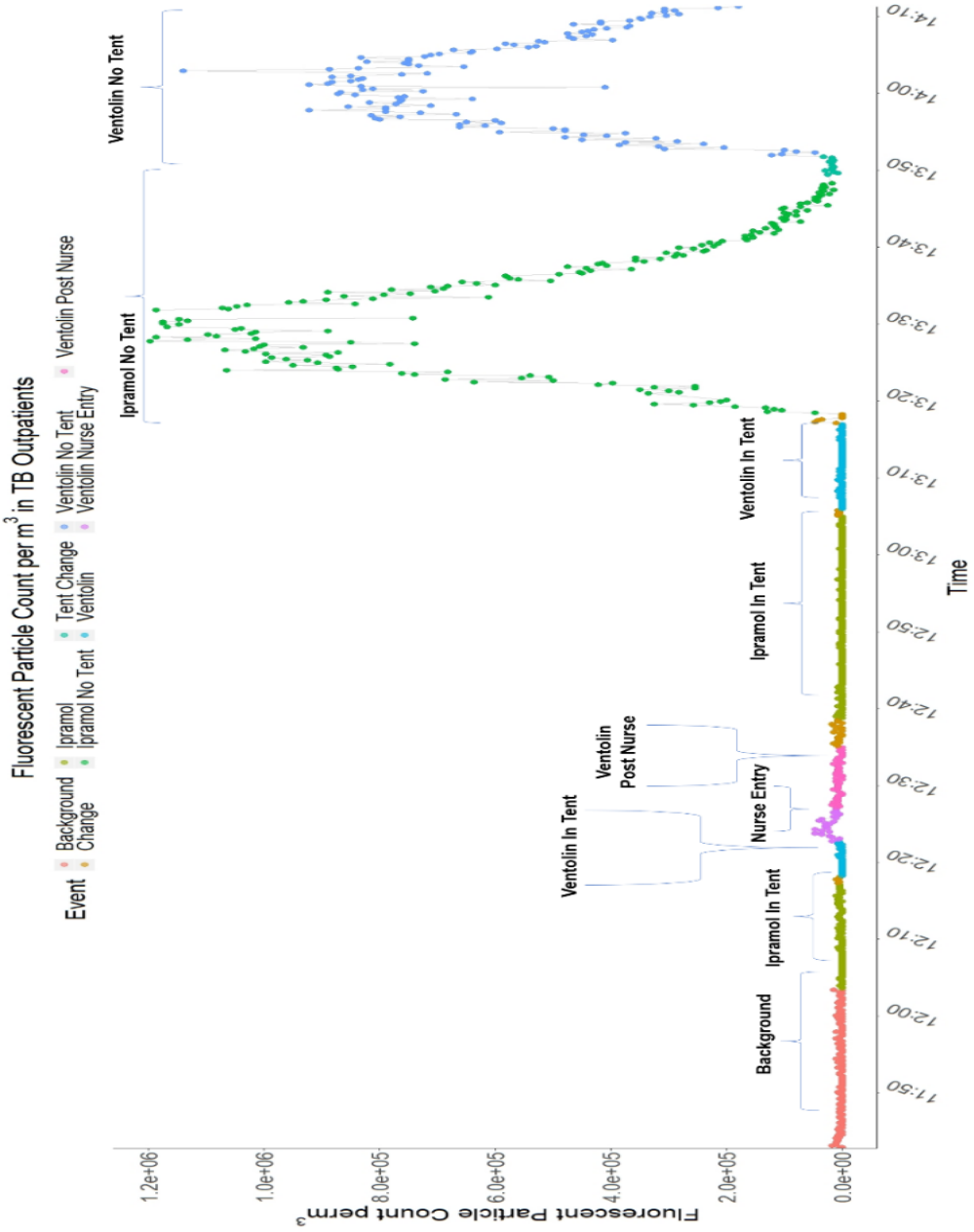

Figure 5.3 Fluorescent particle count per m^3 time series by activity colour.

The study, timeline shown in Figure 5.3, started at 11:42 and finished at 14:11. Background levels were measured for 21 minutes. WIBS was in the same location for both in-tent and out-of-tent nebuliser analysis.

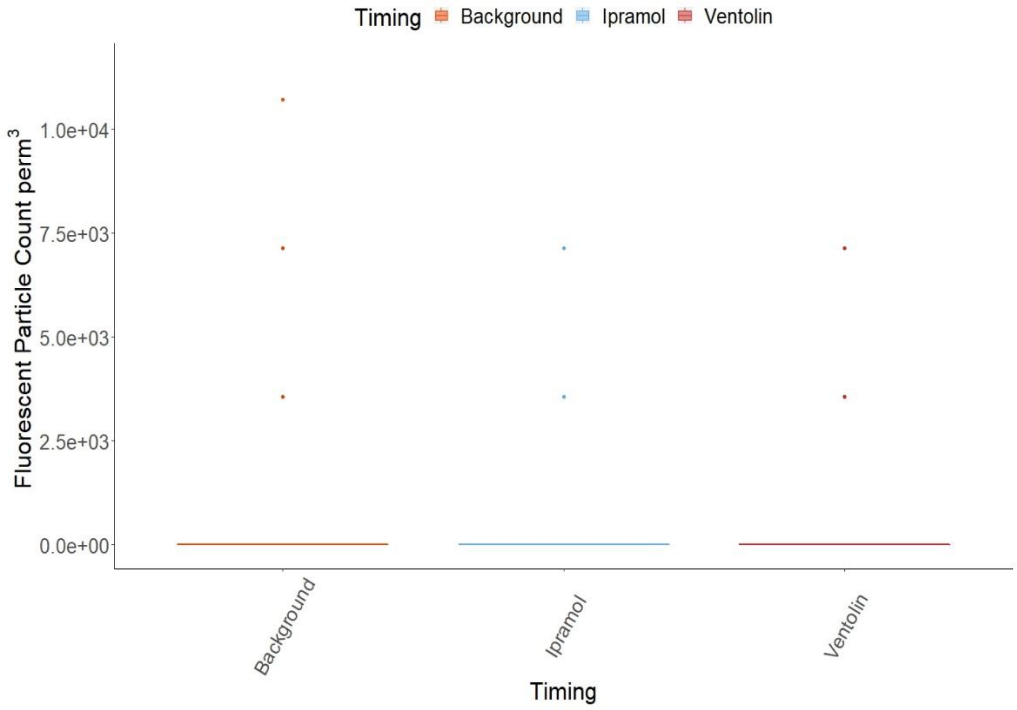

Figure 5.4 Boxplots of comparing fluorescent particle counts per m^3 of background (orange) and drug solutions nebulised in the tent Ipramol (blue) and Ventolin (red).

The mean fluorescent particle count was significantly lower for both in-tent nebulised drugs time periods, ($P<0.001$), than the background (Figure 5.4 and Table 5.1). However, it must be noted that the extractor tent is fitted with a charcoal filter, which may be indirectly filtering all the air in the room while the extractor is on. This may be the reason for nebulised drug time periods yielding lower particle counts than the background.

Table 5.1 Fluorescent Particle statistics for nebuliser solutions and background, with p-values calculated between the observed fluorescent counts from nebuliser drug and background.

Type	Mean ± SD		P-Value
	Fluorescent (Part/m^3 ×10^4)	Fluorescent Particle Count	
Background	0.091 ± 0.20	0.26 ± 0.55	1
Ventolin	0.065 ± 0.16	0.18 ± 0.44	<0.001
Ipramol	0.057 ± 0.15	0.16 ± 0.43	<0.001

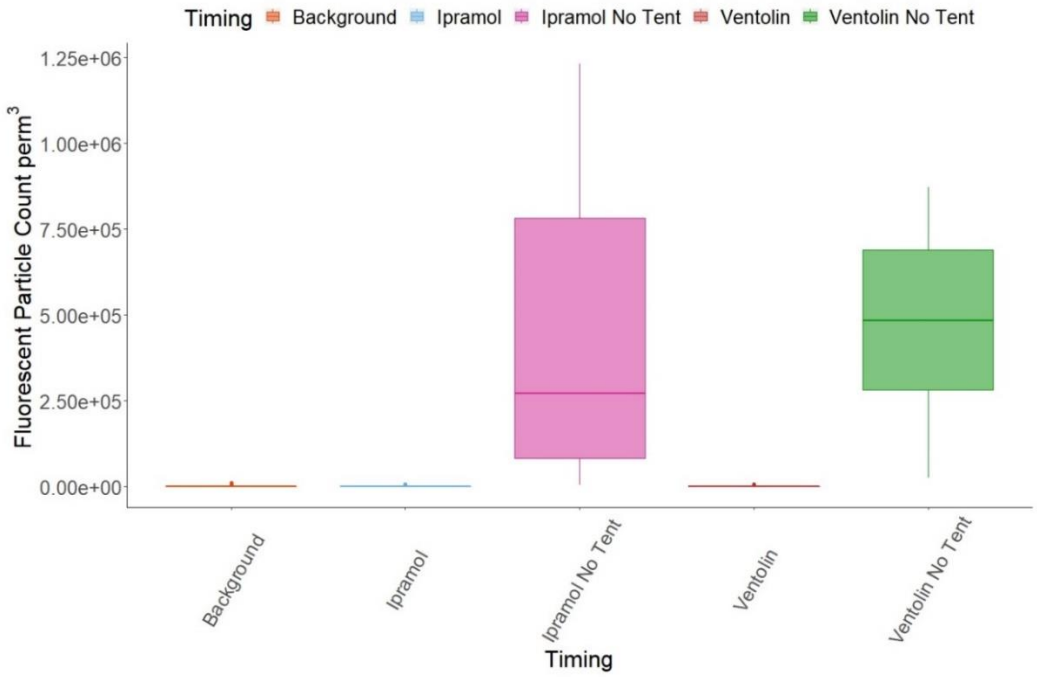

Figure 5.5 Boxplots of fluorescent particle counts per m^3 for background (orange), drug solutions nebulised in the tent Ipramol (blue), Ventolin (red) and outside of tent Ipramol (pink) and Ventolin (green).

Nebulising directly into room air resulted in a 7.03×10^4 and 4.64×10^4-fold increase in particle counts for Ventolin and Ipramol, Figure 5.5 and Table 5.2. Nebulising in the tent resulted in a maximum particle count of 2 and 3 for Ventolin and Ipramol, respectively. Direct room nebulisation resulted in a 1.58×10^4 and 1.15×10^4-fold increase to the maximum particle count over background levels. Using the tent lead to a >99% decrease in fluorescent particles, compared to nebulising drugs outside of the tent, Table 5.2.

Table 5.2 Fluorescent Particle statistics of nebuliser solutions with positive test (outside of tent) and inside of tent.

Tent	Type	Mean ± SD		Max Value		% Increase Without Tent
		Fluorescent (Part/m^3 $\times10^4$)	Fluorescent Particle Count	Fluorescent (Part/m^3 $\times10^4$)	Fluorescent Particle Count	
Yes	Ventolin	0.065 ± 0.16	0.18 ± 0.44	0.71	2	NA
	Ipramol	0.057 ± 0.15	0.16 ± 0.43	0.71	2	NA
No	Ventolin	47.51 ± 23.47	113.05 ± 65.74	87.13	244	99.18
	Ipramol	42.11 ± 37.43	117.93 ± 104.81	123.2	345	99.42

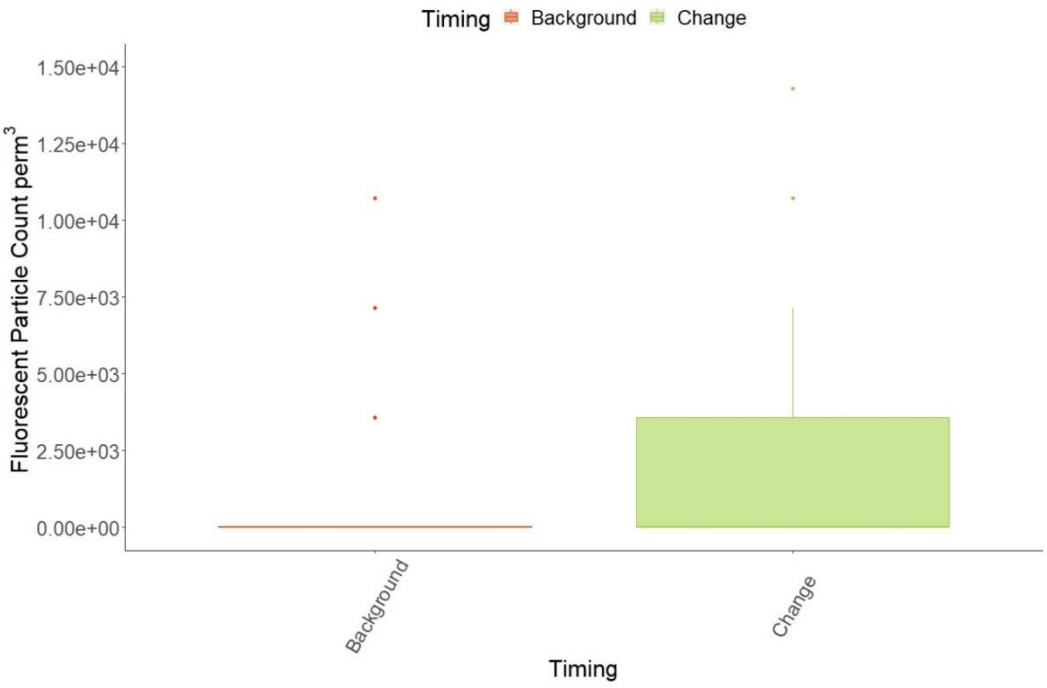

Figure 5.6 Boxplots of fluorescent particle counts per m^3 for background (orange), and change (green).

After a drug sample had run dry while nebulising in the tent, the tent had to be breached (opened) in order to change the nebuliser solutions. The time during drug solution change is referred to as "Change", see Figure 5.6 and Table 5.3.

From Figure 5.6 and Table 5.3 during nebuliser change-over a significant increase in fluorescent particle counts was observed compared to the background ($P<0.001$). However, it must be noted that although this increase is significant it is quite small in terms of particle counts, on average increasing by 0.47 counts, and the maximum counts observed differing by only 1 particle count.

Table 5.3 Fluorescent Particle statistics for background and change period, with p-values calculated between fluorescent particle counts observed for both periods.

Type	Mean ± SD		Max Value		P-Value
	Fluorescent (Part/m^3 ×10^4)	Fluorescent Particle Count	Fluorescent (Part/m^3 ×10^4)	Fluorescent Particle Count	
Background	0.091 ± 0.20	0.26 ± 0.55	1.07	3.00	<0.001
Change	0.261 ± 0.35	0.73 ± 0.97	1.42	4.00	

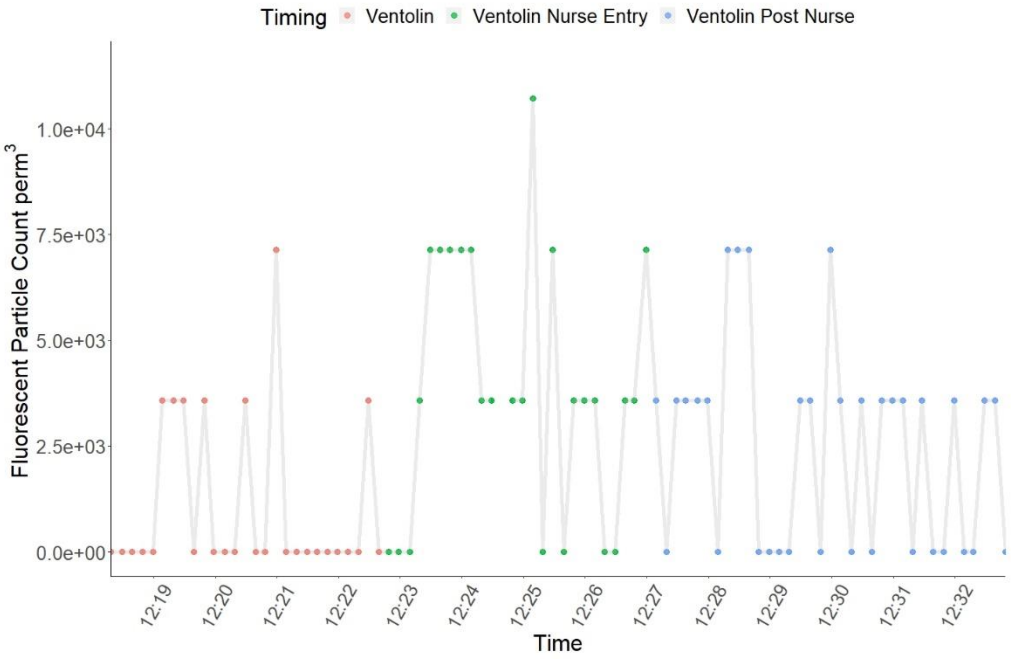

Figure 5.7 Fluorescent particle counts during tent-enclosed salbutamol nebulisation, nurse entry documented.

Considering confounding events, a significant 2-fold increase in mean fluorescent particles on a very low background was noted from 12:23 minutes after Ventolin nebulisation commenced, to Ventolin +6.00 minutes. This was associated with entry of a nurse to the room from 12:22-12:26 (Figure 5.7).

Table 5.4 Fluorescent Particle Count and Statistics for Nurse entry.

Type	Mean ± SD		Max Value		P-Value
	Fluorescent (Part/m^3 $\times 10^4$)	Fluorescent Particle Count	Fluorescent (Part/m^3 $\times 10^4$)	Fluorescent Particle Count	
Ventolin	0.065 ± 0.16	0.18 ± 0.44	0.71	2.00	<0.001
Nurse Entry	0.43 ± 0.36	1.19 ± 1.0	1.43	4.00	

During nebulisation in the tent the WIBS did not detect the nebulised aerosols escaping the tent the only events that the WIBS detected were the fluorescent particles produced by the outside event i.e. like the nurse's entry, Figure 5.7.

5.3.2 Inhalation Rates

Using the particle count and size with average tidal volume of 230 L/30 minutes, the concentrations (mg) of nebulised drug inhaled by a visitor or healthcare professional within the ward during nebulisation therapy can be calculated as follows. Using the fluorescent particle count, from the nebulisers fluorescent signature as developed in chapter 2, during the 4 nebulisation periods of ~ 05:00, 11:00, 16:00 and 20:00 and on average every 30 minutes a person will inhale 1.74×10^{-3} – 2.35×10^{-3} mg of nebuliser solution at average tidal volume. In an effort to isolate fluorescent particles from the nebulised drugs, the background ambient aerosols as calculated by the average particles during the early morning period were subtracted, even if it may not have explicitly removed all ambient aerosols.

Table 5.5 Calculated inhalation rates at nebuliser times (Chapter 3, Table 3.4). All exhaled drug denotes all nebulised drug lost to surrounding environment, patient exhaled denotes inhaled drug that was immediately exhaled into the environment.

Nebuliser Time	mg ($\times10^{-3}$) inhaled of nebulised drug	
	All exhaled	Patient exhaled
05:00:00	1.74	1.20
05:30:00	2.35	1.61
11:00:00	2.25	1.57
11:30:00	1.75	1.12
16:00:00	2.16	1.48
16:30:00	2.08	1.59
20:00:00	2.16	1.57
20:30:00	2.12	1.47

Values provided in Table 5.5 are average values for nebuliser particle concentrations, as we could not discriminate between which patients used the nebulisers and the distance they were from the instrument. The highest inhaled concentration of nebuliser aerosols was 05:00 - 06:00:00 where bystanders were estimated to be inhaling 2.36×10^{-3} mg of the of the exhaled nebuliser aerosols (~0.725 mg) and 1.61×10^{-3} mg of inhaled and immediately exhaled aerosols (~0.325 mg). All exhaled and patient exhaled aerosols are based on nebuliser loss estimates by Clay *et al.* and McGrath *et al.* (Clay and Clarke, 1987b, McGrath et al., 2019).

5.4 **Conclusion**

Nebulising in the tent restricted Ventolin and Ipramol to a maximum particle count of 2 and 3, respectively, Figure 5.4. Nebulising directly into room air resulted in a maximum particle count of 319 and 348 for Ventolin and Ipramol, respectively (Figure 5.5). Nebulising directly into room air resulted in a 7.03×10^4 and 4.64×10^4-fold increase in particle counts for Ventolin and Ipramol, Table 5.2. WIBS monitoring showed 100 % efficacy of the tent in restricting spread of nebulised drug particles. The only time the WIBS detected fluorescent particles was during external events i.e. the nurse's entry, Figure 5.7. The mean fluorescent particle count was significantly lower for both in-tent nebulised drugs time periods, than the background, Table 5.1. A charcoal filter is fitted on the extractor tent, which may be indirectly filtering all the air in the room while the extractor is on. This may be the reason for nebulised drug time periods yielding lower particle counts than the background.

Previous experiments assessing the efficiency of the Demistifier 2000 in limiting Sustained release Lipid Inhalation Targeting (SLIT) cisplatin secondary exposure by Wittgen *et al.* reported air samples were assayed for platinum content by inductively coupled plasma mass spectrometry (ICP-MS) and were indistinguishable from blanks during patient dosing, indicating no cisplatin escaped the demistifier during a 14 hour patient dosing (Wittgen et al., 2006). Air concentrations of cisplatin measured with tent integrity compromised i.e. while taking the patient from the tent were below the limit of quantification (LOQ), similarly, measured air concentrations were below the LOQ following 7 ml nebulisation of SLIT cisplatin inside a tent without a patient. The demistifier tent and filtration mechanism were therefore effective at containing any nebulised liposomal encapsulated cisplatin during patient treatment, when the tent integrity was compromised, and the HEPA filter was capable of effectively clearing large volumes of nebulised drug (Wittgen et al., 2006). Results from this thesis are consistent with those reported by Wittgen *et al.* in that the Demistifier 2000 completely restricts the spread of nebuliser aerosols during nebulisation. After nebulisation a small but significant increase in fluorescent particle counts occurred at one point compared to the background (Figure 5.7), but this time point corresponded to an event outside the tent likely to increase airborne particles - the room door opening with a nurse entering.

From on-ward data, chapter 3 section 3.7, we observed nebulised aerosols contributing a 1564% (×~15.5) increase in hourly average particle concentration, with an on-ward reduction rate of ~1753-2322 particles/min, returning to background levels. This was a 4-bed respiratory ward where most patients required nebuliser therapy, all contributing to this large increase in aerosol concentrations at regular intervals in the daytime, corresponding to medication rounds.

The data from this chapter shows that use of an extractor tent would completely restrict the spread of nebulised drug particles and prevent this large increase in airborne ward particles. Reducing the vast number of nebuliser aerosols released into the ward may also reduce the risk of nebuliser related aerosolised pathogens. Although other external factors may influence how much drug a visitor or health care worker may inhale on the ward, we have calculated on average a person will inhale 1.56×10^{-3} – 2.49×10^{-3} mg of nebuliser solution at average tidal volume. We do not know the infectious dose to cause a nosocomial infection from respired nebuliser aerosols and therefore is not possible to quantify individual risk of transmission via the airborne route, however, the infectious dose is likely to vary according to the pathogen and the vulnerability of the host or patient.

Salbutamol and ipratropium have been reported to generate harmful side effects. In the case of salbutamol, studies have shown it may cause allergic reactions or unwanted pharmacological effects in someone who is oversensitive or has cardiac problems (Libretto, 1994, Montgomery et al., 1994, Beasley et al., 1988). Salbutamol is a short-acting agonist of the $ß_2$ adrenergic receptors (used to widen airways) and may aggravate cardiac conditions including sinus tachycardia (Udezue et al., 1995, Du Plooy et al., 1994), ventricular and supraventricular tachycardia (Kallergis et al., 2005, Patanè et al., 2010) and myocardial ischemia (Fisher et al., 2004, Kochiadakis et al., 2007), especially in cases of acute overuse. Ipratropium type drugs are known as anticholinergic, used to widen airways by blocking the cholinergic nerves. Ipratropium bromide has been associated with increased risk of cardiovascular events (CVE) (acute coronary syndrome, heart failure, or cardiac dysrhythmia) (Ogale et al., 2010) and an increased risk of premature death where it has been suggested that the drying effect that Ipratropium has on lung secretions might lead to mucus plugging (Guite et al., 1999, Ringbaek and Viskum, 2003). During a large clinical trial comparing

ipratropium bromide to a placebo in mild COPD, there was increased cardiovascular morbidity and mortality of marginal significance in the group assigned ipratropium bromide, particularly an increase in the incidence of supra-ventricular tachycardia (Anthonisen et al., 2002). Ipratropium is related to tiotropium, a long acting anticholinergic, which is regularly used to control wheezing and shortness of breath related to lung diseases such as asthma and COPD. However, studies have shown an up to 52% increased risk of mortality associated with the long-term use of tiotropium mist inhalers in patients with COPD. They found a dose of 5 µg of tiotropium was associated with a 46% increased risk of mortality in the five trials and doubling the dose to 10 µg dose was associated with a doubling of the relative risk in four trials (Singh et al., 2011). However, the concentrations that may be inhaled on the ward may not be of the quantity to elicit an adverse cardiac effect, although cumulative inhalation of aerosols has not been documented. Although in relatively small quantities, nebulised drug solutions of 1.56×10^{-3} – 2.49×10^{-3} mg of nebuliser solution inhaled by a bystander at an average tidal volume, may cause an allergic reaction.

Preservatives such as benzalkonium chloride (BAC) have been added to nebuliser solutions to prevent the growth of bacteria. However, it has been reported that BAC containing ipratropium bromide solutions caused a 20% drop in forced expiratory volume (FEV) in asthma patients (Beasley et al., 1987). It was found that BAC caused a dose-dependent bronchoconstriction that persisted for greater than 1 hour. The mean concentration that provoked the decrease in FEV was 0.13-0.2 mg/ml. The bronchoconstrictor effects of BAC, through simulating cholinergic and non-cholinergic airway nerves, have been demonstrated in patients with asthma with no past history of inadvertent bronchoconstriction (Miszkiel et al., 1988b, Miszkiel et al., 1988a).

O'Neil *et al.* observed significant aerosol generation during nebuliser therapy, but only minimal, common environmental bacterial organisms were recovered, which would suggest little infection risk associated with nebuliser therapy (O'neil et al., 2017). The authors noted that the study was limited by using small sample numbers (5 samples for each procedure), a lack of clinical data, having only 1 sampling location for each sample, noncontinuous air sampling, and lack of viral pathogen recovery (O'neil et al., 2017). They also used patients which were under contact precautions for

methicillin-resistant *Staphylococcus aureus* (MRSA), vancomycin-resistant Enterococci (VRE), multidrug-resistant gram-negative organisms (MDROs), and *Clostridioides difficile*. Further studies would need to look at airborne precaution patients (CF, H1N1 patients) and investigate whether viruses can be isolated. It is known that cross infection with *P. aeruginosa* can occur between people with CF (McCallum et al., 2001, Denton et al., 2002), with nebulisation playing a part in its dissemination, indicating that nebulisers may play a role in the dissemination of known airborne pathogens.

Data gathered in this chapter shows that extractor tents such as the Demister 2000 are completely effective in preventing airborne spread of drug particles from nebulised therapy. This suggests that they would also prevent the dispersal of any pathogens that may be exhaled by patients during nebuliser therapy. Although on the respiratory ward, the drug solutions were BAC free, restricting environmental aerosol contamination which must be taken into consideration on wards where BAC solutions are still in use.

5.5 Reference

AGAR, S. L., SHA, J., FOLTZ, S. M., EROVA, T. E., WALBERG, K. G., PARHAM, T. E., BAZE, W. B., SUAREZ, G., PETERSON, J. W. & CHOPRA, A. K. 2008. Characterization of a mouse model of plague after aerosolization of Yersinia pestis CO92. *Microbiology,* 154**,** 1939-1948.

ANTHONISEN, N. R., CONNETT, J. E., ENRIGHT, P. L. & MANFREDA, J. 2002. Hospitalizations and mortality in the Lung Health Study. *American journal of respiratory and critical care medicine,* 166**,** 333-339.

ARI, A., FINK, J. B. & PILBEAM, S. P. 2016. Secondhand aerosol exposure during mechanical ventilation with and without expiratory filters: An in-vitro study.

BARNES, K. L., CLIFFORD, R., HOLGATE, S. T., MURPHY, D., COMBER, P. & BELL, E. 1987. Bacterial contamination of home nebuliser. *British medical journal (Clinical research ed.),* 295**,** 812.

BATEMAN, E. D., HURD, S., BARNES, P., BOUSQUET, J., DRAZEN, J., FITZGERALD, M., GIBSON, P., OHTA, K., O'BYRNE, P. & PEDERSEN, S. 2008. Global strategy for asthma management and prevention: GINA executive summary. *European Respiratory Journal,* 31**,** 143-178.

BEASLEY, C., RAFFERTY, P. & HOLGATE, S. 1987. Bronchoconstrictor properties of preservatives in ipratropium bromide (Atrovent) nebuliser solution. *British medical journal (Clinical research ed.),* 294**,** 1197.

BEASLEY, R., RAFFERTY, P. & HOLGATE, S. 1988. Adverse reactions to the non-drug constituents of nebuliser solutions. *British journal of clinical pharmacology,* 25**,** 283.

BECK-SAGUÉ, C., DOOLEY, S. W., HUTTON, M. D., OTTEN, J., BREEDEN, A., CRAWFORD, J. T., PITCHENIK, A. E., WOODLEY, C., CAUTHEN, G. & JARVIS, W. R. 1992. Hospital outbreak of multidrug-resistant Mycobacterium tuberculosis infections: factors in transmission to staff and HIV-infected patients. *Jama,* 268**,** 1280-1286.

BIVAS-BENITA, M., ZWIER, R., JUNGINGER, H. E. & BORCHARD, G. 2005. Non-invasive pulmonary aerosol delivery in mice by the endotracheal route. *European Journal of Pharmaceutics and Biopharmaceutics,* 61**,** 214-218.

BLAU, H., MUSSAFFI, H., MEI ZAHAV, M., PRAIS, D., LIVNE, M., CZITRON, B. & COHEN, H. 2007. Microbial contamination of nebulizers in the home treatment of cystic fibrosis. *Child: care, health and development,* 33**,** 491-495.

CLAY, M. M. & CLARKE, S. W. 1987a. Effect of nebulised aerosol size on lung deposition in patients with mild asthma. *Thorax,* 42**,** 190-194.

CLAY, M. M. & CLARKE, S. W. 1987b. Wastage of drug from nebulisers: a review. *Journal of the Royal Society of Medicine,* 80**,** 38-39.

COHEN, H. A., KAHAN, E., COHEN, Z., SARRELL, M., BENI, S., GROSMAN, Z. & ASHKENAZI, S. 2006. Microbial colonization of nebulizers used by asthmatic children. *Pediatrics international,* 48**,** 454-458.

CONNOR, T. H., LEONE, M. M., MCDIARMID, M. A., POLOVICH, M., POWER, L. A., REED, L. D. & WHALEN, J. J. 2008. Personal protective equipment for health care workers who work with hazardous drugs.

CONTROL, C. F. D. & PREVENTION 2006. Prevention and control of tuberculosis in correctional and detention facilities: recommendations from CDC. Endorsed by the Advisory Council for the Elimination of Tuberculosis, the National Commission on Correctional Health Care, and the American Correctional Association. *MMWR. Recommendations and reports: Morbidity and mortality weekly report. Recommendations and reports,* 55**,** 1.

DAVIES, A., THOMSON, G., WALKER, J. & BENNETT, A. 2009. A review of the risks and disease transmission associated with aerosol generating medical procedures. *Journal of Infection Prevention,* 10**,** 122-126.

DELCLOS, G. L., GIMENO, D., ARIF, A. A., BURAU, K. D., LUSK, C., STOCK, T., SYMANSKI, E., WHITEHEAD, L. W., ZOCK, J.-P. & BENAVIDES, F. G. 2007. Occupational risk factors and asthma among health care professionals. *American journal of respiratory and critical care medicine,* 175**,** 667-675.

DENTON, M., KERR, K., MOONEY, L., KEER, V., RAJGOPAL, A., BROWNLEE, K., ARUNDEL, P. & CONWAY, S. 2002. Transmission of colistin-resistant Pseudomonas aeruginosa between patients attending a pediatric cystic fibrosis center. *Pediatric pulmonology,* 34**,** 257-261.

DU PLOOY, W., HAY, L., KAHLER, C., SCHUTTE, P. & BRANDT, H. 1994. The dose-related hyper-and-hypokalaemic effects of salbutamol and its arrhythmogenic potential. *British journal of pharmacology,* 111**,** 73-76.

EAMES, I., TANG, J., LI, Y. & WILSON, P. 2009. Airborne transmission of disease in hospitals. The Royal Society.

FENNELLY, K. P., JONES-LÓPEZ, E. C., AYAKAKA, I., KIM, S., MENYHA, H., KIRENGA, B., MUCHWA, C., JOLOBA, M., DRYDEN-PETERSON, S. & REILLY, N. 2012. Variability of infectious aerosols produced during coughing by patients with pulmonary tuberculosis. *American journal of respiratory and critical care medicine,* 186**,** 450-457.

FENNELLY, K. P., MARTYNY, J. W., FULTON, K. E., ORME, I. M., CAVE, D. M. & HEIFETS, L. B. 2004. Cough-generated aerosols of Mycobacterium tuberculosis: a new method to study infectiousness. *American journal of respiratory and critical care medicine,* 169**,** 604-609.

FENNELLY, M. J., SEWELL, G., PRENTICE, M. B., O'CONNOR, D. J. & SODEAU, J. R. 2017. The Use of Real-Time Fluorescence Instrumentation to Monitor Ambient Primary Biological Aerosol Particles (PBAP). *Atmosphere,* 9**,** 1.

FISHER, A. A., DAVIS, M. W. & MCGILL, D. A. 2004. Acute myocardial infarction associated with albuterol. *Annals of Pharmacotherapy,* 38**,** 2045-2049.

FRANCIS, J. 1999. Conducting sputum induction safely. *Institutional Consultation Services Effective TB Solutions. California: Curry National Tuberculosis Center (CNTC)***,** 9.

GARDENHIRE, D. S., BURNETT, D., STRICKLAND, S., RRT-ACCS, A., MYERS, T. R. & RRT-NPS, F. 2017. Aerosol Delivery Devices for Respiratory Therapists.

GORE, B. & SMITH, K. 2011. Tuberculosis infection control: a practical manual for preventing TB, 2011. *San Francisco (CA)*.

GORTAZAR, C., REPERANT, L. A., KUIKEN, T., DE LA FUENTE, J., BOADELLA, M., MARTÍNEZ-LOPEZ, B., RUIZ-FONS, F., ESTRADA-PEÑA, A., DROSTEN, C. & MEDLEY, G. 2014. Crossing the interspecies barrier: opening the door to zoonotic pathogens. *PLoS pathogens,* 10**,** e1004129.

GUITE, H. F., DUNDAS, R. & BURNEY, P. G. 1999. Risk factors for death from asthma, chronic obstructive pulmonary disease, and cardiovascular disease after a hospital admission for asthma. *Thorax,* 54**,** 301-307.

HEALTH, N. I. F. & EXCELLENCE, C. 2010. Chronic Obstructive Pulmonary Disease in Over 16s: Diagnosis and Management.[CG101].

HEALY, D. A., O'CONNOR, D. J., BURKE, A. M. & SODEAU, J. R. 2012. A laboratory assessment of the Waveband Integrated Bioaerosol Sensor (WIBS-4) using individual samples of pollen and fungal spore material. *Atmospheric environment,* 60**,** 534-543.

HEIJERMAN, H., WESTERMAN, E., CONWAY, S., TOUW, D. & GROUP, G. D. F. T. C. W. 2009. Inhaled medication and inhalation devices for lung disease in patients with cystic fibrosis: a European consensus. *Journal of Cystic Fibrosis,* 8**,** 295-315.

HUI, D. S., CHOW, B. K., CHU, L. C., NG, S. S., HALL, S. D., GIN, T. & CHAN, M. T. 2009. Exhaled air and aerosolized droplet dispersion during application of a jet nebulizer. *Chest,* 135**,** 648-654.

HUTCHINSON, G. R., PARKER, S., PRYOR, J. A., DUNCAN-SKINGLE, F., HOFFMAN, P. N., HODSON, M. E., KAUFMANN, M. E. & PITT, T. L. 1996. Home-use nebulizers: a potential primary source of Burkholderia cepacia and other colistin-resistant, gram-negative bacteria in patients with cystic fibrosis. *Journal of clinical microbiology,* 34**,** 584-587.

JAKOBSSON, B.-M., ÖNNERED, A.-B., HJELTE, L. & NYSTRÖM, B. 1997. Low bacterial contamination of nebulizers in home treatment of cystic fibrosis patients. *Journal of Hospital Infection,* 36**,** 201-207.

JARVIS, S., IND, P., THOMAS, C., GOONESEKERA, S., HAFFENDEN, R., ABDOLRASOULI, A., FIORENTINO, F. & SHINER, R. 2014. Microbial

contamination of domiciliary nebulisers and clinical implications in chronic obstructive pulmonary disease. *BMJ open respiratory research,* 1**,** e000018.

JONES, P., MORITZ, V. & PIERCE, R. 1985. Microbial contamination of domiciliary nebuliser therapy equipment. *Australian and New Zealand journal of medicine,* 15**,** 585-589.

KALLERGIS, E. M., MANIOS, E. G., KANOUPAKIS, E. M., SCHIZA, S. E., MAVRAKIS, H. E., KLAPSINOS, N. K. & VARDAS, P. E. 2005. Acute electrophysiologic effects of inhaled salbutamol in humans. *Chest,* 127**,** 2057-2063.

KAYE, P. H., STANLEY, W. R. & FOOT, E. V. J. 2014. *Fluid-Borne Particle Detector*. US 13/957,655.

KOCHIADAKIS, G. E., HAMILOS, M. I., SKALIDIS, E. I., IGOUMENIDIS, N. E., SCHIZA, S. E. & VARDAS, P. E. 2007. Effect of inhaled salbutamol on coronary circulation in humans. *International journal of cardiology,* 117**,** 408-410.

KRADJAN, W. A. & LAKSHMINARAYAN, S. 1985. Efficiency of air compressor-driven nebulizers. *Chest,* 87**,** 512-516.

KRILOV, L. R. 2002. Safety issues related to the administration of ribavirin. *The Pediatric infectious disease journal,* 21**,** 479-481.

LARSON, J. L., LAMBERT, L., STRICOF, R. L., DRISCOLL, J., MCGARRY, M. A. & RIDZON, R. 2003. Potential nosocomial exposure to Mycobacterium tuberculosis from a bronchoscope. *Infection Control & Hospital Epidemiology,* 24**,** 825-830.

LEE, N., HUI, D., WU, A., CHAN, P., CAMERON, P., JOYNT, G. M., AHUJA, A., YUNG, M. Y., LEUNG, C. & TO, K. 2003. A major outbreak of severe acute respiratory syndrome in Hong Kong. *New England Journal of Medicine,* 348**,** 1986-1994.

LI, Y., HUANG, X., YU, I., WONG, T. & QIAN, H. 2005. Role of air distribution in SARS transmission during the largest nosocomial outbreak in Hong Kong. *Indoor air,* 15**,** 83-95.

LIBRETTO, S. E. 1994. A review of the toxicology of salbutamol (albuterol). *Archives of toxicology,* 68**,** 213-216.

LOEB, M., MCGEER, A., HENRY, B., OFNER, M., ROSE, D., HLYWKA, T., LEVIE, J., MCQUEEN, J., SMITH, S. & MOSS, L. 2004. SARS among critical care nurses, Toronto. *Emerging infectious diseases,* 10**,** 251.

MASTRO, T. D., FIELDS, B. S., BREIMAN, R. F., CAMPBELL, J., PLIKAYTIS, B. D. & SPIKA, J. S. 1991. Nosocomial Legionnaires' disease and use of medication nebulizers. *Journal of Infectious Diseases,* 163**,** 667-671.

MCCALLUM, S. J., CORKILL, J., GALLAGHER, M., LEDSON, M. J., HART, C. A. & WALSHAW, M. J. 2001. Superinfection with a transmissible strain of Pseudomonas aeruginosa in adults with cystic fibrosis chronically colonised by P aeruginosa. *The Lancet,* 358**,** 558-560.

MCGRATH, J. A., O'SULLIVAN, A., BENNETT, G., O'TOOLE, C., JOYCE, M., BYRNE, M. A. & MACLOUGHLIN, R. 2019. Investigation of the quantity of exhaled aerosols released into the environment during nebulisation. *Pharmaceutics,* 11**,** 75.

MCWILLIAMS, T., WELLS, A., HARRISON, A., LINDSTROM, S., CAMERON, R. & FOSKIN, E. 2002. Induced sputum and bronchoscopy in the diagnosis of pulmonary tuberculosis. *Thorax,* 57**,** 1010-1014.

MISZKIEL, K., BEASLEY, R. & HOLGATE, S. 1988a. The influence of ipratropium bromide and sodium cromoglycate on benzalkonium chloride-induced bronchoconstriction in asthma. *British journal of clinical pharmacology,* 26**,** 295-301.

MISZKIEL, K., BEASLEY, R., RAFFERTY, P. & HOLGATE, S. 1988b. The contribution of histamine release to bronchoconstriction provoked by inhaled benzalkonium chloride in asthma. *British journal of clinical pharmacology,* 25**,** 157-163.

MOGAYZEL JR, P. J., NAURECKAS, E. T., ROBINSON, K. A., MUELLER, G., HADJILIADIS, D., HOAG, J. B., LUBSCH, L., HAZLE, L., SABADOSA, K. & MARSHALL, B. 2013. Cystic fibrosis pulmonary guidelines: chronic medications for maintenance of lung health. *American journal of respiratory and critical care medicine,* 187**,** 680-689.

MONTGOMERY, H., GILL, J. & PUMPHREY, C. 1994. Unsuspected coronary artery disease revealed by administration of nebulised salbutamol. *British heart journal,* 72**,** 181-181.

MORAWSKA, L., JOHNSON, G., RISTOVSKI, Z., HARGREAVES, M., MENGERSEN, K., CORBETT, S., CHAO, C. Y. H., LI, Y. & KATOSHEVSKI, D. 2009. Size distribution and sites of origin of droplets expelled from the human respiratory tract during expiratory activities. *Journal of Aerosol Science,* 40**,** 256-269.

NARDELL, E. A. 2004. Catching droplet nuclei: toward a better understanding of tuberculosis transmission. American Thoracic Society.

NAZAROFF, W. W. 2004. Indoor particle dynamics. *Indoor air,* 14**,** 175-183.

O'CALLAGHAN, C. & BARRY, P. W. 1997. The science of nebulised drug delivery. *Thorax,* 52**,** S31.

O'RIORDAN, T. G. & SMALDONE, G. C. 1992. Exposure of health care workers to aerosolized pentamidine. *Chest,* 101**,** 1494-1499.

O'NEIL, C. A., LI, J., LEAVEY, A., WANG, Y., HINK, M., WALLACE, M., BISWAS, P., BURNHAM, C.-A. D. & BABCOCK, H. M. 2017. Characterization of aerosols generated during patient care activities. *Clinical Infectious Diseases*.

OGALE, S. S., LEE, T. A., AU, D. H., BOUDREAU, D. M. & SULLIVAN, S. D. 2010. Cardiovascular events associated with ipratropium bromide in COPD. *Chest,* 137**,** 13-19.

ORGANIZATION, W. H. 2008. Epidemic-and pandemic-prone acute respiratory diseases: infection prevention and control in health care (Aide-Memoire). *Geneva: WHO,* 18.

PATANÈ, S., MARTE, F., LA ROSA, F. C. & LA ROCCA, R. 2010. Atrial fibrillation associated with chocolate intake abuse and chronic salbutamol inhalation abuse. *International journal of cardiology,* 145**,** e74-e76.

PECKHAM, D., WILLIAMS, K., WYNNE, S., DENTON, M., POLLARD, K. & BARTON, R. 2016. Fungal contamination of nebuliser devices used by people with cystic fibrosis. *Journal of Cystic Fibrosis,* 15**,** 74-77.

PETERSON, J. W., COMER, J. E., BAZE, W. B., NOFFSINGER, D. M., WENGLIKOWSKI, A., WALBERG, K. G., HARDCASTLE, J., PAWLIK, J., BUSH, K. & TAORMINA, J. 2007. Human monoclonal antibody AVP-21D9 to protective antigen reduces dissemination of the Bacillus anthracis Ames strain from the lungs in a rabbit model. *Infection and immunity,* 75**,** 3414-3424.

PITCHFORD, K. C., COREY, M., HIGHSMITH, A. K., PERLMAN, R., BANNATYNE, R., GOLD, R., LEVISON, H. & FORD-JONES, E. L. 1987. Pseudomonas species contamination of cystic fibrosis patients' home inhalation equipment. *The Journal of pediatrics,* 111**,** 212-216.

RABOUD, J., SHIGAYEVA, A., MCGEER, A., BONTOVICS, E., CHAPMAN, M., GRAVEL, D., HENRY, B., LAPINSKY, S., LOEB, M. & MCDONALD, L. C. 2010. Risk factors for SARS transmission from patients requiring intubation: a multicentre investigation in Toronto, Canada. *PLoS One,* 5**,** e10717.

RINGBAEK, T. & VISKUM, K. 2003. Is there any association between inhaled ipratropium and mortality in patients with COPD and asthma? *Respiratory medicine,* 97**,** 264-272.

SETO, W. 2015. Airborne transmission and precautions: facts and myths. *Journal of Hospital Infection,* 89**,** 225-228.

SIMONDS, A., HANAK, A., CHATWIN, M., MORRELL, M., HALL, A., PARKER, K., SIGGERS, J. & DICKINSON, R. 2010. Evaluation of droplet dispersion during non-invasive ventilation, oxygen therapy, nebuliser treatment and chest physiotherapy in clinical practice: implications for management of pandemic influenza and other airborne infections. *Health technology assessment (Winchester, England),* 14**,** 131-172.

SINGH, S., LOKE, Y. K., ENRIGHT, P. L. & FURBERG, C. D. 2011. Mortality associated with tiotropium mist inhaler in patients with chronic obstructive pulmonary disease: systematic review and meta-analysis of randomised controlled trials. *Bmj,* 342**,** d3215.

SIRIGNANO, W. A. 2010. *Fluid Dynamics and Transport of Droplets and Sprays*, Cambridge University Press.

STILIANAKIS, N. I. & DROSSINOS, Y. 2010. Dynamics of infectious disease transmission by inhalable respiratory droplets. *Journal of the Royal Society Interface,* 7**,** 1355-1366.

THOMPSON, K.-A., PAPPACHAN, J. V., BENNETT, A. M., MITTAL, H., MACKEN, S., DOVE, B. K., NGUYEN-VAN-TAM, J. S., COPLEY, V. R., O'BRIEN, S. & HOFFMAN, P. 2013. Influenza aerosols in UK hospitals during the H1N1 (2009) pandemic–the risk of aerosol generation during medical procedures. *PloS one,* 8**,** e56278.

TORNIMBENE, B., EREMIN, S., ESCHER, M., GRISKEVICIENE, J., MANGLANI, S. & PESSOA-SILVA, C. L. 2018. WHO global antimicrobial resistance surveillance system early implementation 2016–17. *The Lancet Infectious Diseases,* 18**,** 241-242.

UDEZUE, E., D'SOUZA, L. & MAHAJAN, M. 1995. Hypokalemia after normal doses of nebulized albuterol (salbutamol). *The American journal of emergency medicine,* 13**,** 168-171.

VARIA, M., WILSON, S., SARWAL, S., MCGEER, A., GOURNIS, E. & GALANIS, E. 2003. Investigation of a nosocomial outbreak of severe acute respiratory syndrome (SARS) in Toronto, Canada. *Canadian Medical Association Journal,* 169**,** 285-292.

VASSAL, S., TAAMMA, R., MARTY, N., SARDET, A., D'ATHIS, P., BRÉMONT, F., DALPHIN, M., PLÉSIAT, P., RAULT, G. & THUBERT, J. 2000. Microbiologic contamination study of nebulizers after aerosol therapy in patients with cystic fibrosis. *American journal of infection control,* 28**,** 347-351.

VESTBO, J., HURD, S. S., AGUSTÍ, A. G., JONES, P. W., VOGELMEIER, C., ANZUETO, A., BARNES, P. J., FABBRI, L. M., MARTINEZ, F. J. & NISHIMURA, M. 2013. Global strategy for the diagnosis, management, and prevention of chronic obstructive pulmonary disease: GOLD executive summary. *American journal of respiratory and critical care medicine,* 187**,** 347-365.

WEISZHAR, Z. & HORVATH, I. 2013. Induced sputum analysis: step by step. Eur Respiratory Soc.

WITTGEN, B. P., KUNST, P. W., PERKINS, W. R., LEE, J. K. & POSTMUS, P. E. 2006. Assessing a system to capture stray aerosol during inhalation of nebulized liposomal cisplatin. *Journal of aerosol medicine,* 19**,** 385-391.

WITTGEN, B. P., KUNST, P. W., VAN DER BORN, K., VAN WIJK, A. W., PERKINS, W., PILKIEWICZ, F. G., PEREZ-SOLER, R., NICHOLSON, S., PETERS, G. J. & POSTMUS, P. E. 2007. Phase I study of aerosolized SLIT cisplatin in the treatment of patients with carcinoma of the lung. *Clinical Cancer Research,* 13**,** 2414-2421.

WONG, T.-W., LEE, C.-K., TAM, W., LAU, J. T.-F., YU, T.-S., LUI, S.-F., CHAN, P. K., LI, Y., BRESEE, J. S. & SUNG, J. J. 2004. Cluster of SARS among medical students exposed to single patient, Hong Kong. *Emerging infectious diseases,* 10**,** 269.

YU, I. T., LI, Y., WONG, T. W., TAM, W., CHAN, A. T., LEE, J. H., LEUNG, D. Y. & HO, T. 2004. Evidence of airborne transmission of the severe acute respiratory syndrome virus. *New England Journal of Medicine,* 350**,** 1731-1739.

5.6 Appendix

5.6.1 Inhalation calculation

i. Flow Rate of WIBS was measured to be 0.28 L/min

ii. Size of the particle was used to get the volume using the volume of a sphere calculation;

$$\frac{4}{3} \times \pi \times r^3 = X\mu g^3$$

iii. The number of particles in a cubic meter was then used to get the volume of particles per litre;

$$Particles\ m^3 \times X\mu g^3 = X\frac{\mu g^3}{L}$$

iv. Converting this to ml per *L*

$$X\frac{\mu g^3}{m^3} \times 1 \times 10^{-12} = X\frac{ml}{L}$$

v. Convert to mg per *L*

$$X\frac{ml}{m^3} \times 1 \times 10^3 = X\frac{mg}{L}$$

vi. Once in $\frac{mg}{L}$ exposure can be calculated

$$X\frac{mg}{L} \times 230L\ (Tidal\ volume\ for\ 30\ min)$$

$$= Inhaled\ at\ tidal\ volume\ \frac{mg}{230\ L}$$

Chapter 6
Bioaerosol Production from a Shared Lavatory

Table of Contents

6.1 Introduction

Water and aqueous solutions used in hospital facilities are often associated with hospital acquired infections (HAI). Hospital water supplies can become a reservoir for nosocomial pathogens and are frequently colonised by environmental waterborne microbes (Anaissie et al., 2002), mainly bacteria , including *Legionella* sp., (De Giglio et al., 2015), *Pseudomonas* spp., (Trautmann et al., 2001), *Mycobacterium* spp., (Von Reyn et al., 1994, Falkinham III et al., 2015), *Stenotrophomonas* spp., (Weber et al., 1999, Pagnier et al., 2015) and *Achromobacter* sp., (Amoureux et al., 2013). These may induce clinically important opportunistic nosocomial infections in already debilitated hospital patients, arising from sinks, showers or potable water. Outbreaks of gastroenteritis have been associated with the swallowing and inhalation of viral particles as documented by Weinstein *et al.* (Weinstein et al., 2008).

There are, however, other potential aqueous sources of infection in hospitals. It has been well documented that a toilet plume aerosol capable of entraining microorganisms, at least as large as bacteria, is produced by flush toilets (Jessen, 1955, Darlow and Bale, 1959, Blair, 2000, Barker and Bloomfield, 2000, Best et al., 2012). These studies have demonstrated that potentially infectious aerosols from bacteria and viruses present in faeces or during urination may be produced in substantial quantities during flushing. Where sufficiently small, microbe-containing droplets will evaporate to form droplet nuclei bioaerosols small enough to be inhaled deep into the lung or swallowed and viable bacteria may continue to be suspended in air in this manner for long periods (Morawska et al., 2013, Morawska, 2006). Several studies have observed surface contamination of toilet seats and lids, the surrounding floors, and the nearby surfaces by toilet flush aerosols (Jessen, 1955, Darlow and Bale, 1959, Newsom, 1972, Gerba et al., 1975, Barker and Jones, 2005, Best et al., 2012, Yahya et al., 1992). A study of the survival and environmental spread of *Salmonella* sp in domestic homes showed that *Salmonella* incorporates itself both into biofilm material found under the recess of the toilet bowl rim, and even into the scaly biofilm adhering to the toilet bowl surface below the water line, persisting for up to 4 weeks after diarrhoea (Barker and Bloomfield, 2000). The same study showed that mimicking the environmental conditions associated with acute diarrhoea using *Salmonella enteritidis* resulted in

toilet seat and lid contamination associated with toilet flushing, as well as airborne spread immediately after flushing (Barker and Bloomfield, 2000).

Artificial seeding of toilet bowl sidewalls with S. *marcescens* or MS2 bacteriophage established that bioaerosol production continues through multiple flushes, with some bioaerosols lasting up to 60 minutes after flushing, suggesting the long term potential for a contaminated toilet bowl to be an infectious bioaerosol generator (Barker and Jones, 2005). Surface contamination was detected at various locations surrounding the toilet 30 minutes after flushing, with a number of colony forming units (CFU) and plaque forming units (PFU) on both sides of the seat as well as on the cistern and shelf (Barker and Jones, 2005). The potential for airborne dissemination of *C. difficile* spores, especially from patients with recent onset diarrhoea, to contribute to widespread environmental contamination, is recognised by the World Health Organisation (WHO) (McDonald et al., 2018).

Contamination of the toilet environment with non-diarrhoea-causing enteric organisms, potentially allowing patient-to-patient transfer, is a well-recognised phenomenon which causes concern. For example, WHO recommends that patients colonised with Carbapenem-resistant *Enterobacteriaceae* (CRE), *Acinetobacter baumannii* (CRAB) and *Pseudomonas aeruginosa* (CRPsA) should be physically separated from non-colonised or non-infected patients using either a single room or cohorting patients with the same resistant pathogen, and during isolation in single patient rooms it is preferable that patients have their own toilet facilities (Organization, 2017).

16S rRNA profiling of airborne organisms using a Coriolis µ (Bertin Technologies) air to liquid sampler, described in chapter 3, found 8 out of 9 air DNA samples taken on six separate days over three months positive with the largest single group at Phylum level being Firmicutes. The majority belonged to *Clostridiaceae*/*Clostridiales* Families. Actinobacteria formed the next commonest phylum in 5/9 samples, comprising common gastrointestinal species and *Micrococcaceae*. Proteobacteria (72-99% Gammaproteobacteria) were the second commonest phylum in 4 samples with a

low DNA content and the commonest attributable phylum in a sequenced negative control sample. Most of these identified bacteria are potentially of gastrointestinal origin (Flores et al., 2011), the source of this could have been the communal lavatory that was present within the ward. Subsequently, the WIBS study described in this chapter was undertaken in a communal office toilet to investigate the aerosol production from different toilet activities.

Although a wide variety of toilet facilities exist in healthcare settings, patients' toilets are commonly shared and do not have lids, despite the growing evidence of flush related aerosol generation and ensuing surface contamination (Barker and Bloomfield, 2000, Barker and Jones, 2005, Best et al., 2012). Toilet bowls and traps are potentially environmental reservoirs for carbapenemase producing Enterobacterales (CPE), whereby rooms with common waste plumbing can become contaminated from a single source (Smismans et al., 2019). *Smismans et al.* suggested that earlier detection through both patient screening and environmental sampling may have found this unexpected reservoir before spread occurred. It has also been documented that toilet seats may harbour MRSA, even after cleaning. MRSA has been cultured from toilet seats in a children's hospital despite rigorous cleaning. This represents a potential risk for patients who may acquire it by fomite transmission (Giannini et al., 2009), and with the potential for reaerosolisation through flush-related toilet plumes.

Other sources of bioaerosols may be present in the lavatory environment. Different hand-drying methods may carry different risks of spreading potentially harmful pathogens. Paper towels (PT), and electric warm or jet-air-dryers (JAD) are the most common hand drying methods in work environments. Whereas paper towels directly absorb excess moisture from hands, jet air dryers depend on a combination of high-speed air flow and shearing forces to rapidly dry hands by dispersal and evaporation. Various studies have observed an association between the hand drying method and the spread of residual microbes from hands, after hand washing. They have consistently found that jet-air-dryers increase environmental bacterial burdens and dispersal when compared to paper towels (Margas et al., 2013, Best et al., 2014, Best and Redway, 2015, Kimmitt and Redway, 2016, Wilcox et al., 2017, Best et al., 2018).

Multiple significant differences in environmental bacterial contamination were observed in health care settings, with generally lower contamination in PT versus JAD washrooms (Best et al., 2018). This has led to the suggestion that electric hand dryers may not be suited to a clinical setting. This data may also be relevant to an office or school setting, especially during periods of influenza and norovirus activity, when airborne dispersal of pathogens may become a concern.

This study was designed to assess the effect of toilet flushing and hand drying on environmental aerosols in a shared lavatory cubicle using a real-time bioaerosol detector. As well as an observational study, with the gathering of data from in use monitoring of a lavatory cubicle in normal use, an experiment was performed recording aerosols associated with flushing artificial stool in the same cubicle.

6.2 Methods

The lavatory use was monitored using the WIBS over a 5-day period from 13/02/2019 to 17/02/2019. The lavatory contained one water closet (WC) with a plastic seat and lid, a sink, and a hot air hand dryer (HD) (Figure 6.1 Toilet plan). Toilet users completed a diary sheet comprising time of entry, exit, flush, hand dryer and type of use (urination or defaecation). Two "lid up" and two "lid down" days were designated. Toilet generated aerosols using simulated faeces were assessed in the same lavatory. Users were asked during "lid down" days to only lift the lid when about to use the toilet and place the lid back down before toilet flush, the lid remaining down till the next user. On "lid up" days the lid was left up all the time.

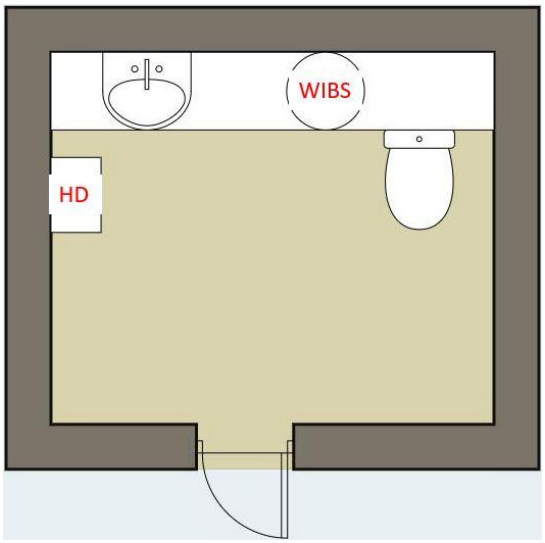

Figure 6.1 Toilet plan.

The artificial stool was made as per one of the recipes described by Penn *et al. (Penn et al., 2018)*. Although a few types of synthetic faeces are described in this publication, time restrictions only allowed the use of one for the artificial defaecation experiment. The recipe used was as follows: 130 g yeast, 43 g microcrystalline cellulose, 75 g psyllium husk, 75 g miso paste, 85 g oleic acid, 9 g NaCl, 9 g $CaCl_2.H_2O$ and 580 ml DI water. Three grams of freeze-dried food-grade *Lactobacillus spp* were added. 100 grams at a time were deposited from a beaker in a simulated defaecation into the bowl.

6.2.2 Wideband Integrated Bioaerosol Sensor (WIBS)

The WIBS-4A was used to collect bioaerosol samples in this study. A more detailed description of its operation are provided by Kaye et al. (Kaye et al., 2014), Fennelly et al. (Fennelly et al., 2017) and Chapter 3.

6.3 Results

Over 5 days, 30 lavatory visits were recorded (Table 6.1). 30-second averaged particle counting periods for the entire campaign were used during the analysis. The exact time of flushing and whether toilet use comprised either urination only (18 visits) or defaecation (12 visits) was noted in a diary by participants. Toilet occupancy period was defined as the sum of pre-flush, flush and post-flush periods. Pre- and post-

flushing are periods of 5 minutes before and after flushing with the flushing itself being a 1-minute period.

6.3.1 Effect of occupancy on toilet aerosols.

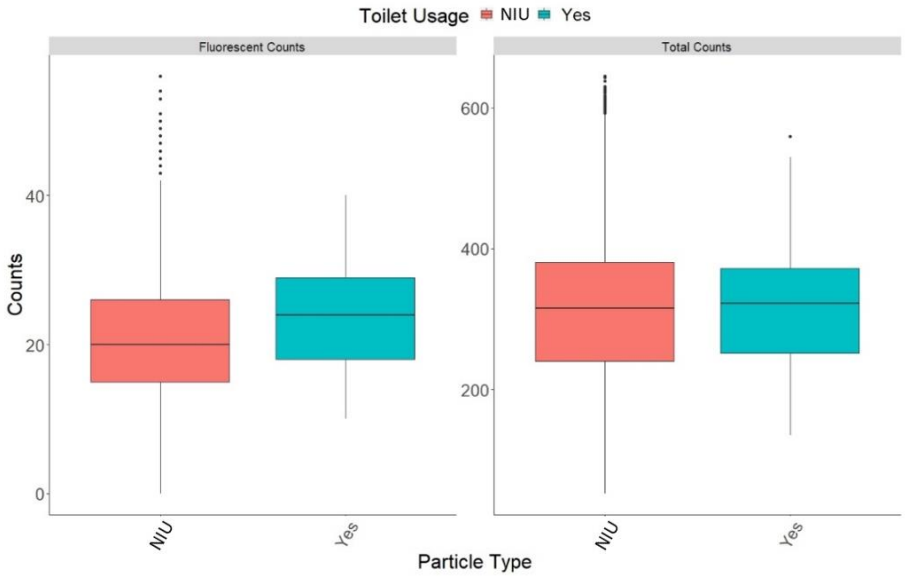

Figure 6.2 Boxplots of fluorescent (left panel) and total particle counts (right panel) for toilet occupancy periods (Yes, blue) and when the toilet was empty (NIU, red).

The mean fluorescent particle count was significantly ($P<0.01$) higher with the toilet occupied (23.57 ± 7.14) compared to unoccupied (20.68 ± 7.78). Conversely, the total particle counts did not differ significantly, $p=0.91$, with lavatory occupation (312.59 ± 87.21) compared with unoccupied (313.22 ± 105.00) (Figure 6.2, Table 6.1).

Table 6.1 Mean ± standard deviation (sd) for fluorescent and total particle counts with calculated p-value between lavatory occupancy.

Particle Type	Particle mean ± sd		P-value
	Toilet Usage		
	NIU	Yes	
Fluorescent count	20.68 ± 7.78	23.57 ± 7.14	<0.01
Total count	313.22 ± 105.00	312.59 ± 87.21	0.91

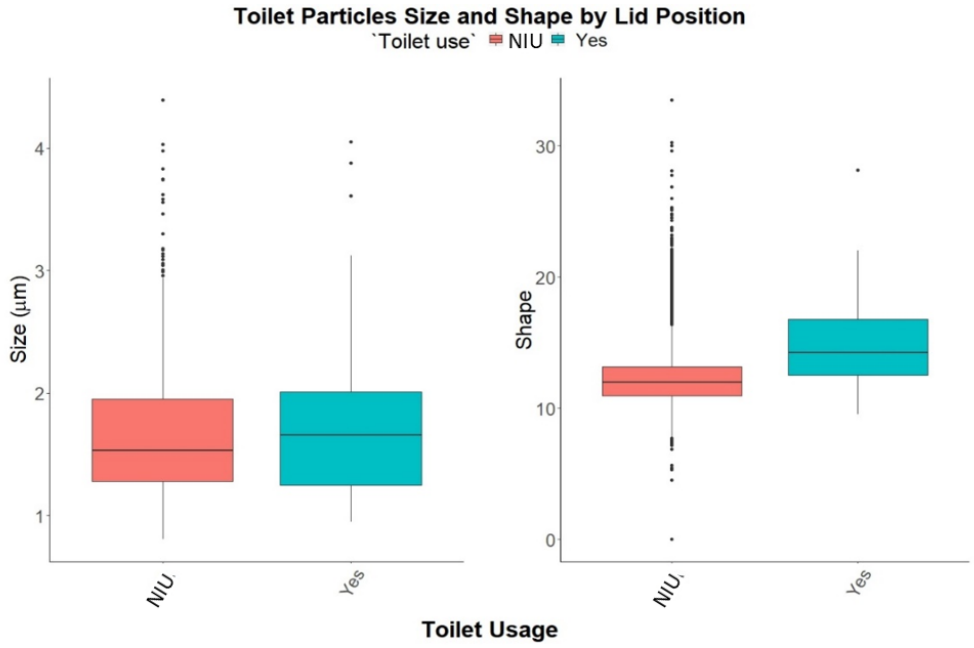

Figure 6.3 Boxplots of fluorescent particle size (left panel) and shape, AF (right panel) for time periods when lavatory was occupied (Yes, blue) and when it was empty (NIU, red)

The fluorescent particle size (µm) and sphericity index (AF) were significantly larger ($P<0.01$) when the toilet was occupied (1.89 µm ± 0.62 µm, 14.94 ± 3.16) compared to empty (1.25 µm ± 0.33 µm, 12.29 ± 2.03) (Figure 6.3, Table 6.2)

Table 6.2 Mean ± sd for fluorescent particle size (µm) and shape with calculated p-value between lavatory occupancy.

Particle Type	Particle mean ± sd Toilet Usage		P-value
	NIU	Yes	
Size (µm)	1.25 ± 0.33	1.88 ± 0.601	<0.01
Sphericity Index (30=linear)	12.30 ± 2.04	14.85 ± 3.05	<0.01

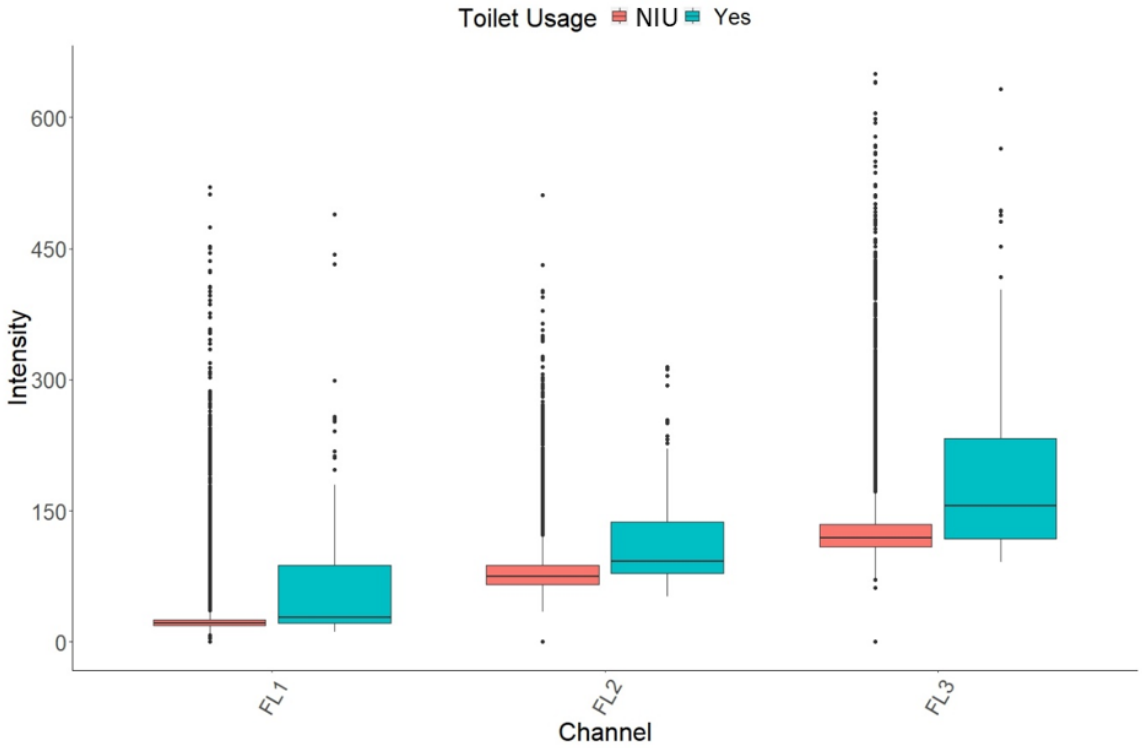

Figure 6.4 Boxplots of fluorescent channel intensities for each fluorescent channel when lavatory was occupied (Yes, blue) to when it was empty (NIU, red).

All channels showed significantly higher fluorescence intensity of particles when the lavatory was occupied compared to when it was unoccupied (P<0.01) (Figure 6.4 and Table 6.3). The largest increase in mean intensity was exhibited in the FL1 channel where with occupancy mean intensity increased ~2.5 fold from 27.98 ± 30.02 to 70.61 ± 87.71 (Table 6.3). The FL2 and FL3 channels also showed similar increases, both increasing 1.5 times their intensity with occupation (Table 6.3).

Table 6.3 Mean ± sd for fluorescent channel intensity with calculated p-value between lavatory occupancy.

Channel	Fluorescent Intensity mean ± sd		P-value
	Toilet Usage		
	NIU	Yes	
FL1	27.98 ± 30.02	70.61 ± 87.71	< 0.01
FL2	82.69 ± 31.44	127.61 ± 73.05	< 0.01
FL3	134.03 ± 54.87	219.34 ± 132.74	< 0.01

This section 6.3.1 has shown that toilet occupancy significantly increases fluorescent particle counts and these particles display altered physical properties, when compared to observations of the unoccupied toilet. However, occupancy does not significantly alter the total particle count or the physical properties of non-fluorescent particles. This would suggest that activities within the lavatory significantly affect the generation of biological particles. The following sections analyse the effect of different events on toilet bioaerosols over time.

6.3.2 Effect of toilet activity on lavatory aerosols

This section will investigate the effect of different toilet activities on particle production and properties.

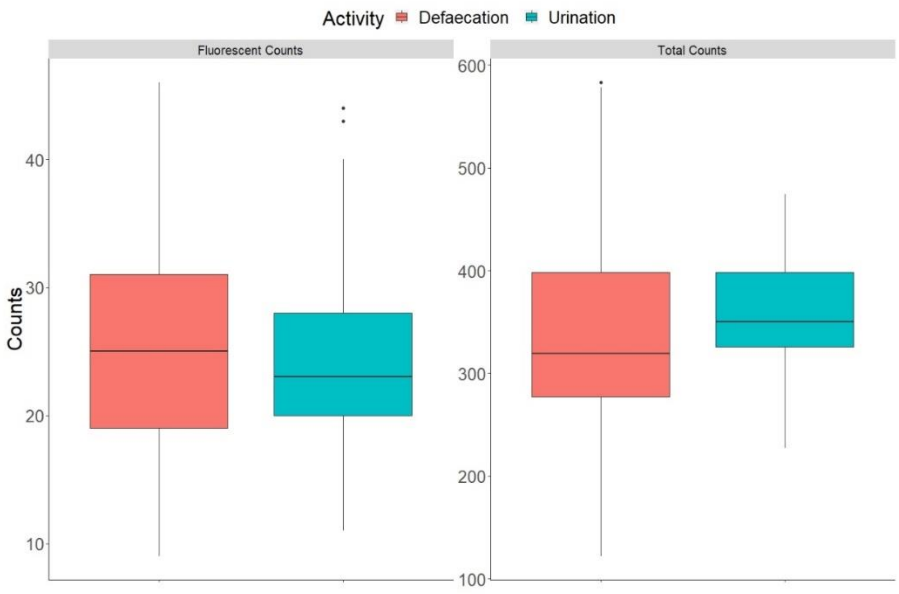

Figure 6.5 Boxplots of fluorescent (left panel) and total particle counts (right panel) for occupancy periods when lavatory was used for defaecation (red) and when it was used for urination only (blue).

Both the mean fluorescent and total particle counts differed significantly between defaecation and urination (Figure. 6.5, Table 6.4). Defaecation is associated with a significantly higher fluorescent particle count (25.41 ± 7.71) than urination (23.73 ± 6.26) ($P<0.01$). However, urination is associated with significantly higher total particle

counts (359.23 ± 51.88) than defaecation (330.87 ± 102.00), Table 6.4. The higher total, but lower fluorescent particle count associated with urination suggests urination produces more non-fluorescent particles than defaecation this may be due to the splashing from urination, as urination is constant it may produce greater turbulence resulting in the greater aerosolisation of non-fluorescent particles.

Table 6.4 Mean ± sd for fluorescent and total particle counts with calculated p-value between lavatory activity.

Lavatory Activity	Particle count mean ± sd	
	Fluorescent	Total
Defaecation	25.41 ± 7.71	330.87 ± 102.00
Urination	23.73 ± 6.26	359.23 ± 51.88
P-value	< 0.01	< 0.01

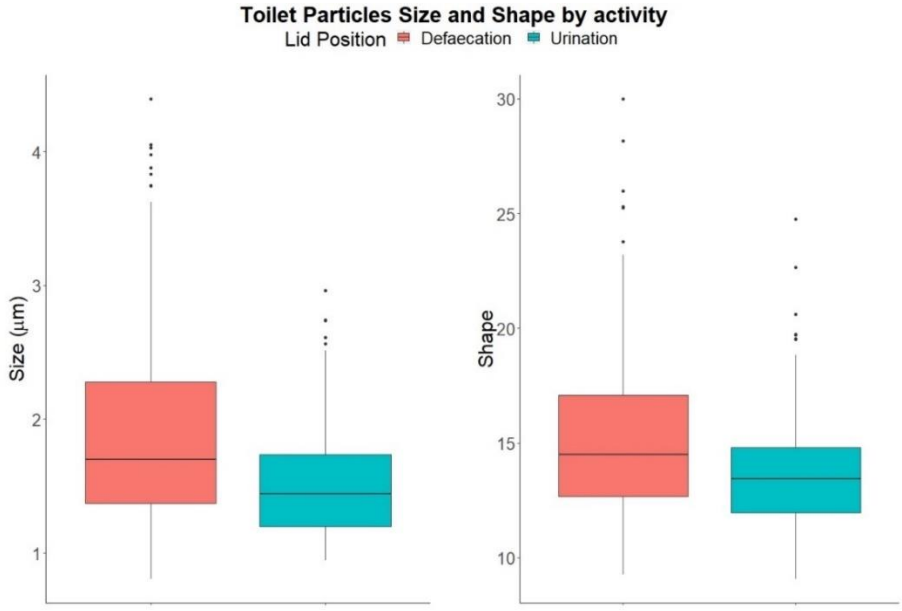

Figure 6.6 Boxplots of fluorescent particle size (left panel) and shape, AF (right panel) for time periods when lavatory was used for defaecation (red) and when it was used for urination (blue).

Fluorescent particle size (µm) and sphericity index (AF) increased significantly (P<0.01) (larger, less spherical particles) when the lavatory was used for defaecation compared to urination (Figure 6.6, Table 6.5).

Table 6.5 Mean ± sd for fluorescent particle size (µm) and shape with calculated p-value between lavatory activity.

Particle Type	Fluorescent particle means ± sd Lavatory Activity		P-value
	Defaecation	Urination	
Size (µm)	1.91 ± 0.73	1.52 ± 0.40	<0.01
AF	15.2 ± 3.54	13.6 ± 2.31	<0.01

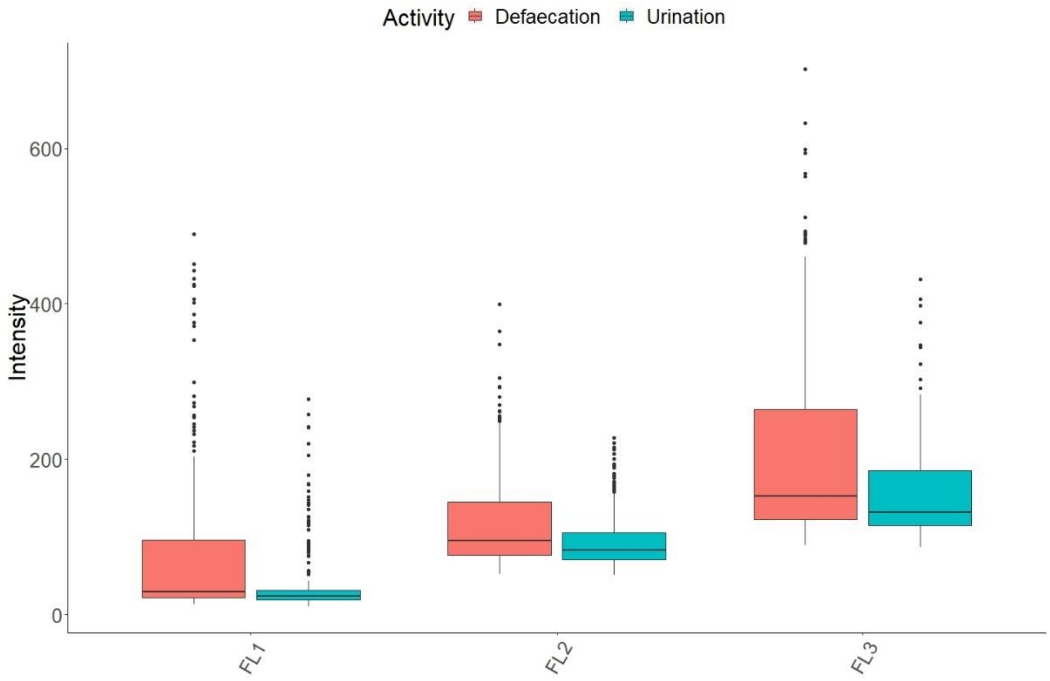

Figure 6.7 Boxplots of fluorescent channel intensities for each fluorescent channel when lavatory was used for defaecation (red) and when it was used for urination (blue). Panel is split into 3 sets of boxplots each representing a fluorescent channel; (left) FL1, (middle) FL2 and (right) FL3.

Significantly higher fluorescence intensity of particles was observed on all channels when the lavatory was used for defaecation compared to urination (P<0.001) (Figure. 6.7, Table 6.6). The largest increase in mean intensity was exhibited in the FL1 channel where defaecation was associated with ~1.8-fold increased mean (Table 6.6). The FL2 and FL3 channels showed increases of ~1.25 and 1.4-fold respectively with defaecation activity compared to urination, Table 6.6.

Table 6.6. Mean ± sd for fluorescent channel intensity with calculated p-value between lavatory activity.

Channel	Toilet Activity		P-value
	Defaecation	Urination	
	Channel Fluorescent Intensity mean ± sd		
FL1	77.47 ± 97.70	41.16 ± 45.32	<0.01
FL2	120.63 ± 64.54	95.96 ± 37.57	<0.01
FL3	210.25 ± 124.31	155.60 ± 61.29	<0.01

Comparing different toilet activities, defaecation results in significantly higher fluorescent counts than urination, with fluorescent particles that are larger, less spherical and of higher fluorescence intensity. Urination results in a higher total particle count. This suggests that defaecation and flushing produce significantly more bioaerosols than urination and flushing.

6.3.3 Effect of toilet lid position on aerosols

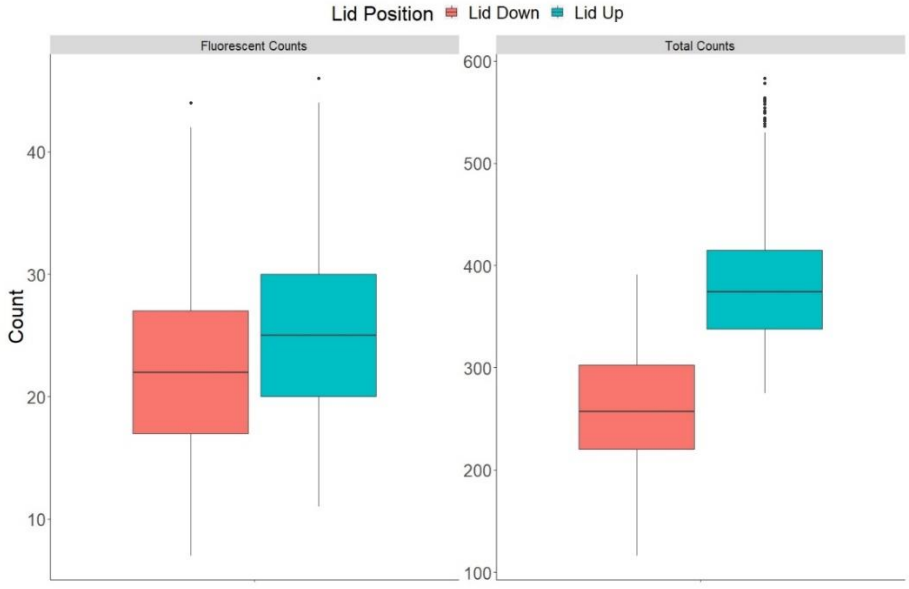

Figure 6.8 Boxplots of fluorescent (left panel) and total particle counts (right panel) for time periods when lavatory was used for lid down (red) and when it was used for lid up (blue).

Both the mean fluorescent and total particle counts differed significantly between days with lid up and days with lid down (Figure 6.8). Significantly higher fluorescent and total particle counts were observed on days where the lid remained up compared to days where lid remained down, ($P<0.01$, Table 6.7).

Table 6.7. Mean ± sd for fluorescent and total particle counts with calculated p-value between lid position.

Particle Type	Particle count mean ± sd		P-value
	Lid Down	Lid Up	
Fluorescent	22.67 ± 7.51	31.63 ± 35.01	< 0.01
Total	256 ± 60.11	397.40 ± 82.14	< 0.01

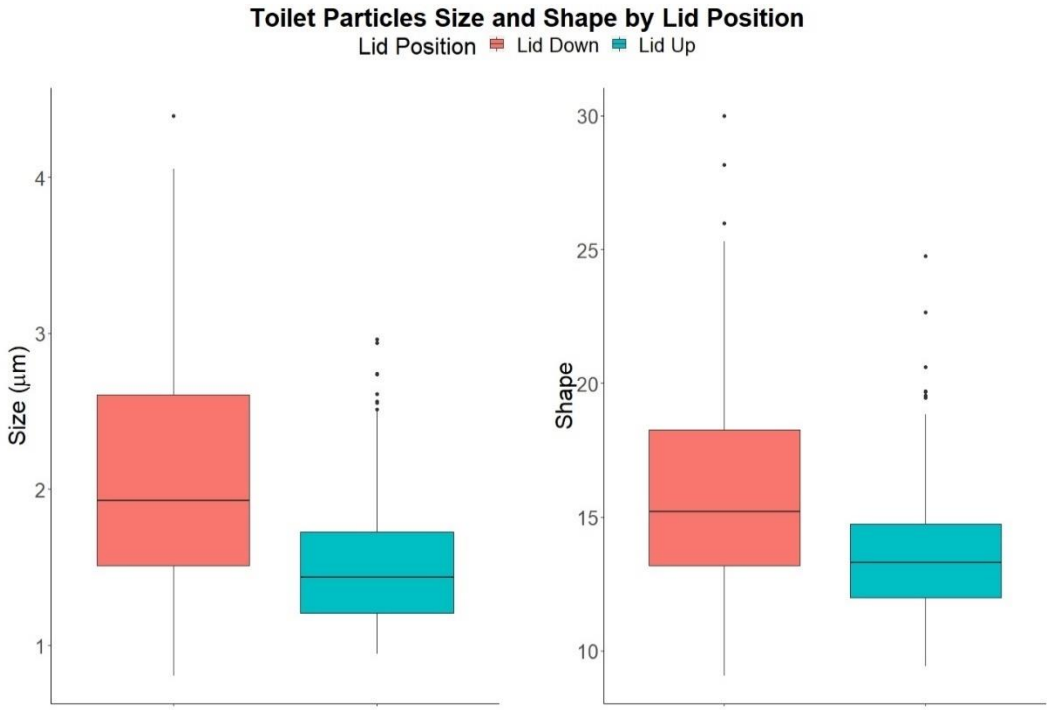

Figure 6.9 Boxplots of fluorescent particle size (left panel) and shape, AF (right panel) for lid down (red) and lid up (blue) time periods.

Leaving the lid down significantly ($P<0.01$) increases both fluorescent particle size (µm) and shape compared to the lid being up (Figure 6.9, Table 6.8). Size (µm) increases by ~ 0.5 µm while particles also become slightly more elongated (13.72 to 15.38) with the lid down compared to up.

Table 6.8 Mean ± sd for fluorescent particle size (µm) and shape with calculated p-value between lid position.

Physical Characteristic	Lid Down	Lid Up	P-value
	Mean ± sd		
Size (µm)	2 ± 0.71	1.57 ± 0.44	<0.01
Shape (AF)	15.38 ± 3.42	13.72 ± 0.44	<0.01

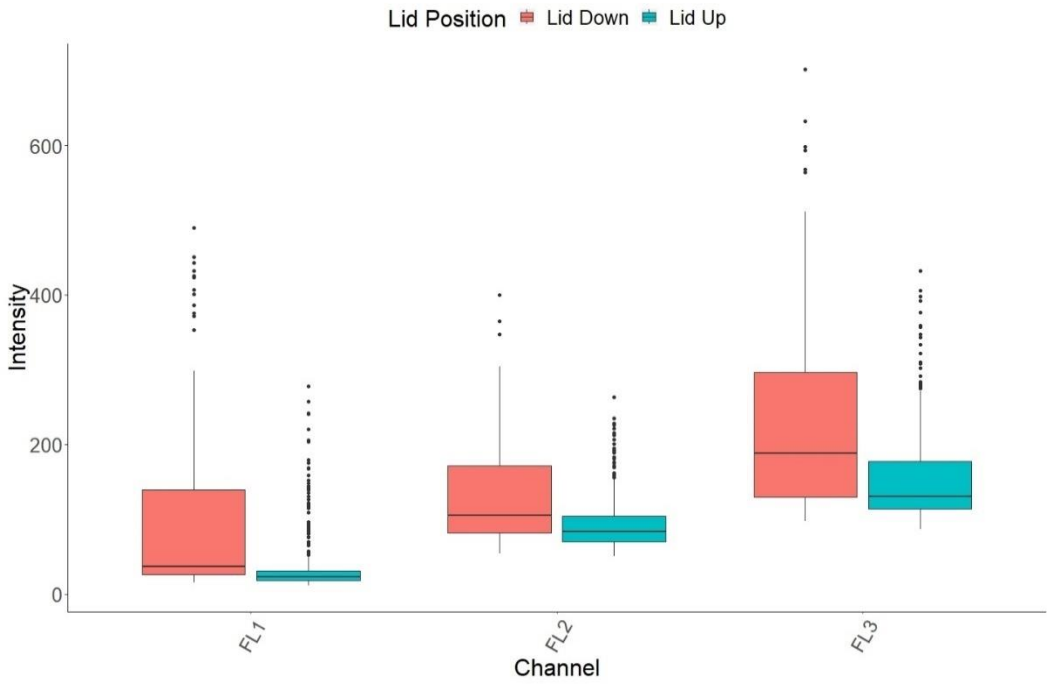

Figure 6.10 Boxplots of fluorescent channel intensities for each fluorescent channel when lid position was down (red) and when it was used up (blue). Panel is split into 3 sets of boxplots each representing a fluorescent channel; (left) FL1, (middle) FL2 and (right) FL3.

Significantly higher fluorescence intensity of particles was observed on all channels when the lid was positioned down compared to leaving the lid up ($P<0.01$) (Figure 6.10 and Table 6.9). The largest increase in mean intensity was exhibited in the FL1 channel where lid down increased mean intensity ~2.5 fold from 39.62 ± 43.81 with lid up to 96.2 ± 109.03 with lid down, Table 6.9. Increases of ~1.4 and 1.5-fold were observed in the FL2 and FL3 channels, respectively, when the lid position was down compared to up, Table 6.9.

Table 6.9 Mean ± sd for fluorescent channel intensity with calculated p-value between lid position.

Channel	Lid Position		P-value
	Down	Up	
	Channel Fluorescent Intensity mean ± sd		
FL1	96.2 ± 109.03	39.62 ± 43.81	<0.01
FL2	133.48 ± 69.38	94.85 ± 37.53	<0.01
FL3	235.62 ± 133.77	154.75 ± 63.25	<0.01

Lid position has a significant effect on the characteristics of airborne particles produced by toilet use. Although having the lid down reduced the fluorescent and total particle counts (Table 6.7), the fluorescent particles that are produced are significantly larger in size and exhibit a higher fluorescent intensity (Table 6.8, 6.9). In other WIBS studies involving airborne pollen and fungal spores, particle fluorescence intensity was related to particle size, with larger particles producing higher fluorescent intensity because of a greater content of fluorescing compounds scaling by volume (Healy et al., 2012, O'Connor et al., 2013). This could suggest that to avoid confounding, fluorescence intensity should be normalised by particle size or volume. However, it is not appropriate to normalise fluorescent intensity by particle size in these observations because of the underlying aqueous nature of the particles. In this system increased particle size may result from smaller droplets with bacteria in them mixing with other droplets without bacteria in them and effectively reducing the size-normalised fluorescence. So absolute fluorescence (Table 6.9), is a better measure than size-normalised intensity in this case. It is not assumed that there is a linear relationship between the size of the droplet and the number of bacteria in it, as it is most likely randomised.

6.3.4 Effect of lid position and toilet activity on produced aerosols

In the previous two sections, 6.3.2 and 6.3.3, defaecation and urination , and lid position were separately assessed for an effect on toilet aerosols. This section will look at the combined effects of both toilet activity and lid position on the production and characteristics of aerosols.

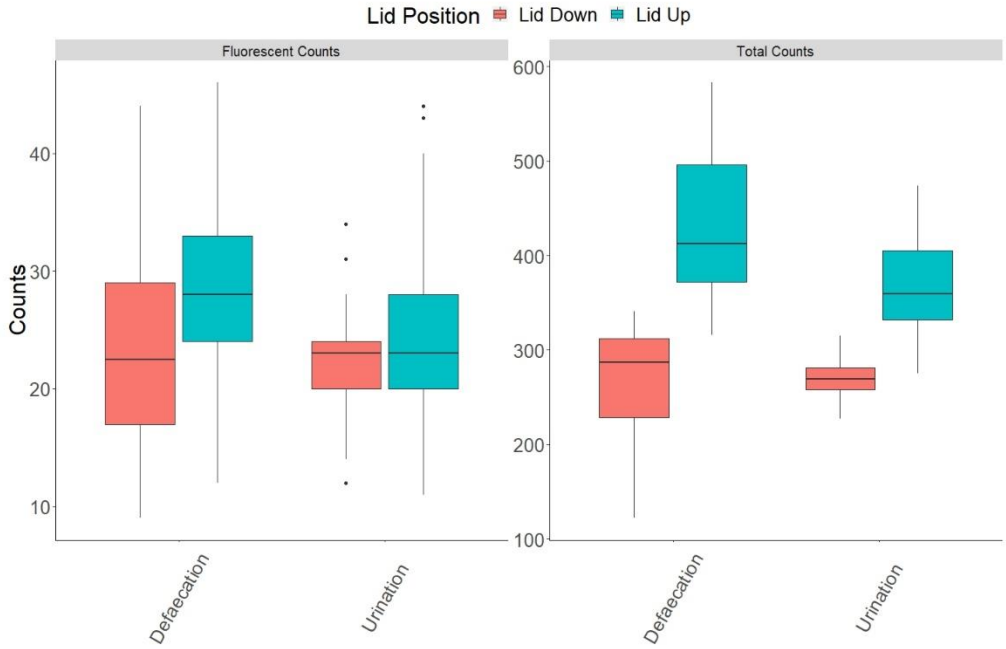

Figure 6.11 Boxplots of fluorescent (left panel) and total particle counts (right panel) for time periods when lid was down (red) and when the lid was up (blue). Both panels are split, left-hand side shows boxplots for defaecation and right-hand side boxplots for urination.

Both the mean fluorescent and total particle counts were significantly lower on lid down days for both defaecation and urination compared to lid up days (Figure 6.11, Table 6.10). The magnitude of the difference was lower for urination. Fluorescent counts produced with the lid down did not differ significantly, P=0.18, between defaecation (23.44 ± 7.70) and urination (22.08 ± 5.24) but were significantly higher for defaecation with lid up flushing (Table 6.10). Total particle counts were significantly higher for defaecation with lid up flushing compared to lid down, and for defaecation versus urination with lid up flushing. A small but significant decrease in

total particle numbers was observed for defaecation vs urination with lid down flushing (Table 6.10).

Table 6.10 Mean ± sd for fluorescent and total particle counts with calculated p-value between lid position and toilet activity.

Activity	Fluorescent Count means ± sd		P-value (Lid)	Total Count means ± sd		P-value (Lid)
	Lid Down	Lid Up		Lid Down	Lid Up	
Defaecation	23.44 ± 7.70	28.32 ± 6.74	< 0.01	267.35 ± 59.65	425.26 ± 75.32	< 0.01
Urination	22.08 ± 5.24	23.91 ± 6.34	< 0.01	270.46 ± 20.72	368.61 ± 44.84	< 0.01
P-value (activity)	0.18	< 0.01	NA	< 0.01	< 0.01	NA

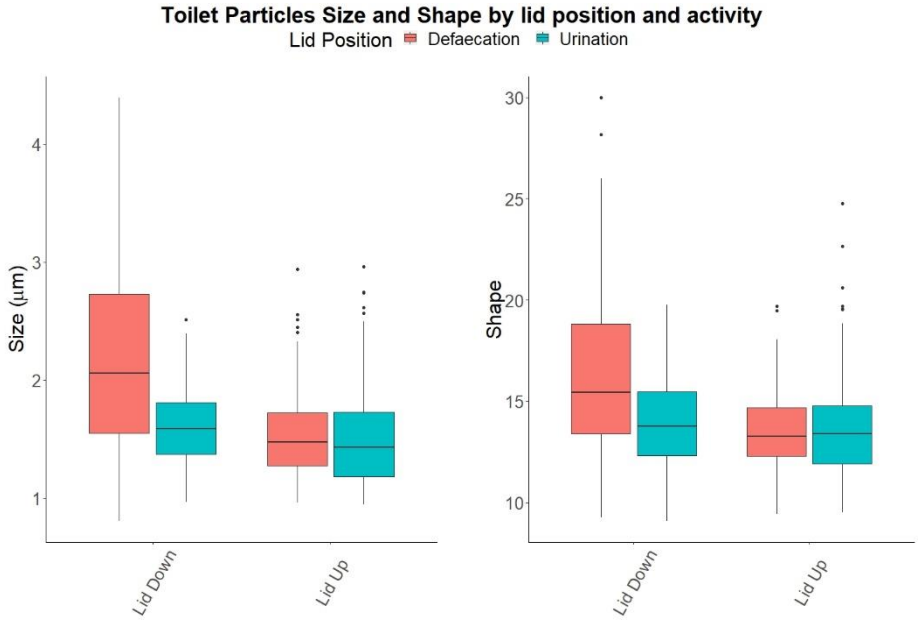

Figure 6.12 Boxplots of fluorescent particle size (µm) (left panel) and shape (right panel) for time periods when lid was down (red) and when its lid was up (blue). Both panels are split, left-hand side is boxplots for defaecation and right-hand side is boxplots for urination.

Positioning the lid down significantly (P<0.01) increased fluorescent particle size (1.53 ± 0.39 µm to 2.17 ± 0.78 µm) and shape (more elongated) (13.48 ± 2.05 to 16.32 ± 3.86) for defaecation compared to lid up (Figure 6.12, Table 6.11). A small but significant (P<0.01), increase in fluorescent particle size was observed with the lid down (1.51 ± 0.4 µm to 1.62 ± 0.37 µm) with no difference, (P = 0.11), in shape

(Figure 6.12, Table 6.11). With the lid positioned up no significant difference was observed between the size (µm), P =0.11, and shape, 0.58, between fluorescent particles produced by defaecation and urination, Table 6.11.

Table 6.11. Mean ± sd for fluorescent particle size (µm) and shape with calculated p-value between lid position and toilet activity.

Toilet Activity	Lid Down	Lid Up	P-Value (Lid)	Lid Down	Lid Up	P-Value (Lid)
	Size (µm) mean ± sd			Shape mean ± sd		
Defaecation	2.17 ± 0.78	1.53± 0.39	< 0.01	16.32 ± 3.86	13.48 ± 2.05	< 0.01
Urination	1.62 ± 0.37	1.51± 0.40	< 0.01	13.87 ± 2.47	13.53 ± 2.30	0.13
P-Value (activity)	<0.01	0.11	NA	<0.01	0.58	NA

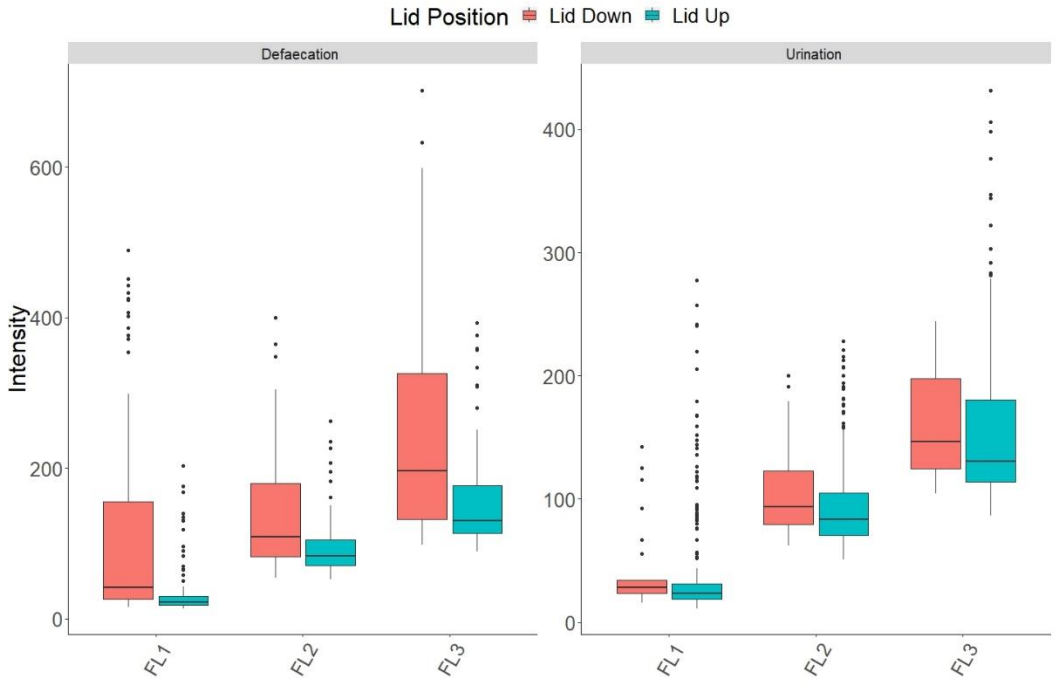

Figure 6.13 Boxplots of fluorescent channel intensities for each fluorescent channel when lid position was down (red) and when it was used up (blue). The two panels represent the toilet activity defaecation (left) and urination (right). Each panel is split into 3 sets of boxplots each representing a fluorescent channel; (left) FL1, (middle) FL2 and (right) FL3.

For defaecation, the particle fluorescent intensity significantly increased in each channel with lid down flushing ($P < 0.01$, Table 6.12). Lid position did not make a statistical difference to fluorescent intensity in any channel with urination (Table 6.12). Positioning the lid down with defaecation produced significantly higher particle intensity in every channel compared to urination ($P<0.01$, Table 6.12). Conversely with the lid up no fluorescent intensity difference was noted in any channel, between particles produced following urination or defaecation (Table 6.12).

Table 6.12 Mean ± sd for fluorescent channel intensity with calculated p-value between lid position.

Activity	Channel	Fluorescent Intensity mean ± sd		P-value (Lid)
		Lid Down	Lid Up	
Defaecation	FL1	105.13 ± 114.69	36.37 ± 37.51	<0.01
	FL2	137.89 ± 72.30	94.96 ± 38.84	<0.01
	FL3	247.68 ±140.00	154.65 ± 64.79	<0.01
Urination	FL1	42.63 ± 35.63	41.00 ± 46.28	0.03
	FL2	106.97 ± 41.09	94.80 ± 37.08	0.08
	FL3	163.24 ± 45.08	154.80 ± 62.79	0.07
P-value (activity)	FL1	<0.01	0.09	NA
	FL2	<0.01	0.78	NA
	FL3	<0.01	0.98	NA

This section highlights the impact lid position has on the physical properties of particles and, interestingly, particle fluorescent intensity with defaecation. Although lid down reduces the amount of fluorescent and total particles produced, it instigates the production of larger, more elongated particles of significantly higher intensity for defaecation when compared to those produced with lid up. Although lid usage also significantly increased particle size associated with urination it did not affect particle shape or particle fluorescent intensity, signifying that the lid down position has a larger effect on defaecation-related toilet activity.

6.3.5 Effect of lid position on aerosols at different times during toilet use

This section observed the effect lid position has on particles produced at different times during toilet use. Toilet use is split into 3 periods; Pre – is a period of 5 minutes before the flush time noted by the user, Flush – refers to a 1 minute period starting when the flush was recorded, and Post is a five minute period after the flush period.

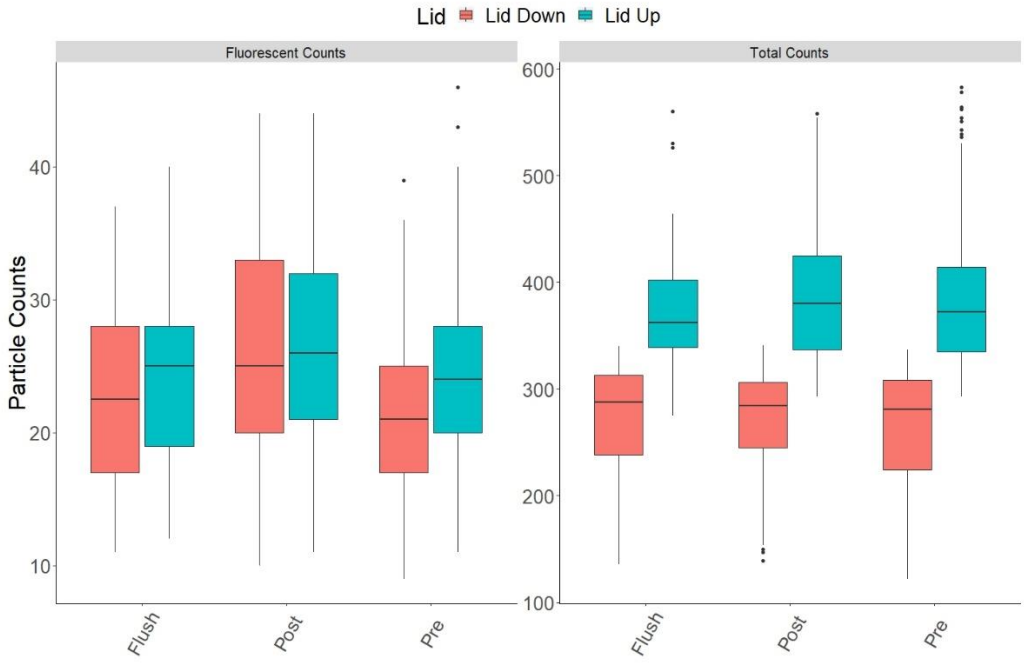

Figure 6.14 Boxplots of fluorescent (left panel) and total particle counts (right panel) for time periods when lid was down (red) and when the lid was up (blue). Both panels are split into pairs of boxplots for each period, first pair of boxplots is for flush-, second pair for post- and third pair for pre-.

Lid down significantly reduced total particle counts during each period by an average of 115.35 particles ($P<0.01$, Table 6.13). Interestingly, lid position did not significantly affect the fluorescent particle counts observed during the Flush or Post period (Table 6.13).

Table 6.13. Mean ± sd for fluorescent and total particle counts for each period with calculated p-value between lid position.

Particle Type	Toilet Timing	Particle count mean ± sd		P-Value
		Lid Down	Lid Up	
Fluorescent Counts	Flush	22.38 ± 7.15	24.35 ± 6.61	0.06
	Post	25.77 ± 7.94	26.19 ± 6.95	0.43
	Pre	21.06 ± 6.13	24.43 ± 6.47	<0.01
Total Counts	Flush	269.26 ± 54.13	377.37 ± 61.1	<0.01
	Post	269.95 ± 53.31	387.91 ± 60.14	<0.01
	Pre	265.22 ± 58.70	385.19 ± 62.85	<0.01

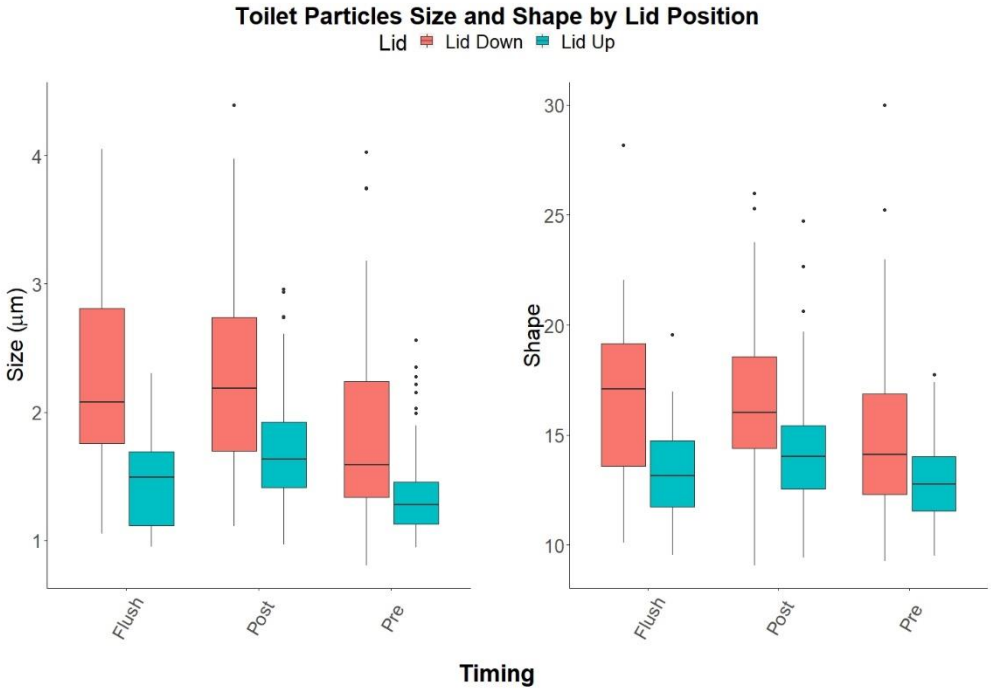

Figure 6.15 Boxplots of fluorescent particle size (µm) (left panel) and shape (right panel) for time periods when lid was down (red) and when the lid was up (blue). Both panels are split into sets of boxplots for each period, first set of boxplots is for flush-, second set for post- and third set for pre-.

Lid down significantly increased particle size and elongated shape across all periods (P<0.01, Figure 6.15, Table 6.14). The largest increase in size was observed during the Flush period when a ~1.5-fold increase in particle size (1.47 ± 0.37 to 2.3 ± 0.78 µm) was shown with the lid down. Similarly, the largest difference in shape was noted

during the Flush period with a ~1.3-fold increase in AF shape (13.40 ± 2.1 to 17.01 ± 3.91) i.e. elongating, Table 6.14.

Table 6.14. Mean ± sd for fluorescent particle size (µm) and shape for each period with calculated p-value between lid position.

Particle Characteristic	Toilet Timing	Mean ± sd		P-Value
		Lid Down	Lid Up	
Size	Flush	2.3 ± 0.78	1.47 ± 0.37	< 0.01
	Post	2.26 ± 0.71	1.68 ± 0.41	< 0.01
	Pre	1.84 ± 0.73	1.33 ± 0.29	< 0.01
Shape (AF)	Flush	17.01 ± 3.91	13.40± 2.1	< 0.01
	Post	16.55 ± 3.39	14.18 ± 2.45	< 0.01
	Pre	15.05 ± 3.94	12.84 ± 1.72	< 0.01

Across all toilet periods, the lid position caused a significant increase in fluorescent particle physical characteristics, with the largest increases noted during the Flush period when size increased by ~ 0.9 µm with shape increasing by ~4 AF i.e. becoming more elongated (Table 6.14).

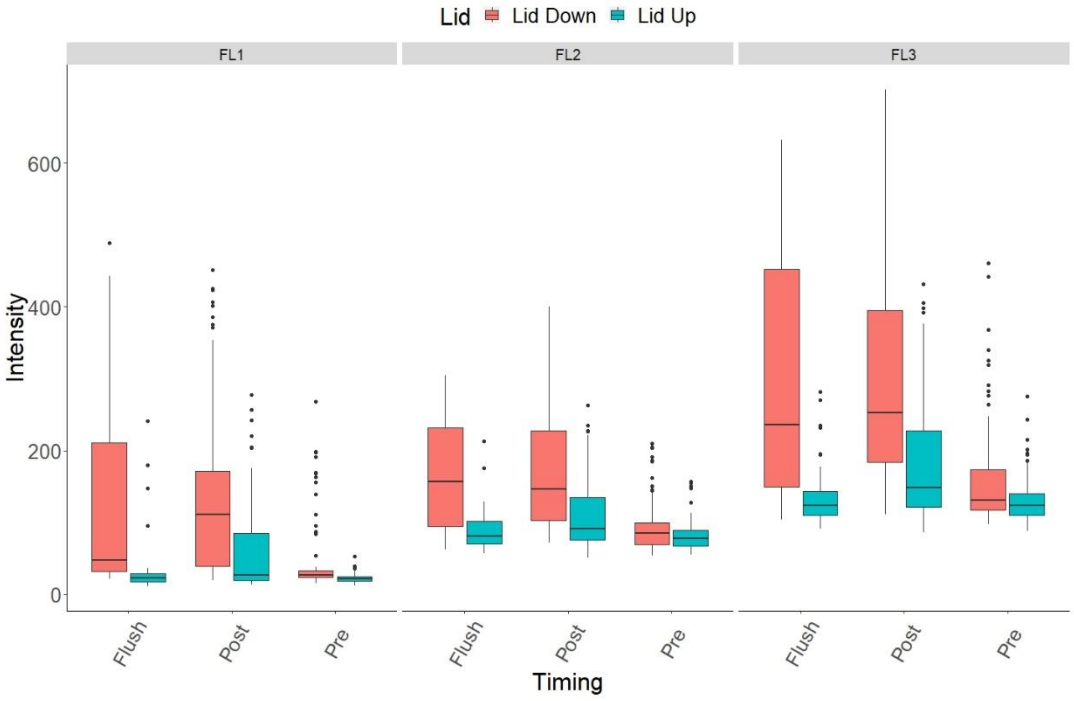

Figure 6.16 Boxplots of fluorescent particle intensity for each fluorescent channel during the different time periods when lid was down (red) and when the lid was up (blue). The three panels represent a fluorescent channel; first panel FL1 (left), FL2 (middle), and FL3 (right). The 3 channel panels are split into sets of boxplots for each period, first set of boxplots is for flush-, second set for post- and third set for pre-.

Figure 6.16 and Table 6.15 show that lid usage increases particle fluorescent intensity in all channels, during nearly all periods when the lid was positioned down ($P<0.01$). The FL2 channel during the pre-period was the only channel and period that did not show an increase of this significance with the lid down (Table 6.15).

Table 6.15. Mean ± sd for fluorescent particle intensity in each channel for each period with calculated p-value between lid position.

Toilet Timing	Channel	Fluorescent Intensity mean ± sd		P-value
		Lid Down	Lid Up	
Flush	FL1	129.37 ± 145.08	36.67± 47.12	<0.01
	FL2	158.75 ± 73.09	89.34 ± 30.67	<0.01
	FL3	290.10 ± 158.91	140.09 ± 46.66	<0.01
Post	FL1	135.07 ± 119.11	56.31 ± 55.20	<0.01
	FL2	163.91 ± 74.92	109.04 ± 46.05	<0.01
	FL3	292.04 ± 136.01	181.56 ± 77.75	<0.01
Pre	FL1	47.40 ± 53.13	22.25 ± 5.88	<0.01
	FL2	95.50 ± 37.86	80.89 ± 18.88	0.02
	FL3	162.69 ± 77.48	129.53 ± 28.98	<0.01

Splitting the toilet visit into three periods showed that fluorescent particle counts were only significantly reduced in the Lid Down period compared to Lid Up during the Pre-Flush periods, (Table 6.13). However, lid positioned down caused a significant increase in particle size and elongation (Table 6.14) and fluorescence intensity in all channels, through all periods (Table 6.15). This suggests Lid Down is associated with changing characteristics of fluorescent particles generated from flushing and these particles remain airborne for longer after flushing.

Although Pre-period showed significant difference for counts, physical and fluorescent particle characteristics with lid position, it may not be necessarily influenced by lid position but instead reflect the background levels. That is, if there is a long period between visits then the background level before the visit should be stable. However, if visits are more frequent then it may be influenced by the last visit. This is the case for days with the lid down when the toilet was visited most frequently. The day showing the most frequent visits was 14th February (a lid down day), which recorded 12 toilet visits, the highest reported on a lid up day was 8 on 13th February. On 15th February (lid down day) 3 visits were listed and the final lid up day 17th February recorded 6 visits.

6.3.6 Toilet activity related aerosols at different toilet times

This section reports the particles produced at different times during different toilet activities. As per section 2.5 toilet use is split into 3 periods; Pre – is a period of 5 minutes before the flush was recorded, Flush – refers to a 1 minute period starting when flush was recorded and Post – is a five minute period after the flush period.

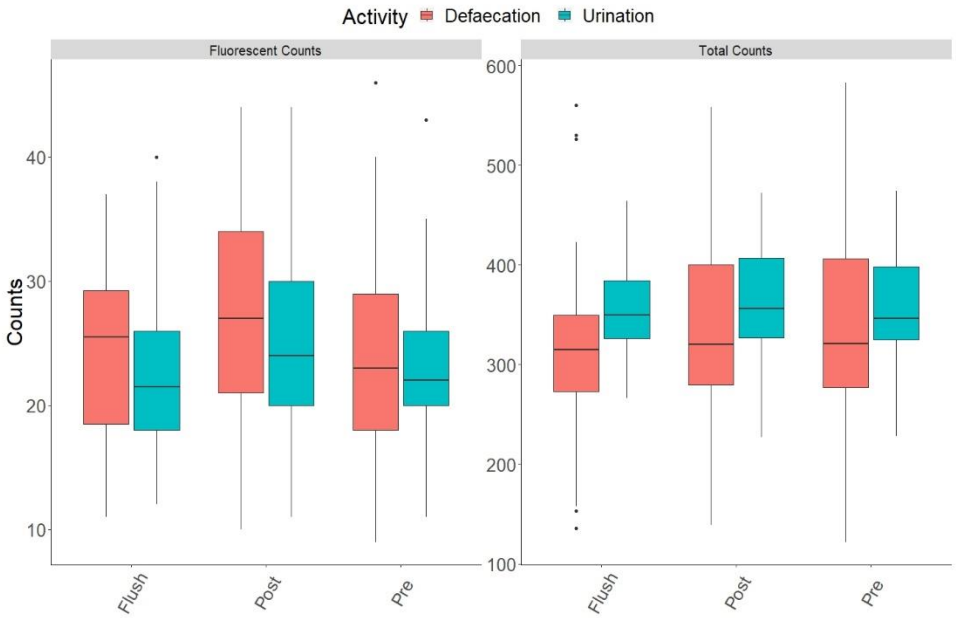

Figure 6.17 Boxplots of fluorescent (left panel) and total particle counts (right panel) for time periods for defaecation (red) and urination (blue). Both panels are split into sets of boxplots for each period, first set of boxplots is for flush-, second set for post- and third set for pre-.

Apart from the Pre period, defaecation was associated with a significant increase in the number of fluorescent particles observed during each time period in comparison to urination (Table 6.16). Conversely, urination related visits had a significantly higher total particle count through each period than defaecation.

Table 6.16 Mean ± sd for fluorescent and total particle counts for each period by toilet activity with calculated p-value between lid position.

Particle type	Timing	Defaecation	Urination	P-value
		Mean ± sd		
Fluorescent	Flush	24.64 ± 6.83	22.3 ± 6.76	0.01
	Post	27.41 ± 7.74	24.86 ± 6.63	0.01
	Pre	23.66 ± 7.49	22.87 ± 5.46	0.3
Total	Flush	319.33 ± 93.88	353.33 ± 50	0.01
	Post	334.33 ± 99.99	363.64 ± 53.40	0.01
	Pre	331.12 ± 106.39	355.90 ± 50.4	0.01

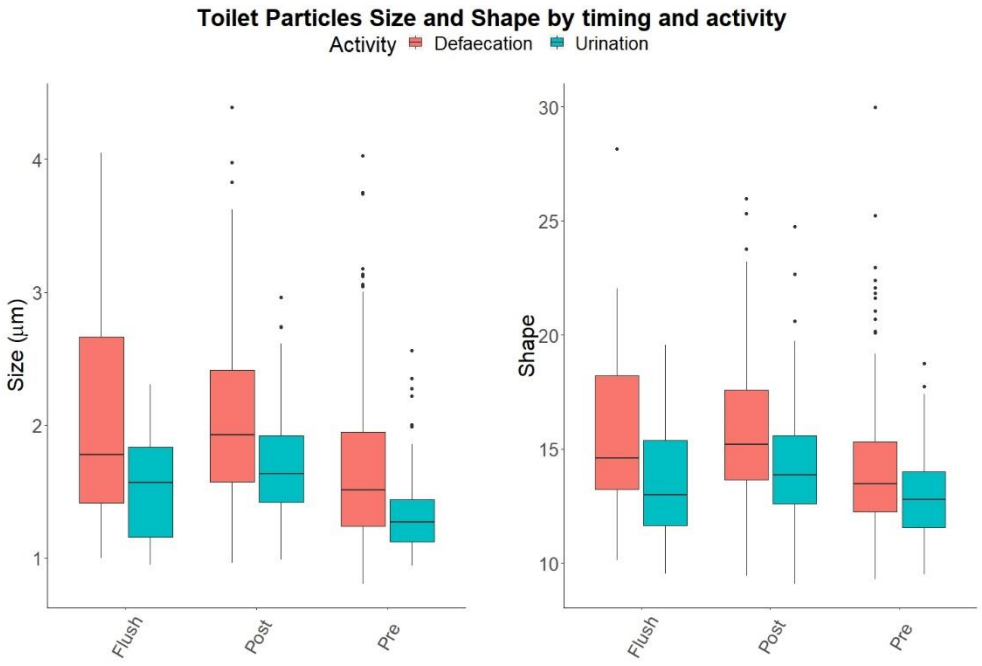

Figure 6.18 Boxplots of fluorescent particle size (µm) (left panel) and shape (right panel) for time periods with defaecation (red) and with urination (blue). Both panels are split into sets of boxplots for each period, first set of boxplots is for flush-, second set for post- and third set for pre-.

Table 6.17 shows particle size significantly increased, and shape elongated across all periods with defaecation in comparison to urination (P<0.01). the largest increase in size (µm) was observed during the flush period where particle size increased by ~0.5 (µm) (1.55 ± 0.38 µm to 2.01 ± 0.83 µm) with defaecation compared to urination.

Similarly, the largest difference in shape was noted during the flush period with a 2.4 AF-fold increase in shape (13.53 ± 2.34 to 15.91 ± 3.79) i.e. elongating, Table 6.17.

Table 6.17 Mean ± sd for fluorescent particle size (µm) and shape for each period by toilet activity with calculated p-value between lid position

Particle type	Timing	Defaecation	Urination	P-value
		Mean ± sd		
Size	Flush	2.01 ± 0.83	1.55 ± 0.38	< 0.01
	Post	2.08 ± 0.69	1.68 ± 0.41	< 0.01
	Pre	1.69 ± 0.66	1.32 ± 0.29	< 0.01
Shape	Flush	15.91 ± 3.79	13.53 ± 2.34	< 0.01
	Post	15.78 ± 3.25	14.21 ± 2.54	< 0.01
	Pre	14.34 ± 3.54	12.87 ± 1.79	< 0.01

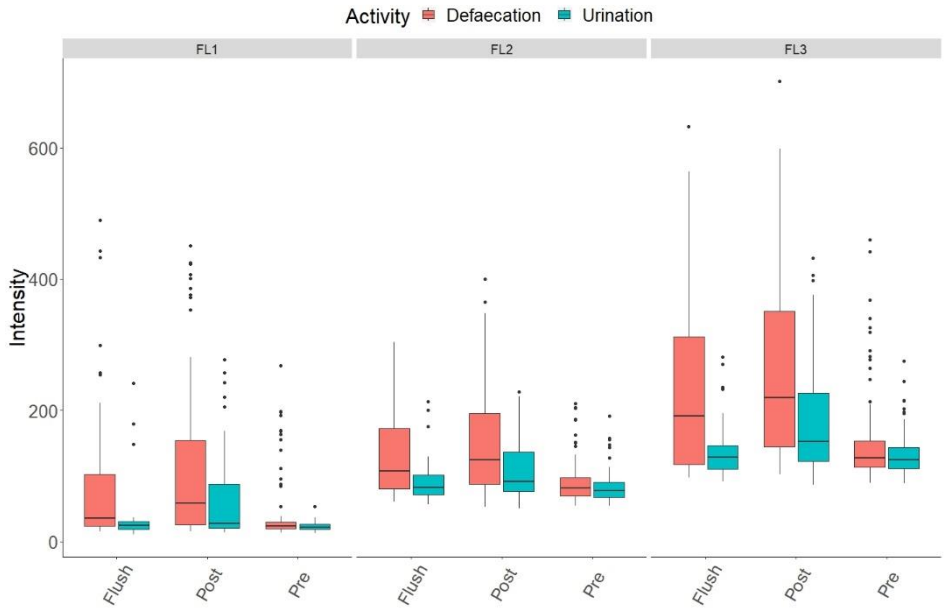

Figure 6.19 Boxplots of fluorescent particle intensity for each fluorescent channel during the different time periods when lid was down (red) and when the lid was up (blue). The three panels represent a fluorescent channel; first panel FL1 (left), FL2 (middle), and FL3 (right). The 3 channel panels are split into sets of boxplots for each period, first set of boxplots is for flush-, second set for post- and third set for pre-.

Figure 6.19 and Table 6.18 show defaecation was associated during all periods, with significantly higher particle fluorescent intensity ($P<0.01$), in all channels compared with urination. Interestingly the highest mean particle fluorescent for each channel was not observed during the flush phase, but instead during the post-flush phase.

Table 6.18 Mean ± sd for fluorescent particle intensity in each channel for each period with calculated p-value between lid position.

Particle type	Timing	Defaecation	Urination	P-value
		Fluorescent intensity means ± sd		
FL1	Flush	100.86 ± 130.38	39.98 ± 51.8	< 0.01
	Post	108.34 ± 109.75	58.18 ± 55.95	< 0.01
	Pre	39.41 ± 45.95	22.66 ± 5.81	< 0.01
FL2	Flush	135.56 ± 69.93	94.03 ± 38.07	< 0.01
	Post	147.04 ± 73.14	108.79 ± 43.54	< 0.01
	Pre	89.68 ± 32.05	82.29 ± 22.21	< 0.01
FL3	Flush	243.52 ± 152.81	145.98 ± 51.99	< 0.01
	Post	260.77 ± 131.51	178.69 ± 73.39	< 0.01
	Pre	149.59 ± 67.19	132.60 ± 32.85	< 0.01

6.3.7 Effect of lid position and toilet activity at different toilet timing

This section examines if toilet activity with lid position produced different particles when examined by different subsections of toilet use time.

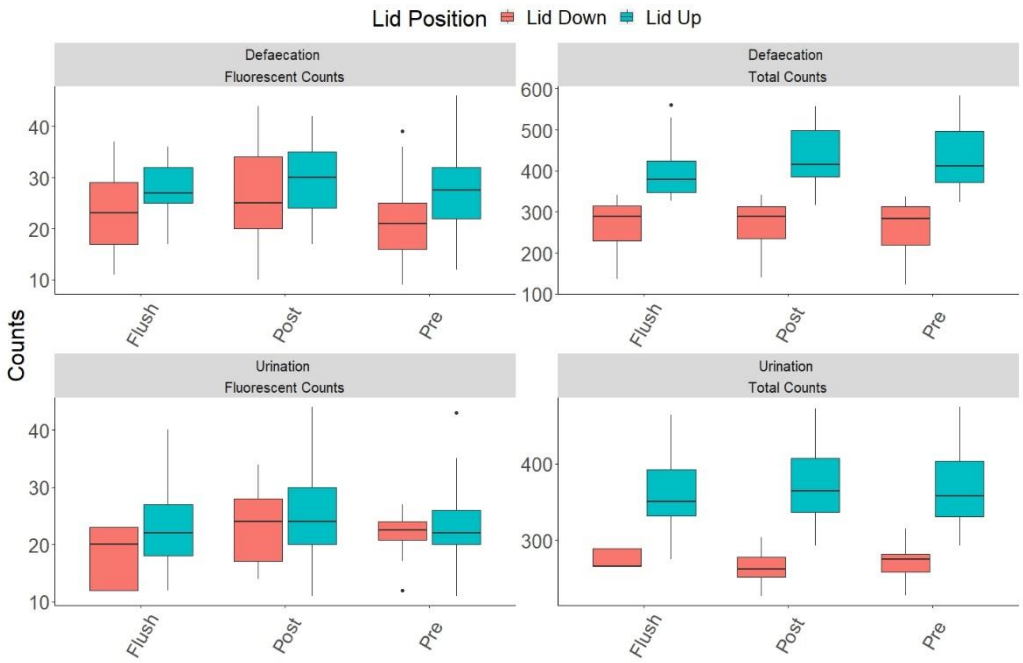

Figure 6.20 Boxplots of fluorescent (left panel) and total particle counts (right panel) for time periods for lid down (red) and lid up (blue). Both panels are split into sets of boxplots for each period, first set of boxplots is for Flush-, second set for Post- and third set for pre-. The panels on top are defaecation related and bottom panels are urination.

Total particle counts for defaecation and urination were significantly reduced during each period with the lid positioned down (Table 6.19, $P<0.01$). Defaecation-related fluorescent particles were significantly reduced ($P<0.01$), with the lid positioned down in all periods, Figure 6.20. No period showed a significantly different fluorescent particle count for urination by lid position.

Table 6.19 Mean ± sd for fluorescent and total particle counts for each period by toilet activity with calculated p-value between lid position.

Timing	Activity	Fluorescent		P-value	Total		P-value
		Lid Down	Lid Up		Lid Down	Lid Up	
		mean ± sd			mean ± sd		
Flush	Urination	18.33 ± 4.78	22.74 ± 6.80	0.03	273.66 ± 11.16	362.19 ± 44.30	<0.01
	Defaecation	22.91 ± 7.23	27.69 ± 4.68	<0.01	268.69 ± 57.23	408.92 ± 77.07	<0.01
Post	Urination	23.45 ± 6.08	25 ± 6.67	0.08	266.09 ± 21.10	372.88 ± 45.68	<0.01
	Defaecation	26.16 ± 8.14	29.19 ± 6.72	<0.01	270.59 ± 56.86	425.80 ± 73.96	<0.01
Pre	Urination	21.75 ± 3.94	23 ± 5.59	0.25	273.67 ± 21.51	365.48 ± 43.56	<0.01
	Defaecation	20.94 ± 6.43	27.63 ± 7.14	<0.01	263.70 ± 62.92	429.33 ± 75.68	<0.01

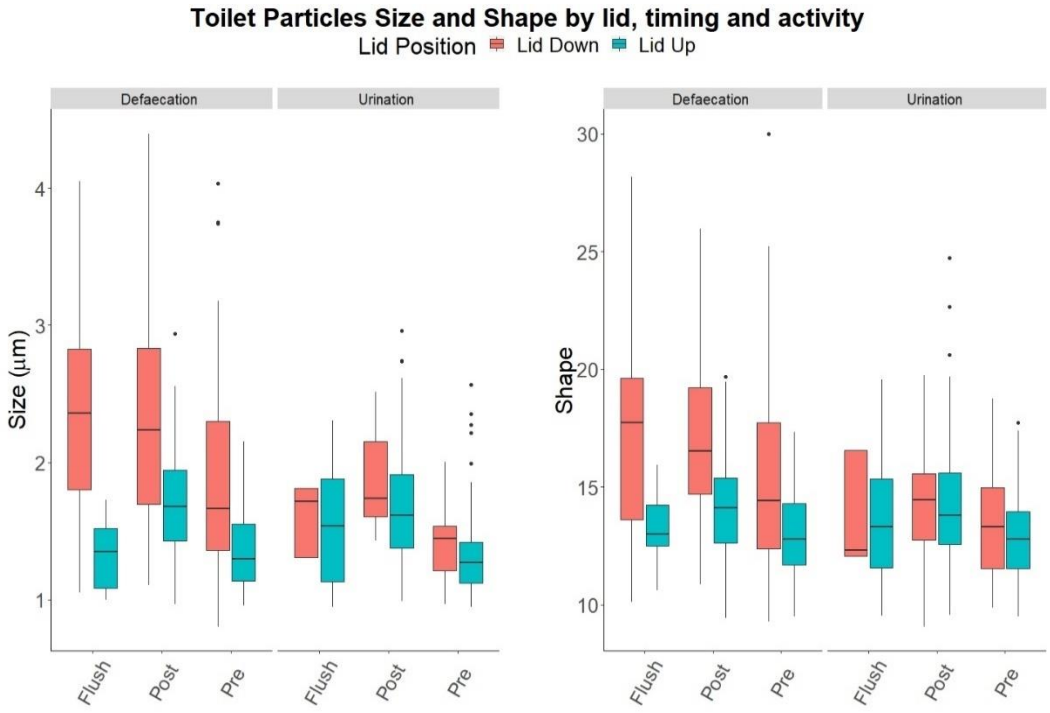

Figure 6.21 Boxplots of size (µm) (left panel) and shape (right panel) for time periods for lid down (red) and lid up (blue). Both panels are split into sets of boxplots for each period, first set of boxplots is for flush-, second set for post- and third set for pre-. The panels (inside-left) are for defaecation related and (inside-right) panels are for urination.

Lid positioned down was associated with a significant increase in size and elongation of defaecation-related fluorescent particles through every period (Figure 6.21, Table 6.20). Urination associated fluorescent particle size was significantly increased pre and post flush, with the lid down, although not to the same extent as defaecation related particles. No period showed a significant difference in shape with lid down for particles related to urination.

Table 6.20 Mean ± sd for fluorescent particle size (µm) and shape for each period by toilet activity with calculated p-value between lid position.

Timing	Activity	Size (µm)		P-value	Shape		P-value
		Lid Down	Lid Up		Lid Down	Lid Up	
		mean ± sd			mean ± sd		
Flush	Urination	1.61 ± 0.22	1.55 ± 0.39	0.35	13.65 ± 2.12	13.52 ± 2.36	0.44
	Defaecation	2.40 ± 0.78	1.31 ± 0.25	0.00	17.45 ± 3.86	13.16 ± 1.37	0.00
Post	Urination	1.86 ± 0.33	1.67 ± 0.42	0.00	14.38 ± 2.54	14.19 ± 2.54	0.16
	Defaecation	2.33 ± 0.73	1.73 ± 0.41	0.00	16.91 ± 3.37	14.15 ± 2.24	0.00
Pre	Urination	1.40 ± 0.3	1.31 ± 0.29	0.00	13.46 ± 2.04	12.80 ± 1.68	0.04
	Defaecation	1.91 ± 0.76	1.37 ± 0.28	0.00	15.33 ± 4.08	12.91± 1.79	0.00

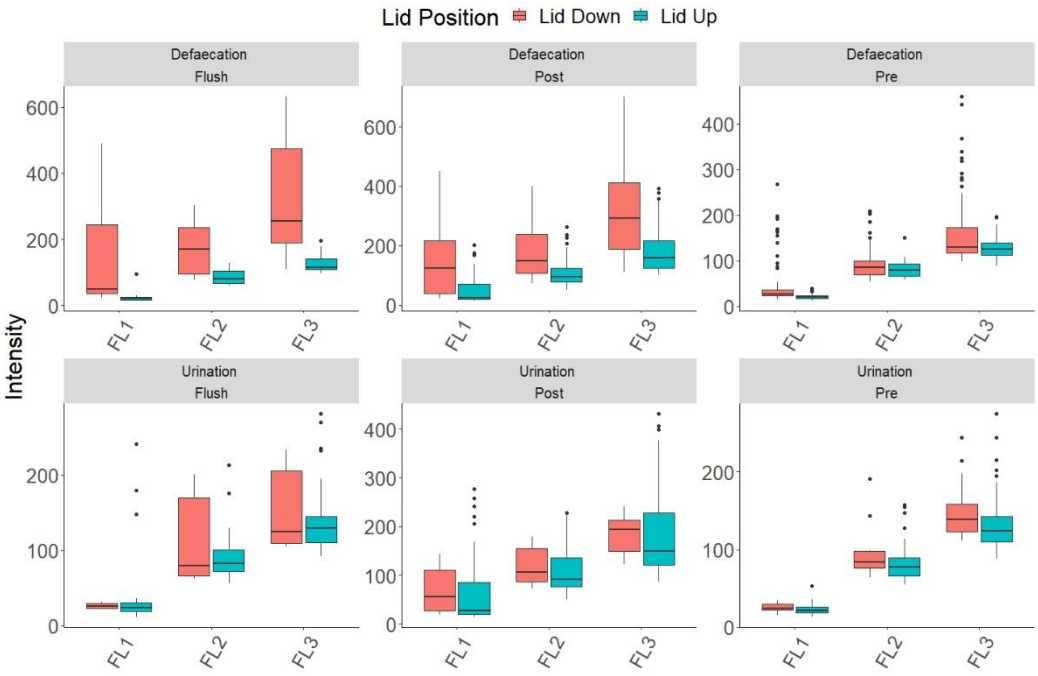

Figure 6.22 Boxplots of fluorescent particle intensity for each fluorescent channel during the different time periods when lid was down (red) and when its lid was up (blue). The three panels represent a fluorescent channel; first panel FL1 (left), FL2 (middle), and FL3 (right). The 3 channel panels are split into sets of boxplots for each period, first set of boxplots is for flush-, second set for post- and third set for pre-. The panels on top are defaecation related and bottom panels are urination

Significant increases in defaecation-related fluorescent particle intensity were noted across all time periods with the lid down opposed to the lid up, in nearly all channels apart from FL2 during the pre-period (Table 6.21). For urination only the FL1 and FL3 channel fluorescence during the pre-period showed significant, particle intensity differences between lid down and the lid being up (P<0.01, Table 6.21).

Table 6.21 Mean ± sd for fluorescent particle intensity in each channel for each period with calculated p-value between lid position.

Toilet Timing	Channel	Urination			Defaecation		
		Fluorescent Intensity mean ± sd		P-value	Fluorescent Intensity mean ± sd		P-value
		Lid Down	Lid Up		Lid Down	Lid Up	
Flush	FL1	26.29 ± 4.8	41.51 ± 55.18	0.36	142.82 ± 149.26	26.64 ± 21.43	< 0.01
	FL2	113.88 ± 75.24	91.83 ± 34.23	0.89	164.61 ±72.44	84.19 ± 21.77	< 0.01
	FL3	153.96 ±69.03	145.10 ± 52.13	0.81	307.87 ± 159.39	129.69 ± 31.85	< 0.01
Post	FL1	66.23 ± 45.554	57.41 ± 57.12	0.03	146.55 ±123.82	53.54 ± 50.52	< 0.01
	FL2	116.38 ±37.41	108.08 ± 44.29	0.15	171.83 ± 76.83	111.47 ± 50.65	< 0.01
	FL3	178.83 ± 40.17	178.68 ± 76.14	0.26	310.91 ± 137.30	188.83 ± 82.10	< 0.01
Pre	FL1	25.08 ±5.46	22.38 ± 5.84	0.01	51.40 ± 56.79	21.96 ± 6.03	< 0.01
	FL2	96.60 ± 36.31	80.62 ±19.65	0.02	95.31 ± 38.39	81.49 ± 17.23	0.07
	FL3	151.27 ± 43.17	130.43 ± 31.10	0.01	164.74 ± 82.19	127.53 ± 23.75	< 0.01

From Table 6.20, we observed lid position down and defaecation toilet activity resulting in particle size (µm) significantly increasing. This would suggest that leaving the lid down may promote particle collisions, that would in turn lead to the formation of agglomerates (clustering of particles) thus increasing particle size (µm).

6.3.8 Particle air-residency time

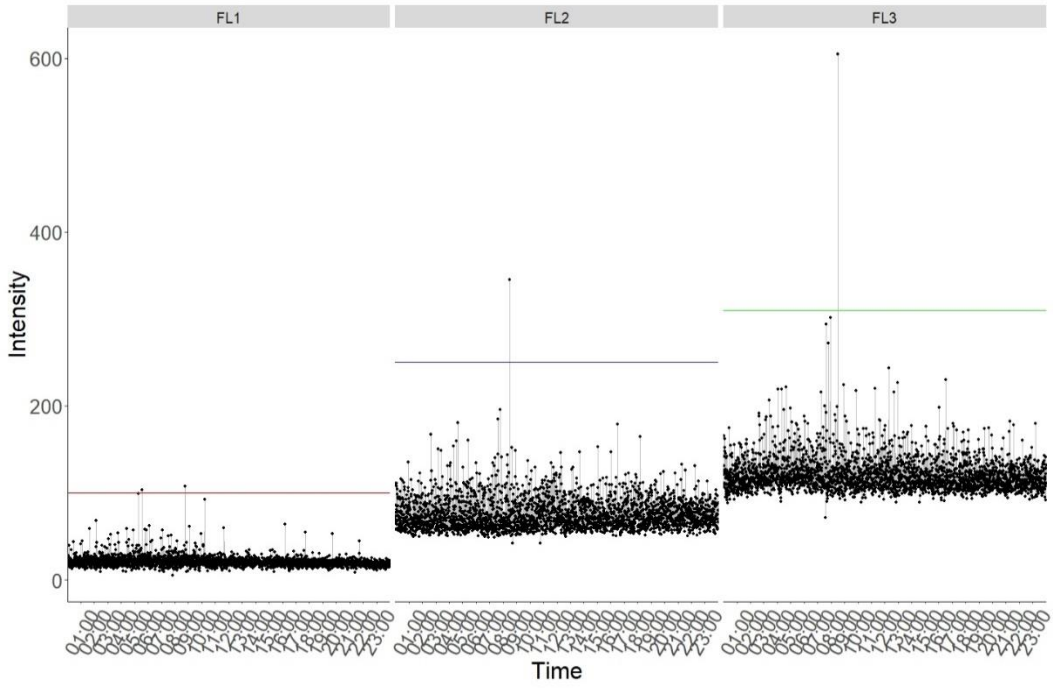

Figure 6.23 Fluorescent intensity recorded on a day with no occupancy. First panel (left) shows the FL1 channel intensity, second panel (middle) FL2 intensity, and third panel (right) FL3 intensity. Coloured line in each panel represents the calculated threshold line of the mean + 9σ of the intensities recorded.

Following on from the previous sections we can see that fluorescent particles, with high intensity, are still airborne for at least 30-seconds post flush, Table 6.21.

To look at the residency time of these particles an intensity threshold was calculated, from which the time of toilet related particles crossing this threshold would be calculated. The threshold was set based on times when the toilet was not occupied (Figure 6.23). This created a baseline of fluorescent intensities for the three channels, the mean intensity + 9σ was adopted as the threshold (Table 6.22).

Table 6.22 Channel with mean intensity and sd with the calculated threshold recorded for unoccupied day.

Channel	Mean intensity	sd	Calculated Threshold
FL1	20.78	6.27	77.17
FL2	75.22	18.03	237.47
FL3	120.64	20.73	307.18

Flushing is taken as a biological aerosol-generating event (as observed by the spike in fluorescent particle numbers). The residency time of event-associated particles is defined as the number of 30 second time intervals after the flush that the mean particle fluorescent intensity stays above the threshold before it returns below it. A time limit of 10 minutes after flushing was set for particles to break threshold, after this it was not considered.

Applying the fluorescent intensity as a simple cut off, 19 events were observed. 14 of these events occurred with the lid positioned down and five with the lid up. Of the 14 events with the lid down, ten of these occurred after defaecation, four after urination. Three of the five events with the lid up occurred with urination with the remaining two with defaecation.

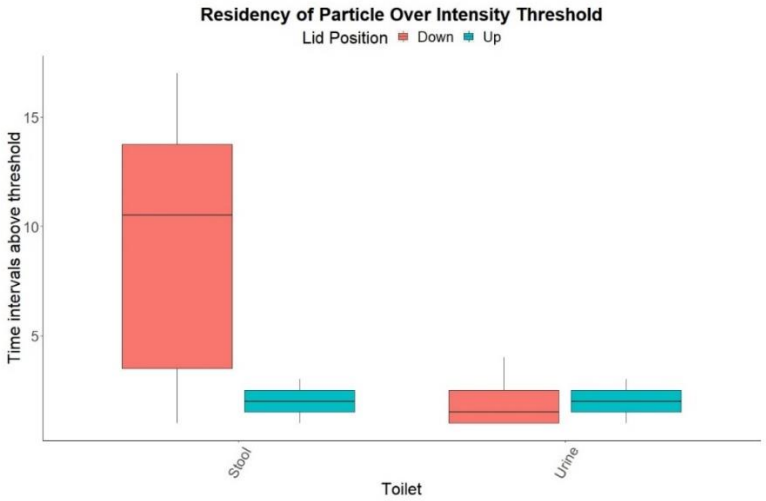

Figure 6.24 Boxplot of time intervals above threshold from toilet-related events. Lid down (red) and lid up (blue). Panel has two sets of boxplots with defaecation (left) and urination (right).

Lid down positioning significantly increased fluorescent particle air residency for defaecation-related particles by ~ 4-fold compared to the lid being up ($P<0.01$, Figure 6.24, Table 6.23). No significant difference was recorded for urination and lid positioning.

Table 6.23 Time intervals above threshold (mean ± sd) by lid position and toilet activity.

Toilet Activity	Lid Down	Lid Up	P-value
	Time intervals above threshold (30-second) Mean ± sd		
Defaecation	8.9 ± 5.92	2 ± 1.41	<0.01
Urination	2 ± 1.41	2 ± 1	1

Of the ten defaecation events that occurred with the lid positioned down, one event resulted in fluorescent particles staying above the threshold for seventeen 30-second time intervals, ~ 8 minutes above background levels post flush. Another event exhibited particles above the threshold for eleven 30-second time intervals when

another occupant had entered the toilet, potentially exposing themselves to those bioaerosols.

From section 6.3.7, lid position down and defaecation toilet activity resulted in a significant increase in particle size (Table 6.20). This would suggest that leaving the lid down promotes particle collisions, that would in turn lead to the formation of agglomerates. Tying this together with results from Table 6.23, it would lead to the possibility of these newly formed agglomerates of bioaerosol particles, promoted by positioning the lid down, staying airborne longer for a longer time-period than those produced when the lid is up. A hypothesis for the process by which these new agglomerates are formed is discussed below.

6.3.9 Catagorisation of toilet-related particles

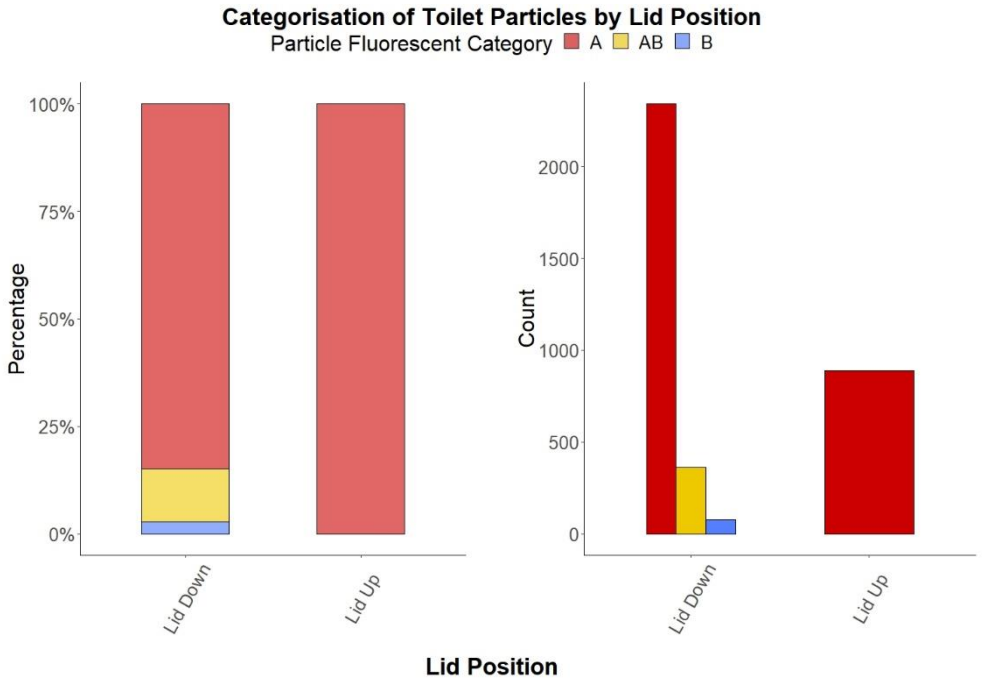

Figure 6.25 Fluorescence properties of toilet related particles. Stacked bar chart panel (Left) represents the % of fluorescent particles in each fluorescent type. Panel (Right) shows the overall particle count distribution in each type. Each panel is split evenly by lid position with lid down (left) and lid up (right).

Fluorescence type distribution is defined by excitation and emission from any of three possible channels alone (A, B or C) or in any combination. Following the annotation introduced by Perring *et al.* particle fluorescence was categorized as one of seven types, which considers each of three fluorescence bandwidths individually, as well as in all possible combinations, described in detail in section 2.1.2 and annotation matrix in Table 1.13 (Perring, 2016).

Figure 6.25 shows the distribution of fluorescent types between lid positions. A larger number of particles of specific fluorescent type were produced with the lid down compared to when the lid was up, owing to particles with higher fluorescent intensity being produced with the lid down, which is associated with fluorescence in more than one channel. Fluorescent type A was the predominant type observed between lid positions. Lid up only produce type A particles whereas lid down saw the production of type A, B, and AB. The greater variety of particle fluorescent types associated with lid down suggests that these particles may be resuspended from surfaces between the toilet rim and seat, with no resuspension observed with lid up.

Table 6.24 Mean number ± sd of particles produced of specific fluorescent type observed between Lid Position.

Lid position	Number in Fluorescent Type mean ± sd		
	A	B	AB
Lid Down	26.30 ± 7.53	25.67 ± 5.51	27.76 ± 8.00
Lid Up	25.4 ± 5.77	0	0

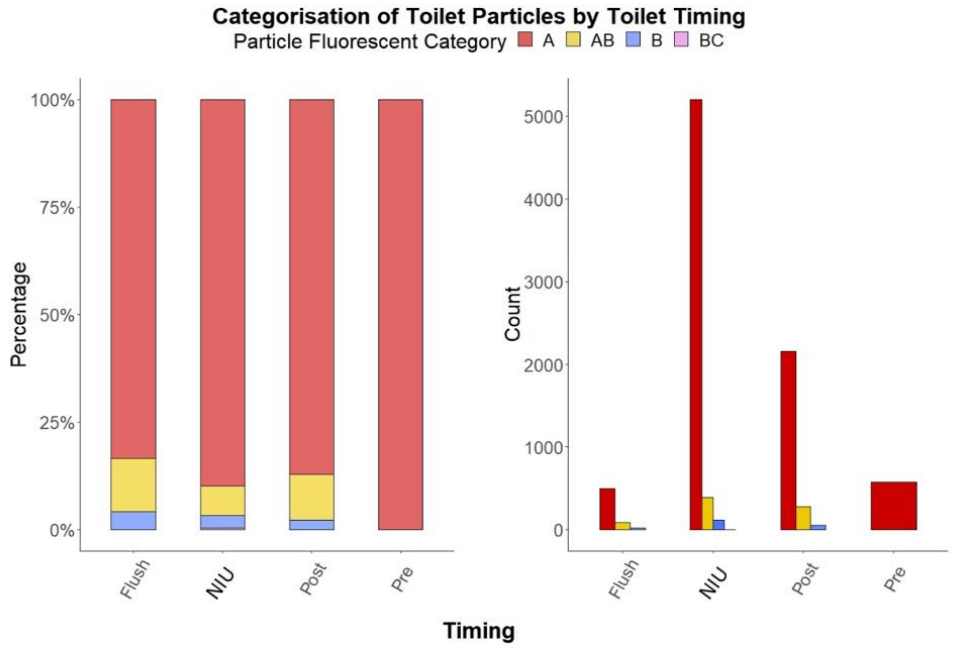

Figure 6.26 Fluorescence properties of toilet related particles. Stacked bar chart panel (Left) represents the % of fluorescent particles in each fluorescent type. Panel (Right) shows the overall total particle count distribution in each type. Each panel is split evenly by time period flush (left), NIU (left-middle), post (right-middle) and pre (right).

NIU represents all the time outside of toilet use i.e. all the time outside of the pre-flush and post- periods. Pre-period only presents particles of fluorescent type A. Flush, post and NIU periods present particles mainly as type A, however, ~10-20% were of B and AB type, Figure 6.26 (left panel). The right panel of Figure 6.26 shows the overall fluorescent type count distribution, clearly the largest total number was observed during the NIU period. However, in terms of mean particles observed per minute, NIU was the lowest (20.89 ± 6.27) and the post period shows highest mean counts per fluorescent type (25.5 ± 7.78 - 27.9 ± 8.27), (Table 6.25). The pre-flush exhibits relatively high readings, however this may be due to toilet use frequency, with little time between occupancy may result in higher particle counts i.e. the higher variability observed.

Table 6.25. Mean number ± sd of particles produced of specific fluorescent type observed per minute within each period.

Toilet Timing	Number in Fluorescent Type mean ± sd per minute			
	A	B	AB	BC
Flush	24.85 ± 5.71	26	27.33 ± 8.74	0
Post	26.60 ± 7.51	25.5 ± 7.78	27.9 ± 8.27	0
Pre	25.13 ± 6.53	0	0	0
NA	20.89 ± 6.27	14.12 ± 8.87	20.47 ± 7.93	4

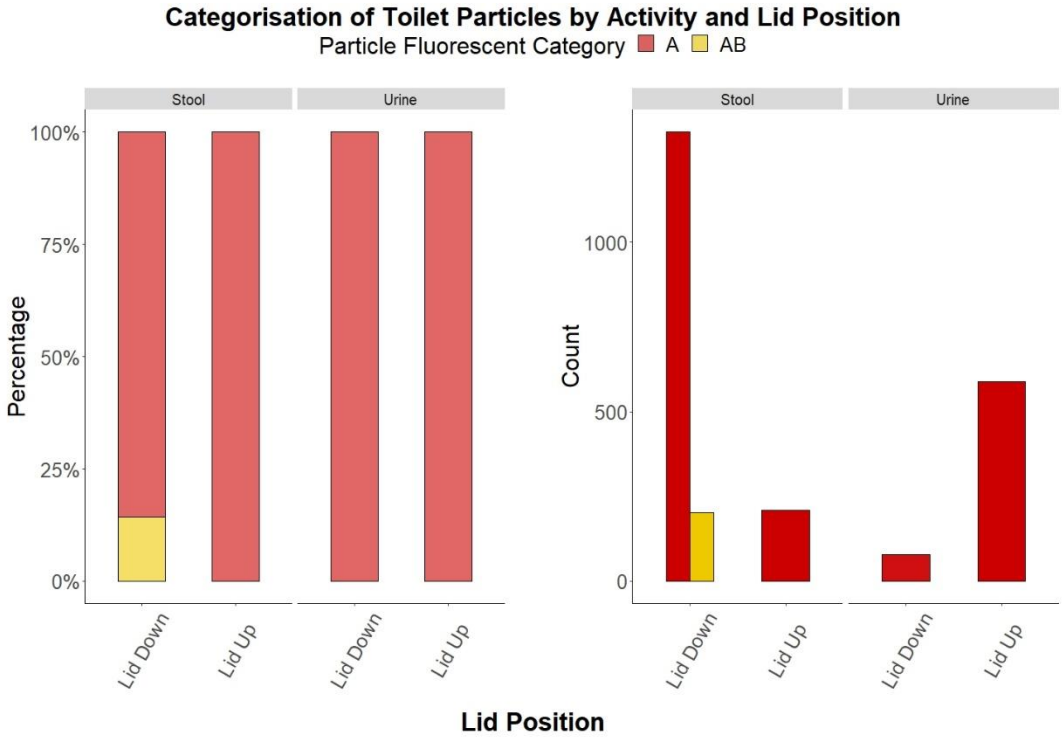

Figure 6.27 Fluorescence properties of toilet related particles. Stacked bar chart panel (Left) represents the % of fluorescent particles in each fluorescent type. Panel (Right) shows the overall particle count distribution in each type. Each panel is split evenly into two sections by toilet activity defaecation (left) and urination (right), these are then again split by lid position with lid down (inside left) and lid up (inside right).

Both defaecation and urination presented most of their associated fluorescent particles as type A, apart from lid down with defaecation activity which also produced ~15%

of its particles as type AB, Figure 6.27 (left panel). Interestingly, urination produces more particles of type A than defaecation produces when the lid was positioned up, a ~2-fold difference. Conversely defaecation produced ~7/8 fold more particles of type A with Lid down than urination does, Table 6.26.

Table 6.26. Mean number ± sd of particles produced by specific fluorescent type observed for defaecation and urination according to lid position.

Toilet Activity	Number in Fluorescent Type		
	Lid Down		Lid Up
	A	AB	A
Defaecation	27.58 ± 7.91	25.25 ± 7.17	26.12 ± 6.10
Urination	26 ± 4.36	0	25.61 ± 5.46

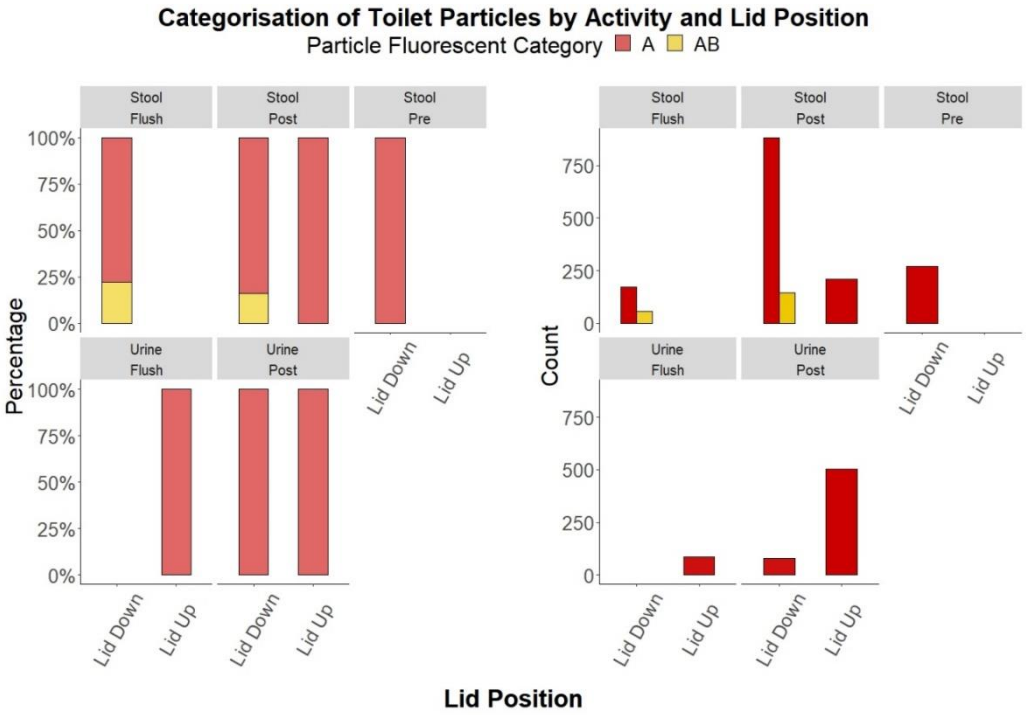

Figure 6.28 Fluorescence properties of toilet related particles. Stacked bar chart panel (Left) represents the % of fluorescent particles in each fluorescent type. Panel (Right) shows the overall particle count distribution in each type. Each panel is split horizontally in two by toilet activity defaecation (top) and urination (bottom). And then both panels are split vertically by time period flush (left), post (middle), and pre (right). There were no particles counted in the Pre period for urination.

The top panels of Figure 6.28 show defaecation produced the majority of type A particles in the post period, and only produced particles of type AB during the flush and post period. Urination did not show particles of any type in the pre period, with the majority of fluorescent type A particles produced during the post period, bottom panel Figure 6.28.

Table 6.27. Mean number ± sd of particles produced of specific fluorescent type observed for defaecation and urination by lid position.

Activity	Lid Position	Toilet Timing				
		Flush		Post		Pre
		A	AB	A	AB	A
Urination	Lid Down	0	0	26 ± 4.35	0	0
	Lid Up	28.66 ± 3.05	0	25.15 ± 5.64	0	0
Defaecation	Lid Down	24.42 ± 6.70	28.5 ± 12.02	28.45 ± 8.13	24.16 ± 6.11	27.1 ± 8.10
	Lid Up	0	0	26.12 ± 6.10	0	0

Section 6.3.9 highlights the toilet-related fluorescent types by lid positioning and toilet activity, as well as the fluorescent types at different toilet times. All of the urination related fluorescent particles presented as type A and while the majority of those associated with defaecation were also fluorescent type A, some presented as type AB, but only occurring during the post-period and with the lid positioned down. The difference in particle characteristics between lid use suggests the possibility of different particle sources. When the lid was down the flushed aerosols were forced through a smaller passage between the lid and the seat, both with surfaces, known to be contaminated (Barker and Bloomfield, 2000). The movement of aerosols through here may re-aerosolise previously settled particles that are there.

6.3.10 Artificial Defaecation

To further control variables of the flush process seen in the observational study, experiments with artificial stool were performed in the same toilet with the lid up. Artificial defaecation was deposited and flushed on four occasions. Three periods were observed for this experiment but due to time constraints no pre period was observed between flushes. A period of twenty-minutes before the initial flush was defined as the pre period. Similar to previous sections the post-flush period was 5 minutes after flush with the flush itself being a 1-minute period. Using one-minute mean values for counts, the following counts were observed.

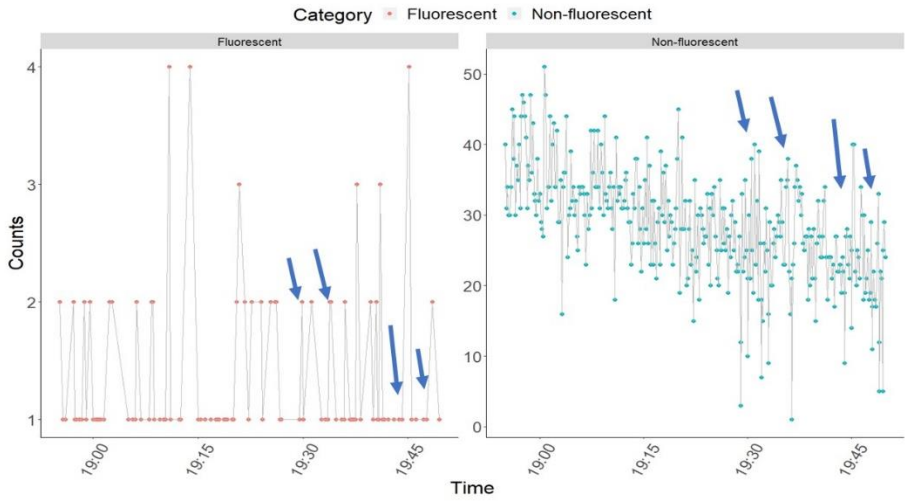

Figure 6.29 Time series of fluorescent and total particle counts for the time period when the lavatory was used for artificial defaecation. Fluorescent (red), and non-fluorescent (Blue). Each panel represents a particle type; (left) fluorescent, and (right) non-fluorescent. The four flushes are marked on each with blue arrows.

From Figure 6.29, there is no apparent change in either fluorescent or total particle counts following flushing. Further particle characteristics are analysed below.

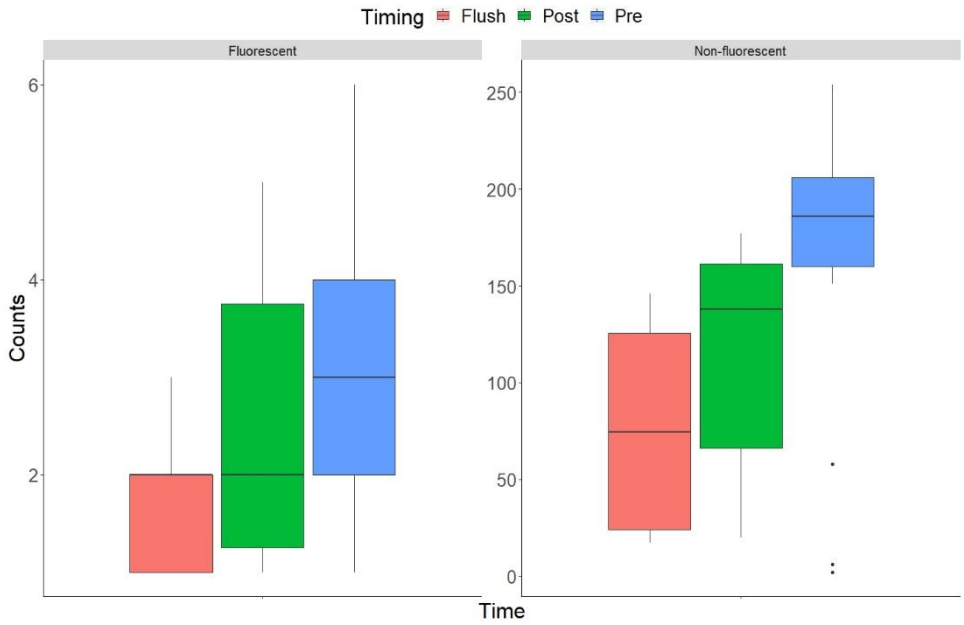

Figure 6.30 Boxplots of mean fluorescent (left panel) and total particle counts (right panel) per minute for time periods when the lavatory was used for the four artificial defaecations flushes. Flush (red), post-flush (green) and Pre (blue).

Both the mean fluorescent and total particle counts did not differ significantly between the flush- and post-periods (Figure 6.30, Table 6.29). Pre was associated with a significantly higher total particle count (169.93 ± 46.55) than either the flush (76.62 ± 58.93) or post (117.25 ± 60.75) periods (P<0.01). However, the background related fluorescent counts did not differ significantly from the flush (1.6 ± 1.3, P = 0.25) or post (2.4 ± 1.59, P = 0.02) periods, Table 6.26.

Table 6.29 Mean ± sd for fluorescent and total particle counts with calculated p-value between flush and post-periods.

Particle Type	Timing	Mean ± sd	P-value
Fluorescent	Flush	1.6 ± 1.3	0.1847655
	Post	2.4 ± 1.59	
	Pre	3.03 ± 1.5	0.25 (flush) 0.02 (post)
Non-fluorescent	Flush	76.62 ± 58.93	0.1558813
	Post	117.25 ± 60.75	
	Pre	169.93 ± 46.55	<0.01(Flush and Post)

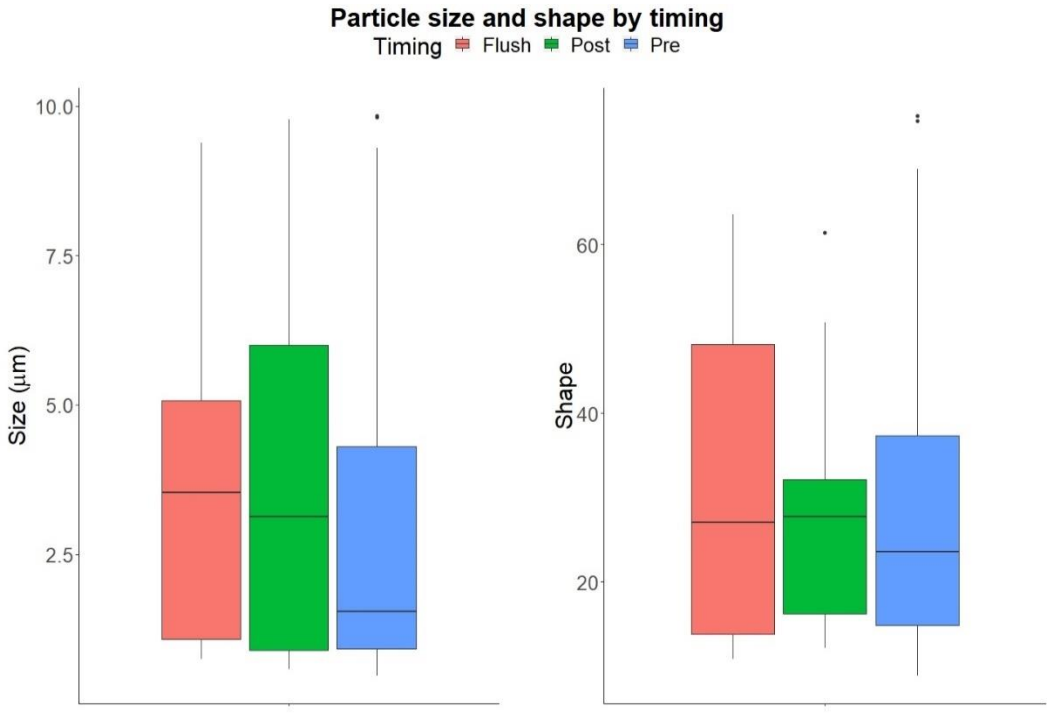

Figure 6.31 Boxplots of fluorescent particle size (left panel) and shape, AF (right panel) for time periods when lavatory was used for artificial defaecation during different timing. Flush (red), post-flush (green) and pre (blue).

The fluorescent particle size (µm) and sphericity index (AF) did not show any significant difference between any period ($P > 0.01$), Figure 6.31.

Table 6.30 Mean ± sd for fluorescent particle size (µm) and shape with calculated p-value between timings.

Timing	Size	AF	P-value
	Mean ± sd		
Flush	3.69 ± 2.93	32.79 ± 21.82	0.85 (post) 0.33 (pre)
Pre	2.79 ± 2.46	28.17 ± 16.72	0.25
Post	3.75 ± 3.2	27.43 ± 12.2	

Ten-second mean fluorescent intensities were observed (Figure 6.32), and the initial flush (marked by an arrow in Figure 6.32), caused a large fluctuation in the FL1 channel, and the highest intensities were observed in the FL2 and FL3 channels.

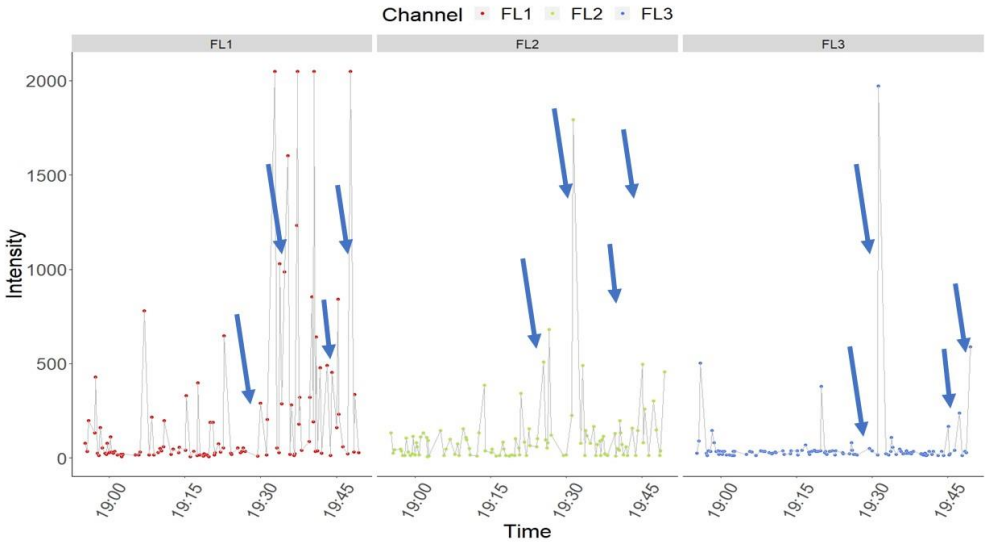

Figure 6.32 Time series of fluorescent channel intensities for time period when the lavatory was used for artificial defaecation. FL1 (red), FL2 (green) and FL3 (Blue). Each panel represents a fluorescent channel; (left) FL1, (middle) FL2 and (right) FL3. Initial flush is marked by an arrow. The four flushes are marked on each with blue arrows.

Figure 6.32, showing the fluorescent intensities over the experiment showed a clear increase in fluorescent intensities immediately after the flush. FL2 and FL3 show highest fluorescent intensity after the flush, while FL1 experienced larger fluctuations after the flush.

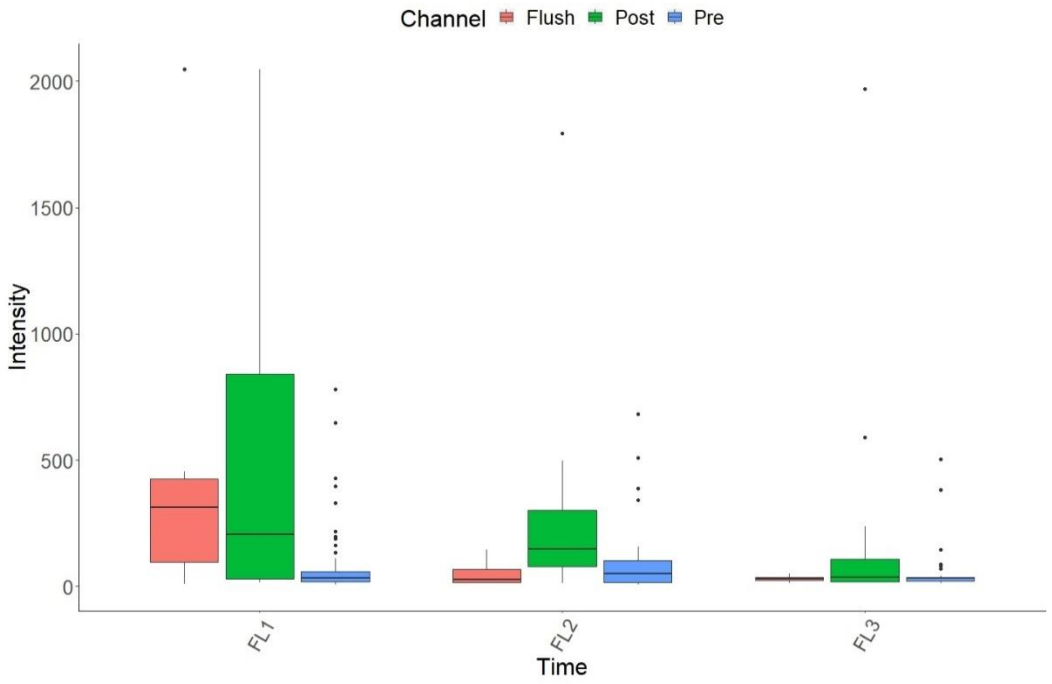

Figure 6.33 Boxplots of fluorescent channel intensities for time periods when the lavatory was used for artificial defaecation during the four deposits. Flush (red), post-flush (green) and pre (blue). Each panel is split into 3 sets of boxplots each representing a fluorescent channel; (left) FL1, (middle) FL2 and (right) FL3.

For flush and background or flush and post periods the particle fluorescent intensity did not differ significantly in the FL2 and FL3 channel ($P > 0.01$, Figure 6.33 and Table 6.31). The flush and post period produced significantly higher particle intensity in the FL1 channel compared to background ($P<0.01$, Table 6.31), and the post period also produced significantly higher fluorescent intensity in the FL2 channel compared to the background. No fluorescent intensity difference was noted in the FL3 channel, between particles in post period and background (Table 6.31).

Table 6.31 Mean ± sd for fluorescent channel intensity with calculated p-value between timings on lower half.

Timing	Channel		
	Mean intensity ± sd		
	FL1	FL2	FL3
Flush	528.38 ± 764.29	51.5 ± 53.13	31.33 ± 12.58
Pre	86.21 ± 143.39	84.62 ± 115.69	46.33 ± 74.74
Post	464.76 ± 618.18	286.93 ± 419.99	200.99 ± 477.58
Channel	P-values		
	Flush vs Post	Flush vs Pre	Pre vs Post
FL1	0.7	<0.01	<0.01
FL2	0.04	0.5	<0.01
FL3	0.5	0.9	0.3

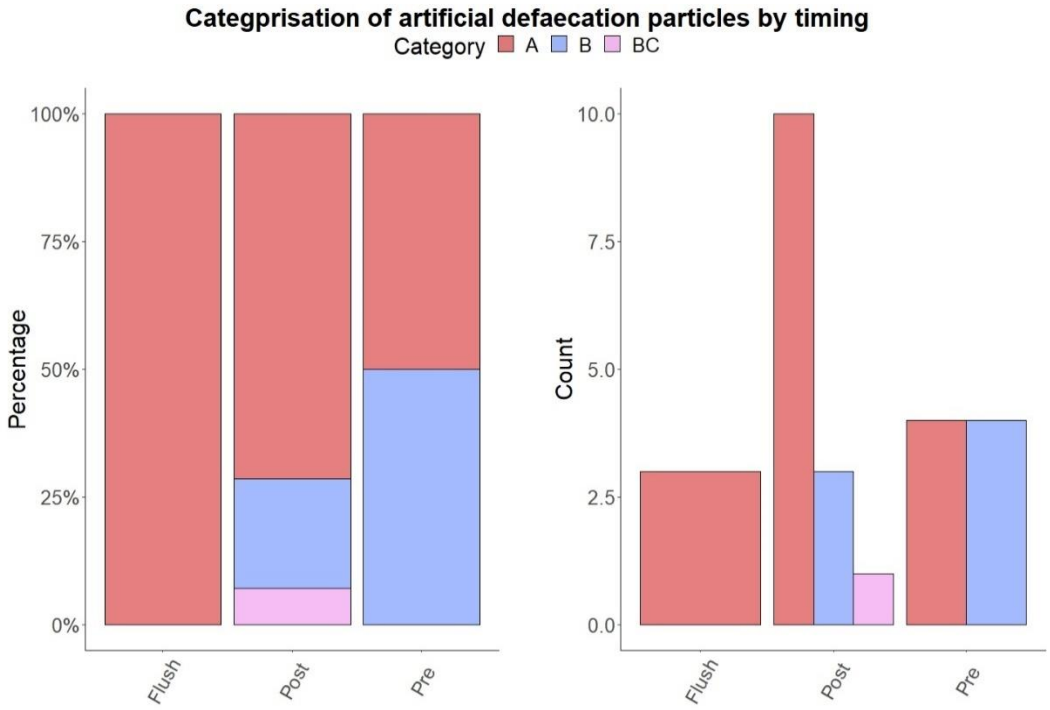

Figure 6.34 Categorisation of artificial defaecation aerosols. (Left) the fluorescent type distribution during toilet phase. (Right) Percentage fluorescent type distribution per toilet phase.

The pre period showed an even split between A and B fluorescent types (Figure 6.34). Flush-period only presents particles of fluorescent type A. Post period present particles mainly as type A, however, ~7-20% were of B and BC type, Figure 6.34 (left panel). The right panel of Figure 6.34 shows the overall fluorescent type count distribution, clearly the largest total number was observed during the post period.

Table 6.32. Percentage fluorescent type distribution of artificial defaecation aerosols per toilet phase.

Timing	Percentage in Fluorescent Type			
	A	B	AB	BC
Flush	100	0	0	0
Pre	50	50	0	0
Post	72	21	0	7

The aerosols categorised here were quite similar compared to those categorisations in Figure 6.26-6.28 describing the observations of actual toilet use. Both sets of aerosols during the flush and post-flush periods presented heavily as fluorescent type A. However, the pre-period differs with the aerosols here showed 50% as type A and 50% as type B, compared to a large majority presenting as type A during the live studies (Figure 6.26). The counts in each category were lower than those observed in the live study, but this may be explained by the weight/size of artificial defaecation deposited in toilet, with larger samples being required to achieve a higher quantity of fluorescent particles. However, Figure 6.32 and Figure 6.33 show particles of high fluorescent intensity once flushing of the artificial defaecation commenced, suggesting that the artificial defaecation model could be effective in replicating defaecation in simulation studies.

6.4 **Empty flushes**

Three empty flushes were performed prior to the toilet campaign. Data is missing from 18:54:10 – 18:56:20 due to a pause in data collection. Three periods were observed for this experiment but due to time constraints no pre period was observed between flushes, a period of three-minutes before initial flush was defined as the pre period. Similar to previous sections the flush itself being a 1-minute period, and two-minutes after flushes is defined as the post period.

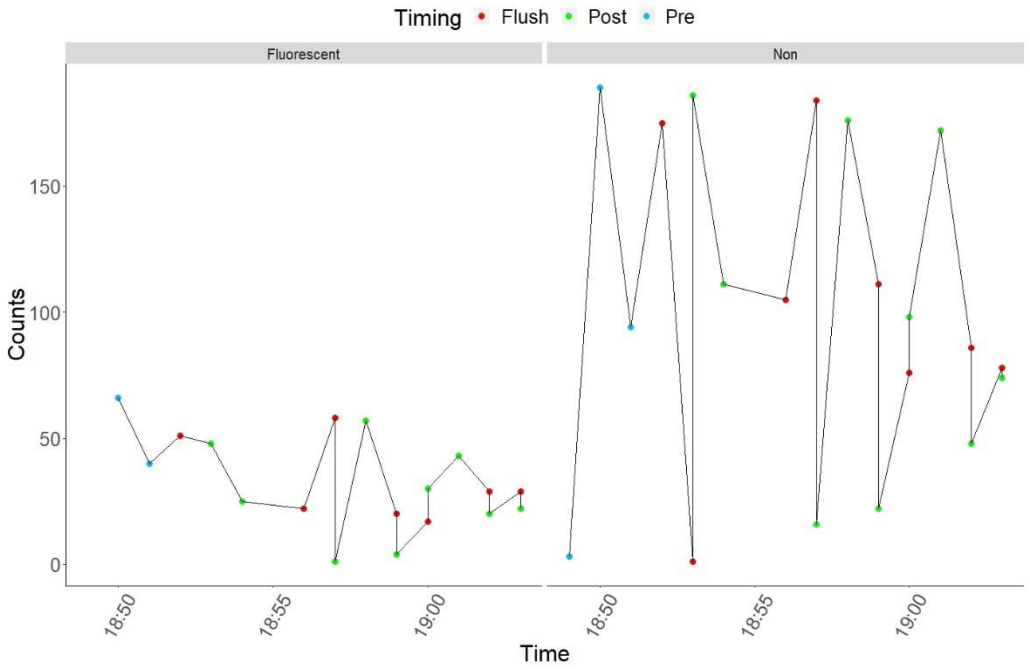

Figure 6.35 Time series of fluorescent and total particle counts for time period when lavatory was used for empty flushes. Fluorescent (left), and non-fluorescent (right). Timing during experiment coloured pre (blue), flush (red) and post (green).

From Figure 6.35, it can be seen there was no change in either fluorescent (left panel) or total counts (right panel) following flushing. Further particle characteristics are analysed below.

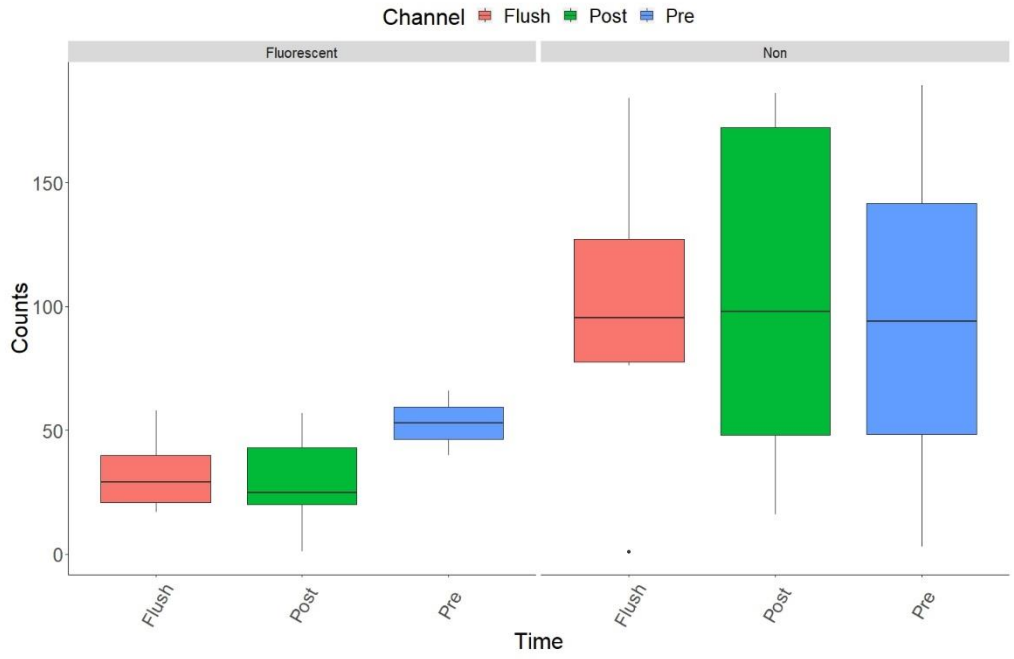

Figure 6.36 Boxplots of fluorescent (left panel) and total particle counts (right panel) per minute for time periods during empty flushing. Colour by timing during experiment pre (blue), flush (red) and post (green).

Both the mean fluorescent and total particle counts did not differ significantly between any time periods (Figure 6.36, Table 6.33).

Table 6.33 Mean ± sd for fluorescent and total particle counts with calculated p-value between flush and post-periods.

Particle Type	Timing	Mean ± sd	P-value
Fluorescent	Post	27.77 ± 18.98	0.75
	Flush	32.3 ± 15.93	
	Pre	53.0 ± 18.38	0.19 (flush) 0.23 (post)
Non-fluorescent	Post	100.33 ± 66.14	0.94
	Flush	102.0 ± 58.37	
	Pre	95.33 93.01	0.9 (flush) 0.8 (post)

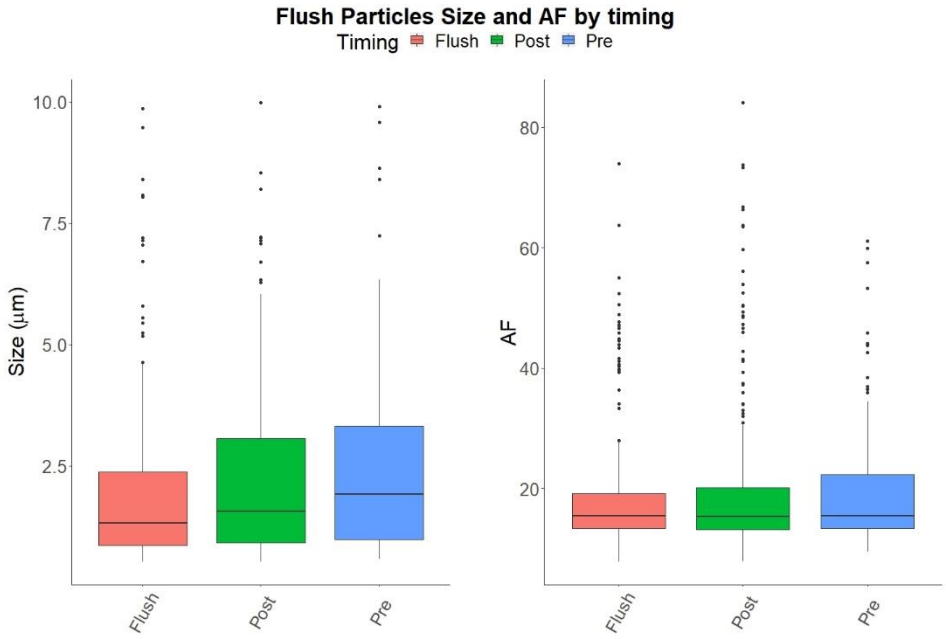

Figure 6.37 Boxplots of fluorescent particle size (left panel) and shape, AF (right panel) for time periods when the lavatory was used for artificial defaecation during different times. Flush (red), post-flush (green) and pre (blue).

The fluorescent particle size (µm) and sphericity index (AF) did not show any significant difference between any period (P>0.01), Figure 6.37 and Table 6.34

Table 6.34 Mean ± sd for fluorescent particle size (µm) and shape with calculated p-value between timings.

Timing	**Mean ± sd**	
	Size (µm)	AF
Pre	1.87 ± 0.56	19.79 ± 2.35
Flush	1.68 ± 0.83	19.16 ± 4.14
Post	1.88 ± 0.78	20.45 ± 4.74

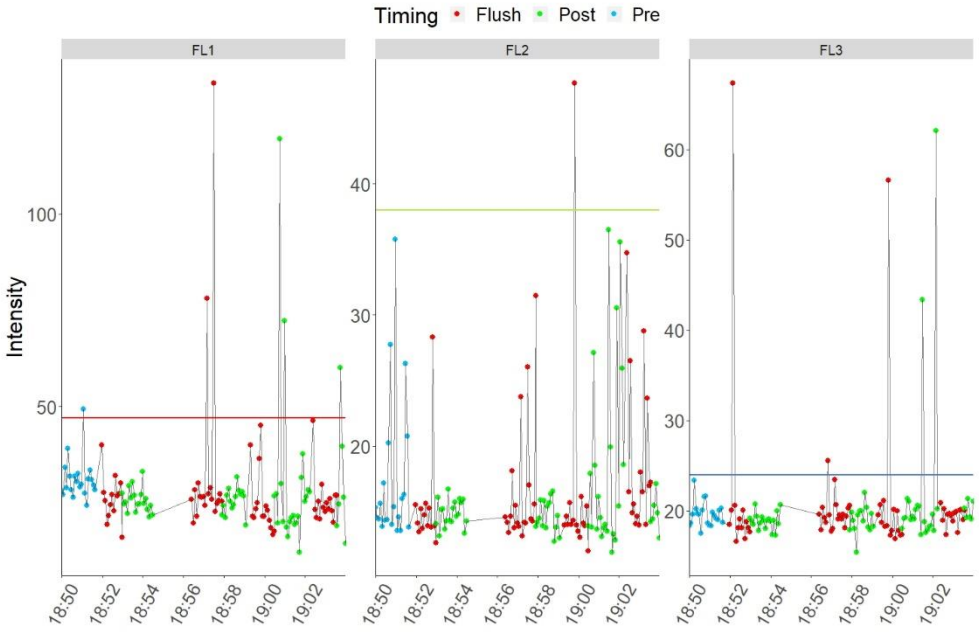

Figure 6.38 Time series of fluorescent channel intensities for time period when lavatory was used for empty flushing. Timing marked by coloured points; Flush (red), post-flush (green) and pre (blue). Each panel represents a fluorescent channel; (left) FL1, (middle) FL2 and (right) FL3.

Ten-second mean fluorescent intensities were observed (Figure 6.38). Flushing caused fluctuations in the FL1 channel, and the highest intensities were observed in the FL2 and FL3 channels during the flush period, Figure 6.38.

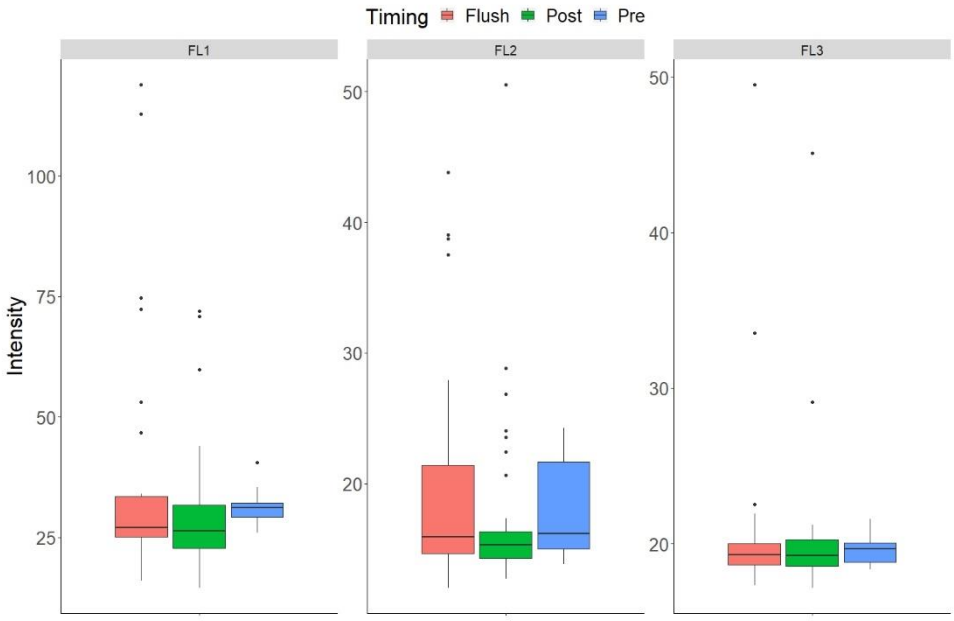

Figure 6.39 Boxplots of fluorescent channel intensities for time periods when the lavatory was used for empty flushing. Colour by timing during experiments are pre (blue), flush (red) and post (green). Each panel is split into 3 sets of boxplots each representing a fluorescent channel; (left) FL1, (middle) FL2 and (right) FL3.

Mean FL1 channel was significantly larger for the pre period compared to the flush- and post-flush periods ($P<0.01$). A significantly higher FL1 mean was observed during flush than the post-flush period. No other channel showed any significant difference between periods. Although the background has the highest mean fluorescent intensity, from Figure 6.38 and Table 6.35 it is clear that particles fluorescing at higher intensity values for FL1 occurred in the flush phase.

Table 6.35 Mean ± sd for fluorescent channel intensity with calculated p-value between timings on lower half.

Timing	Channel		
	Mean intensity ± sd		
	FL1	FL2	FL3
Pre	31.01 ± 4.2	17.22 ± 4.11	19.59 ± 1.01
Flush	27.90 ± 10.68	16.73 ± 4.60	20.55 ± 5.88
Post	27.25 ± 7.05	16.78 ± 4.44	20.61 ± 6.92
Channel	P-values		
	Flush vs. Pre	Post vs. Flush	Pre vs. Post
FL1	<0.01	0.5	<0.01
FL2	0.4	0.4	0.9
FL3	0.5	0.4	0.9

Following the flush analysis, some particles showed high mean fluorescence, even with an empty toilet. (Figure 6.38). Previous research into the dissemination from flushing has revealed that bioaerosol production can occur through multiple flushes (Aithinne et al., 2019, Barker and Jones, 2005). This may be the case here, the toilet was in regular use all day, although no log was kept, and it was not cleaned prior to use so it could be assumed that some residue from occupants throughout the day may have seeded the bowl. These results also suggest that even flushing an empty toilet may result in bioaerosol production.

6.5 Conclusion

The WIBS is able to detect reproducible changes in the numbers and characteristics of airborne particles associated with various phases of toilet use, and changes resulting from interventions such as putting the lid down. The results presented here suggest that placing the lid down before flushing the toilet reduces the number of fluorescent airborne particles produced in the lavatory by flushing following defaecation, in line with previous publications using bacterial culture to detect aerosol spread from flushing (Figure 6.8) (Barker and Jones, 2005, Best et al., 2012). Intriguingly, however, placing the lid down after defaecation activity also significantly increases particle size, shape, particle fluorescent intensity and the residency time of defaecation-related particles in the air. It is recognised that putting the lid down

reduces but does not abolish aerosol spread, and the route of spread in this case is believed to be the gap between the seat and the toilet bowl (Best et al., 2012). However, a change in character of flush-associated particles resulting from putting the lid down has not been reported before.

The ultimate force producing aerosolisation from a toilet flush is the energy expended during the flushing process. Different studies (Johnson et al., 2013, Bound and Atkinson, 1966) support the idea that flush droplet production increases with increased flush energy. Flush energy cannot be measured directly, it is just a label for the extent of agitation the water undergoes throughout the flush. Aeration by mechanical agitation at wastewater plants has been shown to produce large numbers of bioaerosols (Wang et al., 2019, Gregov et al., 2008). Bacteria such as *Klebsiella pneumoniae*, *Mycobacterium tuberculosis*, and *Legionella* spp. have been isolated from the air surrounding aeration basins (Chang and Hung, 2012). Han *et al.* reported that common potential pathogens were detected in bioaerosols in sewage sludge dewatering houses throughout China, such as *Aeromonas caviae, Flavobacterium* sp., and *Staphylococcus lentus (Han et al., 2018)*. Wang et al. found that levels of airborne intestinal bacteria (including *Eubacterium, Faecalibacterium*, and *Lachnospiraceae*) increased from 78 ± 6 CFU/m^3 to 359 ± 18 CFU/m^3 as aeration rate increased. The study by Wang *et al.* produced an interesting observation, using an Anderson six stage sampler. They reported that most airborne bacteria were attached to particles < 4.7 µm at an aeration rate of 0.3 m^3/h, and when increased to 1.2 m^3/h, they were found attached to particles > 4.7 µm (Wang et al., 2019). Thus, it seems plausible that similar increasing particle size effects would occur with any increased flush agitation, albeit on a much smaller scale. This would suggest that if the flush energy were decreased, turbulence would decrease correspondingly, and fewer biological particles would become aerosolised.

There are known differences in aerosolisation capacity associated with different toilet designs. The wash-down toilets in common use in Ireland and the UK release the flush water from the toilet rim where it flows down the bowl walls and washes the waste into the u-bend exit trap way in a turbulent flow (Figure 6.40). This is a “pushing”

action only and does not evacuate the bowl. Instead the waste is simply “pushed” by free flowing turbulent water out of the trapway (Blair, 2000). Siphonic toilets, commonly used in the USA, flush by releasing a submerged jet of water that propels the waste into the trap way to initiate a siphon action that clears the waste, essentially this “pulls” material out of the bowl while the water entering the bowl from the tank through the jet and the rim “pushes” material out. This simultaneous pushing and pulling completely clears the bowl during every flush. (Figure 6.40).

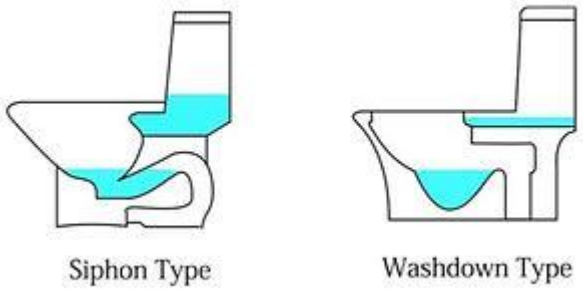

Figure 6.40 Siphonic toilet design vs. washdown type (Binawarehouse, 2019).

Bound and Atkinson *et al.* found that siphonic toilets produce approximately only $1/14^{th}$ as much bioaerosol as the wash-down design for the same flush volume (Bound and Atkinson, 1966).

The author proposes a fluid mechanics-based acoustic turbulence hypothesis to account for the changes seen in flush-related airborne particles on putting the lid down. When significant numbers of particles are present in a fluid, they tend to collide with one another, because of particle movement caused by a mixture of Brownian motion of the particles and turbulent motion of the fluid in which they are confined. If, upon colliding, the particles stick together, the process is termed agglomeration or coagulation and this can lead to a shift in the particle size distribution, the speed of which depends upon the collision rate and the portion of the particles which stick together (Reeks, 2014). Turbulence caused by the toilet flush would induce particle collisions, however, this would be the case whether the lid is up or down.

To account for the results with the lid down, it can be hypothesized that leaving the lid down must somehow promote particle collisions, which in turn leads to the formation of particle clusters. Collisions may be between bacterial aerosols and/or bacterial aerosols and water aerosols; all would increase particle size. The author proposes that the mechanism by which leaving the lid down produces more collisions than when the lid is up may be the phenomenon of acoustic agglomeration. At high acoustic intensities, acoustically induced turbulence promotes particle collisions (Chou et al., 1980, Lee et al., 1981, Tiwary et al., 1984). Orthokinetic and hydrodynamic interactions are the leading mechanisms contributing to this acoustic turbulence (Riera et al., 2015) (Figure 6.41). An orthokinetic interaction mechanism (Brandt and Hiedemann, 1936) refers to particle collisions that occur between two or more suspended particles of dissimilar sizes when they are situated within a distance almost equal to the displacement amplitude of the sound field in the suspended medium, and their relative motion is substantially parallel to the direction of vibration (Riera et al., 2015, Ng et al., 2017). An acoustic field consists of incident waves that are emitted directly from sound sources and scattered waves due to the occurrence of solid particles. Due to differential inertial and fluid forces, particles become entrained at different phases in the oscillations of an acoustic field (Temkin and Leung, 1976). Smaller particles tend to follow acoustic vibrations closely, while larger particles, with larger inertia do not tend to move with the acoustic waves. Consequently, the relative motion between the different sized particles result in collisions, as per Figure 6.41. Particles of high density, large size or the use of high frequency acoustic waves result in less entrainment (Hoffmann and Koopmann, 1996, Gucker and Doyle, 1956).

It is known some particles initially separated by a distance much larger than the acoustic displacement, and particles of a similar size, also agglomerate in an acoustic field. This may be explained by hydrodynamic forces acting on the particles (Zheng and Apfel, 1995). Here the acoustic field generates hydrodynamic forces inducing particles to collide from separation distances much larger than their respective acoustic displacement. These forces particularly govern the agglomeration in monodisperse suspensions (Riera et al., 2015, Ng et al., 2017).

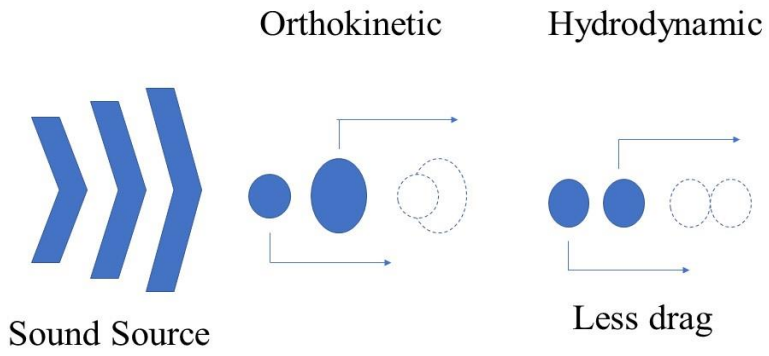

Figure 6.41 Orthokinetic and hydrodynamic mechanism diagram. The relative motions between the different sized particles results in agglomeration (collisions).

The rate of both orthokinetic and hydrodynamic agglomerations are dependent on acoustic intensity (Caperan et al., 1995). Agglomeration efficiency can be elevated by nearly 50% with an increase in sound pressure level (SPL) from 120 dB to 157 dB (Yan et al., 2016). Although agglomeration is favoured by high levels of SPL, it has been shown that particle diameter can increase by one order of magnitude at low SPL, 100-120 dB (Volk and Moroz, 1976). Experiments with monodispersed oil particulates found a mean size increase from 1.5 µm to 4.5 µm with SPL of 140-160 dB (Boulaud et al., 1984). The SPL from flushing of office toilets such as the one used for the current study has been found to range from 60 – 96 dB (Stewart, 2011). The author suggests that when the lid is positioned down it acts as a sound reverberation source by rebounding the SPL produced from flushing, thus increasing the particle collisions within the toilet bowl. Similarly, if the lid acts as a sound source the acoustic waves produced may take the particles from inside the bowl through the gap between the seat and bowl aerosolising them into the air, thus increasing their residency time through the acoustic waves, Figure 6.42.

Another factor that may aid this agglomeration of particles is surface tension between aqueous droplets containing faecal matter. Wetting particles (dust, smoke and fog particles) with fine water or oil spray causes aggregates to be held strongly together by surface tension (Clair, 1949). This would suggest that as the water and faecal mixture inside the bowl is aerosolised, any aqueous agglomerations may hold together more strongly, thus increasing the bioaerosol particle size.

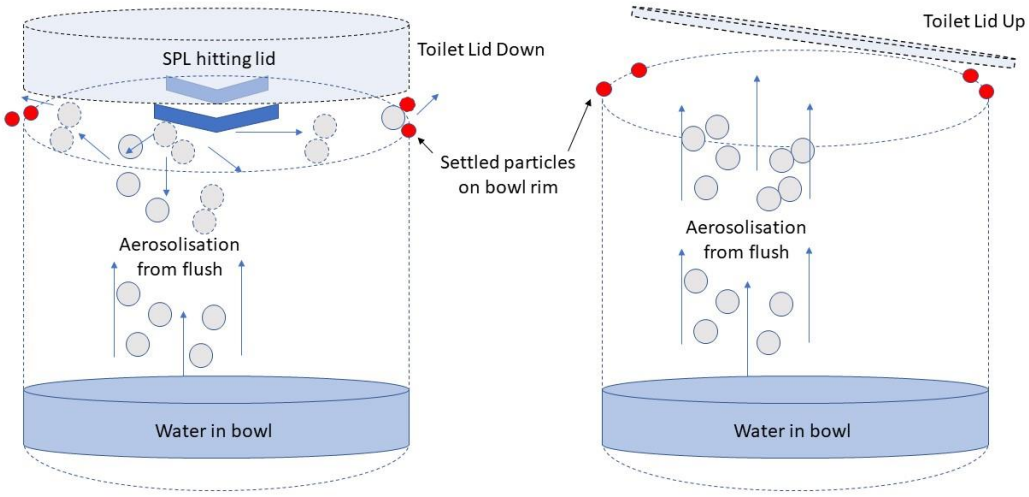

Figure 6.42 Proposed acoustic agglomeration mechanism occurring while the lid is positioned down vs up. Lid positioned down (left) particles that are aerosolised through flush turbulence are then compelled to agglomerate together by the SPL hitting the lid. Particles are then forced out the narrow gap between the toilet rim and seat where they may potentially re-aerosolise settled particles. Positioning the toilet lid up will cause an initial burst of particles which quickly subsides without potentially aerosolising the settled particles on the rim.

Using the annotation system by Perring *et al.* (Perring, 2016), described in section 1.3.3, the fluorescent particle properties from toilet related activities aerosols, section 6.9, exhibit high quantity of particles as type A. All the aerosolised bacterial cultures Perring *et al.* assembled with common fluorescence patterns were below an equivalent size of 1.5 µm. Excluding the spore forming *Bacillus subtilis*, the bacterial bioaerosols were dominated by a single fluorescent category A (Perring et al., 2015). The majority

of the particles categorised by the WIBS in section 6.9 were fluorescent type A, although they were larger in size than the bacteria reported by Perring *et al.* , however, they sampled an aerosol that was desiccated after production, likely to be composed of single bacteria, whereas the bacteria in the current study could be agglomerated as described above.

To control variables of the flush process seen in the observational study, experiments with artificial faeces containing yeast cells and seeded with food bacteria (*Lactobacillus sp*) were observed in the same toilet with the lid up. Fluorescent particle counts did not show any significant difference between each period (Figure 6.29), however, particle intensities showed large increases during and post flush. Flushing gave rise to large fluctuations in fluorescent intensities in FL1, and relatively lower intensity in the FL2 and FL3 channels, with the mean fluorescent intensities significantly larger in the FL1 channel for flush and post periods compared to the background (Table 6.31). The categorised aerosols for the artificial faeces were similar to those collected during the observational study, with the ~70-100% of fluorescent particles during the flush and post phases exhibiting at fluorescent type A, and a relatively smaller quantity of ~20% as B during the post phase (Table 6.32). This suggests that simulated faeces could be effective if used in conjunction with WIBS analysis to assess the effect of toilet design on flush aerosol spread.

Flushing the toilet while empty also showed no increases in fluorescent intensity during flushing or periods around flushing when compared to the background (Table 6.33), however Figure 6.38 shows that during the flush and periods around flushing variation in fluorescent intensity is observed. As the toilet was not specially cleaned before observations were made, and had been in regular use all day, the findings of intermittent highly fluorescent particles observed during and after the flush may represent dispersal of bacterial biofilms resulting from earlier contamination. As recently reported, bioaerosol spread of pathogenic bacteria from faeces can occur during multiple flushes after original contamination (Barker and Jones, 2005, Aithinne et al., 2019)

These results may have significant implication for public access environments e.g. hospitals, where persons shedding gastrointestinal pathogens in stool may contaminate toilets, especially communal toilets. There is scope for testing rational modifications in lid design and flush methodology that the author hypothesizes could reduce this risk. Lid design could easily be adjusted or modified to reduce reverberation from its surface. Sound absorbing materials with low density (e.g., polystyrene foam) are often used for sound proofing due to their effectiveness in attenuating acoustic energy. Recently water-stable cellulose fibre foams that can inhibit microbial growth have been developed (Ottenhall et al., 2018). Their antimicrobial properties have been evaluated with respect to both *E. coli* and and *A. brasiliensis*. The bacterial-reducing effect, bacterial-growth-inhibition and fungal resistance in the insulating materials was described in detail by Ottenhall *et al.* The low-density cellulose fibre foams gained antimicrobial properties by adding chitosan and citric acid to the fibre suspension during the foam-forming process (Ottenhall et al., 2018). A future WIBS study could assess bioaerosol-reducing potential of lining toilet lid covers with this antimicrobial and water-stable material. Another possibility is an existing lid alternative which adds seals between the lid and the bowl (Figure 6.43)

Figure 6.43 Croydex® Safeflush toilet seat (Croydex, 2020).

This is the Safeflush "zero tolerance toilet seat" by Croydex®. This toilet seat features a unique double seal, one seal between the seat and the toilet bowl and another between the seat and the lid. In theory this would prevent dissemination of flush-related bioaerosols. A Croydex® toilet seat model was purchased for this study but unfortunately time restrictions did not allow its analysis. Although the sealed seat may reduce aerosol dispersal, the durability of the seal to cleaning may be a problem i.e. would the use of cleaning products be detrimental to seal integrity.

Another interesting aspect of a future study incorporating WIBS data would be to revisit the 1960s experiments (Bound and Atkinson, 1966) suggesting less turbulent, and quieter siphonic toilet designs used in the USA to minimise the airborne spread of enteric bacteria from flushing compared with the wash-down toilets used in Ireland and the UK. This could be a significant international confounding factor in judging the effect of other interventions and policies in controlling the spread of *C. difficile* or carbapenemase producing Enterobacterales.

6.6 References

AITHINNE, K. A., COOPER, C. W., LYNCH, R. A. & JOHNSON, D. L. 2019. Toilet plume aerosol generation rate and environmental contamination following bowl water inoculation with Clostridium difficile spores. *American journal of infection control,* 47**,** 515-520.

AMOUREUX, L., BADOR, J., FARDEHEB, S., MABILLE, C., COUCHOT, C., MASSIP, C., SALIGNON, A.-L., BERLIE, G., VARIN, V. & NEUWIRTH, C. 2013. Detection of Achromobacter xylosoxidans in hospital, domestic, and outdoor environmental samples and comparison with human clinical isolates. *Appl. Environ. Microbiol.,* 79**,** 7142-7149.

ANAISSIE, E. J., PENZAK, S. R. & DIGNANI, M. C. 2002. The hospital water supply as a source of nosocomial infections: a plea for action. *Archives of internal medicine,* 162**,** 1483-1492.

BARKER, J. & BLOOMFIELD, S. 2000. Survival of Salmonella in bathrooms and toilets in domestic homes following salmonellosis. *Journal of Applied Microbiology,* 89**,** 137-144.

BARKER, J. & JONES, M. 2005. The potential spread of infection caused by aerosol contamination of surfaces after flushing a domestic toilet. *Journal of applied microbiology,* 99**,** 339-347.

BECK-SAGUÉ, C., DOOLEY, S. W., HUTTON, M. D., OTTEN, J., BREEDEN, A., CRAWFORD, J. T., PITCHENIK, A. E., WOODLEY, C., CAUTHEN, G. & JARVIS, W. R. 1992. Hospital outbreak of multidrug-resistant Mycobacterium tuberculosis infections: factors in transmission to staff and HIV-infected patients. *Jama,* 268**,** 1280-1286.

BEST, E., PARNELL, P., COUTURIER, J., BARBUT, F., LE BOZEC, A., ARNOLDO, L., MADIA, A., BRUSAFERRO, S. & WILCOX, M. 2018. Environmental contamination by bacteria in hospital washrooms according to hand-drying method: a multi-centre study. *Journal of Hospital Infection,* 100**,** 469-475.

BEST, E., PARNELL, P. & WILCOX, M. 2014. Microbiological comparison of hand-drying methods: the potential for contamination of the environment, user, and bystander. *Journal of Hospital Infection,* 88**,** 199-206.

BEST, E. & REDWAY, K. 2015. Comparison of different hand-drying methods: the potential for airborne microbe dispersal and contamination. *Journal of Hospital Infection,* 89**,** 215-217.

BEST, E., SANDOE, J. & WILCOX, M. 2012. Potential for aerosolization of Clostridium difficile after flushing toilets: the role of toilet lids in reducing environmental contamination risk. *Journal of Hospital Infection,* 80**,** 1-5.

BINAWAREHOUSE. 2019. *Siphonic & Washdown: Get to know these flushing systems* [Online]. Available: https://www.binawarehouse.com/single-post/2019/06/17/Siphonic-Washdown-Get-to-know-these-flushing-systems [Accessed 21/12/2019 2019].

BLAIR, M. 2000. *Ceramic water closets*, Osprey Publishing.

BOULAUD, D., FRAMBOURT, C., MADELAINE, G. & MALHERBE, C. 1984. Experimental study of the acoustic agglomeration and precipitation of an aerosol. *Journal of Aerosol Science,* 15**,** 247-252.

BOUND, W. H. & ATKINSON, R. I. 1966. Bacterial Aerosol from Water Closets. A Comparison of Two Types of Pan and Two Types of Coyer. *Lancet***,** 1369-70.
BRANDT, O. & HIEDEMANN, E. 1936. The aggregation of suspended particles in gases by sonic and supersonic waves. *Transactions of the Faraday society,* 32**,** 1101-1110.
BRASCHE, S. & BISCHOF, W. 2005. Daily time spent indoors in German homes–baseline data for the assessment of indoor exposure of German occupants. *International journal of hygiene and environmental health,* 208**,** 247-253.
CAPERAN, P., SOMERS, J., RICHTER, K. & FOURCAUDOT, S. 1995. Acoustic agglomeration of a glycol fog aerosol: influence of particle concentration and intensity of the sound field at two frequencies. *Journal of aerosol science,* 26**,** 595-612.
CHANG, C.-W. & HUNG, P.-Y. 2012. Evaluation of sampling techniques for detection and quantification of airborne legionellae at biological aeration basins and shower rooms. *Journal of aerosol science,* 48**,** 63-74.
CHOU, K., LEE, P. & SHAW, D. 1980. Acoustically induced turbulence and shock waves under a traveling-wave condition. *The Journal of the Acoustical Society of America,* 68**,** 1780-1789.
CLAIR, H. W. S. 1949. Agglomeration of smoke, fog, or dust particles by sonic waves. *Industrial & Engineering Chemistry,* 41**,** 2434-2438.
CROYDEX. 2020. *Safeflush toilet seat* [Online]. Available: https://www.croydex.com/products/toilet-seats-and-bath-panels/toilet-seats/white-toilet-seats/safeflush-toilet-seat/924 [Accessed 01/01/2020].
DARLOW, H. & BALE, W. 1959. Infective hazards of water-closets. *Lancet***,** 1196-200.
DE GIGLIO, O., NAPOLI, C., LOVERO, G., DIELLA, G., RUTIGLIANO, S., CAGGIANO, G. & MONTAGNA, M. T. 2015. Antibiotic susceptibility of Legionella pneumophila strains isolated from hospital water systems in Southern Italy. *Environmental research,* 142**,** 586-590.
DELCLOS, G. L., GIMENO, D., ARIF, A. A., BURAU, K. D., LUSK, C., STOCK, T., SYMANSKI, E., WHITEHEAD, L. W., ZOCK, J.-P. & BENAVIDES, F. G. 2007. Occupational risk factors and asthma among health care professionals. *American journal of respiratory and critical care medicine,* 175**,** 667-675.
DU PLOOY, W., HAY, L., KAHLER, C., SCHUTTE, P. & BRANDT, H. 1994. The dose-related hyper-and-hypokalaemic effects of salbutamol and its arrhythmogenic potential. *British journal of pharmacology,* 111**,** 73-76.
FALKINHAM III, J. O., HILBORN, E. D., ARDUINO, M. J., PRUDEN, A. & EDWARDS, M. A. 2015. Epidemiology and ecology of opportunistic premise plumbing pathogens: Legionella pneumophila, Mycobacterium avium, and Pseudomonas aeruginosa. *Environmental health perspectives,* 123**,** 749-758.
FENNELLY, M. J., SEWELL, G., PRENTICE, M. B., O'CONNOR, D. J. & SODEAU, J. R. 2017. The Use of Real-Time Fluorescence Instrumentation to Monitor Ambient Primary Biological Aerosol Particles (PBAP). *Atmosphere,* 9**,** 1.
FLORES, G. E., BATES, S. T., KNIGHTS, D., LAUBER, C. L., STOMBAUGH, J., KNIGHT, R. & FIERER, N. 2011. Microbial biogeography of public restroom surfaces. *PloS one,* 6**,** e28132.

GERBA, C. P., WALLIS, C. & MELNICK, J. L. 1975. Microbiological hazards of household toilets: droplet production and the fate of residual organisms. *Applied microbiology,* 30**,** 229-237.

GIANNINI, M. A., NANCE, D. & MCCULLERS, J. A. 2009. Are toilet seats a vector for transmission of methicillin-resistant Staphylococcus aureus? *American journal of infection control,* 37**,** 505-506.

GREGOV, G., VENGLOVSKI, J., VARGOVA, M., ONDRASOVVICOVA, O., ONDRASOVIC, O., SASÁKOVÁ, N., KUDRIKOVÁ, D. & LAKTIDOVI, K. 2008. Bioaerosols produced by wastewater treatment plant. *Folia Veterinaria,* 52**,** 59-61.

GUCKER, F. T. & DOYLE, G. J. 1956. The amplitude of vibration of aerosol droplets in a sonic field. *The Journal of Physical Chemistry,* 60**,** 989-996.

HAN, Y., WANG, Y., LI, L., XU, G., LIU, J. & YANG, K. 2018. Bacterial population and chemicals in bioaerosols from indoor environment: Sludge dewatering houses in nine municipal wastewater treatment plants. *Science of the Total Environment,* 618**,** 469-478.

HARDIN, B. D., KELMAN, B. J. & SAXON, A. 2003. Adverse human health effects associated with molds in the indoor environment. *Journal of occupational and environmental medicine/American College of Occupational and Environmental Medicine,* 45**,** 470-478.

HEALY, D. A., O'CONNOR, D. J. & SODEAU, J. R. 2012. Measurement of the particle counting efficiency of the "Waveband Integrated Bioaerosol Sensor" model number 4 (WIBS-4). *Journal of Aerosol Science,* 47**,** 94-99.

HOFFMANN, T. L. & KOOPMANN, G. H. 1996. Visualization of acoustic particle interaction and agglomeration: Theory and experiments. *The Journal of the Acoustical Society of America,* 99**,** 2130-2141.

HUNG, C. H., CHU, D. M., WANG, C. L. & YANG, K. D. 1999. Hypokalemia and salbutamol therapy in asthma. *Pediatric pulmonology,* 27**,** 27-31.

HUSMAN, T. 1996. Health effects of indoor-air microorganisms. *Scandinavian journal of work, environment & health***,** 5-13.

JESSEN, C. 1955. Airborne microorganisms: occurrance and control. *Copenhagen: GEC Gad Forlag*.

JOHNSON, D., LYNCH, R., MARSHALL, C., MEAD, K. & HIRST, D. 2013. Aerosol generation by modern flush toilets. *Aerosol Science and Technology,* 47**,** 1047-1057.

KAYE, P. H., STANLEY, W. R. & FOOT, E. V. J. 2014. *Fluid-Borne Particle Detector*. US 13/957,655.

KIMMITT, P. & REDWAY, K. 2016. Evaluation of the potential for virus dispersal during hand drying: a comparison of three methods. *Journal of applied microbiology,* 120**,** 478-486.

LEE, P., CHENG, M. & SHAW, D. 1981. Acoustic and hydrodynamic turbulence-turbulence interaction and its influence on acoustic particulate agglomeration. *NASA STI/Recon Technical Report N,* 82.

MARGAS, E., MAGUIRE, E., BERLAND, C., WELANDER, F. & HOLAH, J. 2013. Assessment of the environmental microbiological cross contamination following hand drying with paper hand towels or an air blade dryer. *Journal of applied microbiology,* 115**,** 572-582.

MCDONALD, L. C., GERDING, D. N., JOHNSON, S., BAKKEN, J. S., CARROLL, K. C., COFFIN, S. E., DUBBERKE, E. R., GAREY, K. W., GOULD, C. V. & KELLY, C. 2018. Clinical practice guidelines for Clostridium difficile infection in adults and children: 2017 update by the Infectious Diseases Society of America (IDSA) and Society for Healthcare Epidemiology of America (SHEA). *Clinical infectious diseases,* 66**,** e1-e48.

MCGRATH, J. A., O'SULLIVAN, A., BENNETT, G., O'TOOLE, C., JOYCE, M., BYRNE, M. A. & MACLOUGHLIN, R. 2019. Investigation of the quantity of exhaled aerosols released into the environment during nebulisation. *Pharmaceutics,* 11**,** 75.

MORAWSKA, L. 2006. Droplet fate in indoor environments, or can we prevent the spread of infection? *Indoor air,* 16**,** 335-347.

MORAWSKA, L., AFSHARI, A., BAE, G., BUONANNO, G., CHAO, C. Y. H., HÄNNINEN, O., HOFMANN, W., ISAXON, C., JAYARATNE, E. R. & PASANEN, P. 2013. Indoor aerosols: from personal exposure to risk assessment. *Indoor Air,* 23**,** 462-487.

NEWSOM, S. 1972. Microbiology of hospital toilets. *The Lancet,* 300**,** 700-703.

NG, B. F., XIONG, J. W. & WAN, M. P. 2017. Application of acoustic agglomeration to enhance air filtration efficiency in air-conditioning and mechanical ventilation (ACMV) systems. *PloS one,* 12**,** e0178851.

O'CONNOR, D. J., HEALY, D. A. & SODEAU, J. R. 2013. The on-line detection of biological particle emissions from selected agricultural materials using the WIBS-4 (Waveband Integrated Bioaerosol Sensor) technique. *Atmospheric environment,* 80**,** 415-425.

ORGANIZATION, W. H. 2017. Guidelines for the prevention and control of carbapenem-resistant Enterobacteriaceae, Acinetobacter baumannii and Pseudomonas aeruginosa in health care facilities.

OTTENHALL, A., SEPPÄNEN, T. & EK, M. 2018. Water-stable cellulose fiber foam with antimicrobial properties for bio based low-density materials. *Cellulose,* 25**,** 2599-2613.

PAGNIER, I., VALLES, C., RAOULT, D. & LA SCOLA, B. 2015. Isolation of Vermamoeba vermiformis and associated bacteria in hospital water. *Microbial pathogenesis,* 80**,** 14-20.

PENN, R., WARD, B. J., STRANDE, L. & MAURER, M. 2018. Review of synthetic human faeces and faecal sludge for sanitation and wastewater research. *Water research,* 132**,** 222-240.

PEREIRA, M. L., KNIBBS, L. D., HE, C., GRZYBOWSKI, P., JOHNSON, G. R., HUFFMAN, J. A., BELL, S. C., WAINWRIGHT, C. E., MATTE, D. L. & DOMINSKI, F. H. 2017. Sources and dynamics of fluorescent particles in hospitals. *Indoor Air*.

PERRING, A. E. 2016. Chamber catalogues of optical and fluorescent signatures distinguish bioaerosol classes. *Atmospheric Measurement Techniques,* 9**,** 3283.

REEKS, M. W. Transport, mixing and agglomeration of particles in turbulent flows. Journal of Physics: Conference Series, 2014. IOP Publishing, 012003.

RIERA, E., GONZÁLEZ-GOMEZ, I., RODRÍGUEZ, G. & GALLEGO-JUÁREZ, J. 2015. Ultrasonic agglomeration and preconditioning of aerosol particles for environmental and other applications. *Power Ultrasonics.* Elsevier.

SAVAGE, N. J., KRENTZ, C. E., KÖNEMANN, T., HAN, T. T., MAINELIS, G., PÖHLKER, C. & HUFFMAN, J. A. 2017. Systematic characterization and fluorescence threshold strategies for the wideband integrated bioaerosol sensor (WIBS) using size-resolved biological and interfering particles. *Atmospheric Measurement Techniques,* 10**,** 4279-4302.

SHINN, E. A., GRIFFIN, D. W. & SEBA, D. B. 2003. Atmospheric transport of mold spores in clouds of desert dust. *Archives of Environmental & Occupational Health,* 58**,** 498.

SMISMANS, A., HO, E., DANIELS, D., OMBELET, S., MELLAERTS, B., OBBELS, D., VALGAEREN, H., GOOVAERTS, A., HUYBRECHTS, E. & MONTAG, I. 2019. New environmental reservoir of CPE in hospitals. *The Lancet Infectious Diseases,* 19**,** 580-581.

STEWART, N. D. 2011. An experience reducing toilet flushing noise reaching adjacent offices. *The Journal of the Acoustical Society of America,* 129**,** 2605-2605.

TEMKIN, S. & LEUNG, C.-M. 1976. On the velocity of a rigid sphere in a sound wave. *Journal of sound and vibration,* 49**,** 75-92.

TIWARY, R., REETHOF, G. & MCDANIEL, O. H. 1984. Acoustically generated turbulence and its effect on acoustic agglomeration. *The Journal of the Acoustical Society of America,* 76**,** 841-849.

TRAUTMANN, M., MICHALSKY, T., WIEDECK, H., RADOSAVLJEVIC, V. & RUHNKE, M. 2001. Tap Water Colonization With Psmdomonas aeruginosa in a Surgical Intensive Care Unit (ICU) and Relation to Psmdomonas Infections of ICU Patients. *Infection Control & Hospital Epidemiology,* 22**,** 49-52.

VARIA, M., WILSON, S., SARWAL, S., MCGEER, A., GOURNIS, E. & GALANIS, E. 2003. Investigation of a nosocomial outbreak of severe acute respiratory syndrome (SARS) in Toronto, Canada. *Canadian Medical Association Journal,* 169**,** 285-292.

VOLK, M. & MOROZ, W. J. 1976. Sonic agglomeration of aerosol particles. *Water, Air, and Soil Pollution,* 5**,** 319-334.

VON REYN, C. F., MARLOW, J., ARBEIT, R., BARBER, T. & FALKINHAM, J. 1994. Persistent colonisation of potable water as a source of Mycobacterium avium infection in AIDS. *The Lancet,* 343**,** 1137-1141.

WANG, Y., LI, L., XIONG, R., GUO, X. & LIU, J. 2019. Effects of aeration on microbes and intestinal bacteria in bioaerosols from the BRT of an indoor wastewater treatment facility. *Science of the total environment,* 648**,** 1453-1461.

WEBER, D. J., RUTALA, W. A., BLANCHET, C. N., JORDAN, M. & GERGEN, M. F. 1999. Faucet aerators: a source of patient colonization with Stenotrophomonas maltophilia. *American journal of infection control,* 27**,** 59-63.

WEINSTEIN, R. A., SAID, M. A., PERL, T. M. & SEARS, C. L. 2008. Gastrointestinal flu: norovirus in health care and long-term care facilities. *Clinical infectious diseases,* 47**,** 1202-1208.

WILCOX, M., BEST, E. & PARNELL, P. 2017. Pilot study to determine whether microbial contamination levels in hospital washrooms are associated with hand-drying method. *Journal of Hospital Infection,* 97**,** 201-203.

WITTGEN, B. P., KUNST, P. W., PERKINS, W. R., LEE, J. K. & POSTMUS, P. E. 2006. Assessing a system to capture stray aerosol during inhalation of nebulized liposomal cisplatin. *Journal of aerosol medicine,* 19**,** 385-391.

WITTGEN, B. P., KUNST, P. W., VAN DER BORN, K., VAN WIJK, A. W., PERKINS, W., PILKIEWICZ, F. G., PEREZ-SOLER, R., NICHOLSON, S., PETERS, G. J. & POSTMUS, P. E. 2007. Phase I study of aerosolized SLIT cisplatin in the treatment of patients with carcinoma of the lung. *Clinical Cancer Research,* 13**,** 2414-2421.

YAHYA, M. T., CASSELLS, J. M., STRAUB, T. M. & GERBA, C. P. 1992. Reduction of microbial aerosols by automatic toilet bowl cleaners. *Journal of Environmental Health***,** 32-34.

YAN, J., CHEN, L. & LI, Z. 2016. Removal of fine particles from coal combustion in the combined effect of acoustic agglomeration and seed droplets with wetting agent. *Fuel,* 165**,** 316-323.

ZHENG, X. & APFEL, R. E. 1995. Acoustic interaction forces between two fluid spheres in an acoustic field. *The Journal of the Acoustical Society of America,* 97**,** 2218-2226.

Chapter 7
Conclusion

Direct, continuous bioaerosol sampling is an established technology utilised for external ambient air characterisation in widely differing environments (Chapter 1, Table 1.9 and Table 1.10). Portable instruments such as the WIBS combine laser scattering and shape detection with signals of particle viability (fluorescence from amino acids and NAD(P)H) to characterise bioaerosols (Chapter 1). The surge in popularity of these instruments is understandable as they possess superior time resolution (millisecond) and continuous real-time readouts, non-destructive technique and no extensive training required for operators to extract data, compared to traditional techniques which are hampered by confined sampling times with processing required over days and weeks to yield data. Although we spend upwards of 80% of life indoors (Brasche and Bischof, 2005) these instruments have not been effectively utilised to monitor indoor air with little research reported on their use in the indoor environment (Pereira et al., 2017). The healthcare environment is a specific indoor environment where limited conventional air quality measurements have traditionally been employed for areas such as operating theatres. Hospital design and practice with regard to airborne spread of infection is similarly based on historical epidemiology and conventional cultures. The overall aim of this thesis was to apply novel technology for the continuous measurement of bioaerosols and other environmental variables to characterise different healthcare environments. The effect of different environmental factors and interventions on the measured variables was then assessed, with a view to defining these effects objectively.

The WIBS-4A instrument, a small consumer air quality monitor called AirVisual Pro (IQAir, Beijing) and an infra-red footfall counter, were deployed in parallel in a 4-bedded bay on the respiratory ward at Cork University Hospital (CUH) (Chapter 3). This to the author's knowledge is the first documented research describing the

simultaneous use of a footfall counter and real-time bioaerosol monitoring in any setting. The patients on the respiratory ward have a range of respiratory illnesses. Environmental airborne bacteria and fungi can exacerbate respiratory diseases like rhinitis, asthma, and pneumonia, (Hardin et al., 2003, Husman, 1996, Shinn et al., 2003), and potential cross infection from respiratory infection can occur. Good air quality is therefore imperative for these patients. Prior to the campaign, as part of refurbishment to incorporate an adult Cystic Fibrosis Unit, the respiratory ward was fitted with wall-mounted plasma disinfection units which had not been activated. The opportunity of evaluating the effect of these units on bioaerosol concentrations using the WIBS in conjunction with conventional air sampling was incorporated into this study.

Initial raw ward data from the WIBS-4A showed large minute-to-minute variations in total and fluorescent particle counts. When averaged over 1, 30 or 60 minutes, a day or more of observations these resolved into particle peaks occurring on a timescale of up to an hour or more. Multiple days of observations (a total of 4 weeks) when plotted diurnally showed four daily fluorescent particle peaks in the daytime (Chapter 3, Figure 3.12). Compared to nocturnal baseline concentrations these peaks represented a 2-300-fold increase in fluorescent particle concentrations. These peaks were also detected in the AirVisual Pro data. The ward events best corresponding to the diurnal peaks were time periods of nebulised drug administration, which have been reported as a source of fluorescent particles (Chapter 3, Figure 3.12). In order to remove this overwhelming influence on particle data, air chamber experiments were necessary. Chapter 4 describes how the fluorescent signatures of the two nebulised drugs used on the ward were obtained using the WIBS-4A threshold, based on the fluorescent signature of nebulised drugs was used to process the ward counts, producing reduced particle numbers defined as fluorescent filtered counts.

Footfall observations (Chapter 3) were extremely consistent over the four-week campaign, with no statistical difference reported between days for any half hour period (Chapter 3, section 3.8.1). This confirmed that ward activity followed a very regular predictable timetable. Highest footfall was recorded during the time period between

07:30-08:00 (this represented night-to-day staff changeover), coinciding with the period of highest fluorescent filtered particle concentrations (Chapter 3, Figure 3.24). This suggested that footfall, or events associated with footfall, were the major bioaerosol generators on the ward apart from nebulised drugs. However, overall footfall counts throughout the day did not show high correlation with the fluorescent filtered counts (Chapter 3, Figure 3.28), suggesting that not all high footfall events resulted in bioaerosol generation.

A significant ~28% reduction in WIBS-measured total and fluorescent filtered particle counts was detected on activating plasma disinfection (Chapter 3, section 3.7). This represents all WIBS time points (one, thirty and sixty-minute time intervals) over the two control weeks and the two plasma disinfection weeks. Interestingly, conventional air sampling at two time points every weekday for four weeks revealed no significant difference in microbial colony counts between the plasma disinfection period and the control period. This could mean that the fluorescent filtered counts were still reflecting some nebulised drugs which were affected by the plasma disinfection (for example by evaporation), rather than representing living organisms. However, as described below in more detail, application of the fluorescent drug threshold does not affect numbers of experimentally aerosolised bacteria detected by WIBS (Chapter 4). Also, on extracting the WIBS-measured fluorescent filtered particle counts over 48 half hour periods corresponding to the conventional sampling times, although 46 recorded a reduction during the plasma disinfection phase, only one half-hour time period reported a significant decrease. This suggests that the high variability of airborne particle numbers over time revealed by fluorescent filtered particle WIBS counts affects the power of the relatively small number of observations possible with conventional cultures to detect real changes in airborne particle numbers. Over the 4-weeks the WIBS observed a high minute-to-minute standard deviation, $\pm$ 1.55 $\times 10^7$ particles / m^3 around a mean of 1.48 $\times 10^7$ particles / m^3. Conventional cultures with the MAS-100 exhibited a relatively lower standard deviation of $\pm$ 341 CFU/ m^3 around a mean of 542 CFU/ m^3 (Chapter 3, Table 3.1 and 3.7). This high variability is easily encompassed by the WIBS but would require multiple air samples per hour with conventional air sampling, and still the extent of the variability may not be accurately

picked up. The low time resolution of conventional air sampling cannot identify high variability. This along with the number of sampling times, highlights inadequacies associated with conventional air sampling in analysing interventions such as air disinfection / cleaning units.

No specific microbial air quality standards for general wards are available, however in comparison to microbial data reported from other hospitals, the conventional counts on the respiratory ward did not suggest it as an outlier (Chapter 3, Figure 3.35). The lack of generally accepted standards for hospital air quality, apart from conventional and ultra-clean operating theatres, is arguably another reflection of the insensitivity and slowness of conventional cultures. In Chapter 4, WIBS data from previous air chamber work with nebulised bacterial suspensions and filtered fluorescent particle numbers from this thesis were used to propose a standard applicable to the respiratory ward.

Air chamber experiments in Chapter 4 detail how the interfering fluorescent drug signals were removed from the WIBS datasets. Drug aerosols exhibited high fluorescence in the FL1 channel, presumably due to the known salbutamol excitation maximum of 278 nm and emission maximum fluorescence at 306 nm. Previous WIBS campaigns have used an instrumental threshold, calculated from the mean + 3σ or mean + 9σ of fluorescent signals recorded inside the instrument (Savage et al., 2017). Instead of using the instrument threshold, the author devised a new threshold using fluorescent data from nebulised aerosols (Chapter 4, Table 4.11). Using the laboratory developed threshold in a controlled setting, a ~95% decrease in aerosolised nebulised drug particle numbers (fluorescent filtered particles) was observed compared to the standard threshold used. Applying the nebulised drug fluorescence thresholds to previously gathered aqueous bacterial aerosol WIBS data produced no significant difference in the classification of bacterial aerosols as fluorescent compared with the raw counts (Chapter 4, Table 4.15).

Previous WIBS studies have only described an instrumental threshold and have not explored the use of observations of the interferants themselves to remove false-

positive aerosols. Chapter 4 has shown that specific interferants can be removed from datasets using their own fluorescent signatures, and, importantly, without loss of bioaerosol data. This chapter also documented the characterisation of aerosolised bacteria. Recently Perring *et al.* provided an extensive characterisation of bioaerosols and provided a new annotation system to categorise bioaerosols allowing for a greater degree of particle classification (Perring, 2016). Although Perring *et al.* categorised a large number of different bioaerosols including bacteria and fungi, they did not observe them at different concentrations. Using an annotation system based on Perring *et al,* aerosolised distilled water samples containing different concentrations of *E. coli* and *B. atropheus* were characterised. Interestingly, it was found that the fluorescent signature observed from the bacteria depended on the bacterial concentration present. As expected, the lower bacterial concentrations resulted in a lower number of fluorescent particles recorded and increasing the concentration increased the number of aerosols classified as fluorescent. However, unexpectedly, the fluorescent signature changed with increasing bacterial concentrations. Lower concentrations resulted in >3 fluorescent types whereas the higher concentrations were represented by two main types (Chapter 4, Table 4.19 and Table 4.22). Chapter 4 demonstrates the ability of the instrument to detect bacterial aerosols even at low concentrations, but also shows the benefit of having different fluorescent channels, in which different types of biological aerosols exhibit different responses.

While the fluorescent nebulised drug particles investigated in Chapters 3 and 4 were classed as an instrument interferent in terms of measuring biological particles, they may also be regarded as having an effect on hospital air quality, with one half hour period of nebulisation producing as much as 6.03×10^8 particles per m^3 (Chapter 3, Figure 3.8). An approach to modify this was therefore considered in Chapter 5. Nebulisers convert liquids into a fine mist of suspended particles, these polydisperse aerosols have a diameter of 1-5 µm, and are instantly inhalable into the respiratory tract. Several studies have emphasized concerns regarding the adverse effects of secondary exposure to nebulised aerosols (inhalation by people other than the intended patient), mainly with respect to cytotoxic drugs like cisplatin (Wittgen et al., 2006, Wittgen et al., 2007). The probability of asthma increases twofold along with

significant associations with bronchial hyperresponsiveness (BHR) following entry into a health care profession performing tasks involving aerosolized medication administration (Delclos et al., 2007). In Chapter 5, in collaboration with Professor Joseph Keane of St James's Hospital, Dublin, an intervention to reduce spread of aerosolised drugs was assessed with the WIBS instrument. The effectiveness of an extractor tent, usually used to enclose TB outpatients during collection of induced sputum samples in restricting access of nebulised drugs to room air, was determined. The tent showed 100% efficacy in restricting the dispersal of the two nebulised drugs in use on the CUH respiratory ward (Chapter 5, Table 5.2). Using the raw particle counts from nebuliser-related peaks in the ward data (Chapter 5, Table 5.5) it was calculated that on average a person at rest would inhale 1.56×10^{-3} – 2.49×10^{-3} mg of nebulised drug solution at average tidal volume per half hour. Pharmacological effects of this dose in bystanders seem unlikely according to the use of nebulised therapeutic doses for children of 0.125 mg/kg (Hung et al., 1999) and intravenous doses of 0.01 mg/kg in baboon studies of salbutamol-induced tachycardia (Du Plooy et al., 1994), however, an allergic response is possible. The risk of nosocomial airborne infection from exhaled nebuliser aerosols is unknown, although case reports suggesting spread of MDR-TB (Beck-Sagué et al., 1992) and SARS (Varia et al., 2003) exist. Eradicating nebuliser aerosol release on the ward using a tent would reduce any potential risk of nebuliser related airborne infection. Little research has been undertaken looking at the mass aerosols produced from nebulisers and the pathogen carrying potential of exhaled aerosols expelled, so this could be an area of future interest. A valved facemask with a filter placed on the exhalation port could be used to administer nebulised drugs to patients, similar to a simulated breathing set up by McGrath *et al.* (McGrath et al., 2019). The filter attached to the mouthpiece would capture any exhaled aerosols by the naturally breathing patient, and this would allow culture and DNA analysis of the captured liquid.

A preliminary analysis of DNA in air samples taken on six separate days over three months on the respiratory ward (Chapter 3, section 3.3) reported *Firmicutes* were the largest single phylum level, followed by *Actinobacteria* and *Bacteroidetes*. These are all commonly associated with soil and/or the human gut. Considering the ward housed

a communal lavatory, shared between 4 patients, and the air sampling location was ~2 m from the lavatory, this suggested the possibility of indirect airborne faecal contamination generated from the lavatory. To investigate this further, in Chapter 6, bioaerosol generation from toilet activities using a shared office lavatory was analysed using the WIBS. Although Johnson *et al.* compiled studies reporting the dispersal of contaminated nuclei generated from toilet flushing (Johnson et al., 2013), Chapter 6 is, to the author's knowledge, the first real-time bioaerosol investigation of toilet generated bioaerosols and interventions such as putting the seat down during flushing.

The WIBS was housed in a shared office lavatory. A timesheet was used to track all time variables, so data could synchronise with the event timestamp, and this assumed complete honesty from the occupant. Previous research in this field has shown dispersal from flushing (Johnson et al., 2013, Aithinne et al., 2019, Barker and Jones, 2005), continuous bioaerosol production through multiple flushes (Barker and Jones, 2005, Aithinne et al., 2019) and contamination of areas from toilet flushing (Barker and Jones, 2005, Best et al., 2012). Use of the toilet with the lid down during the current study (Chapter 6) resulted in particles with high fluorescent intensity remaining airborne for up to 8-minutes post flush, similarly fluorescent particles only lasted 1-minute post flush (Chapter 6, Table 6.23). The WIBS also revealed a small, but significant increase in the fluorescent counts observed with the lid up compared with down with defaecation, but not with urination (Chapter 6, Table 6.23). Although the WIBS has shown that lid down may paradoxically prolong infection risk, with particles remaining airborne longer, fluorescent airborne particles were still produced with the lid up. This suggest there is scope to review toilet systems which may reduce aerosolisation.

Several studies have examined the relationship between lid use and flushing (Gerba et al., 1975, Barker and Jones, 2005, Best et al., 2012) and they all highlighted the risk of not using a toilet lid. However, none of these studies utilised real-time monitoring, and only used conventional sampling using selective culture media. Best *et al.* reported closing the toilet seat lid resulted in a 10-fold reduction in the number of *C. difficile* recovered from air after flushing (Best et al., 2018). They suggested that

the low numbers of *C. difficile* recovered following flushing with the lid closed were aerosols being forced out through gaps between the top of the toilet bowl and seat, and between the lid and the seat (15 and 10 mm gaps, respectively) (Best et al., 2018).

The study by Best *et al.* examined droplets produced by *C. difficile* and they did not look at the air residency times between lid position, instead they used three thirty-minute sampling times from which CFU for *C. difficile* could be recovered. They found that in the first thirty minutes, the majority of *C. difficile* were recovered with the lid up, 10-fold more CFU than with the lid down. However, the number of CFU recovered with the lid down increased in the second 30-minute period, and conversely a 10—fold decrease was observed in the CFU collected with the lid up. Unfortunately, the conventional sampling used, settle plates and an air impactor (AirTrace Environmental portable sampler) cannot provide the time resolution that the WIBS provides, so we do not know when exactly the CFU were recovered with the lid up. They could, for example, have been recovered in the first minute of the 30-minute interval.

A mechanism for the production and dispersal of aerosols generated from flushing, which would account for the differences found between the lid up and lid down, was suggested (Chapter 6 and Figure 6.42). The foundation for this is formed by factors influencing acoustic turbulence with flushing. I hypothesised that leaving the lid down during flushing increases acoustic turbulence due to sound reverberation from the lid, and the increased turbulence increases particle velocity and collisions with increasing particle size. Lid design could be modified to test this hypothesis, for example, preventing reverberation from the lid surface using sound absorbing materials such as the recently developed water-stable, anti-microbial cellulose fibre foams (Ottenhall et al., 2018). An alternative approach to reduce toilet related aerosols without modifying flush turbulence is the commercially available, completely sealed “Safeflush” toilet seat developed by Croydex®. The “Safeflush” was purchased to test in the same shared office setting as was used in Chapter 4, but unfortunately, due to time constraints due to the optical chamber and circuit boards of the WIBS needing repair this study could not be completed. Several studies have reported decreased bioaerosol concentration

with decreased flush energy and turbulence (Aithinne et al., 2019, Johnson et al., 2013, Bound and Atkinson, 1966). Bound and Atkinson *et al.* reported that siphonic toilets produce approximately $1/14^{th}$ as much bioaerosol as a wash-down design for the same flush volume. In the future it would be interesting to see the results of an identical test using the "safeflush" toilet seat or even the proposed modified toilet lid or siphonic toilets to compare results with the results for a normal conventional toilet, as described in Chapter 6.

This thesis demonstrates that continuous observation of healthcare associated environments using bioaerosol detection provides biologically meaningful data allowing a detailed characterisation of these environments. This characterisation facilitates airborne particle source attribution, allows provisional standard setting, and provides a powerful mode of assessment of the results of interventions designed to increase air quality. Figure 7.1 summarises the main research objective as well as the findings of this thesis.

Finally, with regards to the research documented in this these the author suggests further studies into the aerosols produced form nebulised drugs. As mentioned previously little research has been undertaken looking at the mass aerosols produced from nebulisers and the pathogen carrying potential of exhaled aerosols expelled. Future studies could utilise valved facemasks which include filters placed on the exhalation port to administer nebulised drugs to patients, similar to a simulated breathing set up by McGrath *et al.* (McGrath et al., 2019). This would allow the culture and DNA analysis of captured exhaled aerosols from the naturally breathing patient.

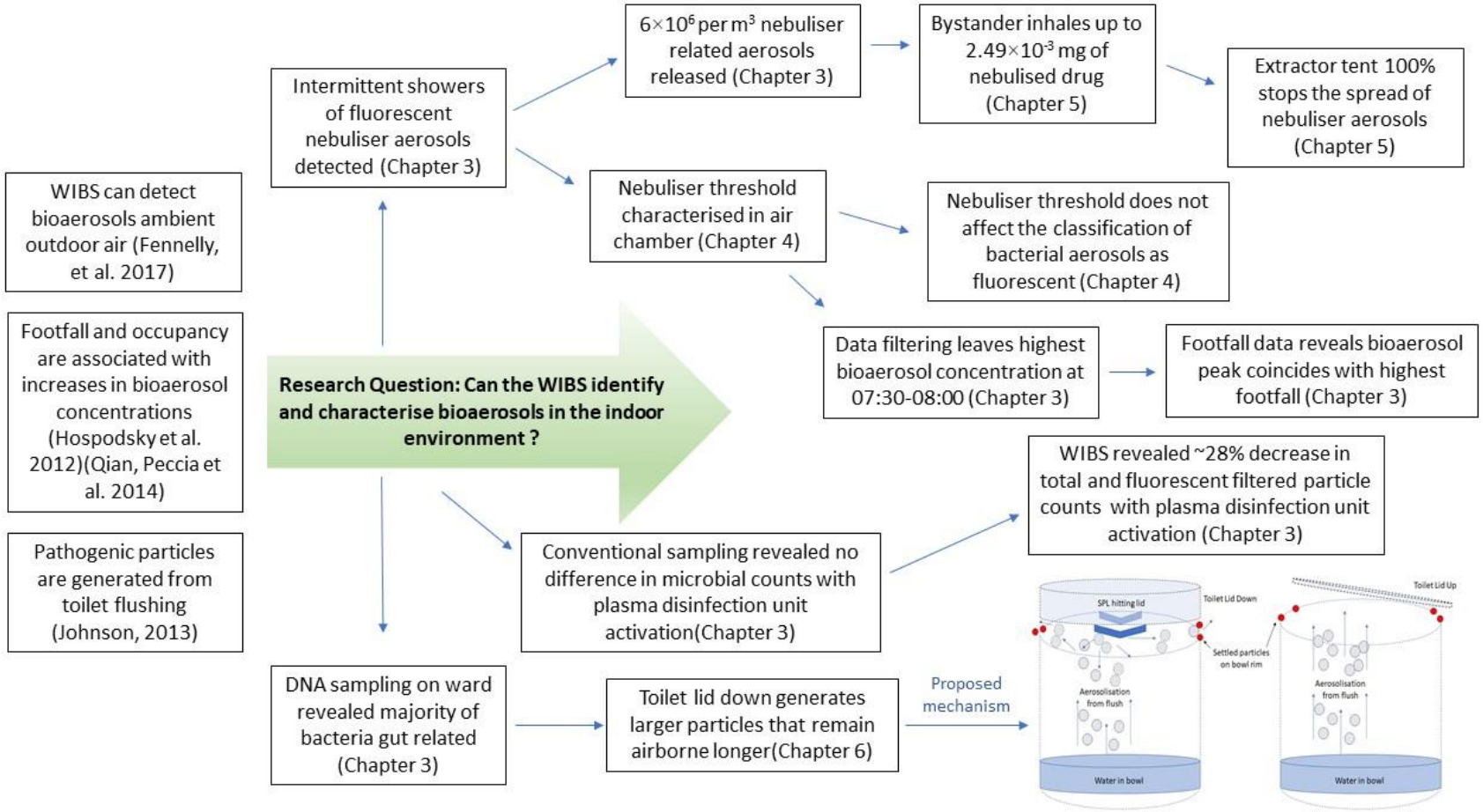

Figure 7.1 Summary of thesis findings

7.1 **References**

AITHINNE, K. A., COOPER, C. W., LYNCH, R. A. & JOHNSON, D. L. 2019. Toilet plume aerosol generation rate and environmental contamination following bowl water inoculation with Clostridium difficile spores. *American journal of infection control,* 47**,** 515-520.

BARKER, J. & JONES, M. 2005. The potential spread of infection caused by aerosol contamination of surfaces after flushing a domestic toilet. *Journal of applied microbiology,* 99**,** 339-347.

BECK-SAGUÉ, C., DOOLEY, S. W., HUTTON, M. D., OTTEN, J., BREEDEN, A., CRAWFORD, J. T., PITCHENIK, A. E., WOODLEY, C., CAUTHEN, G. & JARVIS, W. R. 1992. Hospital outbreak of multidrug-resistant Mycobacterium tuberculosis infections: factors in transmission to staff and HIV-infected patients. *Jama,* 268**,** 1280-1286.

BEST, E., PARNELL, P., COUTURIER, J., BARBUT, F., LE BOZEC, A., ARNOLDO, L., MADIA, A., BRUSAFERRO, S. & WILCOX, M. 2018. Environmental contamination by bacteria in hospital washrooms according to hand-drying method: a multi-centre study. *Journal of Hospital Infection,* 100**,** 469-475.

BEST, E., SANDOE, J. & WILCOX, M. 2012. Potential for aerosolization of Clostridium difficile after flushing toilets: the role of toilet lids in reducing environmental contamination risk. *Journal of Hospital Infection,* 80**,** 1-5.

BOUND, W. H. & ATKINSON, R. I. 1966. Bacterial Aerosol from Water Closets. A Comparison of Two Types of Pan and Two Types of Coyer. *Lancet***,** 1369-70.

BRASCHE, S. & BISCHOF, W. 2005. Daily time spent indoors in German homes–baseline data for the assessment of indoor exposure of German occupants. *International journal of hygiene and environmental health,* 208**,** 247-253.

DELCLOS, G. L., GIMENO, D., ARIF, A. A., BURAU, K. D., LUSK, C., STOCK, T., SYMANSKI, E., WHITEHEAD, L. W., ZOCK, J.-P. & BENAVIDES, F. G. 2007. Occupational risk factors and asthma among health care professionals. *American journal of respiratory and critical care medicine,* 175**,** 667-675.

DU PLOOY, W., HAY, L., KAHLER, C., SCHUTTE, P. & BRANDT, H. 1994. The dose-related hyper-and-hypokalaemic effects of salbutamol and its arrhythmogenic potential. *British journal of pharmacology,* 111**,** 73-76.

GERBA, C. P., WALLIS, C. & MELNICK, J. L. 1975. Microbiological hazards of household toilets: droplet production and the fate of residual organisms. *Applied microbiology,* 30**,** 229-237.

HARDIN, B. D., KELMAN, B. J. & SAXON, A. 2003. Adverse human health effects associated with molds in the indoor environment. *Journal of occupational and environmental medicine/American College of Occupational and Environmental Medicine,* 45**,** 470-478.

HUNG, C. H., CHU, D. M., WANG, C. L. & YANG, K. D. 1999. Hypokalemia and salbutamol therapy in asthma. *Pediatric pulmonology,* 27**,** 27-31.

HUSMAN, T. 1996. Health effects of indoor-air microorganisms. *Scandinavian journal of work, environment & health***,** 5-13.

JOHNSON, D., LYNCH, R., MARSHALL, C., MEAD, K. & HIRST, D. 2013. Aerosol generation by modern flush toilets. *Aerosol Science and Technology,* 47**,** 1047-1057.

MCGRATH, J. A., O'SULLIVAN, A., BENNETT, G., O'TOOLE, C., JOYCE, M., BYRNE, M. A. & MACLOUGHLIN, R. 2019. Investigation of the quantity of exhaled aerosols released into the environment during nebulisation. *Pharmaceutics,* 11**,** 75.

PEREIRA, M. L., KNIBBS, L. D., HE, C., GRZYBOWSKI, P., JOHNSON, G. R., HUFFMAN, J. A., BELL, S. C., WAINWRIGHT, C. E., MATTE, D. L. & DOMINSKI, F. H. 2017. Sources and dynamics of fluorescent particles in hospitals. *Indoor Air*.

PERRING, A. E. 2016. Chamber catalogues of optical and fluorescent signatures distinguish bioaerosol classes. *Atmospheric Measurement Techniques,* 9**,** 3283.

SAVAGE, N. J., KRENTZ, C. E., KÖNEMANN, T., HAN, T. T., MAINELIS, G., PÖHLKER, C. & HUFFMAN, J. A. 2017. Systematic characterization and fluorescence threshold strategies for the wideband integrated bioaerosol sensor (WIBS) using size-resolved biological and interfering particles. *Atmospheric Measurement Techniques,* 10**,** 4279-4302.

SHINN, E. A., GRIFFIN, D. W. & SEBA, D. B. 2003. Atmospheric transport of mold spores in clouds of desert dust. *Archives of Environmental & Occupational Health,* 58**,** 498.

VARIA, M., WILSON, S., SARWAL, S., MCGEER, A., GOURNIS, E. & GALANIS, E. 2003. Investigation of a nosocomial outbreak of severe acute respiratory syndrome (SARS) in Toronto, Canada. *Canadian Medical Association Journal,* 169**,** 285-292.

WITTGEN, B. P., KUNST, P. W., PERKINS, W. R., LEE, J. K. & POSTMUS, P. E. 2006. Assessing a system to capture stray aerosol during inhalation of nebulized liposomal cisplatin. *Journal of aerosol medicine,* 19**,** 385-391.

WITTGEN, B. P., KUNST, P. W., VAN DER BORN, K., VAN WIJK, A. W., PERKINS, W., PILKIEWICZ, F. G., PEREZ-SOLER, R., NICHOLSON, S., PETERS, G. J. & POSTMUS, P. E. 2007. Phase I study of aerosolized SLIT cisplatin in the treatment of patients with carcinoma of the lung. *Clinical Cancer Research,* 13**,** 2414-2421.

AITHINNE, K. A., COOPER, C. W., LYNCH, R. A. & JOHNSON, D. L. 2019. Toilet plume aerosol generation rate and environmental contamination following bowl water inoculation with Clostridium difficile spores. *American journal of infection control,* 47**,** 515-520.

BARKER, J. & JONES, M. 2005. The potential spread of infection caused by aerosol contamination of surfaces after flushing a domestic toilet. *Journal of applied microbiology,* 99**,** 339-347.

BECK-SAGUÉ, C., DOOLEY, S. W., HUTTON, M. D., OTTEN, J., BREEDEN, A., CRAWFORD, J. T., PITCHENIK, A. E., WOODLEY, C., CAUTHEN, G. & JARVIS, W. R. 1992. Hospital outbreak of multidrug-resistant Mycobacterium tuberculosis infections: factors in transmission to staff and HIV-infected patients. *Jama,* 268**,** 1280-1286.

BEST, E., PARNELL, P., COUTURIER, J., BARBUT, F., LE BOZEC, A., ARNOLDO, L., MADIA, A., BRUSAFERRO, S. & WILCOX, M. 2018.

Environmental contamination by bacteria in hospital washrooms according to hand-drying method: a multi-centre study. *Journal of Hospital Infection,* 100**,** 469-475.

BEST, E., SANDOE, J. & WILCOX, M. 2012. Potential for aerosolization of Clostridium difficile after flushing toilets: the role of toilet lids in reducing environmental contamination risk. *Journal of Hospital Infection,* 80**,** 1-5.

BOUND, W. H. & ATKINSON, R. I. 1966. Bacterial Aerosol from Water Closets. A Comparison of Two Types of Pan and Two Types of Coyer. *Lancet,* 1369-70.

BRASCHE, S. & BISCHOF, W. 2005. Daily time spent indoors in German homes–baseline data for the assessment of indoor exposure of German occupants. *International journal of hygiene and environmental health,* 208**,** 247-253.

DELCLOS, G. L., GIMENO, D., ARIF, A. A., BURAU, K. D., LUSK, C., STOCK, T., SYMANSKI, E., WHITEHEAD, L. W., ZOCK, J.-P. & BENAVIDES, F. G. 2007. Occupational risk factors and asthma among health care professionals. *American journal of respiratory and critical care medicine,* 175**,** 667-675.

DU PLOOY, W., HAY, L., KAHLER, C., SCHUTTE, P. & BRANDT, H. 1994. The dose-related hyper-and-hypokalaemic effects of salbutamol and its arrhythmogenic potential. *British journal of pharmacology,* 111**,** 73-76.

GERBA, C. P., WALLIS, C. & MELNICK, J. L. 1975. Microbiological hazards of household toilets: droplet production and the fate of residual organisms. *Applied microbiology,* 30**,** 229-237.

HARDIN, B. D., KELMAN, B. J. & SAXON, A. 2003. Adverse human health effects associated with molds in the indoor environment. *Journal of occupational and environmental medicine/American College of Occupational and Environmental Medicine,* 45**,** 470-478.

HUNG, C. H., CHU, D. M., WANG, C. L. & YANG, K. D. 1999. Hypokalemia and salbutamol therapy in asthma. *Pediatric pulmonology,* 27**,** 27-31.

HUSMAN, T. 1996. Health effects of indoor-air microorganisms. *Scandinavian journal of work, environment & health,* 5-13.

JOHNSON, D., LYNCH, R., MARSHALL, C., MEAD, K. & HIRST, D. 2013. Aerosol generation by modern flush toilets. *Aerosol Science and Technology,* 47**,** 1047-1057.

MCGRATH, J. A., O'SULLIVAN, A., BENNETT, G., O'TOOLE, C., JOYCE, M., BYRNE, M. A. & MACLOUGHLIN, R. 2019. Investigation of the quantity of exhaled aerosols released into the environment during nebulisation. *Pharmaceutics,* 11**,** 75.

PEREIRA, M. L., KNIBBS, L. D., HE, C., GRZYBOWSKI, P., JOHNSON, G. R., HUFFMAN, J. A., BELL, S. C., WAINWRIGHT, C. E., MATTE, D. L. & DOMINSKI, F. H. 2017. Sources and dynamics of fluorescent particles in hospitals. *Indoor Air*.

PERRING, A. E. 2016. Chamber catalogues of optical and fluorescent signatures distinguish bioaerosol classes. *Atmospheric Measurement Techniques,* 9**,** 3283.

SAVAGE, N. J., KRENTZ, C. E., KÖNEMANN, T., HAN, T. T., MAINELIS, G., PÖHLKER, C. & HUFFMAN, J. A. 2017. Systematic characterization and fluorescence threshold strategies for the wideband integrated bioaerosol sensor

(WIBS) using size-resolved biological and interfering particles. *Atmospheric Measurement Techniques,* 10**,** 4279-4302.

SHINN, E. A., GRIFFIN, D. W. & SEBA, D. B. 2003. Atmospheric transport of mold spores in clouds of desert dust. *Archives of Environmental & Occupational Health,* 58**,** 498.

VARIA, M., WILSON, S., SARWAL, S., MCGEER, A., GOURNIS, E. & GALANIS, E. 2003. Investigation of a nosocomial outbreak of severe acute respiratory syndrome (SARS) in Toronto, Canada. *Canadian Medical Association Journal,* 169**,** 285-292.

WITTGEN, B. P., KUNST, P. W., PERKINS, W. R., LEE, J. K. & POSTMUS, P. E. 2006. Assessing a system to capture stray aerosol during inhalation of nebulized liposomal cisplatin. *Journal of aerosol medicine,* 19**,** 385-391.

WITTGEN, B. P., KUNST, P. W., VAN DER BORN, K., VAN WIJK, A. W., PERKINS, W., PILKIEWICZ, F. G., PEREZ-SOLER, R., NICHOLSON, S., PETERS, G. J. & POSTMUS, P. E. 2007. Phase I study of aerosolized SLIT cisplatin in the treatment of patients with carcinoma of the lung. *Clinical Cancer Research,* 13**,** 2414-2421.